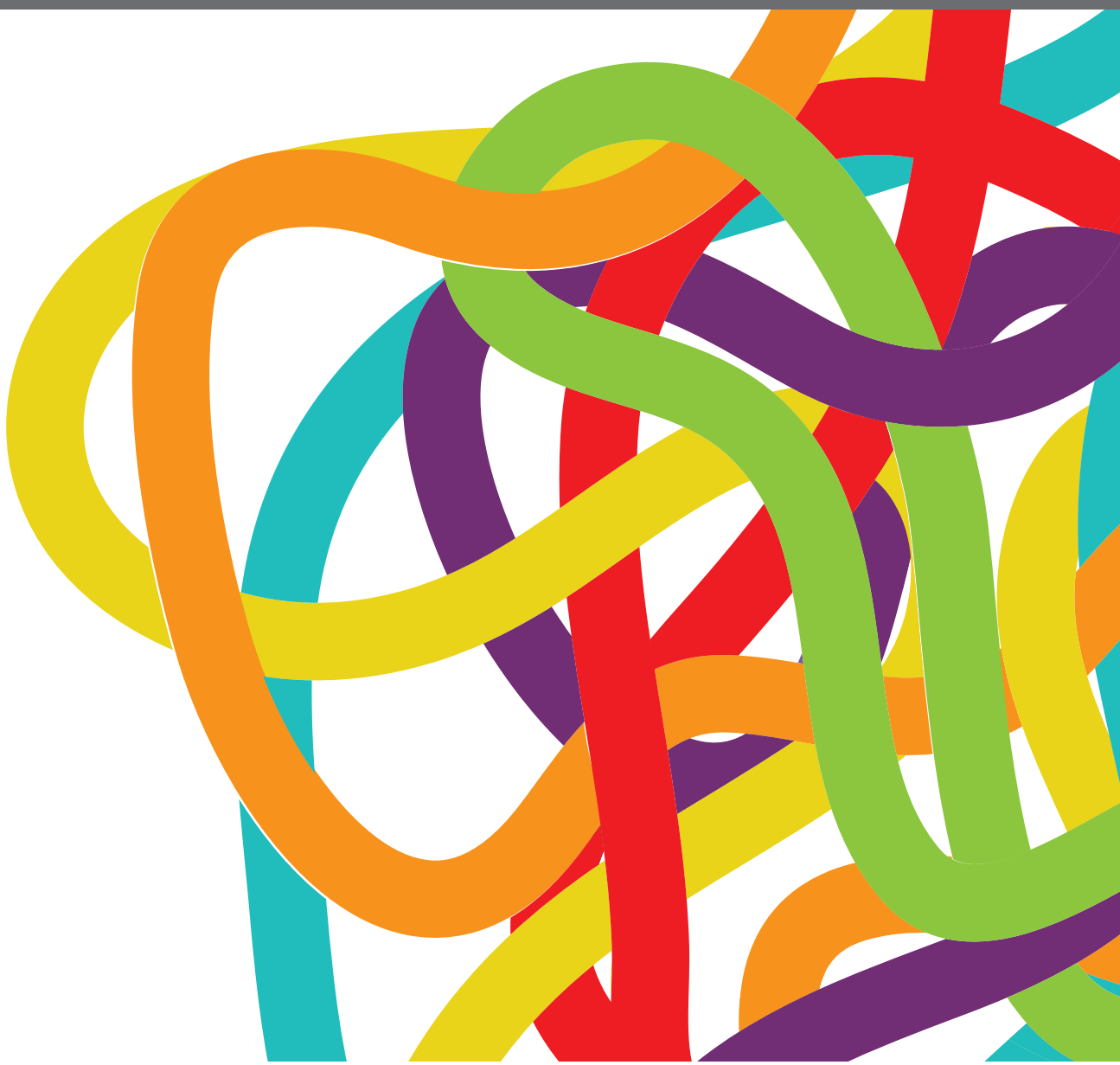
# INFLUENCES IN THE PROGRESSION OF RENAL CELL CARCINOMA

EDITED BY: Andrea Mari, Kouji Izumi and James H. Finke
PUBLISHED IN: Frontiers in Oncology



frontiers Research Topics



# frontiers

**Frontiers eBook Copyright Statement**

The copyright in the text of individual articles in this eBook is the property of their respective authors or their respective institutions or funders. The copyright in graphics and images within each article may be subject to copyright of other parties. In both cases this is subject to a license granted to Frontiers.

The compilation of articles constituting this eBook is the property of Frontiers.

Each article within this eBook, and the eBook itself, are published under the most recent version of the Creative Commons CC-BY licence. The version current at the date of publication of this eBook is CC-BY 4.0. If the CC-BY licence is updated, the licence granted by Frontiers is automatically updated to the new version.

When exercising any right under the CC-BY licence, Frontiers must be attributed as the original publisher of the article or eBook, as applicable.

Authors have the responsibility of ensuring that any graphics or other materials which are the property of others may be included in the CC-BY licence, but this should be checked before relying on the CC-BY licence to reproduce those materials. Any copyright notices relating to those materials must be complied with.

Copyright and source acknowledgement notices may not be removed and must be displayed in any copy, derivative work or partial copy which includes the elements in question.

All copyright, and all rights therein, are protected by national and international copyright laws. The above represents a summary only. For further information please read Frontiers' Conditions for Website Use and Copyright Statement, and the applicable CC-BY licence.

ISSN 1664-8714
ISBN 978-2-83250-636-3
DOI 10.3389/978-2-83250-636-3

## About Frontiers

Frontiers is more than just an open-access publisher of scholarly articles: it is a pioneering approach to the world of academia, radically improving the way scholarly research is managed. The grand vision of Frontiers is a world where all people have an equal opportunity to seek, share and generate knowledge. Frontiers provides immediate and permanent online open access to all its publications, but this alone is not enough to realize our grand goals.

## Frontiers Journal Series

The Frontiers Journal Series is a multi-tier and interdisciplinary set of open-access, online journals, promising a paradigm shift from the current review, selection and dissemination processes in academic publishing. All Frontiers journals are driven by researchers for researchers; therefore, they constitute a service to the scholarly community. At the same time, the Frontiers Journal Series operates on a revolutionary invention, the tiered publishing system, initially addressing specific communities of scholars, and gradually climbing up to broader public understanding, thus serving the interests of the lay society, too.

## Dedication to Quality

Each Frontiers article is a landmark of the highest quality, thanks to genuinely collaborative interactions between authors and review editors, who include some of the world's best academicians. Research must be certified by peers before entering a stream of knowledge that may eventually reach the public - and shape society; therefore, Frontiers only applies the most rigorous and unbiased reviews.
Frontiers revolutionizes research publishing by freely delivering the most outstanding research, evaluated with no bias from both the academic and social point of view. By applying the most advanced information technologies, Frontiers is catapulting scholarly publishing into a new generation.

## What are Frontiers Research Topics?

Frontiers Research Topics are very popular trademarks of the Frontiers Journals Series: they are collections of at least ten articles, all centered on a particular subject. With their unique mix of varied contributions from Original Research to Review Articles, Frontiers Research Topics unify the most influential researchers, the latest key findings and historical advances in a hot research area! Find out more on how to host your own Frontiers Research Topic or contribute to one as an author by contacting the Frontiers Editorial Office: frontiersin.org/about/contact

# INFLUENCES IN THE PROGRESSION OF RENAL CELL CARCINOMA

Topic Editors:
**Andrea Mari,** Careggi University Hospital, Italy
**Kouji Izumi,** Kanazawa University, Japan
**James H. Finke,** Case Western Reserve University, United States

**Citation:** Mari, A., Izumi, K., Finke, J. H., eds. (2022). Influences in the Progression of Renal Cell Carcinoma. Lausanne: Frontiers Media SA.
doi: 10.3389/978-2-83250-636-3

# Table of Contents


05 ***Editorial: Influences in the Progression of Renal Cell Carcinoma***
Mara Bacchiani, Antonio Andrea Grosso, Fabrizio Di Maida, Lorenzo Masieri, Andrea Minervini and Andrea Mari

08 ***The Diagnostic and Immunotherapeutic Value of CD248 in Renal Cell Carcinoma***
Keying Zhang, Chao Xu, Shaojie Liu, Yao Jiang, Xiaolong Zhao, Shanjin Ma, Yu Li, Fa Yang, Yan Wang, Ping Meng, Changhong Shi, Donghui Han, Weihong Wen and Weijun Qin

19 ***Cancer Associated Fibroblasts Promote Renal Cancer Progression Through a TDO/Kyn/AhR Dependent Signaling Pathway***
Li-bo Chen, Shun-ping Zhu, Tian-pei Liu, Heng Zhao, Ping-feng Chen, You-jun Duan and Rong Hu

29 ***SLC39A8/Zinc Suppresses the Progression of Clear Cell Renal Cell Carcinoma***
Lilong Liu, Yaxin Hou, Junyi Hu, Lijie Zhou, Ke Chen, Xiong Yang and Zhengshuai Song

45 ***Review of Prognostic Expression Markers for Clear Cell Renal Cell Carcinoma***
Florent Petitprez, Mira Ayadi, Aurélien de Reyniès, Wolf H. Fridman, Catherine Sautès-Fridman and Sylvie Job

56 ***KDF1, a Novel Tumor Suppressor in Clear Cell Renal Cell Carcinoma***
Jing-min Zheng, Mei-fu Gan, Hong-yuan Yu, Lu-xia Ye, Qing-xin Yu, Yu-hui Xia, Han-xi Zhou, Jia-qian Bao and Yi-qing Guo

69 ***Oncological Outcomes of Patients With Different Pathological Features of pT3a Renal Tumor: A Systematic Review and Quantitative Synthesis***
Pengju Guo, Yongxing Wang, Yili Han, Dechao Wei, Jiahui Zhao, Mingchuan Li, Yongguang Jiang and Yong Luo

82 ***Incidence, Clinical Characteristics, and Survival of Collecting Duct Carcinoma of the Kidney: A Population-Based Study***
Chaopeng Tang, Yulin Zhou, Silun Ge, Xiaoming Yi, Huichen Lv and Wenquan Zhou

91 ***Comparison of Perioperative, Renal Functional, and Oncological Outcomes Between Off-Clamp and On-Clamp Robot-Assisted Partial Nephrectomy for Renal Tumors: An Updated Evidence-Based Analysis***
Yin Huang, Dehong Cao, Zeyu Chen, Bo Chen, Jin Li, Jianbing Guo, Qiang Dong, Qiang Wei and Liangren Liu

102 ***Identification of a Novel Stem Cell Subtype for Clear Cell Renal Cell Carcinoma Based on Stem Cell Gene Profiling***
Hongzhi Wang, Hanjiang Xu, Quan Cheng and Chaozhao Liang

115 ***$CD248^{+}$ Cancer-Associated Fibroblasts: A Novel Prognostic and Therapeutic Target for Renal Cell Carcinoma***
Chao Xu, Keying Zhang, Fa Yang, Xiang Zhou, Shaojie Liu, Yu Li, Shanjin Ma, Xiaolong Zhao, Tong Lu, Shiqi Lu, JiaYu Zhang, Hongji Li, Donghui Han, Weihong Wen and Weijun Qin

128 ***Differentially Expressed Genes in Clear Cell Renal Cell Carcinoma as a Potential Marker for Prognostic and Immune Signatures***
Ying Tong, Yiwen Yu, Hui Zheng, Yanchun Wang, Suhong Xie, Cuncun Chen, Renquan Lu and Lin Guo

140 ***MCM2-7 in Clear Cell Renal Cell Carcinoma: MCM7 Promotes Tumor Cell Proliferation***
Junneng Zhang, Huanzong Zhang, Yinghui Wang and Qingshui Wang

154 ***Adipogenic Transdifferentiation and Regulatory Factors Promote the Progression and the Immunotherapy Response of Renal Cell Carcinoma: Insights From Integrative Analysis***
Shuai Wang, Xiyi Wei, Chengjian Ji, Yichun Wang, Xi Zhang, Rong Cong and Ninghong Song

168 ***Identification of PLAUR-Related ceRNA and Immune Prognostic Signature for Kidney Renal Clear Cell Carcinoma***
Yu Wang, Zhuolun Sun, Shuo Lu, Xu Zhang, Chutian Xiao, Tengcheng Li and Jieying Wu

frontiers | Frontiers in Oncology

TYPE Editorial
PUBLISHED 14 October 2022
DOI 10.3389/fonc.2022.1059615

Check for updates

OPEN ACCESS

EDITED AND REVIEWED BY
Ronald M Bukowski,
Cleveland Clinic, United States

*CORRESPONDENCE
Andrea Mari
andreamari08@gmail.com

SPECIALTY SECTION
This article was submitted to Genitourinary Oncology, a section of the journal Frontiers in Oncology

RECEIVED 01 October 2022
ACCEPTED 03 October 2022
PUBLISHED 14 October 2022

CITATION
Bacchiani M, Grosso AA, Di Maida F, Masieri L, Minervini A and Mari A (2022) Editorial: Influences in the progression of renal cell carcinoma. *Front. Oncol.* 12:1059615. doi: 10.3389/fonc.2022.1059615

COPYRIGHT
© 2022 Bacchiani, Grosso, Di Maida, Masieri, Minervini and Mari. This is an open-access article distributed under the terms of the Creative Commons Attribution License (CC BY). The use, distribution or reproduction in other forums is permitted, provided the original author(s) and the copyright owner(s) are credited and that the original publication in this journal is cited, in accordance with accepted academic practice. No use, distribution or reproduction is permitted which does not comply with these terms.

# Editorial: Influences in the progression of renal cell carcinoma

Mara Bacchiani[1,2], Antonio Andrea Grosso[1,2], Fabrizio Di Maida[1,2], Lorenzo Masieri[1,2], Andrea Minervini[1,2] and Andrea Mari[1,2]*

[1]Department of Urology, University of Florence, Florence, Italy, [2]Department of Experimental and Clinical Medicine, University of Florence, Florence, Italy

KEYWORDS

**renal cell carcinoma, molecular diagnosis, molecular factors, progression, localized renal cancer**

Editorial on the Research Topic
Influences in the progression of renal cell carcinoma

Renal cell carcinoma (RCC) is the most common kidney cancer and represents approximately 2-3% of all human tumors. Clear cell RCC (ccRCC) is the most common histological subtype, followed in the order by papillary (pRCC), chromophobe (chRCC) and collecting duct carcinoma (CDCK) (Tang et al.).

In 2020, there were approximately 74,000 new cases and 15,000 deaths in the United States. Over the years, an annual increase of about 3% in incidence has been shown in most of the world (1). The increasing incidence could be due to the wide use of ultrasound, computed tomography (CT) and magnetic resonance imaging (MRI) during screenings and medical evaluations, since more than 80% of kidney cancers are incidental findings (Liu et al.).

At diagnosis most of renal cancers are asymptomatic, non-palpable, still localized, that is intracapsular (T1 and T2) or locally advanced tumors (2).

Partial nephrectomy is currently recommended by the European Guidelines as the standard surgical treatment for cT1 (<7 cm) renal tumors because its oncologic outcomes are equivalent and its functional outcomes are superior comparing with those of radical nephrectomy (Huang et al.).

Partial nephrectomy has been also extended to clinical T2 renal tumors with promising oncological outcomes (3).

RCC presents a 5-year relative survival rate of 76%, although survival is highly dependent on the stage at diagnosis. Nevertheless, around 30% of patients with localized tumors, developed local recurrence or tumor progression within three to five years (4, 5).

Many studies have been led to identify prognostic factors to individualize surveillance and select high-recurrence risk patients which could benefit from adjuvant therapy.

Tumour grade and histotype are prognostic factors recommended by the EAU guidelines. For example, collecting duct carcinoma from the epithelium of the collecting ducts of Bellini is an aggressive malignant tumor and has a poorer prognosis and more limited response to immunotherapy comparing with most common histotypes (Tang et al.).

Others consolidated prognostic factors are TNM classification, presence of sarcomatoid or rhabdoid features, microvascular invasion (MVI), tumor necrosis, pelvicalyceal system invasion, renal vein invasion and renal sinus invasion, that is infiltration of tumor into the peri-renal fat (6, 7).

On the other hand, the lymphovascular invasion seems not to be significantly correlated to cancer-specific survival (CSS) (Guo et al.).

Positive surgical margin (PSM) is an important predictor of disease-free survival (DFS) in patients with advanced T classification, in fact positive margin determine 18-fold higher risk of recurrence (3), but PSM has no impact on cancer-specific survival after partial nephrectomy for T1 neoplasia because of low cancer progression rate (8). In fact the relationship between PSM and increased risk of recurrence after partial nephrectomy is still uncertain.

Moving from these aggressive pathological characteristics, an individualized risk-based approach might be useful to decide follow-up protocols and postoperative therapies after radical or partial nephrectomy.

There is poor level of evidence about the use of prognostic models in patients with localized RCC, such as Leibovich score and the University of California Integrated Staging System (UISS) score. However, these tools represent a useful guide for patients' enrollment into adjuvant clinical trials.

In this special issue, several studies have been conducted to understand the molecular mechanisms underlying RCC and its recurrence and metastasis process to identify factors which influence the progression of the disease and to provide new molecular and therapeutic strategies for patients with RCC.

A review synthetized that main biological pathways altered in ccRCC are cell cycle, angiogenesis, hypoxia, and immune response (Petitprez et al.). Since the von Hippel–Lindau (VHL) gene has been identified in 1993, VHL gene mutation has been reported in 70% of ccRCC tumors and its hypermethylation in 15%. The VHL gene inactivation conducts to hypoxia-inducible factors (HIF1a-HIF1b) activation and to increasing angiogenesis through vascular endothelial growth factor (VEGF) signaling (Petitprez et al., Wang et al., Tong et al.).

Therefore, anti-angiogenic tyrosine kinase inhibitors (TKI) and monoclonal antibodies against VEGF have become a crucial treatment option for ccRCC patients (9).

VHL mutation might also be involved in immunoregulation by activating the effector T cells and enhancing cytokine level in ccRCC.

Many studies underline that extracellular matrix (ECM) and tumor microenvironment (TME) are crucial for tumor development, tumor progression and metastasis spread (Xu et al.).

In fact, several stromal and immune cells, such as myeloid inhibitory cells, tumor associated macrophages, mesenchymal stem cells and cancer-associated fibroblasts (CAFs), provide vascularization, drop immunitary defence, and build a matrix barrier in order to promote cancer cells' survival.

As soon as the tumor is born, multiple CAFs begin to appear and secrete multiple pro-tumor factors which promote neo-angiogenesis, remodel the ECM, modify immunoregulation and favorite therapeutic resistance (Chen et al.).

Immunohistochemical identification of immune biomarkers, such as CD8 and PD-L1, led to introduction of immune checkpoint inhibitors, such as Pembrolizumab and Nivolumab, which block programmed cell death protein-1 (PD-1), or Ipilimumab, which is cytotoxic T-lymphocyte-associated protein 4 (CTLA-4) inhibitor.

PD-1 immune checkpoint inhibitors, as well as CTLA-4 inhibitors, proved themselves clinically safe and effective by improving objective response rates like progression-free survival (PFS) and overall survival (OS) and have become the first line standard of care in PDL1-positive metastatic disease (Wang et al.).

TME with its complexity is the target of last decade innovative therapies, such as immune checkpoint inhibitors (ICIs) and anti-angiogenic tyrosine kinase inhibitors (TKIs), but is also the origin of many potential therapeutic resistances.

For example the TME activation of angiogenic escape pathways decreased the therapeutic response to TKIs.

CD248, a specific biomarker of activated fibroblasts and pericytes residing in tumor blood vessels, is upregulated in RCC and may represent a novel prognostic and therapeutic target and the antibody-drug targeting CD248 might overcome the immunosuppressive TME and help to destroy cancer (Xu et al., Zhang et al.).

Moreover, adipose-related genes (ARGs) expression is associated with immune cell infiltration and immune microenvironment in ccRCC. The adipogenic transdifferentiation status of tumor cells is closely related to prognosis and ARGs expression may be a novel independent biomarker in the prediction of ccRCC patients' survival (Wang et al.).

Others potential target are AKT and STAT3 signaling pathways, activated by aromatic hydrocarbon receptor (AhR) which is up-regulated by kynurenine (Kyn) produced by CAFs. Alternatively downregulate AhR might improve the antitumoral effects of Sorafenib or Sutinib(Chen et al.).

The urokinase-type plasminogen activator receptor (PLAUR) is upregulated in RCC, such as in several other cancers, and is associated with poor OS and DFS. PLAUR is involved in various malignancy-related processes, including angiogenesis, cell differentiation, proliferation and migration and its expression increases with tumor grade and stage. PLAUR also regulates several immune cells, such as CD4+ T

cells and macrophages, which promote respectively RCC cell proliferation and invasion (Wang et al.).

Malignant cells are characterized by unlimited DNA replication. The minichromosome maintenance proteins (MCM2-7) are essential initiation factors in DNA replication and their expression is increased in ccRCC, especially in patients with a poor prognosis. Therefore, MCM2-7 overexpression is an important biomarker and a potential molecular target (Zhang et al.).

Between tumor suppressor mutated in ccRCC we can count Keratinicyte Differentiation Factor1 (KDF1). Its expression levels correlate negatively with tumor grade and tumor stage, and positively with patients' survival. Overexpression of KDF1 is associated to reduction of ccRCC cells' proliferation, migration and invasion (Zheng et al.).

Other tumor suppressors are Zrt- and Irt-like proteins (ZIP) family members (SLC39A1-14), which function is to pass zinc into the cytoplasm for many biological anti-neoplastic processes. A study showed that down-regulation of SLC39A8 is involved in ccRCC progression and lower expression of SLC39A8 correlates to worse prognosis (Liu et al.).

As these factors may allow a better identification of patients who could respond to immunotherapy by outlining real immune signatures, it is of utmost importance to define appropriate algorithms to correctly define personalized treatments and, eventually, determine bioindicators for cancer monitoring during follow-up.

New molecular-based research on oncogenes, tumor suppressors, cancer associated fibroblasts are needed to identify biomarkers which influence RCC progression and prognosis, to guide the clinical management with personalized treatment strategies and to improve survival outcomes for RCC patients.

## Author contributions

MB: Writing original draft. AG: Writing original draft. FM: Supervision. LM: Conceptualization. AMi: Conceptualization. AMa: Conceptualization, Writing original draft, Supervision. All authors have made a substantial contribution to the manuscript and have read and approved the final manuscript.

## Conflict of interest

The authors declare that the research was conducted in the absence of any commercial or financial relationships that could be construed as a potential conflict of interest.

## Publisher's note

All claims expressed in this article are solely those of the authors and do not necessarily represent those of their affiliated organizations, or those of the publisher, the editors and the reviewers. Any product that may be evaluated in this article, or claim that may be made by its manufacturer, is not guaranteed or endorsed by the publisher.

## References

1. Padala SA, Barsouk A, Thandra KC, Saginala K, Mohammed A, Vakiti A, et al. Epidemiology of renal cell carcinoma. *World J Oncol* (2020) 11:3. doi: 10.14740/WJON1279

2. Brassetti A, Anceschi U, Bertolo R, Ferriero M, Tuderti G, Capitanio U, et al. Surgical quality, cancer control and functional preservation: Introducing a novel trifecta for robot-assisted partial nephrectomy. *Minerva Urol Nefrol* (2020) 72:1. doi: 10.23736/S0393-2249.19.03570-7

3. Bertolo R, Autorino R, Simone G, Derweesh I, Garisto JD, Minervini A, et al. Outcomes of robot-assisted partial nephrectomy for clinical T2 renal tumors: A multicenter analysis (ROSULA collaborative group). *Eur Urol* (2018) 74:2. doi: 10.1016/j.eururo.2018.05.004

4. Ljungberg B, Albiges L, Abu-Ghanem Y, Bedke J, Capitanio U, Dabestani S, et al. European association of urology guidelines on renal cell carcinoma: The 2022 update. *Eur Urol* (2022) 82(4):399–410. doi: 10.1016/j.eururo.2022.03.006

5. Di Martino S, De Luca G, Grassi L, Federici G, Alfonsi R, Signore M, et al. Renal cancer: New models and approach for personalizing therapy. *J Exp Clin Cancer Res* (2018) 37:1. doi: 10.1186/s13046-018-0874-4

6. Klatte T, Rossi SH, Stewart GD. Prognostic factors and prognostic models for renal cell carcinoma: a literature review. *World J Urol* (2018) 36:12. doi: 10.1007/s00345-018-2309-4

7. Anceschi U, Ferriero MC, Tuderti G, Brassetti A, Bertolo R, Capitanio U, et al. Head to head impact of margin, ischemia, complications, score versus a novel trifecta score on oncologic and functional outcomes after robotic-assisted partial nephrectomy: Results of a multicenter series. *Eur Urol Focus* (2021) 7(6):1391–99. doi: 10.1016/j.euf.2020.06.021

8. Schiavina R, Mari A, Bianchi L, Amparore D, Antonelli A, Artibani W, et al. Predicting positive surgical margins in partial nephrectomy: A prospective multicentre observational study (the RECORd 2 project). *Eur J Surg Oncol* (2020) 46:7. doi: 10.1016/j.ejso.2020.01.022

9. Sun M, Shariat SF, Cheng C, Ficarra V, Murai M, Oudard S, et al. Prognostic factors and predictive models in renal cell carcinoma: A contemporary review. *Eur Urol* (2011) 60:4. doi: 10.1016/j.eururo.2011.06.041

frontiers in Oncology

ORIGINAL RESEARCH
published: 12 March 2021
doi: 10.3389/fonc.2021.644612

# The Diagnostic and Immunotherapeutic Value of CD248 in Renal Cell Carcinoma

*Keying Zhang[1†], Chao Xu[1†], Shaojie Liu[1†], Yao Jiang[1], Xiaolong Zhao[1], Shanjin Ma[2], Yu Li[1], Fa Yang[1], Yan Wang[3], Ping Meng[1], Changhong Shi[4], Donghui Han[1*], Weihong Wen[5*] and Weijun Qin[1*]*

[1] Department of Urology, Xijing Hospital, Fourth Military Medical University, Xi'an, China, [2] Department of Urology, Tangdu Hospital, Fourth Military Medical University, Xi'an, China, [3] Department of Emergency, 987th Hospital of the Chinese People's Liberation Army, Baoji, China, [4] Laboratory Animal Center, Fourth Military Medical University, Xi'an, China, [5] Institute of Medical Research, Northwestern Polytechnical University, Xi'an, China

OPEN ACCESS

**Edited by:**
Andrea Mari,
Careggi University Hospital, Italy

**Reviewed by:**
Valentina Devescovi,
Partner Institute for Computational Biology, China
Enrico Checcucci,
Istituto di Candiolo (IRCCS), Italy

***Correspondence:**
Donghui Han
906812205@qq.com
Weihong Wen
wenweih@fmmu.edu.cn
Weijun Qin
qinwj@fmmu.edu.cn

[†]These authors have contributed equally to this work

**Specialty section:**
This article was submitted to Genitourinary Oncology, a section of the journal Frontiers in Oncology

**Received:** 21 December 2020
**Accepted:** 08 February 2021
**Published:** 12 March 2021

**Citation:**
Zhang K, Xu C, Liu S, Jiang Y, Zhao X, Ma S, Li Y, Yang F, Wang Y, Meng P, Shi C, Han D, Wen W and Qin W (2021) The Diagnostic and Immunotherapeutic Value of CD248 in Renal Cell Carcinoma. Front. Oncol. 11:644612. doi: 10.3389/fonc.2021.644612

**Background:** Renal cell carcinoma (RCC) is the most common malignancy in the urinary system. Despite substantial improvements in available treatment options, the survival outcome of advanced RCC is unsatisfactory. Identifying novel biomarkers to assist in early diagnosis and to screen patients who are sensitive to immunotherapy would be beneficial. CD248 is a promising candidate that deserves to be investigated.

**Methods:** The Cancer Genome Atlas (TCGA) data set and clinical specimens were adopted to analyze the expression of CD248 between normal and tumor tissues. Univariate and multivariate Cox regression analyses were employed to identify independent prognostic factors and construct a CD248-based prognostic signature. The correlation among the present signature, tumor-infiltrating immune cells (TIICs), the tumor mutation burden (TMB), and immunomodulatory molecules was evaluated. The weighted gene co-expression network analysis (WGCNA), the enrichment analysis, and the miRNA correlation analysis were performed to explore the underlying mechanism of CD248 in the progression of RCC.

**Results:** The overexpression of CD248 in RCC was related to a poor prognosis, and a CD248-based prognostic signature could precisely stratify patients with RCC with different survival outcomes regardless of the training or testing cohort. The present signature could reflect the immunosuppressive landscape of RCC (i.e., increased infiltration of regulatory T cells and upregulated immune checkpoints), accompanied by deteriorated clinicopathologic indexes. The TMB and immunostimulatory molecules expression also increased with the risk score generated from the present signature. CD248 co-expressed gene sets were identified through the WGCNA algorithm, and several immunosuppressive Gene Ontology (GO) terms and Kyoto Encyclopedia of Genes and Genomes (KEGG) pathways were significantly enriched. The result of CD248-correlated miRNA further emphasized the importance of CD248 in RCC.

**Conclusion:** CD248 is a valuable biomarker to improve the diagnostic and therapeutic efficiency of RCC. The immunosuppressive effect of CD248 co-expressed genes may provide insight for the present study, and miRNA would help to reveal the mechanism of the expressive regulation of CD248.

**Keywords: renal cell carcinoma, CD248, immunotherapy, prognosis, molecular cancer signature**

## INTRODUCTION

Renal cell carcinoma (RCC) is the seventh most common neoplasm in the developed world and the most lethal malignancy in the urinary system (1). As reported, the morbidity of RCC has more than doubled in North America and Western Europe over the past half century and is predicted to rapidly increase in Latin America, Asia, and Africa in the coming decades (2). Actually, RCC is an insidious neoplasm with one-third of cases initially diagnosed as metastatic, whose survival rate is abysmally low. Despite treatment options for RCC have been revolutionized by targeted therapy, the 5-year survival rate of advanced/metastatic RCC is only 12% (3). Immunotherapy with immune checkpoint inhibitors to block PD1, CTLA4, and LAG3 is another promising method to promote the survival outcome of patients with RCC (4–6). However, the low response rate restricts its therapeutic efficacy (7). Hence, identifying novel biomarkers to facilitate the early diagnosis of patients who are asymptomatic and to assist clinicians for screening the ones who are sensitive to immunotherapy would be beneficial for the prognosis of RCC.

Tumor endothelial markers (TEMs) involved with tumor-specific angiogenesis play a crucial role in the development and progression of tumors, among which TEM1 (also known as endosialin or CD248) is specifically overexpressed in tumor-associated fibroblasts and pericytes residing in tumor blood vessels. It has been found that CD248 is an essential molecule associated with cell adhesion, migration, and stromal cell proliferation (8). Once CD248 is knocked out in mice, there was a striking reduction in the growth of the tumors, invasiveness, and metastasis after tumor transplantation, indicating that CD248-positive stroma would promote malignancy (9). Therefore, CD248-characterized tumor vasculature (10) and stroma (11) were regarded as promising targets for the therapy of tumors. However, whether CD248 can predict the prognosis of RCC and guide immunotherapy is largely unknown.

To explore the predictive value of CD248 in RCC, we conducted the present study. The Cancer Genome Atlas (TCGA) data set and clinical specimens were adopted to analyze the expression of CD248 between normal and tumor tissues. Then, we constructed a CD248-based prognostic signature by integrating multiple clinical variables, which acquired the promoted predictive accuracy. The correlation among the present signature, tumor-infiltrating immune cells (TIICs), the tumor mutation burden (TMB), and immunomodulatory molecules was also evaluated. Finally, the weighted gene co-expression network analysis (WGCNA) and enrichment analysis were performed to explore the underlying mechanism of CD248 in the progression of RCC.

## MATERIALS AND METHODS

### Data Source and Preprocessing

Renal cell carcinoma data (895) and non-tumor data (128) were downloaded from the TCGA portal (https://portal.gdc.cancer.gov/). Transcriptomic data [RNA sequencing (RNA-Seq) Fragments Per Kilobase Million (FPKM)], miRNA isoform expression, and clinical information were integrated through ID numbers. The genes measured with multi-probes were replaced with their average *via* limma package (12). All data were processed and analyzed with R software (https://www.r-project.org/).

### The Differential Expression Analysis of CD248

Differentially expressed genes (DEGs) between tumor and normal tissues were analyzed through the Wilcox test. The *p*-value was adjusted with the false discovery rate (FDR), and the filter criteria were FDR $< 0.05$ and $|\log_2$ fold-change [FC]$| > 1$. The expression of CD248 between groups was analyzed through the *t*-test and visualized with the GraphPad Prism 8 (GraphPad Software, San Diego, CA, USA). A body map of the expression of CD248 was obtained from the Gene Expression Profiling Interactive Analysis (GEPIA) website (http://gepia.cancer-pku.cn/), and the expression median was normalized to transcripts per million (TPM).

### Qualitative Evaluation of the Expression of CD248 in RCC

Paraffin-embedded tissue microarrays (Outdo Biotech, Shanghai, China) were deparaffinized, rehydrated, and treated with 3% hydrogen peroxide for 10 min to inhibit endogenous peroxidase activity. Heat-mediated retrieval of antigens was performed in citrate buffer for 2 min. After being blocked with 5% bovine serum albumin (BSA) for 30 min, slides were incubated with rabbit anti-human CD248 primary antibody (1:2,000, ab204914, Abcam, MA, USA) overnight at 4°C. The immunodetection was performed using the standard rapid EnVision technique (Dako, Glostrup, Denmark). Subsequently, slides were washed in distilled water and counterstained with hematoxylin. Digital images for qualitative evaluation were obtained using an optical microscope (BX51, Olympus, Tokyo, Japan).

### The Prognostic Value Analysis of CD248 in RCC

Patients with TCGA-RCC were divided into high expression and low expression groups according to the median expression level of CD248. Then, Kaplan–Meier survival analysis and

receiver operating characteristic (ROC) analysis were performed to evaluate the prognostic value and the predictive accuracy of CD248, respectively. Univariate and multivariate Cox regression analyses were employed to identify the independent prognostic factors of RCC. $p < 0.05$ was considered statistically significant.

## The Construction and Validation of the CD248-based Prognostic Signature

Patients with TCGA-RCC with complete clinical information ($n = 246$) were used as a training cohort, and patients with TCGA-clear cell RCC (ccRCC) with certain clinical information (i.e., age, histological grade, pathological stage, and M status) were selected as a testing cohort ($n = 489$). The training cohort was used to construct a CD248-based prognostic signature, and the testing cohort was used to confirm its performance. The survival R package was adopted to construct the present signature by integrating clinicopathological variables [i.e., age, gender, histological grade, pathological stage, and tumor-node-metastasis (TNM) status] with the expression level of CD248. To avoid overfitting, clinicopathological variables that correlated highly with CD248 were deleted during data analysis. Then, Cox proportional hazards regression was used to build a prognostic risk model, and the regression coefficients were used as weight variables of the model. The risk score of each patient was calculated using the following formula, and the median was employed to separate both cohorts into different risk groups (13):

$$Risk\ score\ = \sum_{i=1}^{n} coefficient\ (gene\ i)^{*} Expression\ value\ of\ (gene\ i)$$

The survival and ROC analysis were performed as mentioned. To visualize the present signature, a nomogram was constructed by the rms R package.

## The Correlation Between the CD248-based Signature and TIICs

The tumor purity and the immune score of patients with TCGA-RCC were assessed through the ESTIMATE R package as previously reported (14). The relative fraction of 22 types of TIICs in each sample was quantified by the CIBERSORT method and the LM22 signature matrix (15, 16). The algorithm ran at 100 permutations with a threshold of $p < 0.05$ to select eligible patients (17). The correlation between the risk score and TIICs was analyzed with the Pearson correlation coefficient test, and the impact of TIICs on clinicopathological features was analyzed with the Wilcox test and the Kruskal–Wallis test. The box plot was prepared with the beeswarm R package.

## The Correlation Between the CD248-based Signature and the Tumor Mutation Burden

Masked somatic mutation data (VarScan) of RCC were retrieved from the TCGA portal. Non-synonymous somatic mutations of each patient were counted by the Perl software (https://www.perl.org/). Then, we used 38 Mb as the estimate of the exome size and calculated the TMB (i.e., mutation density) with the following formula: TMB = total mutation frequency/38. The Wilcox test was adopted to evaluate the relationship between the TMB and the risk score or clinicopathological features. $p < 0.05$ was considered statistically significant.

## The Correlation Between the CD248-based Signature and Immunomodulatory Molecules

Immune checkpoint molecules (i.e., PD1, CTLA4, LAG3, TIM3, BTLA, and VSIR) and immunostimulatory molecules (i.e., CD28, CD27, TNFRSF4, TNFRSF9, and TNFRSF18) play important roles in immunoregulation. In the present study, the expression level of the aforementioned molecules between two risk groups was analyzed with the Wilcox test. The Kaplan–Meier survival analysis was performed using the R software, and the median expression level was used as the cut-off value. $p < 0.05$ was considered statistically significant.

## The Weighted Gene Co-expression Network Analysis and the Enrichment Analysis

Differentially expressed genes (DEGs) co-expressed with CD248 were selected through the Pearson correlation coefficient test and visualized with the pheatmap R package. Filter criteria were |correlation coefficient| $> 0.5$ and $p < 0.001$. The WGCNA was employed to identify CD248 co-expressed modules. Briefly, the gradient method was used to screen out the appropriate power value with an independence degree of 0.9. The cluster analysis was performed to construct a dendrogram, and the module-trait heatmap was painted to identify the phenotype (clinic trait) and the highly correlated expression set (module). Finally, the interested modules were visualized with Cytoscape 3.6.0 and analyzed with GO and KEGG enrichment analysis. FDR $< 0.05$ was used as the threshold.

## CD248 Correlated miRNA Analysis

The software package edgeR was adopted to identify the differentially expressed miRNA (DEmiRNA) between tumor and normal tissues. The filter criteria were FDR $< 0.05$ and $\log_2$ FC $> 1$. Subsequently, CD248-correlated DEmiRNA and survival-related DEmiRNA were selected through the Pearson correlation coefficient test and the Kaplan–Meier survival analysis, respectively. Filter criteria were |correlation coefficient| $> 0.5$ and $p < 0.001$. The intersection of those two kinds of DEmiRNA was visualized with the Venn diagram and the heatmap.

# RESULTS

## The Overexpression of CD248 in Tissues With RCC

Based on the TCGA-RCC data set, 3,086 DEGs were obtained, among which 1,127 genes were downregulated, and 1,959 genes were upregulated in tissues with RCC compared with the normal (FDR $< 0.05$, $|\log_2 FC| > 1$, **Figures 1A,B**). Then, the overexpression of CD248 in tissues with RCC was identified ($p < 0.0001$, **Figure 1C** and **Supporting Data 1**). The body

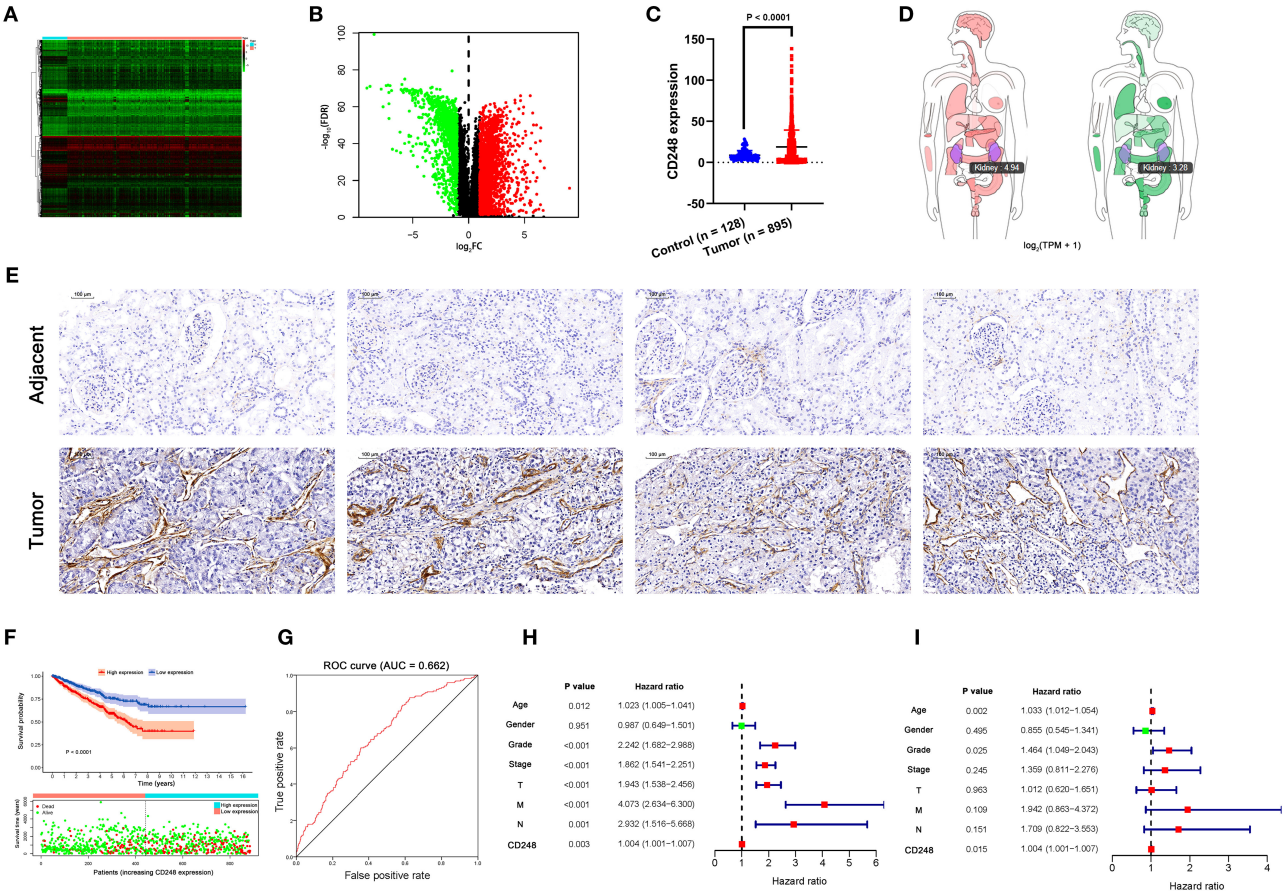



**FIGURE 1 |** The expression and the prognostic value of CD248. **(A)** A heat map of DEGs. Green to red spectrum indicates low to high gene expression. **(B)** A volcano plot of DEGs. Red, green, and black dots represent upregulated, downregulated, and unchanged genes, respectively. **(C)** The overexpression of CD248 in tissues with RCC **(D)** A body map of the expression of CD248 **(E)** Immunohistochemical qualitative evaluation of CD248 in RCC. Scale bar = 100 μm. **(F)** The prognostic value of CD248. Ninety-five percent confidence interval is shown as light-colored background. **(G)** The ROC curve of CD248 **(H)** Univariate Cox regression analysis of CD248 **(I)** Multivariate Cox regression analysis of CD248. Red and green dots represent variables with hazard ratio > 1 and ≤ 1, respectively. $p < 0.05$ was considered statistically significant.

map of CD248 showed that the median expression level in RCC was 4.94, which was much higher than 3.28 in the normal kidney (**Figure 1D**). The results of the immunohistochemical staining indicated overexpression of CD248 in RCC instead of the adjacent normal tissues (**Figure 1E**). As shown in **Figure 1F**, the prognosis was poor in the high-expression CD248 group than in the low-expression group ($p < 0.0001$). Precisely, the overall survival (OS) rate at 5-year for the high-expression group was 58.8%, and the corresponding rate for the low-expression group was 75.3%. The area under the ROC curve (AUC) was 0.662, suggesting that CD248 could accurately predict the OS of patients with RCC (**Figure 1G**). Additionally, univariate and multivariate Cox regression analyses revealed that CD248 could serve as an independent prognostic factor for RCC ($p < 0.05$, **Figures 1H,I**).

## The Prognostic Value of the CD248-based Signature

The training cohort was adopted to construct a CD248-based signature. After deleting clinicopathological variables that would overfit the signature, coefficients were estimated through multivariate Cox regression. Subsequently, the risk score for each patient was calculated with the following formula:

Risk score = (0.0291 × age) + (0.4245 × histological grade) + (0.3303 × pathological stage) + (0.6492 × M status) + (0.0038 × the expression level of CD248)

According to the median risk score 0.8618, individuals in the training cohort were sorted into a high-risk ($n = 123$) and a low-risk group ($n = 123$). The Kaplan–Meier survival analysis showed that the prognosis was worse in the high-risk group than in the low-risk group ($p < 0.0001$, **Figure 2A**). The OS rate at 5 years for the high-risk and the low-risk groups was 31.7 and 77.7%, respectively. Then, we ranked patients with the risk score and analyzed their survival status. As shown in **Figure 2B**, a large amount of death was distributed in the high-risk group. The AUC value for the present signature was 0.889 (**Figure 2C**). To facilitate clinical utility, a nomogram to predict the prognosis of RCC at 3, 5, and 10 years was prepared accordingly (**Figure 2D**).

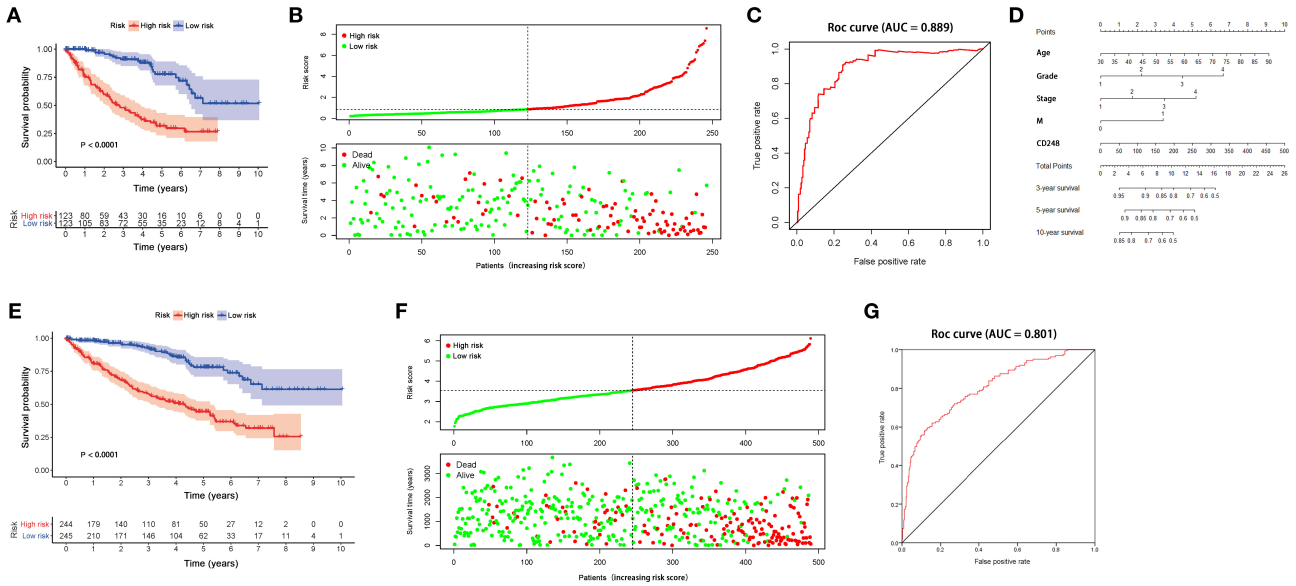



**FIGURE 2 |** The prognostic value of CD248-based signature **(A)** The Kaplan–Meier curve of a training cohort **(B)** The distribution of the risk score and the survival status of each patient in the training cohort **(C)** The ROC curve of the present signature in the training cohort **(D)** A nomogram of the present signature **(E)** The Kaplan–Meier curve of the testing cohort **(F)** The distribution of the risk score and the survival status of each patient in the testing cohort **(G)** The ROC curve of the present signature in the testing cohort. Ninety-five percent confidence interval is shown as light-colored background. $p < 0.05$ was considered statistically significant.

A testing cohort was used to verify the accuracy of the present signature. As shown in **Figures 2E,F**, the survival status of patients with ccRCC differed significantly between the two risk groups ($p < 0.05$). The survival rates at 3 and 5 years in the high-risk group were 58.1 and 44.4%, respectively, while the corresponding rates in the low-risk group were 92.1 and 78.0%, respectively. Moreover, the AUC value of the present signature was 0.801 in the testing cohort (**Figure 2G**).

## The Correlation Between the Present Signature and the Tumor Immune Microenvironment

The ESTIMATE and CIBERSORT algorithms were employed to assess tumor purity and infiltrating immune cells (**Figures 3A,D**). As shown in **Figures 3B,C**, an increased immune score was related to deteriorated histological grade and pathological stage ($p < 0.05$). The fraction of $CD8^+$ T cells and regulatory T cells (Tregs) was positively related to the risk score generated by the present signature ($p < 0.05$, **Figures 3E,F**). Furthermore, a high proportion of $CD8^+$ T cells and Tregs could lead to a poor prognosis of patients with RCC, accompanied by increased histological grade, bad pathological stage, and tumor metastasis ($p < 0.05$, **Figures 3G–K**).

The TMB is a vital factor affecting tumor immune response and immunotherapy. In the present study, with the increase of the risk score generated by the present signature, the TMB significantly increased ($p < 0.05$, **Figure 3L**). Besides, higher TMB was associated with worse histological grade, and the value of the TMB increased with the age of the patients ($p < 0.05$, **Figures 3M,N**).

## The Correlation Between the Present Signature and Immunomodulatory Molecules

The expression level of immunomodulatory molecules was regarded as a promising indicator to guide immunotherapy. We found that the expression of some immune checkpoint molecules (i.e., PD1, CTLA4, and LAG3) increased in the high-risk group ($p < 0.01$, **Figures 4A–C**), while others (i.e., TIM3, BTLA, and VSIR) remained unchanged between the two risk groups ($p > 0.05$, **Figures 4D–F**). The survival analysis indicated that highly expressed PD1 combined with a bad prognosis ($p < 0.0001$, **Figure 4G**), while the expression level of CTLA4 and LAG3 did not significantly affect the OS of patients with RCC ($p > 0.05$, **Figures 4H,I**). In addition to immune checkpoints, the expression of immunostimulatory molecules has been investigated as well. As shown in **Figure 5**, the expression of commonly detected immunostimulatory molecules, such as CD28, CD27, TNFRSF4, TNFRSF9, and TNFRSF18, was upregulated in the high-risk group ($p < 0.05$).

## The Weighted Gene Co-expression Network Analysis and the Enrichment Analysis of CD248 Co-expressed Genes

Through the Pearson correlation coefficient test, 334 DEGs co-expressed with CD248 were selected (|correlation coefficient| $> 0.5$ and $p < 0.001$, **Supporting Data 2**). The top 15 DEGs that positively and negatively correlated with CD248 were adopted to develop a co-expressed heatmap (**Figure 6A**). Subsequently, we identified five distinct CD248 co-expressed modules through the WGCNA

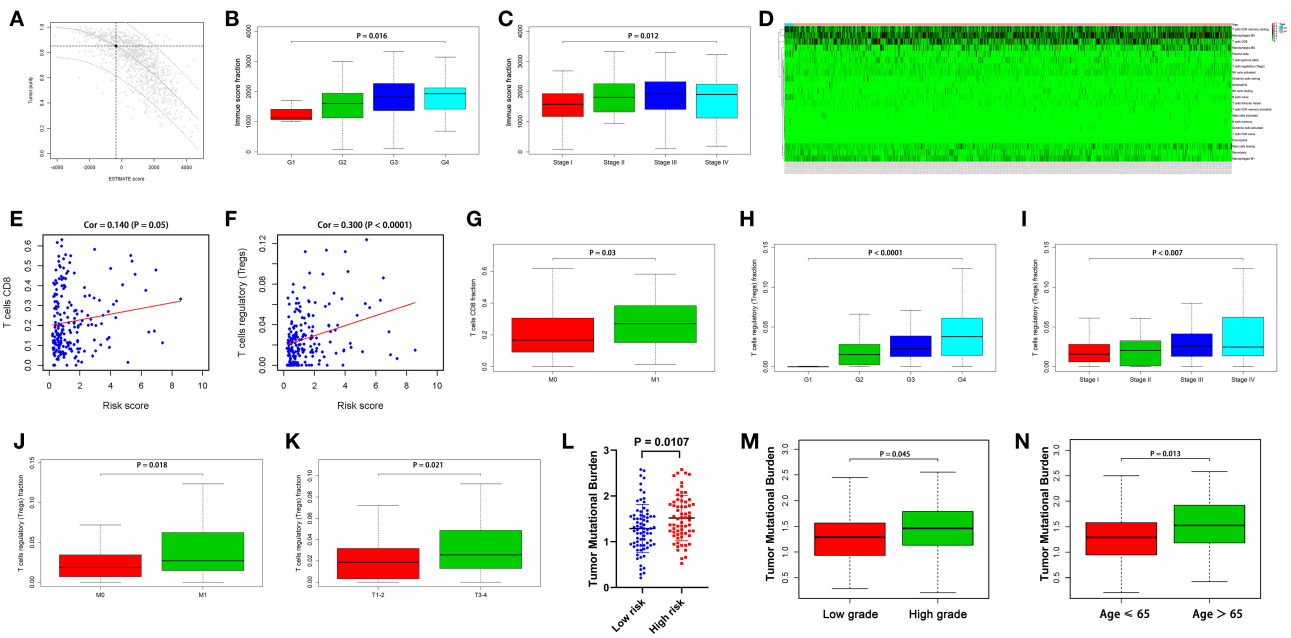



**FIGURE 3 |** The relationship between the present signature and the tumor immune microenvironment **(A)** The tumor purity assessed with the ESTIMATE algorithm **(B)** The immune score and deteriorated histological grade **(C)** The immune score and advanced pathological stage **(D)** TIICs assessed with the CIBERSORT algorithm **(E)** The correlation between the risk score and $CD8^+$ T cells **(F)** The correlation between the risk score and Tregs **(G)** $CD8^+$ T cells fraction and the metastasis of RCC **(H)** Tregs fraction and deteriorated histological grade **(I)** Tregs fraction and advanced pathological stage **(J)** Tregs fraction and the metastasis of RCC **(K)** Tregs fraction and the tumor size **(L)** Increase in the TMB in the high-risk group **(M)** The TMB and deteriorated histological grade **(N)** Increase in the TMB with age. $p < 0.05$ was considered statistically significant.

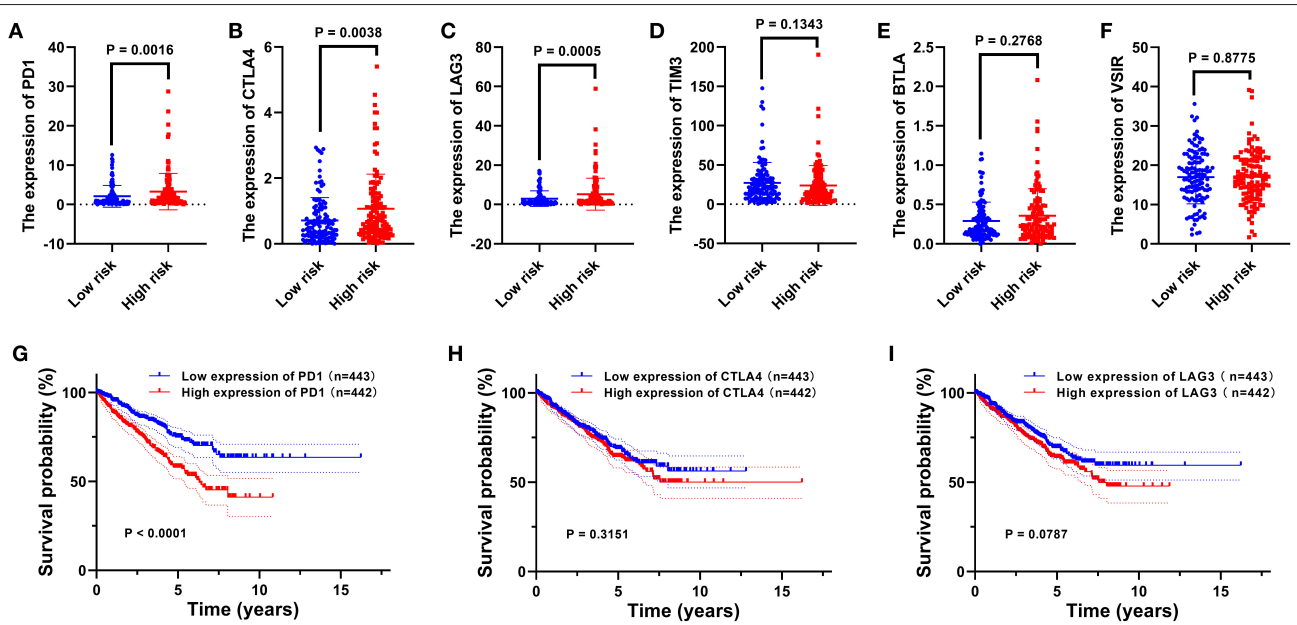



**FIGURE 4 |** The relationship between the present signature and immune checkpoints. Expression analysis of PD1 **(A)**, CTLA4 **(B)**, LAG3 **(C)**, TIM3 **(D)**, BTLA **(E)**, and VSIR **(F)** between two risk groups. The Kaplan–Meier curve of PD1 **(G)**, CTLA4 **(H)**, and LAG3 **(I)**. The median expression level was used as the cut-off value. $p < 0.05$ was considered statistically significant.

(**Figure 6B**). The module-trait heatmap indicated that brown and turquoise modules were significantly associated with the progression of RCC ($p < 0.05$, **Figure 6C**). Then, intramodular and extramodular interactions were visualized, especially the modules marked with brown and turquoise (**Figures 6D,E,H**). With the co-expressed network, several

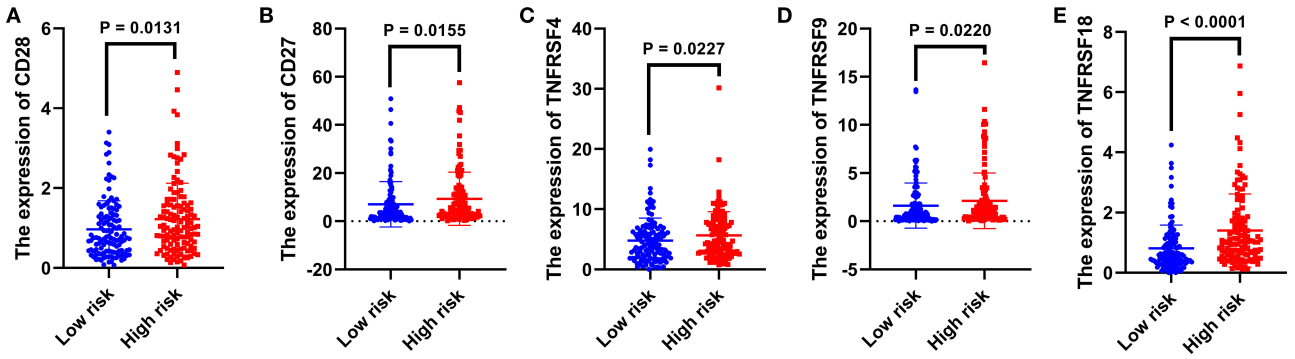



**FIGURE 5 |** The relationship between the present signature and immunostimulatory molecules. The expression analysis of CD28 **(A)**, CD27 **(B)**, TNFRSF4 **(C)**, TNFRSF9 **(D)**, and TNFRSF18 **(E)** between two risk groups. $p < 0.05$ was considered statistically significant.

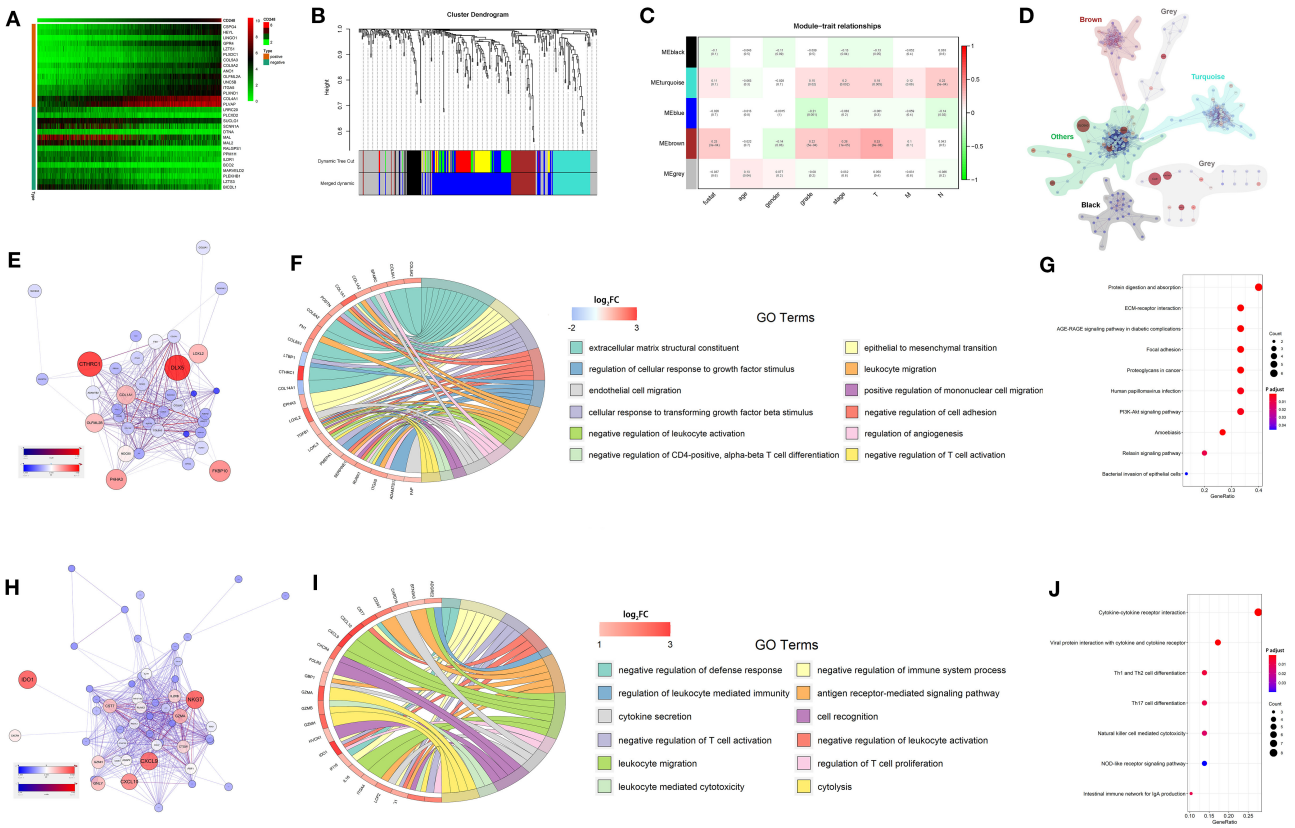



**FIGURE 6 |** The WGCNA and enrichment analysis of CD248 co-expressed genes **(A)** The heatmap of CD248 co-expressed genes **(B)** The identification of co-expressed modules **(C)** The module-trait heatmap **(D)** The interaction among co-expressed modules. The co-expressed network **(E)**, GO enrichment analysis **(F)**, and KEGG enrichment analysis **(G)** of brown modules. The co-expressed network **(H)**, GO enrichment analysis **(I)**, and KEGG enrichment analysis **(J)** of turquoise modules. FDR < 0.05 was considered as statistically significant.

hub genes with maximum intramodular connectivity were identified, which might play a vital role in the progression of RCC.

To explore the underlying mechanism of the brown and turquoise modules on the progression of RCC, GO and KEGG enrichment analysis was performed. As shown in **Figures 6F,I**, "negative regulation of defense response," "negative regulation of immune system process," "negative regulation of leukocyte activation," "negative regulation of cell adhesion," etc. immunosuppressive GO terms were significantly enriched

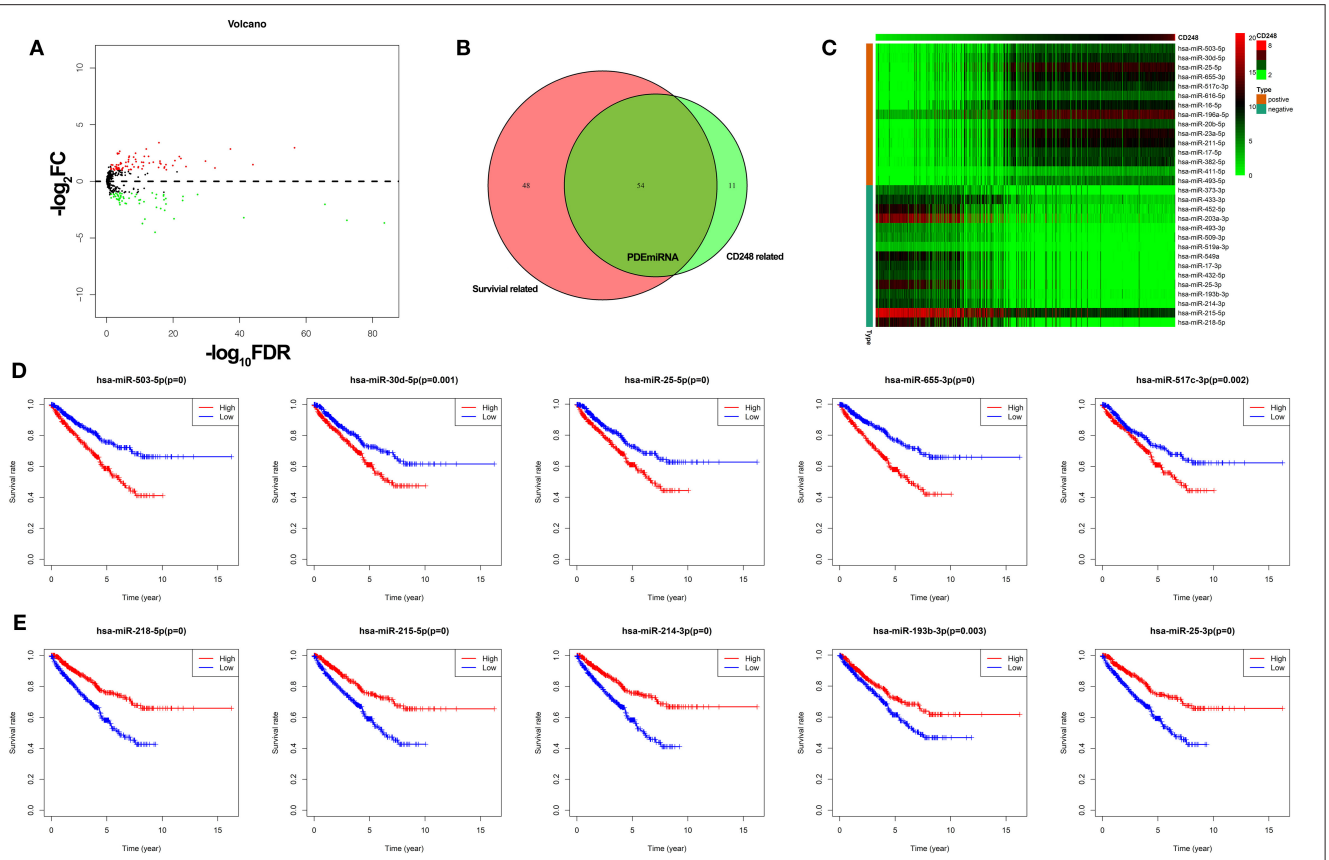



**FIGURE 7 |** The correlation between CD248 and miRNA **(A)** The volcano plot of DEmiRNA. Red, green, and black dots represent upregulated, downregulated, and unchanged genes, respectively. **(B)** The Venn diagram of PDEmiRNA **(C)** The heatmap of the top 15 CD248-correlated PDEmiRNA **(D)** The Kaplan–Meier curve of the top five PDEmiRNA that positively correlated with CD248 **(E)** The Kaplan–Meier curve of the top five PDEmiRNA that negatively correlated with CD248. The median expression level of PDEmiRNA was used as the cut-off value. $p < 0.05$ was considered statistically significant.

(FDR < 0.05). Then, KEGG enrichment analysis showed that several immunomodulatory signaling pathways were significantly enriched, including "PI3K-Akt signaling pathway," "cytokine–cytokine receptor interaction," "Th1 and Th2 cell differentiation," "natural killer cell mediated cytotoxicity," and "NOD-like receptor signaling pathway" (FDR < 0.05, **Figures 6G,J**).

## The Correlation Between CD248 and miRNA

Through the edgeR package, 138 DEmiRNA were obtained (FDR < 0.05, $|\log_2 FC| > 1$, **Figure 7A**), among which 65 DEmiRNA were significantly correlated with the expression of CD248 (correlation coefficient > 0.5 and $p < 0.001$), and 102 DEmiRNA were related with the survival of RCC ($p < 0.05$). Then, 54 CD248-correlated DEmiRNA that related with the prognosis of RCC (PDEmiRNA) were identified (**Figure 7B** and **Supporting Data 3**), and a heatmap of the top 15 PDEmiRNA that positively and negatively correlated with CD248 was developed (**Figure 7C**). Additionally, the top 5 PDEmiRNA that positively correlated with the expression of CD248 (i.e., hsa-miR-503-5p, hsa-miR-30d-5p, hsa-miR-25-5p, hsa-miR-655-3p, and hsa-miR-517c-3p) reflected a bad survival outcome ($p < 0.05$, **Figure 7D**). However, the top five negatively correlated PDEmiRNA (i.e., hsa-miR-218-5p, hsa-miR-215-5p, hsa-miR-214-3p, hsa-miR-193b-3p, and hsa-miR-25-3p) indicated a better prognosis ($p < 0.05$, **Figure 7E**).

## DISCUSSION

The incidence of RCC has increased steadily by about 1% per year, and the high mortality rate remains unchanged worldwide (18). Despite substantial improvements in available treatment options, the 5-year survival rate for advanced/metastatic RCC is <23% (19). In fact, about 30–50% of patients with RCC have missed the best surgical opportunity due to the incidence of the occult (20). Immunotherapy is an emerging method to prolong the OS of RCC. However, the low response rate results in an unsatisfied clinical outcome. Accordingly, various biomarkers have been suggested to assist in the early diagnosis and to guide treatment selection. Chen et al. reported that miR-30a-3p could inhibit the invasion of RCC and serve as a

new prognostic marker (21). miR-142-3p has also proved to be involved with tumorigenesis and the development of RCC (22). In addition to miRNAs, mRNAs including HHLA2 and syntaxin 6 were associated with decreased survival, and corresponding inhibitors held promise as a novel therapy against RCC (23, 24). However, the functional effect of a single gene in the progression of RCC is relatively weak. Identifying sensitive and specific indicators to improve diagnostic and therapeutic efficiency is still urgently needed.

Recently, a great amount of evidence indicates that TEMs have a broad influence in complicated cross-talk between tumor cells and the tumor microenvironment, which would lead to the progression of tumors (25, 26). Thus, TEMs appear to be promising candidates for the early detection of tumors, monitoring, and treatment. As an important part of TEMs, the biological function of CD248 in RCC remains unclear. In the present study, the expression level of CD248 in tissues with RCC was evaluated through the TCGA data set and confirmed in external clinical specimens. Through the qualitative evaluation of immunohistochemistry, we found the overexpression of CD248 in RCC compared with adjacent normal kidney tissues. In addition, highly expressed CD248 was associated with bad prognosis. CD248 could also serve as an independent prognostic factor to predict the OS in patients with RCC, and the predictive accuracy (AUC = 0.662) was regarded as acceptable (27). These findings indicate that the expression level of CD248 could be a new early diagnostic and prognostic marker for RCC. Subsequently, to establish a clinically stratifying system to improve the diagnostic efficiency, we constructed a CD248-based prognostic signature. This signature could stratify patients with TCGA-RCC into two risk groups with statistically different survival outcomes, and the predictive accuracy (AUC = 0.889) was deemed to be excellent (27). The reliability of the present signature was further verified in a testing cohort, and a nomogram was prepared to facilitate its clinical application.

The tumor immune microenvironment, comprising infiltrating immune cells and immune-related proteins (IRPs), has emerged as an important player in the progression of tumors (28, 29). In the present study, we explored the correlation between the present signature and the dysfunctional immune microenvironment. We found that infiltration of Tregs in RCC significantly increased with the risk score generated by the present signature, and a high immune score and high infiltration of Tregs accompanied by bad histological grade, advanced pathological stage, and more chance of metastasis in previous studies (30). Additionally, $CD8^+$ cytotoxic T lymphocytes (CTLs) were positively correlated with the risk score; however, increased CTLs resulted in the metastasis of RCC instead of the killing effect. Thus, we speculate the CTLs-mediated anti-tumor response is counterbalanced by strong immunosuppression of Tregs, which consequentially facilitate the survival and metastasis of cancer cells (31, 32).

The killing efficacy of CTLs is also directly or indirectly regulated by IRPs and TMB (33–35). The immune checkpoints (i.e., PD1, CTLA4, and LAG3) were upregulated in the high-risk group, which might induce the depletion of CTLs, the tumor immune escape, and poor survival outcome. In addition, commonly detected immunostimulatory molecules (i.e., CD28, CD27, TNFRSF4, TNFRSF9, and TNFRSF18) were upregulated in the high-risk group. The TMB—a surrogate for neoantigen level and malignant degree—increased with the risk score generated by the present signature. Based on the immune landscape of high-risk patients, once the immune suppression of CTLs is removed, the self–anti-tumor immune response would be expanded, and high-risk patients might benefit from immunotherapy. Therefore, the present signature could not only contribute to the early diagnosis of patients with RCC but also assist clinicians to screen immunotherapeutic-sensitive patients. Inevitably, a large-scale prospective validation of clinical benefits before widespread adoption is necessary (36).

To explore possible functions of CD248 in RCC, the WGCNA and enrichment analysis were performed. The results suggested that CD248 co-expressed genes could be divided into five modules, among which the brown and turquoise modules were significantly associated with the progression of RCC. Then, the identified prognostic-related modules were analyzed with the GO and the KEGG algorithm. As a result, several immunosuppressive GO terms were significantly enriched, including the negative regulation of leukocyte activation, migration, adhesion, and differentiation, which might provide insight into the depletion of CTLs mentioned above. More accurately, tumor stroma might play an important role in negative immunoregulation since the hub genes (i.e., CTHRC1, COL1A1, LOXL2, P4HA3, and FKBP10) related to immunosuppressive GO terms usually participate in collagen formation. With the immunosuppressive landscape, the expression of CTL effectors (i.e., GZMA, GZMH, and GNLY) would be inhibited. Meanwhile, chemokines (i.e., CXCL9 and CXCL10), inflammatory factors [i.e., interleukin-16 (IL-16), IL-2, and IFI16], and relevant signaling pathways might negatively regulate the activation and migration of CTLs. After verifying them in studies *in vitro* or *in vivo*, novel diagnostic and therapeutic targets might be proposed.

Furthermore, the correlation between CD248 and miRNA was explored, which would be valuable to reveal the potential mechanism of the transcriptomic regulation. Interestingly, the PDEmiRNA that positively or negatively correlated with the expression of CD248 could reflect a bad or good survival outcome, respectively. Therefore, the downregulation of protective PDEmiRNA (CD248 negatively correlated) might contribute to the risk of the overexpression of the gene (i.e., CD248), leading to a poor prognosis. This result further emphasized the importance of CD248 in RCC.

In summary, we identified a valuable biomarker and constructed a reliable prognostic signature that can precisely predict the prognosis of patients with RCC. Additionally, the present signature can effectively screen outpatients with RCC suitable for immunotherapy. The WGCNA, enrichment analysis, and miRNA correlation analysis revealed possible functions and the regulation of the expression of CD248, which may contribute to explain CD248-mediated

progression of RCC and provide potential diagnostic and therapeutic targets.

## DATA AVAILABILITY STATEMENT

Publicly available datasets were analyzed in this study. This data can be found at: https://portal.gdc.cancer.gov.

## AUTHOR CONTRIBUTIONS

KZ, CX, and SL: data acquisition, data analysis, and writing the original draft. KZ, CX, SL, YJ, XZ, SM, and YL: methodology, data interpretation, writing the review, and editing. FY, YW, PM, and CS: literature research and immunohistochemical assay. DH, WW, and WQ: conceptualization, design, and project administration. All authors approved the submitted version.

## FUNDING

The work was supported by grants from the National Natural Science Foundation of China (No. 81772734, 81802935) and the Innovation Capability Support Plan of Shaanxi Province (2020PT-021).

## ACKNOWLEDGMENTS

We thank the TCGA database for the availability of the data.

## SUPPLEMENTARY MATERIAL

The Supplementary Material for this article can be found online at: https://www.frontiersin.org/articles/10.3389/fonc.2021.644612/full#supplementary-material

## REFERENCES

1. Siegel RL, Miller KD, Jemal A. Cancer statistics, 2019. *CA Cancer J Clin*. (2019) 69:7–34. doi: 10.3322/caac.21551
2. Padala SA, Barsouk A, Thandra KC, Saginala K, Mohammed A, Vakiti A, et al. Epidemiology of renal cell carcinoma. *World J Oncol*. (2020) 11:79–87. doi: 10.14740/wjon1279
3. Miller KD, Nogueira L, Mariotto AB, Rowland JH, Yabroff KR, Alfano CM, et al. Cancer treatment and survivorship statistics, 2019. *CA Cancer J Clin*. (2019) 69:363–85. doi: 10.3322/caac.21565
4. Peinemann F, Unverzagt S, Hadjinicolaou AV, Moldenhauer I. Immunotherapy for metastatic renal cell carcinoma: a systematic review. *J Evid Based Med*. (2019) 12:253–62. doi: 10.1111/jebm.12362
5. Topalian SL, Hodi FS, Brahmer JR, Gettinger SN, Smith DC, McDermott DF, et al. Five-year survival and correlates among patients with advanced melanoma, renal cell carcinoma, or non-small cell lung cancer treated with nivolumab. *JAMA Oncol*. (2019) 5:1411–20. doi: 10.1001/jamaoncol.2019.2187
6. Rini BI, Pal SK, Escudier BJ, Atkins MB, Hutson TE, Porta C, et al. Tivozanib versus sorafenib in patients with advanced renal cell carcinoma (TIVO-3): a phase 3, multicentre, randomised, controlled, open-label study. *Lancet Oncol*. (2020) 21:95–104. doi: 10.1016/S1470-2045(19)30735-1
7. Motzer RJ, Escudier B, McDermott DF, George S, Hammers HJ, Srinivas S, et al. Nivolumab versus everolimus in advanced renal-cell carcinoma. *N Engl J Med*. (2015) 373:1803–13. doi: 10.1056/NEJMoa1510665
8. Tomkowicz B, Rybinski K, Foley B, Ebel W, Kline B, Routhier E, et al. Interaction of endosialin/TEM1 with extracellular matrix proteins mediates cell adhesion and migration. *Proc Natl Acad Sci USA*. (2007) 104:17965–70. doi: 10.1073/pnas.0705647104
9. Nanda A, Karim B, Peng Z, Liu G, Qiu W, Gan C, et al. Tumor endothelial marker 1 (Tem1) functions in the growth and progression of abdominal tumors. *Proc Natl Acad Sci USA*. (2006) 103:3351–6. doi: 10.1073/pnas.0511306103
10. Facciponte JG, Ugel S, De Sanctis F, Li C, Wang L, Nair G, et al. Tumor endothelial marker 1-specific DNA vaccination targets tumor vasculature. *J. Clin. Invest*. (2014) 124:1497–511. doi: 10.1172/JCI67382
11. Hong YK, Lee YC, Cheng TL, Lai CH, Hsu CK, Kuo CH, et al. Tumor endothelial marker 1 (TEM1/endosialin/CD248) enhances wound healing by interacting with platelet-derived growth factor receptors. *J. Invest. Dermatol*. (2019) 139:2204–14.e7. doi: 10.1016/j.jid.2019.03.1149
12. Yue C, Ma H, Zhou Y. Identification of prognostic gene signature associated with microenvironment of lung adenocarcinoma. *PeerJ*. (2019) 7:e8128–44. doi: 10.7717/peerj.8128
13. Wan B, Liu B, Huang Y, Yu G, Lv C. Prognostic value of immune-related genes in clear cell renal cell carcinoma. *Aging*. (2019) 11:11474–89. doi: 10.18632/aging.10548
14. Yoshihara K, Shahmoradgoli M, Martínez E, Vegesna R, Kim H, Torres-Garcia W, et al. Inferring tumour purity and stromal and immune cell admixture from expression data. *Nat. Commun*. (2013) 4:2612. doi: 10.1038/ncomms3612
15. Newman AM, Liu CL, Green MR, Gentles AJ, Feng W, Xu Y, et al. Robust enumeration of cell subsets from tissue expression profiles. *Nat. Methods*. (2015) 12:453–7. doi: 10.1038/nmeth.3337
16. Zeng D, Zhou R, Yu Y, Luo Y, Zhang J, Sun H, et al. Gene expression profiles for a prognostic immunoscore in gastric cancer. *Br J Surg*. (2018) 105:1338–48. doi: 10.1002/bjs.10871
17. Ali HR, Chlon L, Pharoah PD, Markowetz F, Caldas C. Patterns of immune infiltration in breast cancer and their clinical implications: a gene-expression-based retrospective study. *PLoS Med*. (2016) 13:e1002194–218. doi: 10.1371/journal.pmed.1002194
18. Zhu WK, Xu WH, Wang J, Huang YQ, Abudurexiti M, Qu YY, et al. Decreased SPTLC1 expression predicts worse outcomes in ccRCC patients. *J. Cell. Biochem*. (2020) 121:1552–62. doi: 10.1002/jcb.29390
19. Motzer RJ, Jonasch E, Agarwal N, Bhayani S, Bro WP, Chang SS, et al. Kidney cancer, version 2.2017, NCCN clinical practice guidelines in oncology. *J Natl Compr Canc Netw*. (2017) 15:804–34. doi: 10.6004/jnccn.2017.0100
20. Qin S, Shi X, Wang C, Jin P, Ma F. Transcription factor and miRNA interplays can manifest the survival of ccRCC patients. *Cancers*. (2019) 11:111668. doi: 10.3390/cancers11111668
21. Chen Y, Zhou J, Wu X, Huang J, Chen W, Liu D, et al. miR-30a-3p inhibits renal cancer cell invasion and metastasis through targeting ATG12. *Transl Androl Urol*. (2020) 9:646–53. doi: 10.21037/tau.2019.12.10
22. Peng X, Pan X, Liu K, Zhang C, Zhao L, Li H, et al. miR-142-3p as a novel biomarker for predicting poor prognosis in renal cell carcinoma patients after surgery. *Int J Biol Markers*. (2019) 34:302–8. doi: 10.1177/1724600819866456
23. Chen L, Zhu D, Feng J, Zhou Y, Wang Q, Feng H, et al. Overexpression of HHLA2 in human clear cell renal cell carcinoma is significantly associated with poor survival of the patients. *Cancer Cell Int*. (2019) 19:101. doi: 10.1186/s12935-019-0813-2
24. Peak TC, Su Y, Chapple AG, Chyr J, Deep G. Syntaxin 6: a novel predictive and prognostic biomarker in papillary renal cell carcinoma. *Sci. Rep. UK*. (2019) 9:3146. doi: 10.1038/s41598-019-39305-z
25. Pietrzyk Ł. Biomarkers discovery for colorectal cancer: a review on tumor endothelial markers as perspective candidates. *Dis. Markers*. (2016) 2016:4912405. doi: 10.1155/2016/4912405
26. Wang X, Zhu Q, Lin Y, Wu L, Wu X, Wang K, et al. Crosstalk between TEMs and endothelial cells modulates angiogenesis and metastasis *via* IGF1-IGF1R signalling in epithelial ovarian cancer. *Br J Cancer*. (2017) 117:1371–82. doi: 10.1038/bjc.2017.297
27. Cho SH, Pak K, Jeong DC, Han ME, Oh SO, Kim YH. The AP2M1 gene expression is a promising biomarker for predicting survival of

patients with hepatocellular carcinoma. *J. Cell. Biochem.* (2019) 120:4140–6. doi: 10.1002/jcb.27699
28. Sobral-Leite M, Salomon I, Opdam M, Kruger DT, Kok M. Cancer-immune interactions in ER-positive breast cancers: PI3K pathway alterations and tumor-infiltrating lymphocytes. *Breast Cancer Res*. (2019) 21:90–102. doi: 10.1186/s13058-019-1176-2
29. McGranahan N, Furness AJ, Rosenthal R, Ramskov S, Lyngaa R, Saini SK, et al. Clonal neoantigens elicit T cell immunoreactivity and sensitivity to immune checkpoint blockade. *Science*. (2016) 351:1463–9. doi: 10.1126/science.aaf1490
30. Wang Y, Yang J, Zhang Q, Xia J, Wang Z. Extent and characteristics of immune infiltration in clear cell renal cell carcinoma and the prognostic value. *Transl Androl Urol*. (2019) 8:609–18. doi: 10.21037/tau.2019.10.19
31. Pol JG, Caudana P, Paillet J, Piaggio E, Kroemer G. Effects of interleukin-2 in immunostimulation and immunosuppression. *J. Exp. Med.* (2020) 217:1247. doi: 10.1084/jem.20191247
32. Pai SI, Marincola FM. Peripheral circulating CD45RA(-)FOXP3(hi) T regulatory (T(R)(eg)) II cells provide a window into the activity of intratumoral T(R)(eg) cells. *Trends Cancer*. (2020) 6:3–6. doi: 10.1016/j.trecan.2019.11.003
33. Mitchell TJ, Rossi SH, Klatte T, Stewart GD. Genomics and clinical correlates of renal cell carcinoma. *World J. Urol.* (2018) 36:1899–911. doi: 10.1007/s00345-018-2429-x
34. Cheng W, Ren X, Zhang C, Cai J, Liu Y, Han S, et al. Bioinformatic profiling identifies an immune-related risk signature for glioblastoma. *Neurology*. (2016) 86:2226–34. doi: 10.1212/WNL.0000000000002770
35. Dudani S, Savard MF, Heng D. An update on predictive biomarkers in metastatic renal cell carcinoma. *Eur Urol Focus*. (2020) 6:34–6. doi: 10.1016/j.euf.2019.04.004
36. Campi R, Sessa F, Corti F, Carrion DM, Mari A, Amparore D, et al. Triggers for delayed intervention in patients with small renal masses undergoing active surveillance: a systematic review. *Minerva Urol. Nefrol.* (2020) 72:389–407. doi: 10.23736/S0393-2249.20.03870-9

**Conflict of Interest:** The authors declare that the research was conducted in the absence of any commercial or financial relationships that could be construed as a potential conflict of interest.

*Copyright © 2021 Zhang, Xu, Liu, Jiang, Zhao, Ma, Li, Yang, Wang, Meng, Shi, Han, Wen and Qin. This is an open-access article distributed under the terms of the Creative Commons Attribution License (CC BY). The use, distribution or reproduction in other forums is permitted, provided the original author(s) and the copyright owner(s) are credited and that the original publication in this journal is cited, in accordance with accepted academic practice. No use, distribution or reproduction is permitted which does not comply with these terms.*

frontiers in Oncology

ORIGINAL RESEARCH
published: 25 March 2021
doi: 10.3389/fonc.2021.628821

# Cancer Associated Fibroblasts Promote Renal Cancer Progression Through a TDO/Kyn/AhR Dependent Signaling Pathway

*Li-bo Chen*[1†], *Shun-ping Zhu*[2†], *Tian-pei Liu*[1], *Heng Zhao*[3], *Ping-feng Chen*[1], *You-jun Duan*[1] *and Rong Hu*[3*]

[1] Department of Urology, The First Affiliated Hospital of University of South China, Hengyang, China, [2] Department of Respiratory, The First Affiliated Hospital of University of South China, Hengyang, China, [3] Department of Radiology, The First Affiliated Hospital of University of South China, Hengyang, China

OPEN ACCESS

**Edited by:**
James H. Finke,
Case Western Reserve University,
United States

**Reviewed by:**
Soumya R. Mohapatra,
German Cancer Research Center (DKFZ), Germany
Sazzad Hassan,
Indiana University Bloomington,
United States

***Correspondence:**
Rong Hu
cclb229@foxmail.com

[†]These authors have contributed equally to this work

**Specialty section:**
This article was submitted to Genitourinary Oncology, a section of the journal Frontiers in Oncology

**Received:** 13 November 2020
**Accepted:** 08 March 2021
**Published:** 25 March 2021

**Citation:**
Chen L-b, Zhu S-p, Liu T-p, Zhao H, Chen P-f, Duan Y-j and Hu R (2021) Cancer Associated Fibroblasts Promote Renal Cancer Progression Through a TDO/Kyn/AhR Dependent Signaling Pathway. Front. Oncol. 11:628821. doi: 10.3389/fonc.2021.628821

Cancer associated fibroblasts (CAFs) play crucial roles in cancer development, however, the specific mechanisms of CAFs associated renal cancer progression remain poorly understood. Our study observed enriched CAFs in high degree malignant tumor tissues from renal cancer patients. These CAFs isolated from tumor tissues are prone to facilitate drugs resistance and promote tumor progression *in vitro* and *in vivo*. Mechanistically, CAFs up-regulated tryptophan 2, 3-dioxygenase (TDO) expression, resulting in enhanced secretion of kynurenine (Kyn). Kyn produced from CAFs could up-regulated the expression of aromatic hydrocarbon receptor (AhR), eventually resulting in the AKT and STAT3 signaling pathways activation. Inhibition of AKT signal prevented cancer cells proliferation, while inhibition of the STAT3 signal reverted drugs resistance and cancer migration induced by kynurenine. Application of AhR inhibitor DMF could efficiently suppress distant metastasis of renal cancer cells, and improve anticancer effects of sorafenib (Sor)/sunitinib (Sun), which described a promising therapeutic strategy for clinical renal cancer.

**Keywords: cancer associated fibroblasts, kynurenine, aromatic hydrocarbon receptor, renal cancer, tryptophan 2, 3-dioxygenase (TDO)**

## INTRODUCTION

Renal cancer is one of most common urogenital neoplasms and has a high risk of distant metastasis (1). Although standard surgery plus novel tyrosine kinases inhibitors, including Sun or Sor, have reported to improve the outcome and prognosis of renal cancer patients in recent years (2). However, many patients still suffered from tumor recurrence and distant metastasis due to the drugs resistance and sustained tumor growth (3). More importantly, it remains poorly understood in the underlying mechanism of renal cancer progression.

Tumor progression is a complex set of proliferative disease, which is determined by diverse factors, including tumor heterogeneity (4), extracellular matrix (5) and tumor microenvironment (6). Several

stromal or immune cells in tumor microenvironment, such as myeloid inhibitory cells (7), tumor associated macrophages (8), mesenchymal stem cells (9) and CAFs (10), have been reported to participate in the tumor progression. Among those cell subpopulations, CAFs have been observed in most solid tumor tissues. Increasing studies suggest that CAFs serves as stromal cells to support cancer development. Previous reports have provided evidence to suggest that cytokines derived from CAFs play crucial roles in regulating tumor behaviors. For example, CAFs are capable of promoting tumor stemness and facilitating cancer cells proliferation through secretion of IGF2 (11). Meanwhile, CAFs could mediate angiogenesis and tumor microenvironment remodeling though secretion of VEGF (12). Clinical and pathological studies also suggested that the distribution of CAFs is tightly correlated to the pro-survival signaling pathways activation in tumor cells (13). However, the potential role of CAFs in renal cancer remains poorly understood and the specific underlying mechanisms of CAFs in renal cancer development have yet to be explored.

In our study, we observed increasing number of CAFs in those high degree malignant tumor tissues from renal cancer patients. Those CAFs isolated from tumor tissues were capable of promoting renal cancer cells proliferation and migration. Meanwhile, we proved that those CAFs also mediated the drugs resistance of renal cancer cells, resulting in poor prognosis in renal cancer patients. We further disclosed the underlying mechanism of CAFs induced tumor progression, which is dependent on a TDO/Kyn/AhR pathway. Our study described that blockade of AhR signals could efficiently improve the outcome of traditional Sor/Sun therapy, which provided a novel sight in clinical renal cancer therapy.

# MATERIALS AND METHODS

## Cell Lines and Reagents

Murine renal cancer cells Renca, human renal cancer cells A498, human skin fibroblasts HFL1 and murine NIH-3T3 fibroblasts were purchased from Cell Bank of Chinese Academy of Sciences (Shanghai, China). All fibroblasts were cultured in DMEM complete culture medium (Gibico, MA, USA) supplemented with 10% fetal bovine serum (Gibco, MA, USA). A498 cells were cultured in 1640/RMPI complete culture medium (Gibico, MA, USA) supplemented with 10% fetal bovine serum (Gibco, MA, USA). Renca cells were cultured in IMDM culture medium (Gibico, MA, USA) supplemented with 10% fetal bovine serum (Gibco, MA, USA). Kyn and Kyn concentration detection Kit were purchased from Abcam (Cambridge, UK). Sorafenib and sunitinib were purchased from Sangon (Shanghai, China). TDO inhibitor LM10, AhR inhibitor PDM2 and DMF, AKT inhibitor capivasertib (Cap) and STAT3 inhibitor S1-109 were purchased from MedChemExpress (L.A, USA).

## Patients' Tumor Tissues and CAFs Collection

Renal tumor samples were obtained after the surgery sterilely at the First Affiliated Hospital, University of South China. All samples were reviewed by a pathologist according to World Health Organization classification. Samples were divided into non-metastatic and metastatic groups according to the subsequent clinical follow-up. Samples were divided into high degree (H-D, stage I and II) and low degree (L-D, stage III and IV) groups according to the pathological diagnose. All samples collection and following analysis were performed according to the declaration of Helsinki and Ethical approval was obtained from the committee of the First Affiliated Hospital, University of South China. For CAFs isolation, tumor tissues from patients or Renca-bearing BalB/C mice were collected and cut into pieces as small as possible. Those tissues were further digested by ACCUMAXTM (Sigma, MA, USA) at 37°C, 5% $CO_2$ incubator for 1~2 hours. The digested cells were collected by filtration (40 μm, Thermo, MA, USA). Half of the cell suspension was stained by CD45 (eBioscience, MA, USA) and CD90 (eBioscience, MA, USA) for cytometry analysis. The rest cells suspension was collected and seeded into 6-well plate containing 2 ml DMEM medium with 10% fetal bovine serum for overnight at 37°C. 12 hours later, the medium was replaced with fresh medium to remove the un-adherent cells. After 2~4 passages, the CD45+/CD90+ positive CAFs were sorted for α-SMA analysis and co-culture. The isolated CAFs were maintained for at most 20 passages.

## Cell Proliferation Detection

Cell proliferation of Renca and A498 were examined by MTT Kit (Solarbio, Beijing, China). Briefly, 2000 tumor cells were seeded into 96-well plate after treatment of CAFs, fibroblasts or signals inhibitors (as described in figure legends). After 0, 24, 48 and 72 hours, 10 μl of MTT solution was added into the 96 wells, following with 3 hours incubation of 2 hours at 37°C. Absorbance was measured at 560 nm on a microplate reader (Bio-Rad, MA, USA). Each experiment was performed for independent three times.

## Transwell Analysis

Cells migrating assay was performed using 8-μm transwell chambers (Thermo, MA, USA). Renca or A498 cells were pre-treated with CAFs, fibroblasts or other inhibitors. Then, $2 \times 10^4$ cells in 150 ul non-serum culture medium were seeded into the upper chambers. 800 ul culture medium containing 10% FBS medium was added into the lower chambers. 24 hours later, transwells were washed with PBS, fixed with formalin and stained with 0.1% crystal violet. Cells were counted in 3 random fields per well under a 100 × microscope. Each experiment was performed in triplicate.

## Cytotoxicity Analysis

Cytotoxicity of Sor and Sun to tumor cells was analyzed using the FITC-Annexin V/PE-PI apoptosis detection kit (BD, NJ, USA). Renca cells were treated with Sun (10 μM) or Sor (5 μM) for 48 hours. A498 were treated with Sor (20 μM) or Sun (15 μM) for 48 hours. Then tumor cells were collected and resuspended with 100 μl staining buffer after chemotherapy treatment. 5 μl FITC-Annexin V staining solution and 2 μl PE-PI staining solution were added into the cells. After incubation of 15 minutes at room

temperature, the cells were washed with PBS and detected by flow cytometry on a C6 flow cytometer (BD, NJ, USA). Each experiment was performed in triplicate.

## Western Blotting

The A498 cells and Renca cells were collected for protein samples with NP40 solution. 25 μg protein samples were separated by SDS-PAGE, followed with transferring to PVDF membranes. Next, samples were examined by immunoblotting with primary antibodies against: α-SMA (1:1000, Abcam, Cambridge, UK), AhR (1:5000, Abcam, Cambridge, UK), phosphorylated-Src (1:500, Abcam, Cambridge, UK), total Src (1:500, Abcam, Cambridge, UK), phosphorylated AKT (1:500, Abcam, Cambridge, UK), total AKT (1:500, Abcam, Cambridge, UK), phosphorylated STAT3 (1:500 Abcam, Cambridge, UK), total STAT3 (Abcam, Cambridge, UK) and β-actin (1:1000, Abcam, Cambridge, UK) respectively at 4°C overnight. Then HRP-conjugated secondary antibody (1:1000, Abcam, Cambridge, UK) was incubated for 1 hour at room temperature, and visualized by using ECL detection kit (Thermo, MA, USA).

## Immunofluorescent Staining

Tumor tissues from patients were kept in 4% PFA overnight, then processed, embedded in paraffin, and sectioned at 4 μm for further study. Sections of tumor tissues from patients were blocked with blocking solution containing 5% bovine serum albumin for 30 min and stained with primary antibodies AhR (1:100; Abcam, Cambridge, UK), phosphorylated AKT (1:300, Abcam, Cambridge, UK) and phosphorylated STAT3 (1:500 Abcam, Cambridge, UK) at 4°C overnight, followed with incubation with secondary antibodies (1:1000; Abcam, Cambridge, UK) for 1 hour at room temperature. Nuclei were stained with the DAPI solution (1 μg/ml). Confocal microscope (Olympus, Tokyo, Japan) was used to visualize the sections. The fluorescence intensity of section and relative protein expression was analyzed by image J software 1.8.0 (NIH, Bethesda, Maryland, USA).

## Kyn Concentration Analysis

Kyn secretion was detected using a Human Kynurenine Elisa Kit (JIANGLAI, Shanghai, China). Briefly, $10^5$ CAFs, HSF or NIH-3T3 cells were cultured in 2 ml culture medium at 37 °C, 5% CO2 incubator. After 48 hours, the culture medium was collected and analyzed for the Kyn concentration. The Kyn concentration analysis were performed according to the guidelines of Human Kynurenine Elisa Kit. Each experiment was performed in three independent times.

## Animal Experiments Protocols

6~8 weeks female BalB/C and NOD-SCID mice were purchased from Huafukang Company (Beijing, China) and maintained in the SPF level. For lung metastasis analysis, $1\times10^6$ Renca cells were injected into BalB/C mice by tail vein. On day 20, mice were sacrificed for lung metastasis analysis. For tumor suppression analysis, we established Renca subcutaneous tumor model by injecting $5\times10^5$ Renca cells into BalB/C mice subcutaneously. We established A498 subcutaneous tumor model by injecting $5\times10^6$ A498 into NOD-SCID mice subcutaneously. Since day 10, mice treated with PBS, Sor (15 mg/kg), Sun (20 mg/kg), DMF (10 mg/kg) or combination twice a week. The overall survival of tumor bearing mice was recorded since day 25. The calculation formula of tumor volume: tumor volume = length × width $^2$/2. All our animal experiments were conducted in accordance with guidelines of Animal Ethics Committee and approved by the Institute Ethics Committee of the First Affiliated Hospital, University of South China.

## Statistical Analysis

Each experiment was performed for at least three independent times. Results were presented as the mean ± SEM and statistical significance was analyzed using GraphPad 6.0 software (La Jolla, California, USA). Statistical significance between groups was calculated by Student's t test for two groups or by one-way ANOVA for more than two groups. Bonferroni analysis were further used for the *post hoc* test. The correlation analysis was performed using GraphPad 6.0 software (La Jolla, California, USA). The survival rates were determined by Kaplan–Meier survival analysis (*$p < 0.05$; **$p < 0.01$; ***$p < 0.001$; ns, no significant difference).

# RESULTS

## CAFs Promoted Tumor Progression in Renal Cancer

Increasing studies have provided evidence that CAFs could regulate tumor progression through secretion of pro-survival cytokines (14). To explore the potential roles of CAFs in renal cancer development, we isolated CD45+/CD90+ cells from tumor tissues and examined their expression of α-SMA (a marker of fibroblasts), in which a higher percentage of CD45+/CD90+ cells was observed in H-D group (**Figure 1A**). Meanwhile, those CD45+/CD90+ cells revealed enhanced α-SMA expression (**Figure 1B**). Those results suggested that high degree malignant tumor tissues possessed a higher proportion of CAFs, which might be associated with the renal cancer progression. Based on this point, we seeded renal cancer cells Renca/A498 into a 24 well plate with a tranwell inert (3 μm) containing CAFs to establish tumor cells/CAFs co-culture system. Notably, tumor cells co-cultured with CAFs revealed strengthened Sor resistance, whereas no similar results were observed in normal fibroblasts cells HSF or NIH-3T3 cells groups (**Figure 1C**). Intriguingly, Renca and A498 also revealed Sun resistance after co-culture with CAFs (**Figure 1D**), indicating that CAFs could mediate the multi-drugs resistance in renal cancer. Additionally, CAFs co-culture promoted cells proliferation of Renca and A498 cells *in vitro* (**Figure 1E**). Next, we further examined the role of CAFs in renal cancer metastasis. The transwell analysis implicated that Renca and A498 cells possessed enhanced capability of migration after CAFs co-culture (**Figure 1F**). Consistently, Renca cells treated with CAFs revealed elevated lung metastasis compared to PBS or NIH-3T3 groups

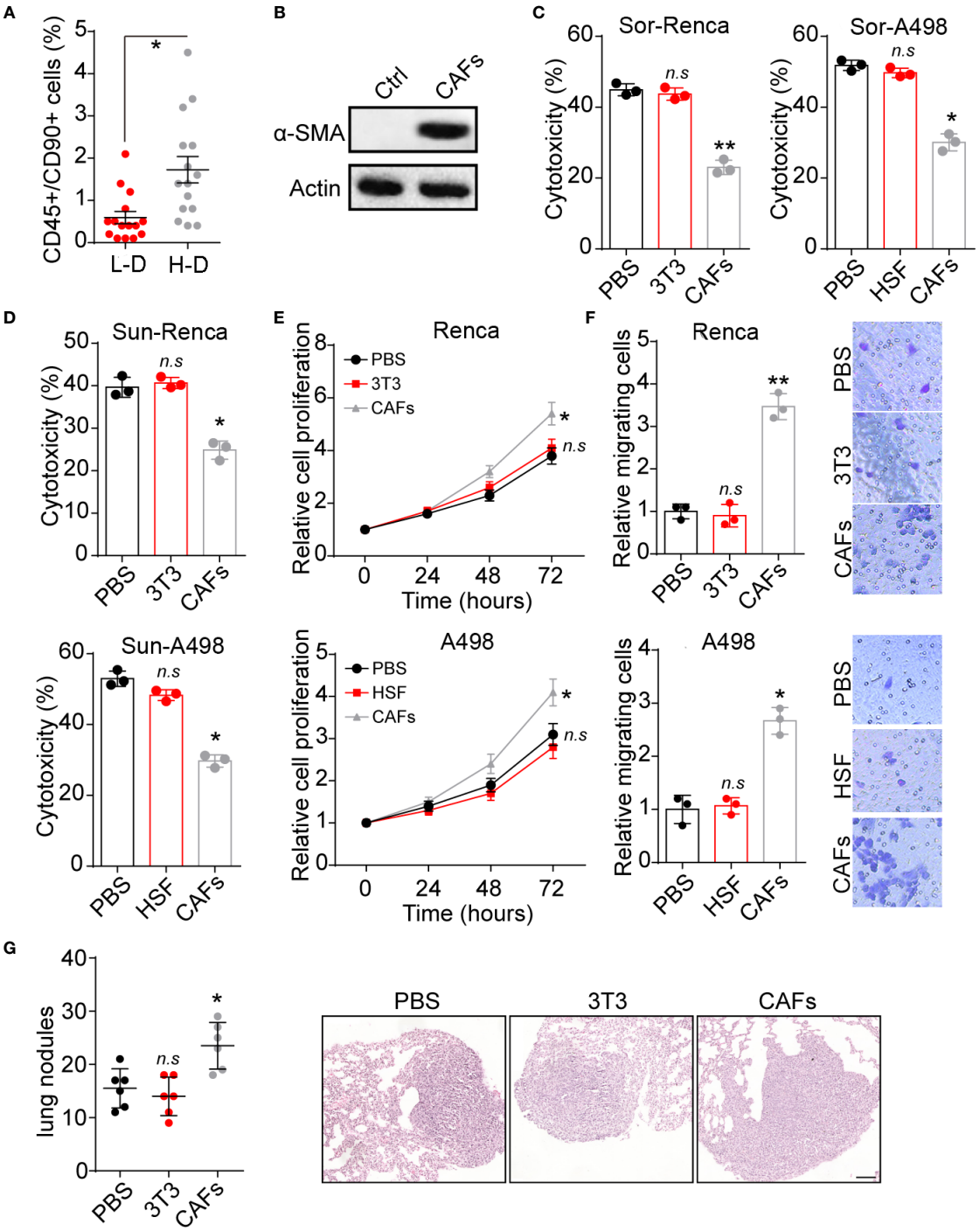



**FIGURE 1** | CAFs promoted renal cancer progression. **(A)** The percentage of CD45+/CD90+ cells subpopulation in tumor tissues from high degree (H-D) and low degree (L-D) malignant renal patients (n=15). **(B)** The western blotting of α-SMA in tumor tissues (ctrl) and CAFs isolated from tumor tissues of renal patients. **(C)** The cytotoxicity of Sor to Renca/A498 co-cultured with NIH-3T3, HSF or CAFs. **(D)** The cytotoxicity of Sun to Renca/A498 co-cultured with NIH-3T3, HSF or CAFs. **(E)** The relative cells proliferation of Renca/A498 co-cultured with NIH-3T3, HSF or CAFs. **(F)** The relative migrating cells numbers and representative images of Renca/A498 co-cultured with NIH-3T3, HSF or CAFs by transwell. **(G)** The lung nodules numbers and representative images of Renca lung metastasis mice models. Renca cells were co-cultured with NIH-3T3 or CAFs and $10^6$ Renca were injected into BalB/C mice by tail vein, which were sacrificed on day 20. The scale bar is 200 μm. Mean ± SEM, n.s, no significant difference; *p < 0.05, **p < 0.01.

(**Figure 1G**), indicating that CAFs could facilitate renal cancer proliferation and metastasis. Together, those results suggested that CAFs promoted tumor progression in renal cancer.

## CAFs Secreted Kyn to Regulate Renal Progression

Next, we further investigated the underlying mechanism of CAFs associated tumor progression. Compelling reports have provided evidence that tryptophan metabolism is tightly correlated to cancer development in diverse tumor types (15). Herein, we examined the expression of tryptophan metabolism associated dioxygenases indoleamine 2,3-dioxygenase 1 (IDO1) and TDO2. Notably, elevated expression of TDO2 was observed in CAFs compared to normal fibroblasts (**Figure 2A**). Consistently, increasing concentration of the tryptophan metabolite Kyn was found in CAFs culture medium (**Figures 2B, C**) compared to HSF or NIH-3T3 cells, indicating enhanced tryptophan metabolism in CAFs. To explore the effects of tryptophan metabolism to tumor cells, we added Kyn into the culture medium of cancer cells and found that Kyn efficiently promoted Sor resistance in Renca and A498 cells. Meanwhile, blockade of TDO by TDO inhibitor LM10 also suppressed the Sor resistance induced by CAFs (**Figure 2D**). The same phenomenon was observed in Sun treatment (**Figure 2E**),

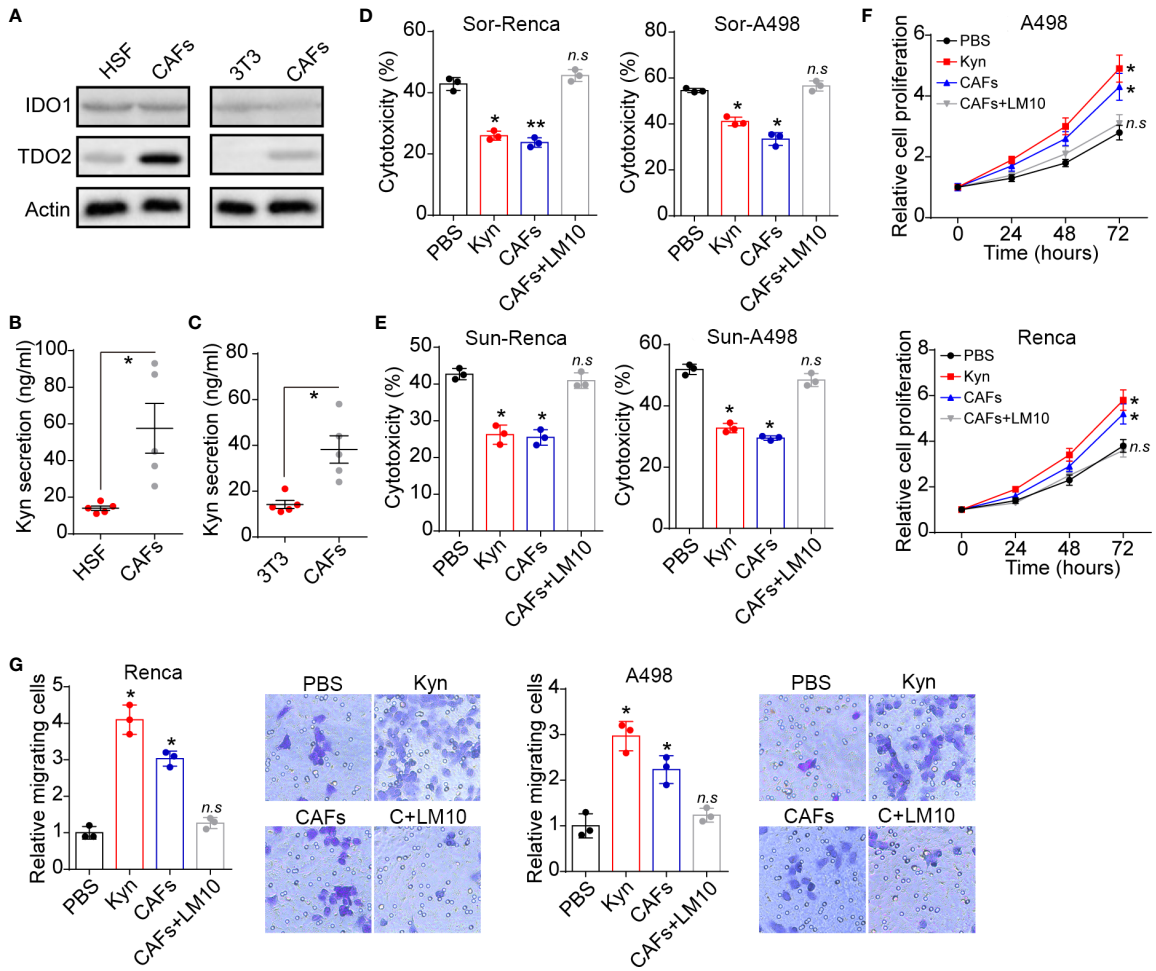



**FIGURE 2** | CAFs secreted Kyn to regulate tumor progression. **(A)** The western blotting of IDO1, TDO2 and β-actin in HSF, NIH-3T3 and CAFs isolated from renal patients (compared to HSF) or Renca bearing mice (compared to Renca). **(B)** The Kyn concentration in culture medium of HSF or CAFs isolated from patients using Elisa analysis ($10^5$ cells in 2 ml culture medium, 48 hours). **(C)** The Kyn concentration in culture medium of NIH-3T3 or CAFs isolated from Renca bearing mice using Elisa analysis ($10^5$ cells in 2 ml culture medium, 48 hours). **(D)** The cytotoxicity of Sor to Renca/A498 treated with Kyn (0.5 μM), CAFs or CAFs combined with LM10 (2 μM). **(E)** The cytotoxicity of Sun to Renca/A498 treated with Kyn (0.5 μM), CAFs or CAFs combined with LM10 (2 μM). **(F)** The relative cell proliferation of Renca/A498 treated with Kyn (0.5 μM), CAFs or CAFs combined with LM10 (2 μM). **(G)** The relative migrating cells numbers and representative images of Renca/A498 treated with Kyn (0.5 μM), CAFs or CAFs combined with LM10 (2 μM). Mean ± SEM, n.s, no significant difference; *p < 0.05, **p < 0.01.

indicating that CAFs secreted Kyn to mediate multidrug resistance in renal cancer. Subsequently, we further examined the cells proliferation and migration of Renca/A498 cells by MTT and transwell analysis. Kyn treatment could significantly promote Renca/A498 cells proliferation and migration, whereas addition of LM10 retarded cells proliferation (**Figure 2F**) and migration (**Figure 2G**). Those results reminded that CAFs regulates renal cancer progression through Kyn.

## Kyn Produced by CAFs Promoted Cells Proliferation Through AhR/AKT Signaling

To investigate the molecular mechanism of Kyn induced tumor progression, we further examined the Kyn downstream signal molecular in renal cancer cells. Intriguingly, elevated expression of AhR was observed in Kyn treated or CAFs co-cultured Renca/A498 cells (**Figure 3A**). More importantly, our immunofluorescent staining results indicated that Kyn treatment facilitated the nucleus entry of AhR in A498 cells (**Figure S1A**), indicating that Kyn induced AhR activation in renal cancer cells. Current study has suggested that activated AhR could mediate the crosstalk between JAK2 and Src (16, 17), resulting in the Src associated pro-survival signaling pathway activation. Herein, we further examined the expression of Src and Src downstream ATK signal. As a result, addition of Kyn efficiently mediated the activation of Src and AKT, whereas blockade of AhR by AhR inhibitor PDM2 reversed the phenomenon (**Figure 3B**). These results suggested that Kyn induced AKT signal activation through AhR axis. To further confirm the role of AhR/AKT axis in tumor progression, we applied AhR inhibitor PDM2 and AKT inhibitor Cap to treat Renca/A498 cells. Blockade of AhR or AKT obviously suppressed the cells proliferation induced by Kyn (**Figure 3C**), indicating that Kyn promoted cells proliferation through AhR/AKT signaling pathway. However, AKT inhibitor Cap treatment was not capable of suppressing the drugs resistance or cells migration (**Figures 3D–F**), reminding us that Kyn might regulate drugs resistance and

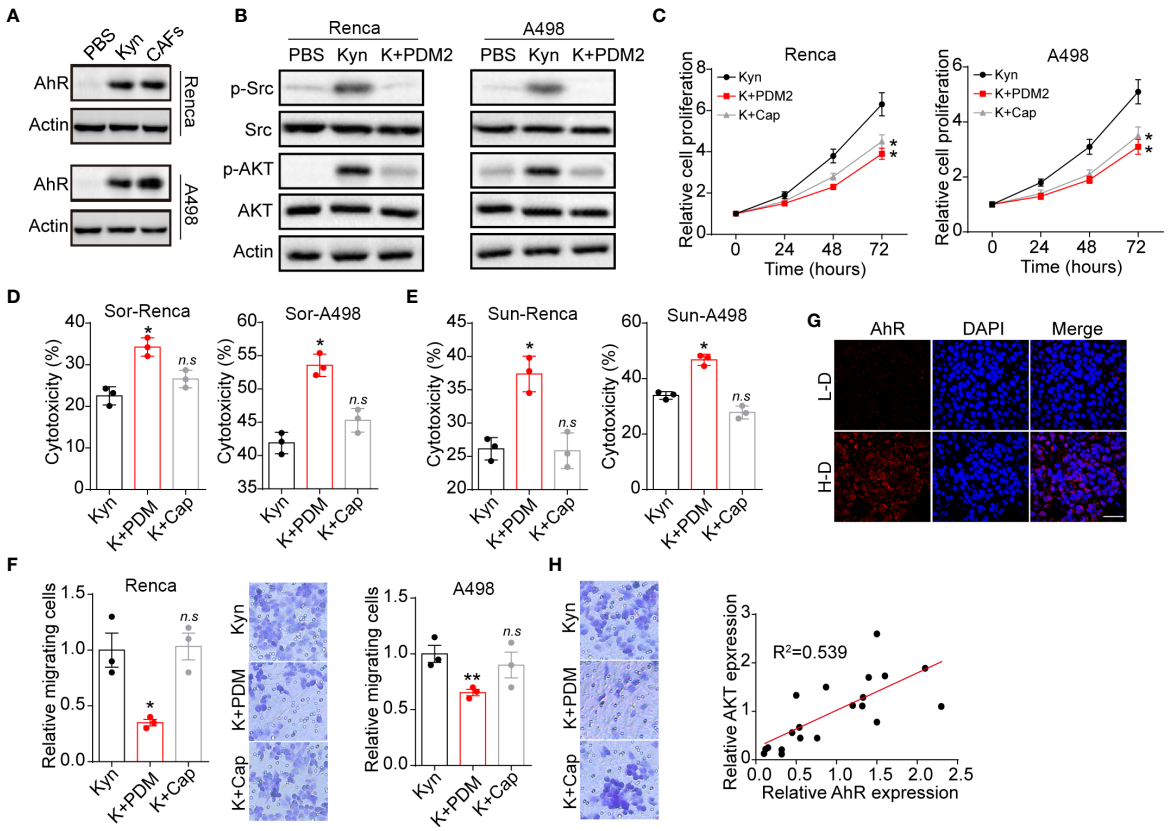



**FIGURE 3** | Kyn facilitated cells proliferation by AhR/ATK signal. **(A)** The western blotting of AhR and β-actin in Renca/A498 treated with PBS, Kyn (0.5 μM) or CAFs co-culture. **(B)** The western blotting of phosphorylated Src, total Src, phosphorylated AKT, total AKT and β-actin in Renca/A498 treated with PBS, Kyn (0.5 μM) or Kyn (0.5 μM) combined with PDM2 (1 nM). **(C)** The relative cells proliferation of Renca/A498 treated with Kyn (0.5 μM) or Kyn (0.5 μM) combined with PDM2 (1 nM)/Cap (10 nM). **(D)** The cytotoxicity of Sor to Renca/A498 treated with Kyn (0.5 μM) or Kyn (0.5 μM) combined with PDM2 (1 nM)/Cap (10 nM). **(E)** The cytotoxicity of Sun to Renca/A498 treated with Kyn (0.5 μM) or Kyn (0.5 μM) combined with PDM2 (1 nM)/Cap (10 nM). **(F)** The relative migrating cells numbers and representative images of Renca/A498 treated with Kyn (0.5 μM) or Kyn (0.5 μM) combined with PDM2 (1 nM)/Cap (10 nM). **(G)** Immunofluorescence staining of AhR in tumor tissues from high degree (H-D) and low degree (L-D) malignant renal patients. The scale bar is 50 μm. **(H)** The correlation analysis of AhR and phosphorylated AKT in tumor tissues from renal patients. Mean ± SEM, n.s, no significant difference, *p < 0.05, **p < 0.01.

migration through different AhR downstream signaling molecular. Next, we further confirmed the curial role of AhR in patients' tumor tissues. The immunofluorescence staining implicated enhanced expression of AhR was observed in high degree malignant tumor tissues compared to low degree malignant tissues (**Figure 3G**). However, no significant difference of AKT expression was observed in H-D and L-D groups (**Figure S1B**), indicating that AKT associated signals might not be involved into the AhR associated drugs resistance in renal cancer. However, a potential correlation ($R^2$>0.5) between AhR and AKT expression was still observed in those renal tumor tissues (**Figure 3H**), indicating that activation of AKT signals was AhR dependent in patients. Those results suggested that Kyn produced by CAFs promoted the cells proliferation through an AhR/AKT signaling pathway.

## Kyn Produced by CAFs Promoted Drugs Resistance and Cells Migration Through AhR/STAT3 Signaling

STAT3, which serves as the Src downstream signaling molecular (18), is a crucial participant in tumor drugs resistance and distant metastasis (19). Herein, we examined the expression of STAT3 in Renca and A498 cells. Activation of STAT3 signal was observed in Kyn treated A498/Renca cells, whereas blockade of AhR suppressed the STAT3 activation (**Figure 4A**). More importantly, blockade of STAT3 signal by STAT3 inhibitor S1-109 obviously suppressed the drugs resistance (**Figures 4B, C**) and cells migration (**Figure 4D**) induced by Kyn. Additionally, we examined the cytotoxicity of our inhibitors, including LM10, PDM2, Cap and S1-109, to exclude the potential influence caused by inhibitors associated cytotoxicity. As a result, no significant cytotoxicity to tumor cells was observed in our inhibitors (**Figure S1C**). Next, the enhanced expression of phosphorylated STAT3 was also found in high degree malignant tumor tissues from renal cancer patients (**Figure 4E**) and tumor tissues from metastatic renal patients (**Figure 4F**), indicating that STAT3 signals are vital for tumor progression and distant metastasis in clinical renal cancer. The correlation analysis also implicated that the expression of phosphorylated STAT3 was related to the AhR expression ($R^2$ = 0.6941) in clinical renal tumor tissues (**Figure 4G**). Together, those results suggested that Kyn regulated renal cancer drugs resistance and metastasis through AhR downstream STAT3 signaling pathway.

## Blockade of AhR Signals Improved Outcome of Chemotherapy in Mice Model

Given the crucial role of AhR in renal cancer progression, it might be feasible to block AhR signals to improve the outcome of Sor/Sun therapy. DMF, an AhR inhibitor, revealed obvious anti-cancer activity and could be administered orally, which is befitting for renal cancer therapy. Herein, we established lung metastatic/subcutaneous Renca bearing mice model and treated mice with PBS, DMF and Sor. As anticipated, blockade of AhR signals by DMF efficiently suppressed the lung metastasis of Renca cells.

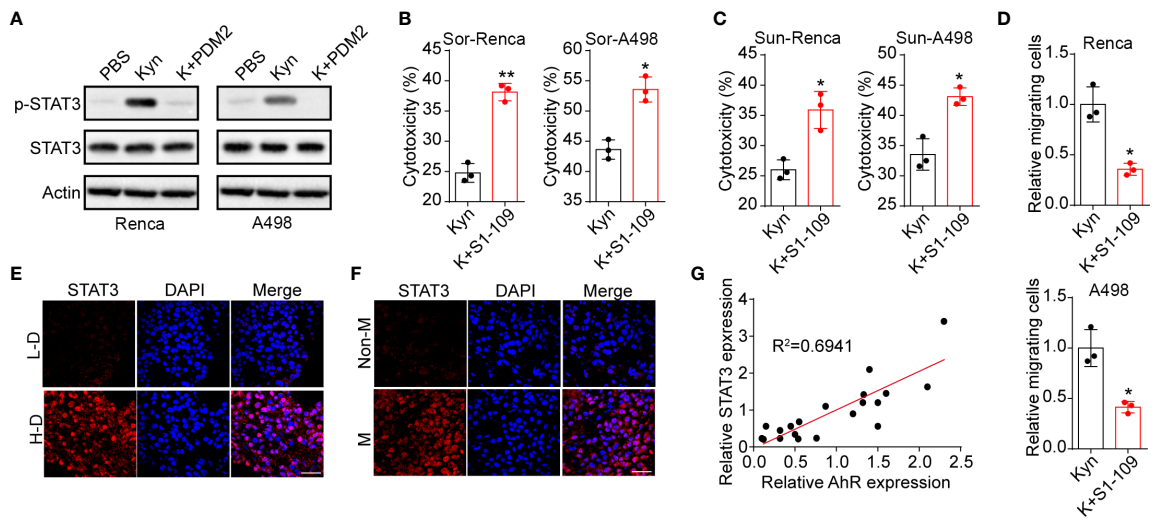



**FIGURE 4** | Kyn regulated cells migration and metastasis through AhR/STAT3 signal. **(A)** The western blotting of phosphorylated STAT3, total STAT3 in Renca/A498 treated with PBS, Kyn (0.5 μM), Kyn (0.5 μM) combined with PDM2 (1 nM). **(B)** The cytotoxicity of Sor to Renca/A498 treated with Kyn (0.5 μM) or Kyn (0.5 μM) combined with S1-109 (2 μM). **(C)** The cytotoxicity of Sun to Renca/A498 treated with Kyn (0.5 μM) or Kyn (0.5 μM) combined with S1-109 (2 μM). **(D)** The relative migrating cells numbers and representative images of Renca/A498 treated with Kyn (0.5 μM) or Kyn (0.5 μM) combined with S1-109 (2 μM). **(E)**, Immunofluorescence staining of phosphorylated STAT3 in tumor tissues from high degree (H-D) and low degree (L-D) renal cancer patients. The scale bar is 50 μm. **(F)** Immunofluorescence staining of phosphorylated STAT3 in tumor tissues from non-metastatic (non-M) and metastatic renal cancer patients. The scale bar is 50 μm. **(G)** The correlative analysis of AhR and phosphorylated STAT3 expression in tumor tissues from renal patients. Mean ± SEM, n.s, no significant difference; *p < 0.05, **p < 0.01.

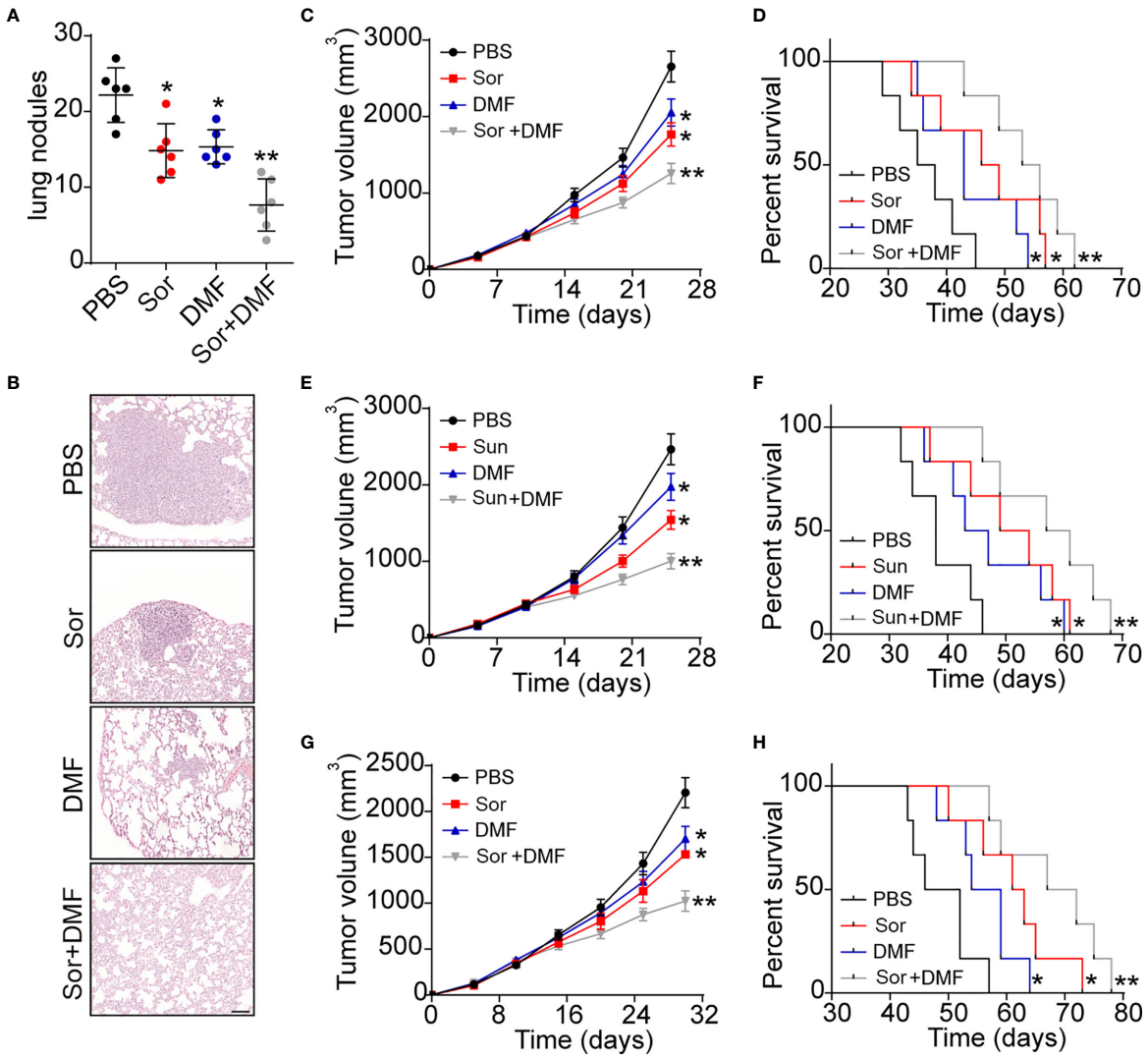



**FIGURE 5** | Blockade of AhR signals improved outcome of chemotherapy in renal cancer. **(A)** The metastasis lung nodules of Renca lung metastasis mice models treated with PBS, DMF, Sor and Sor combined with DMF. **(B)** Representative images of lung tissues from **(A)**. The scale bar is 200 μm. **(C)** The tumor volume of subcutaneous Renca bearing mice treated with PBS, DMF, Sor and Sor combined with DMF. **(D)** The survival time of subcutaneous Renca bearing mice treated with PBS, DMF, Sor and Sor combined with DMF. **(E)** The tumor volume of subcutaneous Renca bearing mice treated with PBS, DMF, Sun and Sun combined with DMF. **(F)** The survival time of subcutaneous Renca bearing mice treated with PBS, DMF, Sun and Sun combined with DMF. **(G)** The tumor volume of subcutaneous A498 bearing mice treated with PBS, DMF, Sor and Sor combined with DMF. **(H)** The survival time of subcutaneous A498 bearing mice treated with PBS, DMF, Sor and Sor combined with DMF. Mean ± SEM, n.s, no significant difference; *$p < 0.05$, **$p < 0.01$.

Meanwhile, DMF/Sor combination group revealed enhanced anticancer effects compared to the single DMF or Sor groups (**Figures 5A, B** and **S1D**). Addition of DMF significantly strengthened the tumor suppressive effects of Sor and prolonged the survival time in subcutaneous Renca bearing mice (**Figures 5C, D**). The synergistic effects were also observed in DMF and Sun combination (**Figures 5E, F**). Next, we further established human derived renal cancer model by subcutaneously injecting A498 into immunodeficient mice. Similarly, combination of DMF and Sor significantly suppressed the A498 tumor growth and prolonged the overall survival time of mice (**Figures 5G, H**). Taken together, those results suggested that blockade of DMF could strengthen the anticancer effects of chemotherapy, which provided an innovative approach for clinical renal cancer treatment.

## DISCUSSION

Despite the advance in cancer diagnose and therapy, the role of CAFs in renal cancer development remains controversial. CAFs

paly a complex role in cancer development through secretion of diverse elements (20). Previous reports focused on the cytokines derived from CAFs, which influenced tumor cells through activation of pro-survival signaling pathway directly. However, cellular metabolism is emerging as critical participant in tumor biological activities, which is frequently associated with tumor progression (21). Here, our study identified the role of CAFs in renal cancer progression, which was dependent on the Kyn associated signaling pathway.

Our study proved that CAFs isolated from tumor tissues contributed to the renal cancer drugs resistance and tumor progression, whereas normal fibroblasts failed to facilitate tumor development *in vitro* and *in vivo*. The Elisa and western blotting analysis suggested that CAFs isolated from tumor tissues revealed strengthened capability of tryptophan metabolism, contributing to the elevated secretion of Kyn in CAFs compared to normal fibroblasts. The Kyn derived from CAFs could efficiently mediate the activation of pro-survival signaling pathways in renal cancer, eventually resulting in cancer development. Compelling reports focused on the cytokines produced by CAFs, such as IGF2, EGF, IL-6 and so on (14). Wang and his colleagues reported that CAFs facilitated cells metastasis of lung cancer through the IL-6/JAK/STAT signaling pathway (22). Apart from cytokines, proteins or compounds produced by CAFs might participate in the tumor process regulation. Li reported that CAFs could facilitate drugs resistance of breast cancer through secretion of type I collagen (23). However, the influence of fibroblasts metabolism to tumor progression has yet to be explored. Kyn has been demonstrated to be an immunosuppressive regulator in innate and adaptive immune response, which is highly correlated to the immune tolerance in cancer development (24). Our study further provided evidence to described the role of Kyn in CAFs associated renal cancer progression. We proved that Kyn produced by CAFs could promote the AhR activation in tumor cells and contribute to the downstream pro-survival signals activation in renal cancer.

AhR, recognized as a ligand-activated basic helixloop-helix transcriptional factor that responses to environmental alternations, has been reported to be associated with tumor growth, drugs resistance and tumor immunosuppression (25). GJ Prud'homme reported that the expression of AhR referred to the cancer stem cells in breast cancer (26). Meanwhile, the sustained activation of the AhR transcription factor could mediate the resistance to BRAF-inhibitors in melanoma (27). Clinical data also suggested that the expression of AhR is highly correlated to the EGFR-TIKs resistance in non-small cell lung cancer (17). Simultaneously, several reports implicated that inhibition of AhR signaling by targeting the AhR proteins or associated ligands is prone to suppress tumor growth and recurrence. In our study, we proved that Kyn derived from CAFs could mediate the AhR activation in renal cancer, contributing to the downstream AKT and STAT3 signaling pathway activation (**Figure 6**). Our study further used AhR inhibitor DMF to be combined with Sor/Sun therapy, which revealed improved tumor suppressive effects and metastasis inhibition. Compared to previous AhR inhibitors, DMF revealed enhanced tumor suppressive effects, as well as good safety. No significant weight loss was observed in our DMF treated mice. Meanwhile, oral administration of DMF enabled the clinical application in renal therapy, which is more appreciate to be combined with Sor/Sun (oral administration) and provides potential clinical implication.

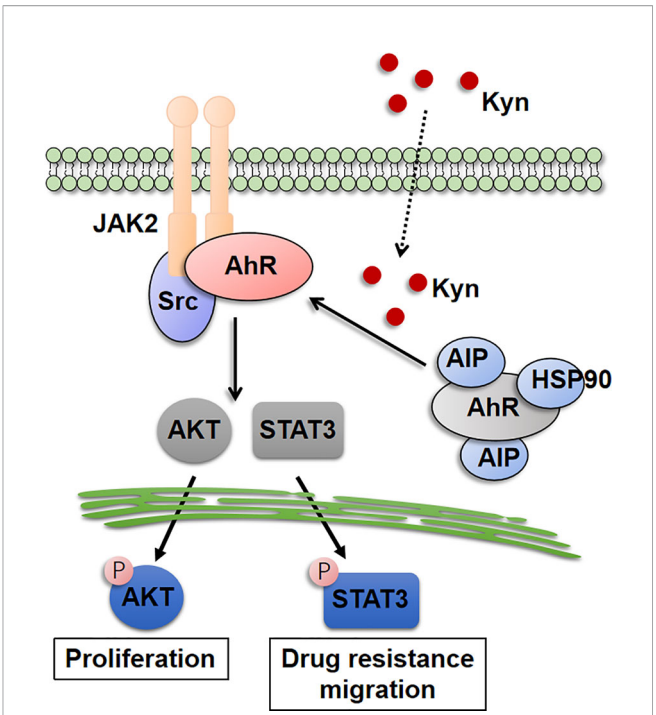



**FIGURE 6** | The schematic diatgram of CAFs induced renal cancer progression.

In conclusion, our study demonstrated that CAFs produced Kyn to promote tumor progression and drugs resistance in renal cancer, which is dependent on the AhR/AKT/STAT3 signaling pathway. Blockade of AhR by DMF could significantly improve the anticancer effects of Sor/Sun, which described a novel strategy for clinical renal cancer therapy.

## DATA AVAILABILITY STATEMENT

The original contributions presented in the study are included in the article/supplementary material. Further inquiries can be directed to the corresponding author.

## ETHICS STATEMENT

The studies involving human participants were reviewed and approved by the committee of the First Affiliated Hospital, University of South China. The patients/participants provided their written informed consent to participate in this study. The animal study was reviewed and approved by the Institute Ethics Committee of the First Affiliated Hospital, University of South China.

## AUTHOR CONTRIBUTIONS

RH conceived the project and wrote the manuscript. L-bC, S-pZ, T-pL, HZ, and Y-jD performed the experiments. L-bC, P-fC, and Y-jD performed data analysis. All authors contributed to the article and approved the submitted version.

## FUNDING

This study was supported by Scientific Research Fund Project of Hunan Provincial Health Commission 20200540.

## ACKNOWLEDGMENTS

We thank all the patients and their family's members for their permission in the study.

## SUPPLEMENTARY MATERIAL

The Supplementary Material for this article can be found online at: https://www.frontiersin.org/articles/10.3389/fonc.2021.628821/full#supplementary-material

## REFERENCES

1. Siegel RL, Miller KD, Jemal A. Cancer statistics, 2019. *CA Cancer J Clin* (2019) 69(1):7–34. doi: 10.3322/caac.21551
2. Capitanio U, Montorsi F. Renal cancer. *Lancet* (2016) 387(10021):894–906. doi: 10.1016/S0140-6736(15)00046-X
3. Tobias K, Sabrina R, Grant S. Prognostic factors and prognostic models for renal cell carcinoma: a literature review. *World J Urol* (2018) 36(12):1943–52. doi: 10.1007/s00345-018-2309-4
4. Marusyk A, Polyak K. Tumor heterogeneity: causes and consequences. *Biochim Biophys Acta* (2020) 1805(1):105–17. doi: 10.1016/j.bbcan.2009.11.002
5. Pickup MW, Mouw JK, Weaver VM. The extracellular matrix modulates the hallmarks of cancer. *EMBO Rep* (2014) 15(12):1243–53. doi: 10.15252/embr.201439246
6. Balkwill FR, Capasso M, Hagemann T. The tumor microenvironment at a glance. *J Cell Sci* (2012) 125(Pt 23):5591–6. doi: 10.1242/jcs.116392
7. Engblom C, Pfirschke C, Pittet MJ. The role of myeloid cells in cancer therapies. *Nat Rev Cancer* (2016) 16(7):447–62. doi: 10.1038/nrc.2016.54
8. Dayoub AS, Brekken RA. TIMs, TAMs, and PS- antibody targeting: implications for cancer immunotherapy. *Cell Commun Signal* (2020) 18 (1):29. doi: 10.1186/s12964-020-0521-5
9. Papaccio F, Paino F, Regad T, Papaccio G, Desiderio V, Tirino V. Concise Review: Cancer Cells, Cancer Stem Cells, and Mesenchymal Stem Cells: Influence in Cancer Development. *Stem Cells Transl Med* (2017) 6(12):2115–25. doi: 10.1002/sctm.17-0138
10. Turner N, Grose R. Fibroblast growth factor signalling: from development to cancer. *Nat Rev Cancer* (2010) 10(2):116–29. doi: 10.1038/nrc2780
11. Liu Y, Yu C, Wu Y, Sun X, Su Q, You C, et al. CD44+ fibroblasts increases breast cancer cell survival and drug resistance via IGF2BP3-CD44-IGF2 signalling. *J Cell Mol Med* (2017) 21(9):1979–88. doi: 10.1111/jcmm.13118
12. De Francesco EM, Lappano R, Santolla MF, Marsico S, Caruso A, Maggiolini M. HIF-1α/GPER signaling mediates the expression of VEGF induced by hypoxia in breast cancer associated fibroblasts (CAFs). *Breast Cancer Res* (2013) 15(4):R64. doi: 10.1186/bcr3458
13. Xing F, Saidou J, Watabe K. Cancer associated fibroblasts (CAFs) in tumor microenvironment. *Front Biosci (Landmark Ed)* (2010) 1(15):166–79. doi: 10.2741/3613
14. Kalluri R. The biology and function of fibroblasts in cancer. *Nat Rev Cancer* (2016) 16(9):582–98. doi: 10.1038/nrc.2016.73
15. Platten M, Nollen EAA, Röhrig UF, Fallarino F, Opitz CA. Tryptophan metabolism as a common therapeutic target in cancer, neurodegeneration and beyond. *Nat Rev Drug Discovery* (2019) 18(5):379–401. doi: 10.1038/s41573-019-0016-5
16. Zhu J, Luo L, Tian L, Yin S, Ma X, Cheng S, et al. Aryl Hydrocarbon Receptor Promotes IL-10 Expression in Inflammatory Macrophages Through Src-STAT3 Signaling Pathway. *Front Immunol* (2018) 9:2033. doi: 10.3389/fimmu.2018.02033
17. Ye M, Zhang Y, Gao H, Xu Y, Jing P, Wu J, et al. Activation of the Aryl Hydrocarbon Receptor Leads to Resistance to EGFR TKIs in Non-Small Cell Lung Cancer by Activating Src-mediated Bypass Signaling. *Clin Cancer Res* (2018) 24(5):1227–39. doi: 10.1158/1078-0432.CCR-17-0396
18. Bromberg JF, Horvath CM, Besser D, Lathem WW, Darnell JE Jr. Stat3 activation is required for cellular transformation by v-src. *Mol Cell Biol* (1998) 18(5):2553–8. doi: 10.1128/MCB.18.5.2553
19. Yu H, Lee H, Herrmann A, Buettner R, Jove R. Revisiting STAT3 signalling in cancer: new and unexpected biological functions. *Nat Rev Cancer* (2014) 14 (11):736–46. doi: 10.1038/nrc3818
20. Liu T, Han C, Wang S, Fang P, Ma Z, Xu L, et al. Cancer-associated fibroblasts: an emerging target of anti-cancer immunotherapy. *J Hematol Oncol* (2019) 12 (1):86. doi: 10.1186/s13045-019-0770-1
21. Pavlova NN, Thompson CB. The Emerging Hallmarks of Cancer Metabolism. *Cell Metab* (2016) 23(1):27–47. doi: 10.1016/j.cmet.2015.12.006
22. Wang L, Zhang F, Cui JY, Chen L, Chen YT, Liu BW. CAFs enhance paclitaxel resistance by inducing EMT through the IL-6/JAK2/STAT3 pathway. *Oncol Rep* (2018) 39(5):2081–90. doi: 10.3892/or.2018.6311
23. Li X, Li Q, Yu X, Li H, Huang G. Reverse of microtubule-directed chemotherapeutic drugs resistance induced by cancer-associated fibroblasts in breast cancer. *Onco Targets Ther* (2019) 12:7963–73. doi: 10.2147/OTT.S211043
24. Cheong JE, Sun L. Targeting the IDO1/TDO2-KYN-AhR Pathway for Cancer Immunotherapy - Challenges and Opportunities. *Trends Pharmacol Sci* (2018) 39(3):307–25. doi: 10.1016/j.tips.2017.11.007
25. Murray IA, Patterson AD, Perdew GH. Aryl hydrocarbon receptor ligands in cancer: friend and foe. *Nat Rev Cancer* (2014) 14(12):801–14. doi: 10.1038/nrc3846
26. Prud'homme GJ, Glinka Y, Toulina A, Ace O, Subramaniam V, Jothy S. Breast cancer stem-like cells are inhibited by a non-toxic aryl hydrocarbon receptor agonist. *PloS One* (2010) 5(11):e13831. doi: 10.1371/journal.pone.0013831
27. Corre S, Tardif N, Mouchet N, Leclair HM, Boussemart L, Gautron A, et al. Sustained activation of the Aryl hydrocarbon Receptor transcription factor promotes resistance to BRAF-inhibitors in melanoma. *Nat Commun* (2018) 9 (1):4775. doi: 10.1038/s41467-018-06951-2

**Conflict of Interest:** The authors declare that the research was conducted in the absence of any commercial or financial relationships that could be construed as a potential conflict of interest.

*Copyright © 2021 Chen, Zhu, Liu, Zhao, Chen, Duan and Hu. This is an open-access article distributed under the terms of the Creative Commons Attribution License (CC BY). The use, distribution or reproduction in other forums is permitted, provided the original author(s) and the copyright owner(s) are credited and that the original publication in this journal is cited, in accordance with accepted academic practice. No use, distribution or reproduction is permitted which does not comply with these terms.*

frontiers in Oncology

ORIGINAL RESEARCH
published: 25 March 2021
doi: 10.3389/fonc.2021.651921

# SLC39A8/Zinc Suppresses the Progression of Clear Cell Renal Cell Carcinoma

*Lilong Liu[1†], Yaxin Hou[1†], Junyi Hu[1], Lijie Zhou[1], Ke Chen[1], Xiong Yang[1*] and Zhengshuai Song[2*]*

*[1] Department of Urology, Union Hospital, Tongji Medical College, Huazhong University of Science and Technology, Wuhan, China, [2] Department of Urology, The Central Hospital of Wuhan, Tongji Medical College, Huazhong University of Science and Technology, Wuhan, China*

Clear cell renal cell carcinoma (ccRCC) is the most frequent and lethal subtype, which has high risk of metastasis or recurrence, accounting for 75–83% of renal cell carcinoma (RCC). Zrt- and Irt-like proteins (ZIP) family members (SLC39A1-14) function to pass zinc into the cytoplasm for many critical biological processes when cellular zinc is depleted. However, the functional analysis of individual ZIP family genes in ccRCC is not clarified. This study aimed to investigate whether ZIP family genes are related to the clinicopathological features and survival of ccRCC patients, and to identify the function of key gene of ZIP family in ccRCC *in vitro*. Through bioinformatics analysis of tumor databases, SLC39A8 was identified as a key gene of ZIP family in ccRCC, which could be used as an effective indicator for diagnosing ccRCC and judging its prognosis. With the progression of tumor, the expression of SLC39A8 decreased progressively. The prognosis of patients with low expression of SLC39A8 is significantly worse. Furthermore, we found that overexpression of SLC39A8 or treatment with low concentration of zinc chloride could effectively inhibit the proliferation, migration and invasion of ccRCC cells. Moreover, the inhibition effect of SLC39A8 overexpression could be enhanced by low concentration zinc supplement. Therefore, this study provides a novel understanding for the role of SLC39A8/zinc in the regulation of ccRCC progression. These findings provide a new direction and target for progressive ccRCC drug development and combination therapy strategies.

**Keywords: ccRCC, bioinformatics analysis, SLC39A8, zinc, progression**

OPEN ACCESS

***Edited by:***
*Lu Yang,*
*Sichuan University, China*

***Reviewed by:***
*Xiao-Jie Lu,*
*Nanjing Medical University, China*
*Chien-Feng Li,*
*National Health Research Institutes, Taiwan*

***Correspondence:**
*Xiong Yang*
*yangxiong1368@hust.edu.cn*
*Zhengshuai Song*
*867703966@qq.com*

*[†]These authors have contributed equally to this work*

***Specialty section:***
*This article was submitted to Genitourinary Oncology, a section of the journal Frontiers in Oncology*

***Received:*** *11 January 2021*
***Accepted:*** *05 March 2021*
***Published:*** *25 March 2021*

***Citation:***
*Liu L, Hou Y, Hu J, Zhou L, Chen K, Yang X and Song Z (2021) SLC39A8/Zinc Suppresses the Progression of Clear Cell Renal Cell Carcinoma. Front. Oncol. 11:651921. doi: 10.3389/fonc.2021.651921*

## INTRODUCTION

The annual incidence rate of kidney cancer in the European Union reached 3.3% leading to approximately 99,200 new cases and 39,100 related deaths in 2018 (1). Renal cell carcinoma (RCC) is one of the most common malignant tumor of renal tubular epithelial cells origin, accounting for 5 and 3% of malignant tumors of males and females (2), and accounts for >90% of kidney cancer cases (3). The classic presentation of RCC includes low backache, hematuria, and a palpable abdominal

mass. But not many patients now present in this manner. About half of the cases are now detected because a kidney mass is accidentally identified during the radiological examination (4). Due to the difficulty of early diagnosis of RCC, around one-third of patients present with metastatic disease at the time of diagnosis (5, 6). Moreover, those with nonmetastatic localized tumors have up to 40% risk of recurrence (5) and 21% risk of metastasis (7) following complete resection. The pathological types of clear cell renal cell carcinoma (ccRCC) is the most frequent and lethal subtype, which has high risk of metastasis or recurrence (8), accounting for 75–83% of RCC (3, 8–10). Currently, targeted therapies have been made in the treatment of ccRCC, including kinase and immune checkpoint inhibitors, which have greatly improved the treatment (11–14). However, there are still some dilemmas waiting to be solved, for example, all the patients do not gain from the treatment, development of drug resistance, loss of efficacy of a particular agent, etc. (11, 13). Hence, it is necessary to further elucidate the molecular mechanisms associated with ccRCC progression and metastasis, contributing to the development of novel therapeutic strategies.

As an essential micronutrient, zinc is the second richest and essential trace element in human body after iron (15), and approximately 98% is localized in the intracellular compartment (16). Most of the intracellular zinc is bound to or at least associated with proteins or complexed by anions (17). As previous studies reported, there were 2,800 human proteins potentially zinc-binding *in vivo*, corresponding to 10% of the human proteome (18). Zinc plays a critical and unique role in many critical biological processes including regulation of gene expression, DNA repair, antioxidant defense, enzyme function, immune function, endocrine function, growth, development, reproduction, and cancer biology (15, 16, 19). Prostate cancer cells have been found to have low levels of zinc, then lower zinc abolish mitochondrial aconitase inhibition, causing genetic/metabolic transformation (20). However, zinc could act as a tumor suppressor agent (20, 21), for example, the accumulation of zinc inhibits growth and proliferation of prostate cells (22), and zinc could induce apoptosis in prostate cancer cells through its direct effects on mitochondrial release of cytochrome C followed by activation of caspases-9 and -3 (23) and inhibition of nuclear factor kappa B (NF-kB) (24, 25). Notably, zinc could also inhibit the invasive and metastatic capabilities of prostate cancer cells (26–28). In addition, the regulation of zinc has also been reported to be associated with head and neck, esophageal, lung, pancreatic, prostate, and breast cancer (29–36).

The solute carrier 30 family (SLC30A/ZnT) and the Zrt- and Irt-like proteins (ZIP/solute carrier 39 family, SLC39A) of zinc transporters are involved in controlling cellular zinc homeostasis in the body (37, 38). When the cellular zinc concentrations are elevated, ZnT family members function to the cytoplasmic zinc balance by exporting zinc out to the extracellular space or by isolating cytoplasmic zinc to the intracellular compartments (37). While ZIP family members serve to pass zinc into the cytoplasm when cellular zinc is depleted (38). The 14 human ZIP family proteins (SLC39A1, 2, 3, 4, 5, 6, 7, 8, 9, 10, 11, 12, 13, 14) are expressed in a wide variety of tissues and function in many different cellular processes (39). To the best of our knowledge, the functional analysis of individual ZIP family genes in patients with ccRCC is not clarified. This study aimed to investigate whether ZIP family genes are related to the clinicopathological features and survival of ccRCC patients. In addition, we also studied the function of key gene (SLC39A8) of ZIP family in ccRCC *in vitro*.

# MATERIALS AND METHODS

## Cancer Database Bioinformatic Analysis

UALCAN, an interactive web-portal to perform to in-depth analyses of The Cancer Genome Atlas (TCGA) gene expression data (40), is publicly available at http://ualcan.path.uab.edu/index.html. This database was used to analyze relative expression of ZIP family genes across tumor and normal samples of ccRCC, as well as the tumor sub-groups based on individual tumor grade. GEPIA (Gene Expression Profiling Interactive Analysis) is a web-based tool to deliver fast and customizable functionalities based on TCGA and Genotype-Tissue Expression (GTEx) data, providing key interactive and customizable functions including differential expression analysis, profiling plotting, correlation analysis, patient survival analysis, similar gene detection and dimensionality reduction analysis (41), is publicly available at http://gepia.cancer-pku.cn/. We used this database to analyze the overall survival (OS) and disease-free survival (DFS) of ZIP family genes in ccRCC with the high and low groups cutoffs were 50% and 50%, the p value <0.05 was considered to have significant differences. Metascape combines functional enrichment, interactome analysis, gene annotation, and membership search to leverage over 40 independent knowledge bases within one integrated portal (42). Functional enrichment analysis of ZIP family genes was conducted with Metascape database (https://metascape.org/gp/index.html). The University of California, Santa Cruz (UCSC) Xena browser was developed as a high-performance visualization and analysis tool for both large public repositories and private datasets (43), available at https://xenabrowser.net/. We downloaded the mRNA expression level data of ZIP family genes in ccRCC tissues and corresponding normal tissues, the clinicopathological and survival data of ccRCC patients from the UCSC Xena browser. ONCOMINE, a cancer microarray database and web-based data-mining platform aimed at facilitating discovery from genome-wide expression analyses (44), is publicly available at https://www.oncomine.org/resource/main.html. Relative expression of SLC39A8 in tumor and normal samples of ccRCC in statistics by Beroukhim et al. (45), Jones et al. (46), Lenburg et al. (47), and Gumz et al. (48) were downloaded from ONCOMINE database. The E-MTAB-1980 cohort (https://www.ebi.ac.uk/arrayexpress/experiments/E-MTAB-1980/) with 101 sample information (49) was used as external validation to evaluate the clinicopathologic significance of SLC39A8 expression and OS in ccRCC patients. The Human Protein Atlas is a Swedish-based program aim to map all the

human proteins in cells, tissues and organs using an integration of various omics technologies, including antibody-based imaging, mass spectrometry-based proteomics, transcriptomics and systems biology (50, 51), is publicly available at https://www.proteinatlas.org. We used this database to determine the expression of protein SLC39A8 in RCC and to account for the difference between tumor and normal samples through antibody-based imaging. Gene Set Enrichment Analysis (GSEA) is a powerful analytical method which derives its power by focusing on gene sets, that is, groups of genes that share common biological function, chromosomal location, or regulation (52). To determine which the hallmark effector gene sets associated with SLC39A8 mRNA expression of the TCGA-KIRC dataset, a GSEA was performed by GSEA software obtained from http://www.broad.mit.edu/gsea. For the enriched gene sets, the false discovery rate (FDR) value <0.25 and P <0.05 after performing 1,000 permutations were considered to be a statistically significant enrichment pathway. A Cancer Dependency Map was developed to identify genes essential for cancer cell proliferation/survival and facilitate the prioritization of therapeutic targets (53). Data evaluating the dependency of SLC39A8 gene for cell survival of renal cancer were downloaded from Depmap portal (https://depmap.org/portal). CERES Dependence Score of 0 and −1 represent the median scores of nonessential and cell-essential genes, respectively (54).

## Tissue Samples

Thirty-two pairs of T3 & T4 human ccRCC tissues and paired adjacent tissues from 32 ccRCC patients were collected by the Department of Urology, Union Hospital, Tongji Medical College (Wuhan, China). Among these, 24 pairs of tissue specimens were preserved in liquid nitrogen for subsequent protein expression analysis by western blotting and mRNA expression analysis by quantitative real-time PCR (qRT-PCR). The remaining eight pairs of samples were fixed with 4% paraformaldehyde for 24–48 h at room temperature and embedded in paraffin after dehydration and transparency for subsequent immuno histochemical (IHC) analysis. This study was fully informed by the patients and was approved by the Human Research Ethics Committee of Huazhong University of science and Technology (Wuhan, China).

## Cell Lines and Cell Culture

The normal human renal epithelial cell line HK2 and the RCC cell lines 786-O, OSRC-2, ACHN, A498 and CAKI-1 were purchased from the American Type Culture Collection (ATCC). All the cell lines were cultured in high glucose Dulbecco's Modified Eagle's medium (DMEM, Servicebio Co., Ltd., China) containing 10% fetal bovine serum (FBS, Gibco, USA) and 1% penicillin–streptomycin (Beijing Solarbio Science & Technology Co., Ltd., China). As for zinc supplementation experiment, the culture medium was replaced with new culture medium containing different concentrations of zinc chloride (a final concentration of 0, 0.5, 5, 10, 20, 50, 75, 100, 150, 200 μM) after the cells adhered completely. All cells were maintained in a cell incubator with 5% CO2, humidified and 37°C atmosphere (Thermo Fisher Scientific, Inc., USA).

## Cell Transfection

Small interfering RNA (siRNA) specifically targeting SLC39A8 (si–SLC39A8) and corresponding negative control siRNA (si-NC) (LOT. NO. R008263554), and the plasmids harboring SLC39A8 (SLC39A8) and a negative control (SLC39A8-NC) were constructed and supplied by Vigene Biology (Vigene, China). 786-O and OSRC-2 cells were transfected by si–SLC39A8, si-NC, SLC39A8, and SLC39A8-NC with lipofectamine® 2000 (Thermo Fisher Scientific, Inc., USA) according to the manufacturer's instructions. Cells were collected 48 h after transfection for subsequent experiments. The si-SLC39A8 sequence was as follows: 5'-CCUUGUAUGCA GGAGAAAUTT-3'.

## Immunohistochemistry

Eight pairs of tissue specimens from ccRCC patients were cut into 5 μm paraffin-embedded sections. The tissue sections were incubated with SLC39A8 rabbit polyclonal antibody (1:200, ABclonal, China) overnight at 4°C, then the immunodetection was performed using secondary antibody at room temperature. Next, the results were visualized by 3,3'-diaminobenzidine and hematoxylin. Finally, the prepared slides were scanned as high-resolution digital images using the Pannoramic MIDI II (3Dhistech, Hungary) histological scanner.

## Western Blotting Experiments

The cell lines and tissue samples protein were extracted by RIPA buffer (Servicebio Co., Ltd., China) containing proteinase inhibitor cocktail and phenylmethanesulfonyl fluoride (PMSF). An equal amount of the above products (total protein) was used for gel electrophoresis and transferred onto nitrocellulose membranes. Then, the membranes were incubated with primary antibodies overnight at 4°C after blocking with 5% milk for 1.5 h. Subsequently, the membranes were incubated with secondary antibodies at room temperature for 1.5 h and the proteins were visualized by ChemiDoc-XRs+ (Bio-Rad Laboratories, Inc., USA). Primary antibodies: GAPDH (1:3,000, Wuhan Boster Biological Technology, Ltd., China), SLC39A8 (1:1,500, ABclonal, China), N-cadherin (1:5,000, Abcam, USA), E-cadherin (1:10,000, Abcam, USA), SNAI1 (1:1,000, Bio-Swamp Life Science Lab, China). All the procedures were carried out according to the manufacturer's instructions.

## RNA Extraction and qRT-PCR

The cell lines and tissue samples total mRNA was extracted by Trizol reagent (Thermo, USA), and the purity and concentration were tested by the NanoDrop 2000 spectrophotometer (NanoDrop Technologies, USA). About 2 μg of the above products were reversely transcribed to complementary DNA (cDNA) according to the manufacturer's instructions. qRT-PCR was carried out using SYBR Green qPCR Master Mix (Vazyme Biotech, China) according to the manufacturer's instructions. Each sample was repeated in triplicate. The relative gene expression level was expressed by the comparative CT method. Specific primers, SLC39A8 (Forward: 5'-TGGTTGCACCCCTCACAAAT-3', Reverse: 5'-CACATGGT GCACTGAAACCG-3'), GAPDH (Forward: 5'-TCGTGGAA

GGACTCATGACC-3', Reverse: 5'-CCAGTGAGCTTCC CGTTCA-3').

## Colony Formation Assay

786-O, OSRC-2 cells and 786-O, OSRC-2 cells transfected with si −SLC39A8, si-NC, SLC39A8, and SLC39A8-NC were seeded into 6-well plates (12-well plates for 786-O and OSRC-2 cells) with 1,000 cells per well. After the cells adhered completely, the culture medium was replaced with new culture medium containing different concentrations of zinc chloride. The cell colonies were fixed by methanol for 12 min and then stained with 0.05% crystal violet dye for 15 min after incubated for 12 days (9 days for 12-well plates).

## Cell Proliferation Assay

786-O, OSRC-2 cells and 786-O, OSRC-2 cells transfected with si −SLC39A8, si-NC, SLC39A8, and SLC39A8-NC were inoculated on 96-well plates with 1,000 cells per well. A cell proliferation assay was carried out per 24 h for a total of 96 h by using a Cell Counting Kit-8 (CCK8, MedChemExpress, USA) according to the manufacturer's instructions. After incubation for 2 h in a cell incubator (Thermo Fisher Scientific, Inc., USA), the absorbance of each well was measured at 450 nm by a spectrophotometer to evaluate the quantity of living cells.

## Transwell Migration and Invasion Experiments

786-O and OSRC-2 cells transfected with si−SLC39A8, si-NC, SLC39A8 (overexpression), and SLC39A8-NC were used for subsequent experiments. Transwell chambers with 8−μm membrane filters and 24-well plates (Corning Inc., USA) were used in the migration and invasion assays. The cells were incubated in DMEM without FBS for 6–8 h, and then collected the cells for later use. For migration assay, $1 \times 10^5$ cells in 200 μl FBS-free DMEM were seeded into the upper chambers, and the lower chambers were filled with 600 μl DMEM containing 10% FBS. For invasion assay, $2 \times 10^5$ cells in 200 μl FBS-free DMEM were seeded into the upper chambers which had been coated with matrigel and incubated at 37°C for 6–8 h, and the lower chambers were also filled with 600 μl DMEM containing 10% FBS. Each group was tested in three replicates. After incubation at a cell incubator (Thermo Fisher Scientific, Inc., USA) with 5% $CO_2$, humidified and 37°C atmosphere, the transwell chambers were transferred to a new 24-well plate, the upper and lower chambers were rinsed with phosphate buffer saline (PBS) twice, then the cells were fixed with 100% methanol for 15 min and stained with 0.05% crystal violet dye for 30 min at room temperature. Finally, the transwell chambers were rinsed in PBS for three times, the cells in the upper chamber were swabbed, and the cells in lower chambers were observed with a light microscope (Nanjing Jiangnan Novel Optics Co., Ltd., China) at 200× magnification, four microscopic fields were randomly selected for cell counting.

## Statistics

Graphpad Prism 6.0 and SPSS statistics software 21.0 were used for statistical analysis. The univariate and multivariate analyses of OS and DFS were performed to further screen the key genes of ZIP family in ccRCC patients. The SLC39A8 mRNA levels were analyzed in different clinicopathological parameters of ccRCC by Student's t-test. The survival curve analysis was used to analyze the relationship between the expression level of SLC39A8 and OS or disease specific survival (DSS) of ccRCC patients. The receiver operating characteristic (ROC) curve was used to analyze the expression level of SLC39A8 to distinguish ccRCC patients and obtain the area under the curve. Rank sum test of ordered data was used to analyze the expression of protein SLC39A8 in RCC through antibody-based imaging from The Human Protein Atlas. Each group of data was presented as mean ± standard deviation (SD). Mean differences were considered statistically significant when $P < 0.05$. *P <0.05, **P <0.01, ***P <0.001, ****P <0.0001.

# RESULTS

## The Relative mRNA Expression of ZIP Family Genes and Their Prognostic Values in ccRCC

To explore the roles of ZIP family genes expression in ccRCC, the expression data from TCGA database were analyzed by using UALCAN. As shown in **Supplementary Figures 1A–N**, the expression of SLC39A1, SLC39A8, SLC39A12 and SLC39A14 in cancer tissues was significantly higher than that in normal tissues, however, the SLC39A3, SLC39A4, SLC39A5, SLC39A6, SLC39A7, SLC39A9 and SLC39A13 were expressed higher in normal tissues, and the expression of SLC39A2, SLC39A10 and SLC39A11 showed no significant difference between cancer and normal tissues. Further, the expression of ZIP family genes based on tumor grade was analyzed. As shown in **Figures 1A–N**, the expression of ZIP family genes was significantly different between normal tissues and cancer tissues of different tumor grades except SLC39A2. In addition, the potential prognostic values of ZIP family genes in ccRCC were investigated by using GEPIA. As shown in **Figures 2A–N**, SLC39A1, SLC39A3, SLC39A5, SLC39A6, SLC39A7, SLC39A8, SLC39A9, and SLC39A10 showed positive relationships between low expression and significant worse OS in patients with ccRCC. However, only SLC39A5, SLC39A8, and SLC39A9 showed positive relationships between low expression and significant worse DFS (**Supplementary Figures 2A–N**). Then, univariate and multivariate analyses of OS and DFS were performed to further find the key gene of ZIP family in ccRCC patients. The results indicated that only SLC39A8 regarded as prognostic factor in both OS and DFS (**Tables 1**, **2**). Thus, we identified SLC39A8 as a key gene of ZIP family in ccRCC.

## Relationship Between the mRNA Levels of SLC39A8 and the Clinicopathological Parameters of Patients With ccRCC

The ONCOMINE and TCGA databases were used to analyze the sequencing data of SLC39A8 in ccRCC. As shown in **Figure 3A**, the expression level of SLC39A8 was significantly lower in cancer

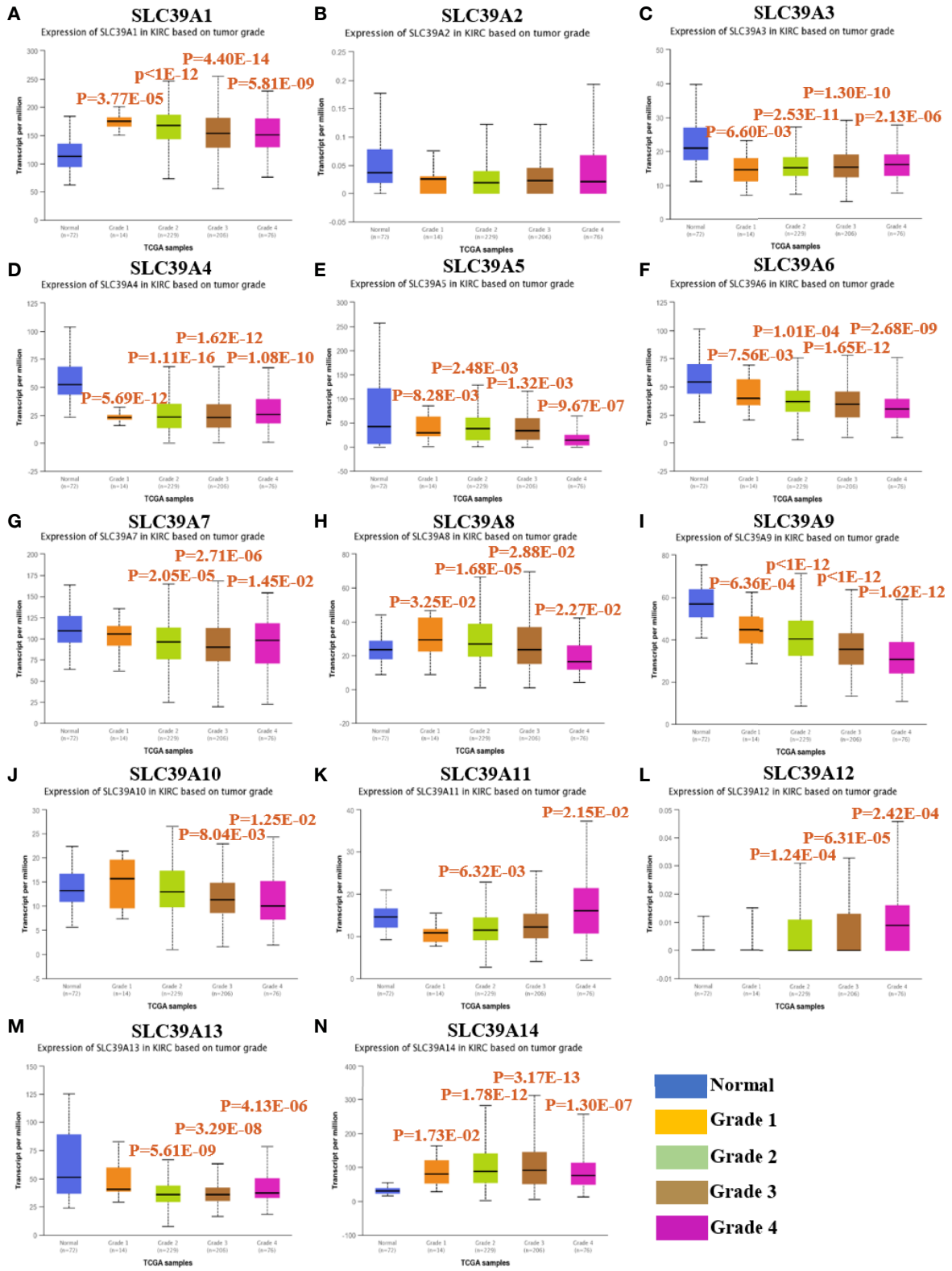



**FIGURE 1** | The expression of ZIP family genes based on tumor grade in patients with ccRCC by using UALCAN database[40]. **(A–N)** SLC39A1, SLC39A2, SLC39A3, SLC39A4, SLC39A5, SLC39A6, SLC39A7, SLC39A8, SLC39A9, SLC39A10, SLC39A11, SLC39A12, SLC39A13, SLC39A14. Mean differences were considered statistically significant when P <0.05.

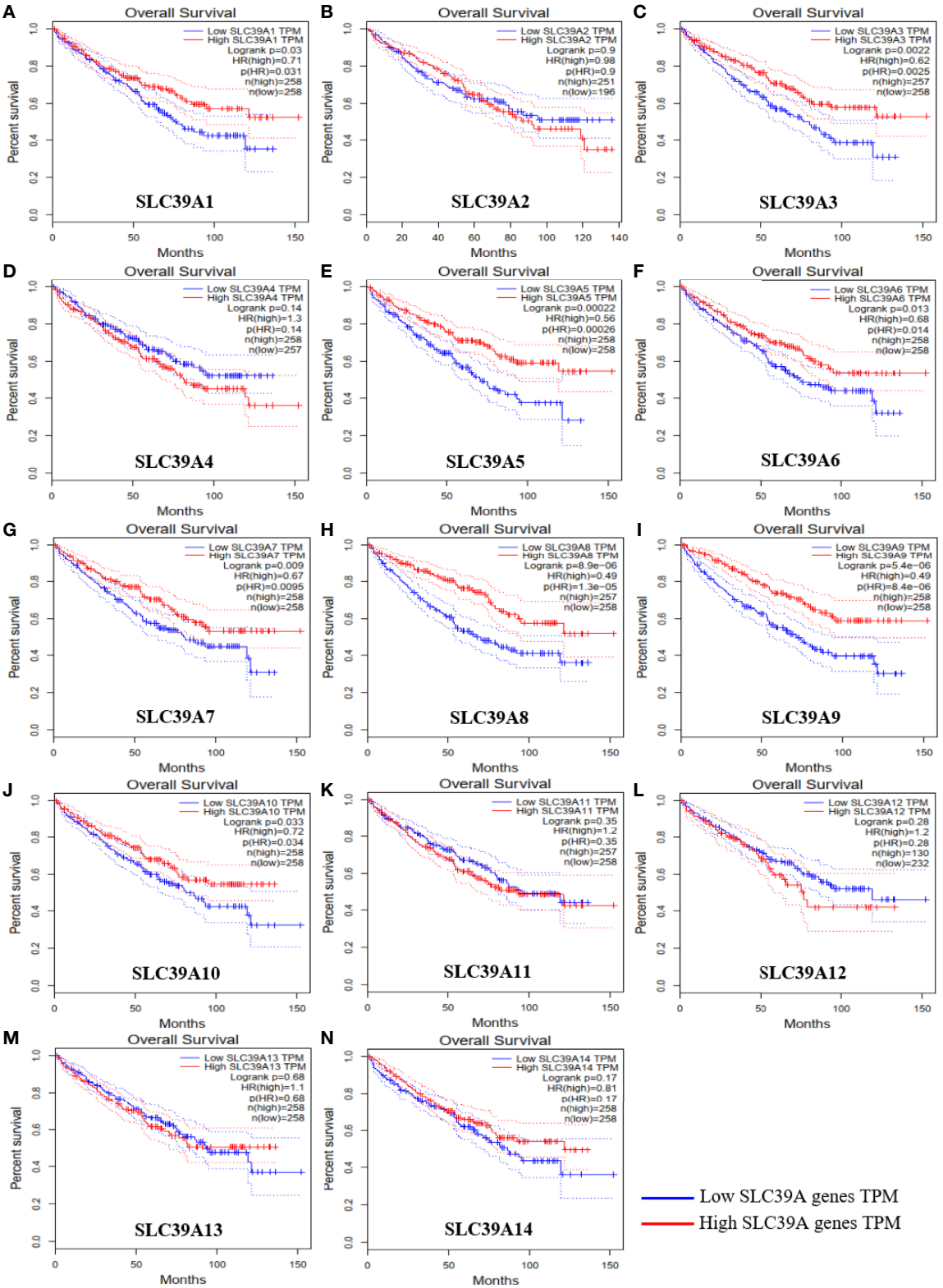



**FIGURE 2** | Overall survival of ZIP family genes in patients with ccRCC by using GEPIA. **(A–N)** SLC39A1, SLC39A2, SLC39A3, SLC39A4, SLC39A5, SLC39A6, SLC39A7, SLC39A8, SLC39A9, SLC39A10, SLC39A11, SLC39A12, SLC39A13, SLC39A14. Mean differences were considered statistically significant when P <0.05.

**TABLE 1 |** Univariate and multivariate analyses of ZIP family genes mRNA level and patient overall survival.

| Variable | Univariate analysis | | | Multivariate analysis | | |
|---|---|---|---|---|---|---|
| | HR | 95%CI | P-value | HR | 95%CI | P-value |
| SLC39A1 | 1.147 | 0.852–1.544 | 0.367 | | | |
| SLC39A2 | 1.296 | 0.962–1.745 | 0.088 | | | |
| SLC39A3 | 1.236 | 0.917–1.665 | 0.164 | | | |
| SLC39A4 | 1.112 | 0.827–1.496 | 0.483 | | | |
| SLC39A5 | 0.581 | 0.429–0.785 | 0.000 | 0.677 | 0.431–1.062 | 0.090 |
| SLC39A6 | 0.885 | 0.658–1.191 | 0.420 | | | |
| SLC39A7 | 1.159 | 0.862–1.559 | 0.329 | | | |
| SLC39A8 | 0.600 | 0.443–0.814 | 0.001 | 0.586 | 0.367–0.935 | 0.025 |
| SLC39A9 | 0.476 | 0.350–0.648 | 0.000 | 0.986 | 0.617–1.575 | 0.953 |
| SLC39A10 | 0.698 | 0.518–0.942 | 0.019 | 1.046 | 0.655–1.670 | 0.850 |
| SLC39A11 | 1.524 | 1.126–2.063 | 0.006 | 0.669 | 0.423–1.058 | 0.086 |
| SLC39A12 | 1.202 | 0.891–1.622 | 0.228 | | | |
| SLC39A13 | 1.820 | 1.342–2.467 | 0.000 | 1.520 | 0.947–2.441 | 0.083 |
| SLC39A14 | 1.038 | 0.772–1.397 | 0.803 | | | |
| Age | 1.771 | 1.305–2.405 | 0.000 | 1.748 | 1.128–2.707 | 0.012 |
| Gender | 0.949 | 0.698–1.292 | 0.741 | | | |
| T stage | 1.915 | 1.628–2.254 | 0.000 | 0.935 | 0.560–1.562 | 0.797 |
| N stage | 3.392 | 1.801–6.389 | 0.000 | 1.383 | 0.653–2.928 | 0.397 |
| M stage | 4.351 | 3.190–5.935 | 0.000 | 1.705 | 0.751–3.873 | 0.202 |
| TNM stage | 1.882 | 1.651–2.145 | 0.000 | 1.393 | 0.810–2.395 | 0.230 |
| Grade | 2.286 | 1.868–2.796 | 0.000 | 1.338 | 0.946–1.893 | 0.100 |
| Recurrence | 2.281 | 0.666–7.816 | 0.189 | | | |

*HR, hazard ratio; CI, confidence interval; TNM, Tumor Node Metastasis. Mean differences were considered statistically significant when P <0.05.*

**TABLE 2 |** Univariate and multivariate analyses of ZIP family genes mRNA level and patient disease-free survival.

| Variable | Univariate analysis | | | Multivariate analysis | | |
|---|---|---|---|---|---|---|
| | HR | 95%CI | P-value | HR | 95%CI | P-value |
| SLC39A1 | 1.422 | 0.995–2.033 | 0.053 | | | |
| SLC39A2 | 1.334 | 0.936–1.901 | 0.111 | | | |
| SLC39A3 | 1.299 | 0.912–1.851 | 0.147 | | | |
| SLC39A4 | 1.011 | 0.711–1.439 | 0.950 | | | |
| SLC39A5 | 0.593 | 0.415–0.848 | 0.004 | 0.503 | 0.302–0.838 | 0.008 |
| SLC39A6 | 1.071 | 0.752–1.525 | 0.705 | | | |
| SLC39A7 | 1.119 | 0.786–1.593 | 0.532 | | | |
| SLC39A8 | 0.406 | 0.278–0.594 | 0.000 | 0.481 | 0.275–0.841 | 0.010 |
| SLC39A9 | 0.481 | 0.335–0.691 | 0.000 | 0.810 | 0.485–1.353 | 0.421 |
| SLC39A10 | 0.777 | 0.546–1.106 | 0.161 | | | |
| SLC39A11 | 1.928 | 1.338–2.776 | 0.000 | 0.716 | 0.399–1.285 | 0.263 |
| SLC39A12 | 0.855 | 0.592–1.234 | 0.403 | | | |
| SLC39A13 | 1.790 | 1.252–2.559 | 0.001 | 1.037 | 0.609–1.765 | 0.895 |
| SLC39A14 | 1.573 | 1.095–2.259 | 0.014 | 1.326 | 0.769–2.287 | 0.310 |
| Age | 1.343 | 0.945–1.911 | 0.100 | | | |
| Gender | 1.389 | 0.939–2.056 | 0.100 | | | |
| T stage | 2.517 | 2.043–3.102 | 0.000 | 0.805 | 0.434–1.494 | 0.493 |
| N stage | 4.690 | 2.293–9.592 | 0.000 | 1.901 | 0.857–4.218 | 0.114 |
| M stage | 8.595 | 5.918–12.483 | 0.000 | 1.340 | 0.519–3.460 | 0.545 |
| TNM stage | 2.678 | 2.247–3.191 | 0.000 | 2.391 | 1.215–4.706 | 0.012 |
| Grade | 3.026 | 2.345–3.904 | 0.000 | 1.319 | 0.907–1.918 | 0.148 |

*HR, hazard ratio; CI, confidence interval; TNM, Tumor Node Metastasis. Mean differences were considered statistically significant when P <0.05.*

tissues than that in normal tissues of ccRCC in statistics by Beroukhim et al. (45), Jones et al. (46), but similar in two studies of Lenburg et al. (47), and Gumz et al. (48). Next, the expression level of SLC39A8 in various subgroups of patients with ccRCC was evaluated. The results indicated that the expression of SLC39A8 in patients with distant metastasis or lymph node metastasis was significantly decreased, and the prognosis of those patients with decreased expression of SLC39A8 was significantly worse. Interestingly, the data from TCGA databases showed that the reduction of SLC39A8 expression was mainly occurred in patients with advanced ccRCC, while the expression level in patients with early ccRCC remained unchanged, even slightly

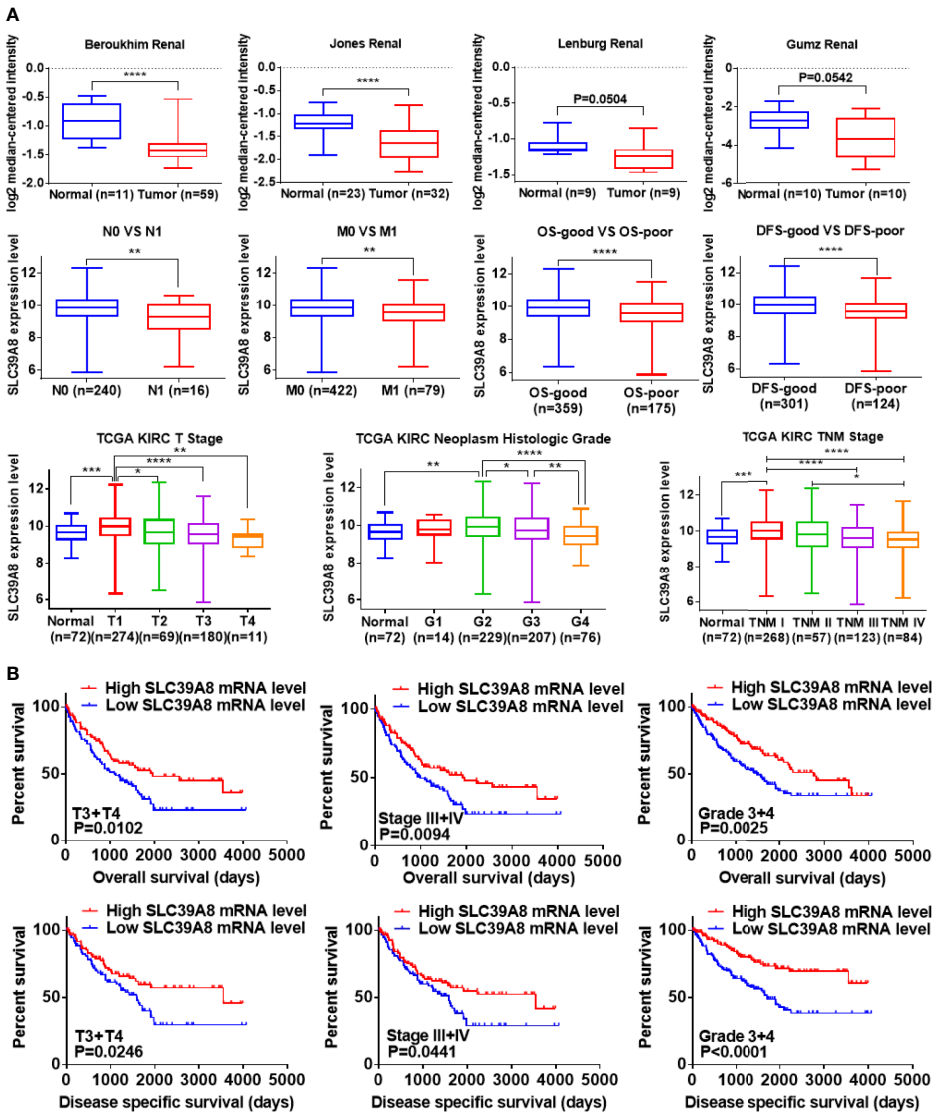



**FIGURE 3** | SLC39A8 was down expression and positively associated with tumor progression and worse prognosis in ccRCC patients. **(A)** ONCOMINE database analysis showed that the mRNA expression levels of SLC39A8 were down-regulated in ccRCC in statistics by Beroukhim et al. (45) and Jones et al. (46), but similar in two studies of Lenburg et al. (47) and Gumz et al. (48). In addition, data analysis based on TCGA showed that with the progression of tumor, the expression of SLC39A8 decreased progressively. **(B)** Survival curve analysis determined that low SLC39A8 expression exhibits a shorter OS and DSS time in progressive ccRCC patients (T3 + T4, Stage III + IV, Grade 3 + 4). OS, overall survival; DSS, disease specific survival. *P <0.05, **P <0.01, ***P <0.001, ****P <0.0001.

increased. Notably, the survival curve analysis determined low SLC39A8 expression patients exhibited a shorter OS and DSS time (**Figure 3B**). In addition, the E-MTAB-1980 cohort was used to check the clinicopathologic significance of SLC39A8 expression, as shown in **Supplementary Figures 3A–E**, the expression of SLC39A8 was decreased in ccRCC patients with distant or lymph node metastasis, and decreased progressively with the increase of T stage and neoplasm histologic grade. Concordant with the results of TCGA database analysis, ccRCC patients with low expression of SLC39A8 had a poor prognosis. These results indicated that SLC39A8 is down-regulated in ccRCC and positively correlated with tumor progression.

To probe the diagnostic significance of low expression of SLC39A8 in ccRCC patients, we analyzed the diagnostic value of SLC39A8 low expression in TCGA data set in various clinicopathological parameters by ROC curve. As shown in **Supplementary Figure 4A**, ROC curve analysis showed that the expression level of SLC39A8 could statistically distinguish ccRCC from normal tissues with an AUC of 0.6378 (P = 0.0043). In addition, we also analyzed the diagnostic value of SLC39A8 expression level in subgroups as follows: N0 vs. N1 stage (AUC = 0.6767, P = 0.0180); M0 vs. M1 stage (AUC=0.6192, P=0.0008); T1 + T2 vs. T3 + T4 stage (AUC = 0.6390, P <0.0001); Stage 1 + Stage 2 vs. Stage 3 + Stage 4 (AUC = 0.6492, P <0.0001);

Grade 1 + Grade 2 vs. Grade 3 + Grade 4 stage (AUC = 5879, P <0.0005); OS-good vs. OS-poor (AUC = 0.6209, P <0.0001); and DFS-good vs. DFS-poor (AUC = 0.6491, P <0.0001). These results suggest that SLC39A8 expression level has diagnostic value for ccRCC patients.

## SLC39A8 Expression in ccRCC Tissues and RCC Cell Lines

As SLC39A8 was down-regulated in the TCGA data set, immunohistochemistry, qRT-PCR, and western blotting experiments were performed to verify the expression levels of SLC39A8 in ccRCC tissues and RCC cell lines. As shown in **Figure 4A**, SLC39A8 protein was mainly located in the plasma membrane of renal tubular epithelial cells from paracancer tissues and cancer cells, the SLC39A8 expression in ccRCC tissues was significantly down-regulated. Moreover, we investigated the expression of protein SLC39A8 in RCC using online database The Human Protein Atlas, the results also indicated that SLC39A8 was down-regulated in RCC (**Supplementary Figure 4B**). At the cell line level, we also found that the expression of SLC39A8 in RCC cell lines was significantly lower than that in HK2 by qRT-PCR and western blotting experiments (**Figure 4B**). In addition, we confirmed SLC39A8 expression in T3 & T4 human ccRCC tissues and paired adjacent tissues by qRT-PCR and western blotting experiments (**Figure 4C**). All the results demonstrated that SLC39A8 expression level was significantly lower in RCC cell lines and T3 & T4 ccRCC tissues.

## The Effect of Zinc Supplementation on Cell Proliferation of ccRCC Cells

Functional enrichment analysis of ZIP family genes was conducted with Metascape. The results showed that ZIP family functions in the cellular import of zinc (**Figure 4D**). The CERES dependence score obtained from Depmap portal showed that SLC39A8 is not a key gene for RCC cells survival (**Supplementary Figure 4C**). Considering that the expression of SLC39A8 is down-regulated in ccRCC cells and SLC39A8 is involved in zinc transport, we speculated that ccRCC cells are in a low intracellular zinc state. Thus, we tried to treat ccRCC cell lines with different concentrations of zinc chloride, and surprisingly, we found that low concentrations (5–75 μM) of zinc supplementation for 48–72 h could significantly inhibit the 786-O and OSRC-2 cells proliferation (**Figure 4E**). The colony formation assay also showed that 10 and 20 μM zinc chloride treatment could significantly inhibit the colonies formation of 786-O and OSRC-2 cells (**Figure 4F**). Since 20 μM zinc treatment could significantly inhibit the growth and colony formation of 786-O and OSRC-2 cells, 20 μM zinc chloride was chosen for the subsequent experiments unless otherwise stated.

## Biological Function of SLC39A8/Zinc in ccRCC Cell Lines

To identify the function of SLC9A8 on the biological behaviors of ccRCC, 786-O and OSRC-2 cell lines were chosen to transfect with si–SLC39A8 to down-regulate the expression of SLC39A8. As shown in **Figure 5A**, SLC39A8 mRNA and protein expression levels were significantly decreased in 786-O & OSRC-2-si –SLC39A8 cells compared with the corresponding control. After transfection, cell proliferation assay and colony formation assay were performed. The results demonstrated that knocking down SLC39A8 could significantly promote cell proliferation, while zinc supplementation could reverse this phenomenon (**Figures 5B, C**). In order to verify this discovery, 786-O and OSRC-2 cells were transfected with SLC39A8 to up-regulate the expression of SLC39A8. As shown in **Figures 5D–F**, overexpression of SLC39A8 could significantly inhibit the proliferation of 786-O and OSRC-2 cells, and zinc supplementation could enhance the inhibitory effect. Next, we investigated the effect of SLC39A8/zinc on the invasion and migration of ccRCC cells. As shown in **Figure 6A**, knocking down SLC39A8 could significantly promote cell invasion and migration, while zinc supplementation could reverse this phenomenon to a certain extent. Conversely, overexpression of SLC39A8 could significantly inhibit cell invasion and migration, and zinc supplementation could enhance this inhibitory effect (**Figure 6B**). These results indicated that SLC39A8/zinc could inhibit the proliferation, migration and invasion of ccRCC cells.

## Mechanism of SLC39A8/Zinc Inhibiting Cell Migration and Invasion

GSEA was performed using TCGA database to obtain more information related to the biological pathways of ccRCC. The results showed that the group with low expression of SLC39A8 was significantly enriched in nine functional gene sets which associated with histone deacetylase (HDAC) or metastasis pathway (**Figure 7A**). Subsequently, we verified the effect of SLC39A8/zinc on epithelial–mesenchymal transition (EMT) in ccRCC cells. 786-O and OSRC-2 cells transfected with si–SLC39A8 (knockdown), SLC39A8 (overexpression), and their corresponding control were used for this study. As shown in **Figure 7B**, through knocking down SLC39A8, western blotting experiments confirmed the enhanced expression of interstitial marker N-Cadherin and transcription factor SNAI1, while the epithelial marker E-Cadherin expression was reduced in 786-O & OSRC-2-si –SLC39A8 cells. However, zinc supplementation reverses this change to some extent. On the other hand, up-regulated expression of E-Cadherin and down-regulated expression of N-Cadherin and SNAI1 were observed in 786-O & OSRC-2-SLC39A8 cells, and this effect could be enhanced by zinc supplementation. These results suggested that the low expression of SLC39A8 in 786-O and OSRC-2 cells induced transition to the interstitial phenotype, on the contrary, overexpression of SLC39A8 induced transition to the epithelial phenotype, and this stimulation was enhanced by low concentration zinc supplement.

# DISCUSSION

Zinc plays a crucial role in various biological events, intracellular and extracellular zinc levels and distributions is critically regulated by two protein families of zinc transporters, ZnT

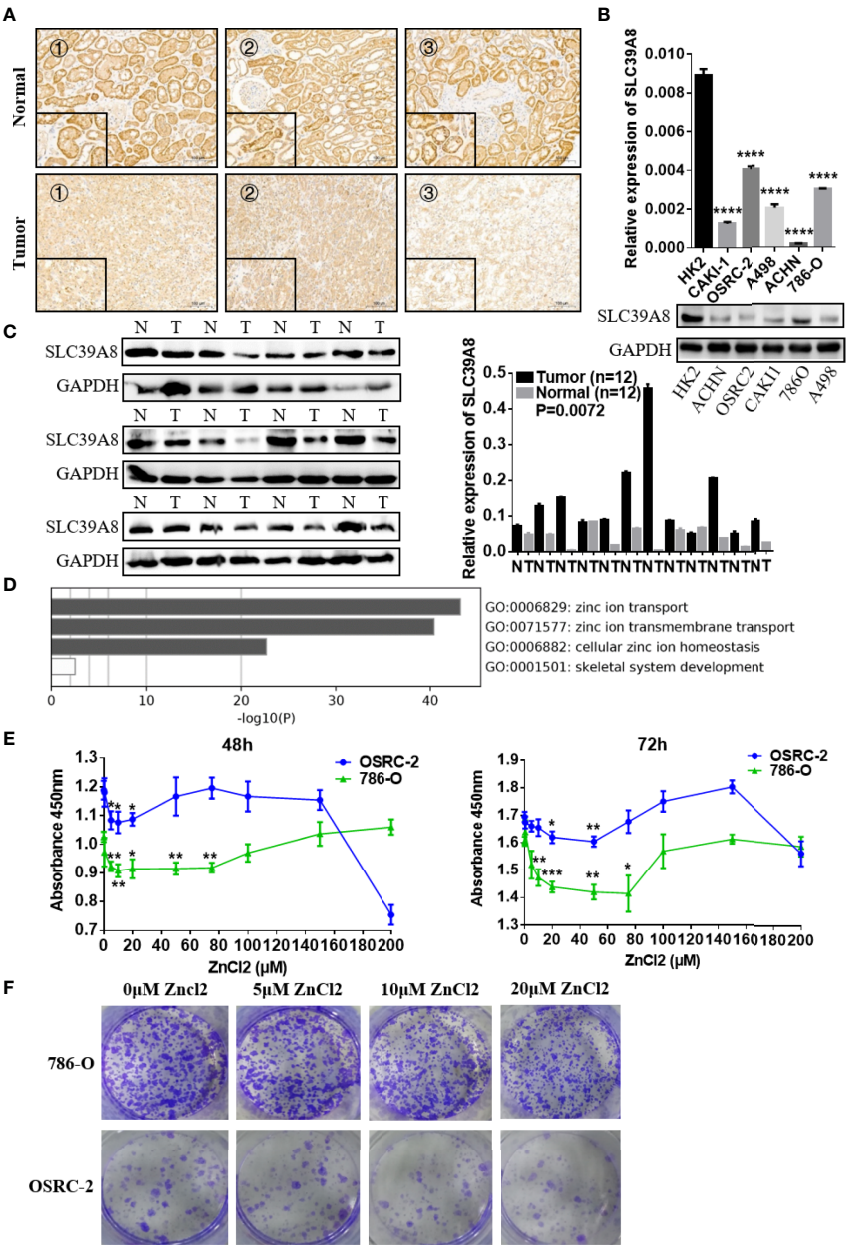



**FIGURE 4** | Function of SLC39A8 and its expression in ccRCC samples and RCC cell lines. **(A)** Immunohistochemistry for SLC39A8 expression in ccRCC tissues and the corresponding normal tissues. The inserted images are the higher magnification picture of a certain part of the same tissue, ×100 and ×400. **(B, C)** Reverse transcription-quantitative PCR assays and western blotting experiments of SLC39A8 expression in normal human renal epithelial cell line HK2 and RCC cell lines (786-O, OSRC-2, ACHN, A498 and CAKI-1) and ccRCC patients. **(D)** Functional enrichment analysis of ZIP family genes by Metascape. The results showed that ZIP family functions in the cellular import of zinc. **(E)** Cell proliferation assay of 786-O and OSRC-2 cells treated with different concentrations of zinc chloride (0–200 μM) for 48–72 h. **(F)** The colony formation assay of 786-O and OSRC-2 cells treated with 0–20 μM zinc chloride. The values of each group were presented as the mean ± standard deviation. *P <0.05, **P < 0.01, ***P < 0.001, ****P < 0.0001.

family functions to export zinc out to the extracellular space (37), and ZIP family serves to pass zinc into the cytoplasm (38). It has been reported that abnormal zinc transporters are associated with many specific diseases, including Alzheimer's disease, diabetes, and cancers (15, 55, 56). For the cancer, zinc generally acts as a suppressive agent (20, 21, 33), accumulating evidence has indicated that zinc deficiency contributed to increased cancer risk, tumor size, tumor stage, and increased unplanned hospitalizations by modified zinc homeostasis, transporter activity and affected ion channel activity (15, 57–

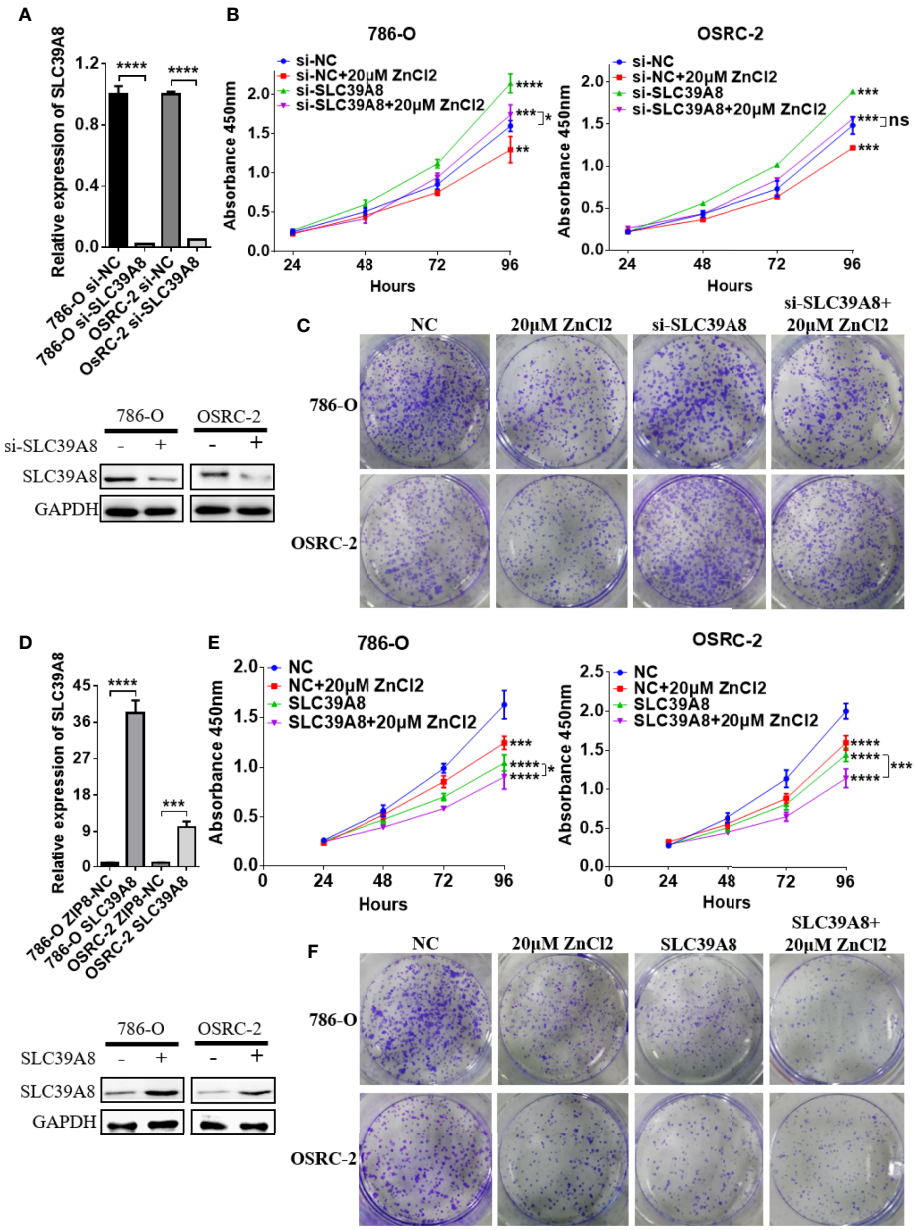



**FIGURE 5** | SLC39A8/zinc inhibits the proliferation of ccRCC cells *in vitro*. **(A)** Quantitative real-time PCR and western blotting experiments of SLC39A8 knockdown in 786-O and OSRC-2 cells. **(B, C)** Cell proliferation assay and colony formation assay detected the effects of SLC39A8 knockdown with or without zinc supplementation on the proliferation of 786-O and OSRC-2 cells. **(D)** Quantitative real-time PCR and western blotting experiments of SLC39A8 overexpression in 786-O and OSRC-2 cells. **(E, F)** Cell proliferation assay and colony formation assay detected the effects of SLC39A8 overexpression with or without zinc supplementation on the proliferation of 786-O and OSRC-2 cells. The values of each group were presented as the mean ± standard deviation. *P < 0.05, **P < 0.01, ***P < 0.001, ****P < 0.0001.

59). However, high dietary zinc intake has been reported to decrease the risk of colon cancer (60). Based on these studies, we can know that the change of expression profile of ZIP family members will inevitably affect the intracellular and extracellular zinc levels, and then affect the occurrence and development of tumors.

In this study, based on TCGA database analysis, we found that the expression of SLC39A1, SLC39A8, SLC39A12 and SLC39A14 were significantly higher in cancer tissues compared to normal tissue, while the SLC39A3, SLC39A4, SLC39A5, SLC39A6, SLC39A7, SLC39A9 and SLC39A13 were expressed higher in normal tissues. However, the low expression of

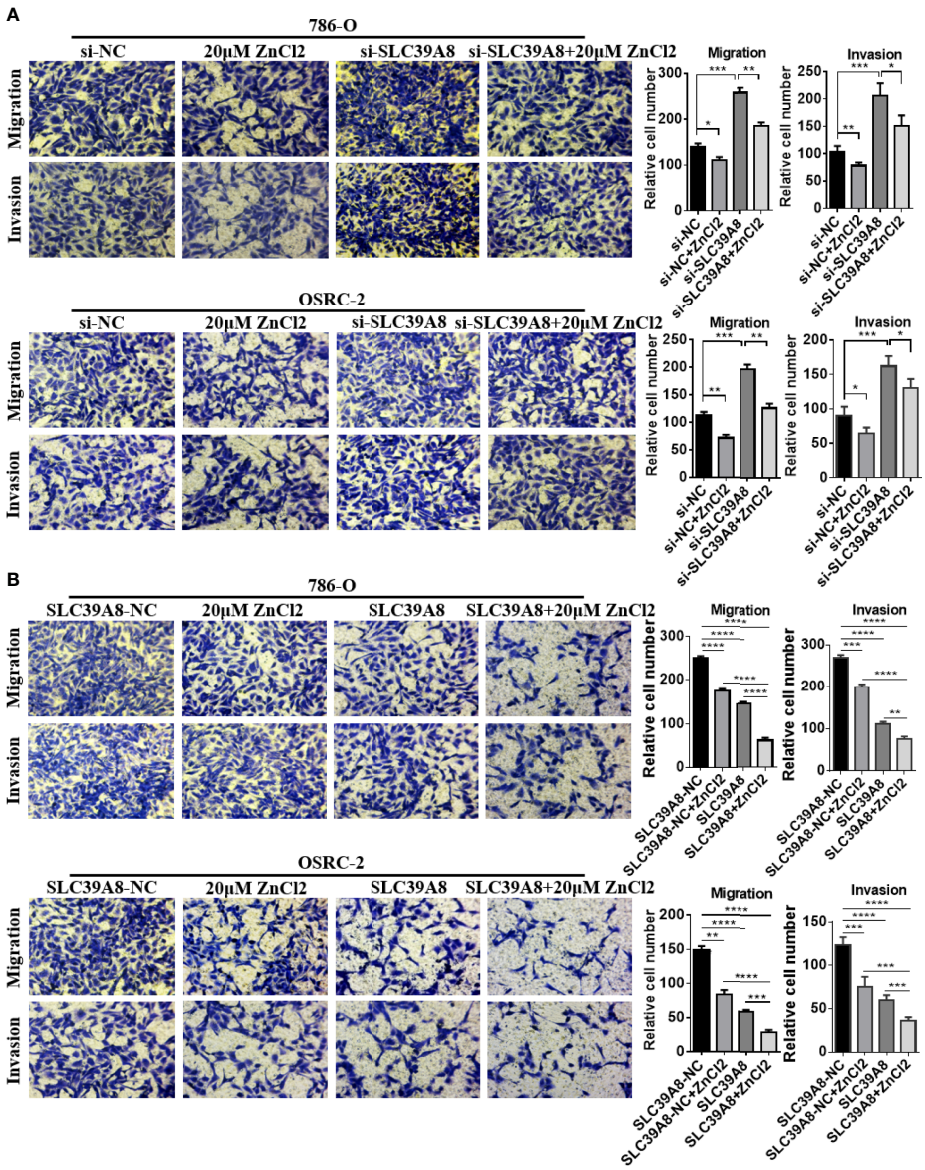



**FIGURE 6** | SLC39A8/zinc inhibits the invasion and migration of ccRCC cells *in vitro*. **(A)** Representative images of migration and invasion assays of SLC39A8 knockdown-786-O and OSRC-2 cells. **(B)** Representative images of migration and invasion assays of SLC39A8 overexpressed-786-O and OSRC-2 cells. Four microscopic fields with ×200 magnification were randomly selected for cell counting, and the data were presented as the mean ± standard deviation. *P < 0.05, **P < 0.01, ***P < 0.001, ****P < 0.0001.

SLC39A1, SLC39A3, SLC39A5, SLC39A6, SLC39A7, SLC39A8, SLC39A9, and SLC39A10 implies a poor OS in patients with ccRCC. This contradiction could be clearly explained by the following analysis, that is, the expression of SLC39A8 is slightly up-regulated in early tumors, but with the increase of tumor grade, its expression level decreased gradually. This indicates that the down-regulation of SLC39A8 is involved in ccRCC progression. In addition, SLC39A8 was identified as a key functional gene of ZIP family in ccRCC by univariate and multivariate analyses. ROC curve analysis also proved that SLC39A8 could be used as an effective index to diagnose ccRCC and judge its prognosis. Considering that SLC39A8 is involved in passing zinc into the cytoplasm (38), as confirmed by functional enrichment analysis, we believe that the decrease of intracellular zinc promotes the progression of ccRCC.

Although multiple advances have been made in systemic therapy for RCC in recent years, metastatic RCC remains incurable (10). Among RCC, ccRCC is the most frequent and lethal subtype with high risk of metastasis and recurrence (8). Thus, effective treatment of progressive ccRCC is the most important part of the treatment of RCC. Previous studies have shown that lower zinc may promote proliferation and inhibit

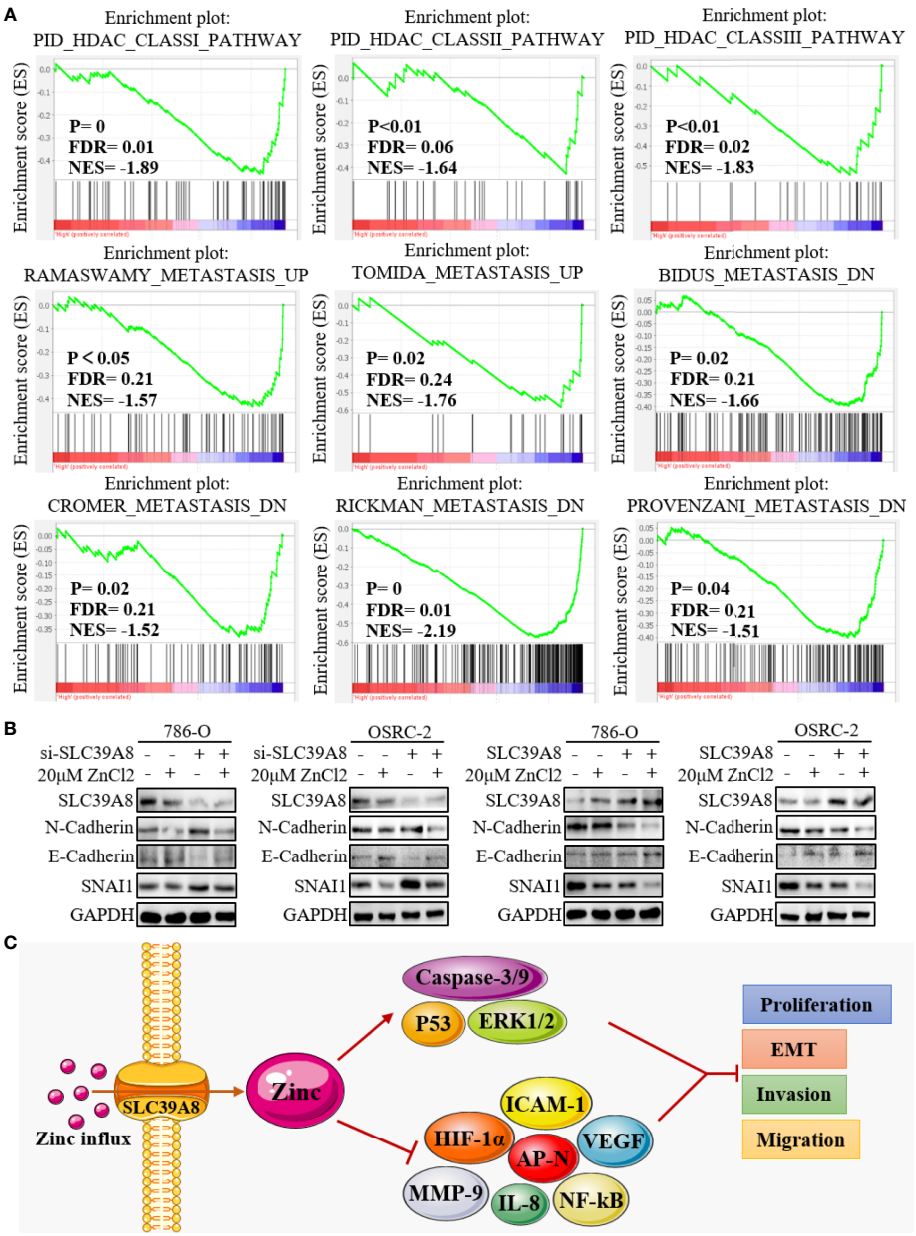



**FIGURE 7** | Mechanism of SLC39A8/zinc inhibiting cell migration and invasion. **(A)** GSEA showed that the group with low expression of SLC39A8 was significantly associated with HDAC and metastasis pathway. **(B)** Western blotting experiments detected the effect of SLC39A8/zinc on EMT in ccRCC cells. 786-O and OSRC-2 cells transfected with si–SLC39A8 (knockdown), SLC39A8 (overexpression), and their corresponding control were used for this study. **(C)** A possible mechanism for SLC39A8/zinc inhibits the EMT of ccRCC cells. HDAC, histone deacetylase; EMT, epithelial-mesenchymal transition; ICAM-1, intercellular adhesion molecule 1; AP-N, aminopeptidase N; NF-kB, nuclear factor kappa B; VEGF, vascular endothelial growth factor; IL-8, interleukin 8; MMP-9, matrix metallopeptidase 9; HIF-1α, hypoxia inducible factor-1α; ERK1/2, extracellular signal-regulated kinase 1/2.

apoptosis of prostate cells (22–25), while zinc supplementation could suppress its EMT through inhibiting intercellular adhesion molecule 1 (ICAM-1) expression and aminopeptidase N (AP-N) activity (27, 28, 33). In addition, zinc sulphate treatment could also reduce the expression of some other angiogenic and metastatic factors, including vascular endothelial growth factor (VEGF), interleukin 8 (IL-8) and matrix metallopeptidase 9 (MMP-9) (27). Moreover, a latest study showed that zinc may inhibit cell proliferation of esophageal cancer cells through Orai1 (a store-operated $Ca^{2+}$ entry channel)-mediated intracellular $Ca^{2+}$ oscillations and revealed a possible molecular basis for zinc-induced cancer prevention (36). In addition, the

mechanisms of zinc inhibiting tumor reported in the existing literature include NF-kB signaling pathway (24, 25), Wnt-3a/β-catenin signaling pathway (61), P53 signaling pathway (62), hypoxia inducible factor-1α (HIF-1α) signaling pathway (63), apoptosis signaling pathway (64), and extracellular signal-regulated kinase 1/2 (ERK1/2) signaling pathway (65), etc. In a word, zinc could inhibit tumors by affecting many different signaling pathways.

In this study, the zinc supplementation experiments confirmed that the treatment with low concentration of zinc chloride could effectively inhibit the proliferation and colonies formation of ccRCC cells. In addition, overexpression of SLC39A8 could significantly inhibit 786-O and OSRC-2 cells proliferation, invasion and migration, and zinc supplementation could satisfactorily enhance this inhibitory effect. Western blotting experiments also confirmed that SLC39A8/zinc could inhibit the EMT of ccRCC cells. Based on these results and existing literatures, we propose a possible mechanism that SLC39A8/zinc inhibit the proliferation, invasion and migration of ccRCC cells (**Figure 7C**). In brief, SLC39A8 serves to pass zinc into the cytoplasm, and intracellular zinc activate P53, ERK1/2 and apoptosis-related genes and pathways, and inhibit NF-kB, ICAM-1, AP-N, IL-8, and HIF-1α related signaling pathways by participating in a series of biological processes, finally leading to increased tumor cell death, and inhibition of EMT, tumor cell proliferation, invasion, and migration.

## CONCLUSION

In this study, SLC39A8 was identified as a key gene of ZIP family in ccRCC, which could be used as an effective indicator for diagnosing ccRCC and judging its prognosis. With the progression of tumor, the expression of SLC39A8 decreased progressively. The prognosis of ccRCC patients with low expression of SLC39A8 is significantly worse. Overexpression of SLC39A8 or treatment with low concentration of zinc chloride could effectively inhibit the proliferation, migration and invasion of ccRCC cells. Moreover, the inhibition effect of SLC39A8 overexpression could be enhanced by low concentration zinc supplement. Therefore, this study provides a novel understanding for the role of SLC39A8/zinc in the regulation of ccRCC progression. These findings provide a new direction and target for progressive ccRCC drug development and combination therapy strategies.

## DATA AVAILABILITY STATEMENT

The original contributions presented in the study are included in the article/**Supplementary Material**. Further inquiries can be directed to the corresponding authors.

## ETHICS STATEMENT

This study was fully informed by the patients and was approved by the Human Research Ethics Committee of Huazhong University of science and Technology (Wuhan, China).

## AUTHOR CONTRIBUTIONS

ZS, XY, and KC designed the study. LL and YH wrote the manuscript. JH and LZ polished the article. LL, YH, JH, and LZ performed the experiment. LL, YH, and XY analyzed the data. ZS and KC helped revised the manuscript. All authors contributed to the article and approved the submitted version.

## FUNDING

This work was supported by the National Natural Science Foundation of China (Grant no. 82002722) and the Science Foundation of Wuhan (grant no. WX20Q20).

## ACKNOWLEDGMENTS

We thank Dr. Hongping Chen (Nanchang University) for guiding us in the zinc supplementation experiments.

## SUPPLEMENTARY MATERIAL

The Supplementary Material for this article can be found online at: https://www.frontiersin.org/articles/10.3389/fonc.2021.651921/full#supplementary-material

**Supplementary Figure 1 |** The relative mRNA expression of ZIP family genes in cancer tissues and corresponding normal tissues in patients with ccRCC by using Uaclan database. **(A–N)** SLC39A1, SLC39A2, SLC39A3, SLC39A4, SLC39A5, SLC39A6, SLC39A7, SLC39A8, SLC39A9, SLC39A10, SLC39A11, SLC39A12, SLC39A13, SLC39A14. Mean differences were considered statistically significant when $P < 0.05$.

**Supplementary Figure 2 |** Disease-free survival of ZIP family genes in patients with ccRCC by using GEPIA. **(A–N)** SLC39A1, SLC39A2, SLC39A3, SLC39A4, SLC39A5, SLC39A6, SLC39A7, SLC39A8, SLC39A9, SLC39A10, SLC39A11, SLC39A12, SLC39A13, SLC39A14. Mean differences were considered statistically significant when $P < 0.05$.

**Supplementary Figure 3 |** The clinicopathologic significance of SLC39A8 expression in the E-MTAB-1980 cohort. **(A–D)** The expression of SLC39A8 in ccRCC patients with distant or lymph node metastasis, and in different subgroups of T stage and neoplasm histologic grade. **(E)** Overall survival analysis of SLC39A8 in ccRCC patients with the high and low groups cutoffs were 35 percent and 35 percent. The p value < 0.05 was considered to have significant differences.

**Supplementary Figure 4 |** Expression and diagnostic value of SLC39A8 in ccRCC patients and its importance in RCC cell lines. **(A)** The diagnostic significance of SLC39A8 low expression in ccRCC patients. **(B)** The antibody-based imaging from online database The Human Protein Atlas indicated that SLC39A8 protein was down-regulated in RCC tissues. **(C)** The CERES dependence score of SLC39A8 in different RCC cell lines, score approach to 0 and −1 represent the median scores of nonessential and cell-essential genes, respectively. Mean differences were considered statistically significant when $P < 0.05$.

## REFERENCES


1. Ferlay J, Colombet M, Soerjomataram I, Dyba T, Randi G, Bettio M, et al. Cancer incidence and mortality patterns in Europe: Estimates for 40 countries and 25 major cancers in 2018. *Eur J Cancer (Oxford Engl 1990)* (2018) 103:356–87. doi: 10.1016/j.ejca.2018.07.005
2. Siegel RL, Miller KD, Jemal A. Cancer statistics, 2020. *CA: A Cancer J For Clin* (2020) 70:7–30. doi: 10.3322/caac.21590
3. Hsieh JJ, Purdue MP, Signoretti S, Swanton C, Albiges L, Schmidinger M, et al. Renal cell carcinoma. *Nat Rev Dis Primers* (2017) 3:17009. doi: 10.1038/nrdp.2017.9
4. Cohen HT, McGovern FJ. Renal-cell carcinoma. *New Engl J Med* (2005) 353:2477–90. doi: 10.1056/NEJMra043172
5. Lam JS, Leppert JT, Belldegrun AS, Figlin RA. Novel approaches in the therapy of metastatic renal cell carcinoma. *World J Urol* (2005) 23:202–12. doi: 10.1007/s00345-004-0466-0
6. Gupta K, Miller JD, Li JZ, Russell MW, Charbonneau C. Epidemiologic and socioeconomic burden of metastatic renal cell carcinoma (mRCC): a literature review. *Cancer Treat Rev* (2008) 34:193–205. doi: 10.1016/j.ctrv.2007.12.001
7. Pichler M, Hutterer GC, Chromecki TF, Jesche J, Kampel-Kettner K, Rehak P, et al. External validation of the Leibovich prognosis score for nonmetastatic clear cell renal cell carcinoma at a single European center applying routine pathology. *J Urol* (2011) 186:1773–7. doi: 10.1016/j.juro.2011.07.034
8. Eggener SE, Yossepowitch O, Kundu S, Motzer RJ, Russo P. Risk score and metastasectomy independently impact prognosis of patients with recurrent renal cell carcinoma. *J Urol* (2008) 180:873–8; discussion 878. doi: 10.1016/j.juro.2008.05.006
9. Kuthi L, Jenei A, Hajdu A, Németh I, Varga Z, Bajory Z, et al. Prognostic Factors for Renal Cell Carcinoma Subtypes Diagnosed According to the 2016 WHO Renal Tumor Classification: a Study Involving 928 Patients. *Pathol Oncol Res POR* (2017) 23:689–98. doi: 10.1007/s12253-016-0179-x
10. Gong J, Maia MC, Dizman N, Govindarajan A, Pal SK. Metastasis in renal cell carcinoma: Biology and implications for therapy. *Asian J Urol* (2016) 3:286–92. doi: 10.1016/j.ajur.2016.08.006
11. Posadas EM, Limvorasak S, Figlin RA. Targeted therapies for renal cell carcinoma. *Nat Rev Nephrol* (2017) 13:496–511. doi: 10.1038/nrneph.2017.82
12. Niinivirta M, Enblad G, Lindskog C, Pontén F, Dragomir A, Ullenhag GJ. Tumoral Pyruvate Kinase L/R as a Predictive Marker for the Treatment of Renal Cancer Patients with Sunitinib and Sorafenib. *J Cancer* (2019) 10:3224–31. doi: 10.7150/jca.30130
13. Di Lorenzo G, Porta C, Bellmunt J, Sternberg C, Kirkali Z, Staehler M, et al. Toxicities of targeted therapy and their management in kidney cancer. *Eur Urol* (2011) 59:526–40. doi: 10.1016/j.eururo.2011.01.002
14. Ljungberg B, Albiges L, Bensalah K, Bex A, Giles R, Hora M, et al. *EAU Guidelines on Renal Cell Carcinoma 2020*. European Association of Urology (2020).
15. Pan Z, Choi S, Ouadid-Ahidouch H, Yang JM, Beattie JH, Korichneva I. Zinc transporters and dysregulated channels in cancers. *Front Biosci (Landmark Ed)* (2017) 22:623–43. doi: 10.2741/4507
16. Vallee BL, Falchuk KH. The biochemical basis of zinc physiology. *Physiol Rev* (1993) 73:79–118. doi: 10.1152/physrev.1993.73.1.79
17. Beyersmann D, Haase H. Functions of zinc in signaling, proliferation and differentiation of mammalian cells. *Biometals Int J Role Metal Ions Biol Biochem Med* (2001) 14:331–41. doi: 10.1007/978-94-017-3728-9_8
18. Andreini C, Banci L, Bertini I, Rosato A. Counting the zinc-proteins encoded in the human genome. *J Proteome Res* (2006) 5:196–201. doi: 10.1021/pr050361j
19. Ho E, Ames BN. Low intracellular zinc induces oxidative DNA damage, disrupts p53, NFkappa B, and AP1 DNA binding, and affects DNA repair in a rat glioma cell line. *Proc Natl Acad Sci U S A* (2002) 99:16770–5. doi: 10.1073/pnas.222679399
20. Costello LC, Franklin RB. The clinical relevance of the metabolism of prostate cancer; zinc and tumor suppression: connecting the dots. *Mol Cancer* (2006) 5:17. doi: 10.1186/1476-4598-5-17
21. Skrajnowska D, Bobrowska-Korczak B. Role of Zinc in Immune System and Anti-Cancer Defense Mechanisms. *Nutrients* (2019) 11(10):2273. doi: 10.3390/nu11102273
22. Liang JY, Liu YY, Zou J, Franklin RB, Costello LC, Feng P. Inhibitory effect of zinc on human prostatic carcinoma cell growth. *Prostate* (1999) 40:200–7. doi: 10.1002/(SICI)1097-0045(19990801)40:3<200::AID-PROS8>3.0.CO;2-3
23. Feng P, Liang JY, Li TL, Guan ZX, Zou J, Franklin R, et al. Zinc induces mitochondria apoptogenesis in prostate cells. *Mol Urol* (2000) 4:31–6. doi: 10.1046/j.1523-1755.2000.00952-3.x
24. Huang L, Kirschke CP, Zhang Y. Decreased intracellular zinc in human tumorigenic prostate epithelial cells: a possible role in prostate cancer progression. *Cancer Cell Int* (2006) 6:10. doi: 10.1186/1475-2867-6-10
25. Uzzo RG, Leavis P, Hatch W, Gabai VL, Dulin N, Zvartau N, et al. Zinc inhibits nuclear factor-kappa B activation and sensitizes prostate cancer cells to cytotoxic agents. *Clin Cancer Res Off J Am Assoc Cancer Res* (2002) 8:3579–83. doi: 10.1093/carcin/23.11.1963
26. Ishii K, Otsuka T, Iguchi K, Usui S, Yamamoto H, Sugimura Y, et al. Evidence that the prostate-specific antigen (PSA)/Zn2+ axis may play a role in human prostate cancer cell invasion. *Cancer Lett* (2004) 207:79–87. doi: 10.1016/j.canlet.2003.09.029
27. Uzzo RG, Crispen PL, Golovine K, Makhov P, Horwitz EM, Kolenko VM. Diverse effects of zinc on NF-kappaB and AP-1 transcription factors: implications for prostate cancer progression. *Carcinogenesis* (2006) 27:1980–90. doi: 10.1093/carcin/bgl034
28. Ishii K, Usui S, Sugimura Y, Yoshida S, Hioki T, Tatematsu M, et al. Aminopeptidase N regulated by zinc in human prostate participates in tumor cell invasion. *Int J Cancer* (2001) 92:49–54. doi: 10.1002/1097-0215(200102)9999:9999<::AID-IJC1161>3.0.CO;2-S
29. Hoang BX, Han B, Shaw DG, Nimni M. Zinc as a possible preventive and therapeutic agent in pancreatic, prostate, and breast cancer. *Eur J Cancer Prev Off J Eur Cancer Prev Org (ECP)* (2016) 25:457–61. doi: 10.1097/CEJ.0000000000000194
30. Jouybari L, Kiani F, Akbari A, Sanagoo A, Sayehmiri F, Aaseth J, et al. A meta-analysis of zinc levels in breast cancer. *J Trace Elements Med Biol Organ Soc Minerals Trace Elements (GMS)* (2019) 56:90–9. doi: 10.1016/j.jtemb.2019.06.017
31. Ressnerova A, Raudenska M, Holubova M, Svobodova M, Polanska H, Babula P, et al. Zinc and Copper Homeostasis in Head and Neck Cancer: Review and Meta-Analysis. *Curr Med Chem* (2016) 23:1304–30. doi: 10.2174/0929867323666160405111543
32. Wang Y, Sun Z, Li A, Zhang Y. Association between serum zinc levels and lung cancer: a meta-analysis of observational studies. *World J Surg Oncol* (2019) 17:78. doi: 10.1186/s12957-019-1617-5
33. Li D, Stovall DB, Wang W, Sui G. Advances of Zinc Signaling Studies in Prostate Cancer. *Int J Mol Sci* (2020) 21(2):667. doi: 10.3390/ijms21020667
34. Hrabeta J, Eckschlager T, Stiborova M, Heger Z, Krizkova S, Adam V. Zinc and zinc-containing biomolecules in childhood brain tumors. *J Mol Med (Berlin Germany)* (2016) 94:1199–215. doi: 10.1007/s00109-016-1454-8
35. Franz MC, Anderle P, Bürzle M, Suzuki Y, Freeman MR, Hediger MA, et al. Zinc transporters in prostate cancer. *Mol Aspects Med* (2013) 34:735–41. doi: 10.1016/j.mam.2012.11.007
36. Choi S, Cui C, Luo Y, Kim SH, Ko JK, Huo X, et al. Selective inhibitory effects of zinc on cell proliferation in esophageal squamous cell carcinoma through Orai1. *FASEB J Off Publ Fed Am Soc Exp Biol* (2018) 32:404–16. doi: 10.1096/fj.201700227RRR
37. Huang L, Tepaamorndech S. The SLC30 family of zinc transporters - a review of current understanding of their biological and pathophysiological roles. *Mol Aspects Med* (2013) 34:548–60. doi: 10.1016/j.mam.2012.05.008
38. Jeong J, Eide DJ. The SLC39 family of zinc transporters. *Mol Aspects Med* (2013) 34:612–9. doi: 10.1016/j.mam.2012.05.011
39. Bowers K, Srai SKS. The trafficking of metal ion transporters of the Zrt- and Irt-like protein family. *Traffic (Copenhagen Denmark)* (2018) 19:813–22. doi: 10.1111/tra.12602
40. Chandrashekar DS, Bashel B, Balasubramanya SAH, Creighton CJ, Ponce-Rodriguez I, Chakravarthi B, et al. UALCAN: A Portal for Facilitating Tumor Subgroup Gene Expression and Survival Analyses. *Neoplasia (N Y NY)* (2017) 19:649–58. doi: 10.1016/j.neo.2017.05.002
41. Tang Z, Li C, Kang B, Gao G, Li C, Zhang Z. GEPIA: a web server for cancer and normal gene expression profiling and interactive analyses. *Nucleic Acids Res* (2017) 45:W98–w102. doi: 10.1093/nar/gkx247

42. Zhou Y, Zhou B, Pache L, Chang M, Khodabakhshi AH, Tanaseichuk O, et al. Metascape provides a biologist-oriented resource for the analysis of systems-level datasets. *Nat Commun* (2019) 10:1523. doi: 10.1038/s41467-019-09234-6
43. Goldman MJ, Craft B, Hastie M, Repečka K, McDade F, Kamath A, et al. Visualizing and interpreting cancer genomics data via the Xena platform. *Nat Biotechnol* (2020) 38:675–8. doi: 10.1038/s41587-020-0546-8
44. Rhodes DR, Yu J, Shanker K, Deshpande N, Varambally R, Ghosh D, et al. ONCOMINE: a cancer microarray database and integrated data-mining platform. *Neoplasia (N Y NY)* (2004) 6:1–6. doi: 10.1016/S1476-5586(04)80047-2
45. Beroukhim R, Brunet JP, Di Napoli A, Mertz KD, Seeley A, Pires MM, et al. Patterns of gene expression and copy-number alterations in von-hippel lindau disease-associated and sporadic clear cell carcinoma of the kidney. *Cancer Res* (2009) 69:4674–81. doi: 10.1158/0008-5472.CAN-09-0146
46. Jones J, Otu H, Spentzos D, Kolia S, Inan M, Beecken WD, et al. Gene signatures of progression and metastasis in renal cell cancer. *Clin Cancer Res Off J Am Assoc Cancer Res* (2005) 11:5730–9. doi: 10.1158/1078-0432.CCR-04-2225
47. Lenburg ME, Liou LS, Gerry NP, Frampton GM, Cohen HT, Christman MF. Previously unidentified changes in renal cell carcinoma gene expression identified by parametric analysis of microarray data. *BMC Cancer* (2003) 3:31. doi: 10.1186/1471-2407-3-31
48. Gumz ML, Zou H, Kreinest PA, Childs AC, Belmonte LS, LeGrand SN, et al. Secreted frizzled-related protein 1 loss contributes to tumor phenotype of clear cell renal cell carcinoma. *Clin Cancer Res Off J Am Assoc Cancer Res* (2007) 13:4740–9. doi: 10.1158/1078-0432.CCR-07-0143
49. Sato Y, Yoshizato T, Shiraishi Y, Maekawa S, Okuno Y, Kamura T, et al. Integrated molecular analysis of clear-cell renal cell carcinoma. *Nat Genet* (2013) 45:860–7. doi: 10.1038/ng.2699
50. Uhlén M, Fagerberg L, Hallström BM, Lindskog C, Oksvold P, Mardinoglu A, et al. Proteomics. *Tissue-Based Map Hum Proteome Sci (N Y NY)* (2015) 347:1260419. doi: 10.1126/science.1260419
51. Uhlén M, Björling E, Agaton C, Szigyarto CA, Amini B, Andersen E, et al. A human protein atlas for normal and cancer tissues based on antibody proteomics. *Mol Cell Proteomics MCP* (2005) 4:1920–32. doi: 10.1074/mcp.M500279-MCP200
52. Subramanian A, Tamayo P, Mootha VK, Mukherjee S, Ebert BL, Gillette MA, et al. Gene set enrichment analysis: a knowledge-based approach for interpreting genome-wide expression profiles. *Proc Natl Acad Sci U S A* (2005) 102:15545–50. doi: 10.1073/pnas.0506580102
53. Tsherniak A, Vazquez F, Montgomery PG, Weir BA, Kryukov G, Cowley GS, et al. Defining a Cancer Dependency Map. *Cell* (2017) 170:564–76.e16. doi: 10.1016/j.cell.2017.06.010
54. Meyers RM, Bryan JG, McFarland JM, Weir BA, Sizemore AE, Xu H, et al. Computational correction of copy number effect improves specificity of CRISPR-Cas9 essentiality screens in cancer cells. *Nat Genet* (2017) 49:1779–84. doi: 10.1038/ng.3984
55. Lyubartseva G, Smith JL, Markesbery WR, Lovell MA. Alterations of zinc transporter proteins ZnT-1, ZnT-4 and ZnT-6 in preclinical Alzheimer's disease brain. *Brain Pathol (Zurich Switzerland)* (2010) 20:343–50. doi: 10.1111/j.1750-3639.2009.00283.x
56. Domínguez-Cruz MG, Muñoz ML, Totomoch-Serra A, García-Escalante MG, Burgueño J, Valadez-González N, et al. Pilot genome-wide association study identifying novel risk loci for type 2 diabetes in a Maya population. *Gene* (2018) 677:324–31. doi: 10.1016/j.gene.2018.08.041
57. Wang J, Zhao H, Xu Z, Cheng X. Zinc dysregulation in cancers and its potential as a therapeutic target. *Cancer Biol Med* (2020) 17:612–25. doi: 10.20892/j.issn.2095-3941.2020.0106
58. Prasad AS, Beck FW, Doerr TD, Shamsa FH, Penny HS, Marks SC, et al. Nutritional and zinc status of head and neck cancer patients: an interpretive review. *J Am Coll Nutr* (1998) 17:409–18. doi: 10.1080/07315724.1998.10718787
59. Fong LY, Taccioli C, Palamarchuk A, Tagliazucchi GM, Jing R, Smalley KJ, et al. Abrogation of esophageal carcinoma development in miR-31 knockout rats. *Proc Natl Acad Sci U S A* (2020) 117:6075–85. doi: 10.1073/pnas.1920333117
60. Lee DH, Anderson KE, Harnack LJ, Folsom AR, Jacobs DRJr. Heme iron, zinc, alcohol consumption, and colon cancer: Iowa Women's Health Study. *J Natl Cancer Institute* (2004) 96:403–7. doi: 10.1093/jnci/djh047
61. Gao K, Zhang Y, Niu J, Nie Z, Liu Q, Lv C. Zinc promotes cell apoptosis via activating the Wnt-3a/β-catenin signaling pathway in osteosarcoma. *J Orthopaedic Surg Res* (2020) 15:57. doi: 10.1186/s13018-020-01585-x
62. Loh SN. The missing zinc: p53 misfolding and cancer. *Metallomics Integrated Biometal Sci* (2010) 2:442–9. doi: 10.1039/c003915b
63. Nardinocchi L, Pantisano V, Puca R, Porru M, Aiello A, Grasselli A, et al. Zinc downregulates HIF-1α and inhibits its activity in tumor cells in vitro and in vivo. *PloS One* (2010) 5:e15048. doi: 10.1371/journal.pone.0015048
64. Feng P, Li T, Guan Z, Franklin RB, Costello LC. The involvement of Bax in zinc-induced mitochondrial apoptogenesis in malignant prostate cells. *Mol Cancer* (2008) 7:25. doi: 10.1186/1476-4598-7-25
65. Wong PF, Abubakar S. High intracellular Zn2+ ions modulate the VHR, ZAP-70 and ERK activities of LNCaP prostate cancer cells. *Cell Mol Biol Lett* (2008) 13:375–90. doi: 10.2478/s11658-008-0009-6


**Conflict of Interest:** The authors declare that the research was conducted in the absence of any commercial or financial relationships that could be construed as a potential conflict of interest.

*Copyright © 2021 Liu, Hou, Hu, Zhou, Chen, Yang and Song. This is an open-access article distributed under the terms of the Creative Commons Attribution License (CC BY). The use, distribution or reproduction in other forums is permitted, provided the original author(s) and the copyright owner(s) are credited and that the original publication in this journal is cited, in accordance with accepted academic practice. No use, distribution or reproduction is permitted which does not comply with these terms.*

frontiers in Oncology

REVIEW
published: 28 April 2021
doi: 10.3389/fonc.2021.643065

# Review of Prognostic Expression Markers for Clear Cell Renal Cell Carcinoma

*Florent Petitprez*[1], *Mira Ayadi*[1], *Aurélien de Reyniès*[1], *Wolf H. Fridman*[2], *Catherine Sautès-Fridman*[2*†] *and Sylvie Job*[1*†]

[1] *Programme Cartes d'Identité des Tumeurs, Ligue Nationale Contre le Cancer, Paris, France,* [2] *Centre de Recherche des Cordeliers, INSERM, Sorbonne Université, Université de Paris, Equipe Inflammation, Complément et Cancer, Paris, France*

OPEN ACCESS

**Edited by:**
*Elena Ranieri,*
*University of Foggia, Italy*

**Reviewed by:**
*Philipp Ivanyi,*
*Hannover Medical School, Germany*
*Ying-Bei Chen,*
*Memorial Sloan Kettering Cancer Center, United States*

***Correspondence:**
*Catherine Sautès-Fridman*
*catherine.fridman@crc.jussieu.fr*
*Sylvie Job*
*sylvie.job@inserm.fr*

[†] *These authors share last authorship*

**Specialty section:**
*This article was submitted to Genitourinary Oncology, a section of the journal Frontiers in Oncology*

**Received:** *17 December 2020*
**Accepted:** *17 February 2021*
**Published:** *28 April 2021*

**Citation:**
*Petitprez F, Ayadi M, de Reyniès A, Fridman WH, Sautès-Fridman C and Job S (2021) Review of Prognostic Expression Markers for Clear Cell Renal Cell Carcinoma. Front. Oncol. 11:643065. doi: 10.3389/fonc.2021.643065*

**Context:** The number of prognostic markers for clear cell renal cell carcinoma (ccRCC) has been increasing regularly over the last 15 years, without being integrated and compared.

**Objective:** Our goal was to perform a review of prognostic markers for ccRCC to lay the ground for their use in the clinics.

**Evidence Acquisition:** PubMed database was searched to identify RNA and protein markers whose expression level was reported as associated with survival of ccRCC patients. Relevant studies were selected through cross-reading by two readers.

**Evidence Synthesis:** We selected 249 studies reporting an association with prognostic of either single markers or multiple-marker models. Altogether, these studies were based on a total of 341 distinct markers and 13 multiple-marker models. Twenty percent of these markers were involved in four biological pathways altered in ccRCC: cell cycle, angiogenesis, hypoxia, and immune response. The main genes (*VHL, PBRM1, BAP1*, and *SETD2*) involved in ccRCC carcinogenesis are not the most relevant for assessing survival.

**Conclusion:** Among single markers, the most validated markers were *KI67, BIRC5, TP53, CXCR4*, and *CA9*. Of the multiple-marker models, the most famous model, ClearCode34, has been highly validated on several independent datasets, but its clinical utility has not yet been investigated.

**Patient Summary:** Over the years, the prognosis studies have evolved from single markers to multiple-marker models. Our review highlights the highly validated prognostic markers and multiple-marker models and discusses their clinical utility for better therapeutic care.

**Keywords: prognostic markers, clear cell renal cell carcinoma (ccRCC), multivariate analysis, independent datasets, cox models**

# INTRODUCTION

Clear cell renal cell carcinoma (ccRCC) is the most common histological subtype of kidney cancers, accounting for around 85% of all renal cell carcinomas (1). Although localized ccRCC can be treated by partial or total surgical ablation of the kidney, advanced ccRCC remains a clinical challenge, with 5-year overall survival (OS) rates of 0–20% (2). Over 90% of ccRCC cases have undergone a loss of heterozygosity of the chromosome 3p, where notably *VHL* is located. Moreover, *VHL* is mutated in 70% of ccRCC tumors and hypermethylated in 15% (3), and inactivating *VHL* mutation is considered the main driver of ccRCC carcinogenesis (4). Loss of *VHL* leads to activation of hypoxia-inducible factors and subsequently to vascular endothelial growth factor (VEGF)-mediated angiogenesis (5). Therefore, tyrosine kinase inhibitors with antiangiogenic properties have become a crucial treatment option for ccRCC patients (6).

Over the past decades, a large series of studies have aimed at finding prognostic markers for ccRCC in order to identify patients who were at higher risk of relapse and death. During this time, technologies have largely evolved—from surface proteins measured by single-molecule immunohistochemistry (IHC) to reverse-transcription quantitative polymerase chain reaction (RTQ-PCR) for mRNA and RNA sequencing (RNA-seq) for mRNA or long non-coding RNAs. Studies gradually incorporated more cases, while assessing an ever-larger number of putative targets, many focusing on angiogenesis-related targets, especially in the context of antiangiogenic therapies (7). Others emphasized immune-based approaches (8), as immune infiltration of tumors is a common prognostic factor in many different types of malignancies (9). Here, we aimed at reviewing prognostic markers that have been proposed for ccRCC during the 15 years between 2003 and 2018 through a thorough analysis of over 2,700 records from the literature.

# MATERIALS AND METHODS

## PubMed Query

A literature search was carried out using PubMed database to identify prognostic expression markers from studies published between 2003 and 2018. The PubMed query was: (clear cell renal cell carcinoma) AND (prognosis OR cancer prognosis OR cancer survival) AND (human OR *Homo sapiens*) AND (expression OR transcription OR transcriptome OR immunohistochemistry OR IHC). The search was conducted in December 2018.

## Study Selection

The following inclusion criteria were applied: original article (not reviews, editorials, conference abstracts); English language; research was performed on human ccRCC tissue samples; and association of the expression level of candidate genes with patient survival was investigated in multivariate analyses in several independent datasets. The following patient survivals were considered: OS, progression-free survival (PFS), relapse-free survival (RFS), disease-free survival (DFS), cancer-specific survival (CSS), and metastasis-free survival (MFS). The studies describing transcriptome-based clusters of samples associated with patient survival were included. Case reports were excluded as well as studies performed on metastatic or advanced cohorts only. Two authors (SJ and FP) evaluated the titles and the abstracts of all 2,730 publications identified by the search strategy, and all 550 publications thought to be potentially relevant were retrieved in full (**Figure 1A**). The same authors then assessed full publications for eligibility. Any study was included in the review with the agreement of both authors.

## Statistical Analysis

The analyses were performed using R software version 3.5.2. We carried out hypergeometric tests on signaling pathways of three databases [Kyoto Encyclopedia of Genes and Genomes (KEGG), Gene Ontology (GO), and Reactome] using the reviewed prognostic markers. We used the gene lists with the most significant hypergeometric test *p*-values to illustrate the prognostic markers within the four mentioned pathways: angiogenesis (GO), hypoxia (Reactome), cell cycle (KEGG), and immunity (Reactome).

# RESULTS

## Literature Evaluation

The PubMed query identified 2,730 publications (**Figure 1A**). Upon review, 2,180 publications were first excluded after title and abstract reading as being irrelevant to the present study, not available, or lacking validation. Of the remaining 550 publications, 301 studies were excluded due to the absence of validation on independent datasets or because of duplicate publication. Thus, the final total number of studies included in the present review was 249 (**Figure 1A** and **Supplementary Table 1**).

## Collection of Prognostic Markers

The 249 selected studies reported 341 distinct prognostic markers, 321 related to coding genes (mRNAs/proteins) and 20 to non-coding RNAs (six long non-coding RNAs, 14 microRNAs). While 169 out of the 249 studies (67.9%) focused on the prognostic impact of a single marker, the 80 remaining studies integrated multiple-marker analyses, 13 of them providing mathematical models computing a risk score (**Figure 1B**). Forty-one percent of markers (45/111) used in single-marker analyses were integrated in multiple-marker models. In the original publications, the expression levels of the prognostic markers were characterized using different technologies mainly represented by IHC, tissue microarray (TMA), RTQ-PCR, microarrays, and RNA-seq technologies (**Figure 1C**). These technologies exploit different types of biomaterials: IHC/TMA technologies generally use formalin-fixed paraffin-embedded (FFPE) samples and quantify a marker at a proteomic level, while RTQ-PCR, microarrays, and RNA-seq use frozen samples and quantify markers at a transcriptomic level. IHC and TMA were the most common identification methodologies used (143/341 targets, 41.9%). Among the 123 out of the 341 markers (36%) identified by two or more methodologies, 50 markers were validated both at the protein level (by IHC/TMA) and at the RNA level (by RTQ-PCR, RNA-seq, or microarrays) (**Supplementary Table 1**).

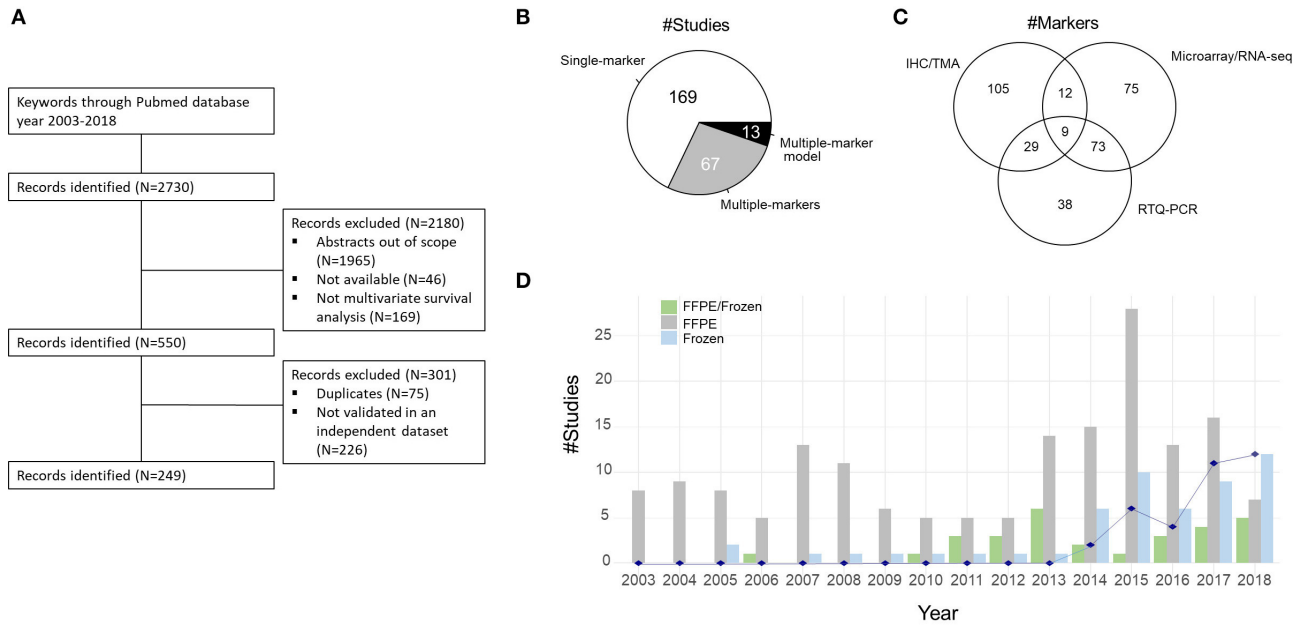



**FIGURE 1 | (A)** Consort diagram showing the selection process of studies included in the literature review. **(B)** Distribution of the studies investigating one marker, several markers, or multiple-marker models. **(C)** Venn diagram of the distribution of technologies used to quantify the expression level of the 341 genes. IHC, immunohistochemistry; TMA, tissue microarray; RNA-seq, RNA sequencing; RTQ-PCR, reverse-transcription quantitative polymerase chain reaction. **(D)** Distribution of the number of studies according to the type of biomaterial over the years: Frozen samples and/or formalin-fixed paraffin-embedded (FFPE) samples. The blue line indicates the number of studies using The Cancer Genome Atlas (TCGA) dataset as training or validation dataset.

Over the years, we have remarked an increase in the number of analyzed frozen samples (**Figure 1D**). This increase is linked, on the one hand, to the growing accessibility to high-throughput technologies (microarrays and then RNA-seq) and, on the other hand, to the public datasets available in genomics data repositories such as Gene Expression Omnibus (GEO), array express, or the GDC data portal of The Cancer Genome Atlas (TCGA) Program. Eighty percent of studies using public datasets as training and/or validation sets use TCGA cohort composed of 532 ccRCC samples (**Figure 1D**). Our review excluded studies resulting from the analysis of familial cohorts and of advanced or metastatic cohorts. The studied cohorts essentially included unselected samples from ccRCC patients who have had a radical or partial nephrectomy, and the samples are primary tumors.

## Main Biological Pathways Related to Prognostic Markers of Clear Cell Renal Cell Carcinoma

As previously stated, we excluded markers identified in a single study on a single cohort. Among the 341 prognostic markers, 250 markers were validated on internal datasets (**Figure 2A**). The 86 markers confirmed in two or more independent studies can be found in **Supplementary Table 2**. Seven markers were found in six or more studies (**Figure 2B**): KI67 (10–22), *BIRC5* (23–32), *TP53* (14, 18, 21, 33–39), *CXCR4* (40–46), *CA9* (47–53), *miR-21* (54–59), and *EZH2* (60–65). Some of them exceed the mere field of ccRCC. For instance, *BIRC5* is able to inhibit cell death and is upregulated in most, if not all, cancers (66); *TP53* is implicated in DNA damage repair and is mutated in a large portion of cancers (67). Of the 17 most reported prognostic markers, some are more tightly related to ccRCC, such as *VHL* (68–71), *PBRM1* (72–75), *CA9* (47–53), or *CAV1* (76–79).

Of the 341 reviewed prognostic markers, 20% are involved in biological pathways altered in ccRCC (80) of which the main ones are cell cycle, angiogenesis, hypoxia, and immune response (**Figure 2C**), which are involved in classical hallmarks of cancer (81).

### Hypoxia and Angiogenesis

*VHL* inactivation, through mutation, hypermethylation, and/or loss of heterozygosity (3), is regarded as the key genetic event leading to ccRCC formation (4). This dysregulation of the Von Hippel–Lindau pathway leads to HIF1α-HIF1β transcription factor activation and increased hypoxia response and neoangiogenesis through VEGF signaling. Expectedly, hypoxia and angiogenesis pathways are importantly represented in the list of prognostic markers that have been identified in the literature (**Figure 2C**). Sixty-nine studies listed at least one gene associated with angiogenesis, and 35 such genes were identified: *AAMP* (82), *ANPEP* (83), *APOLD1* (82), *B4GALT2* (84), *C5* (85), *CAV1* (76–79), *CCL2* (86, 87), *CCR2* (87), *CEACAM1* (82), *CTGF* (83), *CTNNB1* (88–91), *CX3CL1* (82), *CXCL10* (92), *CXCL12* (42), *CXCR2* (93), *CXCR4* (40–46), *EPAS1* (94–96), *FLT1* (14), *GPX1* (82), *HIF1A* (52, 97, 98), *HPSE* (99, 100), *IL6* (82), *JAG1* (101, 102), *MMP2* (103), *NOS3* (82), *NOTCH1* (102, 104, 105), *NRP1* (95), *PDGFRB* (106, 107), *PTEN* (108–110), *SERPINE1* (111–113), *SETD2* (74, 114, 115), *TGFBR2* (116, 117), *THSD7A* (118), *VASH1* (100, 119), *VEGFA* (50, 120, 121). Six markers of hypoxia [*ARNT* (95), *CA9* (47–53), *EPAS1* (94–96), *HIF1A* (52, 97, 98), *VEGFA* (50, 120, 121), and *VHL* (68–71)], representing

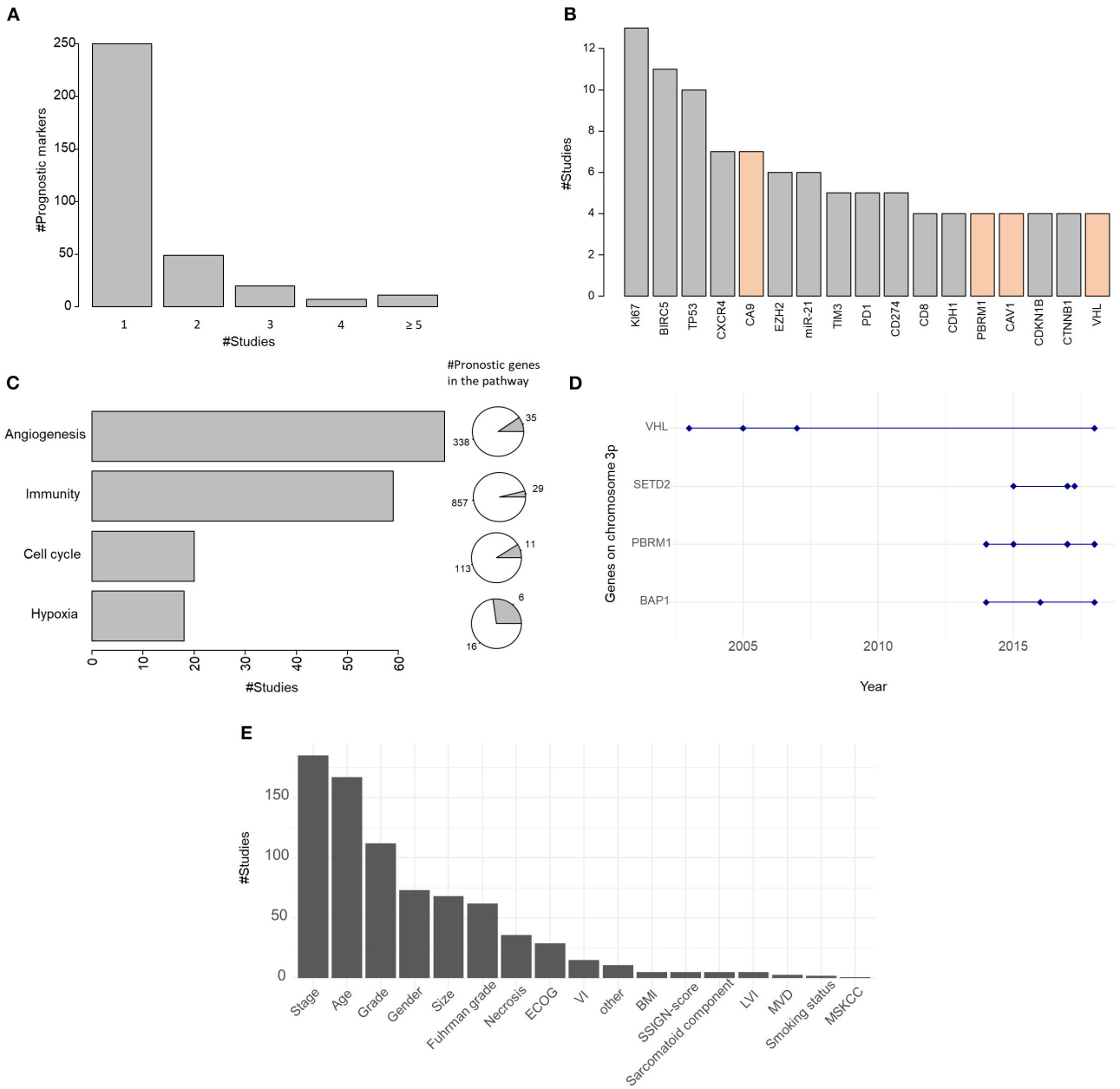



**FIGURE 2 | (A)** Barplot of the number of markers cited in one or more studies. **(B)** Barplot of the most investigated prognostic markers. In orange are indicated prognostic markers specific to clear cell renal cell carcinoma (ccRCC). **(C)** Barplot of the number of studies investigating markers involved in the main biological pathways: angiogenesis, immunity, cell cycle, and hypoxia. Pies on the right represent the proportion of prognostic markers in the pathway. **(D)** Distribution of the studies assessing the prognostic value of genes on chromosome 3p over the years. **(E)** Barplot of the number of studies integrating clinical covariates. ECOG, Eastern Cooperative Oncology Group; VI, vascular invasion; BMI, body mass index; SSIGN, Stage, Size, Grade, and Necrosis; LVI, lymphovascular invasion; MVD, microvessel density; MSKCC, Memorial Sloan Kettering Cancer Center.

about 30% of the genes involved in the hypoxia pathway, are reported as prognostic markers in 18 publications. Of note, three of these markers (*EPAS1*, *HIF1A*, and *VEGFA*) also belong to the angiogenesis pathway.

## Immunity

ccRCC tumors exhibit a rather low mutational burden compared to other tumor types (122). Nonetheless, they have been one of the first tumor types for which immunotherapy with high-dose IL-2 has proved efficient (123), although their responsiveness to immune checkpoint blockade remains rather low, below 30% (124). Moreover, immunity has been repeatedly associated with clinical outcome for this pathology (8). We found 59 articles identifying at least one gene related to immunity (among other pathways) as a prognostic factor in ccRCC. Twenty-nine such genes were identified: *AKT1* (77, 108), *ANAPC5* (125), *ARF1* (82), *BCL2* (39, 126), *C5* (85), *CARD9* (127), *CCR2* (87), *CD274* (26, 128, 128–130), *CD4* (118, 131, 132), *CD44*

(100, 133), *CDH1* (63, 103, 134, 135), *CDK1* (136), *CDKN1A* (17, 18, 137), *CDKN1B* (138–141), *CIITA* (127), *DEFB1* (83, 142), *ICOS* (118, 143), *IKBKE* (144), *IL5RA* (145), *IL6* (82), *MDM2* (34), *NCF2* (127), *PAK1* (146), *PSMD9* (18, 147), *PTEN* (108–110), *RCHY1* (148), *TLR3* (95), *VCAM1* (95, 149), and *VHL* (68–71) (**Figure 2C**). Some of them were independently reported by several publications. For instance, *CXCR4* (40–46), which encodes a receptor for the lymphocyte chemoattractant CXCL12, was identified by seven publications. *ICOS*, a T cell co-stimulatory molecule, was reported as prognostic biomarker by two publications.

### Cell Cycle

Expression of cell cycle-related gene signatures or proteins is generally a marker of the presence of highly proliferative cells and is therefore widely regarded as a biomarker of aggressive malignancy and poor prognosis (150, 151). Here, we have observed 11 such genes, reported in 20 publications: *ANAPC5* (125), *CCND1* (18), *CDC7* (125), *CDK1* (136), *CDKN1A* (17, 18, 137), *CDKN1B* (138–141), *CDKN1C* (18), *CDKN2A* (18, 152), *GADD45G* (127), *MDM2* (34), and *TP53* (14, 18, 21, 33–39).

### Focus on Clear Cell Renal Cell Carcinoma Genes on Chromosome 3p

Over 90% of sporadic ccRCC displays a deletion of chromosome 3p. The ccRCC key event is the alteration of the tumor-suppressor gene VHL (3p25-p26). Its prognostic impact was mainly studied a few years ago (between 2003 and 2007; **Figure 2D**), but the results were not very significant and often associated with specific subcellular locations (69, 70). Its validation as a prognostic marker was then neglected until recently in a study investigating the cumulative roles of *PBRM1* and *VHL* as risk factors (71).

Whole exome sequencing helped to identify the three other frequently mutated genes on chromosome 3p: *PBRM1* (∼40%), *SETD2* (∼12%), and *BAP1* (∼10%) (71). Several studies investigated their prognostic values since 2014. Studies about *PBRM1* (71, 72, 74, 75) were contradictory. While authors of the study (75) validate PBRM1 as an independent predictor of PFS but not of OS, Jiang et al. (74) and Högner et al. (71) showed opposite results. The prognostic value of *BAP1* was dependent on the cellular localization (153) but was only validated by bivariate Cox models (154) or in combination with the expression of *PBRM1* (72). Finally, *SETD2* was studied in three studies (74, 114, 115) in combination or not with the expression of H3K36me3, and all results agreed with the prognostic role of *SETD2*.

In conclusion, despite the high rate of alterations of these four genes on chromosome 3p and their role in ccRCC carcinogenesis and progression, their prognostic value may be ambiguous, explaining why these markers were not in the most reported prognostic markers, except VHL.

## Prognostic Molecular Markers and Clinical Covariates

Our review focused on independent prognostic markers, meaning that their prognostic impacts evaluated by Cox models remain significant after inclusion of other clinical and/or molecular covariates. Here, 242 out of the 249 studies integrated one or more clinical covariates, while seven studies (22, 74, 121, 130, 132, 155, 156) concluded the independence of the prognostic markers only from comparisons with other molecular markers. The studies using one or more bivariate Cox models were integrated in our review despite the lack of a global multivariate Cox model. The selected studies focused on different types of survival: OS, CSS, PFS, DFS, RFS, or MFS. When filled in, the starting times used to compute survival data may also differ between studies using either date at diagnosis or date at surgery. All these aspects make a direct comparison of prognostic values difficult.

**Figure 2E** summarizes the clinical covariates used in the 242 studies. The most represented clinical covariates are age, stage, and grade in adequacy with their known prognostic value. The clinical covariates specific to ccRCC such as Fuhrman grade or Stage, Size, Grade, and Necrosis score (SSIGN score) were also represented but to a lesser extent.

The authors of the reviewed studies present multivariate Cox models in the goal to validate the independence of the molecular predictors they studied. In our point of view, they validate above all the use of clinical and molecular covariates to better predict the survival of patients with ccRCC.

## Risk Multiple-Marker Models

Eighty out of the 249 selected studies investigated the prognostic value of several markers. We distinguish multi-marker analyses ($n = 67$ studies; **Figure 1B**) evaluating several independent predictors in multivariate Cox models and multiple-marker model analyses ($n = 13$ studies) providing a mathematical model that computes a risk score (36, 54, 55, 57, 82, 83, 95, 125, 135, 136, 149, 157, 158). These multiple-marker models were calibrated against a given technology used to quantify expression values (RTQ-PCR, RNA-seq, or nanostring) and used from 2 to 34 markers (**Supplementary Table 3**). Ten out of these multiple-marker models provide a mathematical formula, represented by a weighted sum of the expression values of each prognostic marker with or without clinical covariates. Three studies provided models based on microRNA expression (54, 55, 57). Mlcochova et al. (135) focused on genes involved in epithelial–mesenchymal transition, and Yang et al. (136) computed a risk model using genes in interaction with the nucleotide degrading enzyme gene *RNASEH2A*. Two unsupervised classifications based on whole transcriptome proposed prognostic ccRCC subtyping (157, 158). Brannon et al. (157) identified two subtypes (ccA and ccB), and Beuselinck et al. (158) proposed four subtype names ccrcc1 to ccrcc4. The two classifications identified subtypes related to a worse prognosis (Brannon: ccB; Beuselinck: ccrcc1 and ccrcc4). The classification by Beuselinck et al. (158) was also related to response to antiangiogenic treatment by sunitinib. The now well-established clinico-molecular prognostic model (95), ClearCode34, was built from the classification by Brannon et al. (157) added to clinical covariates (stage and Fuhrman grade). It is the single risk model using clinical and molecular markers.

## Sub-selection of Prognostic Markers for Clinical Utility

We propose a sub-selection of the most validated prognostic predictors with a potential clinical utility. About the single

prognostic markers, we focused on the prognostic markers validated on more than seven independent studies (**Figure 2B**), validated on fewer technologies based on FFPE and frozen samples. We imposed a prognostic impact independent of the classical clinical covariates (stage, Fuhrman grade, age, gender, and grade) on a large set of samples. The five markers (KI67, BIRC5, TP53, CXCR4, and CA9) validated on seven or more independent studies were validated on FFPE and frozen samples and compared with a large set of clinical covariates. KI67 and BIRC5 remained the more confident given their validation on more than 5,000 samples. The quantification of KI67 was used as secondary objective in two clinical trials on ccRCC patients (NCT03575611 and NCT01253668) to evaluate response to treatment. Three clinical trials in ccRCC patients (NCT02787915, NCT00197860, and NCT01924156) integrated the use of BIRC5 to assess survival or response to BIRC5-loaded dendritic cell vaccines.

We have been less strict on the sub-selection of multiple-marker models, as these models are newer. We focused on gene models validated at least in one independent study (**Supplementary Table 3**) and whose clinical use has been evaluated in a clinical trial. Six out of the 13 multiple-marker models were validated in external datasets, but only the clinical utility of the 16-gene assay of Rini et al. (82) and the ccrcc classification of Beuselinck et al. (158) were tested in a phase III (NCT00375674) and a phase II (NCT02960906) clinical trial, respectively.

## DISCUSSION

In this review, we conducted an extensive analysis of the literature on prognostic markers in ccRCC over the last 15 years. Published studies evolved according to technological progresses. The oldest studies mainly focused on the prognosis impact of single genes known to be involved in the ccRCC carcinogenesis such as VHL or HIF1A, mostly validated by IHC. Over the years, the high-throughput technologies allowed the prognosis analysis of the whole transcriptome as well as the integration of non-coding RNA as microRNA and long non-coding RNA showing promising results that still require further validations.

We identified 20% of the 341 reviewed prognostic markers as involved in biological pathways altered in ccRCC of which the main ones are cell cycle, angiogenesis, hypoxia, and immune response. Interestingly, the prognostic immune genes are mainly related to inflammation such as IKBKE that plays a role in regulating inflammatory responses to viral infection (159), the well-known proinflammatory cytokine interleukin-6 (IL6) (160), the complement C5 (161), or the receptor of hyaluronic acid, CD44, involved in inflammation and tissue regeneration (162). These inflammatory markers are mainly related to poor prognosis in agreement with inflammation being a cancer-fueling factor (163).

Among single markers, the most validated markers (KI67, BIRC5, TP53, CXCR4, and CA9) exceed the mere field of ccRCC, except CA9. Two of them, KI67 and BIRC5, were validated on the largest sets of samples, and they are beginning to be used in clinical trials. Among the 13 multiple-marker models proposed in the literature, the most validated ones are the 16-gene assay and the ccrcc1-4 subtyping. Paradoxically, the most famous model, ClearCode34, has been highly validated on several independent datasets, but its clinical utility has not yet been investigated. This review highlights the prognostic molecular predictors that should be investigated in more detail to improve therapeutic care and recommends to focus on the most validated markers or models (KI67, BIRC5, the 16-gene assay, and the ccrcc1-4 subtyping) to be quantified on FFPE samples for an easier clinical use. An important preliminary test should be first to ensure the reproducibility of the quantification on several samples of the same tumor to avoid contradictory conclusions.

Our review has some limitations. Several sources of heterogeneity make difficult the comparison between studies. First, the start points used to compute the survival delays (diagnosis vs. surgery) as well as the type of events (OS, MFS, RFS…) may differ. Another limitation is that we kept markers with a prognostic impact on OS but not RFS or inversely, as well as markers recurrently found to be prognostic even if other studies showed no significance. That is the case of genes mostly studied given their role in the ccRCC carcinogenesis like *VHL* and *BAP1* (164, 165). All the markers proposed in the review were validated in multivariate models in at least two datasets. According to the studies, the multivariate models integrated several genes and/or clinicopathological covariates, but the available clinical annotations strongly differ too. Finally, the increased use of abdominal imaging has resulted in an increase in the number of small renal incidentaloma in recent decades (166). Consequently, the clinical characteristics of the patient cohorts evolved over the 15 years, with an increase of the proportion of early stages. All these heterogeneity sources can explain why some markers can be found to be significantly associated with survival in some studies and not in others. In this context, it is important to note that some markers, notably the ccrcc1-4 molecular subtyping, proved to be related to older therapies, notably antiangiogenic drugs (158), but their predictive power is being considered also for more recent immunotherapies with immune checkpoint inhibitors, as illustrated in clinical trials [BIONIKK trial, NCT02960906 (167)].

In addition to the gene expression markers reviewed here, methylation markers such as the ones that were reviewed by Joosten et al. (168) and mutational markers as the ones reviewed by Mitchell et al. (169) can also be considered and could be integrated in multi-omics prognostic models. Combining the prognostic impact of these omics could improve the accuracy of survival prediction. Altogether, the present comprehensive analysis paves the way to robust and accurate evaluation of the risk of relapse and death for patients with ccRCC.

## AUTHOR CONTRIBUTIONS

FP: conceptualization, methodology, validation, formal analysis, investigation, resources, data curation, writing—review and

editing, and funding acquisition. MA and AR: conceptualization, writing—review and editing, and funding acquisition. WF and CS-F: conceptualization, writing—review and editing, supervision, and project administration. SJ: conceptualization, methodology, validation, formal analysis, investigation, resources, data curation, writing—review and editing, funding acquisition, supervision, and project administration. All authors contributed to the article and approved the submitted version. All authors listed have made substantial, direct, and intellectual contribution to the work and approved it for publication.

## SUPPLEMENTARY MATERIAL

The Supplementary Material for this article can be found online at: https://www.frontiersin.org/articles/10.3389/fonc.2021.643065/full#supplementary-material

**Supplementary Table 1 |** Studies included in the literature review, identified by their PubMed ID. The second column indicates the technologies and the third column the prognostic markers.

**Supplementary Table 2 |** List of the 87 prognostic markers validated on one or more independent studies, identified by the PubMed ID.

**Supplementary Table 3 |** Summary of the 13 multi-marker models.

## REFERENCES


1. Jemal A, Siegel R, Ward E, Murray T, Xu J, Thun MJ. Cancer statistics, 2007. *CA Cancer J Clin.* (2007) 57:43–66. doi: 10.3322/canjclin.57.1.43
2. Ballarin R, Spaggiari M, Cautero N, De Ruvo N, Montalti R, Longo C, et al. Pancreatic metastases from renal cell carcinoma: the state of the art. *World J Gastroenterol.* (2011) 17:4747–56. doi: 10.3748/wjg.v17.i43.4747
3. Sato Y, Yoshizato T, Shiraishi Y, Maekawa S, Okuno Y, Kamura T, et al. Integrated molecular analysis of clear-cell renal cell carcinoma. *Nat Genet.* (2013) 45:860–7. doi: 10.1038/ng.2699
4. Turajlic S, Xu H, Litchfield K, Rowan A, Horswell S, Chambers T, et al. Deterministic evolutionary trajectories influence primary tumor growth: TRACERx renal. *Cell.* (2018) 173:595–610.e11. doi: 10.1016/j.cell.2018.03.043
5. Casuscelli J, Vano Y-A, Fridman WH, Hsieh JJ. Molecular classification of renal cell carcinoma and its implication in future clinical practice. *Kidney Cancer.* (2017) 1:3–13. doi: 10.3233/KCA-170008
6. Lee C-H, Motzer RJ. Kidney cancer in 2016: the evolution of anti-angiogenic therapy for kidney cancer. *Nat Rev Nephrol.* (2017) 13:69–70. doi: 10.1038/nrneph.2016.194
7. D'Aniello C, Berretta M, Cavaliere C, Rossetti S, Facchini BA, Iovane G, et al. Biomarkers of prognosis and efficacy of anti-angiogenic therapy in metastatic clear cell renal cancer. *Front Oncol.* (2019) 9:1400. doi: 10.3389/fonc.2019.01400
8. Vano Y-A, Petitprez F, Giraldo NA, Fridman WH, Sautès-Fridman C. Immune-based identification of cancer patients at high risk of progression. *Curr Opin Immunol.* (2018) 51:97–102. doi: 10.1016/j.coi.2018.03.005
9. Fridman WH, Zitvogel L, Sautès–Fridman C, Kroemer G. The immune contexture in cancer prognosis and treatment. *Nat Rev Clin Oncol.* (2017) 14:717–34. doi: 10.1038/nrclinonc.2017.101
10. Visapää H, Bui M, Huang Y, Seligson D, Tsai H, Pantuck A, et al. Correlation of Ki-67 and gelsolin expression to clinical outcome in renal clear cell carcinoma. *Urology.* (2003) 61:845–50. doi: 10.1016/S0090-4295(02)02404-4
11. Rioux-Leclercq N, Delcros J-G, Bansard J-Y, Epstein JI, Patard J-J, Lobel B, et al. Immunohistochemical analysis of tumor polyamines discriminates high-risk patients undergoing nephrectomy for renal cell carcinoma. *Hum Pathol.* (2004) 35:1279–84. doi: 10.1016/j.humpath.2004.07.002
12. Kankuri M, Söderström K-O, Pelliniemi T-T, Vahlberg T, Pyrhönen S, Salminen E. The association of immunoreactive p53 and Ki-67 with T-stage, grade, occurrence of metastases and survival in renal cell carcinoma. *Anticancer Res.* (2006) 26:3825–33.
13. Tollefson MK, Thompson RH, Sheinin Y, Lohse CM, Cheville JC, Leibovich BC, et al. Ki-67 and coagulative tumor necrosis are independent predictors of poor outcome for patients with clear cell renal cell carcinoma and not surrogates for each other. *Cancer.* (2007) 110:783–90. doi: 10.1002/cncr.22840
14. Klatte T, Seligson DB, LaRochelle J, Shuch B, Said JW, Riggs SB, et al. Molecular signatures of localized clear cell renal cell carcinoma to predict disease-free survival after nephrectomy. *Cancer Epidemiol Biomark Prev.* (2009) 18:894–900. doi: 10.1158/1055-9965.EPI-08-0786
15. Miralles A, Bracamonte L, Soncul H, Diaz del Castillo R, Akhtar R, Bors V, et al. Cardiac tumors: clinical experience and surgical results in 74 patients. *Ann Thorac Surg.* (1991) 52:886–95. doi: 10.1016/0003-4975(91)91241-M
16. Sakai I, Miyake H, Takenaka A, Fujisawa M. Expression of potential molecular markers in renal cell carcinoma: impact on clinicopathological outcomes in patients undergoing radical nephrectomy. *BJU Int.* (2009) 104:942–6. doi: 10.1111/j.1464-410X.2009.08591.x
17. Weber T, Meinhardt M, Zastrow S, Wienke A, Fuessel S, Wirth MP. Immunohistochemical analysis of prognostic protein markers for primary localized clear cell renal cell carcinoma. *Cancer Invest.* (2013) 31:51–9. doi: 10.3109/07357907.2012.749267
18. Gayed BA, Youssef RF, Bagrodia A, Kapur P, Darwish OM, Krabbe L-M, et al. Prognostic role of cell cycle and proliferative biomarkers in patients with clear cell renal cell carcinoma. *J Urol.* (2013) 190:1662–7. doi: 10.1016/j.juro.2013.06.037
19. Gayed BA, Youssef RF, Bagrodia A, Darwish OM, Kapur P, Sagalowsky A, et al. Ki67 is an independent predictor of oncological outcomes in patients with localized clear-cell renal cell carcinoma. *BJU Int.* (2014) 113:668–73. doi: 10.1111/bju.12263
20. Abel EJ, Bauman TM, Weiker M, Shi F, Downs TM, Jarrard DF, et al. Analysis and validation of tissue biomarkers for renal cell carcinoma using automated high-throughput evaluation of protein expression. *Hum Pathol.* (2014) 45:1092–9. doi: 10.1016/j.humpath.2014.01.008
21. Zheng K, Zhu W, Tan J, Wu W, Yang S, Zhang J. Retrospective analysis of a large patient sample to determine p53 and Ki67 expressions in renal cell carcinoma. *J. BUON.* (2014) 19:512–6.
22. Kim SH, Park WS, Park EY, Park B, Joo J, Joung JY, et al. The prognostic value of BAP1, PBRM1, pS6, PTEN, TGase2, PD-L1, CA9, PSMA, and Ki-67 tissue markers in localized renal cell carcinoma: a retrospective study of tissue microarrays using immunohistochemistry. *PLoS ONE.* (2017) 12:e0179610. doi: 10.1371/journal.pone.0179610
23. Parker AS, Kosari F, Lohse CM, Houston Thompson R, Kwon ED, Murphy L, et al. High expression levels of survivin protein independently predict a poor outcome for patients who undergo surgery for clear cell renal cell carcinoma. *Cancer.* (2006) 107:37–45. doi: 10.1002/cncr.21952
24. Kosari F, Parker AS, Kube DM, Lohse CM, Leibovich BC, Blute ML, et al. Clear cell renal cell carcinoma: gene expression analyses identify a potential signature for tumor aggressiveness. *Clin Cancer Res.* (2005) 11:5128–39. doi: 10.1158/1078-0432.CCR-05-0073
25. Byun S-S, Yeo WG, Lee SE, Lee E. Expression of survivin in renal cell carcinomas: association with pathologic features and clinical outcome. *Urology.* (2007) 69:34–7. doi: 10.1016/j.urology.2006.09.024
26. Krambeck AE, Dong H, Thompson RH, Kuntz SM, Lohse CM, Leibovich BC, et al. Survivin and b7-h1 are collaborative predictors of survival and represent potential therapeutic targets for patients with renal cell carcinoma. *Clin Cancer Res.* (2007) 13:1749–56. doi: 10.1158/1078-0432.CCR-06-2129
27. Parker AS, Lohse CM, Leibovich BC, Cheville JC, Sheinin YM, Kwon ED. Comparison of digital image analysis versus visual assessment to assess survivin expression as an independent predictor of survival for patients with clear cell renal cell carcinoma. *Hum Pathol.* (2008) 39:1176–84. doi: 10.1016/j.humpath.2007.12.009

28. Zamparese R, Pannone G, Santoro A, Lo Muzio L, Corsi F, Pedicillo MC, et al. Survivin expression in renal cell carcinoma. *Cancer Invest.* (2008) 26:929–35. doi: 10.1080/07357900802017553
29. Lei Y, Geng Z, Guo-Jun W, He W, Jian-Lin Y. Prognostic significance of survivin expression in renal cell cancer and its correlation with radioresistance. *Mol Cell Biochem.* (2010) 344:23–31. doi: 10.1007/s11010-010-0525-3
30. Shi Z-G, Li S-Q, Li Z-J, Zhu X-J, Xu P, Liu G. Expression of vimentin and survivin in clear cell renal cell carcinoma and correlation with p53. *Clin Transl Oncol.* (2015) 17:65–73. doi: 10.1007/s12094-014-1199-1
31. Ma C, Lu B, Sun E. Clinicopathological and prognostic significance of survivin expression in renal cancer patients: a meta-analysis. *Postgrad Med J.* (2017) 93:186–92. doi: 10.1136/postgradmedj-2016-134105
32. Pu Z, Wang Q, Xie H, Wang G, Hao H. Clinicalpathological and prognostic significance of survivin expression in renal cell carcinoma: a meta-analysis. *Oncotarget.* (2017) 8:19825–33. doi: 10.18632/oncotarget.15082
33. Zigeuner R, Ratschek M, Rehak P, Schips L, Langner C. Value of p53 as a prognostic marker in histologic subtypes of renal cell carcinoma: a systematic analysis of primary and metastatic tumor tissue. *Urology.* (2004) 63:651–5. doi: 10.1016/j.urology.2003.11.011
34. Noon AP, Polański R, El-Fert AY, Kalirai H, Shawki H, Campbell F, et al. Combined p53 and MDM2 biomarker analysis shows a unique pattern of expression associated with poor prognosis in patients with renal cell carcinoma undergoing radical nephrectomy. *BJU Int.* (2012) 109:1250–7. doi: 10.1111/j.1464-410X.2011.10433.x
35. Abolhasani M, Salarinejad S, Asgari M. P53 and MDM2 over-expression and five-year survival of kidney cancer patients undergoing radical nephrectomy–Iranian experience. *Asian Pac J Cancer Prev*. (2015) 16:5043–7. doi: 10.7314/APJCP.2015.16.12.5043
36. Zhan Y, Guo W, Zhang Y, Wang Q, Xu X, Zhu L. A five-gene signature predicts prognosis in patients with kidney renal clear cell carcinoma. *Comput Math Methods Med.* (2015) 2015:842784. doi: 10.1155/2015/842784
37. Cho DS, Joo HJ, Oh DK, Kang JH, Kim YS, Lee KB, et al. Cyclooxygenase-2 and p53 expression as prognostic indicators in conventional renal cell carcinoma. *Yonsei Med J.* (2005) 46:133–140. doi: 10.3349/ymj.2005.46.1.133
38. Shvarts O, Seligson D, Lam J, Shi T, Horvath S, Figlin R, et al. p53 is an independent predictor of tumor recurrence and progression after nephrectomy in patients with localized renal cell carcinoma. *J Urol.* (2005) 173:725–8. doi: 10.1097/01.ju.0000152354.08057.2a
39. Phuoc NB, Ehara H, Gotoh T, Nakano M, Yokoi S, Deguchi T, et al. Immunohistochemical analysis with multiple antibodies in search of prognostic markers for clear cell renal cell carcinoma. *Urology.* (2007) 69:843–8. doi: 10.1016/j.urology.2007.01.069
40. D'Alterio C, Consales C, Polimeno M, Franco R, Cindolo L, Portella L, et al. Concomitant CXCR4 and CXCR7 expression predicts poor prognosis in renal cancer. *Curr Cancer Drug Targets.* (2010) 10:772–81. doi: 10.2174/156800910793605839
41. D'Alterio C, Cindolo L, Portella L, Polimeno M, Consales C, Riccio A, et al. Differential role of CD133 and CXCR4 in renal cell carcinoma. *Cell Cycle Georget Tex.* (2010) 9:4492–500. doi: 10.4161/cc.9.22.13680
42. Wang L, Chen W, Gao L, Yang Q, Liu B, Wu Z, et al. High expression of CXCR4, CXCR7 and SDF-1 predicts poor survival in renal cell carcinoma. *World J Surg Oncol.* (2012) 10:212. doi: 10.1186/1477-7819-10-212
43. Li G, Badin G, Zhao A, Gentil-Perret A, Tostain J, Péoc'h M, et al. Prognostic value of CXCR4 expression in patients with clear cell renal cell carcinoma. *Histol Histopathol.* (2013) 28:1217–22. doi: 10.14670/HH-28.1217
44. Chen D, Gassenmaier M, Maruschke M, Riesenberg R, Pohla H, Stief CG, et al. Expression and prognostic significance of a comprehensive epithelial-mesenchymal transition gene set in renal cell carcinoma. *J Urol.* (2014) 191:479–86. doi: 10.1016/j.juro.2013.08.052
45. An H, Xu L, Zhu Y, Lv T, Liu W, Liu Y, et al. High CXC chemokine receptor 4 expression is an adverse prognostic factor in patients with clear-cell renal cell carcinoma. *Br J Cancer.* (2014) 110:2261–8. doi: 10.1038/bjc.2014.179
46. Li X, Huang Y, Xia J, Chen N, Wei Q, Li X, et al. CXCR4 expression in patients with high-risk locally advanced renal cell carcinoma can independently predict increased risk of disease progression and poor overall survival. *Asian Pac J Cancer Prev*. (2011) 12:3313–8.
47. Li G, Feng G, Gentil-Perret A, Genin C, Tostain J. CA9 gene expression in conventional renal cell carcinoma: a potential marker for prediction of early metastasis after nephrectomy. *Clin Exp Metastasis.* (2007) 24:149–55. doi: 10.1007/s10585-007-9064-z
48. Sandlund J, Oosterwijk E, Grankvist K, Oosterwijk-Wakka J, Ljungberg B, Rasmuson T. Prognostic impact of carbonic anhydrase IX expression in human renal cell carcinoma. *BJU Int.* (2007) 100:556–60. doi: 10.1111/j.1464-410X.2007.07006.x
49. Patard J-J, Fergelot P, Karakiewicz PI, Klatte T, Trinh Q-D, Rioux-Leclercq N, et al. Low CAIX expression and absence of VHL gene mutation are associated with tumor aggressiveness and poor survival of clear cell renal cell carcinoma. *Int J Cancer.* (2008) 123:395–400. doi: 10.1002/ijc.23496
50. Phuoc NB, Ehara H, Gotoh T, Nakano M, Kamei S, Deguchi T, et al. Prognostic value of the co-expression of carbonic anhydrase IX and vascular endothelial growth factor in patients with clear cell renal cell carcinoma. *Oncol Rep.* (2008) 20:525–30.
51. Chamie K, Klöpfer P, Bevan P, Störkel S, Said J, Fall B, et al. Carbonic anhydrase-IX score is a novel biomarker that predicts recurrence and survival for high-risk, nonmetastatic renal cell carcinoma: data from the phase III ARISER clinical trial. *Urol Oncol.* (2015) 33:204.e25–33. doi: 10.1016/j.urolonc.2015.02.013
52. Cros J, Sbidian E, Posseme K, Letierce A, Guettier C, Benoît G, et al. Nestin expression on tumour vessels and tumour-infiltrating macrophages define a poor prognosis subgroup of pt1 clear cell renal cell carcinoma. *Virchows Arch Int J Pathol.* (2016) 469:331–7. doi: 10.1007/s00428-016-1973-2
53. Ingels A, Hew M, Algaba F, de Boer OJ, van Moorselaar RJA, Horenblas S, et al. Vimentin over-expression and carbonic anhydrase IX under-expression are independent predictors of recurrence, specific and overall survival in non-metastatic clear-cell renal carcinoma: a validation study. *World J Urol.* (2017) 35:81–7. doi: 10.1007/s00345-016-1854-y
54. Vergho D, Kneitz S, Rosenwald A, Scherer C, Spahn M, Burger M, et al. Combination of expression levels of miR-21 and miR-126 is associated with cancer-specific survival in clear-cell renal cell carcinoma. *BMC Cancer.* (2014) 14:25. doi: 10.1186/1471-2407-14-25
55. Fritz HKM, Lindgren D, Ljungberg B, Axelson H, Dahlbäck B. The miR(21/10b) ratio as a prognostic marker in clear cell renal cell carcinoma. *Eur J Cancer.* (2014) 50:1758–65. doi: 10.1016/j.ejca.2014.03.281
56. Ge Y-Z, Wu R, Xin H, Zhu M, Lu T-Z, Liu H, et al. A tumor-specific microRNA signature predicts survival in clear cell renal cell carcinoma. *J Cancer Res Clin Oncol.* (2015) 141:1291–9. doi: 10.1007/s00432-015-1927-0
57. Christinat Y, Krek W. Integrated genomic analysis identifies subclasses and prognosis signatures of kidney cancer. *Oncotarget.* (2015) 6:10521–31. doi: 10.18632/oncotarget.3294
58. Tang K, Xu H. Prognostic value of meta-signature miRNAs in renal cell carcinoma: an integrated miRNA expression profiling analysis. *Sci Rep.* (2015) 5:10272. doi: 10.1038/srep10272
59. Liang B, Zhao J, Wang X. A three-microRNA signature as a diagnostic and prognostic marker in clear cell renal cancer: an *in silico* analysis. *PLoS ONE.* (2017) 12:e0180660. doi: 10.1371/journal.pone.0180660
60. Hinz S, Weikert S, Magheli A, Hoffmann M, Engers R, Miller K, et al. Expression profile of the polycomb group protein enhancer of Zeste homologue 2 and its prognostic relevance in renal cell carcinoma. *J Urol.* (2009) 182:2920–5. doi: 10.1016/j.juro.2009.08.014
61. Wagener N, Macher-Goeppinger S, Pritsch M, Hüsing J, Hoppe-Seyler K, Schirmacher P, et al. Enhancer of zeste homolog 2 (EZH2) expression is an independent prognostic factor in renal cell carcinoma. *BMC Cancer.* (2010) 10:524. doi: 10.1186/1471-2407-10-524
62. Liu L, Xu Z, Zhong L, Wang H, Jiang S, Long Q, et al. Prognostic value of EZH2 expression and activity in renal cell carcinoma: a prospective study. *PLoS ONE.* (2013) 8:e81484. doi: 10.1371/journal.pone.0081484
63. Liu L, Xu Z, Zhong L, Wang H, Jiang S, Long Q, et al. Enhancer of zeste homolog 2 (EZH2) promotes tumour cell migration and invasion via epigenetic repression of E-cadherin in renal cell carcinoma. *BJU Int.* (2016) 117:351–62. doi: 10.1111/bju.12702
64. Wang Y, Chen Y, Geng H, Qi C, Liu Y, Yue D. Overexpression of YB1 and EZH2 are associated with cancer metastasis and poor prognosis in renal cell carcinomas. *Tumour Biol.* (2015) 36:7159–66. doi: 10.1007/s13277-015-3417-z

65. Ho TH, Kapur P, Eckel-Passow JE, Christie A, Joseph RW, Serie DJ, et al. Multicenter validation of enhancer of zeste homolog 2 expression as an independent prognostic marker in localized clear cell renal cell carcinoma. *J Clin Oncol.* (2017) 35:3706–13. doi: 10.1200/JCO.2017.73.3238
66. Wheatley SP, Altieri DC. Survivin at a glance. *J Cell Sci.* (2019) 132:jcs223826. doi: 10.1242/jcs.223826
67. Olivier M, Hollstein M, Hainaut P. TP53 mutations in human cancers: origins, consequences, and clinical use. *Cold Spring Harb Perspect Biol.* (2010) 2:a001008. doi: 10.1101/cshperspect.a001008
68. Parker AS, Cheville JC, Lohse CM, Igel T, Leibovich BC, Blute ML. Loss of expression of Von Hippel-Lindau tumor suppressor protein associated with improved survival in patients with early-stage clear cell renal cell carcinoma. *Urology.* (2005) 65:1090–5. doi: 10.1016/j.urology.2004.12.040
69. Schraml P, Hergovich A, Hatz F, Amin MB, Lim SD, Krek W, et al. Relevance of nuclear and cytoplasmic Von Hippel Lindau protein expression for renal carcinoma progression. *Am J Pathol.* (2003) 163:1013–20. doi: 10.1016/S0002-9440(10)63461-X
70. Di Cristofano C, Minervini A, Menicagli M, Salinitri G, Bertacca G, Pefanis G, et al. Nuclear expression of hypoxia-inducible factor-1alpha in clear cell renal cell carcinoma is involved in tumor progression. *Am J Surg Pathol.* (2007) 31:1875–81. doi: 10.1097/PAS.0b013e318094fed8
71. Högner A, Krause H, Jandrig B, Kasim M, Fuller TF, Schostak M, et al. PBRM1 and VHL expression correlate in human clear cell renal cell carcinoma with differential association with patient's overall survival. *Urol Oncol.* (2018) 36:94.e1–e14. doi: 10.1016/j.urolonc.2017.10.027
72. da Costa WH, da Cunha IW, Fares AF, Bezerra SM, Shultz L, Clavijo DA, et al. Prognostic impact of concomitant loss of PBRM1 and BAP1 protein expression in early stages of clear cell renal cell carcinoma. *Urol Oncol.* (2018) 36:243.e1–e8. doi: 10.1016/j.urolonc.2018.01.002
73. da Costa WH, Rezende M, Carneiro FC, Rocha RM, da Cunha IW, Carraro DM, et al. Polybromo-1 (PBRM1), a SWI/SNF complex subunit is a prognostic marker in clear cell renal cell carcinoma. *BJU Int.* (2014) 113:E157–63. doi: 10.1111/bju.12426
74. Jiang W, Dulaimi E, Devarajan K, Parsons T, Wang Q, O'Neill R, et al. Intratumoral heterogeneity analysis reveals hidden associations between protein expression losses and patient survival in clear cell renal cell carcinoma. *Oncotarget.* (2017) 8:37423–34. doi: 10.18632/oncotarget.16965
75. Nam SJ, Lee C, Park JH, Moon KC. Decreased PBRM1 expression predicts unfavorable prognosis in patients with clear cell renal cell carcinoma. *Urol Oncol.* (2015) 33:340.e9–16. doi: 10.1016/j.urolonc.2015.01.010
76. Campbell L, Gumbleton M, Griffiths DFR. Caveolin-1 overexpression predicts poor disease-free survival of patients with clinically confined renal cell carcinoma. *Br J Cancer.* (2003) 89:1909–13. doi: 10.1038/sj.bjc.6601359
77. Campbell L, Jasani B, Edwards K, Gumbleton M, Griffiths DFR. Combined expression of caveolin-1 and an activated AKT/mTOR pathway predicts reduced disease-free survival in clinically confined renal cell carcinoma. *Br J Cancer.* (2008) 98:931–40. doi: 10.1038/sj.bjc.6604243
78. Steffens S, Schrader AJ, Blasig H, Vetter G, Eggers H, Tränkenschuh W, et al. Caveolin 1 protein expression in renal cell carcinoma predicts survival. *BMC Urol.* (2011) 11:25. doi: 10.1186/1471-2490-11-25
79. Ruan H, Li X, Yang H, Song Z, Tong J, Cao Q, et al. Enhanced expression of caveolin-1 possesses diagnostic and prognostic value and promotes cell migration, invasion and sunitinib resistance in the clear cell renal cell carcinoma. *Exp Cell Res.* (2017) 358:269–78. doi: 10.1016/j.yexcr.2017.07.004
80. Sanchez DJ, Simon MC. Genetic and metabolic hallmarks of clear cell renal cell carcinoma. *Biochim Biophys Acta Rev Cancer.* (2018) 1870:23–31. doi: 10.1016/j.bbcan.2018.06.003
81. Hanahan D, Weinberg RA. Hallmarks of cancer: the next generation. *Cell.* (2011) 144:646–74. doi: 10.1016/j.cell.2011.02.013
82. Rini B, Goddard A, Knezevic D, Maddala T, Zhou M, Aydin H, et al. A 16-gene assay to predict recurrence after surgery in localised renal cell carcinoma: development and validation studies. *Lancet Oncol.* (2015) 16:676–85. doi: 10.1016/S1470-2045(15)70167-1
83. Büttner F, Winter S, Rausch S, Hennenlotter J, Kruck S, Stenzl A, et al. Clinical utility of the S3-score for molecular prediction of outcome in non-metastatic and metastatic clear cell renal cell carcinoma. *BMC Med.* (2018) 16:108. doi: 10.1186/s12916-018-1088-5
84. Zhang H, Liu Y, Xie H, Fu Q, Liu Z, Zhu Y, et al. Beta-1,4-galactosyltransferase II predicts poor prognosis of patients with non-metastatic clear-cell renal cell carcinoma. *Tumour Biol.* (2017) 39:1010428317691417. doi: 10.1177/1010428317691417
85. Xi W, Liu L, Wang J, Xia Y, Bai Q, Xiong Y, et al. Enrichment of C5a-C5aR axis predicts poor postoperative prognosis of patients with clear cell renal cell carcinoma. *Oncotarget.* (2016) 7:80925–34. doi: 10.18632/oncotarget.13108
86. Yang Y, Zhai C, Chang Y, Zhou L, Shi T, Tan C, et al. High expression of chemokine CCL2 is associated with recurrence after surgery in clear-cell renal cell carcinoma. *Urol Oncol.* (2016) 34:238.e19–26. doi: 10.1016/j.urolonc.2015.11.026
87. Wang Z, Xie H, Zhou L, Liu Z, Fu H, Zhu Y, et al. CCL2/CCR2 axis is associated with postoperative survival and recurrence of patients with non-metastatic clear-cell renal cell carcinoma. *Oncotarget.* (2016) 7:51525–34. doi: 10.18632/oncotarget.10492
88. Aaltomaa S, Lipponen P, Kärjä V, Lundstedt S, Lappi J, Kosma V-M. The expression and prognostic value of alpha-, beta- and gamma-catenins in renal cell carcinoma. *Anticancer Res.* (2004) 24:2407–13.
89. Krabbe L-M, Westerman ME, Bagrodia A, Gayed BA, Darwish OM, Haddad AQ, et al. Dysregulation of β-catenin is an independent predictor of oncologic outcomes in patients with clear cell renal cell carcinoma. *J Urol.* (2014) 191:1671–7. doi: 10.1016/j.juro.2013.11.052
90. Kovacs G, Billfeldt NK, Farkas N, Dergez T, Javorhazy A, Banyai D, et al. Cytoplasmic expression of β-catenin is an independent predictor of progression of conventional renal cell carcinoma: a simple immunostaining score. *Histopathology.* (2017) 70:273–80. doi: 10.1111/his.13059
91. Lian X, Duan X, Wu X, Li C, Chen S, Wang S, et al. Expression and clinical significance of Von Hippel-Lindau downstream genes: Jade-1 and β-catenin related to renal cell carcinoma. *Urology.* (2012) 80:485.e7–13. doi: 10.1016/j.urology.2012.02.024
92. Liu W, Liu Y, Fu Q, Zhou L, Chang Y, Xu L, et al. Elevated expression of IFN-inducible CXCR3 ligands predicts poor prognosis in patients with non-metastatic clear-cell renal cell carcinoma. *Oncotarget.* (2016) 7:13976–83. doi: 10.18632/oncotarget.7468
93. An H, Xu L, Chang Y, Zhu Y, Yang Y, Chen L, et al. CXC chemokine receptor 2 is associated with postoperative recurrence and survival of patients with non-metastatic clear-cell renal cell carcinoma. *Eur J Cancer.* (2015) 51:1953–61. doi: 10.1016/j.ejca.2015.06.125
94. Biswas S, Charlesworth PJS, Turner GDH, Leek R, Thamboo PT, Campo L, et al. CD31 angiogenesis and combined expression of HIF-1α and HIF-2α are prognostic in primary clear-cell renal cell carcinoma (CC-RCC), but HIFα transcriptional products are not: implications for antiangiogenic trials and HIFα biomarker studies in primary CC-RCC. *Carcinogenesis.* (2012) 33:1717–25. doi: 10.1093/carcin/bgs222
95. Brooks SA, Brannon AR, Parker JS, Fisher JC, Sen O, Kattan MW, et al. ClearCode34: a prognostic risk predictor for localized clear cell renal cell carcinoma. *Eur Urol.* (2014) 66:77–84. doi: 10.1016/j.eururo.2014.02.035
96. Wrzesiński T, Szelag M, Cieślikowski WA, Ida A, Giles R, Zodro E, et al. Expression of pre-selected TMEMs with predicted ER localization as potential classifiers of ccRCC tumors. *BMC Cancer.* (2015) 15:518. doi: 10.1186/s12885-015-1530-4
97. Lidgren A, Hedberg Y, Grankvist K, Rasmuson T, Vasko J, Ljungberg B. The expression of hypoxia-inducible factor 1alpha is a favorable independent prognostic factor in renal cell carcinoma. *Clin Cancer Res.* (2005) 11:1129–35.
98. Schultz L, Chaux A, Albadine R, Hicks J, Kim JJ, De Marzo AM, et al. Immunoexpression status and prognostic value of mTOR and hypoxia-induced pathway members in primary and metastatic clear cell renal cell carcinomas. *Am J Surg Pathol.* (2011) 35:1549–56. doi: 10.1097/PAS.0b013e31822895e5
99. Ren J, Liu H, Yan L, Tian S, Li D, Xu Z. Microvessel density and heparanase over-expression in clear cell renal cell cancer: correlations and prognostic significances. *World J Surg Oncol.* (2011) 9:158. doi: 10.1186/1477-7819-9-158
100. Mikami S, Oya M, Shimoda M, Mizuno R, Ishida M, Kosaka T, et al. Expression of heparanase in renal cell carcinomas: implications for tumor invasion and prognosis. *Clin Cancer Res.* (2008) 14:6055–61. doi: 10.1158/1078-0432.CCR-08-0750

101. Wu K, Xu L, Zhang L, Lin Z, Hou J. High Jagged1 expression predicts poor outcome in clear cell renal cell carcinoma. *Jpn J Clin Oncol.* (2011) 41:411–6. doi: 10.1093/jjco/hyq205
102. Liu Z, Fu Q, Fu H, Wang Z, Xu L, An H, et al. A three-molecule score based on Notch pathway predicts poor prognosis in non-metastasis clear cell renal cell carcinoma. *Oncotarget.* (2016) 7:68559–70. doi: 10.18632/oncotarget.11849
103. Fukata S, Inoue K, Kamada M, Kawada C, Furihata M, Ohtsuki Y, et al. Levels of angiogenesis and expression of angiogenesis-related genes are prognostic for organ-specific metastasis of renal cell carcinoma. *Cancer.* (2005) 103:931–42. doi: 10.1002/cncr.20887
104. An H, Zhu Y, Xu L, Chen L, Lin Z, Xu J. Notch1 predicts recurrence and survival of patients with clear-cell renal cell carcinoma after surgical resection. *Urology.* (2015) 85:483.e9–e14. doi: 10.1016/j.urology.2014.10.022
105. Hu J, Zhang L-C, Song X, Lu J-R, Jin Z. KRT6 interacting with notch1 contributes to progression of renal cell carcinoma, and aliskiren inhibits renal carcinoma cell lines proliferation *in vitro*. *Int J Clin Exp Pathol.* (2015) 8:9182–8.
106. Shim M, Song C, Park S, Choi S-K, Cho YM, Kim C-S, et al. Prognostic significance of platelet-derived growth factor receptor-β expression in localized clear cell renal cell carcinoma. *J Cancer Res Clin Oncol.* (2015) 141:2213–20. doi: 10.1007/s00432-015-2019-x
107. Frödin M, Mezheyeuski A, Corvigno S, Harmenberg U, Sandström P, Egevad L, et al. Perivascular PDGFR-β is an independent marker for prognosis in renal cell carcinoma. *Br J Cancer.* (2017) 116:195–201. doi: 10.1038/bjc.2016.407
108. Pantuck AJ, Seligson DB, Klatte T, Yu H, Leppert JT, Moore L, et al. Prognostic relevance of the mTOR pathway in renal cell carcinoma: implications for molecular patient selection for targeted therapy. *Cancer.* (2007) 109:2257–67. doi: 10.1002/cncr.22677
109. Zhu C, Wei J, Tian X, Li Y, Li X. Prognostic role of PPAR-γ and PTEN in the renal cell carcinoma. *Int J Clin Exp Pathol.* (2015) 8:12668–77.
110. Dai J, Lu Y, Wang J, Yang L, Han Y, Wang Y, et al. A four-gene signature predicts survival in clear-cell renal-cell carcinoma. *Oncotarget.* (2016) 7:82712–26. doi: 10.18632/oncotarget.12631
111. Ohba K, Miyata Y, Kanda S, Koga S, Hayashi T, Kanetake H. Expression of urokinase-type plasminogen activator, urokinase-type plasminogen activator receptor and plasminogen activator inhibitors in patients with renal cell carcinoma: correlation with tumor associated macrophage and prognosis. *J Urol.* (2005) 174:461–5. doi: 10.1097/01.ju.0000165150.46006.92
112. Zubac DP, Wentzel-Larsen T, Seidal T, Bostad L. Type 1 plasminogen activator inhibitor (PAI-1) in clear cell renal cell carcinoma (CCRCC) and its impact on angiogenesis, progression and patient survival after radical nephrectomy. *BMC Urol.* (2010) 10:20. doi: 10.1186/1471-2490-10-20
113. Fuessel S, Erdmann K, Taubert H, Lohse-Fischer A, Zastrow S, Meinhardt M, et al. Prognostic impact of urokinase-type plasminogen activator system components in clear cell renal cell carcinoma patients without distant metastasis. *BMC Cancer.* (2014) 14:974. doi: 10.1186/1471-2407-14-974
114. Liu W, Fu Q, An H, Chang Y, Zhang W, Zhu Y, et al. Decreased expression of SETD2 predicts unfavorable prognosis in patients with nonmetastatic clear-cell renal cell carcinoma. *Medicine.* (2015) 94:e2004. doi: 10.1097/MD.0000000000002004
115. Liu L, Guo R, Zhang X, Liang Y, Kong F, Wang J, et al. Loss of SETD2, but not H3K36me3, correlates with aggressive clinicopathological features of clear cell renal cell carcinoma patients. *Biosci Trends.* (2017) 11:214–20. doi: 10.5582/bst.2016.01228
116. Miyajima A, Asano T, Seta K, Asano T, Kakoi N, Hayakawa M. Loss of expression of transforming growth factor-beta receptor as a prognostic factor in patients with renal cell carcinoma. *Urology.* (2003) 61:1072–7. doi: 10.1016/S0090-4295(02)02553-0
117. Parker AS, Lohse CM, Wu K, Kreinest P, Copland JA, Hilton T, et al. Lower expression levels of the transforming growth factor beta receptor type II protein are associated with a less aggressive tumor phenotype and improved survival among patients with clear cell renal cell carcinoma. *Hum Pathol.* (2007) 38:453–61. doi: 10.1016/j.humpath.2006.08.029
118. Kawashima A, Kanazawa T, Goto K, Matsumoto M, Morimoto-Okazawa A, Iwahori K, et al. Immunological classification of renal cell carcinoma patients based on phenotypic analysis of immune check-point molecules. *Cancer Immunol. Immunother.* (2018) 67:113–25. doi: 10.1007/s00262-017-2060-5
119. Kanomata N, Sato Y, Miyaji Y, Nagai A, Moriya T. Vasohibin-1 is a new predictor of disease-free survival in operated patients with renal cell carcinoma. *J Clin Pathol.* (2013) 66:613–9. doi: 10.1136/jclinpath-2013-201444
120. Yildiz E, Gokce G, Kilicarslan H, Ayan S, Goze OF, Gultekin EY. Prognostic value of the expression of Ki-67, CD44 and vascular endothelial growth factor, and microvessel invasion, in renal cell carcinoma. *BJU Int.* (2004) 93:1087–93. doi: 10.1111/j.1464-410X.2004.04786.x
121. Liang Y-X, He H-C, Han Z-D, Bi X-C, Dai Q-S, Ye Y-K, et al. CD147 and VEGF expression in advanced renal cell carcinoma and their prognostic value. *Cancer Invest.* (2009) 27:788–93. doi: 10.1080/07357900802709167
122. Alexandrov LB, Nik-Zainal S, Wedge DC, Campbell PJ, Stratton MR. Deciphering signatures of mutational processes operative in human cancer. *Cell Rep.* (2013) 3:246–59. doi: 10.1016/j.celrep.2012.12.008
123. Jiang T, Zhou C, Ren S. Role of IL-2 in cancer immunotherapy. *Oncoimmunology.* (2016) 5:e1163462. doi: 10.1080/2162402X.2016.1163462
124. Nishino M, Ramaiya NH, Hatabu H, Hodi FS. Monitoring immune-checkpoint blockade: response evaluation and biomarker development. *Nat Rev Clin Oncol.* (2017) 14:655–68. doi: 10.1038/nrclinonc.2017.88
125. Li P, Ren H, Zhang Y, Zhou Z. Fifteen-gene expression based model predicts the survival of clear cell renal cell carcinoma. *Medicine.* (2018) 97:e11839. doi: 10.1097/MD.0000000000011839
126. Itoi T, Yamana K, Bilim V, Takahashi K, Tomita F. Impact of frequent Bcl-2 expression on better prognosis in renal cell carcinoma patients. *Br J Cancer.* (2004) 90:200–5. doi: 10.1038/sj.bjc.6601454
127. Tan W, Hildebrandt MAT, Pu X, Huang M, Lin J, Matin SF, et al. Role of inflammatory related gene expression in clear cell renal cell carcinoma development and clinical outcomes. *J Urol.* (2011) 186:2071–7. doi: 10.1016/j.juro.2011.06.049
128. Thompson RH, Gillett MD, Cheville JC, Lohse CM, Dong H, Webster WS, et al. Costimulatory B7-H1 in renal cell carcinoma patients: indicator of tumor aggressiveness and potential therapeutic target. *Proc Natl Acad Sci USA.* (2004) 101:17174–9. doi: 10.1073/pnas.0406351101
129. Thompson RH, Kuntz SM, Leibovich BC, Dong H, Lohse CM, Webster WS, et al. Tumor B7-H1 is associated with poor prognosis in renal cell carcinoma patients with long-term follow-up. *Cancer Res.* (2006) 66:3381–5. doi: 10.1158/0008-5472.CAN-05-4303
130. Parker AS, Leibovich BC, Lohse CM, Sheinin Y, Kuntz SM, Eckel-Passow JE, et al. Development and evaluation of BioScore: a biomarker panel to enhance prognostic algorithms for clear cell renal cell carcinoma. *Cancer.* (2009) 115:2092–103. doi: 10.1002/cncr.24263
131. Bromwich EJ, McArdle PA, Canna K, McMillan DC, McNicol A-M, Brown M, et al. The relationship between T-lymphocyte infiltration, stage, tumour grade and survival in patients undergoing curative surgery for renal cell cancer. *Br. J. Cancer.* (2003) 89:1906–8. doi: 10.1038/sj.bjc.6601400
132. Siddiqui SA, Frigola X, Bonne-Annee S, Mercader M, Kuntz SM, Krambeck AE, et al. Tumor-infiltrating Foxp3-CD4+CD25+ T cells predict poor survival in renal cell carcinoma. *Clin Cancer Res.* (2007) 13:2075–81. doi: 10.1158/1078-0432.CCR-06-2139
133. Lim SD, Young AN, Paner GP, Amin MB. Prognostic role of CD44 cell adhesion molecule expression in primary and metastatic renal cell carcinoma: a clinicopathologic study of 125 cases. *Virchows Arch Int J Pathol.* (2008) 452:49–55. doi: 10.1007/s00428-007-0530-4
134. Zhang X, Yang M, Shi H, Hu J, Wang Y, Sun Z, et al. Reduced E-cadherin facilitates renal cell carcinoma progression by WNT/β-catenin signaling activation. *Oncotarget.* (2017) 8:19566–76. doi: 10.18632/oncotarget.15361
135. Mlcochova H, Machackova T, Rabien A, Radova L, Fabian P, Iliev R, et al. Epithelial-mesenchymal transition-associated microRNA/mRNA signature is linked to metastasis and prognosis in clear-cell renal cell carcinoma. *Sci Rep.* (2016) 6:31852. doi: 10.1038/srep31852
136. Yang C-A, Huang H-Y, Yen J-C, Chang J-G. Prognostic value of RNASEH2A-, CDK1-, and CD151-related pathway gene profiling for kidney cancers. *Int J Mol Sci.* (2018) 19:1586. doi: 10.3390/ijms19061586
137. Wang C, Tang K, Li Z, Chen Z, Xu H, Ye Z. Targeted p21(WAF1/CIP1) activation by miR-1236 inhibits cell proliferation and correlates with

favorable survival in renal cell carcinoma. *Urol Oncol.* (2016) 34:59.e23–34. doi: 10.1016/j.urolonc.2015.08.014
138. Pertia A, Nikoleishvili D, Trsintsadze O, Gogokhia N, Managadze L, Chkhotua A. Immunoreactivity of p27: cyclin D3, and Ki67 in conventional renal cell carcinoma. *Int Urol Nephrol.* (2009) 41:243–9. doi: 10.1007/s11255-008-9442-8
139. Pertia A, Nikoleishvili D, Trsintsadze O, Gogokhia N, Managadze L, Chkhotua A. Loss of p27(Kip1) CDKI is a predictor of poor recurrence-free and cancer-specific survival in patients with renal cancer. *Int Urol Nephrol.* (2007) 39:381–7. doi: 10.1007/s11255-006-9077-6
140. Liu Z, Fu Q, Lv J, Wang F, Ding K. Prognostic implication of p27Kip1, Skp2 and Cks1 expression in renal cell carcinoma: a tissue microarray study. *J Exp Clin Cancer Res.* (2008) 27:51. doi: 10.1186/1756-9966-27-51
141. Sgambato A, Camerini A, Genovese G, De Luca F, Viacava P, Migaldi M, et al. Loss of nuclear p27(kip1) and α-dystroglycan is a frequent event and is a strong predictor of poor outcome in renal cell carcinoma. *Cancer Sci.* (2010) 101:2080–6. doi: 10.1111/j.1349-7006.2010.01644.x
142. Rabjerg M, Bjerregaard H, Halekoh U, Jensen BL, Walter S, Marcussen N. Molecular characterization of clear cell renal cell carcinoma identifies CSNK2A1, SPP1 and DEFB1 as promising novel prognostic markers. *APMIS.* (2016) 124:372–83. doi: 10.1111/apm.12519
143. Giraldo NA, Becht E, Vano Y, Petitprez F, Lacroix L, Validire P, et al. Tumor-infiltrating and peripheral blood T-cell immunophenotypes predict early relapse in localized clear cell renal cell carcinoma. *Clin Cancer Res.* (2017) 23:4416–28. doi: 10.1158/1078-0432.CCR-16-2848
144. Hildebrandt MAT, Tan W, Tamboli P, Huang M, Ye Y, Lin J, et al. Kinome expression profiling identifies IKBKE as a predictor of overall survival in clear cell renal cell carcinoma patients. *Carcinogenesis.* (2012) 33:799–803. doi: 10.1093/carcin/bgs018
145. Bamias A, Chorti M, Deliveliotis C, Trakas N, Skolarikos A, Protogerou B, et al. Prognostic significance of CA 125, CD44, and epithelial membrane antigen in renal cell carcinoma. *Urology.* (2003) 62:368–73. doi: 10.1016/S0090-4295(03)00264-4
146. Zhu Y, Xu L, An H, Liu W, Wang Z, Xu J. p21-activated kinase 1 predicts recurrence and survival in patients with non-metastatic clear cell renal cell carcinoma. *Int J Urol.* (2015) 22:447–53. doi: 10.1111/iju.12715
147. Hedberg Y, Ljungberg B, Roos G, Landberg G. Expression of cyclin D1, D3, E, and p27 in human renal cell carcinoma analysed by tissue microarray. *Br J Cancer.* (2003) 88:1417–23. doi: 10.1038/sj.bjc.6600922
148. Wu XR, Sha JJ, Liu DM, Chen YH, Yang GL, Zhang J, et al. High expression of P53-induced Ring-h2 protein is associated with poor prognosis in clear cell renal cell carcinoma. *Eur J Surg Oncol.* (2013) 39:100–6. doi: 10.1016/j.ejso.2012.10.004
149. Yao M, Huang Y, Shioi K, Hattori K, Murakami T, Sano F, et al. A three-gene expression signature model to predict clinical outcome of clear cell renal carcinoma. *Int J Cancer.* (2008) 123:1126–32. doi: 10.1002/ijc.23641
150. Williams GH, Stoeber K. The cell cycle and cancer. *J Pathol.* (2012) 226:352–64. doi: 10.1002/path.3022
151. Otto T, Sicinski P. Cell cycle proteins as promising targets in cancer therapy. *Nat Rev Cancer.* (2017) 17:93–115. doi: 10.1038/nrc.2016.138
152. Ikuerowo SO, Kuczyk MA, von Wasielewski R, Shittu OB, Jonas U, Machtens S, et al. p16INK4a expression and clinicopathologic parameters in renal cell carcinoma. *Eur Urol.* (2007) 51:732–7; discussion: 738. doi: 10.1016/j.eururo.2006.08.010
153. Joseph RW, Kapur P, Serie DJ, Eckel-Passow JE, Parasramka M, Ho T, et al. Loss of BAP1 protein expression is an independent marker of poor prognosis in patients with low-risk clear cell renal cell carcinoma. *Cancer.* (2014) 120:1059–67. doi: 10.1002/cncr.28521
154. Minardi D, Lucarini G, Milanese G, Di Primio R, Montironi R, Muzzonigro G. Loss of nuclear BAP1 protein expression is a marker of poor prognosis in patients with clear cell renal cell carcinoma. *Urol Oncol.* (2016) 34:338.e11–18. doi: 10.1016/j.urolonc.2016.03.006
155. Chang P, Bing Z, Tian J, Zhang J, Li X, Ge L, et al. Comprehensive assessment gene signatures for clear cell renal cell carcinoma prognosis. *Medicine.* (2018) 97:e12679. doi: 10.1097/MD.0000000000012679
156. Cao Y-W, Liu Y, Dong Z, Guo L, Kang E-H, Wang Y-H, et al. Monocarboxylate transporters MCT1 and MCT4 are independent prognostic biomarkers for the survival of patients with clear cell renal cell carcinoma and those receiving therapy targeting angiogenesis. *Urol Oncol.* (2018) 36:311.e15–25. doi: 10.1016/j.urolonc.2018.03.014
157. Brannon AR, Reddy A, Seiler M, Arreola A, Moore DT, Pruthi RS, et al. Molecular stratification of clear cell renal cell carcinoma by consensus clustering reveals distinct subtypes and survival patterns. *Genes Cancer.* (2010) 1:152–63. doi: 10.1177/1947601909359929
158. Beuselinck B, Job S, Becht E, Karadimou A, Verkarre V, Couchy G, et al. Molecular subtypes of clear cell renal cell carcinoma are associated with sunitinib response in the metastatic setting. *Clin Cancer Res.* (2015) 21:1329–39. doi: 10.1158/1078-0432.CCR-14-1128
159. DeLuca C, Kwon H, Lin R, Wainberg M, Hiscott J. NF-kappaB activation and HIV-1 induced apoptosis. *Cytokine Growth Factor Rev.* (1999) 10:235–53. doi: 10.1016/S1359-6101(99)00015-5
160. Kumari N, Dwarakanath BS, Das A, Bhatt AN. Role of interleukin-6 in cancer progression and therapeutic resistance. *Tumour Biol.* (2016) 37:11553–72. doi: 10.1007/s13277-016-5098-7
161. Roumenina LT, Daugan MV, Noe R, Petitprez F, Vano YA, Sanchez-Salas R, et al. Tumor cells hijack macrophage-produced complement C1q to promote tumor growth. *Cancer Immunol Res.* (2019) 7:1091–105. doi: 10.1158/2326-6066.CIR-18-0891
162. Litwiniuk M, Krejner A, Speyrer MS, Gauto AR, Grzela T. Hyaluronic acid in inflammation and tissue regeneration. *Wounds Compend Clin Res Pract.* (2016) 28:78–88.
163. Murata M. Inflammation and cancer. *Environ Health Prev Med.* (2018) 23:50. doi: 10.1186/s12199-018-0740-1
164. Kim BJ, Kim JH, Kim HS, Zang DY. Prognostic and predictive value of VHL gene alteration in renal cell carcinoma: a meta-analysis and review. *Oncotarget.* (2017) 8:13979–85. doi: 10.18632/oncotarget.14704
165. Joseph RW, Kapur P, Serie DJ, Parasramka M, Ho TH, Cheville JC, et al. Clear cell renal cell carcinoma subtypes identified by BAP1 and PBRM1 expression. *J Urol.* (2016) 195:180–7. doi: 10.1016/j.juro.2015.07.113
166. van Oostenbrugge TJ, Fütterer JJ, Mulders PFA. Diagnostic imaging for solid renal tumors: a pictorial review. *Kidney Cancer.* (2018) 2:79–93. doi: 10.3233/KCA-180028
167. Vano Y, Elaidi RT, Bennamoun M, Chevreau CM, Borchiellini D, Pannier D, et al. LBA25 Results from the phase II biomarker driven trial with nivolumab (N) and ipilimumab or VEGFR tyrosine kinase inhibitor (TKI) in naïve metastatic kidney cancer (m-ccRCC) patients (pts): the BIONIKK trial. *Ann Oncol.* (2020) 31:S1157. doi: 10.1016/j.annonc.2020.08.2254
168. Joosten SC, Deckers IA, Aarts MJ, Hoeben A, van Roermund JG, Smits KM, et al. Prognostic DNA methylation markers for renal cell carcinoma: a systematic review. *Epigenomics.* (2017) 9:1243–57. doi: 10.2217/epi-2017-0040
169. Mitchell TJ, Rossi SH, Klatte T, Stewart GD. Genomics and clinical correlates of renal cell carcinoma. *World J Urol.* (2018) 36:1899–911. doi: 10.1007/s00345-018-2429-x

**Conflict of Interest:** The authors declare that the research was conducted in the absence of any commercial or financial relationships that could be construed as a potential conflict of interest.

*Copyright © 2021 Petitprez, Ayadi, de Reyniès, Fridman, Sautès-Fridman and Job. This is an open-access article distributed under the terms of the Creative Commons Attribution License (CC BY). The use, distribution or reproduction in other forums is permitted, provided the original author(s) and the copyright owner(s) are credited and that the original publication in this journal is cited, in accordance with accepted academic practice. No use, distribution or reproduction is permitted which does not comply with these terms.*

frontiers in Oncology

ORIGINAL RESEARCH
published: 31 May 2021
doi: 10.3389/fonc.2021.686678

# KDF1, a Novel Tumor Suppressor in Clear Cell Renal Cell Carcinoma

*Jing-min Zheng[1,2]*, Mei-fu Gan[2†], Hong-yuan Yu[1†], Lu-xia Ye[2], Qing-xin Yu[2], Yu-hui Xia[2], Han-xi Zhou[1], Jia-qian Bao[1] and Yi-qing Guo[1]*

[1] Department of Urology, Taizhou Hospital, Wenzhou Medical University, Linhai, China, [2] Department of Pathology, Taizhou Hospital, Wenzhou Medical University, Linhai, China

KDF1 has been identified as a key regulator of epidermal proliferation and differentiation, but it is unknown whether KDF1 is involved in the pathogenesis of malignancy. No study has reported the expression and function of KDF1 in renal cancer. To explore the pathologic significance of KDF1 in clear cell renal cell carcinoma (ccRCC), the expression level of KDF1 protein in the tumor tissue of ccRCC patients was examined by immunohistochemistry and Western blot while the expression level of KDF1 mRNA was analyzed by using the data from TCGA database. In vitro cell experiments and allogeneic tumor transplantation tests were performed to determine the effects of altered KDF1 expression on the phenotype of ccRCC cells. Both the KDF1 mRNA and protein were found to be decreasingly expressed in the tumor tissue of ccRCC patients when compared with the adjacent non-tumor control tissue. The expression level of KDF1 in the tumor tissue was found to correlate negatively with the tumor grade. Patients with higher KDF1 in the tumor tissue were found to have longer overall survival and disease-specific survival time. KDF1 was shown to be an independent factor influencing the disease-specific survival of the ccRCC patients. Overexpression of KDF1 was found to inhibit the proliferation, migration and invasion of ccRCC cells, which could be reversed by decreasing the expression of KDF1 again. ccRCC cells with KDF1 overexpression were found to produce smaller transgrafted tumors. These results support the idea that KDF1 is involved in ccRCC and may function as a tumor suppressor.

**Keywords: KDF1, clear cell renal cell carcinoma, tumor grade, tumor suppressor, prognosis**

OPEN ACCESS

***Edited by:***
*Kouji Izumi,*
*Kanazawa University, Japan*

***Reviewed by:***
*Ondrej Bonczek,*
*Masaryk Memorial Cancer Institute, Czechia*
*Magdalena Julita Orzechowska,*
*Medical University of Lodz, Poland*
*Emily S. Norton,*
*Mayo Clinic, United States*

****Correspondence:***
*Jing-min Zheng*
*zhengjingmin@enzemed.com*

*[†]These authors have contributed equally to this work and share first authorship*

***Specialty section:***
*This article was submitted to Genitourinary Oncology, a section of the journal Frontiers in Oncology*

***Received:*** *29 March 2021*
***Accepted:*** *05 May 2021*
***Published:*** *31 May 2021*

***Citation:***
*Zheng J-m, Gan M-f, Yu H-y, Ye L-x, Yu Q-x, Xia Y-h, Zhou H-x, Bao J-q and Guo Y-q (2021) KDF1, a Novel Tumor Suppressor in Clear Cell Renal Cell Carcinoma. Front. Oncol. 11:686678. doi: 10.3389/fonc.2021.686678*

## INTRODUCTION

Kidney cancer is one of the ten most commonly diagnosed cancers worldwide and the most lethal of the genitourinary tumors. More than 175,000 people died of kidney cancer in 2018 and the incidence is still rising (1). Clear cell renal cell carcinoma (ccRCC) is a major histological subtype of kidney cancer (accounting for 60-80% of the disease) and the most malignant one of the disease (1). Treatment of ccRCC is not very effective due to its resistance to commonly used chemotherapy and radiation (2). Early surgical resection is still the preferred therapy. However, relapse and metastasis are common even in patients with localized disease after radical nephrectomy (3). Targeted therapy has been introduced to treat ccRCC and has partially extended patients' survival time.

However, none of the therapies result in a durable response (4, 5). Thus, there is an urgent need to further explore the mechanism of ccRCC, find new diagnostic and/or prognostic markers, and develop novel therapies to improve the prognosis of the disease.

In 2013, Lee et al. reported a recessive mutant mouse with a short snout and short limbs, which they designated as shorthand (*shd*) and was further proved to be caused by a mutation in the Keratinocyte Differentiation Factor 1 (KDF1) gene, in an N-ethyl-N-nitrosourea-induced mutagenesis screen (6). *Shd* homozygotes died at birth. Due to the uncontrolled proliferation of basal progenitor cells and a failure of their progeny to differentiate into mature epidermal cells, the *shd* mouse fetuses developed a thick, taut and hyperplastic epidermis with impaired barrier function (6). Later, mutations in KDF1 gene have also been reported in patients with ectodermal dysplasia, affecting the development of eyebrows, teeth, nails, sweat glands and other organs derived from ectoderm (7–9). Evidence from these studies substantiated that KDF1 is a negative regulator of keratinocyte proliferation during epidermis development and an essential promoter for the differentiation of epidermal progenitor cell progeny. Given the key role of KDF1 in the maintenance of the appropriate balance between cell division and differentiation, which is critical for tissue homeostasis and cancer prevention, we speculated that defect in KDF1 might also play a role in the pathogenesis of cancer. To test this idea, in the present study, we examined the expression of KDF1 in the tumor tissue of ccRCC patients in comparison with clinicopathological parameters. Also, we evaluated the effect of altered expression of KDF1 on the phenotype of ccRCC cells.

# MATERIALS AND METHODS

## Patients

The present study included two cohorts of patients: the TCGA cohort and the TZYY cohort. The TCGA cohort included 530 ccRCC patients, including 344 males and 186 females with a median age of 61 years (ranging from 26 to 90 years) at surgery. The RNA sequencing data of tumor tissue and clinicopathologic data for each patient were downloaded from TCGA database (TCGA-KIRC). The RNA sequencing data of 72 normal renal samples were also downloaded from TCGA database and were used as normal controls. The TZYY cohort included 241 ccRCC patients, including 157 males and 84 females with a median age of 59 years (ranging from 28 to 84 years) at surgery. The patients were hospitalized at Department of Urology, Taizhou Hospital, Wenzhou Medical University from 2004 to 2018 and were histologically confirmed ccRCC after partial or radical nephrectomy. All the patients had no other malignancy history and no history of anticancer therapy before surgery. Patients with mixed histological types were excluded. The clinical and pathological data of TZYY cohort patients were collected from medical records and follow-up records. Here, we defined the overall survival time (OS) as the time interval between surgery and the date of death or the last visit, and the disease-specific survival time (DSS) as the time interval between primary surgery and death from ccRCC or the last follow-up visit. For the analysis of disease-specific mortality, deaths as a result of other causes were censored. In the analysis of immunohistochemistry, 39 non-tumor tissue samples were used as controls. The informed consent has been obtained from all the participants. All research work with human participants was in accordance with the ethical standards of the responsible committee on human experimentation and with the Declaration of Helsinki. The present study was approved by the Ethics Committee of Taizhou Hospital (No. K20200821).

## Immunohistochemical Staining and Analysis

Immunohistochemical staining was performed on formalin-fixed Paraffin sections. Briefly, the sections were deparaffinised in xylene, rehydrated with graded ethanols, autoclaved for antigen repair and treated with 3% hydrogen peroxide solution to inactivate the endogenous peroxidase. After blocking for 30 min in 10% fetal calf serum and rinsed in PBS, the sections were incubated overnight at 4°C with the first antibody, such as rabbit anti-human KDF1 antibody (cat.no. PA5-55926, Invitrogen, MA, USA, dilution 1:200) and rabbit anti-human ki-67 antibody (cat.no. 790-4286, Roche, AZ, USA, dilution 1:2). Then, the sections were washed three times, incubated with the second antibody for 30 min, washed again and developed with diaminobenzidine. Finally, each section was counterstained with haematoxylin. Normal homologous serum was used to replace the first antibody as a negative control. According to the immunostaining intensity, the level of KDF1 was scored by two experienced pathologists in a blind manner: 0, negative; 1, weak; 2, medium; 3, strong. The slides with different score obtained by the two pathologists were reviewed again until the agreed score was made.

For the evaluation of the ratio of ki-67 positive cells in the tumor tissues, at least 15 pictures were taken from each section. The number of ki-67 positive nucleus and total nucleus in each picture were counted and the ratio of ki-67 positive nucleus was calculated. The average value of all the pictures from a section was used as the ki-67 positive ratio of the section.

## Cell Culture, Transduction and Treatment

The ccRCC cell lines 786-O and ACHN were obtained from the Cell Bank of the Chinese Academy of Science (Shanghai, China). The cells were cultured in 1640 medium supplemented with 10% fetal bovine serum. In order to obtain ccRCC cells stably over-expressing KDF1, the cells were transduced with a recombinant lentivirus Lenti-KDF1. Lenti-KDF1 was made by inserting KDF1 coding sequence (152-1348 of NM_152365.3) into the NotI/XbaI site of the lentivirus expression vector pCDH-CMV-MCS-EF1. Infection of ccRCC cells was performed when the cells reached about 50% confluence. Stably transduced cells were obtained by screening the cells with 5μg/ml of puromycin, and the overexpression of KDF1 in the cells was verified by RT-PCR and Western blot.

Lentivirus-mediated short hairpin (sh) RNA was employed to inhibit the expression of KDF1 in KDF1-overexpression cells. To produce the KDF1 shRNA expression Lentivirus Lenti-KDF1shRNA, a shRNA targeting KDF1 was synthesized and cloned into the BamH I and EcoR I site of pLVshRNA-EGFP (2A)puro. Following is the shRNA sequence: 5'-GAGGAGTACTATTCTTTCCATCTCGAGATGGAAAGAATAGTACTCCTCTTTTTT-3'.

## RNA Isolation and RT-PCR Analysis

According to the manufacturer's protocol, total cellular RNA was isolated with TRIzol® reagent (cat.no. 9109, Thermo Fisher Scientific, MA, USA.) and cDNA was generated using a PrimeScript TM RT Master Mix kit (cat.no. RR01AM, Takara Biotechnology, Dalian, China). A fragment of cDNA was amplified by using the following primers: KDF1 forward, 5'-GTACCCAGCAAGCCATGA-3' and KDF1 reverse, 5'-CTCCCAGAAAGGGTGTGG-3'.

## Western Blot Analysis

Total protein was extracted using RIPA lysis buffer (cat.no. R0020, Solarbio Technology, Beijing, China) containing Phosphatase Inhibitor and Protease Inhibitor Cocktail (cat.no. C0001,MCE HY-K0023, Targetmol, MA, USA) at 4°C. About 10 μg of total protein was separated by 10% SDS-PAGE and transferred to a PVDF membrane (cat.no. ISEQ00010, Merck KGaA, Darmstadt, Germany). After blocking in the blocking buffer containing 5% skimmed milk powder, the membranes were incubated with the rabbit anti-human KDF1 antibody (cat.no. PA5-55926, Thermo Fisher Scientific, MA, USA, dilution 1:1000) or mice anti-human GAPDH antibody (cat.no. YM3029, Immunoway, TX,USA, dilution 1:1000), overnight at 4°C. Then the membrane was washed and incubated with HRP-conjugated goat anti-rabbit (cat.no. B0201, Immunoway, TX, USA) or rabbit anti-mouse (cat.no. B0101, Immunoway, TX, USA) antibody for 2 h at 37°C. The immunolabeled proteins were detected by chemiluminescence using the Chemiluminescent hRP substrate (Merck KGaA, Darmstadt, Germany). Densitometric analysis was performed using the 1.52a version Image J software (National Institutes of Health, MD, USA).

## Cell Proliferation Assay

A Cell Counting Kit-8 kit (Beyotime Institute of Biotechnology, Shanghai, China) was used in the analysis of cell proliferation according to the manufacturer's instruction. Briefly, 786-O or ACHN cells were seeded into the 96-well plates at a density of $3\times10^3$/well and $5\times10^3$/well, respectively. After 6, 24, 48 and 72 hours, the cells were detected by the Cell Counting Kit-8 kit. Here, the results of 6 h were used as a baseline.

## Cell Migration Assay

A wound healing method was used to evaluate the migration of ccRCC cells. Briefly, when the cells grew to confluence, the cells were treated with serum free medium for 24 h. Then a scratch on the cell monolayer was made with a sterile pipette tip. The detached cells were removed by washing with PBS and then the cells were maintained in serum-free RPMI-1640 medium. At regular time, the images of the culture were captured, the unhealing area of each scratch was measured and the wound healing ratio was calculated. The experiments were performed in triplicate.

## Cell Invasion Assay

The relative invasion ability was measured by using BioCoat Matrigel invasion chambers (24-well plates, 8 μm pores, BD Biosciences, CA, USA). Cells were starved by serum free medium for 24 h prior to invasion assays. Then, $5\times10^4$ ACHN or $1.5\times10^4$ 786-O cells with 200 μL serum-free medium were added to the upper chamber following 500 μL of medium containing 10% FBS being added to the lower chambers. Twenty-four hours later, the cells on the upperside of the membrane were erased and the cells on the downside of the membrane,which have passed through the matrigel and membrane,were fixed with 4% paraformaldehyde, stained with 0.5% crystal violet and counted under Microscope.

## Subcutaneous Xenografts

Four-week old male nude mice were divided randomly into three groups: untransduced cell group, control virus transduced cell group and KDF1 overexpression cell group. Six mice were used in each group. When the untransduced ACHN cells, control virus transduced ACHN cells and KDF1 overexpression ACHN cells grew to nearly 80% confluence, the cells were collected and resuspended in serum-free 1640 medium containing 50% Basement Membrane Extract (cat.no. 2446ML0005, Biofroxx, Einhausen, Germany) at a density of $2\times10^7$/ml. Then, for each mouse, 0.1 ml of respective cells (untransduced ACHN cells for the untransduced cell group, control virus transduced ACHN cells for the control virus transduced cell group, and KDF1 overexpression ACHN cells for the KDF1 overexpression cell group) was transplanted subcutaneously on the side of the body. Six weeks later, the mice were euthanized and the tumors were removed, measured and weighed. All experiments were monitored by the Animal Care Committee of Taizhou Hospital and were performed according to the guidelines of the Animal Care Committee of Taizhou Hospital (No.tyz-2020182). All efforts were made to minimize the number of animals used and their suffering.

## Statistical Analysis

SPSS software (version no. 17.0, IBM, CHI, USA) was used to analyze the data. Multiple comparisons were performed using one-way ANOVA. Independent sample T test was used to compare the difference of KDF1 mRNA expression level between the tumor tissue of ccRCC patients and that of the normal controls. Other differences between two groups in the present study were compared by using Mann-Whitney U test. The Spearman correlation analysis was used to explore the correlation of KDF1 mRNA and protein level (represented by score) with the clinicopathological indices. The Kaplan–Meier method and log-rank test were used for survival analysis. The Cox proportional hazards model was used to determine which variables influenced survival. The variables that significantly

impacted survival in univariate analyses were included in multivariate analyses. All statistical tests were two tailed, and P values <0.05 were considered significant.

# RESULTS

## Results of TCGA Data Analysis

We first analyzed the expression of KDF1 mRNA in the tumor tissue of ccRCC patients by using the data from TCGA database. As shown in **Figure 1A**, the expression level of KDF1 mRNA in the tumor tissue was significantly lower than that in normal renal tissue (8.57 ± 2.45 vs 2.00 ± 2.14 Fragments Per Kilobase per Million (FPKM), p<0.01). Analysis based on Speaman coefficient revealed that the expression level of KDF1 mRNA was negatively correlated with the tumor stage (r=-0.221, p=0.0000003, n=530) and Fuhrman grade (r=-0.249, p=0.000000008, n=522).

To determine the association of KDF1 mRNA level with the survival, patients were divided into two groups: high KDF1 mRNA group and low KDF1 mRNA group according to the cutpoint which was evaluated by using EvaluateCutpoints (http://wnbikp.umed.lodz.pl/Evaluate-Cutpoints/). Analysis based on Kaplan-Meier survival revealed that patients with higher KDF1 mRNA had a longer overall survival time than patients with lower KDF1 mRNA (**Figure 1B**).

## Expression of KDF1 Protein in the Tumor Tissue of ccRCC Patients Detected by Immunohistochemistry and Western Blot

Immunohistochemical staining was performed on the tumor tissue of 241 ccRCC patients while 39 non-tumor renal tissue samples were used as controls. As shown in **Figure 2A**, KDF1 was extensively expressed in the renal tissue, especially in renal tubular epithelial cells. KDF1 was distributed mainly in a cytoplasmic pattern. Compared with the normal renal tissue, the expression level of KDF1 in the tumor tissue of ccRCC patients decreased markedly. Immunostaining for KDF1 was observed mainly in the cytoplasm of cancer cells.

Among the 241 ccRCC patients, 53, 92, 76 and 20 patients were scored as 0, 1, 2 and 3 respectively according to the immunostaining intensity of KDF1. In contrast, among the 39 non-tumor renal tissue samples, 34 were scored as 3 and 5 were scored as 2 (**Figure 2C**).

To confirm the results of immunohistochemistry, the expression of KDF1 in the tumor tissue of 10 ccRCC patients and the corresponding non-tumor tissues was further analyzed by Western blot. As shown in **Figures 2B, D**, results of Western blot analysis indeed showed the decreased expression of KDF1 in ccRCC tumor tissue compared with the non-tumor renal tissue (1 ± 0.25 vs 0.28 ± 0.08, p<0.01).

## Association of KDF1 Protein Level With Clinicopathological Parameters

The association between the expression level of KDF1 protein in the tumor tissue of ccRCC patients and patient's clinicopathological parameters was analyzed based on the score of immunostaining intensity for KDF1. As shown in **Table 1**, higher expression level of KDF1 protein was observed in patients with high tumor grade. No significant difference in the expression level of KDF1 protein was observed in patients with different ages, gender, location of tumor, tumor size,

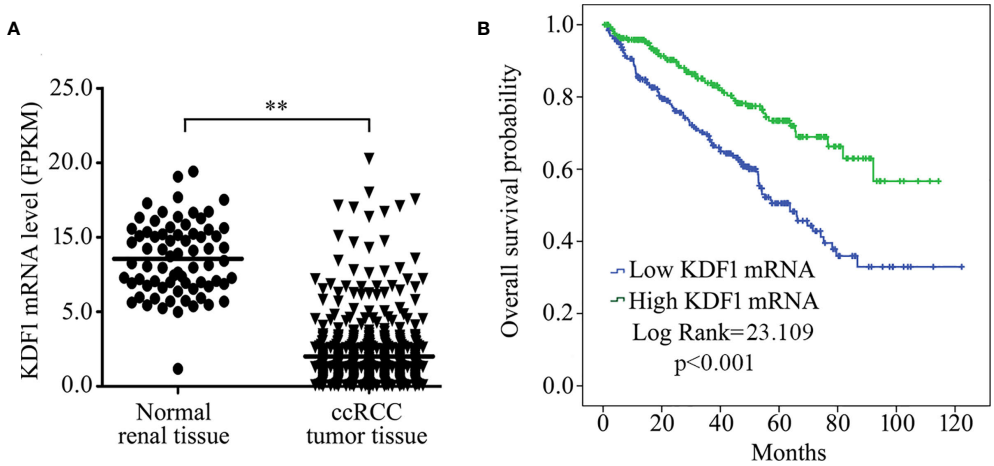



**FIGURE 1** | Expression of KDF1 mRNA in the tumor tissue of patients with clear cell renal cell carcinoma (ccRCC) and its association with overall survival. The expression level of KDF1 mRNA in the tumor tissue of 530 ccRCC patients was compared with that in the 72 normal renal samples **(A)**. Patients were divided into higher KDF1 mRNA subgroup (with the KDF1 mRNA level >1.415 Fragments Per Kilobase per Million (FPKM)) and lower KDF1 mRNA subgroup (with the KDF1 mRNA level ≤1.415 FPKM) according to the level of KDF1 mRNA in the tumor tissue and overall survival were compared between the two subgroups by using Kaplan–Meier method **(B)**. In the analysis of overall survival, 23 patients who died within a month after operation were excluded and a total of 507 patients were included. **p < 0.01. FPKM, Fragments per kilobase Million.

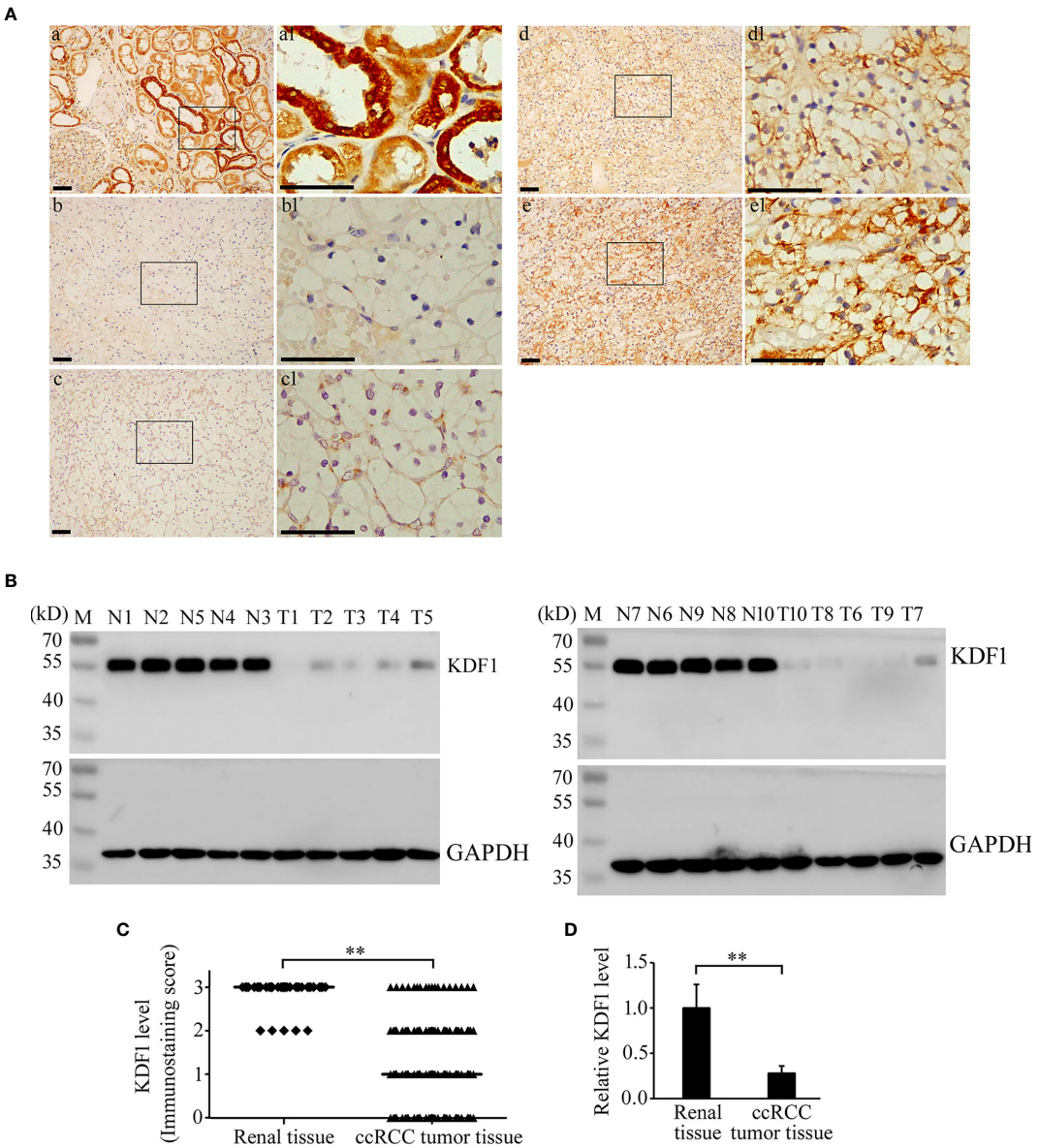



**FIGURE 2** | Expression of KDF1 in the tumor tissue of patients with clear cell renal cell carcinoma (ccRCC). Immunohistochemical staining was performed on the tumor tissue of 241 ccRCC patients while 39 non-tumor renal tissue samples were used as controls. The expression of KDF1 in the tumor tissue of 10 ccRCC patients was confirmed by Western blot while 10 non-tumor renal tissues were used as controls. **(A)** Representative pictures of immunohistochemistry. a: A representative picture from non-tumor renal tissue; b: A representative picture from ccRCC patients showing negative immunostaining for KDF1 (the KDF1 level was scored as 0); c: A representative picture from ccRCC patients showing weak immunostaining for KDF1 (the KDF1 level was scored as 1); d: A representative picture from ccRCC patients showing medium immunostaining for KDF1 (the KDF1 level was scored as 2); e: A representative picture from ccRCC patients showing strong immunostaining for KDF1 (the KDF1 level was scored as 3). **(B)** Results of Western blot analysis for KDF1 in the tumor tissue of 10 ccRCC patients and the matched non-tumor tissue. **(C)** Comparison of the KDF1 protein level between the tumor tissue of ccRCC patients and the non-tumor renal tissue according to the results of immunohistochemistry. **(D)** Quantitative analysis of the KDF1 protein level in the tumor tissue of 10 ccRCC patients compared with the non-tumor renal tissue according to the results of Western blot. a1-e1 is the local amplification of a-e respectively. N1-N10: Non-tumor tissue; T1-T10: ccRCC tumor tissue. **P < 0.01. Scale bar: 50 μm.

tumor stage and the habit of smoking and drinking. Also, we did not find significant influence in the expression of KDF1 protein by the presence of necrosis observed in the tumor tissue samples or the presence of hypertension and diabetes mellitus (**Table 1**). Analysis based on Spearman coefficient revealed that the expression level of KDF1 protein was correlated negatively with the Fuhrman grade (r=-0.215, p=0.001, n=241).

**TABLE 1** | Association between KDF1 protein expression level and clinicopathological parameters.

| Variable | KDF1 expression level in tumor cells (score) | | | | p |
|---|---|---|---|---|---|
| | 0 | 1 | 2 | 3 | |
| **Age (years)** | | | | | |
| <60 number (%) | 20 (15.6) | 49 (38.3) | 49 (38.3) | 10 (7.8) | 0.210 |
| ≥60 number (%) | 25 (21.9) | 43 (37.7) | 38 (33.3) | 8 (7.0) | |
| **Gender** | | | | | |
| Male number (%) | 31 (19.7) | 60 (38.2) | 54 (24.4) | 12 (7.6) | 0.460 |
| Female number (%) | 13 (15.5) | 32 (38.1) | 33 (39.3) | 6 (7.1) | |
| **Tumor size** | | | | | |
| ≤4 cm number (%) | 23 (16.1) | 56 (39.2) | 53 (37.1) | 11 (7.7) | 0.449 |
| >4 cm number (%) | 21 (21.4) | 36 (36.7) | 34 (34.7) | 7 (7.1) | |
| **Stage** | | | | | |
| 1∼2 number (%) | 36 (16.9) | 87 (40.8) | 72 (33.8) | 18 (8.5) | 0.865 |
| 3∼4 number (%) | 8 (28.6) | 5 (17.9) | 15 (53.6) | 0 (0.0) | |
| **Fuhrman grade** | | | | | |
| 1-2 number (%) | 28(15.1) | 67 (36.0) | 73 (39.2) | 18 (9.7) | 0.0004 |
| 3-4 number (%) | 16 (29.1) | 25 (45.5) | 14 (25.5) | 0 (0.0) | |
| **Location** | | | | | |
| Left number (%) | 25 (22.3) | 42(37.5) | 35(31.3) | 10 (8.9) | 0.268 |
| Right number (%) | 19(14.7) | 50 (38.8) | 52 (40.3) | 8 (6.2) | |
| **Smoking** | | | | | |
| Yes number (%) | 15 (22.4) | 26 (38.8) | 22 (32.8) | 4 (6.0) | 0.250 |
| No number (%) | 29 (16.7) | 66 (37.9) | 65(37.4) | 14 (8.0) | |
| **Drinking** | | | | | |
| Yes number (%) | 4 (14.3) | 13 (46.4) | 11 (29.3) | 0 (0.0) | 0.683 |
| No number (%) | 40 (18.8) | 79 (37.1) | 76 (35.7) | 18 (8.5) | |
| **Hypertension** | | | | | |
| Yes number (%) | 18 (20.0) | 38 (42.2) | 29 (32.2) | 5 (5.6) | 0.179 |
| No number (%) | 26 (17.2) | 54 (35.8) | 58 (38.4) | 13 (8.6) | |
| **Diabetes** | | | | | |
| Yes number (%) | 3 (11.5) | 13 (50.0) | 9 (34.6) | 1 (3.8) | 0.876 |
| No number (%) | 41 (18.2) | 79 (35.1) | 88 (39.1) | 17 (7.5) | |
| **Necrosis in tumor** | | | | | |
| Yes number (%) | 5 (13.2) | 13 (34.2) | 18 (47.4) | 2 (5.3) | 0.287 |
| No number (%) | 39 (19.2) | 79 (38.9) | 69 (34.0) | 16 (7.9) | |

*Number, the number of patients.*

## Results of Survival Analysis Based on KDF1 Protein Level in the Tumor Tissue of ccRCC Patients

To determine whether the expression level of KDF1 is associated with the survival, patients were divided into lower KDF1 protein group (including patients of score 0 and 1) and higher KDF1 protein group (including patients of score 2 and 3) according to the immunostaining intensity for KDF1 in the tumor tissue and a survival analysis using Kaplan-Meier method was performed. As shown in **Figure 3**, patients with higher KDF1 protein level in the tumor tissues were found to have a longer OS and DSS when compared with patients with lower KDF1 protein.

Analysis based on Univariable Cox regression revealed that KDF1 protein level in the tumor tissue of ccRCC patients was associated significantly with both OS and DSS along with the age of the patients, the size of the tumors, Fuhrman grade and tumor stage. Analysis based on Multivariable Cox regression revealed that the level of KDF1 protein in the tumor tissue was not associated significantly with the OS of the patients, but it still had a significant association with the DSS along with the tumor stage and tumor Fuhrman grade (**Tables 2** and **3**).

## Effect of Overexpression of KDF1 on the Proliferation, Migration and Invasion of ccRCC Cells

To determine the possible role of KDF1 in ccRCC cells, we first examined the effect of KDF1 overexpression on the phenotype of ACHN and 786-O cells. KDF1 over-expressing ccRCC cells ACHN-KDF1 and 786-O-KDF1 were established through stably transducing ACHN and 786-O cells with the recombinant lentivirus Lenti-KDF1. The increased expression of KDF1 mRNA (16.75 ± 2.98 vs 1 ± 0.24 and 1.19 ± 0.30 in ACHN cells, $p<0.01$; 18.72 ± 1.96 vs 1 ± 0.30 and 1.14 ± 0.37 in 786-O cells, $p<0.01$) and protein (4.06 ± 0.41 vs 1 and 1.04 ± 0.07 in ACHN cells, $p<0.01$; 4.27 ± 0.36 vs 1 and 0.98 ± 0.05 in 786-O cells, $p<0.01$) in the cells was proved by quantitative RT-PCR and Western blot (**Figure 4A**). As shown in **Figure 4**, overexpression of KDF1 significantly inhibited the proliferation (0.74 ± 0.08 vs 1 ± 0.07 and 1.03 ± 0.10 in ACHN cells at 72h, $p<0.01$; 0.89 ± 0.05 vs 1.0 ± 0.14 and 1.04 ± 0.11 in 786-O cells at 72h, $p<0.05$, **Figure 4B**) and invasion (0.56 ± 0.12 vs 1 ± 0.11 and 0.99 ± 0.06 in ACHN cells, $p<0.01$; 0.46 ± 0.05 vs 1 ± 0.10 and 1.01 ± 0.07 in 786-O cells, $p<0.01$, respectively, **Figure 4C**) of ACHN and 786-O cells. However,

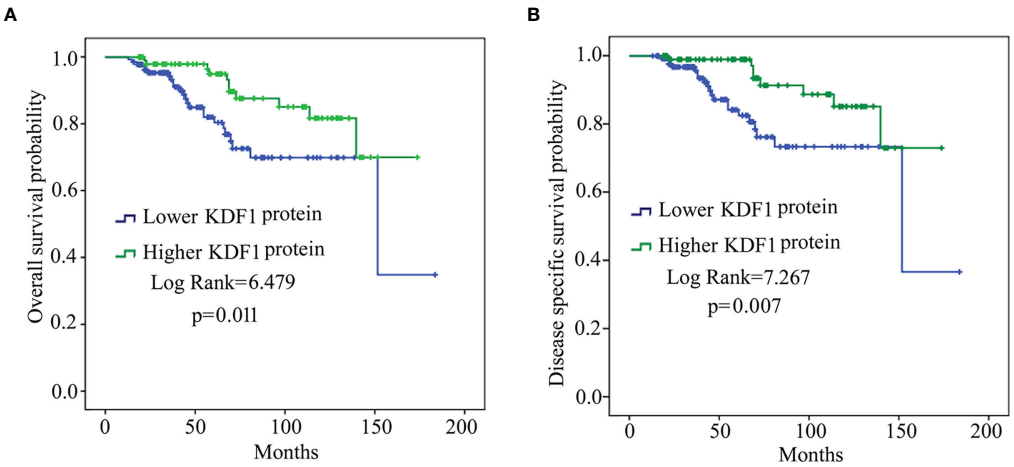



**FIGURE 3** | Results of survival analysis of patients with clear cell renal cell carcinoma (ccRCC) based on KDF1 protein level in the tumor tissue. A total of 241 ccRCC patients were included. The patients were divided into lower KDF1 protein subgroup (with immunostaining score for KDF1 in the tumor tissue being 0 or 1, n=136) and higher KDF1 protein subgroup (with immunostaining score for KDF1 in the tumor tissue being 2 or 3, n=105) according to the level of KDF1 protein in the tumor tissue of the patients. The overall survival **(A)** and disease-specific survival **(B)** were compared between the two subgroups by using Kaplan-Meier method.

significantly decreased migration was only observed in 786-O cells (0.60 ± 0.08 vs 1 ± 0.06 and 1.02 ± 0.09, p<0.01, **Figure 4D**).

## Overexpression of KDF1 Significantly Decreased the Growth of Xenograft Tumors Produced by ACHN Cells

?A3B2 twb 0.24w?>Given that overexpression of KDF1 was found to decrease the proliferation of ccRCC cells *in vitro*, we suppose that overexpression of KDF1 might also reduce the growth of ccRCC tumor. To test this possibility, a xenograft trial was performed by using the untransduced, control virus transduced and KDF1 over-expressing ACHN cells. As shown in **Figure 5A**, ACHN cells over-expressing KDF1 produced much smaller xenograft tumors compared with those produced by the control cells (0.73 ± 0.21 vs 1 ± 0.08 and 0.99 ± 0.14 in size, p<0.01; 0.43 ± 0.08 vs 1 ± 0.20 and 0.89 ± 0.18 in weight, p<0.01). To determine whether the decreased tumors were caused by the decreased proliferation of ccRCC cells, we further examined the expression of ki-67, a molecular marker for proliferation cells, in the tumor tissues. As shown in **Figure 5B**, the percentage of ki-67 positive cells in the tumors derived from the KDF1 overexpression cells was significantly lower compared with that in tumors derived from the control cells (28.11 ± 2.41 vs 35.59 ± 1.91 and 36.32 ±

**TABLE 2** | Univariable and multivariable Cox regression analysis for overall survival.

| Variables | Univariate analysis | | Multivariate analysis | |
|---|---|---|---|---|
| | HR (95.0% CI) | p value | HR (95.0% CI) | p value |
| Age ≤59 vs >59 (years) | 3.15 (1.51-6.58) | 0.002 | 2.15 (1.00-4.65) | 0.051 |
| Stage 1~2 vs 3~4 | 3.82 (1.92-7.61) | 0.0001 | 2.25 (1.06-4.79) | 0.036 |
| Gender Male vs female | 0.98 (0.48-2.01) | 0.954 | | |
| Tumor size ≤4 vs >4 (cm) | 2.05 (1.04-4.04) | 0.038 | 1.41 (0.68-2.91) | 0.356 |
| Fuhrman Grade 1~2 vs 3~4 | 5.17 (2.60-10.29) | 0.000003 | 3.17 (1.48-6.81) | 0.003 |
| KDF1 level Low vs high | 0.40 (0.20-0.83) | 0.014 | 0.52 (0.25-1.10) | 0.085 |
| Hypertension Yes vs no | 0.99 (0.49-1.97) | 0.968 | | |
| Diabetes Mellitus Yes vs no | 0.85 (0.26-2.78) | 0.786 | | |

*HR, hazard ratio; CI, confidence interval.*

**TABLE 3 |** Univariable and multivariable Cox regression analysis for Disease specific survival.

| Variables | Univariate analysis | | Multivariate analysis | |
|---|---|---|---|---|
| | HR (95.0% CI) | p value | HR (95.0% CI) | p value |
| Age ≤59 vs >59 (years) | 2.26 (1.04-4.92) | 0.04 | 1.11 (0.47-2.65) | 0.807 |
| Stage 1~2 vs 3~4 | 5.49 (2.60-11.59) | 0.000008 | 2.55 (1.12-5.81) | 0.026 |
| Gender Male vs female | 0.92 (0.41-2.05) | 0.840 | | |
| Tumor size ≤4 vs >4 (cm) | 3.38 (1.49-7.69) | 0.004 | 2.16 (0.92-5.07) | 0.076 |
| Fuhrman Grade 1~2 vs 3~4 | 9.14 (3.87-21.55) | 0.0000004 | 5.77 (2.32-14.31) | 0.0002 |
| KDF1 level Low vs high | 0.34 (0.15-0.77) | 0.010 | 0.42 (0.18-0.97) | 0.041 |
| Hypertension Yes vs no | 0.91 (0.41-1.99) | 0.806 | | |
| Diabetes Mellitus Yes vs no | 1.11 (0.33-3.68) | 0.868 | | |

*HR, hazard ratio; CI, confidence interval.*

1.93, p<0.01). However, we did not observed difference in the structure of the tumors (**Figure 5C**).

## Knock-Down of KDF1 in KDF1 Over-Expressing Cells Restore the Phenotype of ccRCC Cells

To determine whether the phenotypic changes in KDF1 overexpressing ccRCC cells is caused by the increased KDF1 in the cells, we knocked down the expression of KDF1 in the KDF1 overexpressing cells by transducing them with a shRNA overexpression recombinant lentivirus, which was designed to express a shRNA targeting KDF1. As shown in **Figure 6A**, transduction of the KDF1 over-expressing cells 786-O-KDF1 and ACHN-KDF1 with the lentivirus significantly reduced the expression of KDF1 mRNA (1.47 ± 0.54, 18.22 ± 3.57 and 1 ± 0.22 in the knockdown, KDF1 overexpression and untransduced 786-O cells; 1.41 ± 0.57, 17.71 ± 4.16 and 1 ± 0.21 in the knockdown, KDF1 overexpression and untransduced ACHN cells) and protein (1.06 ± 0.58, 5.02 ± 0.84 and 1 in the knockdown, KDF1 overexpression and untransduced 786-O cells; 1.11 ± 0.56, 4.69 ± 1.00, and 1 in the knockdown, KDF1 overexpression and untransduced ACHN cells) in these cells. In the meanwhile, it markedly reversed the ccRCC cells' inhibition in the proliferation (0.96 ± 0.09, 0.84 ± 0.04 and 1 ± 0.13 in the knockdown, KDF1 overexpression and untransduced 786-O cells at 72 h; 0.94 ± 0.05, 0.72 ± 0.05 and 1 ± 0.10 in the knockdown, KDF1 overexpression and untransduced ACHN cells at 72 h, **Figure 6B**), migration (1.04 ± 0.13, 0.72 ± 0.08 and 1 ± 0.15 in the knockdown, KDF1 overexpression and untransduced 786-O cells; 1.01 ± 0.03, 0.94 ± 0.03 and 1 ± 0.04 in the knockdown, KDF1 overexpression and untransduced ACHN cells, **Figure 6C**) and invasion (0.98 ± 0.10, 0.48 ± 0.08 and 1 ± 0.09 in the knockdown, KDF1 overexpression and untransduced 786-O cells; 1.13 ± 0.20, 0.67 ± 0.16 and 1 ± 0.11 in the knockdown, KDF1 overexpression and untransduced ACHN cells, **Figure 6D**) caused by KDF1 overexpression.

# DISCUSSION

In the present study, we examined the expression of KDF1 in the tumor tissue of ccRCC patients using two cohorts of patients and compared it with the clinicopathological indices of the patients. Analysis based on RNA sequencing data from TCGA database showed that the expression level of KDF1 mRNA decreased markedly in the tumor tissues of ccRCC patients compared with that in the normal renal tissues. The expression level of KDF1 mRNA was found to correlate negatively with tumor grade and tumor stage, and positively with patients' OS. In accordance with the results of mRNA expression, KDF1 protein was also found to be down-regulated in the tumor tissues of ccRCC patients compared with that in the normal renal tissues. The decreased expression of KDF1 in the tumor tissue was further confirmed by Western blot analysis. The level of KDF1 protein in the cancer cells was found to correlate negatively with tumor grade. Patients of ccRCC with higher KDF1 protein in cancer cells were found to have longer OS and DSS and KDF1 was demonstrated to be an independent factor associated with patients' DSS. Based on the above results, we believe that patients with higher KDF1 expression tend to have better prognosis compared with those with lower KDF1 expression. It is believed that renal cell carcinoma including ccRCC is derived from renal tubular epithelial cells. The present clinical finding suggested that down-regulation of KDF1 might be involved in the pathogenesis of ccRCC and KDF1 might function as a tumor suppressor. In support of this idea, in the present study, overexpression of KDF1 was observed to decrease the proliferation, migration and invasion of ccRCC cells, which could be reversed by knocking down the expression of KDF1 in the cells. Also, KDF1 over-expressing ccRCC cells were found to produce significantly smaller tumors in the xenograft tests. Furthermore, decreased ki-67 positive cells were observed in the xenograft tumor tissue derived from the KDF1 overexpression ccRCC cells compared with those xenograft tumors derived from

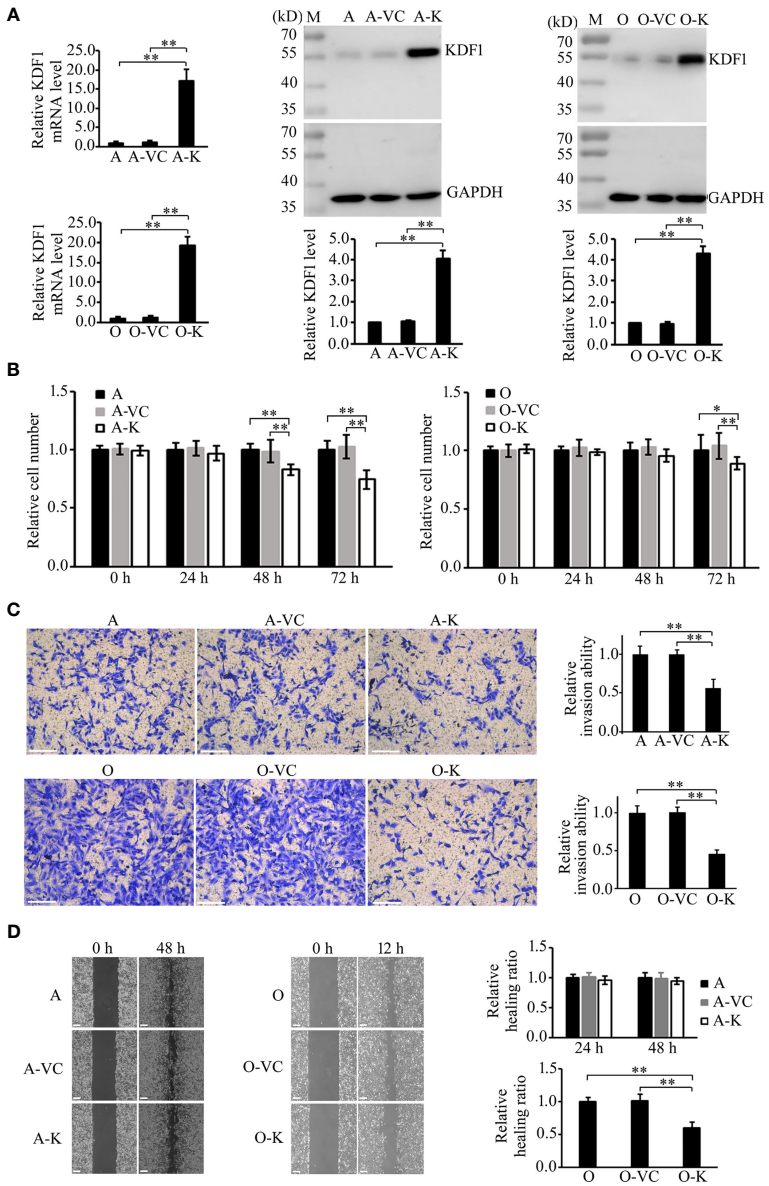



**FIGURE 4** | Effect of KDF1 overexpression on the proliferation, migration and invasion of ccRCC cells. Two ccRCC cell lines, 786-O and ACHN, were used in the experiments. The KDF1 overexpression ccRCC cells, 786-O-KDF1 and ACHN-KDF1, were constructed *via* stably infecting 786-O and ACHN cells with a recombinant KDF1 expression lentivirus. The overexpression of KDF1 in ccRCC cells were confirmed by quantitative RT-PCR and Western blot **(A)** and the influence of KDF1 overexpression in the proliferation **(B)**, migration **(C)** and invasion **(D)** of the ccRCC cells were evaluated by using CCK-8, wound healing and Matrigel invasion chamber methods. All the experiments were repeated at least three times. A, untransduced ACHN cells; A-VC, control virus transduced ACHN cells; A-K, KDF1 overexpression ACHN cells; O, untransduced 786-O cells; O-VC, control virus transduced 786-O cells; O-K, KDF1 overexpression 786-O cells. *$p < 0.05$; **$p < 0.01$. Scale bar, 100μm.

the control ccRCC cells. To our knowledge, this is the first report on the expression and role of KDF1 in ccRCC.

KDF1 was first reported by Lee and his colleagues in a forward genetic study, in which KDF1 was demonstrated to play a key role in the development of normal epidermis through regulating the proliferation and differentiation of keratinocytes (6). Since then, several other studies have reported the involvement of KDF1 in ectodermal organ development (7–9). In particular, mutation of KDF1 has been reported to be associated with tooth agenesis (7, 9). Interestingly, there is an emerging debate about the connection of tooth agenesis to cancer: On the one hand, some family studies indicated that presence of tooth agenesis meant higher incidence of some cancers including colorectal cancer and epithelial ovarian cancer, but on the other hand, some case-controlled molecular studies showed that there was no significant association

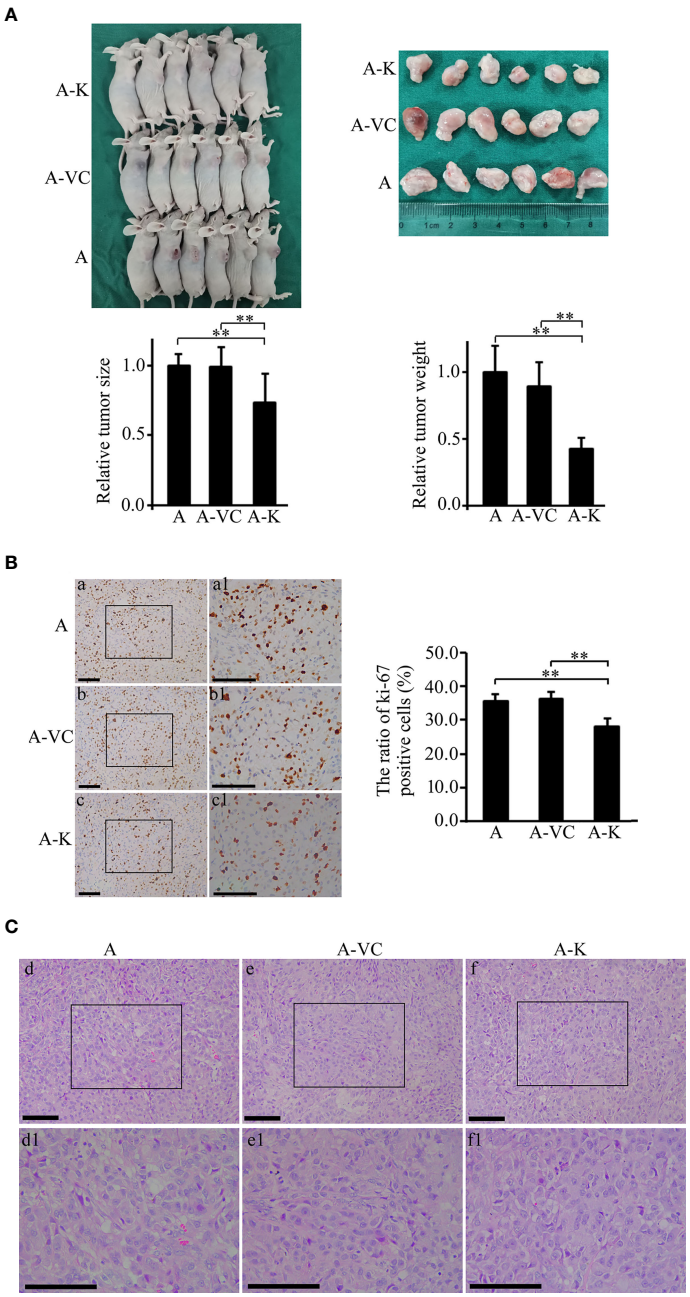



**FIGURE 5** | Overexpression of KDF1 significantly decreased the growth of transgrafted tumors and the ratio of ki-67 positive cells in the tumor. Four-week old male nude mice were randomly divided into non-transduced cell group, control virus transduced cell group and KDF1 overexpression cell group. Six mice were used in each group. For each mouse, $2\times10^6$ cells (untransduced ACHN cells for the untransduced cell group, control virus transduced ACHN cells for the control virus transduced cell group, and KDF1 overexpression ACHN cells for the KDF1 overexpression cell group) were transplanted subcutaneously on the side of the body. Six weeks later, the mice were euthanized and the tumors were removed, measured and weighed. Paraffin sections of the transgrafted tumors were used in Hematoxylin-Eosin (HE) staining and immunohistochemical staining for ki-67. Figure part **(A)** Results of the tumor transplant trial showing that overexpression of KDF1 decreased the growth of transgrafted tumors. Figure part **(B)** Results of immunohistochemical staining for ki-67 showing that overexpression of KDF1 decreased the ratio of ki-67 positive cells in the transgrafted tumors. Figure part **(C)** Results of HE staining showing no structural difference among the tumor tissues. A, the untransduced cell group; A-VC, the control virus transduced cell group; A-K, the KDF1 overexpression cell group. a1-f1 is a partial magnification of a-f, respectively. $^{**}P < 0.01$.

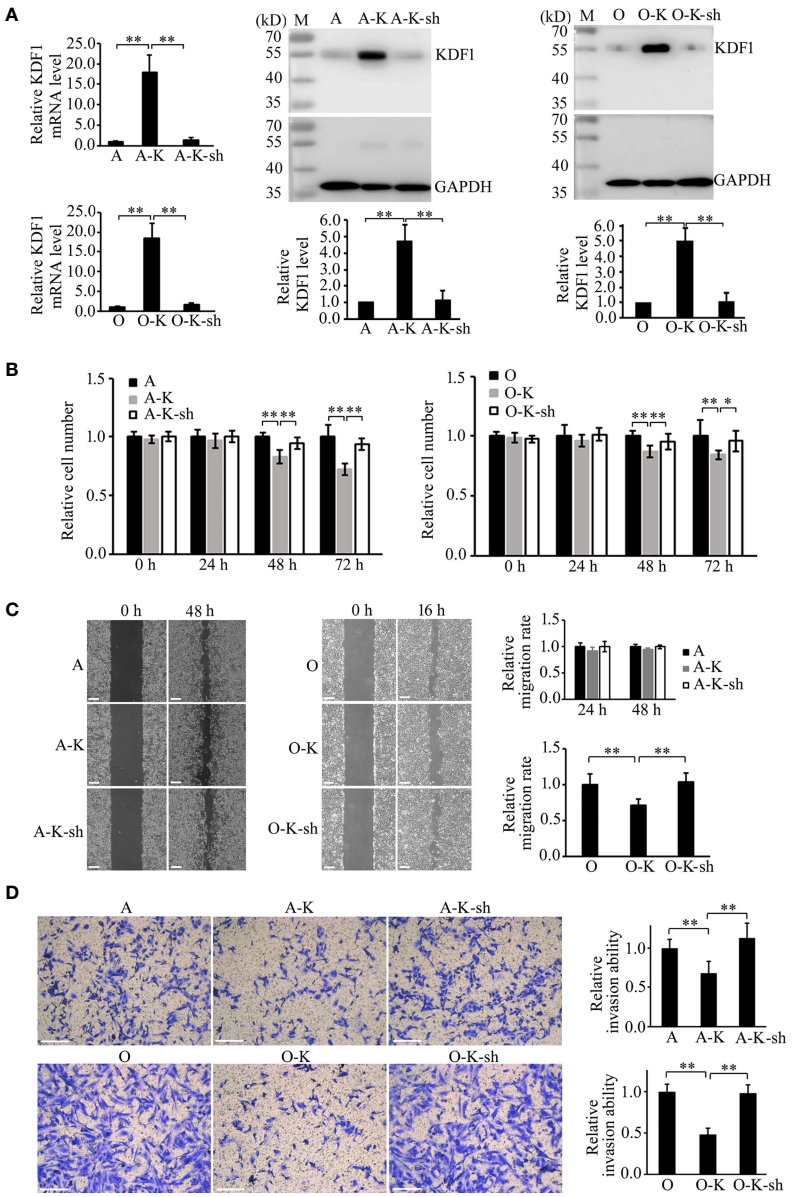



**FIGURE 6** | Knockdown of KDF1 reversed the effect of KDF1 overexpression on the ccRCC cell's proliferation, migration and invasion. A recombinant KDF1 shRNA expression lentivirus was used to knock down the expression of KDF1 in the KDF1 overexpression ccRCC cells. The knockdown of KDF1 expression was confirmed by quantitative RT-PCR and Western blot analysis **(A)** and the influence of KDF1 knockdown in the proliferation **(B)**, migration **(C)** and invasion **(D)** of the KDF1 overexpression ccRCC cells were evaluated by using CCK-8, wound healing and Matrigel invasion chamber methods. All the experiments were repeated at least three times. A, untransduced ACHN cells; A-K, KDF1 overexpression ACHN cells; A-K-sh, the KDF1 knockdown A-K; O, untransduced 786-O cells; O-K, KDF1 overexpression 786-O cells; O-K-sh, the KDF1 knockdown O-K; *$p < 0.05$; **$p < 0.01$. Scale bar, 100μm.

between tooth agenesis and the occurrence of these cancer (10). Given the common signaling pathways shared in tooth development and tumorigenesis (10), the molecular abnormity that caused tooth agenesis may also lead to tumorigenesis. To our knowledge, no study has reported the role of KDF1 in cancer. Thus, the present finding about the involvement of KDF1 in ccRCC not only has broadened the window of understanding the pathological function of KDF1, but has also provided a novel link between tooth agenesis and ccRCC. However, further systematic research should be performed before exact conclusion can be drawn.

As a newly discovered molecule, data about the function of KDF1 is still limited. To make things worse, although it is an evolutionarily conserved protein, there is no homologous experimental structure available that would serve as a good-confidence support for modeling the 3D structure of KDF1 (11). Thus, the functional information deduced from structural bioinformatic analysis about this molecule is quite limited.

According to the prediction of secondary structure, KDF1 is unlikely to be an enzyme or transmembrane transporter or receptor, instead, it might function as a protein-binding adaptor, scaffold and/or cofactor (7). Indeed, stratifin was found to interact genetically with KDF1 (6) and in a recent study, KDF1 was found to regulate skin differentiation through deubiquitination and stabilization of IKKa (12). In addition, *shd* mutant was also found opposite in phenotype to a previously mutant caused by p63 loss (6, 13–15) and in the study carried out by Lee et al., reducing the dosage of p63 rescued many aspects of the *shd* phenotype (6), indicating that KDF1 regulates Keratinocyte differentiation through inhibiting the expression of p63. Stratifin, also known as 14-3-3-σ, is a protein member of 14-3-3 family, which has been reported to be involved in a variety of essential cellular functions including cell proliferation, differentiation, survival, apoptosis, and cytoskeletal integrity (16). As a transcription factor of p53 family, p63 has been well-studied and proved to play a crucial role in the regulation of epidermal cell proliferation and differentiation. In addition, the protein has been reported to be involved in the development of many tumors through regulating the expression of its target genes (17). IKKa is key member of NF-κB signaling system. Through regulating the degradation of IκB, the specific inhibitor of NFκB, IKKα plays a key role in NFκB based signal transduction, which is important in a variety of biological process including inflammation and tumor development (18). Besides, IKKα has also been reported to exert its roles in an NFκB signaling-independent way, which is especially important in the pathogenesis of some cancers (19). Of note, the roles of stratifin, p63 and IKK in tumor development have been demonstrated to be cell context-specific. Both tumor suppressive and promotive roles have been reported for these molecules in different cancers (20–22). Therefore, the functional association of KDF1 with stratifin, p63 and IKK might have pointed a road for dissecting the mechanism underlying the pathogenic role of KDF1 in ccRCC. However, more studies are needed to answer this question.

It should be pointed out that there are some differences in the effects of KDF1 overexpression on the phenotype of the two ccRCC cell lines, 786-O and ACHN. While overexpression of KDF1 significantly reduced the migration of 786-O cells, its influence in the migration of ACHN cells is quietly limited, not reaching the significant level. Again, the influence of KDF1 overexpression in the proliferation of 786-O cells was smaller than that in ACHN cells although it still reached the significant level when compared with the control groups. For the present, we don't know the exact cause for this, but this phenomenon is quite similar to that found in stratifin, p63 and IKK (20–22), three molecules found to be functionally associated with KDF1, and emphasizes the importance of taking the specific cellular context into account when we discuss the function of KDF1.

Limitations are present in the present study. First of all, the population investigated in the present study is not very large, especially in the part of KDF1 protein expression; deviation due to patient selection might be inevitable. Secondly, the present study has not explored the molecular mechanism through which KDF1 exerts its roles. To well dissect the pathologic significance of KDF1, further mechanism research is essential. Thirdly, the present study only used two ccRCC cell lines. Given the fact that the function of KDF1 may be context-specific, it is better to examine the roles of this molecule in more ccRCC cell lines.

In summary, for the first time, the present study investigated the expression and function of KDF1 in the tumor tissue of ccRCC patients. KDF1 was found to be decreasingly expressed in the cancer cells and correlated negatively with the tumor grade and positively the survival of the patients. Overexpression of KDF1 was shown to reduce the proliferation, migration and invasion of ccRCC cells, which could be reversed by re-knock down of KDF1. Also, overexpression of KDF1 was found to inhibit the growth of xenograft tumors. All these suggest that decreased expression of KDF1 is involved in the pathogenesis of ccRCC and KDF1 may function as a tumor suppressor. Thus, the present study has opened a novel window for understanding the pathological function of KDF1 in ccRCC and thrown a novel beam of light on the pathogenic mechanism of the disease. However, further research is still needed to prove our findings and dissect the function of KDF1 in ccRCC.

## DATA AVAILABILITY STATEMENT

The original contributions presented in the study are included in the article/supplementary material. Further inquiries can be directed to the corresponding author.

## ETHICS STATEMENT

The animal study was reviewed and approved by the Animal Care Committee of Taizhou Hospital. All research work concerning human participants was reviewed and approved by the Ethics Committee of Taizhou Hospital.

## AUTHOR CONTRIBUTIONS

J-mZ designed the study, participated in the experiments and analysis of the data, drafted the manuscript and gave final approval of the version to be published. M-fG and H-yY participated in the design of the study, analysis of the data and revision of the manuscript, and gave final approval of the version to be published. L-xY, H-xZ, J-qB, and Y-qG participated in the performance of the experiments, analysis of the data, and gave final approval of the version to be published. Q-xY and Y-hX participated in revision of the manuscript, and gave final approval of the version to be published. All authors contributed to the article and approved the submitted version.

## FUNDING

The project was supported by a Doctor funding from Enze medical center (2017BSKYQDJJ01).

## ACKNOWLEDGMENTS

The authors thank Zi-jing Ye who is affiliated to the research center of Taizhou hospital, for their help in the performance of immunohistochemistry. The authors also thank Cai-ping Xie, who is affiliated to the Department of Pathology, Taizhou Hospital, Wenzhou Medical University, for her help in tumor tissue sample collection.

## REFERENCES

1. Xu W, Atkins MB, McDermott DF. Checkpoint Inhibitor Immunotherapy in Kidney Cancer. *Nat Rev Urol* (2020) 17(3):137–50. doi: 10.1038/s41585-020-0282-3
2. Goyal R, Gersbach E, Yang XJ, Rohan SM. Differential Diagnosis of Renal Tumors With Clear Cytoplasm: Clinical Relevance of Renal Tumor Subclassification in the Era of Targeted Therapies and Personalized Medicine. *Arch Pathol Lab Med* (2013) 137(4):467–80. doi: 10.5858/arpa.2012-0085-RA
3. Gupta K, Miller JD, Li JZ, Russell MW, Charbonneau C. Epidemiologic and Socioeconomic Burden of Metastatic Renal Cell Carcinoma (mRCC): A Literature Review. *Cancer Treat Rev* (2008) 34(3):193–205. doi: 10.1016/j.ctrv.2007.12.001
4. Diamond E, Molina AM, Carbonaro M, Akhtar NH, Giannakakou P, Tagawa ST, et al. Cytotoxic Chemotherapy in the Treatment of Advanced Renal Cell Carcinoma in the Era of Targeted Therapy. *Crit Rev Oncol Hematol* (2015) 96 (3):518–26. doi: 10.1016/j.critrevonc.2015.08.007
5. Blanco AI, Teh BS, Amato RJ. Role of Radiation Therapy in the Management of Renal Cell Cancer. *Cancers (Basel)* (2011) 3(4):4010–23. doi: 10.3390/cancers3044010
6. Lee S, Kong Y, Weatherbee SD. Forward Genetics Identifies Kdf1/1810019J16Rik as an Essential Regulator of the Proliferation-Differentiation Decision in Epidermal Progenitor Cells. *Dev Biol* (2013) 383(2):201–13. doi: 10.1016/j.ydbio.2013.09.022
7. Shamseldin HE, Khalifa O, Binamer YM, Almutawa A, Arold ST, Zaidan H, et al. KDF1, Encoding Keratinocyte Differentiation Factor 1, is Mutated in a Multigenerational Family With Ectodermal Dysplasia. *Hum Genet* (2017) 136 (1):99–105. doi: 10.1007/s00439-016-1741-z
8. Manaspon C, Thaweesapphithak S, Osathanon T, Suphapeetiporn K, Porntaveetus T, Shotelersuk V. A Novel De Novo Mutation Substantiates KDF1 as a Gene Causing Ectodermal Dysplasia. *Br J Dermatol* (2019) 181 (2):419–20. doi: 10.1111/bjd.18007
9. Zeng B, Lu H, Xiao X, Yu X, Li S, Zhu L, et al. KDF1 is a Novel Candidate Gene of non-Syndromic Tooth Agenesis. *Arch Oral Biol* (2019) 97:131–6. doi: 10.1016/j.archoralbio.2018.10.025
10. Bonczek O, Krejci P, Izakovicova-Holla L, Cernochova P, Kiss I, Vojtesek B. Tooth Agenesis: What do We Know and is There a Connection to Cancer? *Clin Genet* (2021) 99(4):493–502. doi: 10.1111/cge.13892
11. Uhlén M, Björling E, Agaton C, Szigyarto CA, Amini B, Andersen E, et al. A Human Protein Atlas for Normal and Cancer Tissues Based on Antibody Proteomics. *Mol Cell Proteomics* (2005) 4(12):1920–32. doi: 10.1074/mcp.M500279-MCP200
12. Li Y, Tang L, Yue J, Gou X, Lin A, Weatherbee SD, et al. Regulation of Epidermal Differentiation Through KDF1-mediated Deubiquitination of Ikkα. *EMBO Rep* (2020) 21(5):e48566. doi: 10.15252/embr.201948566
13. Mills AA, Zheng B, Wang XJ, Vogel H, Roop DR, Bradley A. p63 is a p53 Homologue Required for Limb and Epidermal Morphogenesis. *Nature* (1999) 398(6729):708–13. doi: 10.1038/19531
14. Yang A, Schweitzer R, Sun D, Kaghad M, Walker N, Bronson RT, et al. p63 is Essential for Regenerative Proliferation in Limb, Craniofacial and Epithelial Development. *Nature* (1999) 398(6729):714–8. doi: 10.1038/19539
15. Truong AB, Kretz M, Ridky TW, Kimmel R, Khavari PA. p63 Regulates Proliferation and Differentiation of Developmentally Mature Keratinocytes. *Genes Dev* (2006) 20(22):3185–97. doi: 10.1101/gad.1463206
16. Smith AJ, Daut J, Schwappach B. Membrane Proteins as 14-3-3 Clients in Functional Regulation and Intracellular Transport. *Physiol (Bethesda)* (2011) 26(3):181–91. doi: 10.1152/physiol.00042.2010
17. Perez CA, Pietenpol JA. Transcriptional Programs Regulated by p63 in Normal Epithelium and Tumors. *Cell Cycle* (2007) 6(3):246–54. doi: 10.4161/cc.6.3.3801
18. Quan XX, Hawk NV, Chen W, Coupar J, Lee SK, Petersen DW, et al. Targeting Notch1 and Ikkα Enhanced Nf-κb Activation in CD133(+) Skin Cancer Stem Cells. *Mol Cancer Ther* (2018) 17(9):2034–48. doi: 10.1158/1535-7163.Mct-17-0421
19. The Cancer Genome Atlas Network. Comprehensive Genomic Characterization of Head and Neck Squamous Cell Carcinomas. *Nature* (2015) 517(7536):576–82. doi: 10.1038/nature14129
20. Ta N, Huang X, Zheng K, Zhang Y, Gao Y, Deng L, et al. Mirna-1290 Promotes Aggressiveness in Pancreatic Ductal Adenocarcinoma by Targeting Ikk1. *Cell Physiol Biochem* (2018) 51(2):711–28. doi: 10.1159/000495328
21. Patel A, Garcia LF, Mannella V, Gammon L, Borg TM, Maffucci T, et al. Targeting P63 Upregulation Abrogates Resistance to MAPK Inhibitors in Melanoma. *Cancer Res* (2020) 80(12):2676–88. doi: 10.1158/0008-5472.Can-19-3230
22. Shiba-Ishii A, Kim Y, Shiozawa T, Iyama S, Satomi K, Kano J, et al. Stratifin Accelerates Progression of Lung Adenocarcinoma At an Early Stage. *Mol Cancer* (2015) 14:142. doi: 10.1186/s12943-015-0414-1

**Conflict of Interest:** The authors declare that the research was conducted in the absence of any commercial or financial relationships that could be construed as a potential conflict of interest.

*Copyright © 2021 Zheng, Gan, Yu, Ye, Yu, Xia, Zhou, Bao and Guo. This is an open-access article distributed under the terms of the Creative Commons Attribution License (CC BY). The use, distribution or reproduction in other forums is permitted, provided the original author(s) and the copyright owner(s) are credited and that the original publication in this journal is cited, in accordance with accepted academic practice. No use, distribution or reproduction is permitted which does not comply with these terms.*

frontiers in Oncology

SYSTEMATIC REVIEW
published: 03 June 2021
doi: 10.3389/fonc.2021.678459

# Oncological Outcomes of Patients With Different Pathological Features of pT3a Renal Tumor: A Systematic Review and Quantitative Synthesis

*Pengju Guo†, Yongxing Wang†, Yili Han, Dechao Wei, Jiahui Zhao, Mingchuan Li, Yongguang Jiang* and Yong Luo**

*Department of Urology, Beijing Anzhen Hospital, Capital Medical University, Beijing, China*

**Purpose:** To identify the differences in oncological outcomes for patients with different pT3a renal tumor invasion patterns and pathological features.

**Methods:** The protocol of this study was registered on PROSPERO (CRD42021234475). Relevant studies were identified by searching the PubMed, Cochrane library, Embase, and Web of Science databases. Cancer-specific survival (CSS) was selected as the endpoint. Pooled hazard ratio (HR) and 95% confidence interval (CI) extracted from multivariate Cox models were evaluated to identify the hazard association.

**Results:** A total of 22 studies, which enrolled 12384 patients were included for quantitative synthesis. Sinus fat invasion (SFI) + perinephric fat invasion (PFI) was associated with inferior CSS compared to SFI only ($p = 0.02$). Comparable CSS was observed between SFI and PFI ($p = 0.57$). SFI ± PFI showed inferior CSS compared to PFI only ($p = 0.0002$). The presence of pelvicalyceal system invasion significantly increased the risk of cancer-specific mortality ($p = 0.0005$). Renal vein invasion (RVI) indicated poor oncological outcomes in terms of CSS ($p = 0.002$). The concomitant RVI and fat invasion (FI) significantly increased the risk of deterioration of CSS compared to RVI or FI ($p < 0.0001$). Multiple invasion patterns translated into a significantly decreased CSS ($p < 0.0001$). Aggressive tumor behavior, including lymph node involvement ($p = 0.006$), distant metastases ($p < 0.00001$), sarcomatoid differentiation ($p < 0.0001$), necrosis ($p < 0.0001$), Fuhrman grade III or IV ($p < 0.0001$), positive margin ($p < 0.0001$), and tumor size >7cm ($p < 0.0001$) were the predictors of inferior CSS. The lymphovascular invasion ($p = 0.67$) was indolent in terms of CSS.

**Conclusion:** This study confirmed the heterogenicity of pT3a renal tumors. Multiple invasion patterns could translate into a significantly decreased CSS, and SFI should not be merged in the SFI + PFI group. The presence of PSI or RVI could significantly increase the risk of cancer-specific mortality. Lymph node involvement, distant metastases, sarcomatoid differentiation, necrosis, high Fuhrman grade, positive margin, and size >7cm were the predictors of inferior CSS. A precise-risk grade of CSS for different invasion patterns including comprehensive combinations may be useful for the further refinements of the TNM system.

OPEN ACCESS

***Edited by:***
*Andrea Mari,*
*Careggi University Hospital, Italy*

***Reviewed by:***
*Carlo Terrone,*
*San Martino Hospital (IRCCS), Italy*
*Riccardo Campi,*
*Careggi Hospital, Italy*

****Correspondence:***
*Yongguang Jiang*
*jyganzhen@163.com*
*Yong Luo*
*luoyonganzhen@163.com*

*†These authors have contributed equally to this work*

***Specialty section:***
*This article was submitted to Genitourinary Oncology, a section of the journal Frontiers in Oncology*

***Received:*** *09 March 2021*
***Accepted:*** *06 May 2021*
***Published:*** *03 June 2021*

***Citation:***
*Guo P, Wang Y, Han Y, Wei D, Zhao J, Li M, Jiang Y and Luo Y (2021) Oncological Outcomes of Patients With Different Pathological Features of pT3a Renal Tumor: A Systematic Review and Quantitative Synthesis. Front. Oncol. 11:678459. doi: 10.3389/fonc.2021.678459*

**Systematic Review Registration:** The current study was registered on PROSPERO, and the registration numbers is CRD42021234475.

**Keywords: renal tumor, pT3a, nephrectomy, cancer-specific survival, systematic review**

## INTRODUCTION

Since the publication of the sixth edition of the TNM staging system for renal tumors, the classification of T3a renal tumors has undergone several modifications. Although currently pT3a is defined as a tumor confined to the Gerota's fascia but exhibiting perinephric fat invasion (PFI), sinus fat invasion (SFI), renal vein invasion (RVI), or/and pelvicalyceal system invasion (PSI) regardless of tumor diameter, a realistic controversy is whether pT3a represents a heterogeneous histological group where different elements or a combination may indicate a significant difference in oncological prognosis. The EAU guidelines on renal cell cancer (RCC) state that tumors with SFI might be more aggressive than tumors with PFI, which was consistent with the findings of Thompson et al. (1, 2). However, several studies evaluating oncological outcomes for different pT3a renal tumor invasion patterns have failed to demonstrate the significant difference (3, 4). Lack of consensus on the outcomes of different extrarenal extension patterns may result from the unstandardized definitions for the histological assessment of fat invasion in the early years and discrepancies in study design (2, 5).

Our understanding of the heterogeneous behavior of renal tumors has been well advanced. The increasing interest in adjuvant treatment, immunotherapy and targeted therapies has prompted the need for more accurate staging of renal tumors (5–9). In the clinical context, some pT3a renal tumors are confirmed by postoperative pathology, and their incidence is usually underestimated. Therefore, it is important to accurately predict the prognosis of different pT3a renal tumor invasion patterns to guide the follow-up protocols and evaluate the effect of postoperative therapies on survival. Given the continuing controversy over pT3a renal tumor staging, we undertook a systematic review and quantitative synthesis to determine whether pT3a represents a heterogeneous histological group and evaluate the oncological outcomes for different pT3a renal tumor invasion patterns and pathological features.

## METHODS

This study was conducted according to the Preferred Reporting Items for Systematic Reviews and Meta-analysis (PRISMA) criteria, and the protocol was registered on PROSPERO for the study (CRD42021234475).

### Search Strategy

We searched the PubMed, Cochrane Library, Embase, and Web of Science databases for studies investigating the oncological outcomes of pT3a renal tumors from database inception to April 2021, using search terms integrated subject relevant terms ("renal tumor", "renal neoplasm," "renal cancer," and "renal cell carcinoma") and staging terms ("T3a," "pT3a," "T3," "pT3," "renal vein invasion," and "urinary collecting system"). We also reviewed the references cited in the relevant articles to avoid omissions. The detailed Population, Intervention, Comparison, Outcome and Study design (PICOS) framework of the review was shown in **Table 1**. Only articles written in the English language were searched. All retrieved references were independently screened by two investigators (PG and YW) independently. When discordant decisions occurred, the senior authors (YJ and YL) were consulted to make final decisions.

### Study Selection, Data Extraction, and Quality Assessment

The studies on the oncological outcomes for different pT3a renal tumor invasion patterns and pathological features following partial or radical nephrectomy (PN or RN) were included. Cancer-specific survival (CSS) was considered as the single endpoint of oncological outcomes. Conference abstracts, reviews, commentary, editorials, and letters were excluded but checked for cited references. The studies that did not provide CSS with a hazard ratio (HR) and corresponding 95% confidence interval (CI) or p value in the multivariate cox models were also excluded.

Two investigators independently extracted the data from each study. Extracted data included the name of the first author, year of publication, recruitment period, country or region, study type, sample size, surgery types, and size of pathological features of different pT3a renal tumor invasion patterns. HRs and 95% CIs for CSS associated with different pT3a renal tumor invasion patterns and pathological features were extracted for quantitative synthesis. The quality of included studies was assessed using the Quality In Prognosis Studies (QUIPS) tool (10). The six bias domains when evaluating the literatures were study participation, study attrition, prognostic factor measurement,

**TABLE 1** | The Population, Intervention, Comparison, Outcome and Study design (PICOS) framework of the review.

| Parameter | Inclusion criteria |
|---|---|
| Population (P) | Patients with pathological T3a and clinical or pathological N0-1M0-1 renal tumor. |
| Intervention (I) | Partial or radical nephrectomy |
| Comparison (C) | The cancer-specific survival of patients with different tumor invasion patterns or pathological features. |
| Outcome (O) | Cancer-specific survival with the hazard ratio (HR) and corresponding 95% confidence interval (CI) or p values in the multivariate cox models. |
| Study design (S) | Randomized trials, population-based, single and multi-center observational studies, and retrospective studies which were published in English. |

outcome measurement, study confounding, and statistical analysis and reporting. According to the items and considerations, the overall rating assessments were divided into low, moderate, and high risk of bias for each bias domain.

## Quantitative Synthesis and Analysis

The comparisons of CSS between different tumor invasion patterns were evaluated by the pooled HRs with corresponding 95% CIs. The statistical heterogeneity among studies was evaluated by the Cochrane Q test and quantified by $I^2$ value. $I^2 \leq 50\%$ indicated no or moderate heterogeneity, and a fixed-effect model was applied. On the contrary, $I^2 > 50\%$ indicated obvious heterogeneity, and a random-effect model was applied. The quantitative synthesis of HRs was evaluated by the inverse variance technique, and the quantitative synthesis of risk differences was evaluated by the Mantel-Haenszel test. The sensitivity analysis was conducted by one-removed analysis. Based on the recommendations of the Cochran manual, the evaluation of publication bias was conducted by using Egger's test only when there were 10 or more included studies (11). The certainty of the evidence were evaluated according to the Grading of Recommendations Assessment, Development, and Evaluation (GRADE) approach, which yields four levels of evidence (i.e., very low, low, moderate, and high) (12). All statistical tests were performed using Review Manager 5.4 (Cochrane Collaboration, Oxford, UK) and Stata 15.1 (StataCorp., College Station, Texas). Statistical significance was set at $p < 0.05$, and all specified p values were two-sided.

# RESULTS

Among the 655 potential studies that were identified from the aforementioned databases, 139 studies were excluded due to duplication. After screening the titles and abstracts, 363 studies were found to be unsuitable for full text screening and were excluded. Based on the inclusion criteria, we conducted the full-text evaluation of the remaining 153 studies, among which 23 studies did not focus on the patients with pT3a renal tumor, 16 studies did not report the HRs of the CSS, 52 studies did not compare the CSS for patients with different invasion patterns or pathological features, 13 studies were reviews, 10 study were comments, 13 studies were not published in English, and two studies were case reports. Among the 24 full-text articles assessed for eligibility, two studies that only reported the relevant HRs in the univariate Cox models were also excluded. Finally, 22 studies enrolling 12,384 patients were included in the quantitative synthesis (**Figure 1**) (2–7, 13–28).

The enrolled studies were published between 2005 and 2021, and included 12 (54.5%) studies published over the past five years. All the enrolled studies were retrospective, and the recruited patients had no direct ipsilateral adrenal invasion. The recruited patients were from Asia, Europe, and USA. Ten studies focused only on patients following RN, 12 studies included patients who received PN or RN (**Table 2**). Using the QUIPS tool, the risk of bias for each enrolled study was assessed and the results are shown in **Figure 2**. Also, two enrolled studies used data from the Surveillance, Epidemiology, and End Results

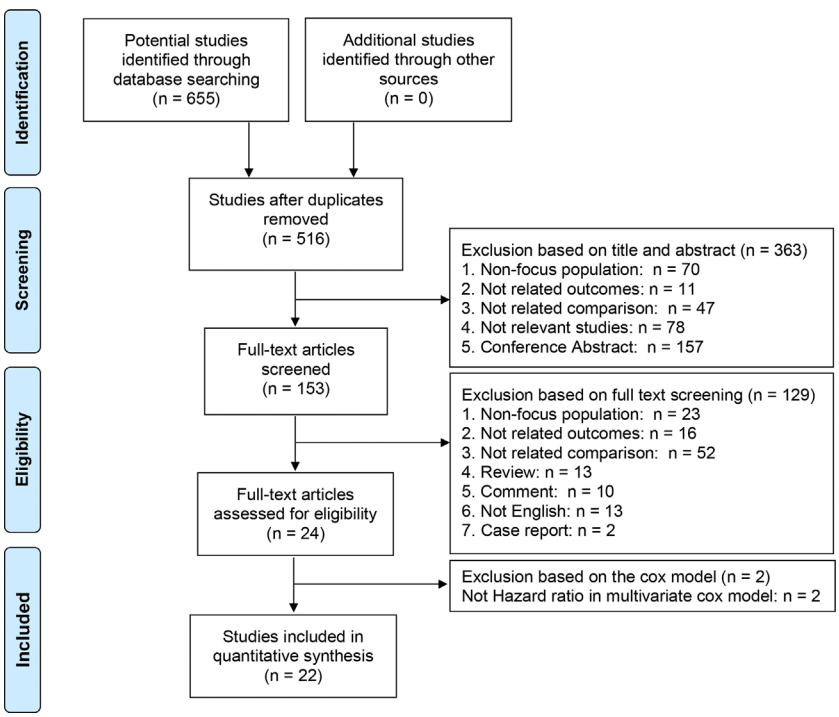



**FIGURE 1** | Flow diagram of study selection.

**TABLE 2 |** Characteristics of the included studies.

| Author | Year | Country | Recruitment period | Study design | Institution | Stage | Surgery type | Outcome | Cox model | Follow-up (mo) |
|---|---|---|---|---|---|---|---|---|---|---|
| Thompson (2) | 2005 | USA | 1970–2002 | RTP | Single | N0-1 M0-1 | RN | CSS | Multi | 72(24–408)* |
| Margulis (13) | 2007 | USA | 1990-2006 | RTP | Single | N0-1 M0-1 | PN, RN | CSS | Uni, Multi | 33.5(6.1–158.6)* |
| Poon (4) | 2009 | USA | 1988–2007 | RTP | Multiple | N0-1 M0-1 | PN, RN | CSS | Uni, Multi | 24(9–48)* |
| Bedke (14) | 2009 | Germany | 1990–2007 | RTP | Single | N0-1 M0-1 | RN | CSS | Uni, Multi | 34.8(14.4–109.2)* |
| Bertini (15) | 2009 | Italy | 1989–2006 | RTP | Single | N0-1 M0-1 | RN | CSS | Uni, Multi | 38(2–240)* |
| Kresowik (16) | 2010 | USA | 1997–2007 | RTP | Single | N0-1 M0-1 | PN, RN | CSS | Multi | 25.3(0–96.4)** |
| Chen (24) | 2017 | China | 2006–2015 | RTP | Single | N0 M0 | RN | CSS | Uni, Multi | 31 (3.4–109.7) |
| Park (17) | 2017 | South Korea | 1997–2012 | RTP | Single | N0 M0 | PN, RN | CSS | Multi | 58.1(37.2–86.5)* |
| Guo (18) | 2019 | China | 1979–2014 | RTP | Multiple | N0 M0 | RN | CSS | Uni, Multi | NA |
| Shah (5) | 2019 | USA | 1970–2011 | RTP | Single | N0 M0 | RN | CSS | Uni, Multi | 111.6(81.6–160.8)* |
| Wang (6) | 2020 | China | 2010–2016 | RTP | Multiple | N0-1 M0-1 | PN, RN | CSS | Multi | 24(10–46)* |
| da Costa (19) | 2012 | Brazil | 1992–2009 | RTP | Single | N0-1 M0-1 | PN, RN | CSS | Multi | 28.6(3–60)** |
| Baccos (20) | 2013 | Italy | 2000–2011 | RTP | Single | N0-1 M0-1 | RN | CSS | Uni, Multi | 31(12–68.2)* |
| Flood (21) | 2020 | Canada | 2011–2017 | RTP | Single | N0-1 M0-1 | RN | CSS | Multi | 33.8(20.6–55.4)* |
| Schiavina (22) | 2015 | Italy | 2000–2013 | RTP | Single | N0-1 M0 | RN | CSS | Uni, Multi | 32(18–62)* |
| Brookman-May (3) | 2015 | Germany | 1992–2010 | RTP | Multiple | N0 M0 | PN, RN | CSS | Multi | NA |
| Peng (23) | 2017 | China | 2007–2012 | RTP | Single | N0 M0 | PN, RN | CSS | Multi | 35.5(10–86)* |
| Oh (7) | 2018 | South Korea | 1988–2015 | RTP | Multiple | N0 M0 | PN, RN | CSS | Uni, Multi | 38.8(NA)** |
| Capitanio (25) | 2018 | Italy | 1988–2015 | RTP | Multiple | N0 M0 | PN, RN | CSS | Multi | 52(NA)** |
| Bailey (26) | 2017 | USA | 2001–2010 | RTP | Single | N0-1 M0-1 | RN | CSS | Uni, Multi | 98.4 (72–129.6)* |
| Garcia Marchinena (27) | 2019 | Argentina | 2000–2016 | RTP | Multiple | N0 M0 | PN, RN | CSS | Uni, Multi | 21(1–194)* |
| Lai (28) | 2021 | China | 2000–2018 | RTP | Single | N0-x M0 | PN, RN | CSS | Uni, Multi | 48(NA)* |

| Author | Year | No.pT3a | No.PFI only (%) | No.SFI only (%) | No.SFI+PFI (%) | No.SFI ± PFI (%) | No.FI (%) | No.RVI ± FI (%) | No.RVI+FI (%) | No.RVI only (%) | No.PSI (%) |
|---|---|---|---|---|---|---|---|---|---|---|---|
| Thompson (2) | 2005 | 205 | 162 (79.0) | 16 (7.8) | 27 (13.2) | 43 (21) | NA | NA | NA | NA | NA |
| Margulis (13) | 2007 | 365 | 199 (54.5) | 96 (26.3) | 70 (19.2) | 166 (45.5) | NA | NA | NA | NA | 331 (90.7) |
| Poon (4) | 2009 | 230 | 167 (72.6) | NA | NA | 63 (27.4) | NA | NA | NA | NA | NA |
| Bedke (14) | 2009 | 106 | 58 (54.7) | 27 (25.5) | 21 (19.8) | 48 (45.3) | NA | NA | NA | NA | NA |
| Bertini (15) | 2009 | 105 | 70 (66.7) | 16 (15.2) | 19 (18.1) | 35 (33.3) | NA | NA | NA | NA | NA |
| Kresowik (16) | 2010 | 110 | 36 (32.7) | 41 (37.2) | 33 (30) | 74 (67.3) | NA | NA | 57 (51.2) | NA | NA |
| Chen (24) | 2017 | 163 | 79 (48.5) | 11 (6.7) | NA | NA | NA | 87 (53.4) | NA | NA | 40 (24.5) |
| Park (17) | 2017 | 266 | 92 (34.6) | 51 (19.2) | 29 (10.9) | 80 (30.1) | 172 (64.7) | 94 (35.3) | 69 (25.9) | 25 (9.4) | NA |
| Guo (18) | 2019 | 1869 | 687 (36.8) | 381 (20.4) | 105 (5.6) | 486 (26.0) | 1173 (62.8) | NA | 696 (37.2) | NA | NA |
| Shah (5) | 2019 | 563 | 114 (20.2) | 51 (9.1) | NA | NA | NA | NA | NA | 163 (29.0) | NA |
| Wang (6) | 2020 | 5290 | 2569 (48.5) | 1975 (37.3) | 746 (14.1) | NA | NA | NA | NA | NA | NA |
| da Costa (19) | 2012 | 46 | NA | NA | NA | NA | 24 (52.1) | NA | 11 (23.9) | 11 (23.9) | NA |
| Baccos (20) | 2013 | 122 | NA | NA | NA | NA | 63 (51.6) | 59 (48.4) | 41 (33.6) | 18 (14.8) | NA |
| Flood (21) | 2020 | 160 | NA | NA | NA | NA | NA | 97 (61) | NA | NA | 24 (15) |
| Schiavina (22) | 2015 | 185 | NA | NA | NA | NA | NA | NA | NA | NA | NA |
| Brookman-May (3) | 2015 | 1247 | NA | NA | NA | NA | 1036 (83.1) | 211 (16.9) | NA | NA | NA |
| Peng (23) | 2017 | 125 | NA | NA | NA | NA | 89 (71.2) | NA | NA | 36 (28.8) | NA |
| Oh (7) | 2018 | 211 | NA | NA | NA | NA | 124 (58.8) | 87 (41.2) | 47 (22.3) | 40 (19.0) | NA |
| Capitanio (25) | 2018 | 309 | 164 | 68 | NA | NA | NA | NA | NA | NA | NA |
| Bailey (26) | 2017 | 325 | NA | NA | NA | NA | NA | NA | NA | NA | 27 (8.3) |
| Garcia Marchinena (27) | 2019 | 293 | 111 (37.9) | 36 (12.3) | 35 (11.9) | 118 (40.3) | 253 (86.3) | 91 (31.1) | 57 (19.5) | 34 (11.6) | 35 (11.9) |
| Lai (28) | 2021 | 89 | NA | NA | NA | NA | 71 (79.8) | 36 (40.4) | 18 (20.2) | 18 (20.2) | NA |

*RTP, retrospective; PN, partial nephrectomy; RN, radical nephrectomy; NOS, Newcastle-Ottawa Scale; NA, not applicable; SFI, sinus fat invasion; PFI, perinephric fat invasion; RVI, renal vein invasion; FI, fat invasion; PSI, pelvicaliceal system invasion.*

**Median (IQR).*

***Mean (range).*

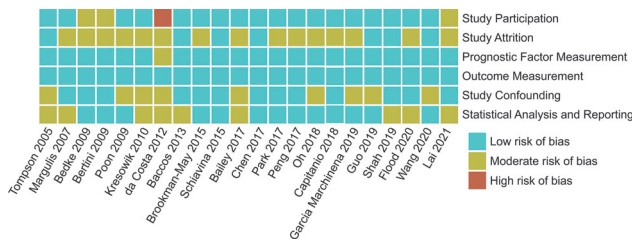



**FIGURE 2** | Risk of Bias for each enrolled studies assessed by QUIPS (Quality In Prognosis Studies) tool.

(SEER) database (6, 18). However, due to the recruitment period and the fact that most reported pathological features were different, it was reasonable to include these two studies. When two studies reported the endpoints of the same pathological features, we selected the most recent outcomes, i.e., those reported by Wang et al., because of the enrolled patients identified between 2010 to 2016 (6).

## Cancer-Specific Survival of Different Invasion Patterns

CSS results were available from 19 studies for different tumor invasion patterns. Although the pooled results revealed that SFI only (n = 631) had comparable CSS to PFI only (n = 903) (HR, 0.92; 95% CI, 0.69–1.23; p = 0.57; $I^2$ = 20%; **Figure 3A**), SFI + PFI (n = 138) was associated with inferior CSS as compared to SFI only (n = 422) (HR, 1.97; 95% CI, 1.13–3.42; p = 0.02; $I^2$ = 2%; **Figure 3B**). SFI ± PFI (n = 126) showed inferior CSS as compared to PFI only (n = 290) (HR, 1.81; 95% CI, 1.33–2.47; p = 0.0002; $I^2$ = 0%; **Figure 3C**). The pooled results revealed that patients with PSI (n = 102) had inferior CSS as compared to those without PSI (n = 676) (HR, 1.91; 95% CI, 1.33–2.75; p = 0.0005; $I^2$ = 0%; **Figure 3D**). Patients with RVI (n = 531) had inferior CSS as compared to those without RVI (n = 1484) (HR, 1.45; 95% CI, 1.15–1.82; p = 0.002; $I^2$ = 47%; **Figure 3E**), and the coexistence of RVI and fat invasion (FI) (n = 168) showed further deterioration of CSS as compared to RVI or FI (n = 477) (HR, 2.13; 95% CI, 1.52–2.99; p = 0.002; $I^2$ = 0%; **Figure 3F**). The multiple invasion pattern (n = 1266) was associated with inferior CSS as compared to single pattern (n = 1226) (HR, 1.77; 95% CI, 1.49–2.09; p < 0.00001; $I^2$ = 0%; **Figure 3G**). Using the GRADE approach, the certainty of SFI only vs. PFI only was low, while that of RVI+FI vs. RVI or FI was high. The certainty of SFI+PFI vs. SFI only, SFI ± PFI vs. PFI only, PSI vs. non-PSI, RVI vs. non-RVI and multiple vs. single pattern were all moderate (**Table 3**).

## Cancer-Specific Survival of Different Pathological Features

The pooled results revealed that lymph node involvement (n = 398; HR, 1.71; 95% CI, 1.17–2.50; p = 0.006; $I^2$, 67%; **Figure 4A**), distant metastases (n = 726; HR, 3.36; 95% CI, 2.88–3.91; p < 0.00001; $I^2$ = 42%; **Figure 4B**), sarcomatoid differentiation (n = 436; HR, 2.09; 95% CI, 1.78–2.46; p < 0.00001; $I^2$ = 12%; **Figure 4C**), Fuhrman grade III or IV (n = 1737; HR, 2.70; 95% CI, 2.18–3.34; p < 0.00001; $I^2$ = 0%; **Figure 4D**), necrosis (n = 640; HR, 1.96; 95% CI, 1.54–2.49; p < 0.00001; $I^2$ = 0%; **Figure 4E**), tumor size >7 cm (n = 1571; HR, 1.77; 95% CI, 1.46–2.15; p < 0.00001; $I^2$ = 1%; **Figure 4F**), and positive margin (n = 28; HR, 7.61; 95% CI, 4.12-14.04; p < 0.00001; $I^2$ = 32%; **Figure 4G**) were associated with inferior CSS. The lymphovascular invasion (LVI) (n = 159; HR, 1.11; 95% CI, 0.69-1.80; p = 0.67; $I^2$ = 0%; **Figure 4H**) was not a predictor of inferior CSS. Using the GRADE approach, the certainty of lymph node involvement and LVI were low. Tumor size >7 cm and necrosis showed moderate certainty. The certainty of metastases, sarcomatoid differentiation, Fuhrman grade III or IV, and positive margin status were all high.

## Sensitivity Analysis

The sequential omission of a single study was conducted to test the stability of pooled results. The merged HRs for CSS did not significantly change, which revealed the robustness of the results. (**Figure 5**).

## Publication Bias

The evaluation of publication bias was conducted using Egger's test only when there were 10 or more included studies. There was no significant publication bias in CSS study of sarcomatoid differentiation (Egger's test p = 0.232).

# DISCUSSION

Classifying tumors from the surgical perspective and optimizing prognostic discrimination are the cardinal principles in the refinements of the TNM system as T3a renal tumor contains a wide range of four patterns of extrarenal extension regardless of tumor diameter and is confirmed by postoperative pathology in general. Nevertheless, the accuracy and rationality of T3a classification have been questioned in the context of inconsistency of individual oncological outcomes reported in the last fifteen years (3, 16, 18, 21). In the current study, we integrated the available clinical evidence and experience by conducting this systematic review and quantitative synthesis.

The major findings of the current study are the following: First, the moderate-certainty evidence suggests that SFI + PFI was associated with inferior CSS as compared to SFI only. The low-certainty evidence of comparable CSS between SFI only and PFI only and the moderate-certainty evidence of inferior CSS of SFI ± PFI compared to PFI only further support the above findings. Several studies, which merged SFI only and SFI + PFI into a single group given the oncological equipoise derived from their cohorts, may be imprecise (2, 15). Second, moderate-certainty evidence suggests that the presence of PSI indicated significantly poor oncological outcome, with a 1.91 times increased risk of cancer-specific mortality (CSM). Although numerous studies have highlighted the adverse effect of PSI on oncological outcomes, the independent prognostic value of PSI has been excluded from the second to seventh edition of AJCC

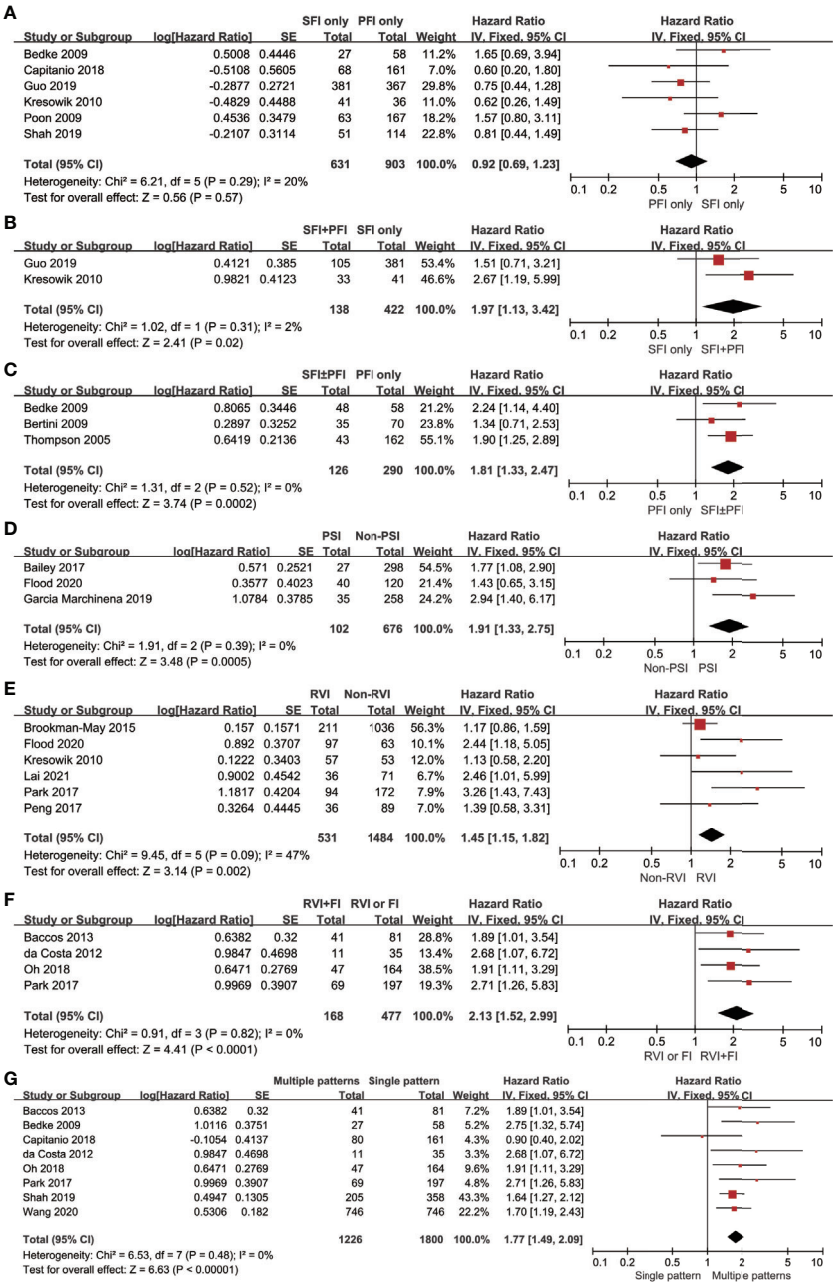



**FIGURE 3** | Forrest plots of hazards ratio (HR) evaluating the significant predictors of cancer-specific survival for different pT3a renal tumor invasion patterns. **(A)**: SFI only vs PFI only; **(B)**: SFI + PFI vs SFI only; **(C)**: SFI ± PFI vs PFI only; **(D)**: PSI vs non-PSI; **(E)**: RVI vs non-RVI; **(F)**: RVI + FI vs RVI or FI; **(G)** Multiple patterns vs Single pattern. SFI, sinus fat invasion; PFI< perinephric fat invasion; PSI, pelvicaliceal system invasion; RVI, renal vein invasion; FI, fat invasion.

TNM system (26, 27, 29–31). Palapattu et al. reported a strong relationship between PSI, lymph node invasion and distant metastases (32). Third, high-certainty evidence suggests that the concomitance of RVI and FI significantly increased the risk of deterioration of CSS as compared to RVI or FI supported the finding that multiple invasion patterns translated into moderate-certainty evidence of significantly decreased CSS. However, most contemporary studies that reported the prognostic heterogeneity of T3a RCC failed to comprehensively explore the survival difference among the various combinations. A precise-risk grade of CSS for different invasion patterns, including comprehensive combinations, may be useful for further refinements of the TNM system. Finally, high-certainty evidence indicates that distant metastases, sarcomatoid differentiation, high Fuhrman grade and positive margin were the predictors of inferior CSS. Tumor size >7cm and necrosis

**TABLE 3 |** The overall quality of evidence according to the GRADE (Grading of Recommendations Assessment, Development, and Evaluation) approach.

| Comparison | Certainty assessment | | | | | | No. of patients | | Effect | | Certainty | Importance |
|---|---|---|---|---|---|---|---|---|---|---|---|---|
| | No. of Studies | Risk of bias | Inconsistency | Indirectness | Imprecision | Large effect | Case | Control | HRs | 95% CI | | |
| SFI only vs PFI only | 6 | not serious | not serious | not serious | serious | No | 631 | 903 | 0.92 | 0.69–1.23 | ⨁⨁◯◯ LOW | IMPORTANT |
| SFI+PFI vs SFI only | 2 | not serious | not serious | not serious | not serious | No | 138 | 422 | 1.97 | 1.13–3.42 | ⨁⨁⨁◯MODERATE | IMPORTANT |
| SFI ± PFI vs PFI only | 3 | not serious | not serious | not serious | not serious | No | 126 | 290 | 1.81 | 1.33–2.47 | ⨁⨁⨁◯ MODERATE | IMPORTANT |
| PSI vs non-PSI | 3 | not serious | not serious | not serious | not serious | No | 102 | 676 | 1.91 | 1.33–2.75 | ⨁⨁⨁◯ MODERATE | IMPORTANT |
| RVI vs non-RVI | 6 | not serious | not serious | not serious | not serious | No | 531 | 1484 | 1.45 | 1.15–1.82 | ⨁⨁⨁◯ MODERATE | IMPORTANT |
| RVI+FI vs RVI or FI | 4 | not serious | not serious | not serious | not serious | Yes | 168 | 477 | 2.13 | 1.52–2.99 | ⨁⨁⨁⨁ HIGH | IMPORTANT |
| Multiple vs Single pattern | 8 | not serious | not serious | not serious | not serious | No | 1226 | 1800 | 1.77 | 1.49–2.09 | ⨁⨁⨁◯ MODERATE | IMPORTANT |
| Node<br>N1 vs N0/x | 6 | not serious | serious | not serious | not serious | No | 398 | 1912 | 1.71 | 1.17–2.5 | ⨁⨁◯◯ LOW | IMPORTANT |
| Metastases<br>M1 vs M0 | 8 | not serious | not serious | not serious | not serious | Yes | 726 | 1844 | 3.36 | 2.88–3.91 | ⨁⨁⨁⨁ HIGH | IMPORTANT |
| Sarcomatoid<br>Yes vs No | 10 | not serious | not serious | not serious | not serious | Yes | 436 | 3185 | 2.09 | 1.78–2.46 | ⨁⨁⨁⨁ HIGH | IMPORTANT |
| Fuhrman grade<br>III or IV vs II or I | 8 | not serious | not serious | not serious | not serious | Yes | 1737 | 1065 | 2.7 | 2.18–3.34 | ⨁⨁⨁⨁ HIGH | IMPORTANT |
| Necrosis<br>Yes vs No | 6 | not serious | not serious | not serious | not serious | No | 640 | 699 | 1.96 | 1.54–2.49 | ⨁⨁⨁◯ MODERATE | IMPORTANT |
| Size<br>>7cm vs ≤ 7cm | 5 | not serious | not serious | not serious | not serious | No | 1571 | 1811 | 1.77 | 1.46–2.15 | ⨁⨁⨁◯ MODERATE | IMPORTANT |
| Margin status<br>positive vs negative | 6 | not serious | not serious | not serious | not serious | Yes | 28 | 1154 | 7.61 | 4.12–14.04 | ⨁⨁⨁⨁ HIGH | IMPORTANT |
| LVI vs non-LVI | 3 | not serious | not serious | not serious | not serious | No | 159 | 290 | 1.11 | 0.69–1.8 | ⨁⨁◯◯ LOW | IMPORTANT |

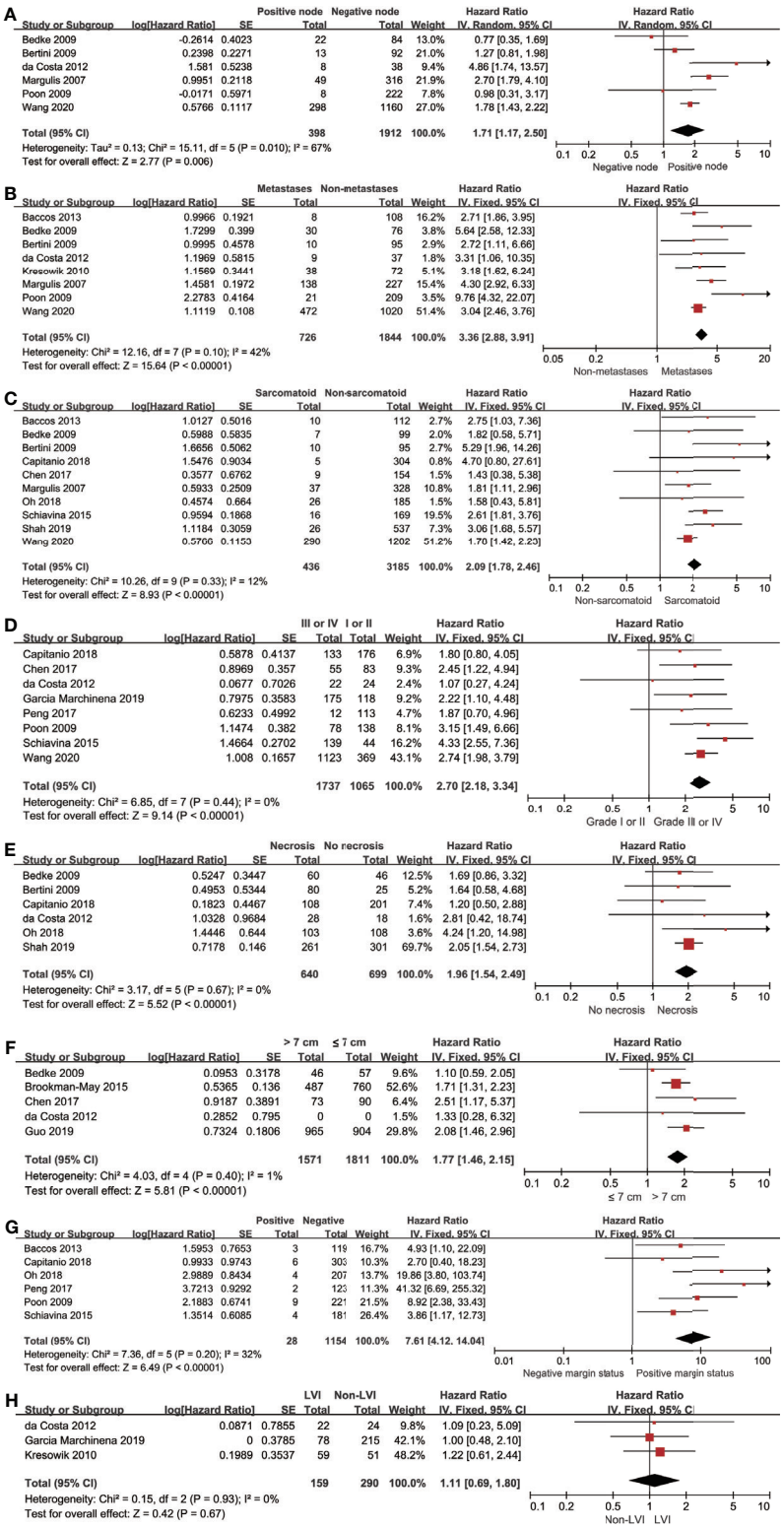



**FIGURE 4** | Forrest plots of Hazards ratio (HR) evaluating the significant predictors of cancer-specific survival for different pathological features of pT3a. **(A)**: lymph node involvement; **(B)**: distant metastases; **(C)**: sarcomatoid differentiation; **(D)**: Fuhrman grade (III, IV vs I, II); **(E)**: tumor necrosis; **(F)**: tumor size (>7 cm vs ≤ 7cm); **(G)**: positive margin status; **(H)**: lymphovascular invasion.

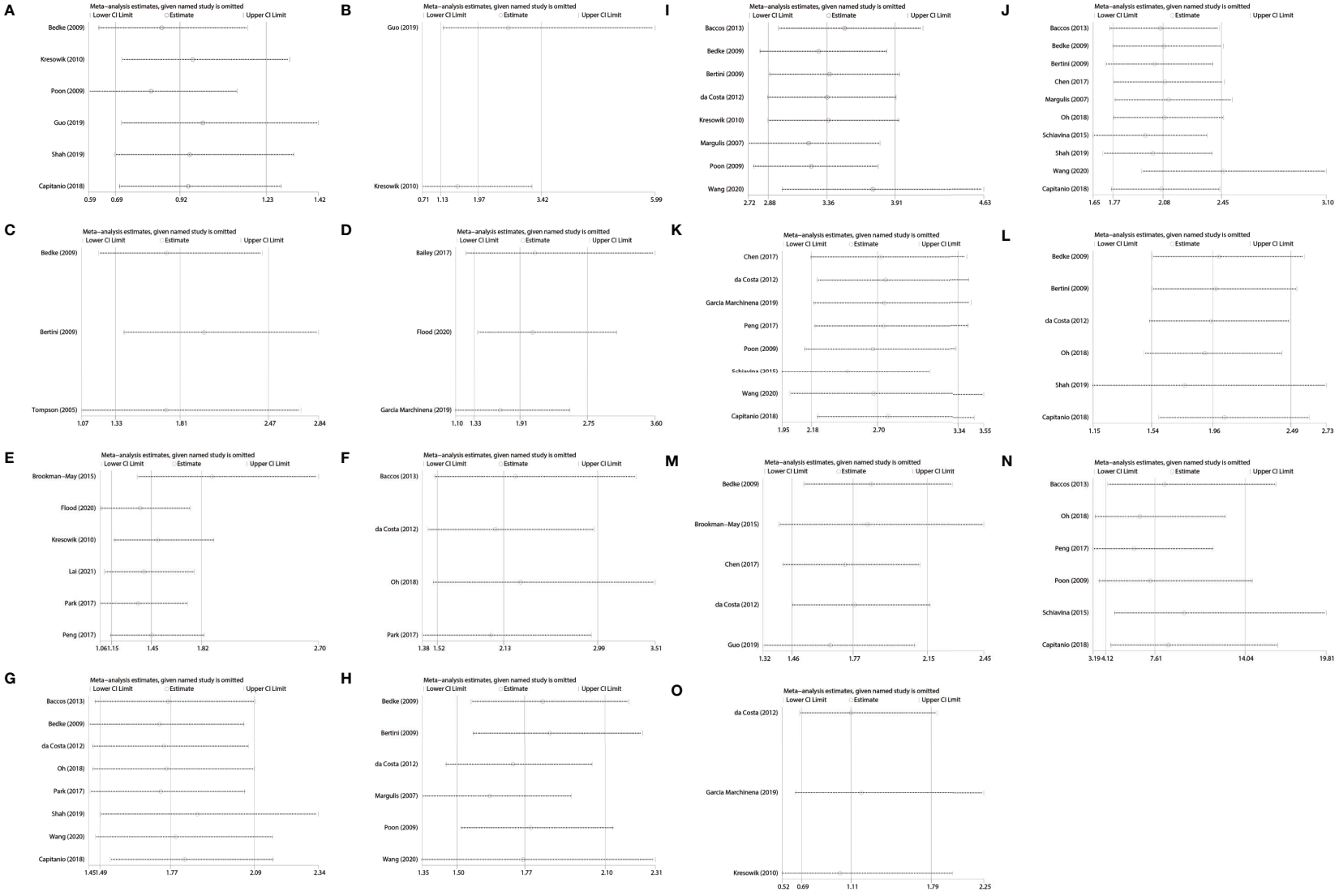



**FIGURE 5** | Sensitive analysis of the included studies by one-removed analysis. **(A)**: SFI only vs PFI only; **(B)**: PFI + SFI vs SFI only; **(C)**: SFI ± PFI vs PFI only; **(D)**: PSI vs non-PSI; **(E)**: RVI vs non RVI; **(F)**: RVI + FI vs RVI or FI; **(G)**: multiple vs single pattern; **(H)**: lymph node involvement; **(I)**: distant metastases; **(J)**: sarcomatoid differentiation; **(K)**: Fuhrman grade (III, IV vs I, II); **(L)**, tumor necrosis; **(M)**: tumor size (> 7 cm vs ≤ 7 cm); **(N)**, positive margin status; **(O)**, lymphovascular invasion; SFI, sinus fat invasion; PFI, perinephric fat invasion; PSI, pelvicaliceal system invasion; RVI, renal vein invasion; FI, fat invasion.

also increased the risk of deterioration of CSS, which represents the moderate-certainty evidence. The low-certainty evidence suggests that lymph node involvement might increase the risk of CSM and the lymphovascular invasion was indolent in terms of CSS. The comparable CSS between SFI only and PFI only and the indolent impact of lymphovascular invasion on the survival are inconsistent with the EAU guidelines on RCC, which underlines the prognostic value of several anatomical and histological factors (1). This may require further validation due to the low-certainty evidence.

The inevitable risk of bias caused by the type of surgery that might affect the results of the included studies should be highlighted, even though it had been adjusted in the studies, which included patients undergoing PN or RN. Several studies reported comparable CSS for upstaged pT3a PN patients compared to pT3a RN patients (33, 34). However, the significantly smaller tumor size of the PN cohort compared to the tumor size of the RN cohort indicated that organ confined tumors are susceptible to receive PN. Given the absence of the standardized pathological protocol of capsular invasion in the early years, the classification of renal capsular invasion patterns was an unreliable prognostic variable in some previous studies (2, 35). The recommended routine histopathological examination of perirenal fat was conducted on a discounted basis among patients with peripheral renal tumor since the specimens of renal sinus fat were not systematically collected during PN, especially in the context of the PN enthusiasm (36). The aforementioned factors might have led to the underreported frequency of SFI. Grignon et al. noted that pT1b and pT2 renal tumors probably represented a shrinking proportion when the renal sinus was carefully evaluated (37). In the last two decades, TNM staging classification system for renal tumors was refined three times, which may affect the accuracy and manifolds of pT3a and the heterogeneity of study designs despite minor changes.

Given the increasing PN implementation, the realistic concern is the positive margin, which occurs more frequently in patients with aggressive features, including pT2a, pT3a, and grade III-IV (38, 39). Shah et al. reported that positive margin significantly increased the rate of recurrence, especially among patients with aggressive pathological features, including pT2-T3a, high Fuhrman grade, and clear cell histology (39). In their study, recurrence was observed in almost one third of patients who were up staged to pT3a after PN (40). Bensalah et al. found that positive margin did not cause a decrease CSS; however, the fact that the mean tumor size was 3.5 ± 2 cm, and almost 90% of the positive margin cohort were patients with T1–2 RCC made their conclusions not necessarily applicable to patients with pT3a patients (41). Although several studies mentioned the controversial impact of positive margin on the oncological prognosis among patients with localized RCC, according to the current results that identified more than seven times risk of CSM in patients with pT3a RCC and postoperative positive margin compared to those with negative margin, the weak recommendation of EAU guidelines for intensive follow-up of patients with positive margin may be imprecise (1, 42, 43).

Several studies have highlighted the impact of tumor size on CSS for T3a renal tumor (3, 18, 22, 39, 44–48). In light of the agreement of some studies in which a cutoff of 7 cm was recommended as a prognosis prediction for T3a renal tumor and the applicability of the refinement for the current TNM classification, only the results that considered tumor diameter as a binary variable by using a cutoff of 7cm were merged in the current study. We found that patients with pT3a renal tumor > 7 cm experienced an additional 77% risk of CSM, which was consistent with the findings of Brookman-May et al, reporting that tumor size was identified with the highest prediction accuracy by increasing 71% risk of CSM with a 7 cm cutoff (3). Although the tumor size did not result as a predictor of prognosis in several studies, which cannot be ignored, this is not necessarily contrary to our results and should be further analyzed in the context of the design of the studies and evaluation of patients (14, 19). Whether the impact of tumor size on prognosis can induce T3a and T1/T2 reintegration needs further validation. Chevinsky et al. reported that pT3a had significantly inferior RFS compared to pT1/T2 (45). Chen et al. found that patients with pT3a renal cell carcinoma showed poorer disease-free survival (DSS) as compared to pT1a, pT1b, pT2a, and pT2b. However, Yoo et al. reported a comparable CSS and DSS between pT2 and pT3a ≤ 7cm (49).

The results of the current study may be used to guide the follow-up protocols and select patients suitable for adjuvant therapy after nephrectomy. A compact interval of surveillance may be vital for patients with aggressive factors. Although limited evidence suggested that compact postoperative imaging intervals did not result in the early detection of recurrence, which would benefit survival, the EAU guidelines on RCC recommend a risk-based approach to stratify follow-up for different patients, based on the individual aggressive anatomical, histological and clinical factors (1, 50). The S-TRAC trail exhibited superior disease-free survival (DFS) with sunitinib support. The PROTECT study also reported an improved DFS in the intention to treat pazopanib 800mg population (51). Among the highest-risk subpopulation, the ATLAS study found that axitinib translated into a 36% and 27% reduction in risk of a DFS event per investigator and by independent review committee, respectively (52). However, the recent SORCE trial results, which focused on the DFS and overall survival (OS) in patients with an intermediate or high risk of recurrence, failed to offer positive evidence of sorafenib (53). A recent meta-analysis revealed that adjuvant use of tyrosine kinase inhibitors (TKI) did not translate into improved OS, but showed a benefit in DFS in overall and high-risk populations (54). Due to the lack of sufficient evidence that adjuvant therapy with vascular endothelial growth factor receptor (VEGFR) –TKI offers survival benefits for patients with high-risk RCC, the EAU guidelines on RCC do not recommend the adjuvant therapy after nephrectomy (1). However, heterogeneity among the enrolled patients could be the main cause of the negative results (55). In light of the non-strict inclusion criteria of previous studies, supplemental randomized trials are necessary to determine whether patients with aggressive patterns or characteristics of pT3a renal tumors may benefit from adjuvant treatment.

The present study has some limitations. First, the retrospective nature of the included studies inevitably led the selection bias.

Second, the inevitable risk of bias caused by the type of surgery might affect the results. Third, most contemporary studies failed to comprehensively explore the survival difference among the various combinations. Fourth, the determination of the patterns of pT3a renal tumor invasion and pathological features were made by different pathologists, probably based on different criteria. Finally, a small sample of some included studies increased the variability of results.

## CONCLUSION

The current study identified the heterogenicity of pT3a renal tumors. Multiple invasion patterns could translate into a significantly decreased CSS, and SFI only should not be merged with the SFI + PFI group. The presence of PSI or RVI could significantly increase the risk of cancer-specific mortality. Lymph node involvement, distant metastases, sarcomatoid differentiation, necrosis, high Fuhrman grade, positive margin, and tumor size >7cm are the predictors of inferior CSS. The follow-up protocols and postoperative therapies after nephrectomy should be conducted with individuation according to a risk-based approach for stratification based on these aggressive pathological characteristics. External validation and a precise-risk grade of CSS for different invasion patterns, including comprehensive combinations, may be useful for the further refinements of the TNM system.

## DATA AVAILABILITY STATEMENT

The original contributions presented in the study are included in the article/supplementary material. Further inquiries can be directed to the corresponding authors.

## AUTHOR CONTRIBUTIONS

PG and YW contributed to the design of the study. YH and DW were responsible for literature search. PG and JZ were responsible for data extraction and analysis. PG and ML were responsible for drafting the manuscript. YJ and YL approved the submitted version. All authors contributed to the article and approved the submitted version.

## FUNDING

This study was supported by the Natural Science Foundation of Beijing Municipality (award no. 7192053).

## REFERENCES

1. Ljungberg B, Albiges L, Bedke J, Bex A, Capitanio U, Giles RH, et al. (2021). Eau Guidelines on Renal Cell Carcinoma. In: *Presented at the EAU Annual Congress Milan 2021.* Arnhem, The Netherlands: EAU Guidelines Office
2. Thompson RH, Leibovich BC, Cheville JC, Webster WS, Lohse CM, Kwon ED, et al. Is Renal Sinus Fat Invasion the Same as Perinephric Fat Invasion for pT3a Renal Cell Carcinoma? *J Urol* (2005) 174(4 Pt 1):1218–21. doi: 10.1097/01.ju.0000173942.19990.40
3. Brookman-May SD, May M, Wolff I, Zigeuner R, Hutterer GC, Cindolo L, et al. Evaluation of the Prognostic Significance of Perirenal Fat Invasion and Tumor Size in Patients With pT1-pT3a Localized Renal Cell Carcinoma in a Comprehensive Multicenter Study of the CORONA Project. Can We Improve Prognostic Discrimination for Patients With Stage pT3a Tumors? *Eur Urol* (2015) 67(5):943–51. doi: 10.1016/j.eururo.2014.11.055
4. Poon SA, Gonzalez JR, Benson MC, McKiernan JM. Invasion of Renal Sinus Fat is Not an Independent Predictor of Survival in pT3a Renal Cell Carcinoma. *BJU Int* (2009) 103(12):1622–5. doi: 10.1111/j.1464-410X.2008.08239.x
5. Shah PH, Lyon TD, Lohse CM, Cheville JC, Leibovich BC, Boorjian SA, et al. Prognostic Evaluation of Perinephric Fat, Renal Sinus Fat, and Renal Vein Invasion for Patients With Pathological Stage T3a Clear-Cell Renal Cell Carcinoma. *BJU Int* (2019) 123(2):270–6. doi: 10.1111/bju.14523
6. Wang Z, Yu K, Zhu Y, Feng C, Liu C, Liu S, et al. Multiple Patterns of Perirenal Fat Invasion are Associated With a Poorer Prognosis Compared With Isolated Invasion: A Proposal for a Revision of T3aN0M0 Tnm Staging System. *Front Oncol* (2020) 10:336. doi: 10.3389/fonc.2020.00336
7. Oh JJ, Lee JK, Do Song B, Lee H, Lee S, Byun SS, et al. Accurate Risk Assessment of Patients With Pathologic T3an0m0 Renal Cell Carcinoma. *Sci Rep* (2018) 8(1):13914. doi: 10.1038/s41598-018-32362-w
8. Ravaud A, Motzer RJ, Pandha HS, George DJ, Pantuck AJ, Patel A, et al. Adjuvant Sunitinib in High-Risk Renal-Cell Carcinoma After Nephrectomy. *N Engl J Med* (2016) 375(23):2246–54. doi: 10.1056/NEJMoa1611406
9. Haas NB, Manola J, Dutcher JP, Flaherty KT, Uzzo RG, Atkins MB, et al. Adjuvant Treatment for High-Risk Clear Cell Renal Cancer: Updated Results of a High-Risk Subset of the ASSURE Randomized Trial. *JAMA Oncol* (2017) 3(9):1249–52. doi: 10.1001/jamaoncol.2017.0076
10. Hayden JA, van der Windt DA, Cartwright JL, Cote P, Bombardier C. Assessing Bias in Studies of Prognostic Factors. *Ann Intern Med* (2013) 158 (4):280–6. doi: 10.7326/0003-4819-158-4-201302190-00009
11. Egger M, Davey Smith G, Schneider M, Minder C. Bias in Meta-Analysis Detected by a Simple, Graphical Test. *BMJ* (1997) 315(7109):629–34. doi: 10.1136/bmj.315.7109.629
12. Guyatt GH, Oxman AD, Vist GE, Kunz R, Falck-Ytter Y, Alonso-Coello P, et al. GRADE: An Emerging Consensus on Rating Quality of Evidence and Strength of Recommendations. *BMJ* (2008) 336(7650):924–6. doi: 10.1136/bmj.39489.470347.AD
13. Margulis V, Tamboli P, Matin SF, Meisner M, Swanson DA, Wood CG. Location of Extrarenal Tumor Extension Does Not Impact Survival of Patients With pT3a Renal Cell Carcinoma. *J Urol* (2007) 178(5):1878–82. doi: 10.1016/j.juro.2007.07.011
14. Bedke J, Buse S, Pritsch M, Macher-Goeppinger S, Schirmacher P, Haferkamp A, et al. Perinephric and Renal Sinus Fat Infiltration in pT3a Renal Cell Carcinoma: Possible Prognostic Differences. *BJU Int* (2009) 103(10):1349–54. doi: 10.1111/j.1464-410X.2008.08236.x
15. Bertini R, Roscigno M, Freschi M, Strada E, Petralia G, Pasta A, et al. Renal Sinus Fat Invasion in pT3a Clear Cell Renal Cell Carcinoma Affects Outcomes of Patients Without Nodal Involvement or Distant Metastases. *J Urol* (2009) 181(5):2027–32. doi: 10.1016/j.juro.2009.01.048
16. Kresowik TP, Johnson MT, Joudi FN. Combined Renal Sinus Fat and Perinephric Fat Renal Cell Carcinoma Invasion has a Worse Prognosis Than Either Alone. *J Urol* (2010) 184(1):48–52. doi: 10.1016/j.juro.2010.03.010
17. Park M, Shim M, Kim M, Song C, Kim CS, Ahn H. Prognostic Heterogeneity in T3aN0M0 Renal Cell Carcinoma According to the Site of Invasion. *Urol Oncol* (2017) 35(7):458.e417–58.e422. doi: 10.1016/j.urolonc.2016.05.019
18. Guo S, Liu Z, Li X, Yao K, Dong P, Chen D, et al. The Prognostic Value of the Site of Invasion in T3aN0M0 Clear Cell Renal Cell Carcinoma. *Urol Oncol* (2019) 37(5):301.e311–301.e317. doi: 10.1016/j.urolonc.2019.01.019
19. da Costa WH, Moniz RR, da Cunha IW, Fonseca FP, Guimaraes GC, de Cassio Zequi S. Impact of Renal Vein Invasion and Fat Invasion in pT3a Renal Cell Carcinoma. *BJU Int* (2012) 109(4):544–8. doi: 10.1111/j.1464-410X.2011.10366.x

20. Baccos A, Brunocilla E, Schiavina R, Borghesi M, Rocca GC, Chessa F, et al. Differing Risk of Cancer Death Among Patients With Pathologic T3a Renal Cell Carcinoma: Identification of Risk Categories According to Fat Infiltration and Renal Vein Thrombosis. *Clin Genitourin Cancer* (2013) 11(4):451–7. doi: 10.1016/j.clgc.2013.05.006
21. Flood TA, Hogan K, Lavallee LT, Breau RH, Morash C, Belanger EC, et al. Evaluation of Individual and Cumulative Sites of Extrarenal Tumor Invasion in pT3a Clear Cell Renal Cell Carcinoma. *Urol Oncol* (2020) 38(2):42.e13–8. doi: 10.1016/j.urolonc.2019.09.030
22. Schiavina R, Borghesi M, Chessa F, Dababneh H, Bianchi L, Della Mora L, et al. The Prognostic Impact of Tumor Size on Cancer-Specific and Overall Survival Among Patients With Pathologic T3a Renal Cell Carcinoma. *Clin Genitourin Cancer* (2015) 13(4):e235–41. doi: 10.1016/j.clgc.2014.06.011
23. Peng D, He ZS, Li XS, Tang Q, Zhang L, Yang KW, et al. Partial Nephrectomy for T3aN0M0 Renal Cell Carcinoma: Shall We Step Forward? *Int Braz J Urol* (2017) 43(5):849–56. doi: 10.1590/S1677-5538.IBJU.2016.0598
24. Chen L, Ma X, Li H, Gu L, Li X, Gao Y, et al. Influence of Tumor Size on Oncological Outcomes of Pathological T3aN0M0 Renal Cell Carcinoma Treated by Radical Nephrectomy. *PLoS One* (2017) 12(3):e0173953. doi: 10.1371/journal.pone.0173953
25. Capitanio U, Stewart GD, Klatte T, Akdogan B, Roscigno M, Marszalek M, et al. Does the Unexpected Presence of Non-organ-confined Disease At Final Pathology Undermine Cancer Control in Patients With Clinical T1n0m0 Renal Cell Carcinoma Who Underwent Partial Nephrectomy? *Eur Urol Focus* (2018) 4(6):972–7. doi: 10.1016/j.euf.2017.02.020
26. Bailey GC, Boorjian SA, Ziegelmann MJ, Westerman ME, Lohse CM, Leibovich BC, et al. Urinary Collecting System Invasion is Associated With Poor Survival in Patients With Clear-Cell Renal Cell Carcinoma. *BJU Int* (2017) 119(4):585–90. doi: 10.1111/bju.13669
27. Garcia Marchinena P, Tobia I, Abreu D, de Cassio Zequi S, Jurado A, Gueglio G, et al. Prognostic Value of Perirenal and/or Sinus Fat Infiltration in Patients With pT3a Renal Cell Carcinoma: A Multicentre Cohort Study. LARCG Group. *Actas Urol Esp* (2019) 43(9):495–502. doi: 10.1016/j.acuro.2019.01.005
28. Lai GS, Li JR, Wang SS, Chen CS, Yang CK, Hung SC, et al. Prognostic Evaluation of the Site of Invasion in Pathological Stage T3a Renal Cell Carcinoma. *In Vivo* (2021) 35(2):1083–9. doi: 10.21873/invivo.12353
29. Verhoest G, Avakian R, Bensalah K, Thuret R, Ficarra V, Artibani W, et al. Urinary Collecting System Invasion is an Independent Prognostic Factor of Organ Confined Renal Cell Carcinoma. *J Urol* (2009) 182(3):854–9. doi: 10.1016/j.juro.2009.05.017
30. Anderson CB, Clark PE, Morgan TM, Stratton KL, Herrell SD, Davis R, et al. Urinary Collecting System Invasion is a Predictor for Overall and Disease-Specific Survival in Locally Invasive Renal Cell Carcinoma. *Urology* (2011) 78 (1):99–104. doi: 10.1016/j.urology.2011.02.039
31. Chen L, Ma X, Li H, Li X, Gao Y, Zhang Y, et al. Invasion of the Urinary Collecting System is an Independent Prognostic Factor in pT3 Renal Cell Carcinoma. *Urol Oncol* (2016) 34(7):293 e211–296. doi: 10.1016/j.urolonc.2016.02.019
32. Palapattu GS, Pantuck AJ, Dorey F, Said JW, Figlin RA, Belldegrun AS. Collecting System Invasion in Renal Cell Carcinoma: Impact on Prognosis and Future Staging Strategies. *J Urol* (2003) 170(3):768–72; discussion 772. doi: 10.1097/01.ju.0000082580.13597.a2
33. Srivastava A, Patel HD, Joice GA, Semerjian A, Gorin MA, Johnson MH, et al. Incidence of T3a Up-Staging and Survival After Partial Nephrectomy: Size-stratified Rates and Implications for Prognosis. *Urol Oncol* (2018) 36(1):12 e17–.e13. doi: 10.1016/j.urolonc.2017.09.005
34. Shvero A, Nativ O, Abu-Ghanem Y, Zilberman D, Zaher B, Levitt M, et al. Oncologic Outcomes of Partial Nephrectomy for Stage T3a Renal Cell Cancer. *Clin Genitourin Cancer* (2018) 16(3):e613–7. doi: 10.1016/j.clgc.2017.10.016
35. Murphy AM, Gilbert SM, Katz AE, Goluboff ET, Sawczuk IS, Olsson CA, et al. Re-Evaluation of the Tumour-Node-Metastasis Staging of Locally Advanced Renal Cortical Tumours: Absolute Size (T2) is More Significant Than Renal Capsular Invasion (T3a). *BJU Int* (2005) 95(1):27–30. doi: 10.1111/j.1464-410X.2005.05244.x
36. Kirkali Z, Algaba F, Scarpelli M, Trias I, Selvaggi FP, Van Poppel H. What Does the Urologist Expect From the Pathologist (and What can the Pathologists Give) in Reporting on Adult Kidney Tumour Specimens? *Eur Urol* (2007) 51(5):1194–201. doi: 10.1016/j.eururo.2006.11.024
37. Grignon D, Paner GP. Renal Cell Carcinoma and the Renal Sinus. *Adv Anat Pathol* (2007) 14(2):63–8. doi: 10.1097/PAP.0b013e318032452e
38. Wood EL, Adibi M, Qiao W, Brandt J, Zhang M, Tamboli P, et al. Local Tumor Bed Recurrence Following Partial Nephrectomy in Patients With Small Renal Masses. *J Urol* (2018) 199(2):393–400. doi: 10.1016/j.juro.2017.09.072
39. Shah PH, Moreira DM, Okhunov Z, Patel VR, Chopra S, Razmaria AA, et al. Positive Surgical Margins Increase Risk of Recurrence After Partial Nephrectomy for High Risk Renal Tumors. *J Urol* (2016) 196(2):327–34. doi: 10.1016/j.juro.2016.02.075
40. Shah PH, Moreira DM, Patel VR, Gaunay G, George AK, Alom M, et al. Partial Nephrectomy is Associated With Higher Risk of Relapse Compared With Radical Nephrectomy for Clinical Stage T1 Renal Cell Carcinoma Pathologically Up Staged to T3a. *J Urol* (2017) 198(2):289–96. doi: 10.1016/j.juro.2017.03.012
41. Bensalah K, Pantuck AJ, Rioux-Leclercq N, Thuret R, Montorsi F, Karakiewicz PI, et al. Positive Surgical Margin Appears to Have Negligible Impact on Survival of Renal Cell Carcinomas Treated by Nephron-Sparing Surgery. *Eur Urol* (2010) 57(3):466–71. doi: 10.1016/j.eururo.2009.03.048
42. Tabayoyong W, Abouassaly R, Kiechle JE, Cherullo EE, Meropol NJ, Shah ND, et al. Variation in Surgical Margin Status by Surgical Approach Among Patients Undergoing Partial Nephrectomy for Small Renal Masses. *J Urol* (2015) 194(6):1548–53. doi: 10.1016/j.juro.2015.06.076
43. Tellini R, Antonelli A, Tardanico R, Fisogni S, Veccia A, Furlan MC, et al. Positive Surgical Margins Predict Progression-Free Survival After Nephron-sparing Surgery for Renal Cell Carcinoma: Results From a Single Center Cohort of 459 Cases With a Minimum Follow-Up of 5 Years. *Clin Genitourin Cancer* (2019) 17(1):e26–31. doi: 10.1016/j.clgc.2018.08.004
44. Shimizu T, Miyake M, Hori S, Iida K, Ichikawa K, Sakamoto K, et al. Clinical Significance of Tumor Size, Pathological Invasion Sites Including Urinary Collecting System and Clinically Detected Renal Vein Thrombus as Predictors for Recurrence in Pt3a Localized Renal Cell Carcinoma. *Diagn (Basel)* (2020) 10(3):154–66. doi: 10.3390/diagnostics10030154
45. Chevinsky M, Imnadze M, Sankin A, Winer A, Mano R, Jakubowski C, et al. Pathological Stage T3a Significantly Increases Disease Recurrence Across All Tumor Sizes in Renal Cell Carcinoma. *J Urol* (2015) 194(2):310–5. doi: 10.1016/j.juro.2015.02.013
46. Chen K, Lee BL, Huang HH, Tan BY, Lee LS, Ng LG, et al. Tumor Size and Fuhrman Grade Further Enhance the Prognostic Impact of Perinephric Fat Invasion and Renal Vein Extension in T3a Staging of Renal Cell Carcinoma. *Int J Urol* (2017) 24(1):51–8. doi: 10.1111/iju.13237
47. Lam JS, Klatte T, Patard JJ, Goel RH, Guille F, Lobel B, et al. Prognostic Relevance of Tumour Size in T3a Renal Cell Carcinoma: A Multicentre Experience. *Eur Urol* (2007) 52(1):155–62. doi: 10.1016/j.eururo.2007.01.106
48. Siddiqui SA, Frank I, Leibovich BC, Cheville JC, Lohse CM, Zincke H, et al. Impact of Tumor Size on the Predictive Ability of the pT3a Primary Tumor Classification for Renal Cell Carcinoma. *J Urol* (2007) 177(1):59–62. doi: 10.1016/j.juro.2006.08.069
49. Yoo C, Song C, Hong JH, Kim CS, Ahn H. Prognostic Significance of Perinephric Fat Infiltration and Tumor Size in Renal Cell Carcinoma. *J Urol* (2008) 180(2):486–91; discussion 491. doi: 10.1016/j.juro.2008.04.034
50. Dabestani S, Beisland C, Stewart GD, Bensalah K, Gudmundsson E, Lam TB, et al. Increased Use of Cross-Sectional Imaging for Follow-Up Does Not Improve Post-Recurrence Survival of Surgically Treated Initially Localized R.C.C.: Results From a European Multicenter Database (R.E.C.U.R.). *Scand J Urol* (2019) 53(1):14–20. doi: 10.1080/21681805.2019.1588919
51. Lenis AT, Donin NM, Johnson DC, Faiena I, Salmasi A, Drakaki A, et al. Adjuvant Therapy for High Risk Localized Kidney Cancer: Emerging Evidence and Future Clinical Trials. *J Urol* (2018) 199(1):43–52. doi: 10.1016/j.juro.2017.04.092
52. Gross-Goupil M, Kwon TG, Eto M, Ye D, Miyake H, Seo SI, et al. Axitinib Versus Placebo as an Adjuvant Treatment of Renal Cell Carcinoma: Results From the Phase III, Randomized ATLAS Trial. *Ann Oncol* (2018) 29 (12):2371–8. doi: 10.1093/annonc/mdy454
53. Eisen T, Frangou E, Oza B, Ritchie AWS, Smith B, Kaplan R, et al. Adjuvant Sorafenib for Renal Cell Carcinoma At Intermediate or High Risk of Relapse: Results From the SORCE Randomized Phase Iii Intergroup Trial. *J Clin Oncol* (2020) 38(34):4064–75. doi: 10.1200/JCO.20.01800
54. Massari F, Di Nunno V, Mollica V, Graham J, Gatto L, Heng D. Adjuvant Tyrosine Kinase Inhibitors in Treatment of Renal Cell Carcinoma: A Meta-Analysis of Available Clinical Trials. *Clin Genitourin Cancer* (2019) 17(2): e339–44. doi: 10.1016/j.clgc.2018.12.011
55. Gu L, Li H, Wang Z, Wang B, Huang Q, Lyu X, et al. A Systematic Review and Meta-Analysis of Clinicopathologic Factors Linked to Oncologic Outcomes for

Renal Cell Carcinoma With Tumor Thrombus Treated by Radical Nephrectomy With Thrombectomy. *Cancer Treat Rev* (2018) 69:112–20. doi: 10.1016/j.ctrv.2018.06.014

**Conflict of Interest:** The authors declare that the research was conducted in the absence of any commercial or financial relationships that could be construed as a potential conflict of interest.

*Copyright © 2021 Guo, Wang, Han, Wei, Zhao, Li, Jiang and Luo. This is an open-access article distributed under the terms of the Creative Commons Attribution License (CC BY). The use, distribution or reproduction in other forums is permitted, provided the original author(s) and the copyright owner(s) are credited and that the original publication in this journal is cited, in accordance with accepted academic practice. No use, distribution or reproduction is permitted which does not comply with these terms.*

frontiers in Oncology

ORIGINAL RESEARCH
published: 14 September 2021
doi: 10.3389/fonc.2021.727222

# Incidence, Clinical Characteristics, and Survival of Collecting Duct Carcinoma of the Kidney: A Population-Based Study

*Chaopeng Tang*†, *Yulin Zhou*†, *Silun Ge*, *Xiaoming Yi*, *Huichen Lv* and *Wenquan Zhou**

*Department of Urology, Jinling Hospital, Jinling School of Clinical Medicine, Nanjing Medical University, Nanjing, China*

**Objective:** To investigate the exact age-adjusted incidence (AAI), clinical characteristics, and survival data of collecting duct carcinoma of the kidney (CDCK) recorded in the Surveillance, Epidemiology, and End Results (SEER) database of the National Cancer Institute.

**Methods:** Patients with CDCK confirmed by microscopic examination from 2004 to 2018 were selected from the SEER database. AAI rates were calculated using SEER*Stat software (version 8.3.9). The Kaplan-Meier method was used to evaluate cancer-specific survival (CSS) rates according to tumor size, tumor stage, and treatment methods, and differences among these variables were assessed by the log-rank test. Cox regression analysis was employed to identify variables independently related to CSS.

**Results:** A total of 286 patients with CDCK were identified from the database. The majority of the patients were white (69.2%), male (67.5%), and married (60.5%), and the median age was 59 years. Most patients with CDCK (74.4%) presented with stages III or IV disease. The diameter of most (59.4%) tumors was less than 7 cm, and the tumors were more commonly found on the left than on the right (55.2% *vs.* 44.8%). The incidence of CDCK decreased over time. The median CSS time was 17 months. In terms of the treatment modalities used, 83.9% of the patients underwent surgery; 32.9% underwent chemotherapy, and 13.6% underwent radiotherapy. The CSS rates at 1, 2, and 5 years were 57.3%, 43.2%, and 30.7%, respectively. In patients with stage IV CDCK treated with surgery alone, chemotherapy alone, and surgery plus chemotherapy, the median survival time was 5 months, 9 months, and 14 months, respectively ($P$ =0.024). Multivariate Cox regression analysis showed surgery, chemotherapy, stage, regional lymph node metastasis, and distant metastasis were independent prognostic factors for patients with CDCK.

**Conclusions:** CDCK is an uncommon malignant renal carcinoma, and its incidence is decreasing based on the analysis of current data. CDCK is a high stage, regional lymph-nodes positive, and metastatic disease. Compared with surgery alone or chemotherapy alone, patients with stage IV could gain survival benefit from surgery combined with chemotherapy.

**Keywords: collecting duct carcinoma, kidney, SEER database, surgery, chemotherapy**

OPEN ACCESS

***Edited by:***
*Kouji Izumi,*
*Kanazawa University, Japan*

***Reviewed by:***
*Tomoyuki Makino,*
*Kanazawa University, Japan*
*Qiu-Qiang Zhang,*
*Zhejiang University, China*

****Correspondence:***
*Wenquan Zhou*
*shzwqzsl@163.com*

*†These authors have contributed equally to this work*

***Specialty section:***
*This article was submitted to Genitourinary Oncology, a section of the journal Frontiers in Oncology*

***Received:*** *18 June 2021*
***Accepted:*** *25 August 2021*
***Published:*** *14 September 2021*

***Citation:***
*Tang C, Zhou Y, Ge S, Yi X, Lv H and Zhou W (2021) Incidence, Clinical Characteristics, and Survival of Collecting Duct Carcinoma of the Kidney: A Population-Based Study. Front. Oncol. 11:727222. doi: 10.3389/fonc.2021.727222*

## INTRODUCTION

Collecting duct carcinoma of the kidney (CDCK), which is believed to arise from the epithelial layer of the collecting ducts of Bellini in the renal medullary, is an uncommon pathological subtype of renal carcinoma and accounts for 0%–3% of all renal malignancies (1–3). According to histologic findings, CDCK is defined as a subtype of renal carcinoma. However, the presentation, imaging findings, and prognosis of CDCK remarkably differ from those of other types of renal cancer. Clinically, CDCK displays characteristics similar to those of upper tract urothelial cell carcinoma (UTUC), which has a poor prognosis and limited response to immunotherapy (3, 4).

No significant differences were observed in terms of the effect of race or sex on the relative survival rates of CDCK in 98 samples recorded from 1973 to 2004 in the Surveillance, Epidemiology, and End Results (SEER) database (5). Wright JL et al. (6) compared cases of CDCK and clear cell renal cell carcinomas (CCRCC) recorded in the SEER database from 2001 to 2005 and found that patients with CDCK had a higher stage and poorer prognosis compared with CCRCC. This result is consistent with the largest report on CDCK by Sui W et al. (7). Abern MR et al. (8) compared the cancer-specific survival (CSS) rates of medullary renal cell carcinoma and CDCK from 1995 to 2007 recorded in the SEER database, and found that the prognosis of both diseases is generally poor; moreover, locally high stage or metastatic disease and not receiving surgery were considered predictors of mortality in the CDCK model.

Although these studies based on the SEER database clarified the clinical characteristics and prognosis of patients with CDCK, they did not investigate the association of variables such as marital status, radiotherapy, and chemotherapy with survival. Considering the rarity of this disease, we analyzed the latest CDCK data in the SEER database from 2004 to 2018 to identify the age-adjusted incidence (AAI) rates, clinical features, independent predictors of CSS rates, and survival outcomes of CDCK.

## MATERIALS AND METHODS

### Study Population

We used the SEER database, which included 18 tumor registries released in April 2021, for analysis. The SEER program collected cancer data from population-based registries representing about 34.6% of the US population. The database was a public and free research resource.

Patients with CDCK were selected based on the code of ICD-0-3: 8319/3: Collecting duct carcinoma. The eligibility criteria were as follows: (a) the labeled tumor sequence number was "one primary only;" (b) the year of diagnosis was between 2004 and 2018; (c) the labeled primary site was selected as "C64.9-Kidney, NOS;" (d) the tumor was microscopically confirmed; and (e) the tumor was unilateral. Patients with an unknown survival time were excluded from this work. The final cohort included 286 CDCK patients who met the eligibility criteria. Flowchart displaying the selection procedure of CDCK cases in the SEER database is shown in **Supplementary Figure 1**.

### Patient Information

The "case listing session" option was used to obtain the information of demographic factors such as age at diagnosis, sex, race, and marital status at diagnosis. Tumor features, including tumor size, tumor site, stage, T, N, and M were also extracted from the database. Furthermore, we collected information on treatment methods, including surgery, radiotherapy, and chemotherapy.

### Statistical Analysis

The AAI rates of CDCK were calculated using SEER*Stat software (version 8.3.9). The incidence rates were adjusted to the 2000 US population. The X-tile software determined 72 and 7 as the optimal cutoff point for age and tumor diameter, respectively. Demographic and clinical factors were analyzed using descriptive statistics, and the chi-square test was used to assess differences among annual incidence rates. Median, 1-year, 2-year, and 5-year overall survival (OS) and CSS rates were estimated using the Kaplan–Meier method. Kaplan–Meier curves were used to assess the CSS rates according to demographics, clinical parameters, and treatment methods, and the log-rank test was used to assess differences among these variables, the analysis was further stratified by tumor stage that could affect the treatment effects. Cox regression analysis was employed to identify variables independently related to CSS. SPSS version 21 was used for statistical analyses, and $P<0.05$ was considered significant.

## RESULTS

### Incidence of CDCK

The overall AAI of CDCK between 2004 and 2018was 0.2990 per 1,000,000 population. **Figure 1** shows that the incidence rate of CDCK decreased annually from 0.4580 per 1,000,000 population

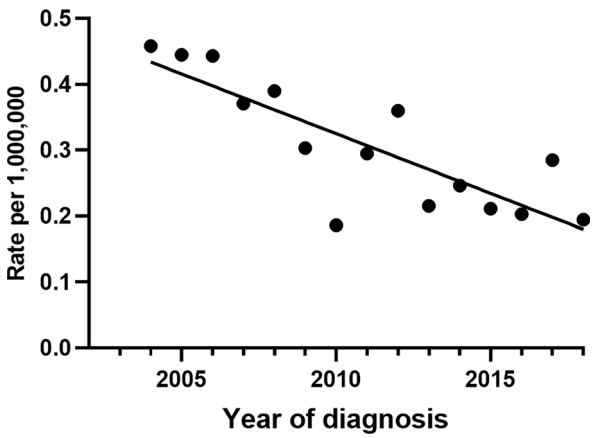



**FIGURE 1** | Incidence of CDCK in the period 2004–2018.

in 2004 to 0.1943 per 1,000,000 population in 2018. A significant difference in incidence rates was observed between these years ($P$ =0.002). The AAI of CDCK showed a decreasing trend over time.

## Clinical Characteristics of CDCK

The demographic characteristics of the patients showed that the median age in this study was 59 years (range: 14–89 years). In terms of marital status, 16.8% of the patients were single, 60.5% were married, and 22.7% were classified as others (including divorced, widowed, unknown, and others). In terms of sex, male patients accounted for 67.5% of the study population, and the male-to-female ratio was 2.08:1. The majority of the patients (69.2%) were white, 21.3% were black, and 9.4% were identified as others (including American Indian/Alaska Native, Asian or Pacific Islander, and unknown). In terms of tumor characteristics, 18.9%, 4.2%, 24.1%, and 50.3% of the patients presented with stages I, II, III, and IV disease, respectively. The proportions of regional lymph nodes and distant metastasis were 40.6% and 42.0%, respectively. Most patients (59.4%) had tumors less than 7 cm in diameter, and the diameter range was 1.2–24.8 cm. Tumors were more commonly located on the left side than on the right side of the body (55.2% *vs.* 44.8%). With regard to the treatment modalities used, surgery was the primary therapy (83.9%) for CDCK patients. Only a few patients received radiotherapy or chemotherapy, and the ratios of patients receiving these treatments relative to the total study population were 13.6% and 32.9%, respectively. Furthermore, beam radiation was the main radiotherapy scheme. The relevant demographic and clinical characteristics of the patients with CDCK are shown in **Table 1**.

**TABLE 1** | Descriptive data of patients with CDCK.

| Variables | Number (%) |
|---|---|
| Marital status | |
| Married | 173 (60.5%) |
| Single | 48 (16.8%) |
| Others | 65 (22.7%) |
| Race | |
| White | 198 (69.2%) |
| Black | 61 (21.3%) |
| Others | 27 (9.4%) |
| Sex | |
| Male | 193 (67.5%) |
| Female | 93 (32.5%) |
| Age (years) | |
| ≤72 | 233 (81.5%) |
| >72 | 53 (18.5%) |
| Tumor site | |
| Left | 158 (55.2%) |
| Right | 128 (44.8%) |
| Surgery | |
| Yes | 240 (83.9%) |
| No | 46 (16.1%) |
| Radiotherapy | |
| Yes | 39 (13.6%) |
| No/Unknown | 247 (86.4%) |
| Chemotherapy | |
| Yes | 94 (32.9%) |
| No/Unknown | 192 (67.1%) |
| Tumor size | |
| ≤7 cm | 170 (59.4%) |
| >7 cm | 102 (35.7%) |
| Unknown | 14 (4.9%) |
| Tumor stage | |
| I | 54 (18.9%) |
| II | 12 (4.2%) |
| III | 69 (24.1%) |
| IV | 144 (50.3%) |
| Unknown | 7 (2.4%) |
| T | |
| T1 | 79 (27.6%) |
| T2 | 18 (6.3%) |
| T3 | 151 (52.8%) |
| T4 | 26 (9.1%) |
| Tx | 12 (4.2%) |
| Regional lymph node metastasis | |
| N0 | 158 (55.2%) |
| N1 | 116 (40.6%) |
| Nx | 12 (4.2%) |
| Distant metastasis | |
| M0 | 162 (56.6%) |
| M1 | 120 (42.0%) |
| Mx | 4 (1.4%) |

## Prognosis of CDCK

The mean follow-up period was 33.6 months (range 0-175 months). The median OS and CSS times were 16 months (95% CI: 11.718–20.282) and 17 months (95% CI: 11.850–22.150), respectively. The OS rates at 1, 2, and 5 years were 55.5%, 39.4%, and 26.8%, respectively. The CSS rates at 1, 2, and 5 years were 57.3%, 43.2%, and 30.7%, respectively. No significant difference was observed between OS and CSS ($P$ =0.137, **Figure 2A**).

Patients with smaller tumors have higher survival rates than those with larger tumors (24 months *vs.* 13 months, $P$ = 0.038). The survival rates were also related to T staging, and the median survival times of T1, T2, T3, and T4 were 81 months, 56 months, 13 months, and 7 months, respectively ($P$ <0.001). A statistical difference was observed between T1 and T3 disease ($P$ <0.001), between T1 and T4 disease ($P$ <0.001), between T2 and T3 disease ($P$ =0.022), between T2 and T4 disease ($P$ =0.001), and between T3 and T4 disease ($P$ =0.040), but not between T1 and T2 disease ($P$ =0.813). The median survival times of patients with and without regional lymph node metastases were 9 and 41 months, respectively ($P$ <0.001). Differences in median survival times between patients with and without distant metastases were statistically significant at 7 and 53 months, respectively ($P$ <0.001). The survival rates were related to tumor stage, and the median survival times for stages I, II, III, and IV were as follows: not reached, 91 months, 26 months, and 7 months, respectively ($P$ <0.001; **Figure 2B**). Pairwise comparison indicated a statistical difference between stage I and stage III disease ($P$ <0.001), between stage I and IV disease ($P$ <0.001), between stage II and III disease ($P$ =0.049), between stage II and IV disease ($P$ <0.001), and between stage III and IV disease ($P$ <0.001), but not between stage I and stage II disease ($P$ =0.706). The CSS rates were significantly higher in surgery patients than non-surgery patients (24 months *vs.* 4 months, $P$ <0.001; **Figure 2C**). A significant difference in CSS rates was also observed between radiotherapy patients and non-radiotherapy patients (8 months *vs.* 23 months, $P$ <0.001). Patients treated with chemotherapy had lower CSS rates than

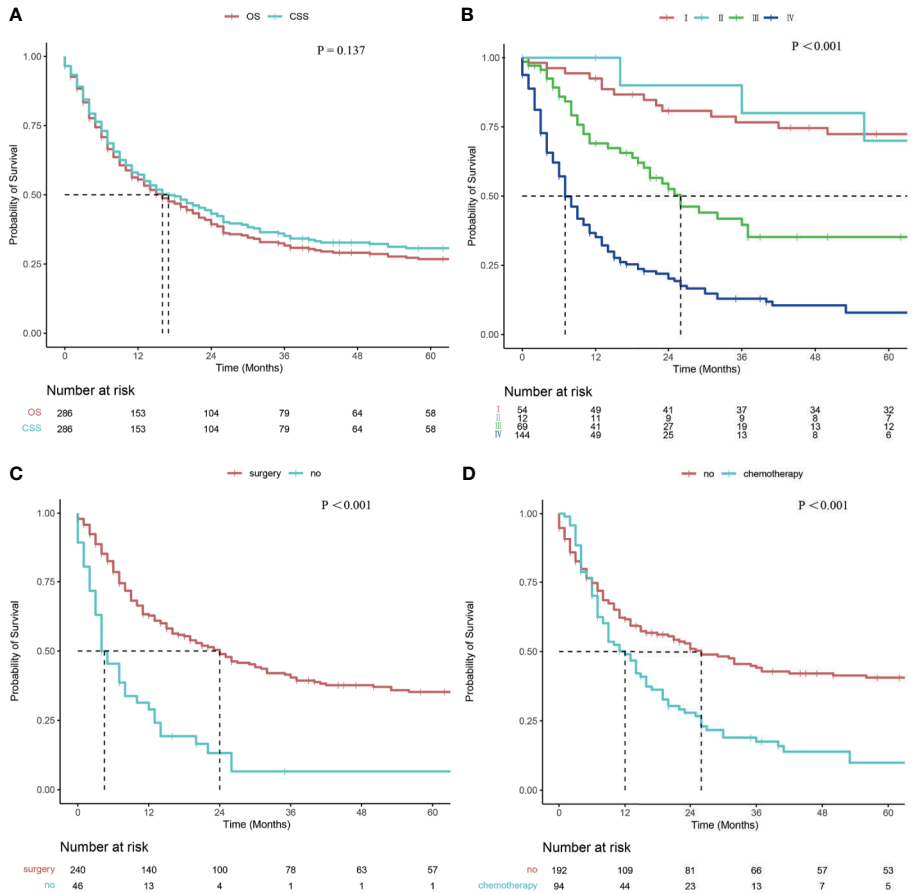



**FIGURE 2** | Survival curve of patients with CDCK evaluated using the Kaplan–Meier method. **(A)** OS and CSS; **(B)** According to the stage; **(C)** According to surgery; **(D)** According to chemotherapy.

those without chemotherapy (12 months *vs.* 26 months, $P$ <0.001; **Figure 2D**). Univariate analysis revealed no significant difference in survival rates with regard to marital status, sex, race, age, and tumor site.

In terms of radiotherapy stratified according to tumor stage, no significant difference was observed in survival rates between patients with stage III or IV ($P$ =0.107, $P$ =0.520, respectively). In terms of surgery stratified according to tumor stage, patients presenting with stage I or IV CDCK who underwent surgery had higher survival rates than those patients without surgery ($P$ <0.001, and $P$ =0.017, respectively; **Figures 3A, B**). However, no significant differences were observed in patients presenting with stage III disease ($P$ =0.715), and all patients presenting with stage II CDCK underwent surgery. In terms of chemotherapy stratified according to tumor stage, patients presenting with stage IV CDCK who underwent chemotherapy had higher survival rates than patients without chemotherapy ($P$ =0.014; **Figure 3C**). However, no significant differences were observed in patients presenting with stages II and III ($P$ =0.069, and $P$ =0.779, respectively). All patients who presented with stage I disease did not undergo chemotherapy. Patients presenting with stage IV CDCK who underwent surgery plus chemotherapy had higher survival rates than those who underwent surgery or chemotherapy alone (14 months, 5 months, and 9 months, respectively; $P$ = 0.024; **Figure 3D),** while survival rates were similar between patients who underwent surgery or chemotherapy alone ($P$ = 0.505). However, there were no significant differences in survival rates between patients with stage III treated with surgery plus chemotherapy or surgery alone (23 months *vs.* 29 months; $P$ = 0.850).

Variables exerting significant differences in survival rates were enrolled in the multivariate Cox regression analysis. The results of this analysis are shown in **Table 2**. Univariate Cox regression analysis suggested that no surgery (HR: 2.983; 95%CI: 2.080–4.277; $P$ <0.001), radiotherapy (HR: 2.291; 95%CI: 1.579–3.322; $P$ <0.001), chemotherapy (HR: 1.805; 95%CI: 1.339–2.432; $P$ <0.001), tumor size >7 cm (HR: 1.429; 95%CI: 1.055–1.937; $P$=0.021), regional lymph node metastasis (HR: 2.724; 95%CI: 2.004–3.701; $P$ <0.001), stage III(HR:2.953; 95%CI 1.636–5.331; $P$ <0.001), stage IV(HR: 7.514; 95%CI 4.407–12.813; $P$ <0.001), T3(HR: 2.268; 95%CI 1.557–3.303; $P$ <0.001), T4(HR: 3.599; 95% CI 2.132–6.074; $P$ <0.001), and distant metastasis (HR: 4.204; 95%CI: 3.084–5.730; $P$ <0.001) were risk factors for prognosis. Finally, multivariate Cox analysis revealed that surgery,

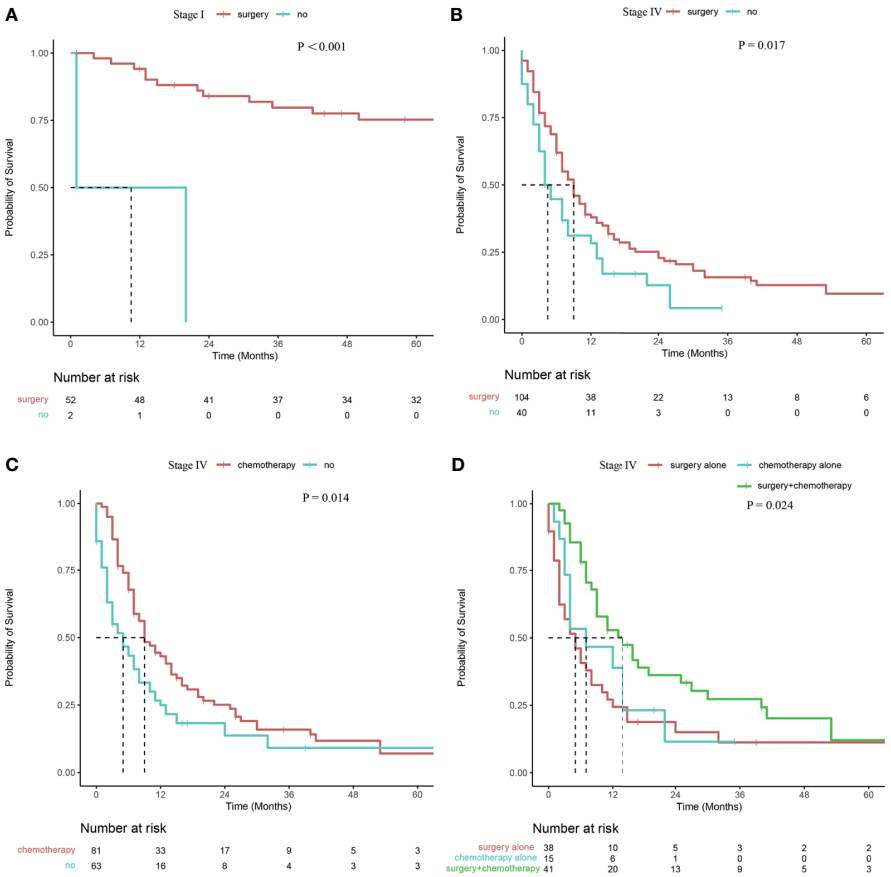



**FIGURE 3** | Survival curve of patients with CDCK evaluated using the Kaplan–Meier method **(A, B)** Surgery stratified according to tumor stage; **(C)** Chemotherapy stratified according to tumor stage; **(D)** Surgery and/or chemotherapy alone stratified according to tumor stage.

chemotherapy, stage, regional lymph node metastasis, and distant metastasis were independent prognostic factors for CDCK patients.

## DISCUSSION

CDCK, also known as Bellini duct carcinoma, is a relatively uncommon and aggressive malignant tumor originating from the epithelial layer of the collecting ducts of Bellini in the renal medullary (9). Studies suggest that patients with CDCK are associated with a high incidence of early mortality; specifically, 60% –70% of patients died within 3 years of diagnosis (10). The first observation that Bellini duct epithelial cells are the source of tumor development was reported by Cromie W et al. (11). However, Fleming and Lewi identified the disease as a unique renal cell carcinoma in 1986 (12). Our literature search revealed that studies on CDCK are gradually increasing. However, the specific incidence and AAI of CDCK remain unclear; indeed, the literature reports a CDCK incidence rate of only 0%–2% of all renal malignancies (1, 2). Our results showed that the overall AAI of CDCK between 2004 and 2018 was 0.299 per 1,000,000 population, and numbers showed a decreasing trend annually.

In a cohort of 227 CDCK cases reported from 1995 to 2007 in the SEER database, the median CSS time was 30 months. However, in another cohort of 160 CDCK cases from 2001 to 2005 in the SEER database, the median survival time was only 5 months (6). Our study showed that the median CSS and OS of 286 CDCK patients were 17 and 16 months, respectively; these results are consistent with the largest known cohort regarding CDCK (7). A previous study based on the SEER dataset reported that the 1- and 3-year CSS rates for CDCK were 70% and 58%, respectively, and we reported that the OS rates at 1, 2, and 5 years were 55.5%, 39.4%, and 26.8%, respectively. Moreover, the CSS rates at 1, 2, and 5 years were 57.3%, 43.2%, and 30.7%, respectively, consistent with the findings of May et al. (i.e.,60.4%, 47.3%, and 40.3%, respectively) (13), thus indicating that over 50% of the CDCK patients died within 2 years. Inconsistences between the results recorded in the present work and previous reports based on the SEER dataset may be due to differences in the inclusion criteria among studies.

In our study, the ages of the patients ranged from 14 years to 89 years, with a median age of 59 years. Males were more likely to

**TABLE 2 |** Univariate and multivariate analyses of the CSS of the patients.

| | Univariate | | Multivariate | |
|---|---|---|---|---|
| **Variables** | **HR (95%CI)** | ***P* value** | **HR (95%CI)** | ***P* value** |
| Marital status | | | | |
| Married | 1 | | | |
| Single | 0.840 (0.562–1.254) | 0.394 | | |
| Others | 0.807 (0.553–1.178) | 0.267 | | |
| Race | | | | |
| White | 1 | | | |
| Black | 0.752 (0.518–1.092) | 0.134 | | |
| Others | 0.819 (0.487–1.377) | 0.452 | | |
| Sex | | | | |
| Male | 1 | | | |
| Female | 0.803 (.586–1.100) | 0.172 | | |
| Age | | | | |
| ≤72 | 1 | | | |
| >72 | 1.091 (0.741–1.606) | 0.660 | | |
| Tumor site | | | | |
| Left | 1 | | | |
| Right | 1.151 (0.861–1.540) | 0.342 | | |
| Surgery | | | | |
| Yes | 1 | | 1 | |
| No | 2.983 (2.080–4.277) | <0.001 | 1.814 (1.126–2.924) | 0.014 |
| Radiotherapy | | | | |
| No/Unknown | 1 | | 1 | |
| Yes | 2.291 (1.579–3.322) | <0.001 | 1.184 (0.800–1.753) | 0.398 |
| Chemotherapy | | | | |
| No/Unknown | 1 | | 1 | |
| Yes | 1.805 (1.339–2.432) | <0.001 | 0.454 (.312–.661) | <0.001 |
| Tumor size | | | | |
| ≤7 cm | 1 | | 1 | |
| >7 cm | 1.429 (1.055–1.937) | 0.021 | 1.153 (0.820–1.622) | 0.412 |
| Unknown | 1.585 (0.828–3.037) | 0.165 | 0.958 (0.401–2.293) | 0.924 |
| Tumor stage | | | | |
| I | 1 | | 1 | |
| II | 1.168 (0.390–3.494) | 0.782 | 0.793 (0.180–3.503) | 0.760 |
| III | 2.953 (1.636–5.331) | <0.001 | 2.218 (0.997–4.934) | 0.051 |
| IV | 7.514 (4.407–12.813) | <0.001 | 2.565 (1.055–6.236) | 0.038 |
| Unknown | 4.133 (1.377–12.401) | 0.011 | 2.340 (0.386–14.173) | 0.355 |
| T | | | | |
| T1 | 1 | | 1 | |
| T2 | 1.081 (0.522–2.235) | 0.834 | 1.371 (0.486–3.870) | 0.551 |
| T3 | 2.268 (1.557–3.303) | <0.001 | 1.381 (0.775–2.461) | 0.274 |
| T4 | 3.599 (2.132–6.074) | <0.001 | 1.566 (0.828–2.962) | 0.168 |
| Tx | 2.002 (0.892–4.493) | 0.092 | 0.467 (0.136–1.605) | 0.226 |
| Regional lymph node metastasis | | | | |
| N0 | 1 | | 1 | |
| N1 | 2.724 (2.004–3.701) | <0.001 | 1.448 (1.001–2.096) | 0.049 |
| Nx | 2.478 (1.192–5.150) | 0.015 | 2.268 (0.773–6.649) | 0.136 |
| Distant metastasis | | | | |
| M0 | 1 | | | |
| M1 | 4.204 (3.084–5.730) | <0.001 | 3.256 (1.844–5.750) | <0.001 |
| Mx | 1.686 (0.414–6.867) | 0.466 | 1.346 (0.173–10.479) | 0.777 |

develop CDCK than females, and the ratio of males to females was 2.08:1. This result is consistent with previous reports (8, 14), that is, CDCK is frequently found in middle-aged and older patients and more often observed in men than in women. Moreover, tumors occurring on the left side have a slight advantage over those on the right side.

Hematuria is the most common presentation of CDCK, followed by abdominal pain, weight loss, and palpable masses. The clinical symptoms of CDCK vary according to tumor size, location, and invasion. Some patients are diagnosed by physical examination because they have no symptoms (15), whereas other patients are diagnosed with symptoms at the site of metastasis (16, 17). Unfortunately, the absence of information on symptoms in the database prevented us from understanding the characteristics of patients' symptoms in the present study.

The preoperative diagnosis of CDCK is limited by the lack of specific radiological features. When the tumor is small, the imaging features supporting the diagnosis of CDCK include

solitary tumor, medullary location, weak and heterogeneous enhancement, renal sinus involvement, infiltrative growth, and continuous renal contour (9, 18). However, when the tumor is large, the expansive growth of the tumor obscures these features; thus, distinguishing CDCK from other common cortical renal cell carcinomas is difficult (19). Studies (20, 21) found that CDCK showed high 18-fluorine fluorodeoxyglucose ($^{18}$F-FDG) uptake in local and distant metastases; therefore, $^{18}$F-FDG-PET/CT may be an appropriate method to assess the extent of the disease.

Given the lack of specific imaging findings, distinguishing CDCK from other tumors by imaging alone is extremely challenging. Therefore, the correct diagnosis still depends on pathological examination. The International Society of Urological Pathology believes that a tumor should present with the following pathological features to be diagnosed as CDCK: (1) tumor involving the renal medullary, (2) predominant tubule formation, (3) present with desmoplastic stromal reaction, (4) cytologic features are high grade, (5) infiltrative growth pattern, and (6) other RCC subtypes of urothelial carcinoma should be excluded (22).

CDCK needs to be differentiated from urothelial carcinoma, renal medullary carcinoma, papillary renal cell carcinoma type 2, and unclassified renal cell carcinoma (23). Differentiating CDCK from UTUC is especially critical. Immunohistochemistry can be used to determine the origin of the tumors based on the staining characteristics of each cell type for differential diagnosis. A number of markers suggest that CDCK expresses some specific biological markers, including UEA-1, PNA, HMW-CK, and Fez1 (24). Collecting ducts express PAX8, and p63 is a marker that is commonly used for urothelial differentiation. Albadine R et al. (25) found that the combination of PAX8 and p63 can accurately differentiate between CDCK and UTUC. The diagnosis of CDCK was supported when PAX8+/p63−, the sensitivity and specificity were 85.7% and 100%, respectively; by contrast, the diagnosis of UTUC was supported when PAX8−/p63+, the sensitivity and specificity were 88.2% and 100%, respectively.

The majority of patients with CDCK present with highly metastatic features and an advanced TNM stage at diagnosis (15). The lymph nodes, lungs, liver, bones, and adrenal glands are the most frequent distant metastases sites (26). In this study, regional lymph node metastasis occurred in 116 out of 286 cases, and distant metastasis occurred in 120 out of 286 cases. We found that CSS rates decreased with increasing tumor stage. Our finding is consistent with the results of previous studies (7), which showed that advanced-stage disease is an independent predictor for poor survival. Our study showed that the hazard ratios of survival rates in patients with CDCK of stages II, III, and IV were 1.168, 2.953, and 7.514 times higher than that in patients with stage I CDCK, respectively. Compared with that of T1, the hazard ratios of survival rates in T2, T3, and T4 were 1.081, 2.268, and 3.599, respectively. The hazard ratio of the survival rates of patients with lymph node metastases was 2.724 times higher than that of patients without lymph node metastases. The hazard ratio for the survival of patients with metastases was 4.204 higher compared with that of patients without distant metastases. Multivariate Cox regression analysis showed that stage, regional lymph node metastasis, and distant metastasis were independent prognostic factors for CDCK patients.

Although limited reports established that targeted therapy and immunotherapy could be beneficial for patients with advanced CDCK (27–30), the prognosis of patients with CDCK remains poor, cytoreductive nephrectomy may be the only potentially curable option for patients with CDCK (8, 27, 31). The majority of the reported patients were treated with radical nephrectomy, while a few cases were treated with partial nephrectomies (32, 33). Given the aggressive nature of CDCK, radical nephrectomy is usually recommended (15), partial nephrectomy may be a treatment option in the management of low-grade CDCK (32). In our study, surgery, including cryosurgery, nephrectomy, and ureterectomy, was the first option. Of 286 patients, 240 received surgery. The median survival times of surgery and non-surgery patients were 24 and 4 months, respectively, and a significant difference in CSS rate was observed between these patients. Considering that CDCK is prone to lymph node metastasis, lymph node metastasis was found in 40.6% of the patients in this study. Therefore, the hilar lymph node should be removed during surgery.

Literature related to CDCK chemotherapy is limited. Because of the similarity of the clinical features of CDCK and urothelial cancer, some researchers believe that the chemotherapy regimen for urothelial cancer may be effective for patients with CDCK. Milowsky MI et al. (34) used doxorubicin and gemcitabine for postoperative chemotherapy in a CDCK patient. Although early treatment effects were favorable, the patient died 10 months after a diagnosis of bone and liver metastasis. Peyromaure M et al. (35) reported two CDCK patients who received postoperative chemotherapy, including gemcitabine and cisplatin, and remained disease-free for 27 and 9 months postoperatively. In the present study, however, the median survival time of patients who underwent chemotherapy was significantly lower than that of patients without chemotherapy. The inconsistent results compared with other reports may be contributed to differences in composition between the two groups, that is, 1, 12, and 81 out of 94 patients with chemotherapy had stage II, III, and IV tumors, respectively; by contrast, 54, 11, 57, and 63 out of 192 patients without chemotherapy had I, II, III, and IV tumors, respectively. Stratified analysis was performed to exclude the interference of the confounding factors on the treatment effect. In terms of chemotherapy stratified according to tumor stage, patients with stage IV CDCK who underwent chemotherapy had higher survival rates than patients without chemotherapy. However, no significant differences were found among patients with stages I, II, and III. In terms of surgery stratified according to tumor stage, patients presenting with stage I or IV CDCK who underwent surgery had higher survival rates than those patients without surgery. However, no significant differences were observed in patients presenting with stage III disease. Patients presenting with stage IV CDCK who underwent surgery plus chemotherapy had higher survival rates than those who underwent surgery or chemotherapy alone, these results are consistent with the previous literature (7). Considering that

CDCK has genetic characteristics that differ from those of UTUC, chemotherapy regimens used for uroepithelial carcinoma are unsuitable for the former (36), and new regimens used to treat this disease should be investigated.

Although this study used the SEER database to provide considerable information on CDCK, it still presents a number of limitations. First, this study is retrospective in nature. Second, because the treatment regimen and time of chemotherapy administration are unclear, studies on the specific effects of the drug type may be limited. Finally, the lack of a centralized pathological review may lead to the misclassification of this disease. Despite these limitations, however, this study is of great benefit to clinicians seeking to assess the prognosis of CDCK and formulate appropriate treatment plans for the disease.

## CONCLUSIONS

This study used the SEER database to investigate patients with CDCK, which is a rare malignant carcinoma. Patients presenting with stage I and IV CDCK who underwent surgery had higher survival rates than patients without surgery, and patients presenting with stage IV CDCK who underwent chemotherapy had higher survival rates than patients without chemotherapy. Surgery plus chemotherapy has a survival benefit for patients presenting with stage IV compared with surgery alone or chemotherapy alone. New chemotherapy regimens should be investigated on the basis of the genetic characteristics of CDCK.

## DATA AVAILABILITY STATEMENT

All raw data in this article can be obtained in the SEER program: https://seer.cancer.gov/.

## ETHICS STATEMENT

Since the data from the SEER registry were de-identified and publicly available, no institutional review board approval was necessary and no informed consent was signed for this study.

## AUTHOR CONTRIBUTIONS

CT, XY, and WZ: study concept and design. CT and YZ: analysis data and drafting of the manuscript. SG, HL, and YZ: critical revision of the manuscript. All authors contributed to the article and approved the submitted version.

## FUNDING

This study was supported by the National Natural Science Foundation of China (No. 82072836).

## ACKNOWLEDGMENTS

We would like to thank the Surveillance, Epidemiology, and End Results (SEER) database of the National Cancer Institute for data provided.

## SUPPLEMENTARY MATERIAL

The Supplementary Material for this article can be found online at: https://www.frontiersin.org/articles/10.3389/fonc.2021.727222/full#supplementary-material

## REFERENCES

1. Gupta R, Billis A, Shah RB, Moch H, Osunkoya AO, Jochum W, et al. Carcinoma of the Collecting Ducts of Bellini and Renal Medullary Carcinoma Clinicopathologic Analysis of 52 Cases of Rare Aggressive Subtypes of Renal Cell Carcinoma With a Focus on Their Interrelationship. *Am J Surg Pathol* (2012) 36(9):1265–78. doi: 10.1097/PAS.0b013e3182635954
2. Karakiewicz PI, Trinh Q-D, Rioux-Leclercq N, de la Taille A, Novara G, Tostain J, et al. Collecting Duct Renal Cell Carcinoma: A Matched Analysis of 41 Cases. *Eur Urol* (2007) 52(4):1140–6. doi: 10.1016/j.eururo.2007.01.070
3. Chao D, Zisman A, Pantuck AJ, Gitlitz BJ, Freedland SJ, Said JW, et al. Collecting Duct Renal Cell Carcinoma: Clinical Study of a Rare Tumor. *J Urol* (2002) 167(1):71–4. doi: 10.1016/s0022-5347(05)65385-2
4. Orsola A, Trias I, Raventós CX, Español I, Cecchini L, Orsola I. Renal Collecting (Bellini) Duct Carcinoma Displays Similar Characteristics to Upper Tract Urothelial Cell Carcinoma. *Urology* (2005) 65(1):49–54. doi: 10.1016/j.urology.2004.08.012
5. Pepek JM, Johnstone PA, Jani AB. Influence of Demographic Factors on Outcome of Collecting Duct Carcinoma: A Surveillance, Epidemiology, and End Results (SEER) Database Analysis. *Clin Genitourin Cancer* (2009) 7(2): E24–7. doi: 10.3816/CGC.2009.n.017
6. Wright JL, Risk MC, Hotaling J, Lin DW. Effect of Collecting Duct Histology on Renal Cell Cancer Outcome. *J Urol* (2009) 182(6):2595–9. doi: 10.1016/j.juro.2009.08.049
7. Sui W, Matulay JT, Robins DJ, James MB, Onyeji IC, RoyChoudhury A, et al. Collecting Duct Carcinoma of the Kidney: Disease Characteristics and Treatment Outcomes From the National Cancer Database. *Urol Oncol* (2017) 35(9):540.e13–.e18. doi: 10.1016/j.urolonc.2017.04.010
8. Abern MR, Tsivian M, Polascik TJ, Coogan CL. Characteristics and Outcomes of Tumors Arising From the Distal Nephron. *Urology* (2012) 80(1):140–6. doi: 10.1016/j.urology.2012.03.034
9. Moch H, Cubilla AL, Humphrey PA, Reuter VE, Ulbright TM. The 2016 WHO Classification of Tumours of the Urinary System and Male Genital Organs-Part A: Renal, Penile, and Testicular Tumours. *Eur Urol* (2016) 70 (1):93–105. doi: 10.1016/j.eururo.2016.02.029
10. Tokuda N, Naito S, Matsuzaki O, Nagashima Y, Ozono S, Igarashi T. Collecting Duct (Bellini Duct) Renal Cell Carcinoma: A Nationwide Survey in Japan. *J Urol* (2006) 176(1):40–3. doi: 10.1016/S0022-5347(06)00502-7
11. Cromie W, Davis C, Deture F. Atypical Carcinoma of Kidney. *Urology* (1979) 13:315–7. doi: 10.1016/0090-4295(79)90434-5
12. Fleming S, Lewi HJE. Collecting Duct Carcinoma of the Kidney. *Histopathology* (1986) 10(11):1131–41. doi: 10.1111/j.1365-2559.1986.tb02553.x
13. May M, Ficarra V, Shariat SF, Zigeuner R, Chromecki T, Cindolo L, et al. Impact of Clinical and Histopathological Parameters on Disease Specific Survival in Patients With Collecting Duct Renal Cell Carcinoma: Development of a Disease Specific Risk Model. *J Urol* (2013) 190(2):458–63. doi: 10.1016/j.juro.2013.02.035

14. Ciszewski S, Jakimów A, Smolska-Ciszewska B. Collecting (Bellini) Duct Carcinoma: A Clinical Study of a Rare Tumour and Review of the Literature. *Can Urol Assoc* (2015) 9(9-10):E589–93. doi: 10.5489/cuaj.2932
15. Qian X, Wang Z, Zhang J, Wang Q, Zhou P, Wang S, et al. Clinical Features and Prognostic Outcome of Renal Collecting Duct Carcinoma: 12 Cases From a Single Institution. *Cancer Manage Res* (2020) 12:3589–95. doi: 10.2147/cmar.S244094
16. Hasan A, Abozied H, Youssef A, Fayad S, Ismail A. A Rare Case of Collecting Duct Carcinoma With First Presentation of Respiratory Symptoms. *Urol Case Rep* (2020) 33:101367–. doi: 10.1016/j.eucr.2020.101367
17. Thangarasu M, Raghavan D, Muthu R, Prabhakar V, Prakash S. Collecting Duct Carcinoma of Kidney: Masquerading as Genitourinary Tuberculosis - Lessons Learnt. *Urol Case Rep* (2020) 29:101100. doi: 10.1016/j.eucr.2019.101100
18. Yoon SK, Nam KJ, Rha SH, Kim JK, Cho KS, Kim B, et al. Collecting Duct Carcinoma of the Kidney: CT and Pathologic Correlation. *Eur J Radiol* (2006) 57(3):453–60. doi: 10.1016/j.ejrad.2005.09.009
19. Pickhardt PJ, Siegal CL, McLarnery JK. Collecting Duct Carcinoma of the Kidney: Are Imaging Findings Suggestive of the Diagnosis? *Am J Roentgenol* (2001) 176(3):627–33. doi: 10.2214/ajr.176.3.1760627
20. Marx K, Bauer J, Guillou L, Delaloye AB, Prior J. Bellini Duct Carcinoma Visualization on F-18 FDG PET/CT. *Clin Nucl Med* (2009) 34(8):541–2. doi: 10.1097/RLU.0b013e3181abb768
21. Lyu Z, Liu L, Li H, Wang H, Liu Q, Chen T, et al. Imaging Analysis of 13 Rare Cases of Renal Collecting (Bellini) Duct Carcinoma in Northern China: A Case Series and Literature Review. *BMC Med Imaging* (2021) 21(1):42. doi: 10.1186/s12880-021-00574-8
22. Srigley JR, Delahunt B, Eble JN, Egevad L, Epstein JI, Grignon D, et al. The International Society of Urological Pathology (ISUP) Vancouver Classification of Renal Neoplasia. *Am J Surg Pathol* (2013) 37(10):1469–89. doi: 10.1097/PAS.0b013e318299f2d1
23. Fleming S. Distal Nephron Neoplasms. *Semin Diagn Pathol* (2015) 32(2):114–23. doi: 10.1053/j.semdp.2015.02.004
24. Bansal P, Kumar S, Mittal N, Kundu AK. Collecting Duct Carcinoma: A Rare Renal Tumor. *Saudi J Kidney Dis Transplant* (2012) 23(4):810–2. doi: 10.4103/1319-2442.98166
25. Albadine R, Schultz L, Illei P, Ertoy D, Hicks J, Sharma R, et al. PAX8 (+)/P63 (-) Immunostaining Pattern in Renal Collecting Duct Carcinoma (CDC): A Useful Immunoprofile in the Differential Diagnosis of CDC Versus Urothelial Carcinoma of Upper Urinary Tract. *Am J Surg Pathol* (2010) 34(7):965–9. doi: 10.1097/PAS.0b013e3181dc5e8a
26. Mennitto A, Verzoni E, Peverelli G, Alessi A, Procopio G. Management of Metastatic Collecting Duct Carcinoma: An Encouraging Result in a Patient Treated With Cabozantinib. *Clin Genitourinar Cancer* (2018) 16(3):E521–3. doi: 10.1016/j.clgc.2018.03.010
27. Pagani F, Colecchia M, Sepe P, Apollonio G, Claps M, Verzoni E, et al. Collecting Ducts Carcinoma: An Orphan Disease. Literature Overview and Future Perspectives. *Cancer Treat Rev* (2019) 79:1–7. doi: 10.1016/j.ctrv.2019.101891
28. Zeng Y, Zhang W, Li Z, Zheng Y, Wang Y, Chen G, et al. Personalized Neoantigen-Based Immunotherapy for Advanced Collecting Duct Carcinoma: Case Report. *J ImmunoTher Cancer* (2020) 8(1):e000217. doi: 10.1136/jitc-2019-000217
29. Flippot R, Damarla V, McGregor BA. Management of Metastatic Renal Cell Carcinoma With Variant Histologies. *Urol Clinics N Am* (2020) 47(3):319–27. doi: 10.1016/j.ucl.2020.04.003
30. Ito K. Recent Advances in the Systemic Treatment of Metastatic non-Clear Cell Renal Cell Carcinomas. *Int J Urol* (2019) 26(9):868–77. doi: 10.1111/iju.14027
31. Alhalabi O, Karam JA, Tannir NM. Evolving Role of Cytoreductive Nephrectomy in Metastatic Renal Cell Carcinoma of Variant Histology. *Curr Opin Urol* (2019) 29(5):521–5. doi: 10.1097/mou.0000000000000661
32. Matsumoto H, Wada T, Aoki A, Hoshii Y, Takahashi M, Aizawa S, et al. Collecting Duct Carcinoma With Long Survival Treated by Partial Nephrectomy. *Int J Urol* (2001) 8(7):401–3. doi: 10.1046/j.1442-2042.2001.00321.x
33. Kopec N, Kopcza P, Wrona A, Salagierski M. Nephron Sparing Surgery for Metastatic Collecting Duct Carcinoma. *Cent Eur J Urol* (2019) 72(4):374–7. doi: 10.5173/ceju.2019.0055
34. Milowsky MI, Rosmarin A, Tickoo SK, Papanicolaou N, Nanus DM. Active Chemotherapy for Collecting Duct Carcinoma of the Kidney - A Case Report and Review of the Literature. *Cancer* (2002) 94(1):111–6. doi: 10.1002/cncr.10204
35. Peyromaure M, Thiounn N, Scotte F, Vieillefond A, Debre B, Oudard S. Collecting Duct Carcinoma of the Kidney: A Clinicopathological Study of 9 Cases. *J Urol* (2003) 170(4):1138–40. doi: 10.1097/01.ju.0000086616.40603.ad
36. Becker F, Junker K, Parr M, Hartmann A, Füssel S, Toma M, et al. Collecting Duct Carcinomas Represent a Unique Tumor Entity Based on Genetic Alterations. *PloS One* (2013) 8(10):e78137. doi: 10.1371/journal.pone.0078137


**Conflict of Interest:** The authors declare that the research was conducted in the absence of any commercial or financial relationships that could be construed as a potential conflict of interest.

**Publisher's Note:** All claims expressed in this article are solely those of the authors and do not necessarily represent those of their affiliated organizations, or those of the publisher, the editors and the reviewers. Any product that may be evaluated in this article, or claim that may be made by its manufacturer, is not guaranteed or endorsed by the publisher.

*Copyright © 2021 Tang, Zhou, Ge, Yi, Lv and Zhou. This is an open-access article distributed under the terms of the Creative Commons Attribution License (CC BY). The use, distribution or reproduction in other forums is permitted, provided the original author(s) and the copyright owner(s) are credited and that the original publication in this journal is cited, in accordance with accepted academic practice. No use, distribution or reproduction is permitted which does not comply with these terms.*

frontiers in Oncology

ORIGINAL RESEARCH
published: 21 September 2021
doi: 10.3389/fonc.2021.730662

# Comparison of Perioperative, Renal Functional, and Oncological Outcomes Between Off-Clamp and On-Clamp Robot-Assisted Partial Nephrectomy for Renal Tumors: An Updated Evidence-Based Analysis

*Yin Huang[1,2†], Dehong Cao[1†], Zeyu Chen[1,2], Bo Chen[1,2], Jin Li[1,2], Jianbing Guo[1], Qiang Dong[1], Qiang Wei[1*] and Liangren Liu[1*]*

[1] Department of Urology/Institute of Urology, West China Hospital, Sichuan University, Chengdu, China, [2] West China School of Medicine, Sichuan University, Chengdu, China

**Objectives:** We aimed to report the latest and largest pooled analysis and evidence update to compare the perioperative, renal functional, and oncological outcomes between off-clamp and on-clamp robot-assisted partial nephrectomy (RAPN) for renal tumors.

**Patients and methods:** We performed a systematic literature search using PubMed, Embase, and Web of Science up to August 2021 for studies that compared the efficacy and/or safety between off-clamp and on-clamp RAPN for renal tumors. Outcomes measured were operating time, estimated blood loss (EBL), conversion rate, length of stay (LOS), complication rate, transfusion rate, long-term % decrease in estimated glomerular filtration rate (eGFR), positive surgical margin rate, and recurrence rate.

**Results:** A total of 21 eligible articles involving 4,493 patients (1,274 off-clamp *versus* 3,219 on-clamp) were included for the evidence synthesis. Baseline characteristics of the two groups were similar in all outcomes except that lower R.E.N.A.L. score and smaller tumor size were observed in the off-clamp group. Pooled analysis showed shorter operative time, higher EBL, and lower complication rate in the off-clamp group. No significant difference was observed in the conversion rate, LOS, and transfusion rate. The recurrence rates were similar in the two groups, while a lower positive surgical margin rate was observed in the off-clamp group. Finally, the off-clamp group had a superior postoperative renal functional outcome.

**Conclusions:** Given the presence of heterogeneity and potential bias, urologists should select the clamp strategy based on their experience and patient-specific factors.

**Keywords: robot-assisted partial nephrectomy, off-clamp, on-clamp, kidney cancer, renal function**

OPEN ACCESS

***Edited by:***
*Kouji Izumi,*
*Kanazawa University, Japan*

***Reviewed by:***
*Yunxiang Li,*
*North Sichuan Medical College, China*
*Alessandro Antonelli,*
*University of Verona, Italy*

****Correspondence:***
*Qiang Wei*
*weiqiang339@126.com*
*Liangren Liu*
*liangren_liu517@126.com*

*†These authors have contributed equally to this work*

***Specialty section:***
*This article was submitted to Genitourinary Oncology, a section of the journal Frontiers in Oncology*

***Received:*** *25 June 2021*
***Accepted:*** *25 August 2021*
***Published:*** *21 September 2021*

***Citation:***
*Huang Y, Cao D, Chen Z, Chen B, Li J, Guo J, Dong Q, Wei Q and Liu L (2021) Comparison of Perioperative, Renal Functional, and Oncological Outcomes Between Off-Clamp and On-Clamp Robot-Assisted Partial Nephrectomy for Renal Tumors: An Updated Evidence-Based Analysis. Front. Oncol. 11:730662. doi: 10.3389/fonc.2021.730662*

## INTRODUCTION

Renal cancer is one of the most common malignant tumors, with an estimated 73,750 new cases and 14,830 deaths in the USA in 2020 (1). In the past few years, partial nephrectomy (PN) has been considered as the standard surgical procedure for cT1 (<7 cm) renal tumors due to its equivalent oncological outcomes, better preservation of renal function, and superior overall survival compared with radical nephrectomy (2, 3). As a minimally invasive operation, robot-assisted PN (RAPN) is being increasingly performed globally, which has superiority in dissection and intracorporeal suturing (4, 5). As we all know, the major goals of PN are to control tumors, avoid intraoperative and postoperative complications, and preserve renal function (6). Three factors have been validated associated with postoperative renal function, including preoperative renal function, quantity of preserved renal parenchyma, and warm ischemia time (WIT), of which WIT was regarded as a major modifiable factor for renal function preservation (7).

In recent years, under the condition of more and more surgeons performing the RAPN with zero ischemia technique, namely, the off-clamp approach to minimize the WIT (8), plenty of studies have been conducted to identify whether the off-clamp RAPN is superior to the on-clamp in efficacy and safety, especially in postoperative renal function preservation (9–29). However, consensus of which clamping technique in RAPN is optimal with respect of perioperative, renal functional, and oncological outcomes remains controversial.

There were two published meta-analyses that compared the efficacy and safety of on-clamp and off-clamp RAPN, which both did not assert that the off-clamp approach is the optimal clamping technique in RAPN (30, 31). Whereafter, six novel original studies of the same topic have been published during 2019–2020 (24–29). Thus, we reported a pooled analysis and evidence update to compare the perioperative, renal functional, and oncological outcomes between off-clamp and on-clamp RAPN for renal tumors.

## MATERIALS AND METHODS

### Literature Search

The present evidence-based analysis was conducted following the PRISMA (Preferred Reporting Items for Systematic Reviews and Meta-Analysis) 2020 statement (32) and was prospectively registered in the PROSPERO (CRD42021228512). The PRISMA 2020 checklist is shown in **Supplementary Table S1**. We performed a systematic literature search using PubMed, Embase, and Web of Science up to August 2021 for studies that compared the efficacy and/or safety between off-clamp and on-clamp RAPN for renal tumors and published in English. We searched the databases using the following terms: "robot-assisted", "robotic-assisted", "robot", "robotic", "partial nephrectomy", "nephron sparing surgery", "clamp", "clamping", "off-clamp", and "on-clamp". The detailed search strategy is presented in **Supplementary Table S2**. In addition, the reference lists of all eligible studies were manually reviewed. Two investigators searched and evaluated the included studies independently. Any disagreement in literature search was resolved by consensus.

### Identification of Eligible Studies

Studies were included if they met the following criteria: (1) the study design was randomized controlled, cohort, or case–control; (2) studies were conducted in adults with renal tumors; (3) studies comparing off-clamp RAPN with on-clamp RAPN; (4) at least one perioperative (operating time, estimated blood loss (EBL), conversion rate, length of stay (LOS), complication rate, and transfusion rate), renal functional (postoperative estimated glomerular filtration rate (eGFR) decrease and serum creatine increase during follow-up), or oncological (positive surgical margins rate and recurrence rate) outcome was evaluated; and (5) sufficient data to calculate odds ratio (OR) or weighted mean difference (WMD).

We excluded reviews, letters, editorial comments, case reports, conference abstracts, pediatric articles, unpublished articles, and non-English articles. We defined the off-clamp RAPN as the RAPN performed without any hilar clamping procedure, and the on-clamp RAPN was identified as clamping the main renal artery during the entire procedure. Thus, studies that focused on selective-clamp RAPN, super-selective clamp RAPN, and early-unclamping RAPN were also excluded.

### Data Extraction

Data extraction was performed by two investigators independently. Any disagreement was resolved by the third investigator to make a final decision. We extracted the following data from included studies: first author, publication year, study period, country of study, study design, sample size, age, body mass index (BMI), American Society of Anesthesiologist (ASA) score, preoperative eGFR, preoperative serum creatinine, tumor size, R.E.N.A.L. score, follow-up time, operating time, EBL, conversion rate, LOS, complication rate, transfusion rate, long-term (postoperative 6 months or longer) % decrease in eGFR, positive surgical margin rate and recurrence rate. When continuous variables in the study were reported as median with range or interquartile range, we calculated the mean ± standard deviation through the validated mathematical method (33, 34). When data were missing or not reported in the study, we contacted the corresponding authors to obtain completed data if available.

### Quality Assessment

The Newcastle–Ottawa Scale (NOS) was used for evaluating the quality of included studies (35), and studies with seven to nine points were regarded as high quality (36). In addition, we assessed the level of evidence for each study according to the Oxford Centre for Evidence-Based Medicine Levels of Evidence Working Group (37). Two investigators independently evaluated the quality and level of evidence for eligible studies, and any discrepancy was resolved through discussion.

### Statistical Analysis

Evidence synthesis was performed in Review Manager 5.3 version (Cochrane Collaboration, Oxford, UK). The WMD and OR were applied for the comparison of continuous and dichotomous variables, respectively. All metrics were reported with 95% confidential intervals (CIs). The heterogeneity in studies was assessed through the chi-squared ($\chi^2$) test

(Cochran's *Q*) and inconsistency index ($I^2$) (38). $\chi^2$ *p* value < 0.05 or $I^2$ > 50% were considered as significant heterogeneity. A random-effect model was used to estimate the combined WMD or OR when significant heterogeneity was detected ($\chi^2$ *p* value < 0.05 or $I^2$ > 50%). Otherwise, the fixed-effect model was applied. In addition, we performed one-way sensitivity analyses to evaluate the effect of included studies on the combined results for outcomes with significant heterogeneity. Publication bias was evaluated visually by creating funnel plots *via* Review Manager 5.3 version (Cochrane Collaboration, Oxford, UK), as well as by conducting Egger's regression tests (39) using Stata 12.0 version (Stata Corp, College Station, TX, USA) for outcomes with 10 or more included studies. *p* value < 0.05 was considered as statistically significant publication bias.

# RESULTS

## Literature Search and Study Characteristics

The flowchart of the systematic search and selection process is presented in **Figure 1**. A total of 1,736 relevant articles in PubMed (n = 283), Embase (n = 974), and Web of Science (n = 479) were yielded through systematic literature search. After removing duplicate papers, 968 titles and abstracts were reviewed. Finally, 21 full-text articles involving 4,493 patients (1,274 off-clamp *versus* 3,219 on-clamp) were included for the pooled analysis (9–29). Of these articles, 7 were prospective cohort studies (9, 10, 12, 13, 16, 18, 25, 27), 10 were retrospective cohort studies (11, 14, 15, 17, 19–21, 23, 24, 29), and 3 were prospective randomized studies (22, 26, 28). **Table 1** shows the characteristics, level of evidence, and quality score of each included study. The median (range) quality score was 7 (5–8), and 15 studies were identified as high quality (9, 11, 12, 14, 16–24, 28, 29). The details of quality assessment of all eligible studies are presented in **Supplementary Table S3**.

## Demographic Characteristics

There were no significant differences among the two groups in terms of age (WMD: -0.16; 95% CI: -0.73, 0.41; $p = 0.58$), gender (male/total, OR: 0.99; 95% CI: 0.85, 1.15; $p = 0.87$), BMI (WMD: 0.19; 95% CI: -0.18, 0.56; $p = 0.32$), ASA score (WMD: 0.02; 95% CI: -0.08, 0.13; $p = 0.66$), preoperative eGFR (WMD: 0.89; 95% CI: -0.33, 2.11; $p = 0.15$), and preoperative serum creatine

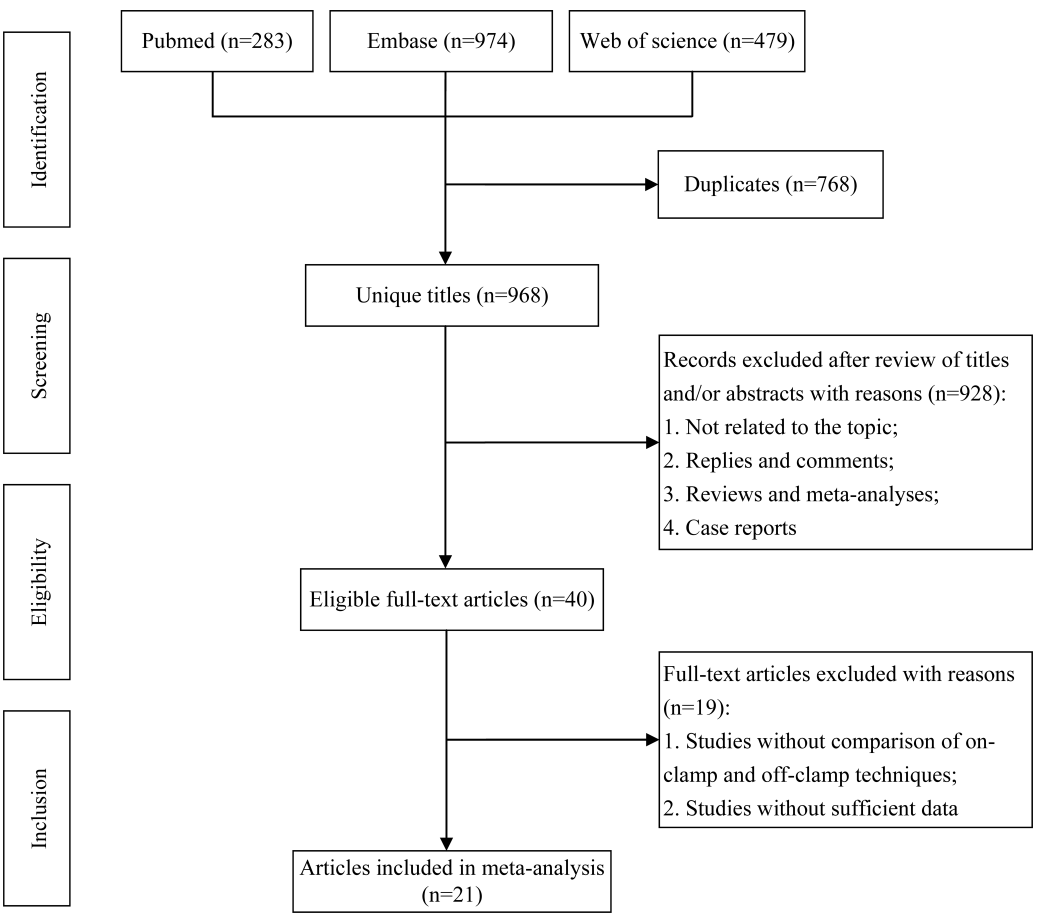



**FIGURE 1** | Flowchart of the systematic search and selection process.

**TABLE 1** | Baseline characteristics of include studies and methodological assessment.

| Authors | Study period | Country | Study design | Patients (n) Off-clamp/ on-clamp | Median follow-up (months) | Level of evidence | Quality score |
|---|---|---|---|---|---|---|---|
| White et al. (9) | 2008 | USA | Prospective | 8/20 | 15 | 2b | 8 |
| Novak et al. (10) | 2009–2010 | USA | Prospective | 22/35 | – | 4 | 6 |
| Tanagho et al. (11) | 2008–2011 | USA | Retrospective | 29/29 | 9 | 2b | 7 |
| Kaczmarek et al. (12) | 2007–2011 | USA | Prospective | 49/283 | 13.5 | 2b | 8 |
| Krane et al. (13) | 2010-2011 | USA | Prospective | 19/18 | 3.8 | 2b | 6 |
| Acar et al. (14) | 2010–2013 | Turkey | Retrospective | 30/14 | 18.9 | 2b | 8 |
| Komninos et al. (15) | 2007–2013 | Korea | Retrospective | 23/114 | – | 4 | 6 |
| Ener et al. (16) | 2009–2015 | Turkey | Prospective | 12/22 | – | 2b | 7 |
| Peyronnet et al. (17) | 2010–2014 | France | Retrospective | 26/104 | 12 | 2b | 8 |
| Rosen et al. (18) | 2008–2016 | USA | Prospective | 41/82 | 9.2 | 2b | 7 |
| Anderson et al. (19) | 2009–2015 | USA | Retrospective | 50/50 | 9 | 2b | 7 |
| Mari et al. (20) | 2011–2014 | Italy | Retrospective | 120/120 | 40 | 2b | 8 |
| Taweemonkongsap et al. (21) | 2010–2016 | Thailand | Retrospective | 12/27 | 18 | 2b | 8 |
| Anderson et al. (22) | 2013–2017 | USA | Prospective | 40/30 | 3 | 1b | 7 |
| Bertolo et al. (23) | 2007–2017/2010–2017 | USA/Italy | Retrospective | 200/400 | – | 2b | 7 |
| Guo et al. (24) | 2015–2017 | China | Retrospective | 48/45 | 12 | 2b | 8 |
| Anceschi et al. (25) | 2013–2019 | USA/Italy | Prospective | 27/27 | 13 | 2b | 6 |
| Antonelli et al. (26) | 2014–2018 | Italy | Prospective | 91/129 | – | 1b | 6 |
| Beksac et al. (27) | 2006–2018 | USA | Prospective | 39/375 | – | 2b | 5 |
| Antonelli et al. (28) | 2015–2018 | Italy | Prospective | 164/160 | – | 1b | 7 |
| Mellouki et al. (29) | 2011–2019 | France | Retrospective | 224/1135 | 38 | 2b | 7 |

(WMD: -0.01; 95% CI: -0.06, 0.03; $p = 0.60$). However, the two groups were significantly different in baseline characteristics in terms of R.E.N.A.L. score (WMD: -0.55; 95% CI: -0.93, -0.17; $p = 0.004$) and tumor size (WMD: -0.37; 95% CI: -0.67, -0.08; $p = 0.01$) (**Table 2**).

## Operating Time

Data of operating time were synthesized from 17 studies including 2,636 patients (833 off-clamp *versus* 1,803 on-clamp) (9–16, 18–24, 26, 27). Pooled analysis revealed a significant shorter operating time in the off-clamp group (WMD: -18.93; 95% CI: -33.87, -4.00; $p = 0.01$) with a significant heterogeneity ($I^2 = 96\%$, $p < 0.00001$) (**Figure 2A**). A visual assessment of the funnel plot indicated the presence of slight publication bias (**Figure 3A**). However, Egger's test was not statistically significant ($p = 0.737$).

## EBL

Analysis of EBL was conducted in 16 studies with 3,338 patients (835 off-clamp *versus* 2503 on-clamp) (9, 11–16, 18–22, 24, 26, 27, 29). Pooled analysis detected a significantly higher EBL in the off-clamp group (WMD: 20.27; 95% CI: 6.11, 34.44; $p = 0.005$) with a statistically significant heterogeneity ($I^2 = 79\%$, $p < 0.00001$) (**Figure 2B**). Funnel plots revealed a slight publication bias (**Figure 3B**) while no statistically significant publication bias was detected through Egger's test ($p = 0.061$).

## Conversion Rate

Seven studies involving 577 patients (206 off-clamp *versus* 371 on-clamp) were included in the analysis (14, 15, 17, 21, 22, 24, 25). Pooled results demonstrated that the rate of conversion to radical or open surgery was similar between the two groups (OR: 1.57; 95% CI: 0.54, 4.60; $p = 0.41$), and no significant heterogeneity was observed ($I^2 = 0\%$, $p = 0.88$) (**Figure 2C**).

**TABLE 2** | Demographics and clinical characteristics of included studies.

| Outcomes | Studies | No. of patients | WMD or OR | 95% CI | p-value | Heterogeneity | | | |
|---|---|---|---|---|---|---|---|---|---|
| | | Off-clamp/On-clamp | | | | $Chi^2$ | df | p-value | $I^2$ (%) |
| Age (years) | (19) | 1,129/3,107 | -0.16 | [-0.73, 0.41] | 0.58 | 15.61 | 18 | 0.62 | 0 |
| Gender (male) | (17) | 670/1,568 | 0.99 | [0.85, 1.15] | 0.87 | 17.48 | 16 | 0.87 | 8 |
| BMI (kg/m$^2$) | (16) | 952/2,309 | 0.19 | [-0.18, 0.56] | 0.32 | 10.01 | 15 | 0.82 | 0 |
| ASA score | (6) | 263/582 | 0.02 | [-0.08, 0.13] | 0.66 | 3.42 | 5 | 0.63 | 0 |
| R.E.N.A.L. score | (17) | 1,101/2,967 | -0.55 | [-0.93, -0.17] | 0.004[a] | 106.75 | 16 | <0.00001 | 85 |
| Tumor size (cm) | (19) | 1,199/2,842 | -0.37 | [-0.67, -0.08] | 0.01[a] | 238.44 | 18 | <0.00001 | 92 |
| Preoperative eGFR (mL/min/1.73 m$^2$) | (17) | 968/1,925 | 0.89 | [-0.33, 2.11] | 0.15 | 60.37 | 16 | <0.00001 | 73 |
| Preoperative sCr (mg/dL) | (6) | 229/251 | -0.01 | [-0.06, 0.03] | 0.60 | 5.50 | 5 | 0.36 | 9 |

[a]*Statistically significant.*

*BMI, body mass index; ASA, American Society of Anesthesiologists; eGFR, estimated glomerular filtration rate; sCr, serum creatine; WMD, weighted mean difference; OR, odds ratio; CI, confidence interval.*

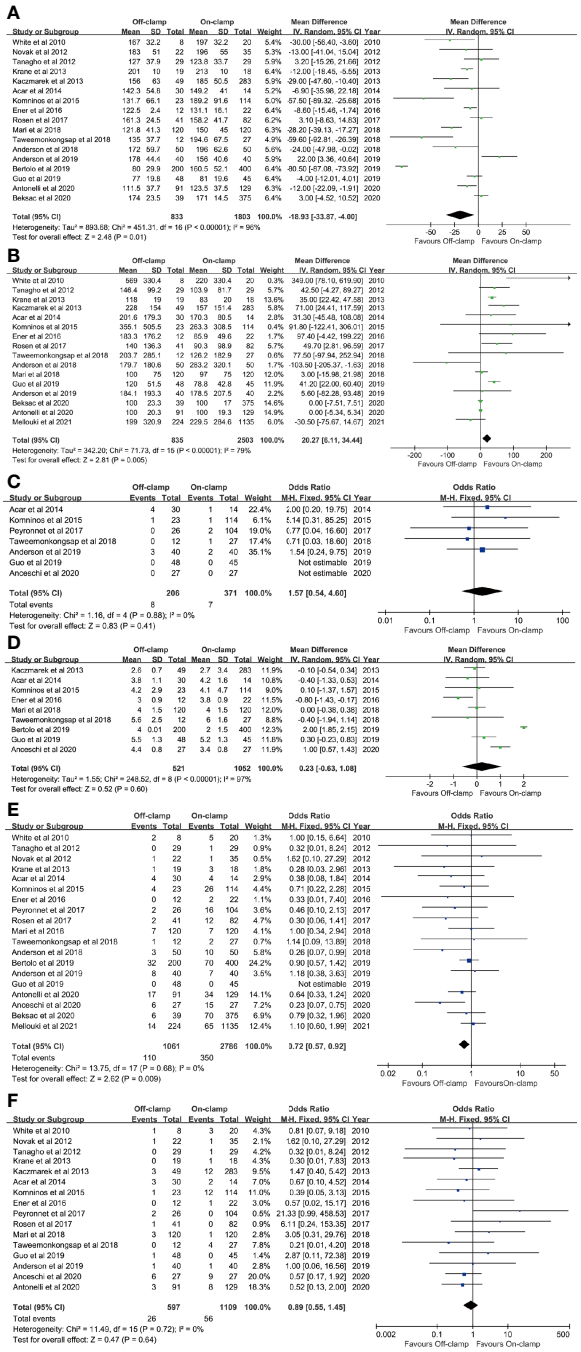



**FIGURE 2** | Forest plots of perioperative outcomes: **(A)** operating time, **(B)** estimated blood loss, **(C)** conversion rate, **(D)** length of stay, **(E)** complication rate, and **(F)** transfusion rate.

## LOS

Nine articles reported the data of LOS, including 1,573 patients (521 off-clamp *versus* 1,052 on-clamp) (12, 14–16, 20, 21, 23–25). No significant difference was detected among the two groups (WMD: 0.23; 95% CI: -0.63, 1.08; $p$ = 0.60), but statistically significant heterogeneity was observed ($I^2$ = 97%, $p$ < 0.00001) (**Figure 2D**).

## Complication rate

Data of the complication rate (including intraoperative and/or postoperative complications) were available in 19 studies with a total of 3,847 patients (1,061 off-clamp versus 2,786 on-clamp) (9–11, 13–27, 29). Pooled analysis revealed a significantly lower rate of complication in the off-clamp group compared with the

on-clamp group (OR: 0.72; 95% CI: 0.57, 0.92; $p$ = 0.009) (**Figure 2E**). No significant heterogeneity ($I^2$ = 0%, $p$ = 0.68) and statistical (Egger's test, $p$ = 0.067) or visual (**Figure 3C**) evidence of publication bias were detected.

## Transfusion Rate

There were 16 articles that reported the data of transfusion rate between the two groups, including 1,706 patients (597 off-clamp *versus* 1,109 on-clamp) (9–18, 20–22, 24–26). Evidence synthesis observed a similar transfusion rate in the two groups (OR: 0.89; 95% CI: 0.55, 1.45; $p$ = 0.64) without significant heterogeneity ($I^2$ = 0%, $p$ = 0.72) (**Figure 2F**) and statistical (Egger's test, $p$ = 0.368) or visual (**Figure 3D**) evidence of publication bias.

## Positive Surgical Margin Rate

Eighteen studies with 3,664 patients (1,000 off-clamp *versus* 2,664 on-clamp) were included in the analysis for positive surgical margin rate (9–11, 13–15, 17–27, 29). Pooled analysis indicated that the off-clamp group had a significantly lower positive surgical margin rate (OR: 0.54; 95% CI: 0.36, 0.79; $p$ = 0.002) (**Figure 4A**). No significant heterogeneity ($I^2$ = 0%, $p$ = 0.92) and statistical (Egger's test, $p$ = 0.946) or visual (**Figure 3E**) evidence of publication bias were observed.

## Recurrence Rate

Data of recurrence rate were obtained from nine studies with 2,462 patients (576 off-clamp *versus* 1,886 on-clamp) (12, 13, 15, 17, 20, 22, 24, 25, 29). No significant difference was observed between the two groups for recurrence rate (OR: 0.89; 95% CI: 0.52, 1.54; $p$ = 0.69), and no significant heterogeneity ($I^2$ = 0%, $p$ = 0.87) was detected (**Figure 4B**).

## Long-Term % Decrease in eGFR

Ten articles were included in the analysis for long-term % decrease in eGFR, involving 1,417 patients (566 off-clamp *versus* 851 on-clamp) (11–13, 18–22, 24, 28). Evidence synthesis showed that the off-clamp group had a significantly lower long-term % decrease in eGFR (WMD: -3.17; 95% CI: -5.81, -0.54; $p$ = 0.02) with a significant heterogeneity ($I^2$ = 81%, $p$ < 0.00001) (**Figure 5**). Both funnel plot (**Figure 3F**) and Egger's test ($p$ = 0.423) did not detect publication bias.

## Sensitivity Analysis

We conducted one-way sensitivity analyses for comparison of operating time, EBL, LOS, and long-term % decrease in eGFR to evaluate the influence of each individual study on the combined WMD through removing the individual study one by one. Sensitivity analyses revealed that the new combined WMD remained constant after exclusion of any individual study for operating time (**Figure 6A**), EBL (**Figure 6B**), LOS (**Figure 6C**), and long-term % decrease in eGFR (**Figure 6D**). However, when we excluded the data reported by Antonelli et al. in 2021 (28), the heterogeneity for the long-term % decrease in eGFR disappeared ($I^2$ = 21%, $p$ = 0.26), suggesting that this study accounts for most of the heterogeneity.

# DISCUSSION

At present, RAPN has been performed widely as a favorable surgical procedure for patients with localized renal tumors since its superiority in dissection, intracorporeal suturing, and preservation of renal function (40, 41). As we all know, there

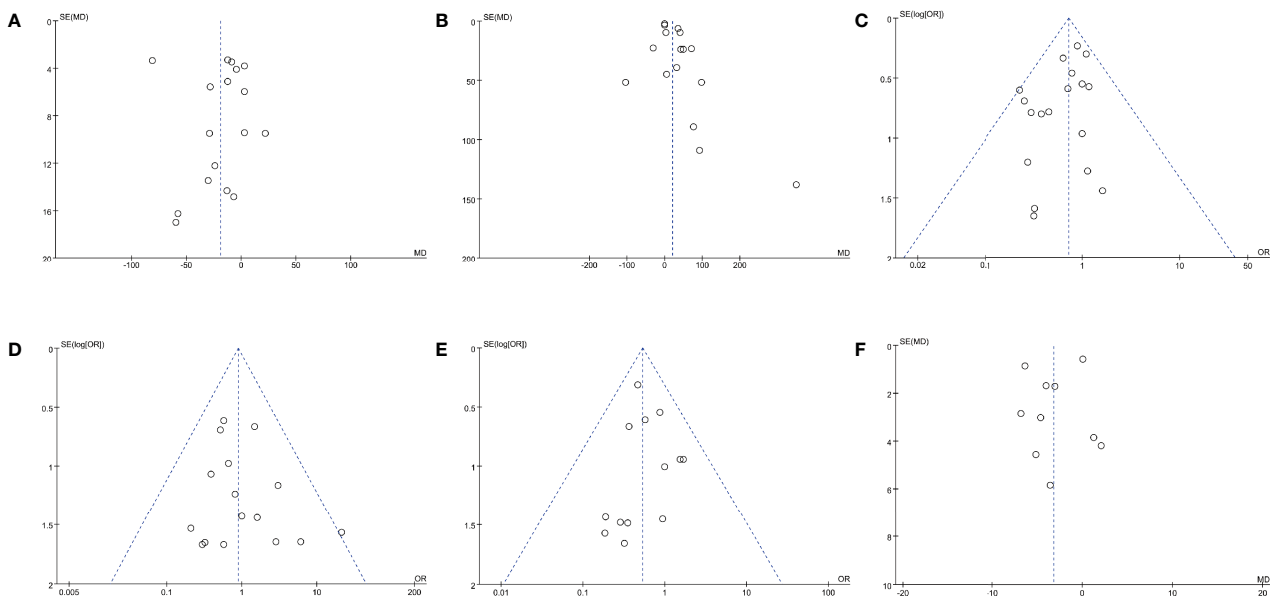



**FIGURE 3** | Funnel plots of **(A)** operating time, **(B)** EBL, **(C)** complication rate, **(D)** transfusion rate, **(E)** positive surgical margins rate, and **(F)** long-term % decrease in eGFR.

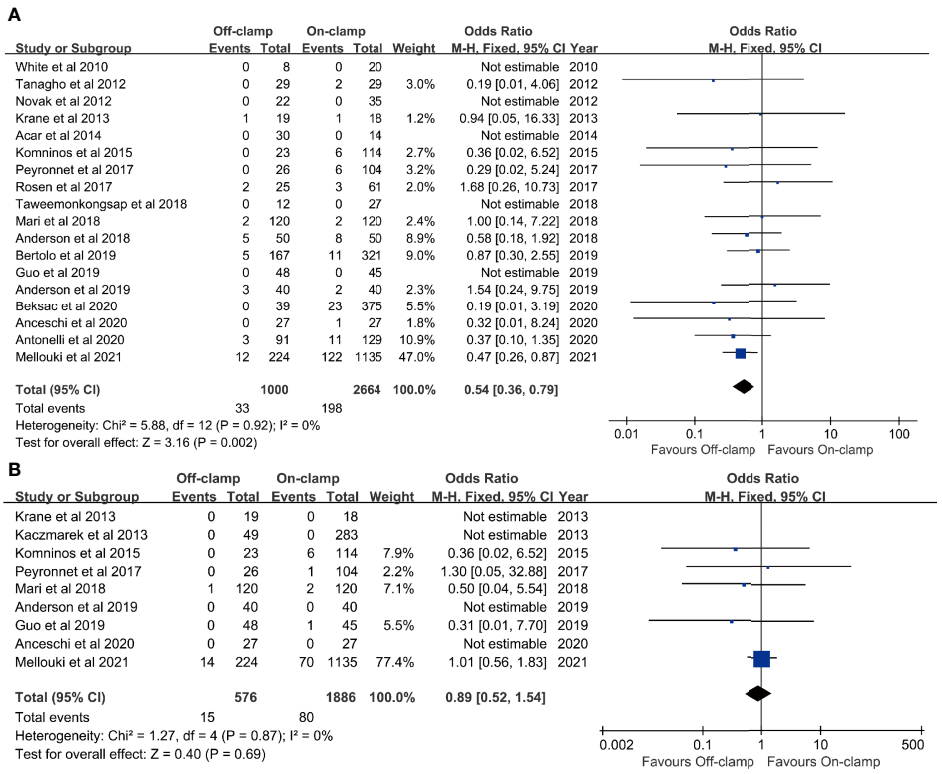



**FIGURE 4** | Forest plots of oncological outcomes: **(A)** positive surgical margins rate and **(B)** recurrence rate.

are three factors that have been regarded as major predictors of postoperative renal function: preoperative renal function, quantity of preserved renal parenchyma, and WIT (42). In 2009, White et al. firstly reported a comparative study of RAPN with or without clamping of the renal artery, which initially evaluated the efficacy and safety of the zero ischemia technique in RAPN (9). After that, numerous cohort studies that focused on the comparison of off-clamp RAPN with on-clamp RAPN have been published. However, the perioperative, oncological, and renal functional outcomes of the two clamping techniques in RAPN were still a matter of wide debate all over the world (14, 17, 22, 24, 30, 31). Under these conditions, we performed the latest and largest systematic review and pooled analysis of 21 comparative studies including 4,493 patients, and our results revealed several important findings.

First, results on perioperative outcomes showed a significantly shorter operating time in the off-clamp group, however, which may attribute to the selective bias that the off-clamp group had a lower R.E.N.A.L. score and smaller tumor size. Similarly, data from the CLOCK Randomized

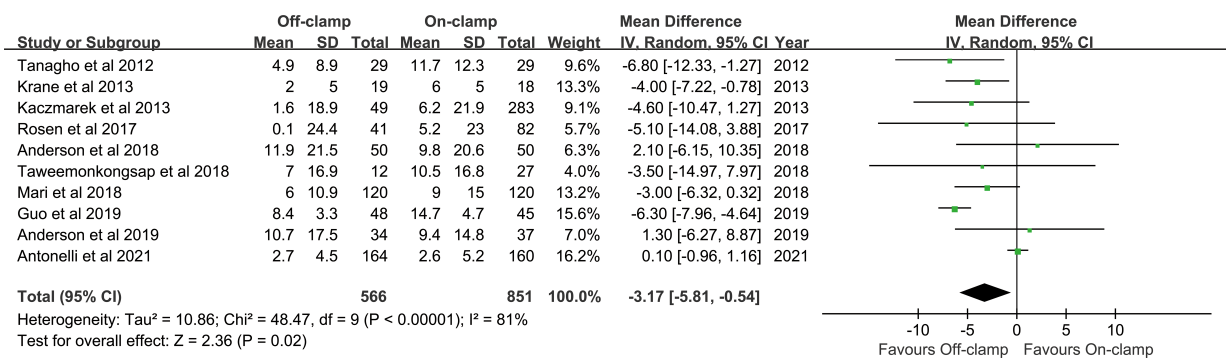



**FIGURE 5** | Forest plots of renal functional outcome: long-term % decrease in eGFR.

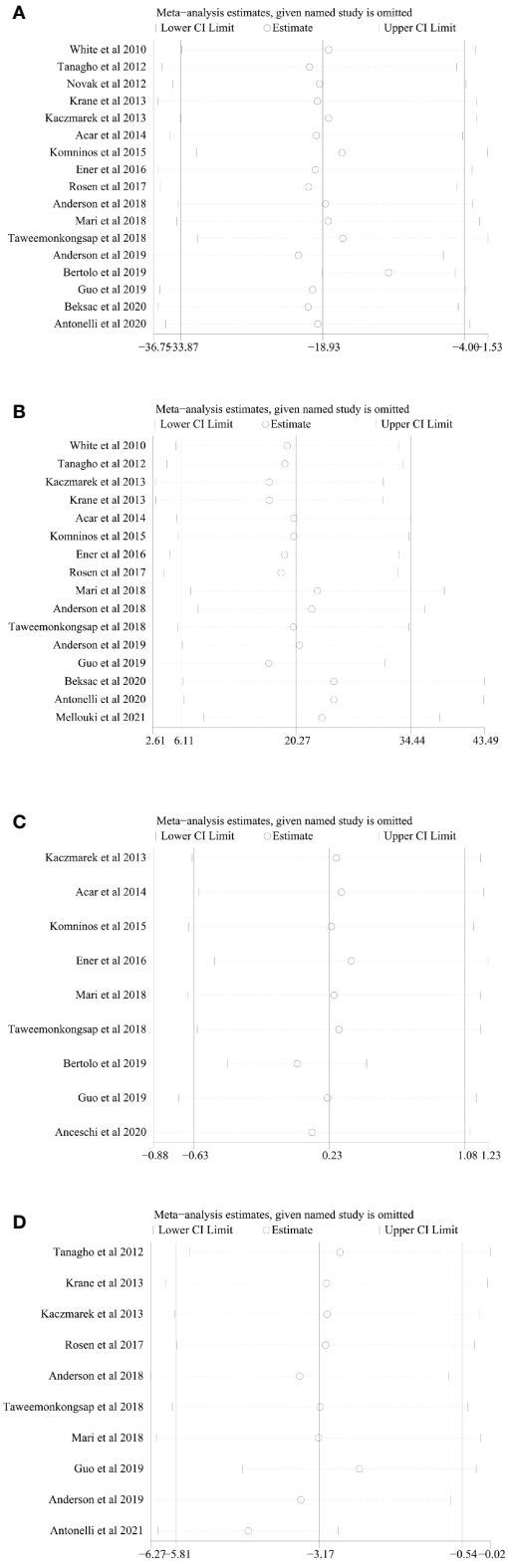



**FIGURE 6** | Sensitivity analysis of **(A)** operating time, **(B)** estimated blood loss, **(C)** length of stay, and **(D)** long-term % decrease in eGFR.

Clinical Trial indicated that the transition from off-clamp to on-clamp RAPN is also associated with renal mass diameter and complexity (43). In addition, shorter operative time in the off-clamp group was likely related to the lower complexity of tumors in the group and the avoidance of renal pedicle dissection in the technique (17, 23). Higher EBL was observed in the off-clamp group, reasonably due to the natural result of unclamping the renal vessels during the surgical procedure (12). Although the difference of EBL was statistically significant, its clinical relevance was limited since the transfusion rates were similar in the two clamping techniques. Moreover, we observed a lower complication rate in the off-clamp group. However, as mentioned previously, the difference may also be related to the smaller tumor size and the lower complexity of tumors in the off-clamp group (44). Patients who underwent on-clamp RAPN may be more technically challenging (19). Furthermore, conversion rates and LOS were similar in the two groups.

Second, analyses of the oncological outcomes in the two clamping techniques revealed a lower positive surgical margin rate in the off-clamp group but similar rates of recurrence in the two groups, which contradicts previous meta-analyses that did not observe a significant difference in the positive surgical margin rate (30, 31). However, the reason for these findings was still unclear. We might still assume that the complexity of tumors and clamping technique itself may influence the tumor dissection technique, leading to the different positive surgical margin rate in the two groups. On the other hand, a retrospective study reported by Shah et al. found that positive surgical margins after PN were associated with an increased risk of recurrence (45), while the relationship between positive surgical margins and recurrence after RAPN is still uncertain.

Third, a pooled analysis of renal functional outcome evaluated by a long-term % decrease in eGFR showed that the off-clamp group had a superior preservation of postoperative renal function. The present result was consistent with the finding of the meta-analysis reported by Cacciamani et al. (31), but contradicted the report of Antonelli et al. (30). Although there was significant heterogeneity in the long-term % decrease in eGFR, the difference remained significant when we excluded the main sources of heterogeneity (WMD: -4.48; 95% CI: -6.14, -2.82; $p < 0.00001$). However, it is worth noting that superior functional outcomes of the off-clamp group which are reported by previous observational studies (11, 13, 24) have not been confirmed in any RCTs (22, 28), indicating potential selection bias in our meta-analysis. Moreover, short-term renal functional outcomes after RAPN are still controversial (12, 15). Unfortunately, we failed to evaluate the short-term change in eGFR of the two groups since the deficiency of data and the data of change in serum creatine, which is another important measurement of postoperative change in renal function, were also insufficient to conduct pooled analysis.

Our study reported the latest and largest evidence-based analysis that directly and exclusively compared the perioperative, renal functional, and oncological outcomes of off-clamp and on-clamp RAPN in patients with renal tumors. However, we must acknowledge several limitations of the present

study. Primarily, there were only three prospective randomized studies (9.5%) included in our pooled analysis. Most of the included studies were retrospective or prospective cohort design, without proper control of confounders. Furthermore, significant heterogeneity was observed in several outcomes including operating time, EBL, LOS, and long-term % decrease in eGFR. Although we performed sensitivity analyses to evaluate the stability of results, the derivation of heterogeneity was still unclear for several outcomes. Considering the potential confounders, results of the present pooled analysis should be interpreted with caution. Finally, we failed to provide a more comprehensive evaluation of the postoperative renal functional outcomes in the two groups due to the insufficient data of short-term change in eGFR and the increase of serum creatine after RAPN.

Notwithstanding several limitations of our study, we reported the latest and largest meta-analysis that added six novel articles (four cohort studies (24, 25, 27, 29) and two prospective randomized studies (26, 28) published during 2019–2021 on the bases of previous studies, which makes our evidence more credible. Our evidence-based analysis validated previous studies reporting the superiority of the off-clamp technique in RAPN (9, 10, 12, 20), especially in patients who require preservation of renal function (e.g., solitary kidney or chronic kidney disease) (23). More well-designed, large-scale prospective randomized studies with long-term follow-up are needed to further compare the perioperative, oncological, and renal functional superiority in these two clamping approaches in RAPN.

## CONCLUSION

Pooled analyses demonstrated that off-clamp was an effective and safe technique with superiority in operating time, EBL, complications, positive surgical margins, and long-term preservation of renal function compared with the on-clamp approach in RAPN. Given the presence of heterogeneity and potential bias, urologists should select the clamp strategy based on their experience and patient-specific factors.

## DATA AVAILABILITY STATEMENT

The raw data supporting the conclusions of this article will be made available by the authors, without undue reservation.

## ETHICS STATEMENT

Ethical review and approval were not required for the study on human participants in accordance with the local legislation and institutional requirements.

## AUTHOR CONTRIBUTIONS

(I) Conception and design: YH and DC. (II) Administrative support: QD, LL, and QW. (III) Provision of study materials or patients: YH and DC. (IV) Collection and assembly of data: YH, DC, ZC, BC, JG, and JL. (V) Data analysis and interpretation: YH and DC. (VI) Manuscript writing: YH, DC, ZC, BC, JL, JG, QD, LL, and QW. All authors contributed to the article and approved the submitted version.

## FUNDING

This study was funded by the National Natural Science Foundation of China (Grant Number 82000721) and Programs from the Department of Science and Technology of Sichuan Province (Grant Number 2020YJ0054).

## SUPPLEMENTARY MATERIAL

The Supplementary Material for this article can be found online at: https://www.frontiersin.org/articles/10.3389/fonc.2021.730662/full#supplementary-material

## REFERENCES

1. Siegel RL, Miller KD, Jemal A. Cancer Statistics, 2020. *CA: Cancer J Clin* (2020) 70(1):7–30. doi: 10.3322/caac.21590
2. Campbell S, Uzzo RG, Allaf ME, Bass EB, Cadeddu JA, Chang A, et al. Renal Mass and Localized Renal Cancer: AUA Guideline. *J Urol* (2017) 198(3):520–9. doi: 10.1016/j.juro.2017.04.100
3. Ljungberg B, Albiges L, Abu-Ghanem Y, Bensalah K, Dabestani S, Fernández-Pello S, et al. European Association of Urology Guidelines on Renal Cell Carcinoma: The 2019 Update. *Eur Urol* (2019) 75(5):799–810. doi: 10.1016/j.eururo.2019.02.011
4. Khalifeh A, Autorino R, Eyraud R, Samarasekera D, Laydner H, Panumatrassamee K, et al. Three-Year Oncologic and Renal Functional Outcomes After Robot-Assisted Partial Nephrectomy. *Eur Urol* (2013) 64(5):744–50. doi: 10.1016/j.eururo.2013.03.052
5. Sukumar S, Rogers CG. Robotic Partial Nephrectomy: Surgical Technique. *BJU Int* (2011) 108(6 Pt 2):942–7. doi: 10.1111/j.1464-410X.2011.10457.x
6. Hung AJ, Cai J, Simmons MN, Gill IS. "Trifecta" in Partial Nephrectomy. *J Urol* (2013) 189(1):36–42. doi: 10.1016/j.juro.2012.09.042
7. Mir MC, Ercole C, Takagi T, Zhang Z, Velet L, Remer EM, et al. Decline in Renal Function After Partial Nephrectomy: Etiology and Prevention. *J Urol* (2015) 193(6):1889–98. doi: 10.1016/j.juro.2015.01.093
8. Gill IS, Eisenberg MS, Aron M, Berger A, Ukimura O, Patil MB, et al. "Zero Ischemia" Partial Nephrectomy: Novel Laparoscopic and Robotic Technique. *Eur Urol* (2011) 59(1):128–34. doi: 10.1016/j.eururo.2010.10.002
9. White WM, Goel RK, Haber G-P, Kaouk JH. Robotic Partial Nephrectomy Without Renal Hilar Occlusion. *BJU Int* (2010) 105(11):1580–4. doi: 10.1111/j.1464-410X.2009.09033.x
10. Novak R, Mulligan D, Abaza R. Robotic Partial Nephrectomy Without Renal Ischemia. *Urology* (2012) 79(6):1296–301. doi: 10.1016/j.urology.2012.01.065
11. Tanagho YS, Bhayani SB, Sandhu GS, Vaughn NP, Nepple KG, Figenshau RS. Renal Functional and Perioperative Outcomes of Off-Clamp *Versus* Clamped Robot-Assisted Partial Nephrectomy: Matched Cohort Study. *Urology* (2012) 80(4):838–43. doi: 10.1016/j.urology.2012.04.074
12. Kaczmarek BF, Tanagho YS, Hillyer SP, Mullins JK, Diaz M, Trinh QD, et al. Off-Clamp Robot-Assisted Partial Nephrectomy Preserves Renal Function: A Multi-Institutional Propensity Score Analysis. *Eur Urol* (2013) 64(6):988–93. doi: 10.1016/j.eururo.2012.10.009

13. Krane LS, Mufarrij PW, Manny TB, Hemal AK. Comparison of Clamping Technique in Robotic Partial Nephrectomy: Does Unclamped Partial Nephrectomy Improve Perioperative Outcomes and Renal Function? *Can J Urol* (2013) 20(1):6662–7.
14. Acar Ö, Esen T, Musaoğlu A, Vural M. Do We Need to Clamp the Renal Hilum Liberally During the Initial Phase of the Learning Curve of Robot-Assisted Nephron-Sparing Surgery? *TheScientificWorldJournal* (2014) 2014:498917. doi: 10.1155/2014/498917
15. Komninos C, Shin TY, Tuliao P, Han WK, Chung BH, Choi YD, et al. Renal Function Is the Same 6 Months After Robot-Assisted Partial Nephrectomy Regardless of Clamp Technique: Analysis of Outcomes for Off-Clamp, Selective Arterial Clamp and Main Artery Clamp Techniques, With a Minimum Follow-Up of 1 Year. *BJU Int* (2015) 115(6):921–8. doi: 10.1111/bju.12975
16. Ener K, Canda AE, Altınova S, Atmaca AF, Alkan E, Asil E, et al. Impact of Robotic Partial Nephrectomy With and Without Ischemia on Renal Functions: Experience in 34 Cases. *Turkish J Urol* (2016) 42(4):272–7. doi: 10.5152/tud.2016.67790
17. Peyronnet B, Khene ZE, Pradère B, Seisen T, Verhoest G, Masson-Lecomte A, et al. Off-Clamp *Versus* On-Clamp Robotic Partial Nephrectomy: A Multicenter Match-Paired Case-Control Study. *Urologia Internationalis* (2017) 99(3):272–6. doi: 10.1159/000471772
18. Rosen DC, Paulucci DJ, Abaza R, Eun DD, Bhandari A, Hemal AK, et al. Is Off Clamp Always Beneficial During Robotic Partial Nephrectomy? A Propensity Score-Matched Comparison of Clamp Technique in Patients With Two Kidneys. *J Endourology* (2017) 31(11):1176–82. doi: 10.1089/end.2017.0450
19. Anderson BG, Potretzke AM, Du K, Vetter J, Figenshau RS. Off-Clamp Robot-Assisted Partial Nephrectomy Does Not Benefit Short-Term Renal Function: A Matched Cohort Analysis. *J Robotic Surg* (2018) 12(3):401–7. doi: 10.1007/s11701-017-0745-6
20. Mari A, Morselli S, Sessa F, Campi R, Di Maida F, Greco I, et al. Impact of the Off-Clamp Endoscopic Robot-Assisted Simple Enucleation (ERASE) of Clinical T1 Renal Tumors on the Postoperative Renal Function: Results From a Matched-Pair Comparison. *Eur J Surg Oncol J Eur Soc Surg Oncol Br Assoc Surg Oncol* (2018) 44(6):853–8. doi: 10.1016/j.ejso.2018.01.093
21. Taweemonkongsap T, Suk-Ouichai C, Chotikawanich E, Jitpraphai S, Woranisarakul V, Ramart P, et al. The Impact of Arterial Clamping Technique in Robot-Assisted Partial Nephrectomy on Renal Function and Surgical Outcomes: Six-Year Experience at Siriraj Hospital, Thailand. *Urologia Internationalis* (2018) 100(3):301–8. doi: 10.1159/000486319
22. Anderson BG, Potretzke AM, Du K, Vetter JM, Bergeron K, Paradis AG, et al. Comparing Off-Clamp and On-Clamp Robot-Assisted Partial Nephrectomy: A Prospective Randomized Trial. *Urology* (2019) 126:102–9. doi: 10.1016/j.urology.2018.11.053
23. Bertolo R, Simone G, Garisto J, Nakhoul G, Armanyous S, Agudelo J, et al. Off-Clamp *vs* on-Clamp Robotic Partial Nephrectomy: Perioperative, Functional and Oncological Outcomes From a Propensity-Score Matching Between Two High-Volume Centers. *Eur J Surg Oncol J Eur Soc Surg Oncol Br Assoc Surg Oncol* (2019) 45(7):1232–7. doi: 10.1016/j.ejso.2018.12.005
24. Guo J, Zhang C, Zhou X, Wang G, Fu B. Robot-Assisted Retroperitoneal Laparoscopic Partial Nephrectomy Without Hilar Occlusion *VS* Classic Robot-Assisted Retroperitoneal Laparoscopic Partial Nephrectomy: A Retrospective Comparative Study. *Med (Baltimore)* (2019) 98(38):e17263. doi: 10.1097/md.0000000000017263
25. Anceschi U, Brassetti A, Bertolo R, Tuderti G, Ferriero MC, Mastroianni R, et al. On-Clamp *Versus* Purely Off-Clamp Robot-Assisted Partial Nephrectomy in Solitary Kidneys: Comparison of Perioperative Outcomes and Chronic Kidney Disease Progression at Two High- Volume Centers. *Minerva Urologica e Nefrologica = Ital J Urol Nephrol* (2020). doi: 10.23736/s0393-2249.20.03795-9
26. Antonelli A, Cindolo L, Sandri M, Bertolo R, Annino F, Carini M, et al. Safety of on- *vs* Off-Clamp Robotic Partial Nephrectomy: Per-Protocol Analysis From the Data of the CLOCK Randomized Trial. *World J Urol* (2020) 38(5):1101–8. doi: 10.1007/s00345-019-02879-4
27. Beksac AT, Okhawere KE, Rosen DC, Elbakry A, Dayal BD, Daza J, et al. Do Patients With Stage 3-5 Chronic Kidney Disease Benefit From Ischaemia-Sparing Techniques During Partial Nephrectomy? *BJU Int* (2020) 125(3):442–8. doi: 10.1111/bju.14956
28. Antonelli A, Cindolo L, Sandri M, Veccia A, Annino F, Bertagna F, et al. Is Off-Clamp Robot-Assisted Partial Nephrectomy Beneficial for Renal Function? Data From the CLOCK Trial. *BJU Int* (2021). doi: 10.1111/bju.15503
29. Mellouki A, Bentellis I, Morrone A, Doumerc N, Beauval JB, Roupret M, et al. Evaluation of Oncological Outcomes of Robotic Partial Nephrectomy According to the Type of Hilar Control Approach (On-Clamp *vs* Off-Clamp), A Multicentric Study of the French Network of Research on Kidney Cancer-UROCCR 58-Nct03293563. *World J Urol* (2021). doi: 10.1007/s00345-020-03558-5
30. Antonelli A, Veccia A, Francavilla S, Bertolo R, Bove P, Hampton LJ, et al. On-Clamp *Versus* Off-Clamp Robotic Partial Nephrectomy: A Systematic Review and Meta-Analysis. *Urologia J* (2019) 86(2):52–62. doi: 10.1177/0391560319847847
31. Cacciamani GE, Medina LG, Gill TS, Mendelsohn A, Husain F, Bhardwaj L, et al. Impact of Renal Hilar Control on Outcomes of Robotic Partial Nephrectomy: Systematic Review and Cumulative Meta-Analysis. *Eur Urol Focus* (2019) 5(4):619–35. doi: 10.1016/j.euf.2018.01.012
32. Page MJ, McKenzie JE, Bossuyt PM, Boutron I, Hoffmann TC, Mulrow CD, et al. The PRISMA 2020 Statement: An Updated Guideline for Reporting Systematic Reviews. *BMJ (Clinical Res ed)* (2021) 372:n71. doi: 10.1136/bmj.n71
33. Wan X, Wang W, Liu J, Tong T. Estimating the Sample Mean and Standard Deviation From the Sample Size, Median, Range and/or Interquartile Range. *BMC Med Res Method* (2014) 14:135. doi: 10.1186/1471-2288-14-135
34. Luo D, Wan X, Liu J, Tong T. Optimally Estimating the Sample Mean From the Sample Size, Median, Mid-Range, and/or Mid-Quartile Range. *Stat Methods Med Res* (2018) 27(6):1785–805. doi: 10.1177/0962280216669183
35. Wells G, Shea B, O'Connell D, Peterson J, Welch V, Losos M, et al. *The Newcastle-Ottawa Scale (NOS) for Assessing the Quality of Nonrandomised Studies in Meta-Analyses* (2011). Available at: http://www.ohri.ca/programs/clinical_epidemiology/oxford.asp.
36. Kim SR, Kim K, Lee SA, Kwon SO, Lee JK, Keum N, et al. Effect of Red, Processed, and White Meat Consumption on the Risk of Gastric Cancer: An Overall and Dose¯Response Meta-Analysis. *Nutrients* (2019) 11(4):826. doi: 10.3390/nu11040826
37. Howick J, Chalmers I, Glasziou P, Greenhalgh T, Heneghan C, Liberati A, et al. *Explanation of the 2011 Oxford Centre for Evidence-Based Medicine (OCEBM) Levels of Evidence (Background Document): Oxford Centre for Evidence-Based Medicine*. Available at: https://www.cebm.ox.ac.uk/resources/levels-of-evidence/explanation-of-the-2011-ocebm-levels-of-evidence/.
38. Higgins JP, Thompson SG. Quantifying Heterogeneity in a Meta-Analysis. *Stat Med* (2002) 21(11):1539–58. doi: 10.1002/sim.1186
39. Egger M, Davey Smith G, Schneider M, Minder C. Bias in Meta-Analysis Detected by a Simple, Graphical Test. *BMJ (Clinical Res ed)* (1997) 315(7109):629–34. doi: 10.1136/bmj.315.7109.629
40. Hu JC, Treat E, Filson CP, McLaren I, Xiong S, Stepanian S, et al. Technique and Outcomes of Robot-Assisted Retroperitoneoscopic Partial Nephrectomy: A Multicenter Study. *Eur Urol* (2014) 66(3):542–9. doi: 10.1016/j.eururo.2014.04.028
41. Rassweiler JJ, Autorino R, Klein J, Mottrie A, Goezen AS, Stolzenburg JU, et al. Future of Robotic Surgery in Urology. *BJU Int* (2017) 120(6):822–41. doi: 10.1111/bju.13851
42. Rod X, Peyronnet B, Seisen T, Pradere B, Gomez FD, Verhoest G, et al. Impact of Ischaemia Time on Renal Function After Partial Nephrectomy: A Systematic Review. *BJU Int* (2016) 118(5):692–705. doi: 10.1111/bju.13580
43. Antonelli A, Cindolo L, Sandri M, Annino F, Carini M, Celia A, et al. Predictors of the Transition From Off to On Clamp Approach During Ongoing Robotic Partial Nephrectomy: Data From the CLOCK Randomized Clinical Trial. *J Urol* (2019) 202(1):62–8. doi: 10.1097/ju.0000000000000194
44. Greco F, Autorino R, Altieri V, Campbell S, Ficarra V, Gill I, et al. Ischemia Techniques in Nephron-Sparing Surgery: A Systematic Review and Meta-Analysis of Surgical, Oncological, and Functional Outcomes. *Eur Urol* (2019) 75(3):477–91. doi: 10.1016/j.eururo.2018.10.005
45. Shah PH, Moreira DM, Okhunov Z, Patel VR, Chopra S, Razmaria AA, et al. Positive Surgical Margins Increase Risk of Recurrence After Partial

Nephrectomy for High Risk Renal Tumors. *J Urol* (2016) 196(2):327–34. doi: 10.1016/j.juro.2016.02.075

**Conflict of Interest:** The authors declare that the research was conducted in the absence of any commercial or financial relationships that could be construed as a potential conflict of interest.

**Publisher's Note:** All claims expressed in this article are solely those of the authors and do not necessarily represent those of their affiliated organizations, or those of the publisher, the editors and the reviewers. Any product that may be evaluated in this article, or claim that may be made by its manufacturer, is not guaranteed or endorsed by the publisher.

*Copyright © 2021 Huang, Cao, Chen, Chen, Li, Guo, Dong, Wei and Liu. This is an open-access article distributed under the terms of the Creative Commons Attribution License (CC BY). The use, distribution or reproduction in other forums is permitted, provided the original author(s) and the copyright owner(s) are credited and that the original publication in this journal is cited, in accordance with accepted academic practice. No use, distribution or reproduction is permitted which does not comply with these terms.*

frontiers in Oncology

ORIGINAL RESEARCH
published: 29 November 2021
doi: 10.3389/fonc.2021.758989

# Identification of a Novel Stem Cell Subtype for Clear Cell Renal Cell Carcinoma Based on Stem Cell Gene Profiling

*Hongzhi Wang*[1,2,3], *Hanjiang Xu*[1,2,3], *Quan Cheng*[4] *and Chaozhao Liang*[1,2,3]*

[1] Department of Urology, The First Affiliated Hospital of Anhui Medical University, Hefei, China, [2] Institute of Urology, Anhui Medical University, Hefei, China, [3] Anhui Province Key Laboratory of Genitourinary Diseases, Anhui Medical University, Hefei, China, [4] Department of General Surgery, the First Affiliated Hospital of Nanjing Medical University, Nanjing, China

Clear cell renal cell carcinoma (ccRCC) is the most common subtype of renal cancer and is characterized by high rates of metastasis. Cancer stem cell is a vital cause of renal cancer metastasis and recurrence. However, little is known regarding the change and the roles of stem cells during the development of renal cancer. To clarify this problem, we developed a novel stem cell clustering strategy. Based on The Cancer Genome Atlas (TCGA) and the International Cancer Genome Consortium (ICGC) genomic datasets, we used 19 stem cell gene sets to classify each dataset. A machine learning method was used to perform the classification. We classified ccRCC into three subtypes—stem cell activated (SC-A), stem cell dormant (SC-D), and stem cell excluded (SC-E)—based on the expressions of stem cell-related genes. Compared with the other subtypes, C2(SC-A) had the highest degree of cancer stem cell concentration, the highest level of immune cell infiltration, a distinct mutation landscape, and the worst prognosis. Moreover, drug sensitivity analysis revealed that subgroup C2(SC-A) had the highest sensitivity to immunotherapy CTLA-4 blockade and the vascular endothelial growth factor receptor (VEGFR) inhibitor sunitinib. The identification of ccRCC subtypes based on cancer stem cell gene sets demonstrated the heterogeneity of ccRCC and provided a new strategy for its treatment.

**Keywords: clear cell renal cell cancer (ccRCC), stem cell, subtype, gene expression, immune microenvironment**

OPEN ACCESS

***Edited by:***
*Andrea Mari,*
*Careggi University Hospital, Italy*

***Reviewed by:***
*Gian Maria Busetto,*
*University of Foggia, Italy*
*Mohammed Imran Khan,*
*Western University, Canada*

***Correspondence:**
*Chaozhao Liang*
*liang_chaozhao@ahmu.edu.cn*

***Specialty section:***
*This article was submitted to Genitourinary Oncology, a section of the journal Frontiers in Oncology*

***Received:*** *15 August 2021*
***Accepted:*** *02 November 2021*
***Published:*** *29 November 2021*

***Citation:***
*Wang H, Xu H, Cheng Q and Liang C (2021) Identification of a Novel Stem Cell Subtype for Clear Cell Renal Cell Carcinoma Based on Stem Cell Gene Profiling. Front. Oncol. 11:758989. doi: 10.3389/fonc.2021.758989*

## INTRODUCTION

Renal cancer accounts for 3% of all adult malignancies worldwide, and its incidence have been increasing in recent years. Clear cell renal cell carcinoma (ccRCC) is the most common subtype of renal cancer, jeopardizing 70%–80% of renal cell carcinoma (RCC) patients. Over 30% of ccRCC patients have distant metastasis at the time of diagnosis, and one-third of patients with localized ccRCC will develop metastasis after nephrectomy (1–3). The 5-year survival rate of localized ccRCC

**Abbreviations:** ccRCC, clear cell renal cell carcinoma; CSC, cancer stem cell; SC-A, stem cell activated; SC-D, stem cell dormant; SC-E: stem cell excluded; OS: overall survival; TMB: tumor mutation burden.

is about 65%; however, it drops to 10%–20% after cancer metastasis (4). Surgery remains the major approach for the treatment of localized ccRCC; nevertheless, novel therapeutic strategies are urgently needed for metastatic patients.

Significant achievements have been made in treating advanced ccRCC in the last two decades, such as the application of tyrosine kinase and mammalian target of rapamycin (mTOR) inhibitors or monoclonal antibodies against vascular endothelial growth factor (VEGF) (5, 6). Combination therapy with these inhibitors prolonged the life span of patients. However, most tumors will progress within 2 years. Recently, new approaches for boosting the immune response to renal tumors with immune checkpoint inhibitors, which block programmed cell death protein-1 (PD-1) or cytotoxic T-lymphocyte-associated protein 4 (CTLA-4) on T cells, have shown promising effects in a subset of patients (7). Fundamentally, improving the outcome of renal cancer patients will require personalized treatment strategies specific to the biological characteristic of each tumor.

Stem cells are defined as cells with the ability to self-renew and differentiate into mature cells of a particular tissue (8). Cancer stem cells (CSCs) are a subpopulation of cancer cells with a higher self-renewal ability and the ability to reproduce the heterogeneity of tumors (9). CSCs have been characterized in various cancers and have been proven to contribute to drug resistance, tumor recurrence, and distant metastasis; however, the situation in kidney cancer remains obscure (10–12). Some studies have indicated that targeting the Notch, Hedgehog, and Wnt signaling pathways could inhibit the self-renewal and pluripotency ability of ccRCC cancer stem cells (13, 14). DKK3 and Notch3, which are members of the Wnt and Notch pathways, have been proven to be indicators of the prognosis of renal cancer patients (13). IL8/CXCR1 signaling was proven to promote the sphere formation and self-renewal capability of renal tumor cells (15). Both IL8 and CXCR1 are significantly correlated with patient survival. These studies indicated that the genes expressed in renal CSCs (RCSCs) could be effective prognostic factors. However, the functional significance and the prognostic value of stem cell-related genes in ccRCC are still scarcely investigated and need to be further clarified.

In the present study, we aimed to identify the subclasses of ccRCC with different CSC properties based on the expressions of stem cell-related genes. We divided ccRCC into three clusters with different features and prognosis. In addition, we proved the stability and reliability of this clustering with an independent dataset using the unsupervised clustering method. Moreover, we comprehensively analyzed the prognosis of the RCSC subtypes, relationship with immune cells and genes, the sensitivity of the immune checkpoint inhibitor treatment, and potential changes in the biological process. Classification of the stem cell gene-related subtypes may contribute to formulating the optimal treatment for renal cancer patients.

# RESULTS

## NMF Identifies Three Subclasses in ccRCC

An analysis flowchart was designed to systematically depict our study (**Figure 1**). Three hundred and ninety-two stem cell-related genes were enrolled for subsequent non-negative matrix factorization (NMF) analysis. The training set comprising 263 ccRCC samples from The Cancer Genome Atlas (TCGA) was clustered based on the expressions of the aforementioned 392 candidate genes using NMF consensus clustering. Cophenetic correlation coefficients, dispersion, and silhouette were calculated to identify the best $k$ value; $k = 3$ was proven to be the optimal number of clusters (three subclasses were assigned: C1, C2, and C3) (**Figure 2A**). Based on the present classification, the consensus heatmap showed sharp and crisp boundaries, indicating the applicability and robust clustering of these samples (**Figure 2B**). To validate the subtype classification, we conducted $t$-distributed stochastic neighbor embedding (t-SNE)

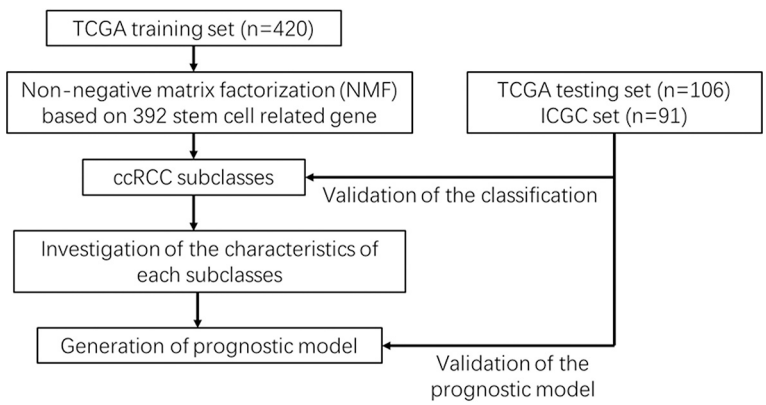



**FIGURE 1** | Workflow chart.

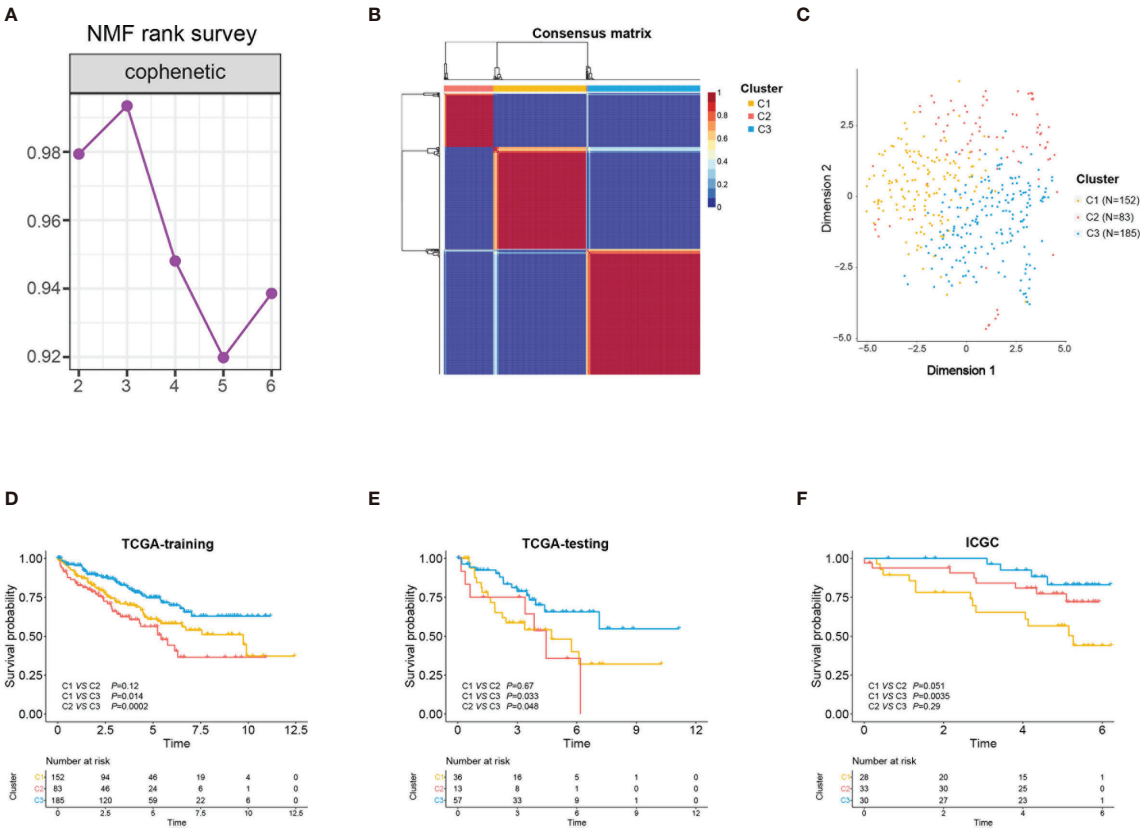



**FIGURE 2** | Identification of three stem cell subtypes using non-negative matrix factorization (NMF) consensus clustering in clear cell renal cell carcinoma (ccRCC) The Cancer Genome Atlas (TCGA) training cohort. **(A)** NMF clustering using 392 stem cell-associated genes. Cophenetic correlation coefficients for $k$ = 2–6 are shown. **(B)** Consensus heatmap for ccRCC samples when $k$ = 3. **(C)** $t$-Distributed stochastic neighbor embedding (t-SNE) analysis supported the stratification into three stem cell subtypes. *Dots with different colors* represent different samples in the subclasses. **(D–F)** Overall survival of the three subclasses (C1, C2, C3) in TCGA training and testing sets and the International Cancer Genome Consortium (ICGC) cohort.

to reduce the dimension of the features and found that samples in the same subclass generally gather in the same region. This indicates that the subclasses were mostly accordant with the t-SNE distribution patterns (**Figure 2C**). Additionally, to validate this classification, we performed an independent analysis on TCGA testing set and the International Cancer Genome Consortium (ICGC) dataset, the results of which also demonstrated that there were three distinct molecular subclasses. Based on the classification, a significant prognostic difference was observed in both TCGA testing set and the ICGC dataset (**Figures 2D–F**).

## Correlation of the ccRCC Subclass With Stem Cell-Related Signatures

Considering that the clustering was based on stem cell-related genes, we further investigated whether the different subclasses had distinct stem cell characteristics. Firstly, 19 stem cell-related biological process scores were calculated using the GSVA R package based on TCGA training cohort. Three subtypes showed significantly different stem cell-related signatures and clinicopathological characteristics (**Figure 3A**). Similar trends were identified in the ICGC cohort (**Supplementary Figure S1**). The results showed that C1 was related to the negative regulation of stem cell maintenance (**Figure 3B**), while C2 and C3 were correlated with positive stem cell maintenance (**Figure 3C**). Moreover, the scores of the stem cell proliferation signatures were highest in C2 (**Figure 3E**). Compared with C3, the C2 subtype was characterized by higher stem cell proliferation and differentiation scores (**Figures 3D, E**). Hence, we defined C1 as the stem cell excluded (SC_E) subclass, C2 as the stem cell activated (SC_A) subclass, and C3 as the stem cell dormant (SC_D) subclass.

To further characterize the subclasses, the expressions of the RCSC surface markers (CD44, CXCRL8, CXCR4, and ENG) and the stem cell-related pathways such as hypoxia-inducible factor (HIF), Notch, Wnt, and Hedgehog were investigated. Subclass C2(SC_A) had the highest expression of RCSC marker genes (**Figure 4E**). Moreover, subclasses C2(SC_A) and C3(SC_D) had higher normal stem cell and CSC gene markers (**Figures 4A, C**). Generally, compared to that in subclasses C2(SC_A) and C3

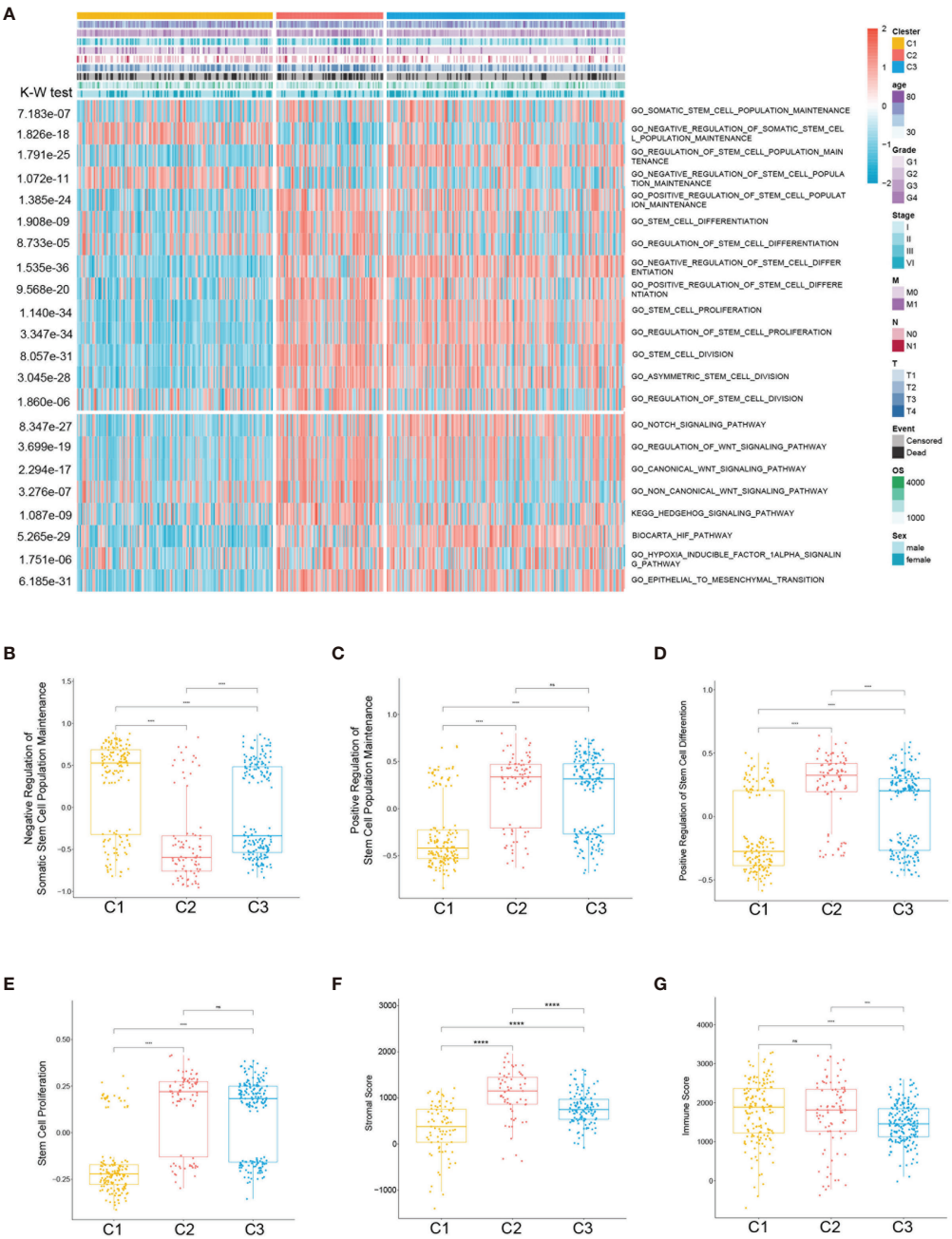



**FIGURE 3** | Association between the stem cell-associated signatures and the clear cell renal cell carcinoma (ccRCC) subclasses. **(A)** Heatmap of the specific stem cell-associated signatures. **(B–E)** Box plot of the signature scores for the stem cell-associated signatures distinguished by different subclasses. Box plot of the stromal **(F)** and immune **(G)** scores from estimates of the three subclasses. The *p*-values are labeled *above each box plot* with *asterisks*. *ns*, no significance. ***$p < 0.001$, ****$p < 0.0001$.

(SC_D), HIF, Notch, Wnt, and Hedgehog were less activated in subclass C1(SC_E) (**Figures 4B, D, F, G**). Besides, the immune and stromal scores of the subclasses were calculated using the ESTIMATE (estimation of stromal and immune cells in malignant tumours using expression data) algorithm. As shown in **Figures 3F, G**, subclass C2(SC_A) had the highest stromal and immune cell infiltration scores.

## Correlation of the ccRCC Subclasses With Immune Infiltration

Considering the significant differences in the immune and stromal scores displayed among the subclasses, immune and stromal cell infiltration was explored to depict their microenvironment landscape based on TCGA training cohort. Using the single-sample gene set enrichment analysis (ssGSEA)

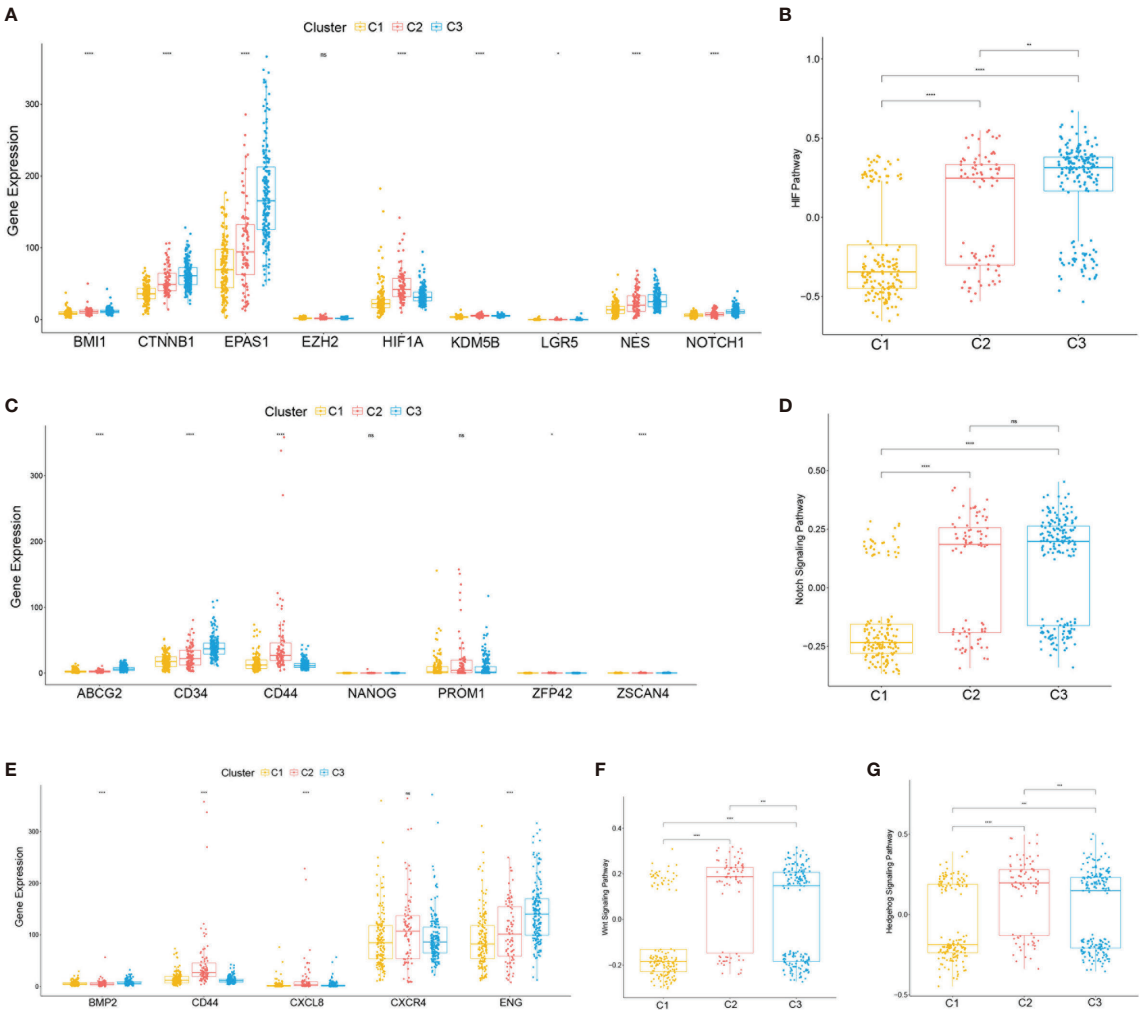



**FIGURE 4** | Expressions of clear cell renal cell carcinoma (ccRCC) stem cell-related genes and pathways. **(A, C, E)** Expression levels of cancer stem cell marker genes **(A)**, normal stem cell marker genes **(C)**, and ccRCC cancer stem cell marker genes **(E)**. **(B, D, F, G)** Box plot of the status of ccRCC cancer stem cell-related pathways. The *p*-values are labeled *above each box plot* with *asterisks*. *ns*, no significance. $^{*}p < 0.05$, $^{**}p < 0.01$, $^{***}p < 0.001$, $^{****}p < 0.0001$.

algorithm, the abundance rates of the 28 immune-related cell types were quantified and presented in a heatmap (**Figure 5A**). Subclass C2(SC_A) showed a significantly different immune cell infiltration compared with the other two subclasses. Stromal cells, especially fibroblasts, which have an important role in renal cancer progression, showed different infiltration status in the three subtypes (**Figures 5B, C**). Moreover, we explored the association between subclasses and the expressions of potentially targetable immune checkpoint genes, which have been used for drug inhibitors in clinical trials or approved for specific cancer treatment (**Figure 5D**). Subclass C2(SC_A) had the highest expressions of most of these genes.

## Correlation of the ccRCC Subclasses With Mutations and Copy Number Variations

The tumor genomic landscape has been demonstrated to be associated with antitumor immunity. To investigate whether differences exist in the somatic mutation frequencies across the ccRCC subclasses and to observe the different patterns of mutations among the ccRCC clusters, somatic mutation data from TCGA database were analyzed. **Figures 6A–C** show the landscape of the top 20 mutated genes in the three subtypes. There was no significant difference in the mutation count of the three subclasses (**Figure 6E**). However, the tumor mutation burden (TMB) (**Figure 6D**) and the fraction genome altered (**Figure 6F**) were significantly higher in subclass C1(SC_E) compared to those in subclasses C2(SC_A) and C3(SC_D).

## Transcriptome Features of the ccRCC Subclasses

To better characterize the three ccRCC subclasses, gene differential analysis was conducted. Genes with an adjusted *p*-value less than 0.01 and an absolute log2 fold change larger than 1 were considered significantly differential. Only those genes

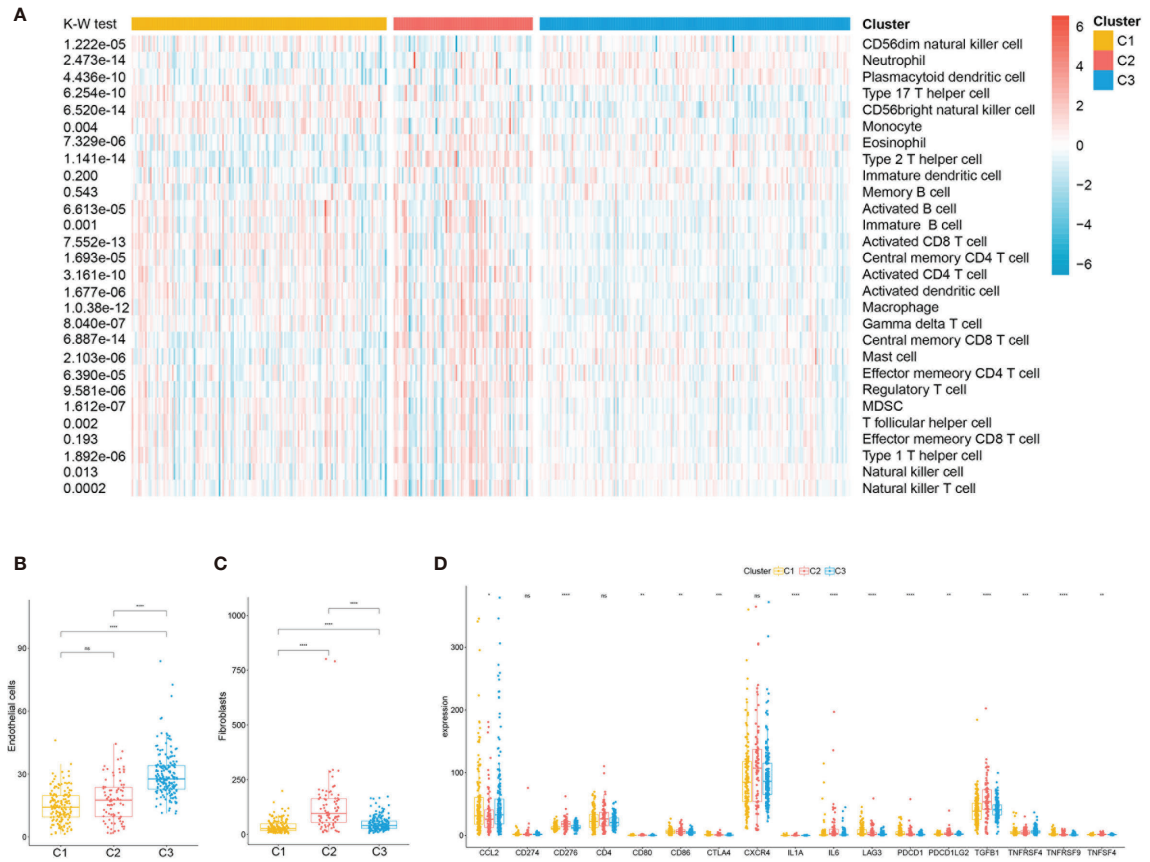



**FIGURE 5** | Immune characteristics of the three subclasses in The Cancer Genome Atlas (TCGA) training set. **(A)** Heatmap describing the abundance of immune cell populations in C1, C2, and C3. Box plot of the abundance of endothelial **(B)** and fibroblasts **(C)** distinguished by different subclasses. **(D)** Expression levels (in fragments per kilobase of transcript per million mapped reads, FPKM) of 17 immune checkpoint genes in the three clear cell renal cell carcinoma (ccRCC) subclasses. *ns*, no significance. $^{*}p < 0.05$, $^{**}p < 0.01$, $^{***}p < 0.001$, $^{****}p < 0.0001$.

which showed significant differences in two possible comparisons were considered subclass-specific genes. Finally, all of the 1,695 subclass-specific genes were identified, including 172 specific genes for C1(SC_E), 1,485 specific genes for C2(SC_A), and 38 specific genes for C3(SC_D). Subsequently, gene ontology (GO) enrichment analysis of the subclass-specific genes was performed using clusterProfiler in the R package. The significantly enriched biological processes are shown in **Figure 7**. Subclass C2(SC_A), which was enriched in extracellular matrix organization and extracellular structure organization, had significantly different enriched pathways compared with the other subclasses (**Figure 7B**).

## Prediction of the Therapeutic Response of the ccRCC Stem Cell Subtypes to Immune Checkpoint Inhibitors and Target Therapy

Based on the above results, we further evaluated the response of the three subtypes to immunotherapy. In RCC, the blockade of PD-1 and CTLA-4 has become the new treatment approach in patients with intermediate- and high-risk metastatic tumors, whereas monotherapy with the PD-1 inhibitor nivolumab is the second-line or third-line treatment approach after failure of VEGF tyrosine kinase inhibitors (16). In 2019, the United States Food and Drug Administration (FDA) approved the combination use of PD-1 blockade and anti-angiogenic therapy for the treatment of patients with advanced RCC (17). To predict the sensitivity to immunotherapy of the different clusters, we performed subclass mapping to compare the expression profiles of the three stem cell subtypes with 47 melanoma patients who were treated with immunotherapy (18). The subclass mapping results indicated that the C2(SC_A) subtype might be more sensitive to anti-CTLA-4 treatments (**Figure 8A**).

Since VEGF receptor (VEGFR) target therapy is a more conventional therapy for patients with advanced ccRCC, we selected five conventional target therapy agents (sunitinib, sorafenib, axitinib, pazopanib, and rapamycin) and evaluated the responses of the three subtypes. We constructed a prediction model on the Genomics of Drug Sensitivity in Cancer (GDSC) cell line dataset using ridge regression and evaluated the prediction accuracy using 10-fold cross-validation. We

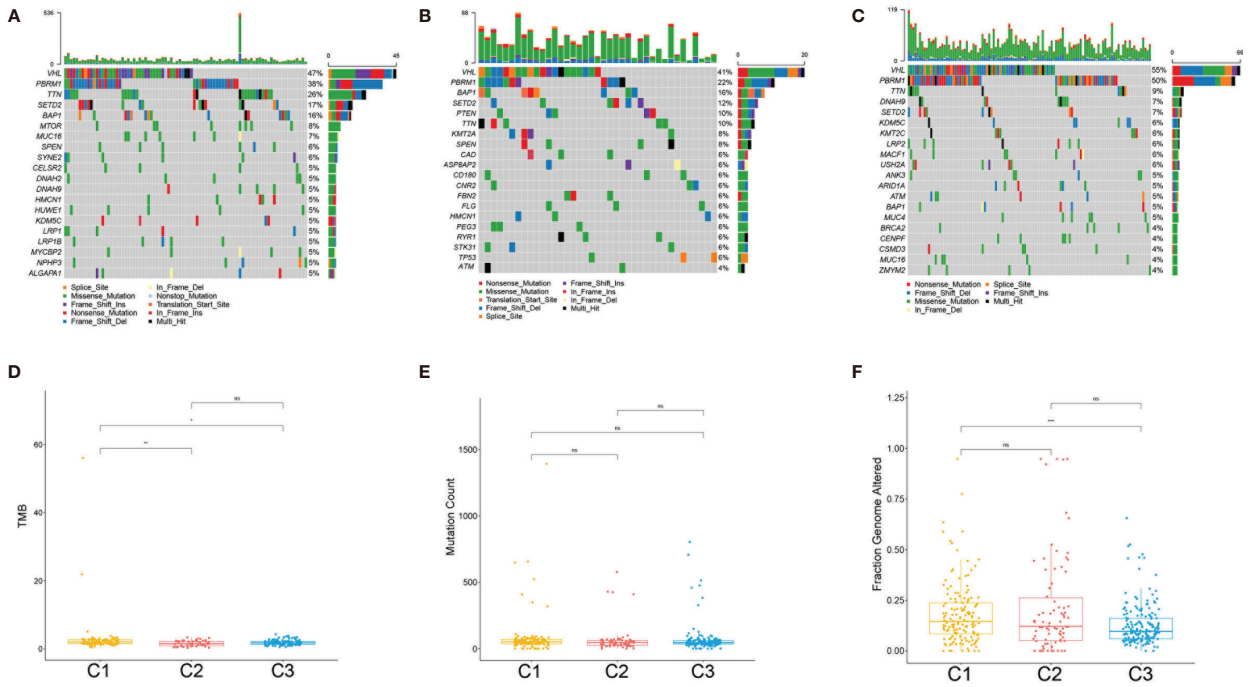



**FIGURE 6** | Association between the clear cell renal cell carcinoma (ccRCC) subclasses and mutations. **(A–C)** Oncoprint of the mutation status of the top 20 genes in subclasses C1(SC_E), C2(SC_A), C3(SC_D). **(D–F)** The tumor mutation burden **(D)**, mutation count **(E)**, and fraction genome altered **(F)** in the three subclasses. *ns*, no significance. $^{*}p < 0.05$, $^{**}p < 0.01$, $^{***}p < 0.001$.

estimated the half-maximal inhibitory concentration ($IC_{50}$) of each sample in the training set based on the prediction models for the four target therapy agents. Regarding sunitinib and pazopanib, subclass C2(SC_A) was the most sensitive (**Figures 8C, E**), while for sorafenib, subclass C3(SC_D) had the worst sensitivity. Subclasses C1(SC_E) and C2(SC_A) showed similar sensitivity values (**Figure 8B**). Regarding axitinib, subclass C3(SC_D) was the most sensitive (**Figure 8F**), while for rapamycin, subclass C1(SC_E) was the most sensitive (**Figure 8D**).

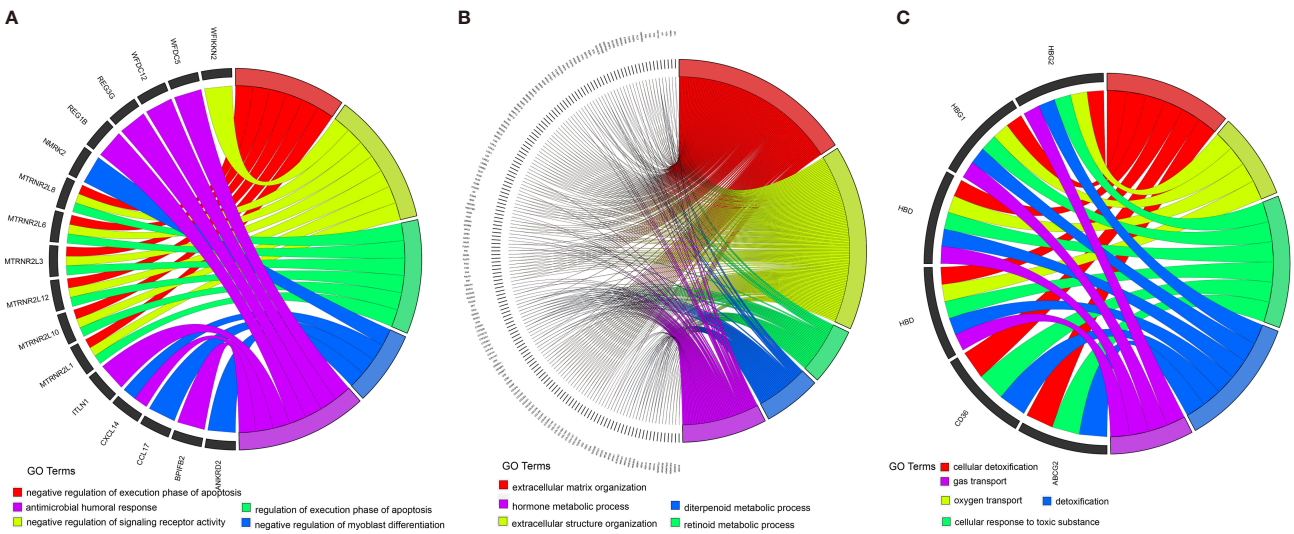



**FIGURE 7** | Enrichment analysis of the differentially expressed genes in three different subclasses: C1 **(A)**, C2 **(B)**, and C3 **(C)**.

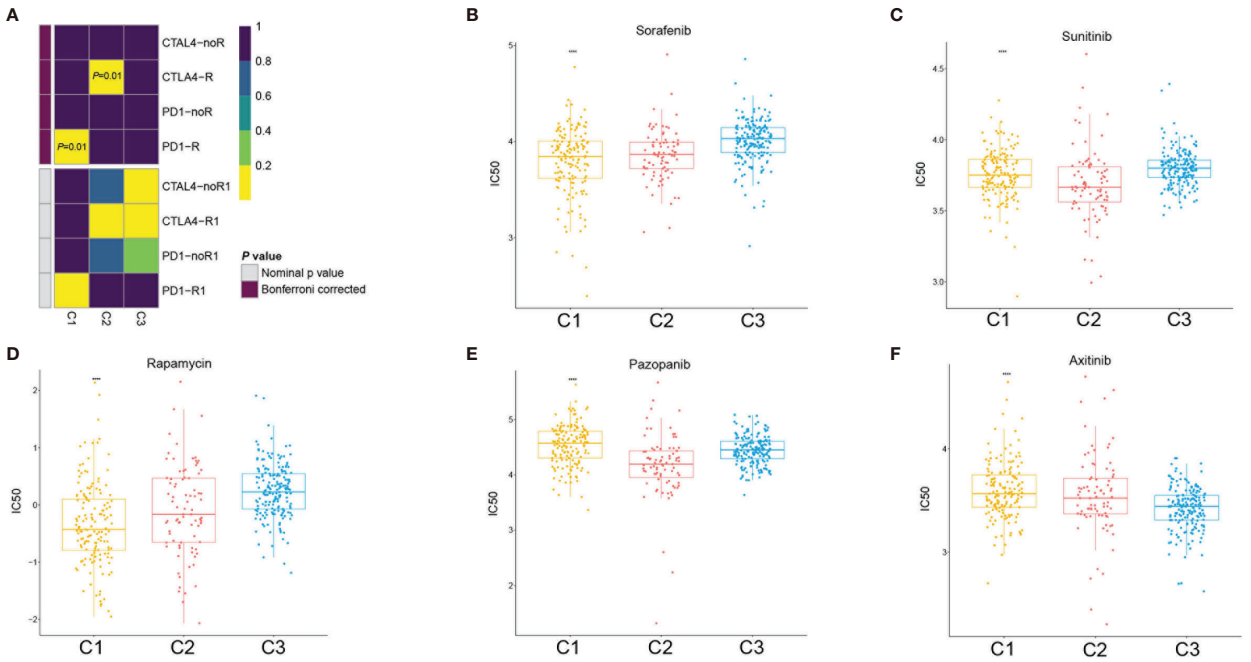



**FIGURE 8** | Immunotherapy and target therapy response prediction in the clear cell renal cell carcinoma (ccRCC) subclasses. **(A)** Response of the three ccRCC subclasses to PD-1 and CTLA-4 immunotherapy. **(B–F)** Sensitivity of the three ccRCC subclasses to sorafenib **(B)**, sunitinib **(C)**, rapamycin **(D)**, pazopanib **(E)**, and axitinib **(F)**. ****$p < 0.0001$.

## Construction of a Prognostic Model Based on Key Genes

To better characterize the prognosis of each patient, we constructed a risk model based on the key genes. The key genes were extracted from the stem cell-related genes using the NMF package in R. Twenty key genes were identified. Then, we applied least absolute shrinkage and selection operator (LASSO) Cox regression analysis to select the most useful predictive features and identified four genes (*A2M*, *CFL1*, *FN1*, and *PSME2*) with non-zero regression coefficients (**Figures 9A, B**). Ultimately, a six-gene risk signature was built, and the risk score of each patient was calculated using the following formula:

Signature risk core = (−0.00205964493004206 × *A2M* expression) + (0.00157204565454328 × *CFL1* expression) + (0.00199772913455084 × *FN1* expression) + (0.0181057563160569 × *PSME2* expression). Increased expressions of *PSME2*, *FN1*, and *CFL1* correlated with higher risk scores and worse survival outcomes (**Figure 9C**). More importantly, the risk score could stratify patients into a high- and a low-risk group with significantly different survival outcomes (**Figure 9D**). Similar results were found in TCGA testing set and the ICGC dataset (**Figures 9E, F**).

# DISCUSSION

Although a variety of ccRCC classifications based on gene expression have been developed in recent years, a consensus in molecular subtype has not yet been achieved. To identify the ccRCC subgroups associated with CSC and patient prognosis, a ccRCC classification was developed in this study based on 392 genes retrieved from Molecular Signatures Database. Three subclasses of ccRCC with different prognosis were identified. Subsequently, the stem cell signature, immune infiltration, mutation landscape, and clinicopathological characteristics of the subclasses and their sensitivity to immunotherapy were investigated. The results showed that three subclasses were distinct, with significantly different stem cell and immune cell infiltration signatures. Drug sensitivity analysis demonstrated that subclass C2(SC_A) was sensitive toward CTLA-4 inhibitors and sunitinib. In addition, based on the marker genes of each cluster, we constructed a risk model to predict the prognosis of patients. This risk model could stratify patients with different prognosis, and it was validated in an external cohort.

The progression of cancer was accompanied by the gradual loss of differentiation ability and the gain of stem cell-like characteristics (12). Inhibiting the self-renewal capacity and the tumorigenicity of ccRCC significantly suppressed tumor growth and metastasis (19, 20). Given that a relapse in ccRCC has been attributed to the maintenance of ccRCC stemness cells, possessing stem cell properties that lead to therapy resistance (21), there is an urgent need for the development of prognostic biomarkers associated with stem cell properties. Malta et al. developed a novel transcriptome stemness index called mRNAsi (mRNA expression-based stemness index) to evaluate the stemness based on the one-class logistic regression machine

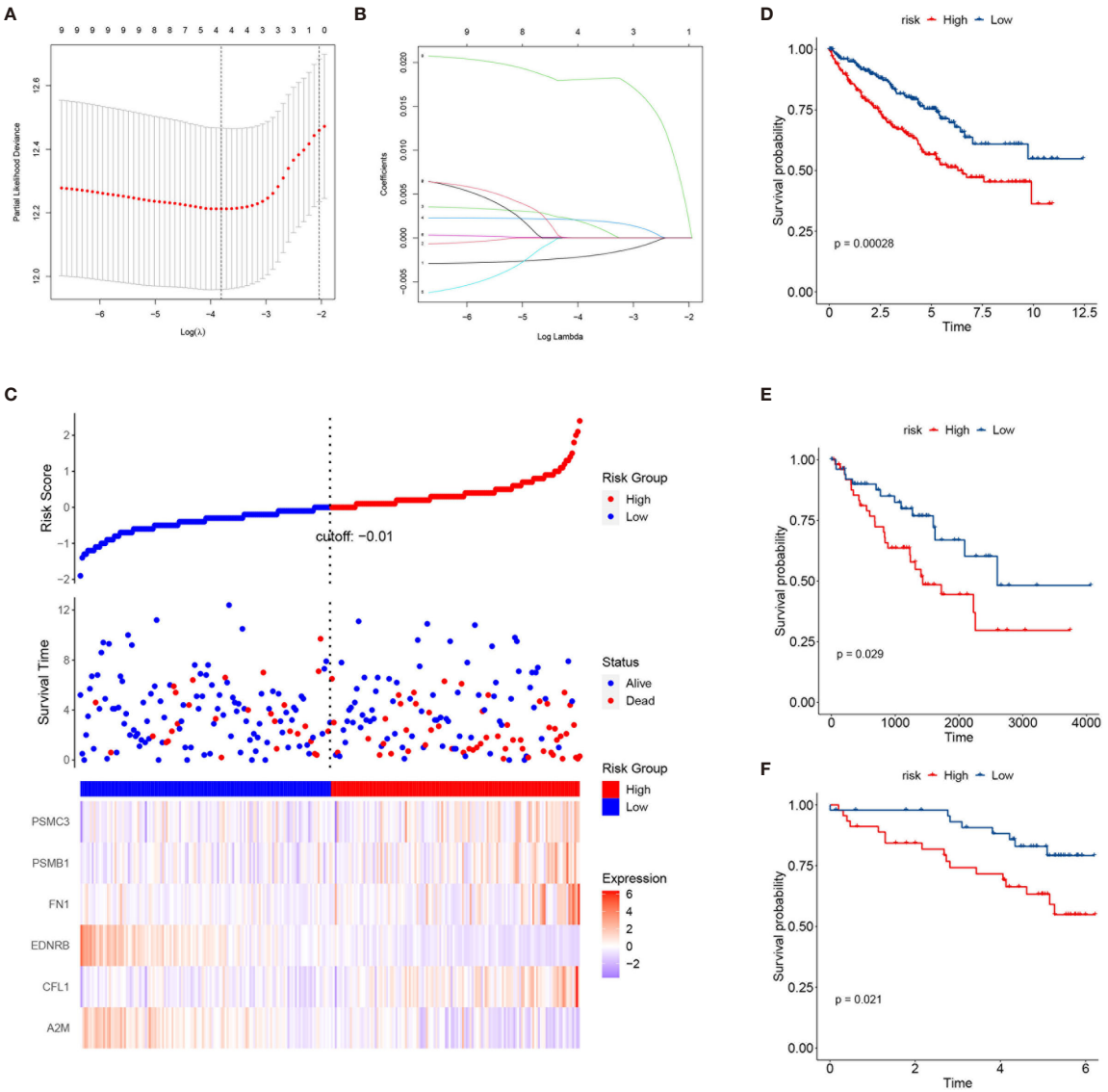



**FIGURE 9** | Construction of a risk prediction model based on the key genes in the three subclasses. **(A)** Tuning parameter (*λ*) screening in the least absolute shrinkage and selection operator (LASSO) regression model. **(B)** LASSO coefficient profiles of the common genes. **(C)** From *top to bottom* are the risk score distribution, survival overview, and heatmap analysis of six genes. **(D–F)** Kaplan–Meier plots of overall survival (OS) according to the risk scores in The Cancer Genome Atlas (TCGA) training set **(D)**, TCGA testing set **(E)**, and the International Cancer Genome Consortium (ICGC) cohort **(F)**.

learning algorithm (22). However, the mRNAsi was higher in normal renal tissue compared with that in renal tumor and showed no correlation with the survival outcomes of patients. This contradicts usual biological experiment results that demonstrate CSC properties to indicate worse prognosis. A novel stem cell-related prognostic evaluation model is needed.

Based on stem cell-related genes, three subtypes with different survival outcomes were identified. The results showed that subclass C1(SC_E) was distinct with the negative regulation of stem cell maintenance; however, subclasses C2(SC_A) and C3 (SC_D) displayed distinct stem cell signatures and were characterized by positive regulation of stem cell maintenance. Moreover, subclass C2(SC_A) was also highly correlated with stem cell division and differentiation. The signature differences between subclasses C2(SC_A) and C3(SC_D) may be caused by the dormancy of CSCs (23, 24). Renal CSC surface markers, such as CD44, CXCR4, and CD105(ENG), were highly expressed in subclasses C2(SC_A) and C3(SC_D) (10, 11). BMP2 and CXCL8, which could promote the self-renewal of RCSCs, also had higher expressions in subclasses C2(SC_A) and C3(SC_D) (15, 25). The HIF, Notch, Wnt, and Hedgehog signaling pathways were reported to promote renal cancer progression by regulating the self-renewal and stemness maintenance of RCSCs (14, 26–28). Hence, we also investigated their status in the different

subclasses. Compared to that in subclass C1(SC_E), these pathways were significantly activated in subclasses C2(SC_A) and C3(SC_D). These results demonstrated the validity of this classification. Moreover, these signaling pathways were also differently expressed in subclasses C2(SC_A) and C3(SC_D). These results indicated that these pathways were not only implicated in stemness maintenance but also associated with the proliferation and differentiation of RCSCs.

A recent study has demonstrated that stem cell properties are microenvironment defined during tumor progression (29, 30). Hence, we analyzed the stromal and immune infiltration levels in the three subtypes using R package ESTIMATE. The C2(SC_A) subtype had higher stromal and immune scores. Subsequent analysis further corroborated the C2(SC_A) subtype as possessing distinct stromal and immune features, including high infiltration of fibroblasts, T cells, and macrophages. Heterogeneous stromal cells in the tumor microenvironment can profoundly boost cancer progression (31). Carcinoma-associated fibroblasts (CAFs) form the chief components of the tumor microenvironment in multiple types of malignancies (32). By providing a supporting niche for CSCs, CAFs could facilitate tumor formation and induce chemoresistance (31). This may partly be explained by the concurrence of a high stem cell maintenance score and fibroblast infiltration. Macrophages abundantly exist in the immune milieu, where they share the microenvironment with CSCs. Macrophage-initiated WNT signaling could contribute to the maintenance of stemness, leading to the characteristics of chemoresistance and invasiveness in ovarian cancer (33). A similar phenomenon was found in lung cancer. A positive feedback interaction between macrophages and cancer cells could promote the stemness of cancer cells (34). Tumor-associated macrophages have been demonstrated to contribute to the maintenance of breast CSC populations through triggering the production of the inflammatory cytokines interleukin 1 (IL-1), IL-6, and IL-8, which, in turn, reinforce the CSC states (35). Interestingly, previous studies proved that IL-8 could boost the CSC-like properties of ccRCC (15). Besides, the activation of the Notch signaling pathway could promote the expansion of ccRCC-derived CSCs and induce chemotaxis simultaneously (27). Th17 cells are another type of immune cells that appear to support CSCs. Th17 cell-associated cytokines could transform dormant stem cells into an active state (36). This is consistent with our finding that subclass C2(SC_A) had a higher infiltration of Th17 helper cells. Tumor-specific antigens are usually generated by somatic mutation and can influence the response of patients to immunotherapy (37, 38). Hence, we comprehensively analyzed the mutation status of the three subclasses. Although there was no significant difference in the TMB among the three subtypes, C1(SC_E) had higher mutation counts and fraction genome altered than the other subclasses. These differences might influence their response to immunotherapy. *VHL* mutation is the most common mutation in ccRCC (39). However, evidence of the relationship between the mutation status of the *VHL* gene and ccRCC remains few and contradictory. Some studies suggested that *VHL* mutation could activate effector T cells and promote the secretion of cytokines (40). However, a recent study has proposed that wild-type *VHL* positively correlated with the expression of programmed death-ligand 1 (PD-L1) (41). In the present study, we found that subclass C2(SC_A) had a relatively lower *VHL* mutation frequency. *PBRM1* is another commonly mutated gene in ccRCC. A previous study indicated that $CD8^+$ T-cell-infiltrated tumors had relatively fewer *PBRM1* mutations (42). Similarly, we found that the mutation frequency of *PBRM1* was significantly lower in subclass C2(SC_A), which had the highest immune cell infiltration. Moreover, the mutation landscape showed that subclass C1 had the highest mTOR mutation frequency. Correspondingly, patients in subclass C1 were most sensitive to the mTOR inhibitor rapamycin. This demonstrated the reliability of the present study. More studies are needed to investigate the relationship between somatic mutations and immune infiltration.

Considering the close interactions between CSCs and the immune system, developing therapeutic strategies that target immune checkpoints might pave the way to eradicating CSCs. At present, immunotherapy has obtained global attention in cancer management. The efficacy and safety of PD-1 immune checkpoint inhibitors and CTLA-4 inhibitors have been applied clinically and have shown promising outcomes (43, 44). Due to the interaction between PD-1 and PD-L1 in tumor-infiltrating lymphocytes and tumor cells, T-cell exhaustion, tumor-specific T-cell dysfunction, and immune evasion by tumor cells were triggered. Exhausted T cells could produce additional inhibitory molecules to promote the progression of cancer; however, this process could be reversed by a combined PD-1 and CTLA-4 blockade. Treating a mouse tumor model with PD-L1 and CTLA-4 inhibitors could promote the elimination of CSCs (45).

Redirecting immune suppression by targeting checkpoints has brought about clinical response in some RCC patients, and a combination treatment involving checkpoint blockade is now the standard of therapy in advanced RCC patients. However, a substantial subset of patients is not sensitive to checkpoint blockade. The identification of a reliable evaluation system to predict the response to checkpoint blockade is essential to improve the clinical efficacy of these therapies (46). Moreover, the immune checkpoint gene *CXCR4*, which is also a marker of RCSC, was highly expressed in subclass C2(SC_A). Targeting the tumor microenvironment may provide a promising therapeutic avenue as the eliminated CSCs could be replenished by non-CSCs for the existence of a survival niche (47). The highest expressions of immune checkpoint genes indicated the sensitivity of subclass C2(SC_A) to immunotherapy. The results demonstrated that anti-CTLA-4 therapy and sunitinib are promising for patients in subclass C2(SC_A). The results of our study provide a novel insight into the combination of anti-CTLA-4 therapy and sunitinib, which requires further validation in future research.

Besides, to better characterize the prognosis of each patient, we constructed a risk model based on the key genes (*A2M*, *CFL1*, *FN1*, and *PSME2*). The risk scores could classify patients into the

high- and low-risk groups with significantly different survival outcomes. In addition, the effectiveness of this risk model was validated in TCGA testing set and the ICGC dataset.

In summary, in this study, we explored the stem cell-related process landscape of ccRCC and identified three subclasses with different stem cell activities. We systematically analyzed the differences of these subclasses in the tumor microenvironment, immune cell infiltration, immunotherapy/target therapy response, and the corresponding pathways and constructed a risk model. The results of this study provide a basis and reference for the treatment and prognostic prediction of ccRCC.

With the development of target therapy and immunotherapy, various drugs have been used for the clinical treatment of advanced ccRCC. The VEGFR inhibitor, anti-checkpoint therapy, and the combination of both showed promising efficacy (48, 49). However, few references were established for the selection of a proper treatment plan. The novel developed stem cell subtypes are critical for selecting suitable therapies for ccRCC patients. Patients in the stem cell activated subtype (SC-A) could benefit more from anti-CTLA-4 and sunitinib treatment. For those in the stem cell excluded subtype, an anti-PD-1 therapy might be more suitable. However, there are limitations in the present study. This study was conducted based on an existing public dataset. These findings need to be validated in larger ccRCC patient cohorts with immunotherapy and target therapy experience.

# MATERIALS AND METHODS

## Patients and Samples

The RNA sequencing data (raw counts) of 530 and 91 ccRCC patient samples with corresponding clinical information were download from The Cancer Genome Atlas (TCGA; http://cancergenome.nih.gov/) and the International Cancer Genome Consortium (ICGC; www.icgc.org), respectively. Patients with 0 day overall survival (OS) were removed; 526 TCGA samples were retained for further analysis. Subsequently, the dataset from TCGA was randomly divided into a training set and a testing set. The gene expression data of 91 ccRCC samples from the ICGC were used for external validation. In total, 662 ccRCC patients were enrolled in the present study. The gene somatic mutation data (MAF files) of ccRCC were retrieved from TCGA.

## Identification of ccRCC Subclasses

Human stem cell-related biological processes were downloaded from the Molecular Signatures Database (https://www.gsea-msigdb.org/gsea/msigdb/index.jsp). A total of 392 genes from 19 stem cell-related biological processes were obtained (**Supplementary Table S1**). These genes were FPKM (fragments per kilobase of transcript per million mapped reads) normalized and used for subsequent non-negative matrix factorization (NMF) analysis using the R NMF package in the training set. NMF is an unsupervised learning technique that has been used to extract meaningful information from high-dimensional data (50). In detail, the best *k*-value was defined according to the cophenetic correlation coefficients, dispersion, and silhouette. The iteration was set as $n_{run} = 100$. This method was also applied to the testing and external validation sets using the same candidate genes. The first value of *k* for which the cophenetic coefficient starts decreasing was chosen as the optimal number for clustering. A *t*-distributed stochastic neighbor embedding (t-SNE)-based approach was then used to validate the sample clustering using the mRNA expression data of the above stem cell-related genes.

## Gene Set Variation Analysis

Gene set variation analysis (GSVA) is a non-parametric and unsupervised gene set enrichment method that can estimate the scores of certain pathways or signatures based on transcriptomic data. Using the GSVA R package, each sample received 19 scores corresponding to 19 stem cell-related signatures. Subsequently, differences in the signatures of the different clusters were calculated using the *t*-test in R.

## Estimation of Immune Infiltration

The microenvironment cell populations counter (MCP-counter), a method based on transcriptomic data, was used to assess the absolute abundance of two stromal cell populations (endothelial cells and fibroblasts) (51). Furthermore, another approach applied for the qualification of the immune infiltration of 28 immune cells used in this research was single-sample gene set enrichment analysis (ssGSEA), which calculated an enrichment score (ES) representing the variations of the pathway activities within a single sample (51). In addition, immune scores and stromal scores were calculated using the ESTIMATE algorithm, which can reflect the infiltration level of stromal and immune cells.

## Enrichment Analysis

Kyoto Encyclopedia of Genes and Genomes (KEGG) pathway enrichment and Gene Ontology (GO) analysis were performed with the R package "clusterProfiler."

## Target Therapy and Immunotherapy Sensitivity Prediction

The sensitivity of patients to target therapy drugs was evaluated based on the GDSC database (https://www.cancerrxgene.org/) (52). $IC_{50}$ values were estimated using the R package pRRophetic (53). In detail, the $IC_{50}$ was calculated by ridge regression and the prediction accuracy was evaluated using 10-fold cross-validation based on the GDSC training set. The response to anti-PD-1 and anti-CTLA-4 therapy was predicted by comparing the expression profiles of three subtypes with 47 melanoma patients who respond to the immunotherapy using subclass mapping (https://www.genepattern.org/).

## Construction of a Prognostic Model

Univariate Cox regression was used to screen the mRNAs affecting the OS of patients ($p < 0.05$). Thereafter, survival-related genes were screened with the LASSO multivariate Cox regression algorithm using the R package "glmnet" (version 3.0). Finally, the signature genes and coefficients in the risk score

signature were constructed based on the most proper penalty parameter $\lambda$. The risk score formula used was:

$$\text{Risk score} = \Sigma_{i=1}^{n} \ \text{Coef}_i * \text{Exp}_i$$

where $\text{Coef}_i$ is the coefficient and $\text{Exp}_i$ is the normalized expression of each gene in the signature. The risk score system was constructed using the training set and evaluated in the testing set. Patients were stratified into a high-risk group and a low-risk group based on the median risk score.

### Statistical Analysis

All statistical analysis was performed using R programming (https://www.r-project.org/). Unpaired Student's *t*-test was used to compare two groups with normally distributed variables. For the comparison of three groups, one-way analysis of variance and the Kruskal–Wallis test were used as parametric and non-parametric methods, respectively. Contingency table variables were analyzed with the chi-square test or Fisher's exact tests. Survival analysis was carried out using the Kaplan–Meier method and compared using the log-rank test. A *p*-value less than 0.05 was considered as statistically significant.

## DATA AVAILABILITY STATEMENT

The original contributions presented in the study are included in the article/**Supplementary Material**. Further inquiries can be directed to the corresponding author.

## AUTHOR CONTRIBUTIONS

HW designed the study and drafted the manuscript. HW and HX collected, analyzed, and interpreted the data. QC and CL participated in revising the manuscript. All authors contributed to the article and approved the submitted version.

## FUNDING

This work was supported by Research Fund of Anhui Institute of Translational Medicine (grant number: ZHYX2020A003).

## ACKNOWLEDGMENTS

We thank Dr. Jianming Zeng (University of Macau) and all the members of his bioinformatics team, biotrainee, for generously sharing their experience and codes.

## SUPPLEMENTARY MATERIAL

The Supplementary Material for this article can be found online at: https://www.frontiersin.org/articles/10.3389/fonc.2021.758989/full#supplementary-material

## REFERENCES

1. Hoffman AM, Cairns P. Epigenetics of Kidney Cancer and Bladder Cancer. *Epigenomics* (2011) 3:19–34. doi: 10.2217/epi.10.64
2. Linehan WM, Rathmell WK. Kidney Cancer. *Urologic Oncol* (2012) 30:948–51. doi: 10.1016/j.urolonc.2012.08.021
3. Sudarshan S, Karam JA, Brugarolas J, Thompson RH, Uzzo R, Rini B, et al. Metabolism of Kidney Cancer: From the Lab to Clinical Practice. *Eur Urol* (2013) 63:244–51. doi: 10.1016/j.eururo.2012.09.054
4. Znaor A, Lortet-Tieulent J, Laversanne M, Jemal A, Bray F. International Variations and Trends in Renal Cell Carcinoma Incidence and Mortality. *Eur Urol* (2015) 67:519–30. doi: 10.1016/j.eururo.2014.10.002
5. Motzer RJ. Perspective: What Next for Treatment? *Nature* (2016) 537:S111. doi: 10.1038/537S111a
6. Busch J, Seidel C, Goranova I, Erber B, Peters R, Friedersdorff F, et al. Categories of Response to First Line Vascular Endothelial Growth Factor Receptor Targeted Therapy and Overall Survival in Patients With Metastatic Renal Cell Carcinoma. *Eur J Cancer* (2014) 50:563–9. doi: 10.1016/j.ejca.2013.10.017
7. Motzer RJ, Escudier B, McDermott DF, George S, Hammers HJ, Srinivas S, et al. Nivolumab Versus Everolimus in Advanced Renal-Cell Carcinoma. *N Engl J Med* (2015) 373:1803–13. doi: 10.1056/NEJMoa1510665
8. Reya T, Morrison SJ, Clarke MF, Weissman IL. Stem Cells, Cancer, and Cancer Stem Cells. *Nature* (2001) 414:105–11. doi: 10.1038/35102167
9. Nassar D, Blanpain C. Cancer Stem Cells: Basic Concepts and Therapeutic Implications. *Annu Rev Pathol* (2016) 11:47–76. doi: 10.1146/annurev-pathol-012615-044438
10. Bussolati B, Bruno S, Grange C, Ferrando U, Camussi G. Identification of a Tumor-Initiating Stem Cell Population in Human Renal Carcinomas. *FASEB J* (2008) 22:3696–705. doi: 10.1096/fj.08-102590
11. Gassenmaier M, Chen D, Buchner A, Henkel L, Schiemann M, Mack B, et al. CXC Chemokine Receptor 4 Is Essential for Maintenance of Renal Cell Carcinoma-Initiating Cells and Predicts Metastasis. *Stem Cells* (2013) 31:1467–76. doi: 10.1002/stem.1407
12. Grange C, Tapparo M, Collino F, Vitillo L, Damasco C, Deregibus MC, et al. Microvesicles Released From Human Renal Cancer Stem Cells Stimulate Angiogenesis and Formation of Lung Premetastatic Niche. *Cancer Res* (2011) 71:5346–56. doi: 10.1158/0008-5472.Can-11-0241
13. Fendler A, Bauer D, Busch J, Jung K, Wulf-Goldenberg A, Kunz S, et al. Inhibiting WNT and NOTCH in Renal Cancer Stem Cells and the Implications for Human Patients. *Nat Commun* (2020) 11:929. doi: 10.1038/s41467-020-14700-7
14. Qu L, Wu Z, Li Y, Xu Z, Liu B, Liu F, et al. A Feed-Forward Loop Between lncARSR and YAP Activity Promotes Expansion of Renal Tumour-Initiating Cells. *Nat Commun* (2016) 7:12692. doi: 10.1038/ncomms12692
15. Corrò C, Healy ME, Engler S, Bodenmiller B, Li Z, Schraml P, et al. IL-8 and CXCR1 Expression is Associated With Cancer Stem Cell-Like Properties of Clear Cell Renal Cancer. *J Pathol* (2019) 248:377–89. doi: 10.1002/path.5267
16. Amin A, Hammers H. The Evolving Landscape of Immunotherapy-Based Combinations for Frontline Treatment of Advanced Renal Cell Carcinoma. *Front Immunol* (2018) 9:3120. doi: 10.3389/fimmu.2018.03120
17. Escudier B. Combination Therapy as First-Line Treatment in Metastatic Renal-Cell Carcinoma. *New Engl J Med* (2019) 380:1176–8. doi: 10.1056/NEJMe1900887
18. Roh W, Chen PL, Reuben A, Spencer CN, Prieto PA, Miller JP, et al. Integrated Molecular Analysis of Tumor Biopsies on Sequential CTLA-4 and PD-1 Blockade Reveals Markers of Response and Resistance. *Sci Transl Med* (2017) 9(379):eaah3560. doi: 10.1126/scitranslmed.aah3560
19. Ge Y, Weygant N, Qu D, May R, Berry WL, Yao J, et al. Alternative Splice Variants of DCLK1 Mark Cancer Stem Cells, Promote Self-Renewal and

Drug-Resistance, and can be Targeted to Inhibit Tumorigenesis in Kidney Cancer. *Int J Cancer* (2018) 143:1162–75. doi: 10.1002/ijc.31400
20. Lawson DA, Bhakta NR, Kessenbrock K, Prummel KD, Yu Y, Takai K, et al. Single-Cell Analysis Reveals a Stem-Cell Program in Human Metastatic Breast Cancer Cells. *Nature* (2015) 526:131–5. doi: 10.1038/nature15260
21. Hu J, Guan W, Liu P, Dai J, Tang K, Xiao H, et al. Endoglin Is Essential for the Maintenance of Self-Renewal and Chemoresistance in Renal Cancer Stem Cells. *Stem Cell Rep* (2017) 9:464–77. doi: 10.1016/j.stemcr.2017.07.009
22. Malta TM, Sokolov A, Gentles AJ, Burzykowski T, Poisson L, Weinstein JN, et al. Machine Learning Identifies Stemness Features Associated With Oncogenic Dedifferentiation. *Cell* (2018) 173:338–54.e315. doi: 10.1016/j.cell.2018.03.034
23. Talukdar S, Bhoopathi P, Emdad L, Das S, Sarkar D, Fisher PB. Dormancy and Cancer Stem Cells: An Enigma for Cancer Therapeutic Targeting. *Adv Cancer Res* (2019) 141:43–84. doi: 10.1016/bs.acr.2018.12.002
24. Triana-Martínez F, Loza MI, Domínguez E. Beyond Tumor Suppression: Senescence in Cancer Stemness and Tumor Dormancy. *Cells* (2020) 9(2):346. doi: 10.3390/cells9020346
25. Wang L, Park P, La Marca F, Than KD, Lin CY. BMP-2 Inhibits Tumor-Initiating Ability in Human Renal Cancer Stem Cells and Induces Bone Formation. *J Cancer Res Clin Oncol* (2015) 141:1013–24. doi: 10.1007/s00432-014-1883-0
26. Myszczyszyn A, Czarnecka AM, Matak D, Szymanski L, Lian F, Kornakiewicz A, et al. The Role of Hypoxia and Cancer Stem Cells in Renal Cell Carcinoma Pathogenesis. *Stem Cell Rev Rep* (2015) 11:919–43. doi: 10.1007/s12015-015-9611-y
27. Xiao W, Gao Z, Duan Y, Yuan W, Ke Y. Notch Signaling Plays a Crucial Role in Cancer Stem-Like Cells Maintaining Stemness and Mediating Chemotaxis in Renal Cell Carcinoma. *J Exp Clin Cancer Res* (2017) 36:41. doi: 10.1186/s13046-017-0507-3
28. Lu J, Wei JH, Feng ZH, Chen ZH, Wang YQ, Huang Y, et al. miR-106b-5p Promotes Renal Cell Carcinoma Aggressiveness and Stem-Cell-Like Phenotype by Activating Wnt/β-Catenin Signalling. *Oncotarget* (2017) 8:21461–71. doi: 10.18632/oncotarget.15591
29. Lenos KJ, Miedema DM, Lodestijn SC, Nijman LE, van den Bosch T, Romero Ros X, et al. Stem Cell Functionality is Microenvironmentally Defined During Tumour Expansion and Therapy Response in Colon Cancer. *Nat Cell Biol* (2018) 20:1193–202. doi: 10.1038/s41556-018-0179-z
30. Chang WH, Lai AG. Aberrations in Notch-Hedgehog Signalling Reveal Cancer Stem Cells Harbouring Conserved Oncogenic Properties Associated With Hypoxia and Immunoevasion. *Br J Cancer* (2019) 121:666–78. doi: 10.1038/s41416-019-0572-9
31. Su S, Chen J, Yao H, Liu J, Yu S, Lao L, et al. CD10(+)GPR77(+) Cancer-Associated Fibroblasts Promote Cancer Formation and Chemoresistance by Sustaining Cancer Stemness. *Cell* (2018) 172:841–856.e816. doi: 10.1016/j.cell.2018.01.009
32. Kalluri R. The Biology and Function of Fibroblasts in Cancer. Nature Reviews. *Cancer* (2016) 16:582–98. doi: 10.1038/nrc.2016.73
33. Raghavan S, Mehta P, Xie Y, Lei YL, Mehta G. Ovarian Cancer Stem Cells and Macrophages Reciprocally Interact Through the WNT Pathway to Promote Pro-Tumoral and Malignant Phenotypes in 3D Engineered Microenvironments. *J Immunother Cancer* (2019) 7:190. doi: 10.1186/s40425-019-0666-1
34. Lu CH, Yeh DW, Lai CY, Liu YL, Huang LR, Lee AY, et al. USP17 Mediates Macrophage-Promoted Inflammation and Stemness in Lung Cancer Cells by Regulating TRAF2/TRAF3 Complex Formation. *Oncogene* (2018) 37:6327–40. doi: 10.1038/s41388-018-0411-0
35. Lu H, Clauser KR, Tam WL, Fröse J, Ye X, Eaton EN, et al. A Breast Cancer Stem Cell Niche Supported by Juxtacrine Signalling From Monocytes and Macrophages. *Nat Cell Biol* (2014) 16:1105–17. doi: 10.1038/ncb3041
36. Shahid A, Bharadwaj M. The Connection Between the Th17 Cell Related Cytokines and Cancer Stem Cells in Cancer: Novel Therapeutic Targets. *Immunol Lett* (2019) 213:9–20. doi: 10.1016/j.imlet.2019.07.001
37. Patel SJ, Sanjana NE, Kishton RJ, Eidizadeh A, Vodnala SK, Cam M, et al. Identification of Essential Genes for Cancer Immunotherapy. *Nature* (2017) 548:537–42. doi: 10.1038/nature23477
38. Chan TA, Yarchoan M, Jaffee E, Swanton C, Quezada SA, Stenzinger A, et al. Development of Tumor Mutation Burden as an Immunotherapy Biomarker: Utility for the Oncology Clinic. *Ann Oncol* (2019) 30:44–56. doi: 10.1093/annonc/mdy495
39. Zhang J, Wu T, Simon J, Takada M, Saito R, Fan C, et al. VHL Substrate Transcription Factor ZHX2 as an Oncogenic Driver in Clear Cell Renal Cell Carcinoma. *Science* (2018) 361:290–5. doi: 10.1126/science.aap8411
40. Hsieh JJ, Le VH, Oyama T, Ricketts CJ, Ho TH, Cheng EH. Chromosome 3p Loss-Orchestrated VHL, HIF, and Epigenetic Deregulation in Clear Cell Renal Cell Carcinoma. *J Clin Oncol* (2018) 36:Jco2018792549. doi: 10.1200/jco.2018.79.2549
41. Kammerer-Jacquet SF, Crouzet L, Brunot A, Dagher J, Pladys A, Edeline J, et al. Independent Association of PD-L1 Expression With Noninactivated VHL Clear Cell Renal Cell Carcinoma-A Finding With Therapeutic Potential. *Int J Cancer* (2017) 140:142–8. doi: 10.1002/ijc.30429
42. Braun DA, Hou Y, Bakouny Z, Ficial M, Sant' Angelo M, Forman J, et al. Interplay of Somatic Alterations and Immune Infiltration Modulates Response to PD-1 Blockade in Advanced Clear Cell Renal Cell Carcinoma. *Nat Med* (2020) 26:909–18. doi: 10.1038/s41591-020-0839-y
43. Wei SC, Duffy CR, Allison JP. Fundamental Mechanisms of Immune Checkpoint Blockade Therapy. *Cancer Discov* (2018) 8:1069–86. doi: 10.1158/2159-8290.Cd-18-0367
44. Killock D. Immunotherapy: Interferon in Anti-CTLA-4 Responses. Nature Reviews. *Clin Oncol* (2016) 13:652–3. doi: 10.1038/nrclinonc.2016.166
45. Zheng F, Dang J, Zhang H, Xu F, Ba D, Zhang B, et al. Cancer Stem Cell Vaccination With PD-L1 and CTLA-4 Blockades Enhances the Eradication of Melanoma Stem Cells in a Mouse Tumor Model. *J Immunother* (2018) 41:361–8. doi: 10.1097/cji.0000000000000242
46. Díaz-Montero CM, Rini BI, Finke JH. The Immunology of Renal Cell Carcinoma. *Nat Rev Nephrol* (2020) 16:721–35. doi: 10.1038/s41581-020-0316-3
47. Plaks V, Kong N, Werb Z. The Cancer Stem Cell Niche: How Essential is the Niche in Regulating Stemness of Tumor Cells? *Cell Stem Cell* (2015) 16:225–38. doi: 10.1016/j.stem.2015.02.015
48. Motzer RJ, Penkov K, Haanen J, Rini B, Albiges L, Campbell MT, et al. Avelumab Plus Axitinib Versus Sunitinib for Advanced Renal-Cell Carcinoma. *N Engl J Med* (2019) 380:1103–15. doi: 10.1056/NEJMoa1816047
49. Rini BI, Plimack ER, Stus V, Gafanov R, Hawkins R, Nosov D, et al. Pembrolizumab Plus Axitinib Versus Sunitinib for Advanced Renal-Cell Carcinoma. *N Engl J Med* (2019) 380:1116–27. doi: 10.1056/NEJMoa1816714
50. Gaujoux R, Seoighe C. A Flexible R Package for Nonnegative Matrix Factorization. *BMC Bioinf* (2010) 11:367. doi: 10.1186/1471-2105-11-367
51. Becht E, Giraldo NA, Lacroix L, Buttard B, Elarouci N, Petitprez F, et al. Estimating the Population Abundance of Tissue-Infiltrating Immune and Stromal Cell Populations Using Gene Expression. *Genome Biol* (2016) 17:218. doi: 10.1186/s13059-016-1070-5
52. Yang W, Soares J, Greninger P, Edelman EJ, Lightfoot H, Forbes S, et al. Genomics of Drug Sensitivity in Cancer (GDSC): A Resource for Therapeutic Biomarker Discovery in Cancer Cells. *Nucleic Acids Res* (2013) 41:D955–61. doi: 10.1093/nar/gks1111
53. Geeleher P, Cox N, Huang RS. Prrophetic: An R Package for Prediction of Clinical Chemotherapeutic Response From Tumor Gene Expression Levels. *PloS One* (2014) 9:e107468. doi: 10.1371/journal.pone.0107468

**Conflict of Interest:** The authors declare that the research was conducted in the absence of any commercial or financial relationships that could be construed as a potential conflict of interest.

**Publisher's Note:** All claims expressed in this article are solely those of the authors and do not necessarily represent those of their affiliated organizations, or those of the publisher, the editors and the reviewers. Any product that may be evaluated in this article, or claim that may be made by its manufacturer, is not guaranteed or endorsed by the publisher.

*Copyright © 2021 Wang, Xu, Cheng and Liang. This is an open-access article distributed under the terms of the Creative Commons Attribution License (CC BY). The use, distribution or reproduction in other forums is permitted, provided the original author(s) and the copyright owner(s) are credited and that the original publication in this journal is cited, in accordance with accepted academic practice. No use, distribution or reproduction is permitted which does not comply with these terms.*

frontiers in Oncology

ORIGINAL RESEARCH
published: 14 December 2021
doi: 10.3389/fonc.2021.773063

# CD248$^+$ Cancer-Associated Fibroblasts: A Novel Prognostic and Therapeutic Target for Renal Cell Carcinoma

*Chao Xu[1†], Keying Zhang[1†], Fa Yang[1†], Xiang Zhou[2], Shaojie Liu[1], Yu Li[1], Shanjin Ma[3], Xiaolong Zhao[1], Tong Lu[1], Shiqi Lu[4], JiaYu Zhang[1], Hongji Li[1], Donghui Han[1*], Weihong Wen[4*] and Weijun Qin[1*]*

[1] Department of Urology, Xijing Hospital, Fourth Military Medical University, Xi'an, China, [2] Department of Clinical Laboratory, Innovation Port Hospital of Xi'an Jiaotong University, Xi'an Jiaotong University, Xi'an, China, [3] Department of Urology, Tangdu Hospital, Fourth Military Medical University, Xi'an, China, [4] Department of Medical Research, Northwestern Polytechnical University, Xi'an, China

**Background:** The tumor microenvironment (TME) plays an important role in the progression of renal cell carcinoma (RCC). Cancer-associated fibroblasts (CAFs) are considered to constitute a major component of the TME and participate in various tumor-promoting molecular events. We have previously confirmed that CD248 represents a promising biomarker of CAFs, which may provide insight into CAF-based tumor-promoting effects. However, CAF-mediated tumor progression and the potential mechanism of CD248 remain largely unknown in RCC patients.

**Methods:** Expression profiling and clinical data of RCC patients were obtained from The Cancer Genome Atlas (TCGA) database. An MCP-counter algorithm and Kaplan–Meier survival analysis were performed to explore the prognostic value of CAFs and CD248, respectively. A Pearson correlation coefficient test and Student's *t*-test were employed to evaluate the relationship between immunosuppressive TME and CD248 or CAFs. Immunohistochemistry and immunofluorescence staining were performed to confirm CD248 expression within CAFs. CD248-specific siRNA was used to investigate the potential function of CD248 in CAF tumor promotion. Differentially expressed genes (DEGs), weighted gene co-expression network analysis (WGCNA), and enrichment analysis were conducted to clarify the function of CD248$^+$ CAFs in RCC progression and the associated regulatory mechanism.

**Results:** CD248 overexpression and CAF infiltration could predict poor RCC prognosis, which may involve the immunosuppressive TME. CD248 may serve as a promising CAFs biomarker and be involved with the tumor-promoting effect of CAFs. Moreover, CD248$^+$ CAF infiltration may contribute to RCC progression and an immunosuppressive TME through cell-extracellular matrix (ECM) interactions and metabolism regulation.

OPEN ACCESS

**Edited by:**
*James H. Finke, Case Western Reserve University, United States*

**Reviewed by:**
*Jennifer D. Wu, Northwestern University, United States*
*Jiaxing Lin, The First Affiliated Hospital of China Medical University, China*

***Correspondence:**
*Weijun Qin*
*qinwj@fmmu.edu.cn*
*Weihong Wen*
*wenweih@fmmu.edu.cn*
*Donghui Han*
*906812205@qq.com*

*†These authors have contributed equally to this work*

**Specialty section:**
*This article was submitted to Genitourinary Oncology, a section of the journal Frontiers in Oncology*

**Received:** *11 October 2021*
**Accepted:** *19 November 2021*
**Published:** *14 December 2021*

**Citation:**
*Xu C, Zhang K, Yang F, Zhou X, Liu S, Li Y, Ma S, Zhao X, Lu T, Lu S, Zhang J, Li H, Han D, Wen W and Qin W (2021) CD248$^+$ Cancer-Associated Fibroblasts: A Novel Prognostic and Therapeutic Target for Renal Cell Carcinoma. Front. Oncol. 11:773063. doi: 10.3389/fonc.2021.773063*

**Conclusion:** CD248+ CAFs participate in the regulation of RCC progression and immunosuppressive TME, which may represent a novel prognostic and therapeutic target for RCC.

**Keywords: renal cell carcinoma, CD248, CAFs, TME, prognostic biomarker**

## INTRODUCTION

Renal cell carcinomas (RCCs) are characterized by a high degree of heterogeneity and composed of different subtypes with their own biological properties and therapeutic responses, which lead to different clinical outcomes (1). High infiltration of stromal and immune components and the plasticity of the tumor microenvironment (TME) are the most common features of RCC (2, 3). Like a protective nest, the TME shelters cancer cells by providing vascular nourishment, suppressing immunity, and establishing a matrix barrier (4). Over the past decade, there have been an increased number of innovative therapeutic strategies targeting TME for RCC, among which immune checkpoint blockade (ICIs) and anti-angiogenic tyrosine kinase inhibitors (TKIs) have attracted keen attention (5, 6). However, the acquisition of therapeutic resistance in most patients has limited their further clinical application (7), which is closely correlated with the perfect linkage between tumor parenchymal and TME (8). Consequently, an in-depth understanding of the components of the TME in RCC is conducive to constructing a tumor-specific framework and developing a novel target for RCC therapy.

Cancer-associated fibroblasts (CAFs) have emerged as a potential target to destroy the TME network, given the cross-linkage role of CAFs in tumor initiation and progression (9). Once the tumor is established, multiple CAF-associated pro-tumor factors begin to appear, in which CAFs are both synthesized and remodeled into the extracellular matrix (ECM) to support tumor proliferation and metastasis, and also function as regulators of neo-angiogenesis, immunoregulation, and therapeutic resistance (10). Histopathological analysis also demonstrated that the infiltration of CAFs and CAF-related signals were predictive of a poor prognosis (11, 12). However, due to the non-specificity of conventional biomarkers, such as αSMA, FAP, PDGFRα/β, and FSP1 (S100A4) (13), a deficiency of specific biomarkers to distinguish CAFs from other components in the TME presents a challenge to the identification of potential functions and potential as a target for RCC treatment.

CD248, also known as endosialin or tumor endothelial marker 1 (TEM1), is rarely expressed in normal tissues and is primarily expressed on stromal cells, including activated fibroblasts, as well as the perivascular cells of tumors or inflammatory diseases (14). Recent reports have focused on CD248 as a specific biomarker of activated fibroblasts, including CAFs in tumors and myofibroblasts in organ fibrosis (15–18). Studies have confirmed that CD248 was overexpressed in CAFs of hepatocellular carcinoma (HCC), which promoted the polarization of tumor-associated macrophages (TAMs) to the M2 phenotype, an inhibitory maker in TME, by regulating growth arrest-specific protein 6 (GAS6) (19). In addition, the knockdown of CD248 in mice showed significant suppression mediated by stromal cells in tumor growth, invasion, and metastasis following tumor transplantation (20). Therefore, the potential role of CD248 as a specific biomarker for CAFs makes it an ideal target for the TME of RCCs. However, the characteristics of CD248+ CAFs in RCC progression and the associated regulatory mechanisms remain largely unknown.

The aim of the present study was to uncover the role that CD248+ CAFs play in the TME of RCCs. Clinical specimens and expression profile assays from the Cancer Genome Atlas (TCGA) and Gene Expression Omnibus (GEO) were analyzed to identify the contribution of CD248 to RCC progression. We found that CD248 expression is highly correlated with CAF infiltration in the TME. Using immunostaining techniques, we confirmed that CD248 was specifically located on CAFs. We also found that CD248 participated in stromal-related signal regulation and the knockdown of CD248 weakened the invasive ability of fibroblasts. Finally, we evaluated the prognostic value of CD248+ CAFs in RCC and analyzed their related genes with a weighted gene co-expression network analysis (WGCNA) and enrichment analysis to explore the underlying mechanism of CD248+ CAFs in regulating the TME of RCC.

## MATERIALS AND METHODS

### Data Source and Processing

A total of 895 RCC samples and 128 normal samples were downloaded from the TCGA database (https://portal.gdc.cancer.gov/). Transcriptomic data (Fragments Per Kilobase Million [FPKM]) and the clinical information were integrated using ID numbers. For samples from the same patients, gene expression was averaged using *limma* package of R software. All data were processed by R software (https://www.r-project.org/). In addition, the gene expression profiling dataset (GSE167093) was downloaded from the GEO database (https://www.ncbi.nlm.nih.gov/geo/), including 152 pairs of RCC and para-cancer tissues, and an additional 450 RCC samples. Moreover, the RNA-sequencing dataset for si-CD248 and si-Con (PRJNA608053) was downloaded from the National Center for Biotechnology Information (NCBI) (https://www.ncbi.nlm.nih.gov/).

### CAF Calculation and TME Estimation

MCP-counter algorithm (21) was performed to calculate the CAF scores of patients from the TCGA cohort. Moreover, the CAFs with high CD248 expression were defined as CD248+ CAF and the CAFs with low CD248 expression were defined as CD248- CAF. The median of CD248 expression was employed as the cutoff value. The ESTIMATE algorithm in the estimate

package of the R software was employed for TME analysis (22). Three scoring forms, including stromal score, immune score, and ESTIMATE score, corresponded to the proportion of stromal and immune components as well as the sum of both. Therefore, the calculated score could reflect the composition of TME.

## Survival Analysis

A Kaplan–Meier survival analysis was performed to evaluate the prognostic value of the variables, including CD248 expression, stromal, and immune scores; CAF infiltration score; and the $CD248^+$ CAF infiltration score. The TCGA-KIRC and KIRP cohorts were further analyzed to validate the effect of $CD248^+$ CAFs on the patient survival outcomes.

## Enrichment Analysis

Using gene set enrichment analysis (GSEA) software (version 4.1.0), the Hallmark and C2 Kegg gene set v7.2 were used for the enrichment analysis. Gene sets with NOM $p < 0.05$ and false discovery rate (FDR) $q < 0.05$ were considered to be significant. The "clusterprofiler" R package was used to perform GO and KEGG enrichment analyses. GO terms and KEGG pathways with a $p$-value < 0.05 were considered to be significantly enriched.

## WGCNA of $CD248^+$ CAF-Related Differentially Expressed Genes

To obtain the DEGs from the TCGA cohort, we divided the samples into two groups according to the medium level of CD248 expression and CAF score. The differential gene expression between these two groups was performed using R software. Genes with an adjusted $p$-value < 0.05 and $|\log_2 FC| > 1$ were considered to be significant. The transcription factor (TF) list was retrieved from the Cistrome website (https://cistrome.org), and differentially expressed TFs (DEFs) were identified by matching with the DEGs. WGCNA R package was used for the co-expression analysis, and the most significant modules were selected for an enrichment analysis. Cytospace software (version 3.6.0) was employed to visualize the protein–protein interaction (PPI) networks.

## Cell Culture and Transfection

HFL-1 cells were purchased from the Chinese Academy of Science (Shanghai, China). The cellular identities were confirmed by STR profiling, and all cell lines underwent routine mycoplasma testing. Cells were maintained in DMEM/F12 (Gibco) supplemented with 10% FBS (Gibco) and 1% penicillin-streptomycin (Invitrogen). Transfections were performed by applying OPTI-MEM and Lipofectamine 3000 in accordance with the manufacturer's instructions. si-CD248 and si-Con were purchased from GenePharma (Shanghai, China) and introduced into the cells at a concentration of 50 nM. The transfected cells were harvested at 36 h post-transfection.

## Western Blotting

The total protein samples were prepared from cell pellets and the concentration was determined using a Bradford assay (ThermoFisher Scientific). Equal amounts of the protein samples were loaded on 10% sodium dodecyl sulfate-polyacrylamide gel (SDS-PAGE) and transferred onto a polyvinylidene fluoride (PVDF) membrane (ThermoFisher Scientific). The membrane was blocked with 5% skim milk, and incubated with the following primary antibodies overnight at 4°C: anti-CD248 (1:1,000, Abcam, #ab48185) and anti-GAPDH (1:2,000, Proteintech, #10494-1-AP). The membranes were next incubated with horseradish peroxidase (HRP)-conjugated secondary antibodies for 1 h at room temperature prior to visualization.

## RT-qPCR

Cells were harvested and the total RNA was isolated with TRIzol. Reverse transcription (RT) was conducted using PrimeScript™ RT Master Mix (TaKaRa, Japan). Next, qPCR was performed using an SYRB Green II kit (#DRR041A; TaKaRa, Japan). The following primers were used: homo-CD248-forward (F): 5'-CTCAACCAACTATCCCCAAGTC-3' and reverse (R): 5'-GCCTGGGTTCTGATACCTGG-3'; homo-GAPDH-F: 5'-AG GTCGGTGTGAACGGATTTG-3' and R: 5'-TGTAGACCA TGTAGTTGAGGTCA-3'.

## Cell Invasion Assays

The invasive ability of HFL-1 cells was determined using a Transwell assay. HFL-1 cells transfected with si-CD248s or si-Con were seeded into the upper chamber. The DMEM medium supplemented with serum was placed into the lower chamber. The cells on the lower side of the filters were defined as invasive cells.

## Tissue Staining

The paraffin-embedded tissue used for the present assay was collected from the patients undergoing a radical operation at our institute. The subjects provided written informed consent. All protocols were authorized by the Ethics Committee of The First Affiliated Hospital of Air Force Military Medical University. For immunohistochemistry (IHC) staining, after deparaffinization and rehydration, sections were applied for antigen retrieval in a citrate solution. After blocking in goat serum (MXB, China) for 40 min, the sections were incubated with a primary CD248 antibody (Abcam, #ab204914) in a humidified box overnight at 4°C. Next, the sections were incubated with the corresponding HRP-labeled secondary antibodies (Abcam, #ab05718) for 30 min at room temperature prior to visualization with a 3,3'-Diaminobenzidine system (MXB, China). Sections were counterstained with hematoxylin and dehydrated in ascending concentrations of ethanol followed by clearance with xylene. The samples were observed under a Nikon light microscope after being sealed onto slides with neutral balsam. For immunofluorescence (IF) staining, the samples were blocked in goat serum for 1 h at room temperature, followed by an incubation with the following primary antibodies: anti-CD248 (Abcam, #ab204914) and anti-α-SMA (Invitrogen, #MA1-06110). The sections were then incubated with Alexa Fluor 488 (Abcam, #ab150077)- and Alexa Fluor 594 (Abcam, #150117)-conjugated secondary antibodies. The nucleus was counterstained with DAPI before being sealed with glycerin. For Masson's staining, the sections were stained with corresponding reagents according to the manufacturer's protocol after deparaffinization and rehydration (Servicebio, China).

## Statistical Analysis

The statistical significance of the mean value of the variables between the two groups was calculated using an unpaired Student's *t*-test or Pearson's correlation coefficient test using R software. All data were presented as the mean ± standard error of the mean (SEM) of at least three independent experiments. Differences were considered significant at a threshold of $p < 0.05$.

# RESULTS

## CD248 Upregulation Is Correlated With RCC Deterioration and a Tumor-Promoting TME

In the TCGA cohort, we compared CD248 expression between normal ($n = 128$) and tumor ($n = 934$) samples from RCC patients and found a significant upregulation of CD248 expression ($p < 0.001$, **Figure 1A**). The normal-tumor paired samples from the same patients yielded a consistent result ($n = 128$, $p < 0.0001$, **Figure 1B**). Likewise, CD248 expression in 152 RCC samples was also significantly higher than that of 152 paired normal samples in the GEO cohort ($p < 0.001$, **Figure S1A**). Moreover, according to the median expression of CD248, the overall survival (OS) rate of RCC patients in the CD248 high-expression group at 5 years was 57.5%, compared with 74.9% for the low-expression group ($p < 0.001$, **Figure 1C**). The clinicopathological correlation analysis indicated that CD248 expression was upregulated as the RCC progressed ($p < 0.05$, **Figure 1D** and **Figure S1B**).

A GSEA of the KEGG pathway was used to analyze the pathways located downstream of CD248 (**Figure 1E**). The results showed that CD248 was positively associated with the activation of pathways related to TME remodeling, including the epithelial–mesenchymal transition (EMT), stromal and ECM signals, immunoregulation, and neo-angiogenesis signals. CH248 was also associated with an inhibition of metabolism-related pathways ($p < 0.05$). An MCP-counter algorithm was performed to determine the relationship between upregulated CD248 and the TME. As a result, the infiltration of tumor epithelial cells, cytotoxic T cells, natural killer (NK) cells, monocytic macrophages, myeloid dendritic cells (MDCS), endothelial cells (ECs), and CAFs was increased in the CD248 high-expression group (**Figure 1F**).

To explore the impact of the TME on RCC prognosis, stromal or immune scores (i.e., a commonly used index to represent the TME) were calculated through the ESTIMATE algorithm. As

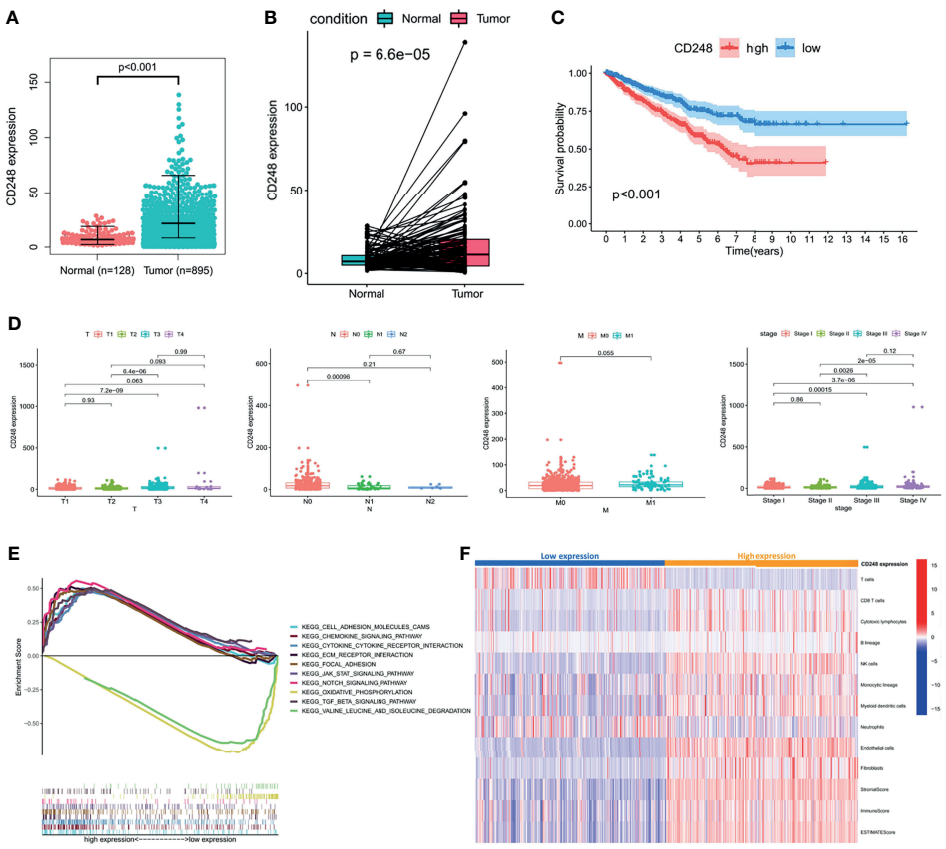



**FIGURE 1** | The role of CD248 in RCC progression. **(A, B)** CD248 overexpression in RCC. **(C)** Kaplan–Meier analysis of the OS in high and low CD248-expressing patients with RCC in the TCGA cohort. **(D)** Clinicopathological correlation of CD248 in RCC. **(E)** GSEA of KEGG pathways analysis. **(F)** Heatmap of TME cells was shown after grouping by CD248. $p < 0.05$ was considered statistically significant.

shown in **Figure S2**, deteriorated tumor progression and a reduced OS rate were detected in the high-score group compared with the low-score group, according to the median scores ($p < 0.05$). Briefly, both CD248 expression and CD248-related TME could predict a poor prognosis.

## CD248 Upregulation Is Correlated With a CAF-Mediated Tumor-Promoting Effect

As the major component of the TME, CAFs participate in various tumor-prompting molecular events. In the present study, the high CAF infiltration group showed a poorer prognosis compared to that of the low infiltration group with the OS rate at 5 years (56.4% and 78.1%, respectively) according to the median CAF infiltration score ($p < 0.001$, **Figure 2A**). Furthermore, RCC patients with a high CAF infiltration have a significantly higher pathological stage and risk of metastasis compared to those in the low infiltration group ($p < 0.001$, **Figure 2B**). Moreover, CAF infiltration was positively associated with the TME score ($p < 0.05$, **Figure 2C**; $p < 0.001$, **Figure 2D**).

Considering that the prognostic value of both CD248 and CAFs was related to the TME, together with our previous findings that CD248 contributes to tumor-promoting regulation of CAFs in HCC (19), we proposed to explore the relationship between CD248 and CAFs in RCC progression. **Figures 3A, B** show that CD248 expression was significantly associated with CAF infiltration (Cor = 0.67, $p < 0.0001$). Using RCC tissue staining, we observed that the expression pattern of CD248 and collagen (mainly CAF synthesis) was similar in the tumor interstitium (**Figure 3C**). Furthermore, CD248 was colocalized with α-SMA (a CAF biomarker) in the RCC sections (**Figure 3D**). Hierarchical clustering results showed that upregulated CD248 was positively correlated with mesenchymal activation, including EMT, ECM-related signals, TGFβ signals, and pan-fibroblast TGFβ response (F-TBRS) in TCGA RCC patients (**Figure 3E**). HFL-1 cells (a fibroblasts cell line) with CD248 knocked down showed a decreased-invasion ability in a Transwell assay ($p < 0.0001$, **Figure 3F** and **Figure S3A**; $p < 0.001$, **Figure 3G**), which indicated that CD248 might contribute to a CAF-mediated tumor-promoting effect.

## Regulatory Mechanism of CD248 in CAF-Mediated Tumor-Promoting Molecular Events

The RNA-Seq profile of HFL-1 cells (i.e., control group and CD248 knockdown group) was analyzed using R software. From this process, 2,104 DEGs were obtained, from which 1,084 genes were upregulated, and 1,019 genes were downregulated in the

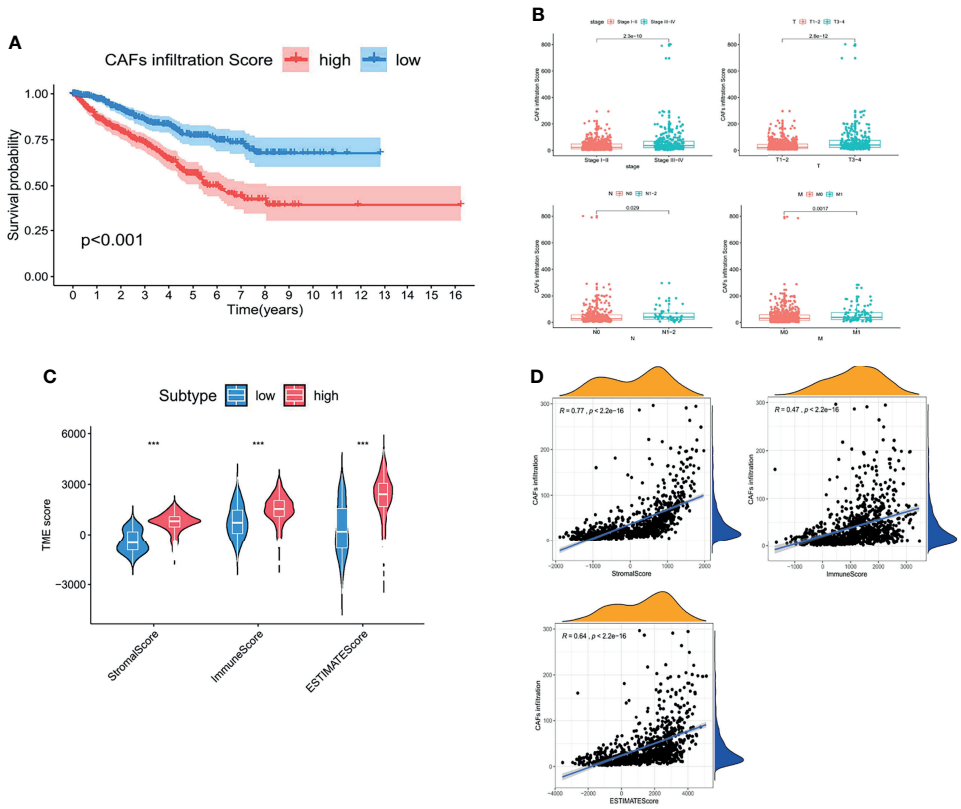



**FIGURE 2** | CAFs constituted the major component of the TME and promoted RCC progression. **(A)** Kaplan–Meier analysis of the OS associated with high and low CAF infiltration. **(B)** Clinicopathological correlation of CAF infiltration in RCC. **(C)** Violin plot of the comparison of stromal and immune and ESTIMATE scores based on high and low CAF infiltration groups. **(D)** Correlation analysis between the CAF infiltration score and TME scores. $p < 0.05$ was considered statistically significant.

CD248 knockdown group compared with the control group (FDR < 0.05, $|\log_2 FC| > 1$, **Figure 4A**). Subsequently, 1,519 DEGs were correlated with CD248 expression and 32 DEFs were selected (Cor = 0.5, $p < 0.05$). The GO enrichment analysis showed that CD248-related genes were primarily enriched in three types of functions, including cell–cell and cell–cytokine interactions, tumor angiogenesis, and cellular proliferation. Chord plots and corresponding PPI networks were constructed

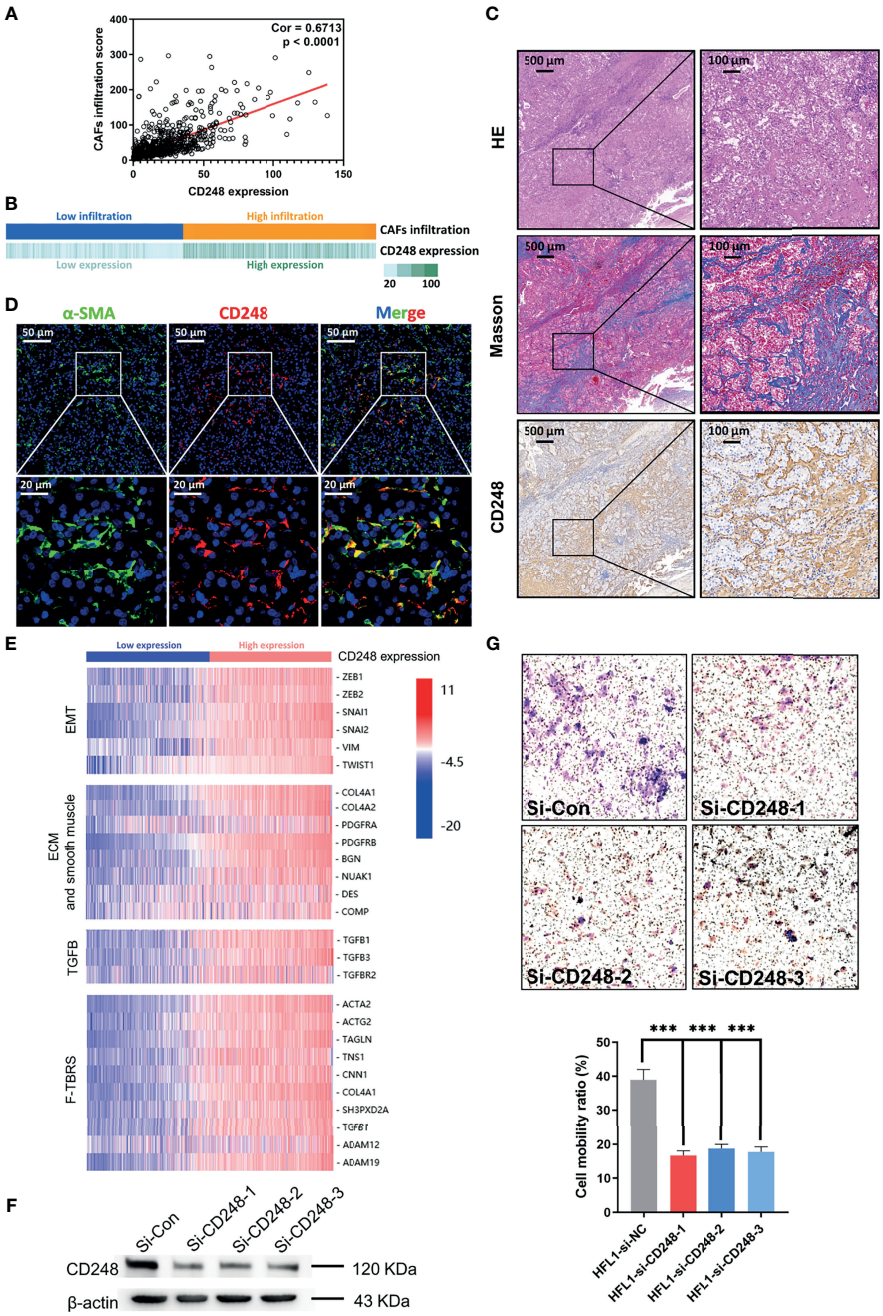



**FIGURE 3** | CD248 is a specific biomarker for CAFs. **(A)** Correlation analysis between CD248 expression and CAF infiltration. **(B)** Correlation bar chart between CD248 expression and CAF infiltration. **(C)** H&E, Masson, and IHC staining for CD248 in RCC tumor lesions. Scale bar = 500 μm. **(D)** Dual IF staining showing the colocalization of α-SMA (green) and CD248 (red) in RCC tumor lesions. Scale bar = 50 μm. **(E)** Hierarchical clustering in the TCGA cohort. **(F)** Western blot showing the effective knockdown of CD248 in the HFL-1 cell line. **(G)** Images of the Transwell assay results following the knockdown of CD248 in HFL-1 cell lines, and representational statistical analysis of the Transwell assay. $n = 3$. Data are shown as the mean ± SEM. Representative images are shown. $p < 0.05$ was considered statistically significant. ***$p < 0.001$.

for visualization (FDR < 0.05, **Figures 4B–G**). Moreover, an integrated PPI of those three above sub-networks was constructed to explore the regulatory mechanism between different GO terms (**Figure 4H**). As a result, several hub DEFs with maximum intramodular connectivity were identified (e.g., SOX4, EGR1, LEF1, FOS, MITF, KLF4, TCF7, and KDM6B), which might involve CD248-mediated tumor-promoting regulation in CAFs (**Figure 4H**). A KEGG analysis of the integrated PPI was performed, and immunoregulation, tumor progression, and neo-angiogenesis pathways were significantly enriched (FDR < 0.05, **Figure 4I**), among which the cytokine–cytokine receptor interaction, PI3K-Akt signaling pathway, and MAPK signaling pathway exhibited the maximum intramodular enrichment.

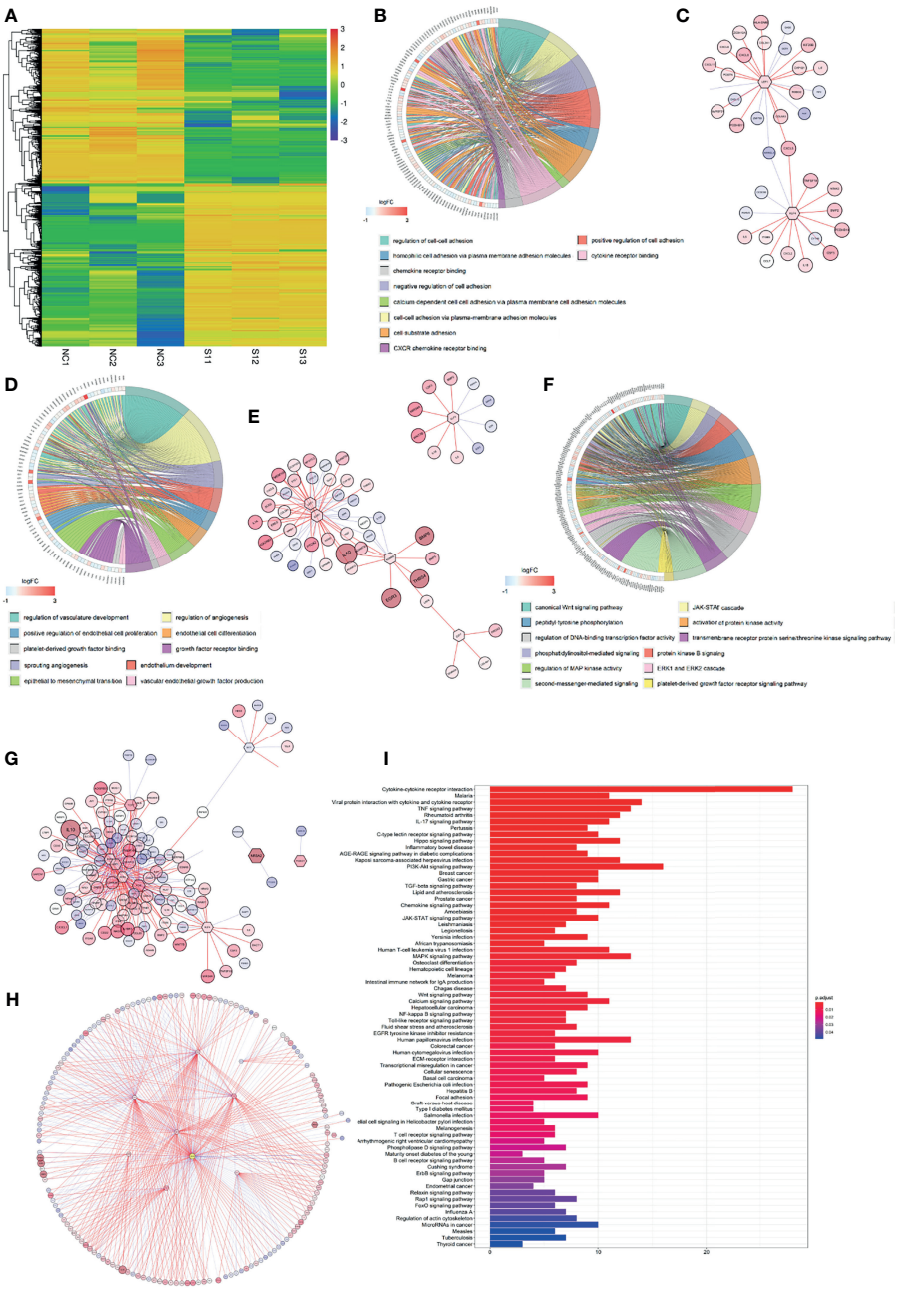



**FIGURE 4** | CD248 promotes the role of CAFs in the TME. **(A)** Hierarchical clustering in the RNA-seq from the CD248 knockdown HFL-1 cell line. **(B, D, F)** Chord charts for the GO enrichment analysis. The left semicircle represents the genes and the right semicircle represents the functions of these gene sets involved in regulation. **(C, E, G)** PPI networks for each of the gene sets. **(H)** The total PPI network. **(I)** KEGG pathways enrichment analysis. $p < 0.05$ was considered to be statistically significant.

## CD248+ CAFs Are Associated With an Immunosuppressive TME in RCC Progression

To further investigate the function of CD248 in CAF-mediated tumor promotion, CAFs exhibiting upregulated CD248 were defined as CD248+ CAFs according to the median expression level. As shown in **Figure 5A**, a high infiltration of CD248+ CAFs in RCC patients was related to a poorer OS. In particular, the OS rate at 5 years was 58.3% in the high infiltration group, whereas this index was 77.5% in the low infiltration group ($p < 0.001$). Additionally, increased CD248+ CAF infiltration could indicate worse tumor stage, local invasion, and metastasis of RCC ($p < 0.01$, **Figure 5B**). The similar prognostic value of CD248+ CAFs in the two major subtypes of RCC (i.e., clear-cell RCC and papillary RCC) were further validated in TCGA-KIRC and KIRP cohorts ($p < 0.01$, **Figures S4A, B**).

Since both CD248 and CAFs were associated with immunoregulation, the CD248+ CAF-mediated RCC tumor-promoting effect may be involved. Moreover, CD248+ CAF infiltration was positively correlated with the TME scores, particularly the immune score ($p < 0.0001$, **Figure 5C**). The results of the MCP-counter algorithm revealed that increased CD248+ CAF infiltration was accompanied by a higher infiltration of CD8+ T cells, NK cells, monocytic macrophages, and MDCS ($p < 0.001$, **Figures 5D, E**). However, the expression level of several T-cell depletion biomarkers (i.e., PDCD1, CTLA4, LAG3, FOXP3, and HAVCR2) and TAM type 2 polarization biomarkers (i.e., CD163, MS4A4A, and MSR1) were significantly increased in the high CD248+ CAF group ($p < 0.001$, **Figure 5F**). This indicates that CD248+ CAFs might be associated with an immunosuppressive TME in RCC progression.

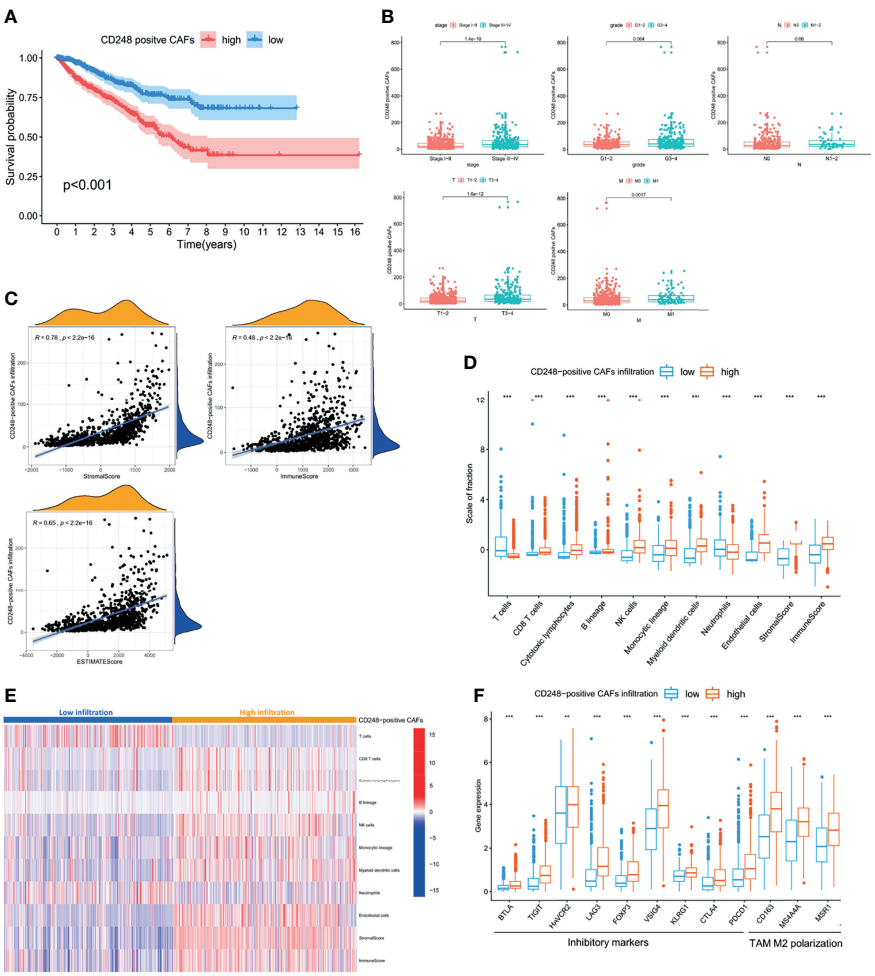



**FIGURE 5** | CD248+ CAF infiltration was suggestive of a poor prognosis in RCC patients and immunosuppression. **(A)** Kaplan–Meier analysis of the OS associated with high and low CD248+ CAF infiltration. **(B)** Clinicopathological correlation of CD248+ CAF infiltration in RCC. **(C)** Correlation analysis between the CAF infiltration score and TME scores. **(D)** Box plot of the comparison of cells in the TME based on high and low CD248+ CAF infiltration groups. **(E)** Heatmap of TME cells shown after grouping by CD248+ CAFs. **(F)** Box plot of the comparison of inhibitory immune molecules based on high and low CD248+ CAF infiltration groups. $p < 0.05$ was considered statistically significant. $^{**}p < 0.01$; $^{***}p < 0.001$.

## Regulatory Mechanism of CD248+ CAFs in RCC Immunosuppression

A total of 3,186 and 2,617 DEGs that correlated with both CD248 and CAFs were recognized in the TCGA cohort, respectively (FDR < 0.05, $|\log_2 FC| > 1$, **Figures 6A, B**). CD248+ CAF-correlated DEGs were identified, among which 1,245 were upregulated and 313 DEGs were downregulated (**Figures 6C, D**). Through a GO and KEGG enrichment analysis, those CD248+ CAF-correlated DEGs were mainly enriched in the activation of immunoregulation pathways, cell–cell and cell–ECM interactions, and inhabitation of metabolism-related pathways (i.e., oxidative phosphorylation and amino acid metabolism) ($p < 0.05$, **Figures 6E–G**).

To accurately identify hubs of gene clusters of immunoregulation and tumor promotion, 1,558 CD248+ CAF-correlated DEGs were analyzed through the WGCNA method

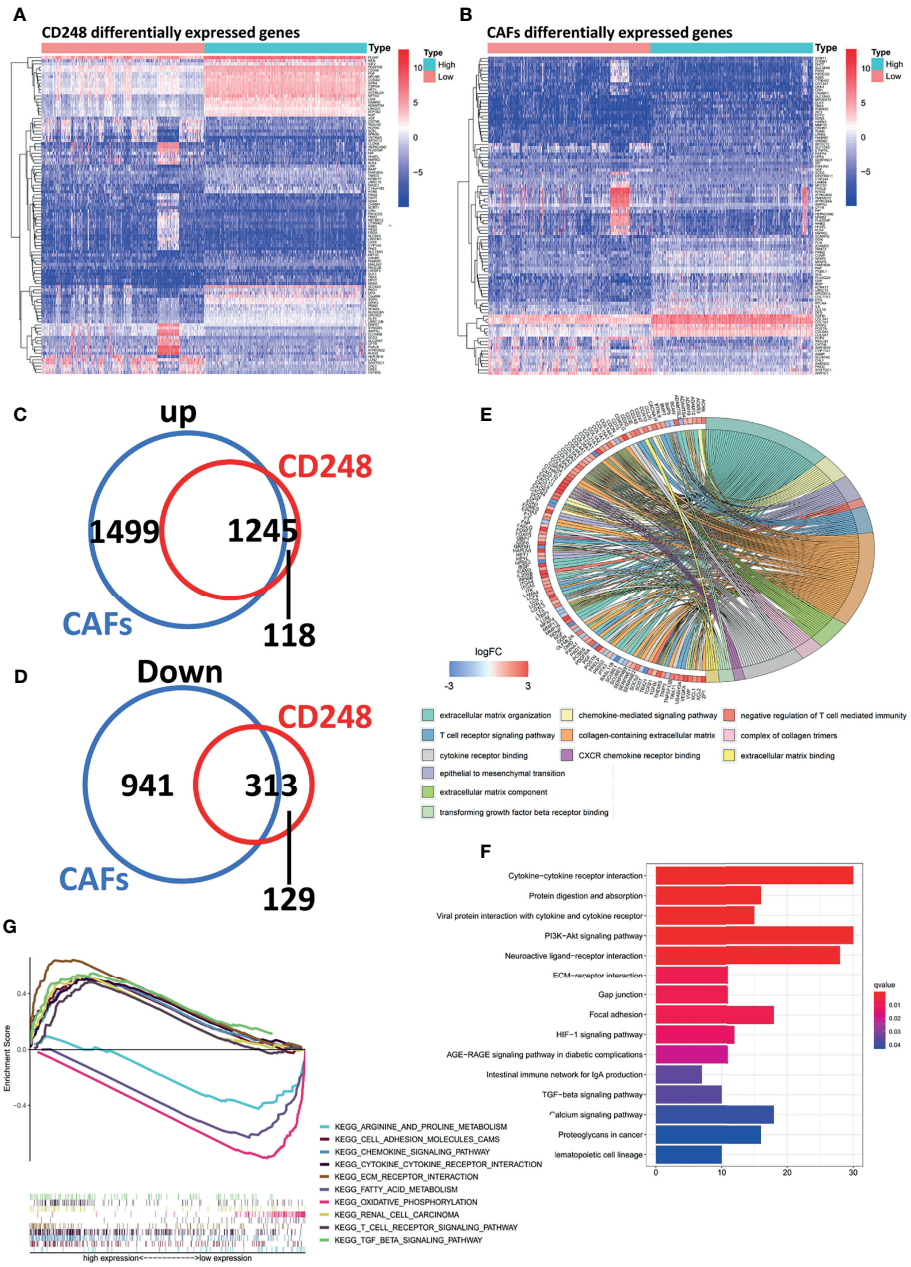



**FIGURE 6** | Recognition of regulatory DEGs for CD248+ CAFs and enrichment analysis. **(A)** Heatmap showing DEGs based on median CD248 expression. **(B)** Heatmap showing DEGs based on the median CAF infiltration. **(C, D)** The intersection of DEGs associated between CD248 and CAFs. **(E)** GO function enrichment analysis. **(F)** KEGG pathway analysis. **(G)** GSEA of KEGG pathway analysis. $p < 0.05$ was considered statistically significant.

(**Figure 7A** and **Figures S5A, B**). These 1,558 DEGs were then categorized into 32 modules (i.e., gene clusters), and we selected eight modules that were significantly associated with clinicopathological variables (Cor > 0.3, $p < 0.001$, **Figure 7B**). GO terms and KEGG pathway enrichment analysis were employed for the functional annotation of the eight modules (**Figure 7C**). Apart from the classical functions of CAFs in ECM remodeling, cell–ECM interactions, and cellular migration (**Figures S6A–C**), CD248+ CAF-correlated DEGs were also enriched in the terms of immune cell activation and cell–cytokine interactions (**Figure 7D** and **Figures S6D–E**). In addition, the metabolism process (i.e., fatty acid, glycolysis, and amino acid metabolism) and cell cycle (i.e., promoting mitosis and relieving proliferation inhibitory signals) terms were significantly

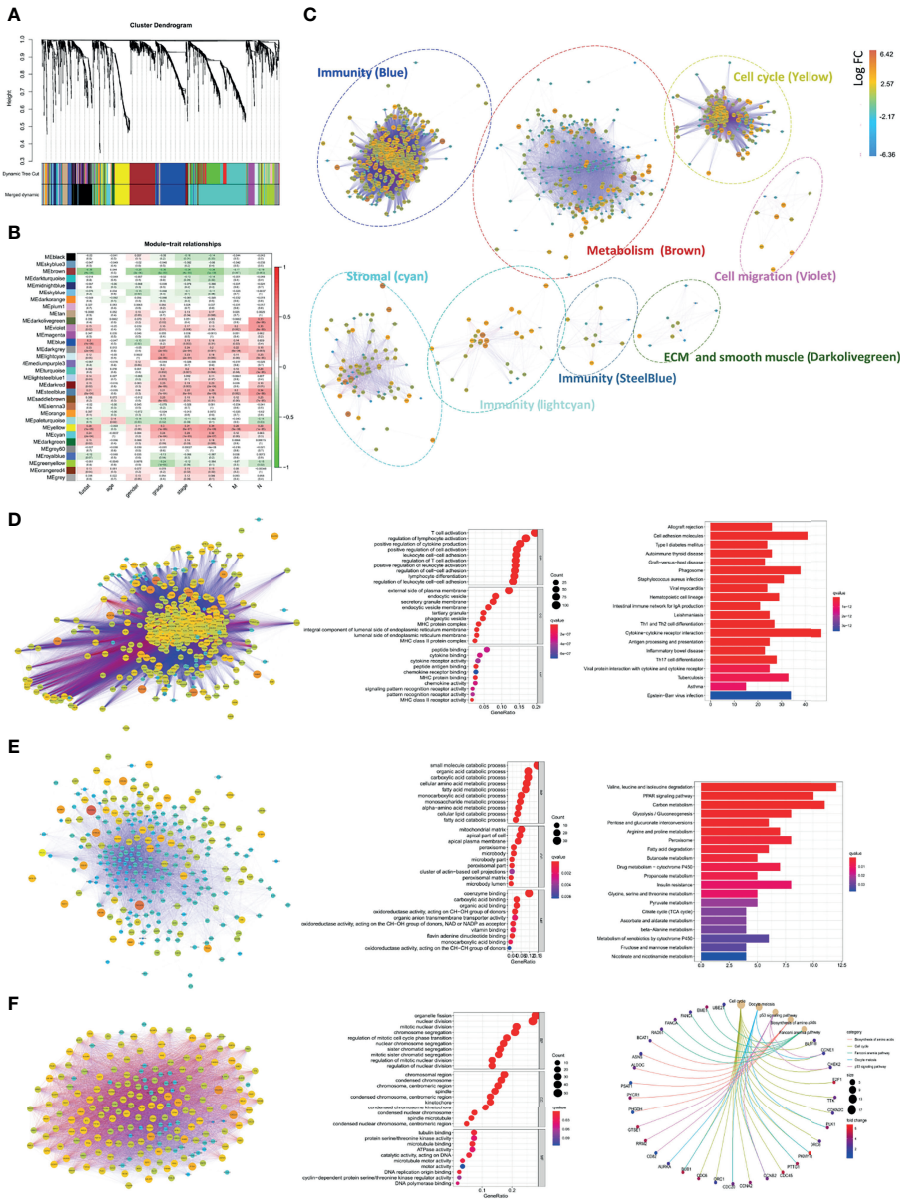



**FIGURE 7** | Comprehensive annotation for the functions of CD248+ CAFs regulatory DEGs. **(A)** Clustering dendrograms of genes and clinicopathological variables, with dissimilarity based on topological overlap, together with assigned module colors. **(B)** Module–trait associations. The rows correspond to module gene sets, and columns correspond to a trait. Cells contain the corresponding correlation and *p*-value. The table is color-coded by correlation according to the color legend. **(C)** PPI network for the 8 selected gene modules. The function of each module is marked. Labels are colored according to the color legend. **(D)** PPI network and bubble diagram of the GO analysis and bar chart of KEGG pathway analysis for the "Blue" module. **(E)** PPI network and bubble diagram of the GO analysis and bar chart of KEGG pathways analysis for the "Brown" module. **(F)** PPI network and bubble diagram of the GO analysis and Circos chart of the KEGG pathway analysis for the "Yellow" module. $p < 0.05$ was considered statistically significant.

enriched (**Figures 7E, F**). For visualization, corresponding PPI networks of each module were simultaneously constructed.

## DISCUSSION

The incidence of RCC has increased annually, accounting for approximately 90%–95% of neoplasms in the kidneys (23). Among patients with RCC, about 40% of patients miss surgery due to the occult progression of the tumor (24). In addition, despite undergoing timely surgical treatment, approximately 28% of patients experience relapse or develop metastasis with a low 5-year survival (25). Fortunately, therapeutic strategies for RCC have rapidly evolved throughout the last decade, among which ICIs or TKIs alone or in combination have been regarded as the standard treatment in advanced RCC (26); however, a moderate tumor mutation burden (TMB) and an inverse correlation between infiltrating $CD8^+$ T cells and prognosis of patients have limited the further utility of ICIs (27, 28). Moreover, a low complete response rate and the activation of angiogenic escape pathways decreased the therapeutic expectation of TKIs (29). Apparently, the complexity of TME brings new anti-tumor targets, but also hides the potential therapeutic resistance mechanism. Therefore, the identification of stable and effective targets from a dynamic alteration of TME will be of central significance for RCC treatment.

As the dominant member of the TME, CAFs participate in all stages of tumor progression, including tumorigenesis and metastasis (30), in which CAFs support the TME *via* cell–cell interactions and the secretion of regulators to promote neo-angiogenesis, accumulate inhibitory immune cells, remodel the ECM, and promote EMT, including vascular endothelial growth factor A (VEGFA), TGFβ, CXCL12, CCL2, IL6, and MMPs, among others (31). Therefore, targeting CAFs to transform the TME from being tumor-promoting to tumor-suppressive represents a recent research hotspot and effective strategy. However, the limitations of specific biomarkers for the identification of CAFs prevent us from further understanding the biology and functions of CAFs in tumorigenesis. CD248 is a single transmembrane glycoprotein that has been reported as a specific biomarker of activated fibroblasts, which is rarely expressed in normal tissues and is upregulated in the stroma of tumors and chronic inflammatory diseases, enabling it to function as a specific biomarker for CAFs (18, 32). In the present study, we first recognized that CD248 overexpression was associated with adverse prognostic outcomes and disease progression in RCC. The GSEA of KEGG pathway analysis revealed that CD248 participated in TME-related signatures, including stroma-related, cell–cell, and cell–ECM interactions, immunoregulation, and EMT signatures. In addition, CD248 overexpression was accompanied by increased infiltration of $CD8^+$ T cells, NK cells, monocytic macrophages, and MDCS, which confirmed that CD248 has a remarkable capacity to recruit immune cells. Since high stromal and immune cell infiltration is associated with a poor prognosis in RCC patients, CD248 may influence RCC progression by regulating the TME.

We next identified that the high infiltration of CAFs was inversely correlated with the clinical outcomes of RCC patients and positively associated with the complexity of the TME, suggesting that CAFs play a dominant role in the TME. Since CD248 expression in CAFs has previously been reported (18, 19), when coupled with CD248-related signatures significantly enriched in the stroma and ECM pathways, we suspected that the upregulation of CD248 might correlate with the CAF-mediated tumor-promoting effect. Indeed, a high correlation between CD248 expression and CAF infiltration was detected in the present study. Additionally, CD248 was significantly accumulated in the ECM enriched region, and was colocated with αSMA, which is a reliable biomarker for fibroblasts (33). CD248 overexpression indicated the activation of stromal-related signatures (e.g., EMT), cell–ECM interactions, TGFβ, and F-TBRS-related signals, which were highly involved in CAF functions. Furthermore, the knockdown of CD248 weakened the invasive ability of fibroblasts. Through the analysis of the differentiation between si-CD248 and si-Con-treated HFL1 cells, we found that fibroblasts could regulate cytokine release and related receptor expression through CD248, and participate in matrix adhesion, angiogenesis, and other functions.

To further investigate the function of CD248 in CAF-mediated tumor-promoting regulation, CAFs with upregulated CD248 were defined as $CD248^+$ CAFs. We initially determined that the high infiltration of $CD248^+$ CAFs in the TME decreased the OS rate of RCC patients and were indicative of RCC deterioration. Moreover, the increase of $CD248^+$ CAFs in the tumor reflected the complexity of TME components, in which there was an increase in the stromal and immune ingredients and was accompanied by the proliferation of epithelial cells. In addition, $CD248^+$ CAFs could recruit $CD8^+$ and cytotoxic T cells, as well as promote the infiltration of monocytic macrophages, NK cells, and MDCS. However, immunosuppression is one of the most important characteristics of TME in RCC (34), and increased $CD248^+$ CAF infiltration was associated with a suppressive immune microenvironment, in which exhausted T cells and M2-type TAMs were expansively infiltrated. Thus, participation in the suppressive immune microenvironment was one of the reasons that $CD248^+$ CAFs lead to a poor prognosis of RCC patients. Furthermore, to comprehensively explore the mechanisms of $CD248^+$ CAFs in RCC progression, we identified a total of 1,558 DEGs related to $CD248^+$ CAFs. Through the GO and KEGG enrichment analysis, we found that $CD248^+$ CAF-correlated DEGs were primarily enriched in the functions and pathways associated with cell–cell and cell–ECM interactions, immunoregulation, and metabolism. To accurately identify the hub gene clusters of immunoregulation and tumor promotion, we next categorized these related DEGs into eight functional modules based on the WGCNA analysis, and selected the most significant modules associated with tumor progression. As a result, $CD248^+$ CAFs might influence immunity, stromal-related signatures, cell adhesion, cell cycle, and metabolism to promote tumor deterioration. In particular, $CD248^+$ CAFs both contribute to the upregulation of exhausted immune biomarkers and also regulate cytokine and chemokine secretion and expression of related receptors, which resulted in an immunosuppressive TME. Additionally, forming and remodeling the ECM to block

normal immune cell infiltration and facilitating the invasion of epithelial cells might be another mechanism by which CD248$^+$ CAFs promote tumor progression (35). Nutrient limitation has been shown to be a critical feature of TME (36), and the depression of certain amino acids (e.g., arginine or accumulation of fatty acids) can lead to immunosuppressive effects (37). In the present study, we found that high CD248$^+$ CAF infiltration generally leads to metabolic inhibition. Finally, sustaining proliferative signatures and evading growth suppressors to facilitate tumor disordered amplification is another pathway that CD248$^+$ CAFs use to facilitate tumor progression.

In summary, CD248$^+$ CAFs participate in the regulation of RCC progression and an immunosuppressive TME, which may represent a novel prognostic and therapeutic target for RCC. The antibody (19), antibody–drug conjugates (ADCs) (38), vaccine (39), and even CAR-T cells targeting CD248$^+$ CAFs might become promising strategies for the destruction of the cancer nest and overcoming the immunosuppressive TME.

## DATA AVAILABILITY STATEMENT

The original contributions presented in the study are included in the article/**Supplementary Material**. Further inquiries can be directed to the corresponding authors.

## ETHICS STATEMENT

The studies involving human participants were reviewed and approved by the Ethics Committee of The First Affiliated Hospital of Air Force Military Medical University. The patients/participants provided their written informed consent to participate in this study.

## AUTHOR CONTRIBUTIONS

CX, KZ, and FY: data acquisition, data analysis, and writing original draft. CX, KZ, FY, XZ, SJL, XLZ, and HL: methodology, data interpretation, writing review, and editing. WQ, WW, and DH: conceptualization, design, and project administration. All authors contributed to the article and approved the submitted version.

## FUNDING

This work was partly supported by grants from the National Natural Science Foundation of China (No. 81772734) and the Innovation Capability Support Program of Shaanxi (Program No. 2020PT-021).

## ACKNOWLEDGMENTS

The authors would like to thank the TCGA databases that were analyzed in this study.

## SUPPLEMENTARY MATERIAL

The Supplementary Material for this article can be found online at: https://www.frontiersin.org/articles/10.3389/fonc.2021.773063/full#supplementary-material

## REFERENCES

1. Brugarolas J, Rajaram S, Christie A, Kapur P. The Evolution of Angiogenic and Inflamed Tumors: The Renal Cancer Paradigm. *Cancer Cell* (2020) 6:771–3. doi: 10.1016/j.ccell.2020.10.021
2. Zhang Y, Narayanan S, Mannan R, Raskind G, Wang X, Vats P, et al. Single-Cell Analyses of Renal Cell Cancers Reveal Insights Into Tumor Microenvironment, Cell of Origin, and Therapy Response. *Proc Natl Acad Sci USA* (2021) 118(24):e2103240118. doi: 10.1073/pnas.2103240118
3. Şenbabaoğlu Y, Gejman R, Winer A, Liu M, Van Allen E, de Velasco G, et al. Tumor Immune Microenvironment Characterization in Clear Cell Renal Cell Carcinoma Identifies Prognostic and Immunotherapeutically Relevant Messenger RNA Signatures. *Genome Biol* (2016) 1:231. doi: 10.1186/s13059-016-1092-z
4. Hanahan D, Coussens L. Accessories to the Crime: Functions of Cells Recruited to the Tumor Microenvironment. *Cancer Cell* (2012) 3:309–22. doi: 10.1016/j.ccr.2012.02.022
5. Braun D, Bakouny Z, Hirsch L, Flippot R, Van Allen E, Wu C, et al. Beyond Conventional Immune-Checkpoint Inhibition - Novel Immunotherapies for Renal Cell Carcinoma. *Nat Rev Clin Oncol* (2021) 4:199–214. doi: 10.1038/s41571-020-00455-z
6. Pitt J, Marabelle A, Eggermont A, Soria J, Kroemer G, Zitvogel L. Targeting the Tumor Microenvironment: Removing Obstruction to Anticancer Immune Responses and Immunotherapy. *Ann Oncol Off J Eur Soc Med Oncol* (2016) 8:1482–92. doi: 10.1093/annonc/mdw168
7. Rini B, Plimack E, Stus V, Gafanov R, Hawkins R, Nosov D, et al. Pembrolizumab Plus Axitinib Versus Sunitinib for Advanced Renal-Cell Carcinoma. *New Engl J Med* (2019) 12:1116–27. doi: 10.1056/NEJMoa1816714
8. Anderson N, Simon M. The Tumor Microenvironment. *Curr Biol CB* (2020) 16:R921–5. doi: 10.1016/j.cub.2020.06.081
9. Barrett R, Puré E. Cancer-Associated Fibroblasts and Their Influence on Tumor Immunity and Immunotherapy. *eLife* (2020) 9:e57243. doi: 10.7554/eLife.57243
10. Kobayashi H, Enomoto A, Woods S, Burt A, Takahashi M, Worthley D. Cancer-Associated Fibroblasts in Gastrointestinal Cancer. *Nat Rev Gastroenterol Hepatol* (2019) 5:282–95. doi: 10.1038/s41575-019-0115-0
11. Calon A, Lonardo E, Berenguer-Llergo A, Espinet E, Hernando-Momblona X, Iglesias M, et al. Stromal Gene Expression Defines Poor-Prognosis Subtypes in Colorectal Cancer. *Nat Genet* (2015) 4:320–9. doi: 10.1038/ng.3225
12. Ji J, Eggert T, Budhu A, Forgues M, Takai A, Dang H, et al. Hepatic Stellate Cell and Monocyte Interaction Contributes to Poor Prognosis in Hepatocellular Carcinoma. *Hepatol (Baltimore Md)* (2015) 2:481–95. doi: 10.1002/hep.27822
13. Öhlund D, Handly-Santana A, Biffi G, Elyada E, Almeida A, Ponz-Sarvise M, et al. Distinct Populations of Inflammatory Fibroblasts and Myofibroblasts in Pancreatic Cancer. *J Exp Med* (2017) 3:579–96. doi: 10.1084/jem.20162024
14. Valdez Y, Maia M, Conway E. CD248: Reviewing its Role in Health and Disease. *Curr Drug Targets* (2012) 3:432–9. doi: 10.2174/138945012799424615
15. Matsushima S, Aoshima Y, Akamatsu T, Enomoto Y, Meguro S, Kosugi I, et al. CD248 and Integrin Alpha-8 Are Candidate Markers for Differentiating Lung Fibroblast Subtypes. *BMC Pulmonary Med* (2020) 1:21. doi: 10.1186/s12890-020-1054-9
16. Smith S, Eardley K, Croft A, Nwosu J, Howie A, Cockwell P, et al. CD248+ Stromal Cells Are Associated With Progressive Chronic Kidney Disease. *Kidney Int* (2011) 2:199–207. doi: 10.1038/ki.2011.103
17. Wilhelm A, Aldridge V, Haldar D, Naylor A, Weston C, Hedegaard D, et al. CD248/endosialin Critically Regulates Hepatic Stellate Cell Proliferation

During Chronic Liver Injury *via* a PDGF-Regulated Mechanism. *Gut* (2016) 7:1175–85. doi: 10.1136/gutjnl-2014-308325
18. Fujii S, Fujihara A, Natori K, Abe A, Kuboki Y, Higuchi Y, et al. TEM1 Expression in Cancer-Associated Fibroblasts Is Correlated With a Poor Prognosis in Patients With Gastric Cancer. *Cancer Med* (2015) 11:1667–78. doi: 10.1002/cam4.515
19. Yang F, Wei Y, Han D, Li Y, Shi S, Jiao D, et al. Interaction With CD68 and Regulation of GAS6 Expression by Endosialin in Fibroblasts Drives Recruitment and Polarization of Macrophages in Hepatocellular Carcinoma. *Cancer Res* (2020) 18:3892–905. doi: 10.1158/0008-5472.Can-19-2691
20. Nanda A, Karim B, Peng Z, Liu G, Qiu W, Gan C, et al. Tumor Endothelial Marker 1 (Tem1) Functions in the Growth and Progression of Abdominal Tumors. *Proc Natl Acad Sci United States America* (2006) 9:3351–6. doi: 10.1073/pnas.0511306103
21. Becht E, Giraldo N, Lacroix L, Buttard B, Elarouci N, Petitprez F, et al. Estimating the Population Abundance of Tissue-Infiltrating Immune and Stromal Cell Populations Using Gene Expression. *Genome Biol* (2016) 1:218. doi: 10.1186/s13059-016-1070-5
22. Yoshihara K, Shahmoradgoli M, Martínez E, Vegesna R, Kim H, Torres-Garcia W, et al. Inferring Tumour Purity and Stromal and Immune Cell Admixture From Expression Data. *Nat Commun* (2013) 4:2612. doi: 10.1038/ncomms3612
23. Koul H, Huh J, Rove K, Crompton L, Koul S, Meacham R, et al. Molecular Aspects of Renal Cell Carcinoma: A Review. *Am J Cancer Res* (2011) 2:240–54.
24. Qin S, Shi X, Wang C, Jin P, Ma F. Transcription Factor and miRNA Interplays Can Manifest the Survival of ccRCC Patients. *Cancers* (2019) 11 (11):1668. doi: 10.3390/cancers11111668
25. Sánchez-Gastaldo A, Kempf E, González Del Alba A, Duran I. Systemic Treatment of Renal Cell Cancer: A Comprehensive Review. *Cancer Treat Rev* (2017) 60:77–89. doi: 10.1016/j.ctrv.2017.08.010
26. Díaz-Montero C, Rini B, Finke J. The Immunology of Renal Cell Carcinoma. *Nat Rev Nephrol* (2020) 12:721–35. doi: 10.1038/s41581-020-0316-3
27. Yarchoan M, Hopkins A, Jaffee E. Tumor Mutational Burden and Response Rate to PD-1 Inhibition. *New Engl J Med* (2017) 25:2500–1. doi: 10.1056/NEJMc1713444
28. Fridman W, Zitvogel L, Sautès-Fridman C, Kroemer G. The Immune Contexture in Cancer Prognosis and Treatment. *Nat Rev Clin Oncol* (2017) 12:717–34. doi: 10.1038/nrclinonc.2017.101
29. Zhou L, Liu X, Sun M, Zhang X, German P, Bai S, et al. Targeting MET and AXL Overcomes Resistance to Sunitinib Therapy in Renal Cell Carcinoma. *Oncogene* (2016) 21:2687–97. doi: 10.1038/onc.2015.343
30. Chen X, Song E. Turning Foes to Friends: Targeting Cancer-Associated Fibroblasts. *Nat Rev Drug Discovery* (2019) 2:99–115. doi: 10.1038/s41573-018-0004-1
31. Kalluri R. The Biology and Function of Fibroblasts in Cancer. *Nat Rev Cancer* (2016) 9:582–98. doi: 10.1038/nrc.2016.73
32. Di Benedetto P, Ruscitti P, Liakouli V, Del Galdo F, Giacomelli R, Cipriani P. Linking Myofibroblast Generation and Microvascular Alteration: The Role of CD248 From Pathogenesis to Therapeutic Target (Review). *Mol Med Rep* (2019) 2:1488–98. doi: 10.3892/mmr.2019.10429
33. Chen Y, Kim J, Yang S, Wang H, Wu C, Sugimoto H, et al. Type I Collagen Deletion in αsma Myofibroblasts Augments Immune Suppression and Accelerates Progression of Pancreatic Cancer. *Cancer Cell* (2021) 4:548–65.e546. doi: 10.1016/j.ccell.2021.02.007
34. Drake C, Stein M. The Immunobiology of Kidney Cancer. *J Clin Oncol Off J Am Soc Clin Oncol* (2018) 36(36):JCO2018792648. doi: 10.1200/jco.2018.79.2648
35. Yoshida G. Regulation of Heterogeneous Cancer-Associated Fibroblasts: The Molecular Pathology of Activated Signaling Pathways. *J Exp Clin Cancer Res CR* (2020) 1:112. doi: 10.1186/s13046-020-01611-0
36. Martínez-Reyes I, Chandel N. Cancer Metabolism: Looking Forward. *Nat Rev Cancer* (2021) 21(10):669–80. doi: 10.1038/s41568-021-00378-6
37. Bader J, Voss K, Rathmell J. Targeting Metabolism to Improve the Tumor Microenvironment for Cancer Immunotherapy. *Mol Cell* (2020) 6:1019–33. doi: 10.1016/j.molcel.2020.05.034
38. Rouleau C, Gianolio D, Smale R, Roth S, Krumbholz R, Harper J, et al. Anti-Endosialin Antibody-Drug Conjugate: Potential in Sarcoma and Other Malignancies. *Mol Cancer Ther* (2015) 9:2081–9. doi: 10.1158/1535-7163.Mct-15-0312
39. Ugel S, Facciponte J, De Sanctis F, Facciabene A. Targeting Tumor Vasculature: Expanding the Potential of DNA Cancer Vaccines. *Cancer Immunol Immunother CII* (2015) 10:1339–48. doi: 10.1007/s00262-015-1747-8

**Conflict of Interest:** The authors declare that the research was conducted in the absence of any commercial or financial relationships that could be construed as a potential conflict of interest.

**Publisher's Note:** All claims expressed in this article are solely those of the authors and do not necessarily represent those of their affiliated organizations, or those of the publisher, the editors and the reviewers. Any product that may be evaluated in this article, or claim that may be made by its manufacturer, is not guaranteed or endorsed by the publisher.

*Copyright © 2021 Xu, Zhang, Yang, Zhou, Liu, Li, Ma, Zhao, Lu, Lu, Zhang, Li, Han, Wen and Qin. This is an open-access article distributed under the terms of the Creative Commons Attribution License (CC BY). The use, distribution or reproduction in other forums is permitted, provided the original author(s) and the copyright owner(s) are credited and that the original publication in this journal is cited, in accordance with accepted academic practice. No use, distribution or reproduction is permitted which does not comply with these terms.*

frontiers in Oncology

ORIGINAL RESEARCH
published: 16 December 2021
doi: 10.3389/fonc.2021.776824

# Differentially Expressed Genes in Clear Cell Renal Cell Carcinoma as a Potential Marker for Prognostic and Immune Signatures

*Ying Tong[1†], Yiwen Yu[1†], Hui Zheng[1], Yanchun Wang[1], Suhong Xie[1], Cuncun Chen[1], Renquan Lu[1,2*] and Lin Guo[1,2*]*

[1] Department of Clinical Laboratory, Fudan University Shanghai Cancer Center, Shanghai, China, [2] Department of Oncology, Shanghai Medical College, Fudan University, Shanghai, China

OPEN ACCESS

**Edited by:**
Andrea Mari,
Careggi University Hospital, Italy

**Reviewed by:**
Antonio Andrea Grosso,
Careggi University Hospital, Italy
Riccardo Tellini,
Careggi University Hospital, Italy

***Correspondence:**
Renquan Lu
renquanlu@fudan.edu.cn
Lin Guo
guolin500@hotamil.com

[†]These authors have contributed equally to this work and share first authorship

**Specialty section:**
This article was submitted to Genitourinary Oncology, a section of the journal Frontiers in Oncology

**Received:** 14 September 2021
**Accepted:** 24 November 2021
**Published:** 16 December 2021

**Citation:**
Tong Y, Yu Y, Zheng H, Wang Y, Xie S, Chen C, Lu R and Guo L (2021) Differentially Expressed Genes in Clear Cell Renal Cell Carcinoma as a Potential Marker for Prognostic and Immune Signatures. Front. Oncol. 11:776824. doi: 10.3389/fonc.2021.776824

Clear cell renal cell carcinoma (ccRCC) is characterized by the inactivation of the von Hippel–Lindau (*VHL*) gene. Of note, no other gene is mutated as frequently as *VHL* in ccRCC, turning out that patients with inactivated *VHL* constitute the majority of ccRCC-related character. Thus, differentially expressed genes (DEGs) and their molecular networks caused by *VHL* mutation were considered as important factors for influencing the prognosis of ccRCC. Here, we first screened out six DEGs (*GSTA1*, *GSTA2*, *NAT8*, *FABP7*, *SLC17A3*, and *SLC17A4*) which downregulated in ccRCC patients with *VHL* non-mutation than with the mutation. Generally, most DEGs with high expression were associated with a favorable prognosis and low-risk score. Meanwhile, we spotted transcription factors and their kinases as hubs of DEGs. Finally, we clustered ccRCC patients into three subgroups according to the expression of hub proteins, and analyzed these subgroups with clinical profile, outcome, immune infiltration, and potential Immune checkpoint blockade (ICB) response. Herein, DEGs might be a promising biomarker panel for immunotherapy and prognosis in ccRCC. Moreover, the ccRCC subtype associated with high expression of hubs fit better for ICB therapy.

**Keywords: differentially expressed genes, hubs, immune infiltration, subgroups, immune checkpoint blockade, clear cell renal clear cell carcinoma**

## INTRODUCTION

Renal cell carcinoma (RCC) has become a common but deadly genitourinary malignancy with an increasing incidence, with an estimate of 73,750 new cases and 14,830 death cases in the US alone (1). Of note, due to its being symptomless in the early stage and poorer prognosis, the clear cell type has already taken up to approximately 80% of all RCC subtypes, constituting the majority of cancer-related deaths (2). In the early stage, clear cell renal cell carcinoma (ccRCC) patients can be treated with surgical or ablative strategies with a great outcome, whereas, metastases will still happen in approximately 30% of ccRCC patients (3) with a high mortality rate in advanced phases due to poor responses to radiotherapy and chemotherapy (4). It is reported that the incidence of somatic von Hippel–Lindau (*VHL*) mutations in sporadic ccRCC occupies up to 91% (5). Understanding

differentially expressed genes (DEGs) and their molecular networks caused by *VHL* mutation has been and will continue to be critical to the development to improve both treatment and management of ccRCC patients.

It is known to all that a part of patients has pronounced clinical response with therapeutic intervention; however, other patients still gained minimal or no clinical benefit when provided the same treatment in the same tumor type. More literature uncovered the complexity and diversity of the immune context of the tumor microenvironment (TME) and its influence on response to therapy (6, 7). TME formed by many distinct and interacting cell populations, response, and survival benefit is typically limited to a subset of patients. Thus, patients should be divided into subgroups to investigate separately in clinical research studies. Based on the putative role of TME in influencing the prognosis, immune infiltration analysis has attracted increasing attention in recent years. Identification and comprehensive characterization subtypes are needed for designing novel immunotherapies so as to better improve the response and outcomes of ccRCC patients. Immune checkpoint blockade (ICB) can elicit durable clinical responses by reactivating an exhausted immune response and unprecedented clinical benefit in a subset of patients across multiple types of solid tumors (8–10). For patients with a favorable immune microenvironment, ICB can be used to enhance the preexisting antitumor immunity of these patients and further improve their survival (11).

Seeking factors that specifically influence the prognosis in ccRCC is critical to improving the treatment and management of ccRCC patients. Investigation and characterization of DEGs are vital for seeking prognosis influencing factors. Thus, we first screened out six DEGs between ccRCC patients with *VHL* mutation and non-mutation. Proverbially, a broad network of molecular changes is involved in influencing and modulating DEGs. Thereupon, we analyzed the upstream regulating kinases and transcription factors (TFs) of DEGs by a systems biology approach and defined them as hub proteins. Moreover, the complexity and diversity of TME signify that only a part of patients benefits from therapeutic intervention. So, we clustered ccRCC patients into three subgroups according to their expression of hub proteins, and whereafter analyzed with clinical profile, outcomes and immune infiltration. In general, our results demonstrated that DEGs might be supposed as promising prognostic biomarkers in ccRCC and might have clinical implications for personalized immunotherapy.

# MATERIALS AND METHODS

## ccRCC Datasets

Protein expression of 84 adjacent normal tissues and 110 ccRCC samples were derived from the Clinical Proteomic Tumor Analysis Consortium (CPTAC). Raw counts of RNA-sequencing data (level 3) of patients with ccRCC (n = 530) and the corresponding clinical data were downloaded from TCGA data portal, in which the method of acquisition and application complied with the guidelines and policies. Data on overall survival (OS) were extracted from TCGA cohort.

## Differential Genes Expression Analysis of ccRCC

The raw count data of mRNA profile in ccRCC from TCGA dataset include both *VHL* wild-type and mutation groups. Volcano plots were used to filtrate the DEGs *via* Limma package (version: 3.40.2) of R software. DEGs was constructed using fold-change values and adjusted P. The adjusted P-value was analyzed to correct for false positive results in TCGA or GTEx. Adjusted P <0.05 and Log (Fold Change) >1 or Log (Fold Change) <−1 were charactered as the thresholds for the screening of DEGs.

## Protein Expression Analysis

We explored the total protein expression level of DEGs between primary tumor and normal tissues through the *CPTAC* (Clinical proteomic tumor analysis consortium) dataset in the *UALCAN* portal (http://ualcan.path.uab.edu/analysis-prot.html), an interactive web resource for analyzing cancer Omics data. The available dataset of clear cell RCC was selected.

## Functional Enrichment Analysis of DEGs

With the screened DEGs, Kyoto Encyclopedia of Genes and Genomes (KEGG) pathways analysis and gene ontology (GO) enrichment analysis were performed on the online tool *Metascape* (http://metascape.org/gp/index.html#/main/step1).

## Spearman Correlation Analysis

The dataset was comprised of mRNA-seq data of ccRCC cohort from TCGA. Spearman's correlation analysis was used to describe the correlation among DEGs without a normal distribution. The multi-gene correlation map was realized by the R software package pheatmap. The value in the sphere represented the correlation p-value and the bigger sphere represents the stronger correlation.

## Infer Upstream Regulatory Networks

Upstream regulatory networks from signatures of DEGs were inferred by X2K Web. Transcription Factor Enrichment Analysis (TFEA) is the first step of the X2K pipeline, which was predicted to regulate DEGs by performing gene set enrichment analysis using ChIP-seq experiments (ChEA). Secondly, Protein–Protein Interaction (PPI) Expansion was the expansion of enriched TFs, achieved by identifying proteins which physically interact with these TFs through the Genes2Networks (G2N) algorithm. Finally, Kinase Enrichment Analysis (KEA) was the third step of the X2K pipeline, which performed enrichment analysis based on the list of proteins from the PPI network using kinase–substrate interaction databases.

## Prognostic Risk Signatures

The prognostic risk signatures of DEGs were established by the least absolute shrinkage and selection operator (LASSO) regression analysis in the TCGA set. Coefficients of selected features were shown by λ parameter. Signatures were screened

out by selecting the optimal penalty parameter λ correlated with 10-fold cross-validation using the R software package glmnet. Partial likelihood deviance versus log (λ) was drawn using LASSO Cox regression model. Kaplan–Meier survival analysis with log-rank test was also used to compare the survival difference between low-risk and high-risk group. The analytical methods were performed by R software. The hazards ratio was calculated based on Cox PH Model.

## Immune Score and Immune Infiltration Analysis

In the "Immune-Gene" module of the TIMER2 web, we explored the association between the expressions of hub genes and immune infiltrates across in the ccRCC. To make reliable immune infiltration estimations and immune cell distribution score, we took advantage of the immunedeconv, an R package which integrates some state-of-the-art algorithms, namely, MCPCOUNTER and EPIC. The p-values and the correlation (cor) values in ccRCC were achieved *via* the purity-adjusted Spearman's rank correlation test. The data were visualized as a heatmap and a scatter plot.

## Characterization of ccRCC Subgroups and Immune Signature Analysis in Subgroups

Raw counts of RNA-sequencing data and corresponding clinical information of ccRCC were obtained from TCGA dataset. ConsensusClusterPlus (v1.54.0) for consistency analysis was implemented by R software package. Clustering heatmaps were conducted *via* R software package pheatmap. The gene expression heatmap retains genes with SD >0.1.

## Immune Checkpoint Analysis

CD274, CTLA4, HAVCR2, LAG3, PDCD1, PDCDILG2, TIGIT, and SIGLEC15 were genes relevant to immune-checkpoint, and expression values of these eight genes were extracted. Immune checkpoints related gene expression were implemented by packages ggplot2 of R foundation for statistical computing (version 4.0.3). The significance of the three groups has passed the Kruskal–Wallis test.

## Predict Potential ICB Response

We collected the RNA-sequencing data and corresponding clinical information of ccRCC from TCGA dataset. Potential ICB response was predicted with TIDE algorithm (12).

# RESULTS

## Analysis of Differentially Expressed Genes in ccRCC

Since the inactivation of the *VHL* is the signature initiating event in ccRCC, we examined the DEGs between ccRCC patients with *VHL* mutation and non-mutation using Volcano plots. Six genes (*GSTA1*, *GSTA2*, *NAT8*, *SLC17A3*, *SLC17A4*, and *FABP7*) were screened out, downregulating in ccRCC patients with wild-type *VHL* compared to patients with the mutation (**Figure 1A**). Enrichment analyses using GO were performed to investigate the potential roles of DEGs, indicating that DEGs were involved in both the processes of glutathione metabolic and the pathways in cancer (**Figure 1B**). To better explore the roles of DEGs in ccRCC, we evaluated the protein expressions of DEGs in cancerous and normal tissues. As the *CPTAC* dataset exhibited, the total protein expression levels of GSTA1, GSTA2, NAT8, SLC17A3, and SLC17A4 were much lower in cancerous than those in normal tissues (**Figure 1C**). Meanwhile, to probe the consistency of DEGs in ccRCC, we performed Spearman correlation analysis in TCGA database. As the average Pearson correlation emerged above, DEGs tended to be positively correlated with each other (**Figure 1D**). Above all, DEGs were involved in the pathway of carcinogenesis with a low expression in ccRCC on the whole.

## Prognostic Analysis of DEGs Signature in ccRCC

Although enrichment analyses have provided a potential forecast that DEGs may participate in the cancer pathway, our knowledge of DEGs was still limited to its expression difference. On this basis, we envisaged to analyze the prognostic signature of DEGs in the TCGA set. Firstly, we divided the ccRCC patients into high-expression and low-expression groups according to the expression levels of DEGs and further investigated the correlation between DEGs expression and the prognosis of patients, mainly using the datasets of TCGA. Analysis from *GEPIA2* indicated that the high expressions of *GSTA2*, *NAT8*, *SLC17A3*, and *SLC17A4* were linked to favorable prognosis of OS (**Figure 2A**). LASSO coefficients of DEGs were shown by lambda parameter (λ) (**Figure 2B**). LASSO Cox regression model was performed to get the optimal lambda value that came from the minimum partial likelihood deviance (λmin = 0.0015), which was related with DEGs that significantly associated with OS (**Figure 2C**). Furthermore, DEGs-based risk score was constructed based on their Cox coefficients: Riskscore = (−0.0636) ∗ GSTA1+ (−0.0558) ∗ GSTA2+ (−0.0968) ∗ NAT8 + (−0.0223) ∗ SLC17A3 + (−0.054) ∗ SLC17A4 + (0.0447) ∗ FABP7. The dotted line represented the median risk score and divided the patients into low-risk and high-risk group. The survival status of all patients was shown in the training group, while a heatmap presented the expression profiles of DEGs in both low-risk and high-risk group (**Figure 2D**). Finally, the prognostic signature of DEGs showed that larger AUC values in a time-dependent ROC analysis was positively related to a better predictive ability of multi-gene model for 1-, 3-, and 5-year OS (**Figure 2E**). To sum up, high expressions of *GSTA2*, *NAT8*, *SLC17A3*, and *SLC17A4* forebode a favorable prognosis, while the lower expression of all DEGs except *FABP7* might predict a higher risk of ccRCC.

## Spot the Major Hub Proteins of the DEGs

Many human cancers are dependent on the inappropriate activity of oncogenic TFs (13), turning out that TFs were well-connected nodes which had a strong capacity of modulating adjacent genes. In order to extensively investigate DEGs mentioned above, and also their role within signaling networks

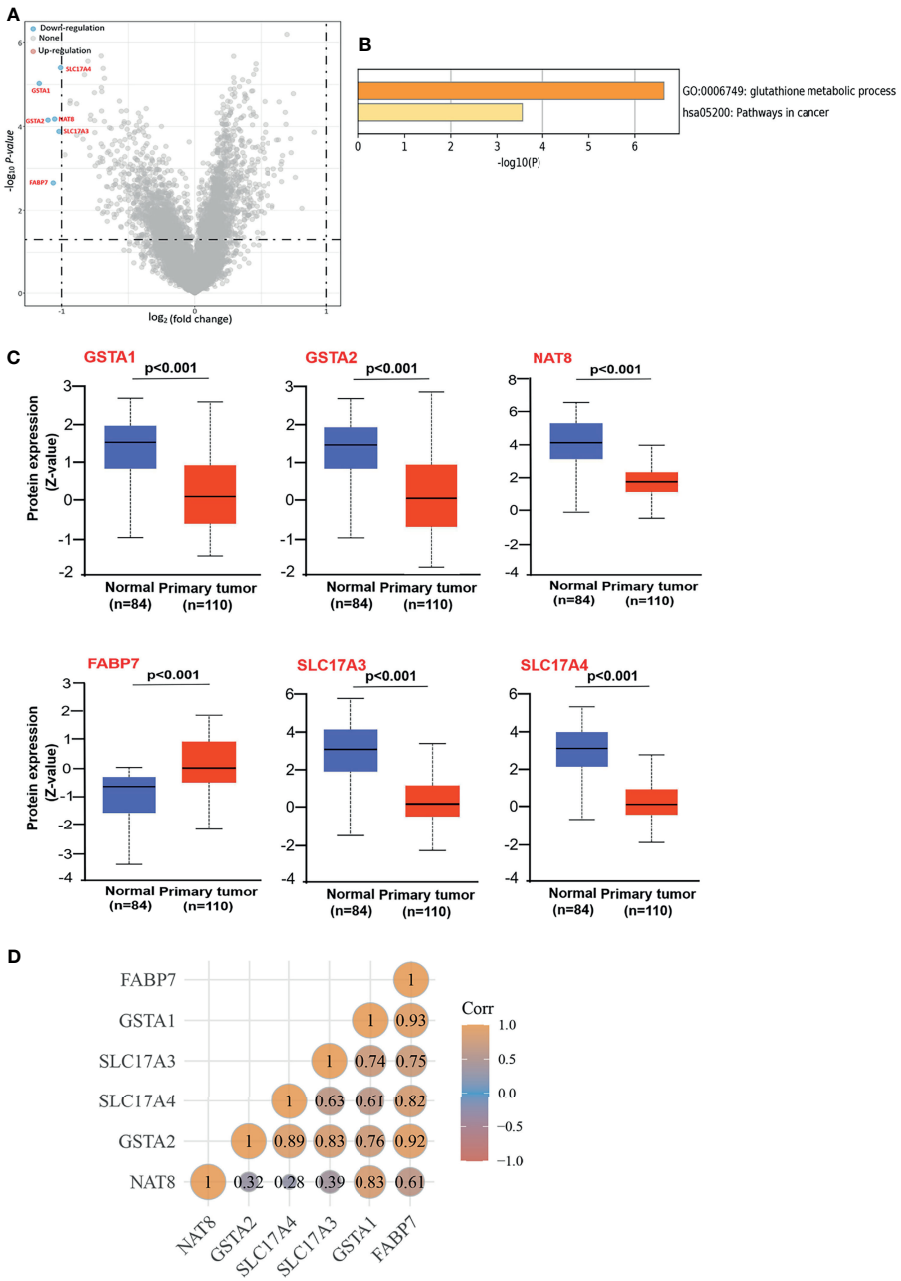



**FIGURE 1** | Screening out the DEGs and identifying their characteristics, **(A)** Volcano plots to screen out the DEGs between patients with wild-type and mutation VHL. The blue point indicates the down-expressed mRNAs with statistical significance. The default set of the threshold was fold change ≥2, P ≤0.05. **(B)** GO Enrichment analyses of DEGs. GO, gene ontology. **(C)** Based on the CPTAC dataset, we analyzed the total protein expression level of GSTA1, GSTA2, NAT8, FABP7, SLC17A4, and SLC17A4 in normal tissue and primary tissue of ccRCC. **(D)** Spearman correlation analysis between DEGs. The value represents the correlation p-value, and the darker the color represents a stronger correlation.

or their transcriptional regulatory mechanisms, we conducted TFEA, screening out three TFs of DEGs with high predictive value, which were MYOD1, NANOG and TP63 as **Figure 3A** manifested. Moreover, results of Protein–Protein Interaction (PPI) networks established a basic abstraction of multiple complex pathways, controlling the major cellular and molecular machinery which could determine the disease. By identifying proteins that physically interact with MYOD1, NANOG, and TP63, a subnetwork of connected TFs and their interacting proteins was visualized as a ball-and-stick diagram (**Figure 3B**). Since protein kinases are responsible for cellular transduction signaling and their hyperactivity, we conducted a Kinase Enrichment Analysis (KEA), and filtered the top predicted kinases that probably regulated the expanded PPI

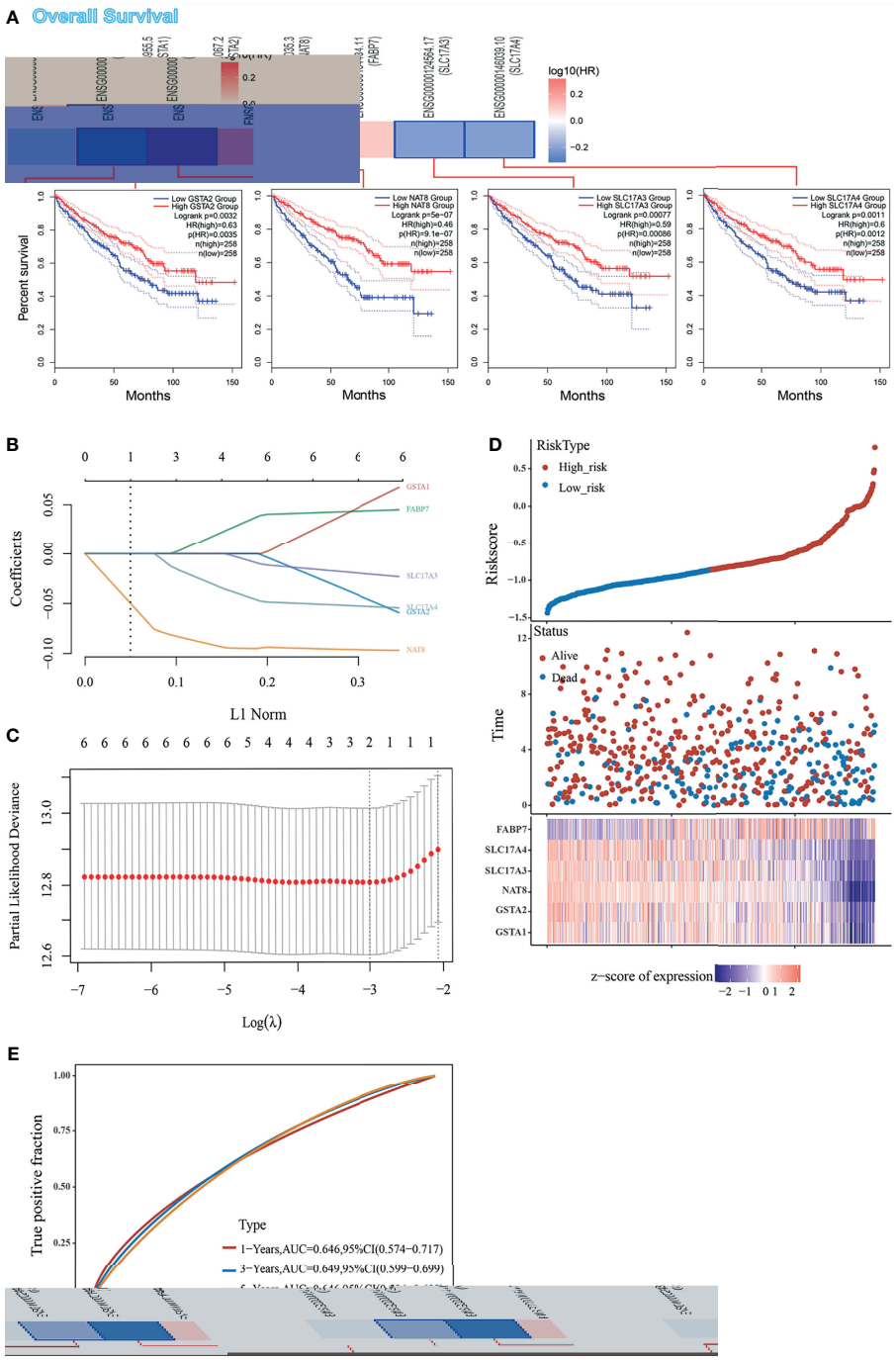



**FIGURE 2** | Prognostic value of DEGs in ccRCC cohort form TCGA set, **(A)** The correlation between OS and DEGs expression, and Kaplan–Meier curves performed by GEPIA2 tool describes the OS. **(B)** Coefficients of DEGs are shown by lambda parameter. **(C)** Partial likelihood deviance versus log (λ) was drawn using LASSO Cox regression model. **(D)** Patients were divided into low- and high-risk groups according to risk score (upper). Survival status of the patients (middle) and expression profiles of the DEGs (below) are shown corresponding to the risk score. **(E)** Time-dependent ROC analysis of the DEGs. The AUC value predicts the prediction ability of the model.

network (**Figure 3C**). Furthermore, the eXpression2Kinases (X2K) network was performed to infer upstream regulatory network (**Figure 3D**). Generally, MYOD1, NANOG, and TP63, along with 20 kinases mentioned in **Figure 3C**, were all supposed to be hub proteins of the DEGs. Phosphorylation orchestrates the activity and stability of hub genes, where alterations in phosphorylation pathways were of great importance to the networks mentioned above.

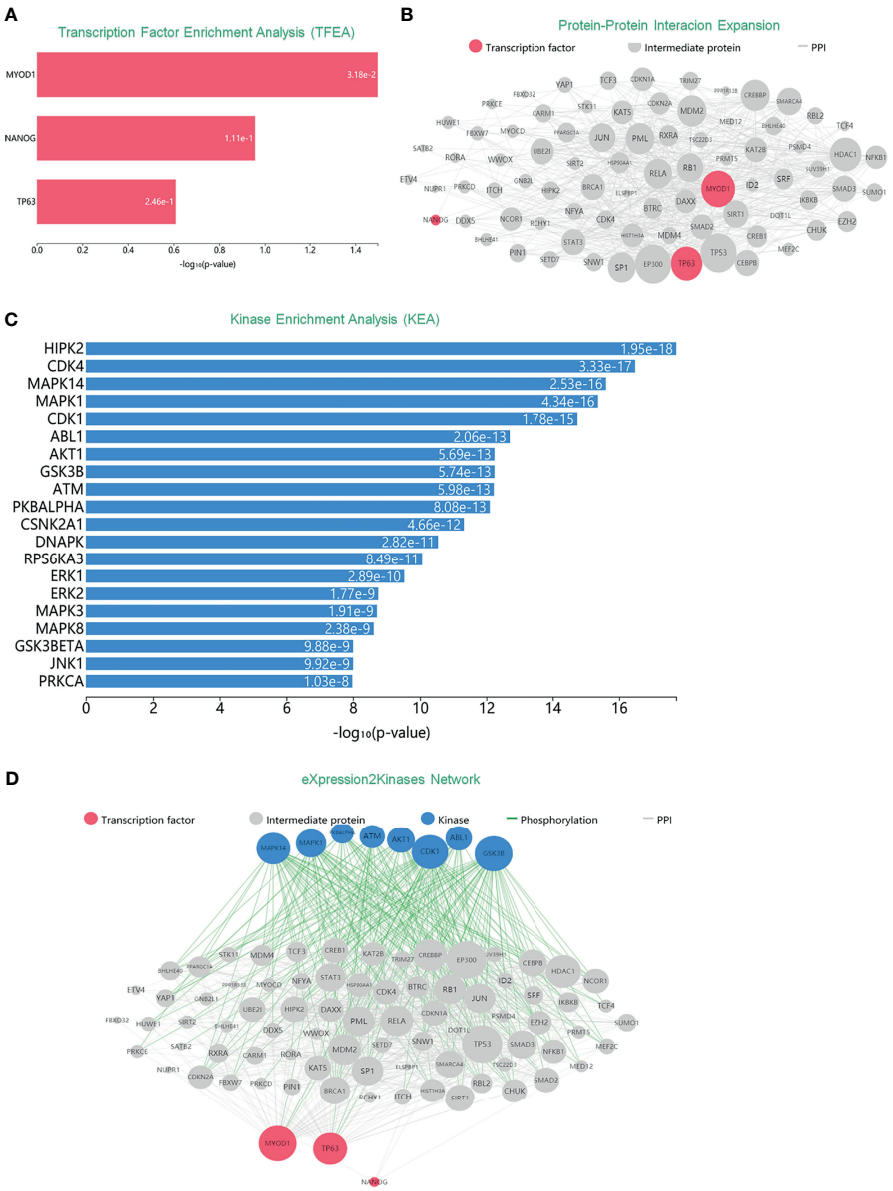



**FIGURE 3** | Inferred upstream regulatory networks of DEGs. **(A)** TFEA was used to predict TFs. Top predicted TFs (MYOD1, NANOG, and TP63) are displayed as a bar graph. **(B)** PPI expands the list of enriched TFs. Gray edges indicate the interaction between two proteins. The size of nodes is relative to the level of expression degree. **(C)** KEA predicts the protein kinases that are likely the regulators of the expanded PPI network. **(D)** The eXpression2Kinases network displays the inferred upstream regulatory network of the DEGs.

## Analysis of Hub Proteins Identifies Distinct Subgroups of ccRCC

PTMs are involved in varieties of cellular activities, and phosphorylation is one of the most extensively studied PTM (14). To further investigate the molecular mechanism of hub genes, we performed KEGG and GO enrichment analyses. Results indicated that most of these genes were linked to orchestrating a range of intracellular processes including cell growth, proliferation, division and so on (**Figure 4A**). In recent years, the concept of precision medicine has promoted the subgroups of individual research objects, and different subgroups have different pathogenic mechanisms and clinical prognostic characteristics. To achieve a general and overall evaluation of hub genes among ccRCC patients, we classified the cohort (n = 530) into three different subtypes *via* consistency analysis according to the expression level of hub genes (**Figure 4B**). Remarkably, all hub genes were considerably high expressed in C1 subgroup while low expressed in C3 (**Figure 4C**). To investigate the clinical profile of three subtypes, tumor stage and the degree of progression of the

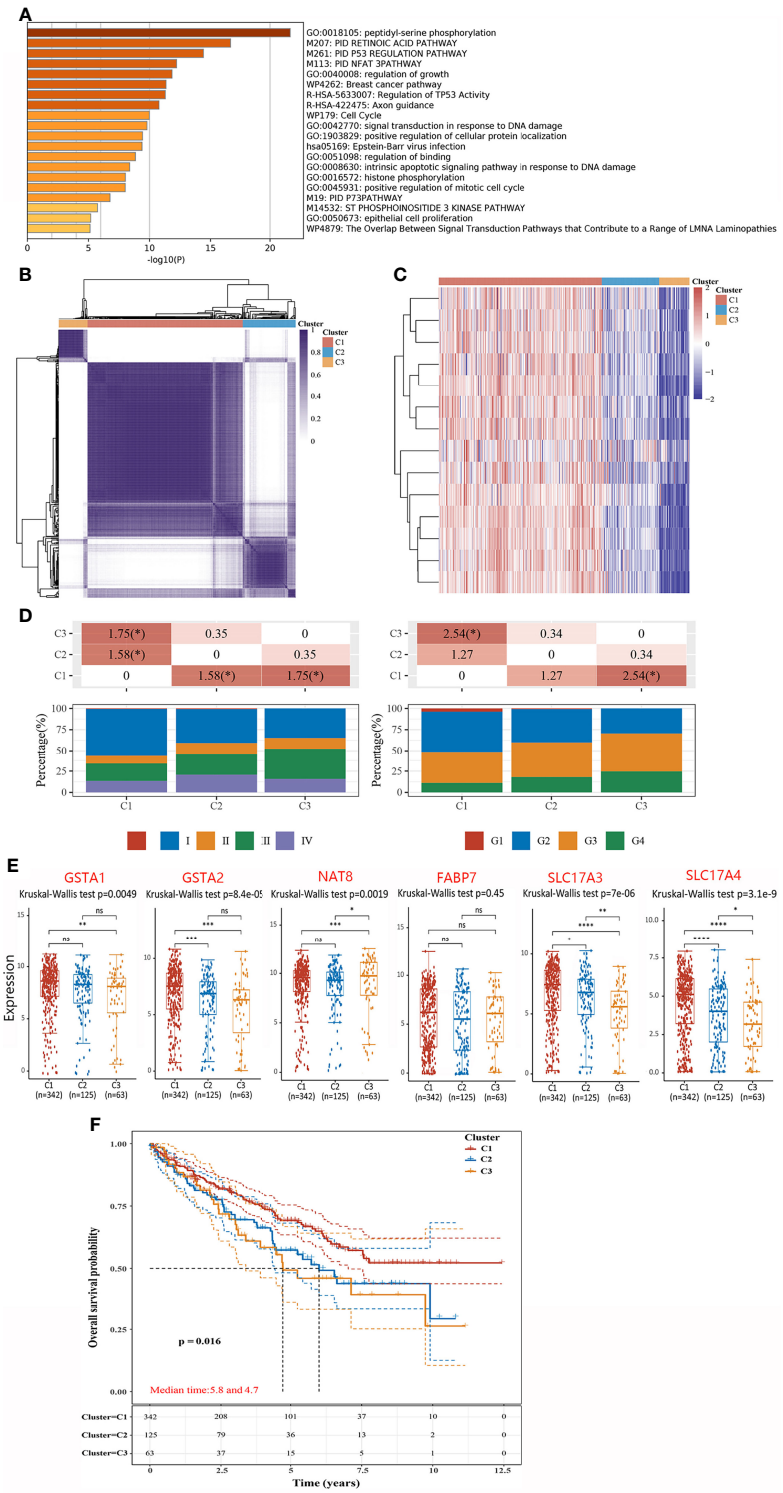



**FIGURE 4** | Integrated cluster assignments analysis of ccRCC patients and characteristics described of them. **(A)** GO Enrichment analyses based on hub genes. **(B)** Heatmap depicting consensus clustering solution (clusters = 3). **(C)** Heatmaps showing the expression of hubs in three subgroups. Red represents high expression and blue represents low expression. **(D)** Distributions of tumor stage (left) and the degree of progression of the primary tumor (right) in three subgroups. The table above represents the distribution of a certain clinical feature in any two subgroups. The significance p-value was analyzed by chi-square test, where the value is –log10 (p value), if marked with *, it means that there is a significant difference in the distribution of the clinical feature in the corresponding two groups ($p < 0.05$). **(E)** The expressions of DEGs in three subgroups. **(F)** Kaplan–Meier curves describe the OS for three subgroups. *P < 0.05, **P < 0.01,***P < 0.001, ns, no significance.

primary tumor were compared among patients in three subtypes. Clinically, cluster C1 presented a strikingly higher frequency of Stage I and early grade (G1 + G2), and a lower frequency of advanced grade (G3 + G4) than the other two subtypes did (**Figure 4D**). Likewise, expression levels of DEGs except *FABP7* were higher in C1 than those in C3 (**Figure 4E**). Upon stratification of the three clusters according to specific data sets, significant differences in OS were observed between the three subtypes. Notably, subtype C1 had the highest OS rate among the three clusters. In comparison, patients with subtype C3 had a worse OS than the other two ($p = 0.016$) (**Figure 4F**). In general, hub genes were serviceable for delineating ccRCC clusters, and the DEGs have the prognostic values in clustered ccRCC subtypes. Namely, the subtype with higher expressions of DEGs might be associated with better OS.

## Immune Infiltration Analysis of ccRCC Subtypes

Inflammation and immune evasion are considered as hallmarks of cancer progression, highlighting the direct involvement of immune cells (15). As the prognostic value of DEGS for ccRCC patients subjected to OS has already been estimated, we explored whether the DEGs could influence the immune infiltration in ccRCC patients. The relationship between the expression distribution of DEGs and infiltration levels of immune cell types was analyzed to estimate the effect of DEGs on the immune microenvironment. In terms of EPIC algorithms, a significantly positive correlation was observed between most of the DEGs and infiltration levels of T cell CD8+ and endothelial cell. While analyzed by MCPCOUNTER algorithms, most of the DEGs positively correlated to T cell CD8+, NK cell, Macrophage, Neutrophil, and endothelial cell (**Figure 5A**). Given the heterogeneity of TME across ccRCC patients (16), it is quite likely that the immune cells might also vary across these subgroups. Thus, we calculated several types of immune cells between three subgroups by EPIC and MCPCOUNTER algorithms. According to EPIC algorithms, a higher number of immune-associated cells such as, CD4+, CD8 T cells, and endothelial cell were produced in subtype C1 than in other subtypes. Additionally, assessed with MCPCOUNTER algorithms, B cell, monocyte, macrophage, myeloid dendritic cell, neutrophil, and endothelial cell were more aggressively to subtype C1 (**Figure 5B**). It was noted that DEGs were positively related to immune cell score and a higher number of immune-associated cells distributed in subtype C1, showing higher expression of DEGs contribute an enhanced immune microenvironment in C1.

## Immune Checkpoint and Predicts ICB Response

Immune checkpoint molecules are ligand–receptor pairs that exert inhibitory or stimulatory effects on immune responses (17). Most of them have been deemed to express on cells of the adaptive immune system, particularly on T cells, and also innate immune system (18). We explored the expression values of immune checkpoint molecules (SIGLEC15, TIGIT, CD274, HAVCR2, PDCD1, CTLA4, LAG3, and PDCD1LG2). Indeed, the expressions of CD274, HAVCR2, and PDCD1LG2 were unanimously higher in C1 than the other two subtypes (**Figure 6A**) and were in accordance with the infiltration levels of principally immune cells assessed in previous sections. Moreover, cancer immunotherapies by ICB aimed to assist the immune system to recognize and attack cancer cells (19). We next evaluated ICB clinical response by Tumor Immune Dysfunction and Exclusion (TIDE), a computational method to model two primary mechanisms of tumor immune evasion (12). As reported, a higher TIDE score forebodes a poorer efficacy of ICB therapy and less favorable survival after ICB treatment. Excitingly, the immune response samples were higher in C1 than in C3. On the contrary, the TIDE score was significantly lower in C1 than in C3 (**Figure 6B**). According to our results, subtype C1 fits better for ICB therapy.

# DISCUSSION

Over 400,000 individuals are affected by renal cell carcinoma worldwide per year, while approximately 70% are diagnosed as ccRCC. Although surgical resection, treated as a primary therapy for localized tumors, can achieve a great outcome, there still exist 30% of ccRCC patients suffering from metastases, with a 5-year survival rate of 8–12% (20). Since the von Hippel–Lindau (*VHL*) gene has been identified in 1993, the *VHL* mutations have been reported as one of the genetic determinants which promote the initiation and progression of ccRCC (5, 21, 22). After years of exploring different prognostic markers in ccRCC, it still remains a challenge for us to find a stable and reliable biomarker to predict the OS. In our study, we used volcano plots to identify the DEGs between ccRCC patients with wild-type *VHL* and *VHL* mutation. Six genes (*GSTA1*, *GSTA2*, *NAT8*, *SLC17A3*, *SLC17A4* and *FABP7*) were screened out, given their downregulation in ccRCC patients with wild-type *VHL*. Furthermore, GO enrichment analysis illustrated that DEGs mentioned above were all involved in the pathway of cancer. Moreover, a prognostic analysis on DEGs and surprisingly found that *GSTA2*, *NAT8*, *SLC17A3*, and *SLC17A4* turned out to be inversely related to OS. Additionally, apart from *FABP7*, all DEGs could function as risk associated genes, while a lower expression might be related with a higher risk of ccRCC patients.

During the past few years, numerous studies have validated the role of multiple TF targets in cancer. Of note, the substantial potential of TFs to modulate several pathways of both cancer and other diseases has already drawn great attention (23, 24). In the present study, MYOD1, NANOG, and TP63 were the TFs that modulated DEGs. Moreover, the construction of a PPIs network provided insights for a basic abstraction of larger complex pathways which controlled the major cellular and molecular machinery determining the disease (25, 26). Here, a subnetwork based on the three TFs visualized the correlation among TFs and proteins interacted with them. Furthermore, results from KEA suggested that protein kinases might regulate the expanded PPI network. On the basis of expanded PPI network and KEA, we

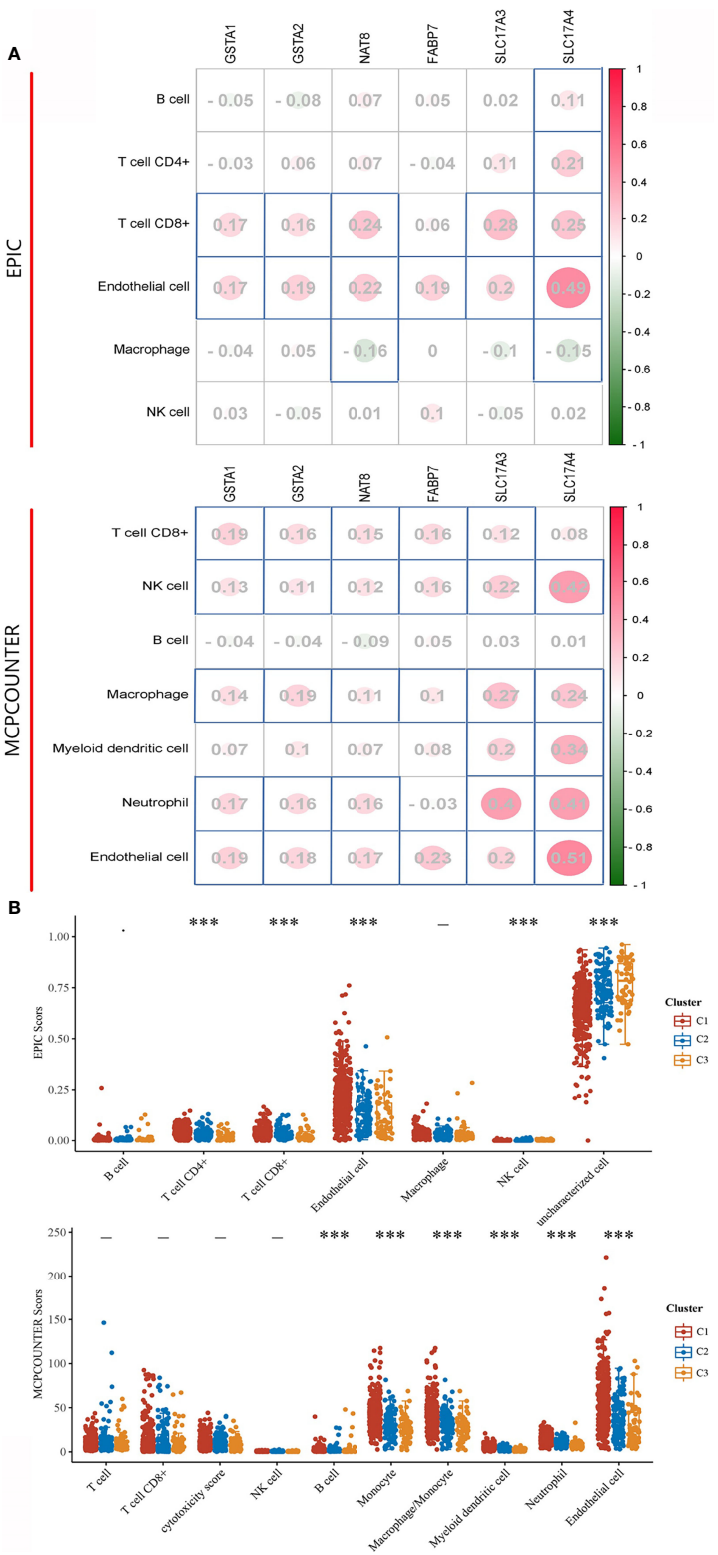



**FIGURE 5** | Immune signature of DEGs and three subgroups in ccRCC. **(A)** The correlations between DEG and immune cells. The corresponding P-values were shown in parenthesis. The left panel shows varieties of immune cells and algorithms. **(B)** The abundance score of infiltrating immune cells across each subgroup. The significance of the three groups passed by the Kruskal–Wallis test. ***P < 0.001, -: no significance.

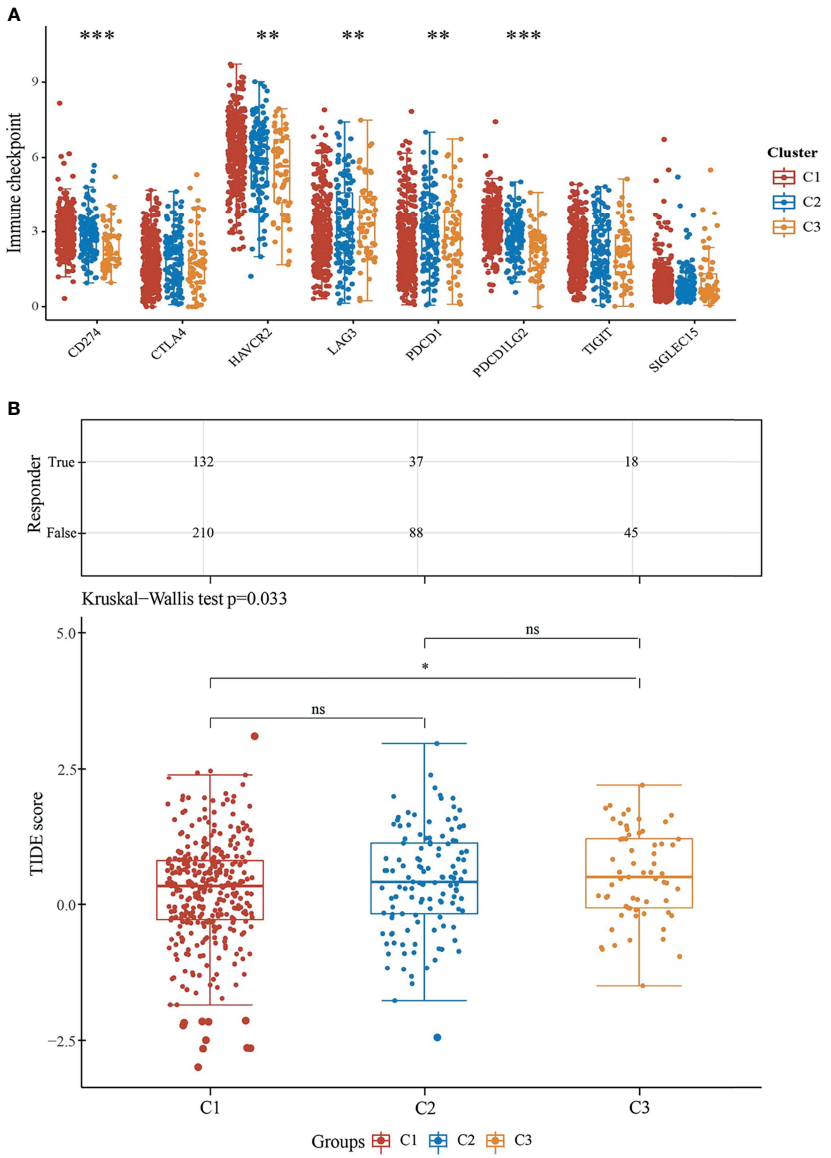



**FIGURE 6** | Predictive ICB response of ccRCC subgroups. **(A)** Expressions of eight immune checkpoint molecules in three subgroups. The significance of the three groups and above passed the Kruskal–Wallis test. **(B)** Statistical table of immune response samples (upper) and the distribution of immune response scores (underneath) in ccRCC subgroups in prediction. **P < 0.01, ***P < 0.001, ns, no significance.

deemed that TFs and kinases had the capability of modulate adjacent genes. Because of their high connectivity, these proteins are called hub proteins (or hubs) and they are of critical importance to PPI networks and whole biological systems (27, 28). Thus, MYOD1, NANOG, and TP63, along with 20 kinases mentioned in **Figure 3C**, were all supposed to be hub proteins of the DEGs.

During the recent years, the term "precision medicine" has come into our sight and has become more and more popular both in scientific and political perspectives (29). Consequently, stratified medicine and tailored therapy have been scientifically developed so as to promote the clinical application (30). To achieve a general and overall evaluation of hub genes among ccRCC patients, we classified the cohort (n = 530) into three different subtypes *via* consistency analysis according to the expression level of hub genes. Meanwhile, the expression of DEGs, clinical characterization, and prognosis in three subtypes were analyzed as well. Surprisingly, we found that each subtype was associated with distinct clinical characteristics and DEGs expression profiles, contributing to different outcomes in OS.

There is a large volume of published studies describing the role of immune cells in host defense against both cancer and infection (15). Meanwhile, the immune-related signature has already been observed in such cancers as pancreatic cancer,

glioblastoma, and most importantly, renal carcinoma (31–33), with plenty of specialized cell types involved in (34). It is known that *VHL* mutations can be widely detected in ccRCC; moreover, it has been suggested that *VHL* mutations might drive the activation of effector T cells as well as enhance cytokine level in ccRCC (35), indicating a potential but crucial role that immune infiltration might play. Although a large body of evidence points to the extent and functional orientation of the T cell infiltrate as important in therapy response (36, 37), recent studies also confirm a role for other components of the TME, such as B cells (38), myeloid lineage cells (39), NK cells (40), and macrophage (41). As the prognostic value of DEGs for ccRCC patients has been evaluated in our study, we aimed to get a better knowledge of the nature and differences of immune infiltration in ccRCC, especially in three subgroups. The correlations between DEGs and infiltrating immune cells, including B cells, CD4+T cells, CD8+T cells, endothelial cells, macrophages, and nature killer (NK) cells, were analyzed by EPIC and MCPCOUNTER algorithms. Considering the heterogeneity of TME among three subgroups of ccRCC classified above, we deeply investigated whether there existed differences among C1 to C3. Fortunately, results from both EPIC and MCPCOUNTER algorithms illustrated a higher number of immune-related cells in C1 than in other subgroups, implying a positive relation between DEGs and immune cell score, which might become a promising predictive panel for immunotherapy. Furthermore, the composition of the TME has been shown to influence response to ICB (42). Recent breakthroughs uncovered that ICB could take advantages of immune cell infiltration in tumors to reinvigorate an efficacious antitumoral immune response (42, 43). Our study confirmed that cluster C1 was supposed to have a higher efficacy of ICB therapy which was associated with a higher expression of immune checkpoint molecules and immune cell infiltration. According to our results, subtype C1 fits better for ICB therapy, suggesting a potential role of DEGs and hubs as a promising predictive strategy for ICB therapy response. Further studies will be performed to further investigate differences in immune microenvironment and ICB therapy response between patients with and without *VHL* mutation.

In conclusion, our study aimed to promote the evaluation of ccRCC prognosis and filtered out six DEGs which could be recognized as a promising prognostic panel for ccRCC and also a potential indicator for immunotherapy. Moreover, hub genes were identified in this study in classified ccRCC patients into three subgroups, proposing to provide a more specific evaluation of the prognosis, respectively and accurately. Furthermore, the ccRCC subtype associated with high expression of hubs fits better for ICB therapy, providing potential therapeutic implications for rational immunotherapy strategies.

## DATA AVAILABILITY STATEMENT

The original contributions presented in the study are included in the article/**Supplementary Material**. Further inquiries can be directed to the corresponding authors.

## AUTHOR CONTRIBUTIONS

Conceptualization, RL and LG. Formal analysis, YT. Writing—original draft, YY. Visualization, HZ. Methodology, YW. Software, SX and CC. All authors contributed to the article and approved the submitted version.

## FUNDING

This study was supported by the National Natural Science Foundation of China (Nos. NSF-81772774, NSF-81772808, and NSF-81800190), the National Science and Technology Major Project (2020ZX09201-013), and the Science and Technology Commission of Shanghai Municipality (19ZR1410300).

## ACKNOWLEDGMENTS

The results shown here are in part based upon data generated by TCGA Research Network.

## SUPPLEMENTARY MATERIAL

The Supplementary Material for this article can be found online at: https://www.frontiersin.org/articles/10.3389/fonc.2021.776824/full#supplementary-material

## REFERENCES

1. Siegel RL, Miller KD, Jemal A. Cancer Statistics, 2020. *CA Cancer J Clin* (2020) 70(1):7–30. doi: 10.3322/caac.21590
2. Perazella MA, Dreicer R, Rosner MH. Renal Cell Carcinoma for the Nephrologist. *Kidney Int* (2018) 94(3):471–83. doi: 10.1016/j.kint.2018.01.023
3. Jonasch E, Gao J, Rathmell WK. Renal Cell Carcinoma. *BMJ* (2014) 349: g4797. doi: 10.1136/bmj.g4797
4. Diamond E, Molina AM, Carbonaro M, Akhtar NH, Giannakakou P, Tagawa ST, et al. Cytotoxic Chemotherapy in the Treatment of Advanced Renal Cell Carcinoma in the Era of Targeted Therapy. *Crit Rev Oncol Hematol* (2015) 96 (3):518–26. doi: 10.1016/j.critrevonc.2015.08.007
5. Gossage L, Eisen T, Maher ER. VHL, The Story of a Tumour Suppressor Gene. *Nat Rev Cancer* (2015) 15(1):55–64. doi: 10.1038/nrc3844
6. Lazăr DC, Avram MF, Romoşan I, Cornianu M, Tăban S, Goldiş A. Prognostic Significance of Tumor Immune Microenvironment and Immunotherapy: Novel Insights and Future Perspectives in Gastric Cancer. *World J Gastroenterol* (2018) 24(32):3583–616. doi: 10.3748/wjg.v24.i32.3583
7. Beavis PA, Slaney CY, Kershaw MH, Gyorki D, Neeson PJ, Darcy PK. Reprogramming the Tumor Microenvironment to Enhance Adoptive Cellular Therapy. *Semin Immunol* (2016) 28(1):64–72. doi: 10.1016/j.smim.2015.11.003
8. Grosser R, Cherkassky L, Chintala N, Adusumilli PS. Combination Immunotherapy With CAR T Cells and Checkpoint Blockade for the

Treatment of Solid Tumors. *Cancer Cell* (2019) 36(5):471–82. doi: 10.1016/j.ccell.2019.09.006
9. Pardoll DM. The Blockade of Immune Checkpoints in Cancer Immunotherapy. *Nat Rev Cancer* (2012) 12(4):252–64. doi: 10.1038/nrc3239
10. Garon EB, Rizvi NA, Hui R, Leighl N, Balmanoukian AS, Eder JP, et al. Pembrolizumab for the Treatment of Non-Small-Cell Lung Cancer. *N Engl J Med* (2015) 372(21):2018–28. doi: 10.1056/NEJMoa1501824
11. Li B, Cui Y, Nambiar DK, Sunwoo JB, Li R. The Immune Subtypes and Landscape of Squamous Cell Carcinoma. *Clin Cancer Res Off J Am Assoc Cancer Res* (2019) 25(12):3528–37. doi: 10.1158/1078-0432.CCR-18-4085
12. Jiang P, Gu S, Pan D, Fu J, Sahu A, Hu X, et al. Signatures of T Cell Dysfunction and Exclusion Predict Cancer Immunotherapy Response. *Nat Med* (2018) 24(10):1550–8. doi: 10.1038/s41591-018-0136-1
13. Yeh JE, Toniolo PA, Frank DA. Targeting Transcription Factors: Promising New Strategies for Cancer Therapy. *Curr Opin Oncol* (2013) 25(6):652–8. doi: 10.1097/01.cco.0000432528.88101.1a
14. Singh V, Ram M, Kumar R, Prasad R, Roy BK, Singh KK. Phosphorylation: Implications in Cancer. *Protein J* (2017) 36(1):1–6. doi: 10.1007/s10930-017-9696-z
15. Biswas SK. Metabolic Reprogramming of Immune Cells in Cancer Progression. *Immunity* (2015) 43(3):435–49. doi: 10.1016/j.immuni.2015.09.001
16. Hu J, Chen Z, Bao L, Zhou L, Hou Y, Liu L, et al. Single-Cell Transcriptome Analysis Reveals Intratumoral Heterogeneity in ccRCC, Which Results in Different Clinical Outcomes. *Mol Ther J Am Soc Gene Ther* (2020) 28(7):1658–72. doi: 10.1016/j.ymthe.2020.04.023
17. Bitar L, Schumann U, König R, Zipp F, Schmidt MHH. Targeting Immune Modulators in Glioma While Avoiding Autoimmune Conditions. *Cancers* (2021) 13(14):3524–46. doi: 10.3390/cancers13143524
18. Zhang Y, Zheng J. Functions of Immune Checkpoint Molecules Beyond Immune Evasion. *Adv Exp Med Biol* (2020) 1248:201–26. doi: 10.1007/978-981-15-3266-5_9
19. Mahoney KM, Rennert PD, Freeman GJ. Combination Cancer Immunotherapy and New Immunomodulatory Targets. *Nat Rev Drug Discov* (2015) 14(8):561–84. doi: 10.1038/nrd4591
20. Harlander S, Schonenberger D, Toussaint NC, Prummer M, Catalano A, Brandt L, et al. Combined Mutation in Vhl, Trp53 and Rb1 Causes Clear Cell Renal Cell Carcinoma in Mice. *Nat Med* (2017) 23(7):869–77. doi: 10.1038/nm.4343
21. Jonasch E, Walker CL, Rathmell WK. Clear Cell Renal Cell Carcinoma Ontogeny and Mechanisms of Lethality. *Nat Rev Nephrol* (2021) 17(4):245–61. doi: 10.1038/s41581-020-00359-2
22. Linehan WM, Ricketts CJ. The Cancer Genome Atlas of Renal Cell Carcinoma: Findings and Clinical Implications. *Nat Rev Urol* (2019) 16(9):539–52. doi: 10.1038/s41585-019-0211-5
23. Bushweller JH. Targeting Transcription Factors in Cancer - From Undruggable to Reality. *Nat Rev Cancer* (2019) 19(11):611–24. doi: 10.1038/s41568-019-0196-7
24. Lee TI, Young RA. Transcriptional Regulation and Its Misregulation in Disease. *Cell* (2013) 152(6):1237–51. doi: 10.1016/j.cell.2013.02.014
25. Li Z, Ivanov AA, Su R, Gonzalez-Pecchi V, Qi Q, Liu S, et al. The OncoPPi Network of Cancer-Focused Protein-Protein Interactions to Inform Biological Insights and Therapeutic Strategies. *Nat Commun* (2017) 8:14356. doi: 10.1038/ncomms14356
26. De Las Rivas J, Fontanillo C. Protein-Protein Interaction Networks: Unraveling the Wiring of Molecular Machines Within the Cell. *Briefings Funct Genomics* (2012) 11(6):489–96. doi: 10.1093/bfgp/els036
27. Higurashi M, Ishida T, Kinoshita K. Identification of Transient Hub Proteins and the Possible Structural Basis for Their Multiple Interactions. *Protein Sci Publ Protein Soc* (2008) 17(1):72–8. doi: 10.1110/ps.073196308
28. Vandereyken K, Van Leene J, De Coninck B, Cammue BPA. Hub Protein Controversy: Taking a Closer Look at Plant Stress Response Hubs. *Front Plant Sci* (2018) 9:694. doi: 10.3389/fpls.2018.00694
29. Ramos P, Bentires-Alj M. Mechanism-Based Cancer Therapy: Resistance to Therapy, Therapy for Resistance. *Oncogene* (2015) 34(28):3617–26. doi: 10.1038/onc.2014.314
30. Konig IR, Fuchs O, Hansen G, von Mutius E, Kopp MV. What Is Precision Medicine? *Eur Respir J* (2017) 50(4):1700391. doi: 10.1183/13993003.00391-2017
31. Zhang J, Yan A, Cao W, Shi H, Cao K, Liu X. Development and Validation of a VHL-Associated Immune Prognostic Signature for Clear Cell Renal Cell Carcinoma. *Cancer Cell Int* (2020) 20(1):584. doi: 10.1186/s12935-020-01670-5
32. Gleeson FC, Levy MJ, Jackson RA, Murphy SJ, Halling KC, Kipp BR, et al. Endoscopic Ultrasound may be Used to Deliver Gene Expression Signatures Using Digital mRNA Detection Methods to Immunophenotype Pancreatic Ductal Adenocarcinoma to Facilitate Personalized Immunotherapy. *Pancreatology* (2020) 20(2):229–38. doi: 10.1016/j.pan.2019.12.002
33. Liu Y, Wu J, Huang W, Weng S, Wang B, Chen Y, et al. Development and Validation of a Hypoxia-Immune-Based Microenvironment Gene Signature for Risk Stratification in Gastric Cancer. *J Transl Med* (2020) 18(1):201. doi: 10.1186/s12967-020-02366-0
34. Binnewies M, Roberts EW, Kersten K, Chan V, Fearon DF, Merad M, et al. Understanding the Tumor Immune Microenvironment (TIME) for Effective Therapy. *Nat Med* (2018) 24(5):541–50. doi: 10.1038/s41591-018-0014-x
35. Sun Y, Xia Y, Liu X, Liu J, He W, Ye H, et al. Dexmedetomidine Alleviates LPS–induced Acute Lung Injury *via* Regulation of the P38/HO−1 Pathway. *Mol Med Rep* (2020) 22(3):2442–50. doi: 10.3892/mmr.2020.11330
36. Sharma P, Allison JP. The Future of Immune Checkpoint Therapy. *Sci (New York NY)* (2015) 348(6230):56–61. doi: 10.1126/science.aaa8172
37. Ribas A, Wolchok JD. Cancer Immunotherapy Using Checkpoint Blockade. *Sci (New York NY)* (2018) 359(6382):1350–5. doi: 10.1126/science.aar4060
38. Horii M, Matsushita T. Regulatory B Cells and T Cell Regulation in Cancer. *J Mol Biol* (2021) 433(1):166685. doi: 10.1016/j.jmb.2020.10.019
39. Zhang L, Li Z, Skrzypczynska KM, Fang Q, Zhang W, O'Brien SA, et al. Single-Cell Analyses Inform Mechanisms of Myeloid-Targeted Therapies in Colon Cancer. *Cell* (2020) 181(2):442–59.e29. doi: 10.1016/j.cell.2020.03.048
40. Shimasaki N, Jain A, Campana D. NK Cells for Cancer Immunotherapy. *Nat Rev Drug Discov* (2020) 19(3):200–18. doi: 10.1038/s41573-019-0052-1
41. Ruffell B, Coussens LM. Macrophages and Therapeutic Resistance in Cancer. *Cancer Cell* (2015) 27(4):462–72. doi: 10.1016/j.ccell.2015.02.015
42. Petitprez F, Meylan M, de Reyniès A, Sautès-Fridman C, Fridman WH. The Tumor Microenvironment in the Response to Immune Checkpoint Blockade Therapies. *Front Immunol* (2020) 11:784. doi: 10.3389/fimmu.2020.00784
43. House IG, Savas P, Lai J, Chen AXY, Oliver AJ, Teo ZL, et al. Macrophage-Derived CXCL9 and CXCL10 Are Required for Antitumor Immune Responses Following Immune Checkpoint Blockade. *Clin Cancer Res Off J Am Assoc Cancer Res* (2020) 26(2):487–504. doi: 10.1158/1078-0432.CCR-19-1868

**Conflict of Interest:** The authors declare that the research was conducted in the absence of any commercial or financial relationships that could be construed as a potential conflict of interest.

**Publisher's Note:** All claims expressed in this article are solely those of the authors and do not necessarily represent those of their affiliated organizations, or those of the publisher, the editors and the reviewers. Any product that may be evaluated in this article, or claim that may be made by its manufacturer, is not guaranteed or endorsed by the publisher.

*Copyright © 2021 Tong, Yu, Zheng, Wang, Xie, Chen, Lu and Guo. This is an open-access article distributed under the terms of the Creative Commons Attribution License (CC BY). The use, distribution or reproduction in other forums is permitted, provided the original author(s) and the copyright owner(s) are credited and that the original publication in this journal is cited, in accordance with accepted academic practice. No use, distribution or reproduction is permitted which does not comply with these terms.*

frontiers in Oncology

ORIGINAL RESEARCH
published: 21 December 2021
doi: 10.3389/fonc.2021.782755

# MCM2-7 in Clear Cell Renal Cell Carcinoma: MCM7 Promotes Tumor Cell Proliferation

*Junneng Zhang*[1*], *Huanzong Zhang*[1], *Yinghui Wang*[1] *and Qingshui Wang*[2*]

[1] Laboratory Medicine Department, The Fifth Hospital of Xiamen, Xiamen, China, [2] Key Laboratory of Optoelectronic Science and Technology for Medicine of Ministry of Education, College of Life Sciences, Fujian Normal University, Fuzhou, China

**Background:** Clear cell renal cell carcinoma (ccRCC) accounts for 60-70% of renal cell carcinoma (RCC) cases. Finding more therapeutic targets for advanced ccRCC is an urgent mission. The minichromosome maintenance proteins 2-7 (MCM2-7) protein forms a stable heterohexamer and plays an important role in DNA replication in eukaryotic cells. In the study, we provide a comprehensive study of MCM2-7 genes expression and their potential roles in ccRCC.

**Methods:** The expression and prognosis of the MCM2-7 genes in ccRCC were analyzed using data from TCGA, GEO and ArrayExpress. MCM2-7 related genes were identified by weighted co-expression network analysis (WGCNA) and Metascape. CancerSEA and GSEA were used to analyze the function of MCM2–7 genes in ccRCC. The gene effect scores (CERES) of MCM2-7, which reflects carcinogenic or tumor suppressor, were obtained from DepMap. We used clinical and expression data of MCM2-7 from the TCGA dataset and the LASSO Cox regression analysis to develop a risk score to predict survival of patients with ccRCC. The correlations between risk score and other clinical indicators such as gender, age and stage were also analyzed. Further validation of this risk score was engaged in another cohort, E-MTAB-1980 from the ArrayExpress dataset.

**Results:** The mRNA and protein expression of MCM2-7 were increased in ccRCC compared with normal tissues. High MCM2, MCM4, MCM6 and MCM7 expression were associated with a poor prognosis of ccRCC patients. Functional enrichment analysis revealed that MCM2-7 might influence the progress of ccRCC by regulating the cell cycle. Knockdown of MCM7 can inhibit the proliferation of ccRCC cells. A two-gene risk score including MCM4 and MCM6 can predict overall survival (OS) of ccRCC patients. The risk score was successfully verified by further using Arrayexpress cohort.

**Conclusion:** We analyze MCM2-7 mRNA and protein levels in ccRCC. MCM7 is determined to promote tumor proliferation. Meanwhile, our study has determined a risk score model composed of MCM2-7 can predict the prognosis of ccRCC patients, which may help future treatment strategies.

**Keywords: ccRCC, MCM2-7, WGCNA, Lasso, cell cycle, proliferation**

OPEN ACCESS

***Edited by:***
*Andrea Mari,*
*Careggi University Hospital, Italy*

***Reviewed by:***
*Luca Lambertini,*
*Careggi University Hospital, Italy*
*Guangzhen Wu,*
*Dalian Medical University, China*

****Correspondence:***
*Junneng Zhang*
*15959391919@163.com*
*Qingshui Wang*
*wangqingshui@fjnu.edu.cn*

***Specialty section:***
*This article was submitted to Genitourinary Oncology, a section of the journal Frontiers in Oncology*

***Received:*** *24 September 2021*
***Accepted:*** *02 December 2021*
***Published:*** *21 December 2021*

***Citation:***
*Zhang J, Zhang H, Wang Y and Wang Q (2021) MCM2-7 in Clear Cell Renal Cell Carcinoma: MCM7 Promotes Tumor Cell Proliferation. Front. Oncol. 11:782755. doi: 10.3389/fonc.2021.782755*

# INTRODUCTION

Renal cell carcinoma (RCC) is one of the common urinary system tumors (1). It accounts for about 90% of all renal malignancies, of which clear cell renal cell carcinoma (ccRCC) is the most common pathological subtype, accounting for about 75% of renal cell carcinoma (2). The latest statistics show that the incidence of ccRCC is increasing at a rate of 2% per year (3). At present, early ccRCC patients mainly rely on surgical treatment, but most early patients have no specific symptoms, so about 1/3 of patients have already metastasized at the time of diagnosis (4). Patients with metastasis and recurrence not only lose the chance of radical surgery, but also easily tolerate traditional radiotherapy and chemotherapy. Although molecularly targeted drugs have made some progress, most patients will eventually become resistant to targeted drugs. Therefore, mining novel targeted biomarkers related to the diagnosis and treatment of ccRCC is one of the current hot spots in cancer research, and it is also a top priority.

The minichromosome maintenance proteins (MCM) family is a highly conserved DNA unwinding protein complex (5). The MCM protein is an essential replication initiation factor and was originally identified as a protein required for the maintenance of minichromosomes in saccharomyces cerevisiae (6). The most famous of these are MCM2, MCM3, MCM4, MCM5, MCM6, and MCM7, which are composed of six structurally related proteins (7). When MCM2-7 forms a hexamer, it has helicase activity in cells. They are evolutionarily conserved in all eukaryotes. The normal function of MCMs protein is necessary for DNA replication. In the G phase of eukaryotic mitosis, the MCM2-7 complex binds to the chromosome to complete the assembly of the pre-replication complex. After entering the S phase, the MCM2-7 complex is activated by kinase, which induces downstream polymerase-primer synthase assembly. At the same time, it combines with DNA polymerase to form a functional replication fork, which starts DNA unwinding and replication. MCM2-7 must bind to the starting point in the G phase. Without the binding of MCM2-7, DNA replication will not proceed. MCM2-7 is a potential marker of cell proliferation, and an increase in the level of MCM2-7 indicates the proliferation of malignant cells. Accumulating evidence indicates that MCM2-7 is related to the progression and prognosis of malignant tumors (8). However, MCM2-7 remains poorly understood in ccRCC.

This study aimed to provide a systematic and comprehensive study of MCM2-7 gene expression and illuminate their potential roles in ccRCC. We systematically integrated the expression profiles of MCM2-7 and elucidated the potential regulatory mechanisms by bioinformatics analyses. Meanwhile, the personalized prognostic features for ccRCC patients were developed based on MCM2-7 related genes. The research may help to establish a foundation for further intensive MCM2-7-related research in individualized treatment of ccRCC.

# MATERIALS AND METHODS

## Gene Expression Extraction

RNA sequencing data of ccRCC and clinical data were downloaded from The Cancer Genome Atlas (TCGA) database (https://www.cancer.gov/tcga). According to the previous study, we selected the patients with copy number loss for chromosome 3p, VHL mutation, or both (9, 10). The microarray dataset GSE66272, GSE36895, GSE46699, and GSE53757 were downloaded from the Gene Expression Omnibus (GEO) database (https://www.ncbi.nlm.nih.gov/geo/), which were performed on Affymetrix Human Genome U133 Plus 2.0 Array platform. The method for extracting microarray gene expression values is based on our previous research (11). Then, we used ComBat for batch effect removal to homogenize the gene expression data from GSE66272, GSE36895, GSE46699, and GSE53757. The ccRCC gene expression data of E-MTAB-1980 used for validation cohort were obtained from ArrayExpress (https://www.ebi.ac.uk/arrayexpress).

## Patients and Specimens

The research was composed of 50 ccRCC tissues and 50 normal renal sample from 50 ccRCC patients, who had a renal resection at the Fifth Hospital of Xiamen between June 2019 and January 2021. The standard requirements for patients included in the study were as follows: (1) histologically proven ccRCC; (2) no history of other malignancy tumor; (3) no prior neoadjuvant chemotherapy. The study was performed with the approval of the Ethics Committee of Fifth Hospital of Xiamen and complied with the Helsinki Declaration. Written informed consent was obtained from all patients involved.

## RNA Isolation and RT-qPCR

In the research, total RNA was extracted from ccRCC tissues and cells using TRIzol (Invitrogen, CA, USA) according to the manufacturer's protocol. Total RNA was reverse transcripted with mRNA reverse transcription kit (Takara, Japan).

RT-qPCR were performed using a SYBR green kit (Vazyme, China) with a Bio-Rad iQ5 (Bio-Rad, USA). Specific primers for RT-qPCR were designed to detect the mRNA level for MCM7 gene. GAPDH was used as internal control to normalize the mRNA levels. All primers were synthesized by Sangon Biotech (Shanghai, China), and the sequences are listed in **Supplementary Table 1**. Relative mRNA level in comparison to controls were determined using $2^{-\Delta ct}$ method.

## Validation of Protein Expression of the MCM2-7 Genes

The Human Protein Atlas (THPA) provides information on the cell and tissue distribution of 26,000 human proteins. It uses specific antibodies to identify protein expression in tumor tissues and normal tissues. In the research, we explored the protein expression of MCM2-7 genes (MCM2, MCM3, MCM4, MCM5, MCM6, MCM7) in ccRCC tissues and normal tissues.

## Single-Cell Analysis

CancerSEA (12) (http://biocc.hrbmu.edu.cn/CancerSEA/) depicts single cell functional status maps that contain 14

functional states (including stemness, proliferation, EMT, differentiation, invasion, apoptosis, DNA damage, hypoxia, metastasis, angiogenesis, DNA repair, inflammation, quiescence, and cell cycle) obtained from 25 types of tumors including 41900 individual cells. In the research, CancerSEA was used to evaluate the potential roles of MCM2-7 genes in ccRCC.

## Weighted Gene Correlation Network Analysis (WGCNA)

WGCNA is a common algorithm used to build gene co-expression networks and was performed by the WGCNA R package. The WGCNA hypotheses that the co-expression gene network follows the scale less distribution firstly, defines the adjoining function of the gene co-expression correlation matrix and gene network formation, the matrix of similarity was constructed using a power of β=3 (4GEOs), β=9 (TCGA) and a scale-free $R^2 = 0.95$. The adjacency matrix was then translated into a topological overlap matrix (TOM). Furthermore, median linkage hierarchical clustering was analyzed using the TOM-based dissimilarity measure with a minimum size of 20.

## Functional Enrichment Analysis

In order to further analyze the specific biological process methods of the potential targets we obtained, we use Metascape (13) (http://metascape.org) to conduct pathway and process enrichment analysis. Metascape is a web-based portal that combines gene, interactome analysis and annotation functional enrichment.

## LASSO Analysis

The Least absolute shrinkage and selection operator (LASSO) was conducted to construct MCM2-7 genes risk predictive model with the help of "survival" and "glmnet" packages in R software. LASSO is a common method used in high-dimensional data regression, which can select prognosis-related gene pairs of ccRCC by shrinking regression coefficients. The optimal penalty weight of the Lasso-Cox model was found in a grid search manner in a 10-fold cross-validation process. Then, the coefficients of most gene pairs reduced to zero, and a small number of gene pairs with nonzero coefficients were closely correlated with the prognosis of ccRCC.

## DepMap

The Cancer Dependency Map (https://depmap.org/portal/) developed CERES, a computational method to estimate gene-dependency levels from CRISPR-Cas9 essentiality screens while accounting for the copy number-specific effect (14, 15). Dependency scores for MCM2-7 genes in RCC cells were calculated using the CERES algorithm. A negative score indicates that the cell line grows slower when the specific gene is knocked down, while a positive score indicates that the cell line grows faster after the specific gene is knocked down (16).

## Cells Culture and Transfection

The cell lines 786-O and A-498 were obtained from American Type Culture Collection (ATCC, Manassas, VA, USA). 786-O cells and A-498 cells were respectively cultured in PRMI 1640 (Gibco by Life Technologies, Grand Island, NY, USA) and MEM Alpha medium (Gibco by Life Technologies, Grand Island, NY, USA) containing 10% fetal bovine serum (FBS, BI, Kibbutz Beit Haemek, Israel) and 100 U/mL penicillin and 0.1 mg/mL streptomycin (BBI life sciences, shanghai, China) at 37 °C in a humidified incubator with 5% $CO_2$. The sequence of shRNA targeting MCM7 was cloned into pLVX vector. The transfection was performed using lipofectamine 2000 (Invitrogen, Carlsbad, CA, USA) according to the manufacturer' s guidelines.

## CCK-8 Assay

Cell proliferation was measured by CCK-8 assay. 786-O and A-498 cells were seeded onto five 96-well plates ($2\times10^4$ cells/well) in triplicate and cultured for 24, 48 and 72 hours. Four hours before absorbance measuring, 10 μL CCK-8 solution was added. The absorbance was measured at 450 nm with a microplate reader after incubated at 37°C for 2 hours.

## Drug Sensitivity Evaluation

GSCALite (http://bioinfo.life.hust.edu.cn/web/GSCALite/) is a website used for genomic cancer analysis and drug sensitivity analysis. In the research, we use the GSCALite database to evaluate the drug sensitivity of MCM2-7 genes to identify potential molecular compounds for targeted immunotherapy.

## Statistical Analysis

In this research, a statistical correlation was calculated by t-test. Unpaired samples used unpaired t-test and paired samples used paired t-test. Overall survival (OS) was evaluated by the Kaplan-Meier method, and survival curves were compared by log-rank test. All p values < 0.05 were considered statistically significant.

# RESULTS

## The Expression and the Prognostic Significance of MCM2-7 in ccRCC

Four datasets, including GSE66272, GSE36895, GSE46699, and GSE53757, were obtained from GEO. GSE66272 contains 27 ccRCC tissues and 27 paired adjacent normal kidney tissues. GSE46699 contains 29 ccRCC tissues and 23 adjacent normal kidney tissues. GSE46699 contains 67 ccRCC tissues and 63 adjacent normal kidney tissues. GSE53757 contains 72 ccRCC tissues and 72 paired adjacent normal kidney tissues. The platform used to generate data for the four datasets was the Affymetrix Human Genome U133 Plus 2.0 Array. Before the identifying of MCM2-7 expression, the normalization and batch effects removal from the four GEO datasets was conducted by the 'sva' package and was named as 4GEOs (**Figures 1A**).

We analyzed overall expression differences in MCM2-7 genes using 4GEOs. As shown in **Figures 1B–G**, the expression of the

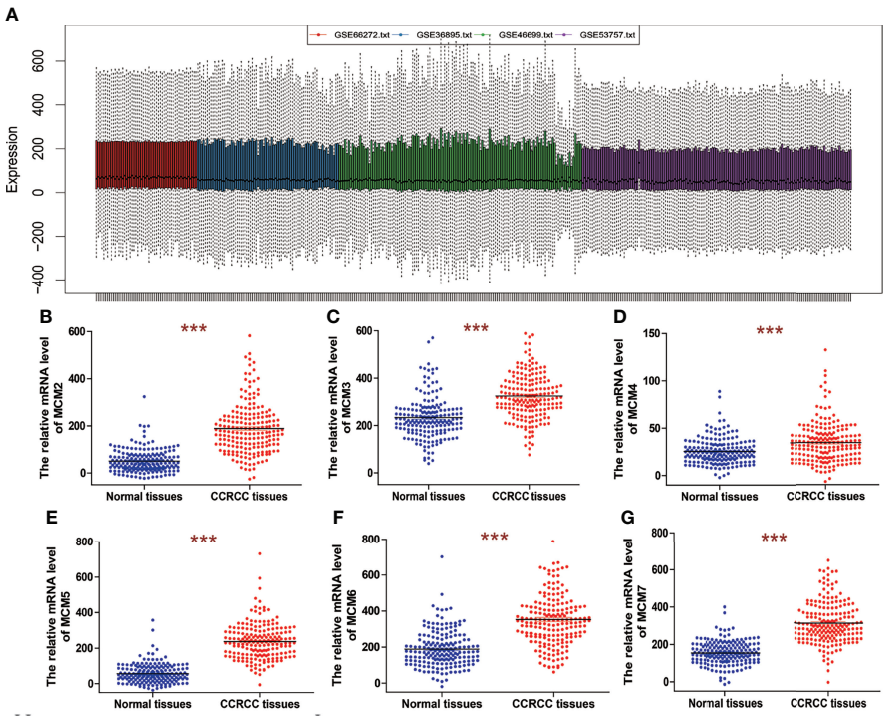



**FIGURE 1** | The mRNA expression of MCM2-7 in ccRCC. **(A)** Removing batch effect between GSE66272, GSE36895, GSE46699 and GSE53757. **(B–G)** The expression of MCM2 **(B)**, MCM3 **(C)**, MCM4 **(D)**, MCM5 **(E)**, MCM6 **(F)** and MCM7 **(G)** in ccRCC tissues compared with normal tissues. ***p < 0.001.

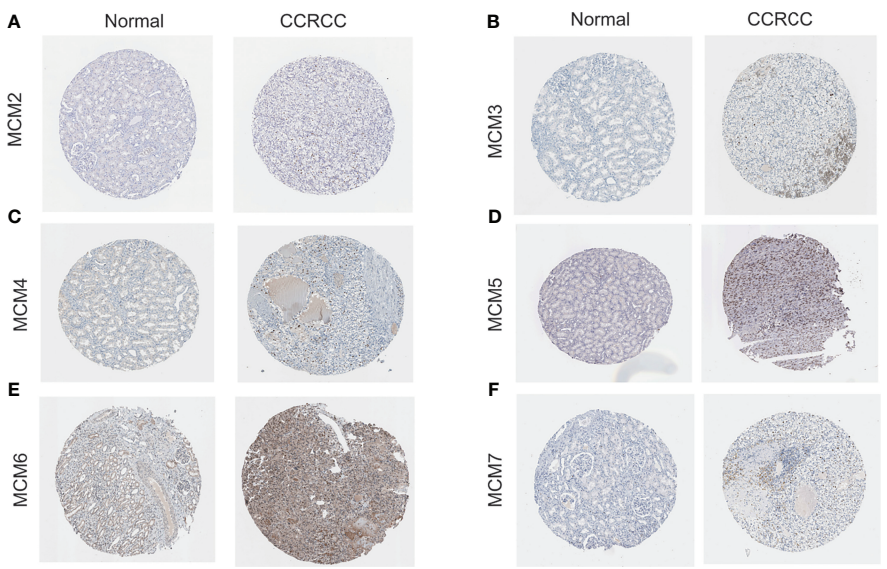



**FIGURE 2** | The protein expression of MCM2-7 in ccRCC. **(A–F)** Representative immunohistochemistry analysis of MCM2 **(A)**, MCM3 **(B)**, MCM4 **(C)**, MCM5 **(D)**, MCM6 **(E)** and MCM7 **(F)** from the human protein atlas database.

MCM2-7 genes in the ccRCC tissues was significantly higher than that in normal kidney tissues. In addition, we examined the IHC results from the Human Protein Atlas project and found that MCM2 was lowly expressed in ccRCC tissues but no detectable expression in normal tissues (**Figures 2A**), MCM3 has moderately expressed in ccRCC tissues but no detectable expression in normal tissues (**Figures 2B**), MCM4 was highly expressed in ccRCC tissues but moderately expressed in

normal tissues (**Figures 2C**), MCM5 was moderately expressed in ccRCC tissues but no detectable expression in normal tissues (**Figures 2D**), MCM6 was moderately expressed in ccRCC tissues but lowly expressed in normal tissues (**Figures 2E**), MCM7 was lowly expressed in ccRCC tissues but no detectable expression in normal tissues (**Figures 2F**). These results indicated that the mRNA and protein level of MCM2-7 were increased in ccRCC tissues compared with normal kidney tissues.

To explore the significance of MCMs gene members in clinical prognosis, we used Kaplan-Meier survival analysis to prepare overall survival (OS) for ccRCC patients (**Figures 3**). The Kaplan-Meier survival curve indicated that high MCM2, MCM3, MCM4, MCM6 and MCM7 expression were associated with a poor prognosis of ccRCC; However, the expression of MCM5 was not significantly associated with OS in ccRCC patients.

## MCM2-7 Were Associated With Cell Cycle Activated Pathways in ccRCC

Analysis of pathway activity by GSCA revealed that MCM2, MCM3, MCM4, MCM5, MCM6 and MCM7 might strongly activate the apoptosis, cell cycle and DNA damage response as well as inhibit RAS/MAPK pathways and hormone ER (**Figure 4A**). Next, we performed GSEA based on the expression of MCM2-7 to identify the related pathways and underlying mechanisms using 4GEO database. GSEA of TCGA database suggested that MCM2, MCM3, MCM4, MCM5, MCM6 and MCM7 were related to cell cycle (**Figures 4B–G**).

WGCNA was performed to identify the highly correlated genes and co-expression networks of MCM2-7 gene in ccRCC patients. 4GEOs database and TCGA database were used to build WGCNA. We calculated the network topology for soft-thresholding powers from 1 to 30 to choose the best threshold. As shown in **Figures 5A, D**, power value 3 and 9 were the lowest power for the scale-free topology for the 4GEOs and TCGA database respectively. Additionally, soft power showed a higher average connectivity degree (**Figures 5B, E**). Then, we set power=3 (4GEOs) and 9 (TCGA) to produce a hierarchical clustering tree. Modules were identified with a merging threshold of 0.25 (**Figures 5C, F**). Among all modules, the magenta module with 448 genes was the most relevant for MCM2-7 expression in the 4GEOs database, and the salmon module with 546 genes was the most relevant for MCM2-7 expression in the TCGA database. The intersection of the 4GEOs and TCGA databases contained 154 genes (**Figure 5G** and **Supplementary Table 2**). Enrichment analysis revealed that 154 genes were enriched in cell cycle, cell division, microtubule cytoskeleton organization involved in mitosis and DNA replication (**Figure 5H**). The functions of 154 genes in single ccRCC cells were explored *via* CancerSEA and were found to be positively associated with the cell cycle (**Figure 5I**). These results indicated that MCM2-7 would be relevant to ccRCC cells proliferation.

## Knockdown of MCM7 Inhibits ccRCC Cell Proliferation

To identify the effect of MCM2-7 on the proliferation of ccRCC cells, we investigated genome-wide CRISPR-based loss-of-function screens derived from DepMap. Every gene exhibited

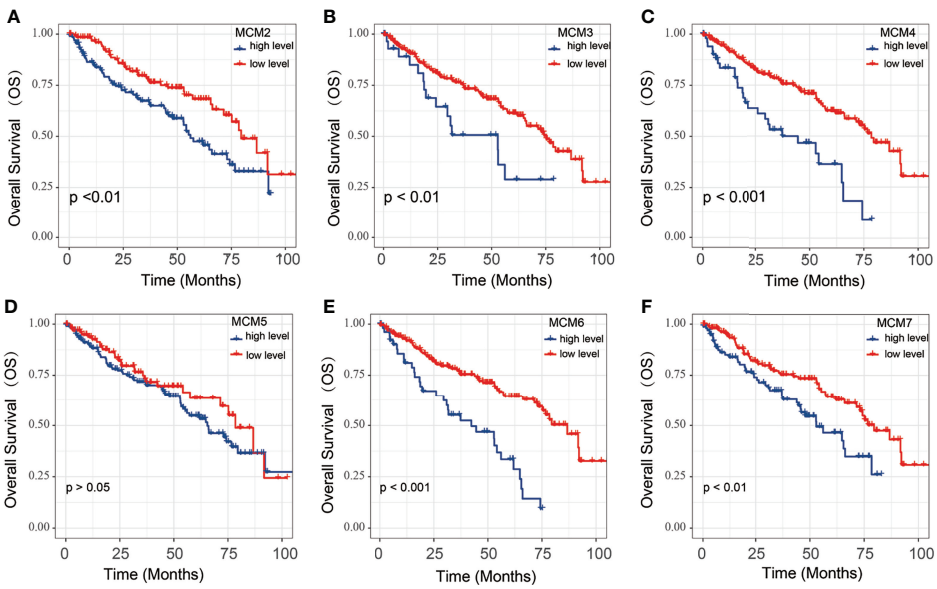



**FIGURE 3** | The OS of MCM2-7 for ccRCC patients. **(A–F)** Overall analysis for the prognostic value of MCM2 **(A)**, MCM3 **(B)**, MCM4 **(C)**, MCM5 **(D)**, MCM6 **(E)** and MCM7 **(F)** expression for OS in ccRCC patients by Kaplan-Meier analysis based on TCGA. The Kaplan-Meier method was used to draw survival curves, and the log-rank test was performed to evaluate survival difference with the best cut-off value.

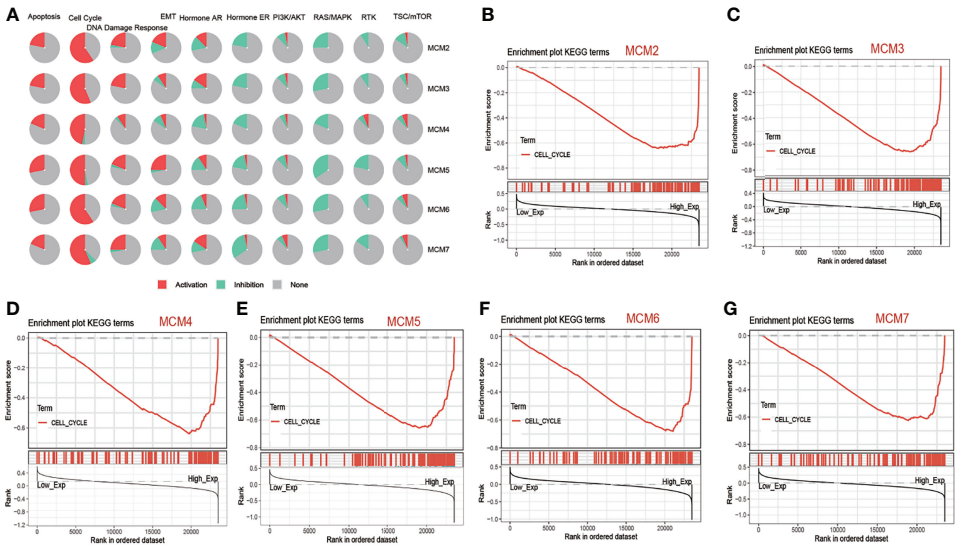



**FIGURE 4** | The function of MCM2-7 in ccRCC. **(A)** Pathway activity of MCM2-7 genes from GSCA. **(B)** Enriched gene sets between high and low expression sample groups based on the MCM2 **(B)**, MCM3 **(C)**, MCM4 **(D)**, MCM5 **(E)**, MCM6 **(F)** and MCM7 **(G)** level in ccRCC using GSEA.

different tendencies as potential oncogenes or tumor suppressor genes according to the definition of the CERES, the CERES of MCM2-7 are illustrated in **Figure 6A**. Among six MCMs genes, MCM7 showed a strong tendency towards oncogenes. Next, we examined MCM7 expression in tumor tissues and adjacent normal tissues from 50 ccRCC patients. Results indicated that MCM7 was high expressed in ccRCC tissues compared with normal renal tissues (**Figure 6B**). And then we knocked down MCM7 expression in 786-O and A-498 cells using shRNA (**Figure 6C**). The results of the CCK-8 assay confirmed that MCM7 knockdown significantly inhibited the proliferation of 786-O and A-498 cells (**Figures 6D, E**).

## Prognosis Model of MCM2-7 Genes Constructed and Survival Analysis

MCM2-7 genes were performed to construct a prognostic model using Lasso-Cox proportional hazards regression (**Figures 7A, B**). The resulting optimal prognostic signature for predicting the overall survival consists of 2 MCM2-7 genes: MCM4 and MCM6. Risk score = (0.005 * MCM4 expression) + (0.081 * MCM6 expression). Each ccRCC patient was assigned a risk score based on the risk score formula and divided into low-risk score and high-risk score groups according to the best cut-off in two groups. Kaplan-Meier curves analysis showed that the overall survival of the low-risk group was substantially longer than the high-risk group (**Figure 7C**). To explore the mechanisms between low score and high score groups, the GSEA approach was performed to identify the potential pathways between different risk score groups. GSEA analysis reveals that the high-risk score group may through involved in cell cycle (**Figure 7D**). Moreover, high-risk score groups also had a worse prognosis in disease-free survival (**Figure 7E**).

Next, we evaluated the association between the risk score and tumor stage or tumor recurrence. **Figure 8A** shows that the risk score was significantly higher in stage III and IV patients than in grade I and II patients. **Figure 8B** shows that the risk score was significantly higher in recurrence patients than in without recurrence patients, indicating that a high-risk score was associated with high malignancy. Moreover, Kaplan-Meier analyses of the patients with low-risk score and high-risk score ccRCC based on clinical factors including age, sex and tumor grade were also performed (**Figure 9**). These results further confirmed the robust stratification ability of the MCM2-7-based risk score.

## Validation of the Prognostic Model

To validate the stability and reliability of the prognostic model, we first downloaded 101 samples with complete clinical information as the validation data set from the E-MTAB-1980-ccRCC database. For each patient, the risk score was calculated using the prognostic model. Patients were divided into the low-risk score and high-risk score groups respectively. Kaplan-Meier curve analysis showed that ccRCC patients with high-risk score had a poor OS than those in the low-risk score group (**Figure 10A**). Moreover, the AUC of 3-year OS was 0.71, indicating good accuracy (**Figure 10B**).

## Construction of a Clinical Prognostic Prediction Model

Based on five variables including age, gender, lymph and risk score, a survival nomogram was created to precisely calculate the probability of survival at 1-year, 3-year and 5-year (**Figure 11A**). The calibration plots suggested that the nomogram performed well in comparison with the ideal model (**Figure 11B**). We hold the opinion that the nomogram may have good accuracy for long-term survival prediction in ccRCC.

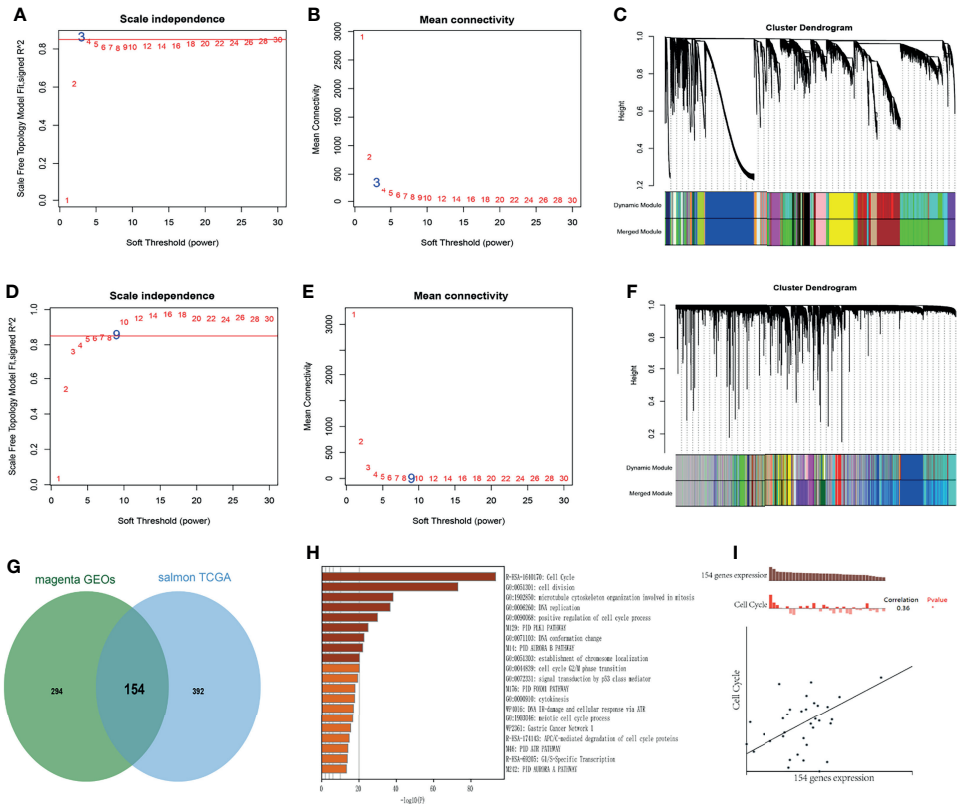



**FIGURE 5** | Identification of co-expression module genes associated with MCM2-7 using the WGCNA. **(A)** Relationship between scale-free topology model fit and soft-thresholds (powers) in 4GEOs database. **(B)** Relationship between the mean connectivity and various soft-thresholds in 4GEOs database. **(C)** Dendrogram of modules identified by WGCNA in 4GEOs database. **(D)** Relationship between scale-free topology model fit and soft-thresholds (powers) in TCGA database. **(E)** Relationship between the mean connectivity and various soft-thresholds in TCGA database. **(F)** Dendrogram of modules identified by WGCNA in TCGA database. **(G)** The intersection of magenta module for 4GEOs database and salmon module for TCGA database contained 154 genes. **(H)** Results of KEGG analysis of 154 genes. **(I)** Single-cell analysis indicated that 154 genes were involved in regulation of the cell cycle.

## The Relationship of the Drug Sensitivity and MCM2-7

The relationship between drug sensitivity and the relative expression levels of MCM2-7 was explored by using GSCA analysis based on the data from the Cancer Drug Sensitivity Genomics Database (GDSC). We hypothesize that a positive correlation between the expression of these genes and the IC50 of the drug being studied will indicate that CCRCC patients develop resistance, and vice versa. High MCM2, MCM3, MCM4, MCM5, MCM6 and MCM7 expression were associated with higher drug resistance to 17-AAG, RDEA119, Trametinib and selumetinib. while there are associated with higher drug sensitivity to AR-42, AT-7519 and BMS345541 et al. (**Figure 12**).

# DISCUSSION

DNA replication is an important issue in the study of tumor occurrence and development. MCM2-7 plays a central role in replication by forming a hexamer ring complex around DNA (17). One of the characteristics of malignant cells is unlimited DNA replication. Therefore, some DNA replication proteins are considered as promising cancer biomarkers. The MCM2-7 is also believed to be closely related to tumor growth and malignant progression. Increased level of MCM2-7 has been detected in various tumor tissues and cell lines.

MCM2 is highly expressed in NSCLC and has certain clinical significance for judging the development and prognosis of NSCLC (18). Knockdown of MCM2 inhibits the expression of cyclin D1 and cyclin-dependent hormone 4 (CDK4), and increases the expression of p21 and p53, indicating that MCM2 silencing triggers cell cycle arrest and induces apoptosis (19). MCM2 is also highly expressed in colorectal cancer and is positively correlated with lymph node metastasis, depth of invasion and Dukes staging (20). In breast cancer, the mRNA and protein levels of MCM2 are increased and tend to increase gradually as the malignancy of tumors increases (21, 22).

Previous studies have shown that overexpression of MCM3 enhances the cell growth, migration, and invasion of medulloblastoma cells (23). Phosphorylated MCM3 promotes the

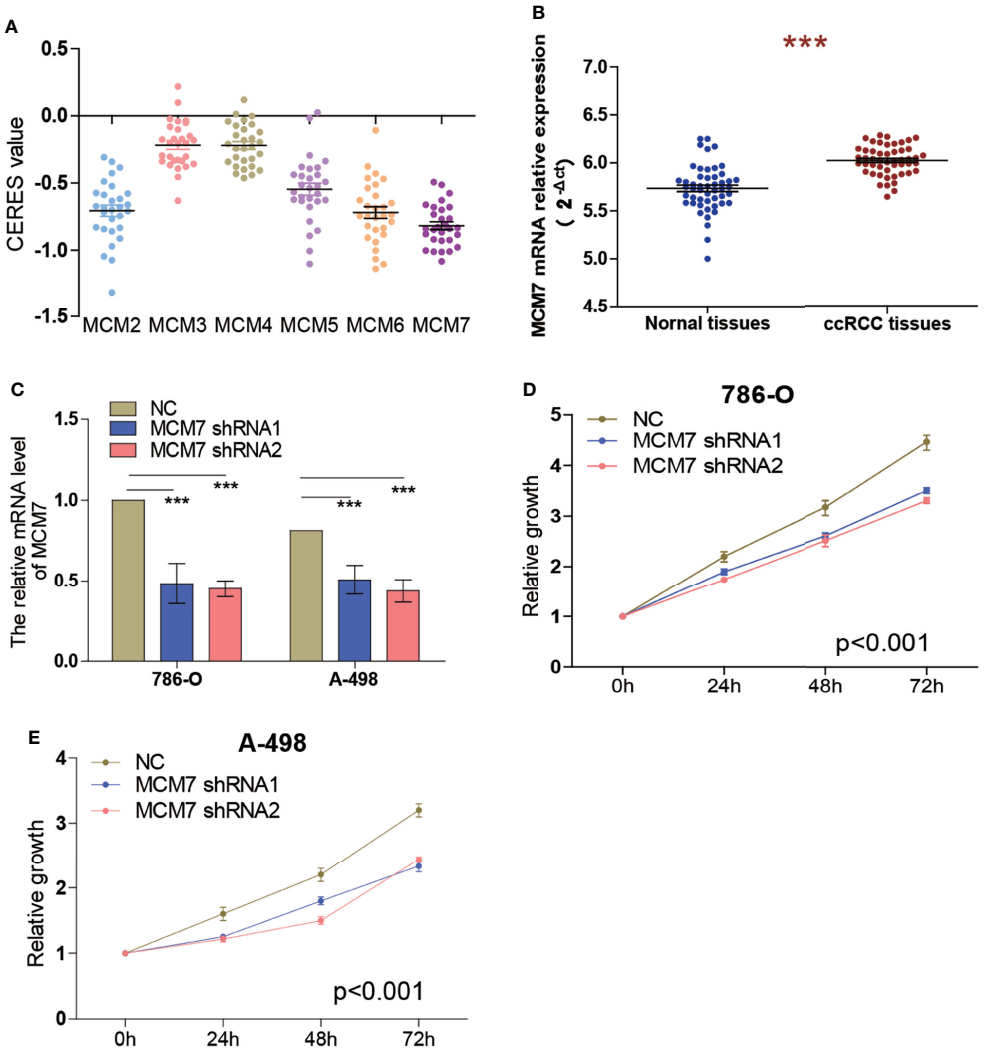



**FIGURE 6** | Knockdown of MCM7 inhibits ccRCC cell proliferation. **(A)** Gene effect scores of MCM2-7 in RCC cells from RNAi and CRISPR/Cas9 screens. **(B)** The expression of MCM7 was measured by RT-qPCR from 50 ccRCC patients, results were presented as $2^{-\Delta Ct}$. **(C)**The MCM7 expression changes were confirmed by real-time PCR in the ccRCC cells (786-O and A-498) after transfecting shRNAs. **(D, E)** The proliferation ability of 786-O **(D)** and A-498 **(E)** cells was measured by the CCK8 assay after transfecting shRNAs. ***p < 0.001.

proliferation of renal cancer cells and inhibits apoptosis (24). These results indicate that MCM3 may be related to tumor proliferation, migration, and invasion. Increased level of MCM3 has also been observed in liver cancer, salivary gland tumors, prostate cancer, melanoma, and cervical squamous cell carcinoma (23, 25–28). These studies indicate that MCM3 may be a potential proliferation marker for the diagnosis of certain tumors.

The increased level of MCM4 is related to the development and pathological stages of esophageal cancer (29). The expression of MCM4 is related to the metastasis of melanoma, and related to the poor prognosis of melanoma patients (30). Increased expression of MCM4 is associated with poor prognosis in patients with hepatocellular carcinoma (31). In addition, the down-regulation of MCM4 inhibited the growth, migration and invasion of lung adenocarcinoma cells (32).

The increased level of MCM5 has been found in various cancers, including lung cancer, malignant skin diseases, gastric adenocarcinoma, bladder cancer, oral squamous cell carcinoma, and cervical cancer (33–37). Higher MCM5 level is significantly related to tumor size, histopathological stage, lymph node metastasis and prognosis. In addition, the overexpression of MCM5 can promote the proliferation and invasion of lung cancer cells (38). Knockdown of MCM5 can inhibit the proliferation of renal cell carcinoma (39).

Patients with a high level of MCM6 were found to have poorer survival and a higher risk of death in craniopharyngioma, non-small cell lung cancer, and mantle cell lymphoma (40–42). High MCM6 level is also associated with a higher histological grade in breast cancer, low-grade chondrosarcoma and endometrioid endometrial adenocarcinoma (40, 43).

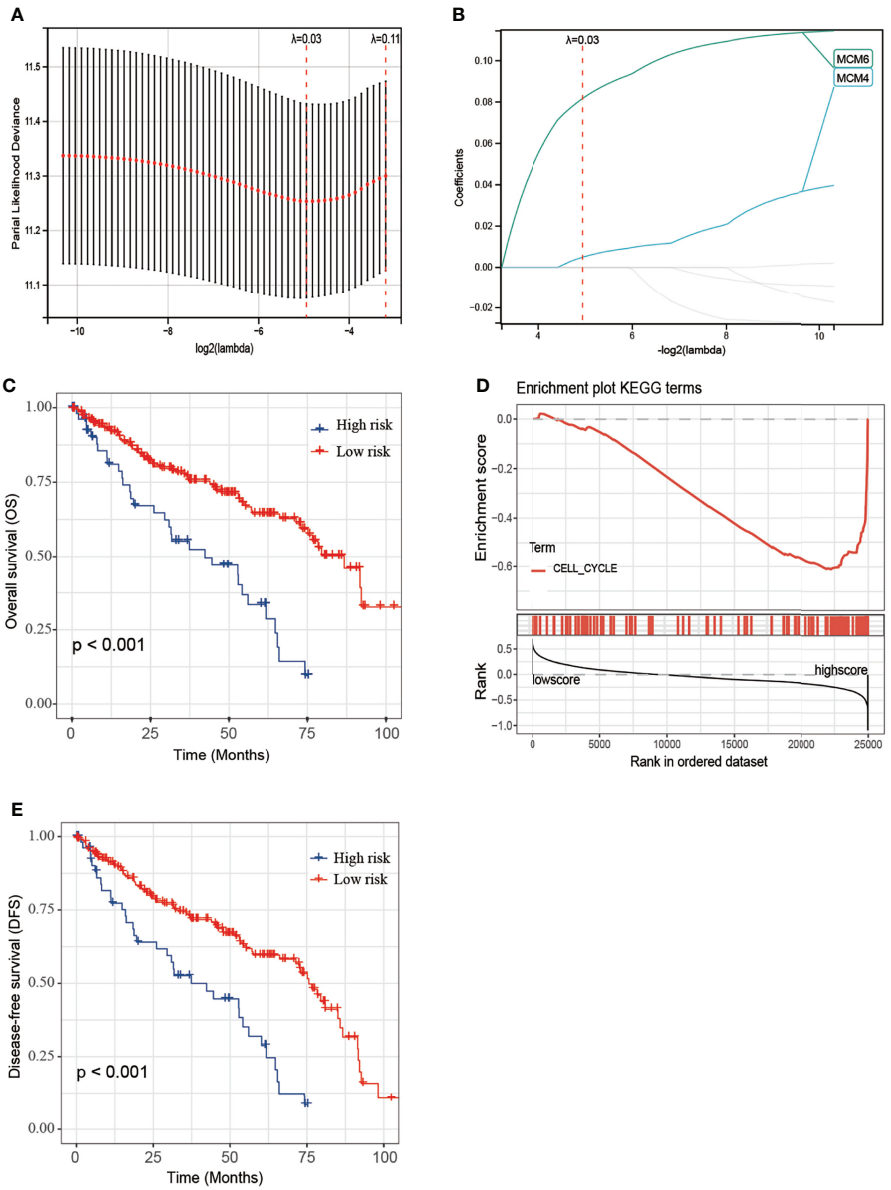



**FIGURE 7** | Construction of MCM2-7 genes-based classifier to predict prognosis in ccRCC patients. **(A)** Partial likelihood deviance of OS for the LASSO coefficient profiles. **(B)** LASSO coefficient profiles of MCM2-7 genes for OS. **(C)** Kaplan-Meier curves to compare overall survival of low-risk and high-risk groups. **(E)** Enriched gene sets between high and low score groups in ccRCC using GSEA. **(D)** Kaplan-Meier curves to compare disease-free survival of low-risk and high-risk groups. The Kaplan-Meier method was used to draw survival curves, and the log-rank test was performed to evaluate survival difference with the best cut-off value.

MCM7 is up-regulated in lung adenocarcinoma and is associated with poor prognosis (44). The up-regulated level of MCM7 is a useful biomarker in the early diagnosis of gastric cancer (45). Knockdown of MCM7 can inhibit the proliferation of gastric cancer cells (46). Inhibition of MCM7 can promote autophagy and apoptosis of skin melanoma cells (47).

Some studies have investigated the expression of MCMs protein in RCC. Expression level of MCM2, MCM5, MCM6, and MCM7 were found to be overexpressed in RCC compared to paired adjacent normal tissue. In addition, a high-level of MCM2, MCM4 or MCM6 was also associated with poorer DFS for RCC patients (48). MCM5 promoted the proliferation of RCC cells and correlates with the progression and prognosis of RCC patients (39). Two studies suggested that MCM2 can be used as a proliferation marker in RCC (49, 50). However, these studies contained all histological types of RCC, including ccRCC, chromophobe RCC, papillary RCC and transitional cell carcinoma. Few studies have been specifically conducted on

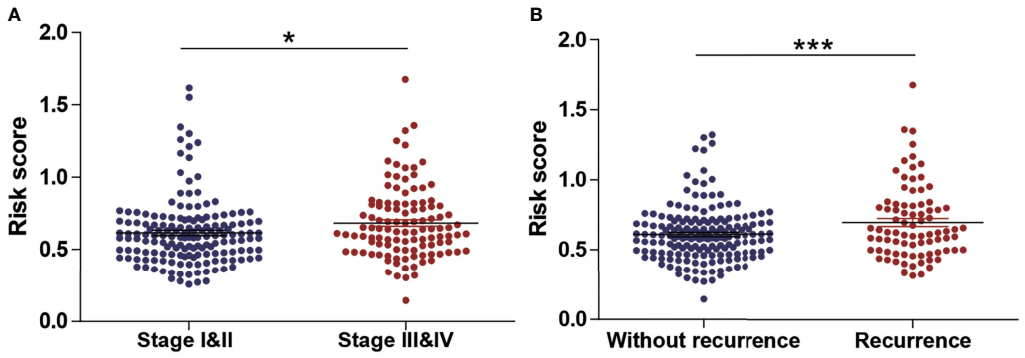



**FIGURE 8** | The Relationship Between risk score and Other Clinicopathological Characteristics. **(A, B)** The distribution of risk score in ccRCC patients with low and high stage **(A)**, recurrence and without recurrence **(B)**. NS, $p > 0.05$; *$p < 0.05$; ***$p < 0.001$.

MCMs expression in ccRCC. Only one study reported MCM6 as a potential prognostic marker in ccRCC (51). To the best of our knowledge, this is the first report investigating the expression levels, co-expression network, potential mechanism of MCM2–7 in ccRCC. This study may have important implications for improving the prognosis of ccRCC patients.

In the study, we analyzed the mRNA and protein expression of MCM2-7 in ccRCC, and the results showed that they were all up-regulated in ccRCC compared with normal tissues. The results of survival analysis demonstrated that a high level of MCM2, MCM3, MCM4, MCM6 and MCM7 were potential factors for the poor prognosis of ccRCC patients.

Next, GSEA analysis was performed to elucidate potential functions of MCM2-7 in ccRCC. Interestingly, for the MCM2-7 high-expression phenotype most gene sets were significantly enriched in the cell cycle pathways. The results indicated that MCM2-7 might influence the progression of ccRCC by regulating the cell cycle. The co-expressed gene of MCM2-7 was identified by WGCNA. The most highly rated gene ontology term of pathway was regulation of cell cycle, which is closely related to cancer growth. The result is plausible because the disturbance in cell cycle can lead to the progression of cancer by affecting chromosomal instability, genomic and proliferation. Other highly ranked terms included cell division, microtubule cytoskeleton organization involved in mitosis, DNA replication and positive regulation of cell cycle process.

Large-scale studies based on CRISPR/Cas9 gene loss-of-function screening provide conditions for studying whether tumor cell proliferation and survival depend on the existence or expression of specific genes. Most tumors have many genetic changes, some of which are considered to be driving factors for tumorigenesis (16, 52). DepMap uses the CRISPR-Cas9 tool to knock out each gene individually to identify candidate genes that are critical to tumor survival. The CERES algorithm was used to calculate the dependency scores of MCM2-7 genes, and the results showed that among the 6 genes, MCM7 was the most essential gene. Therefore, we knocked down MCM7 in ccRCC cells and observed its effect on cell proliferation. The results showed that knocking down MCM7 can inhibit the proliferation of ccRCC cells.

In the past few years, studies on single prognostic biomarkers in ccRCC have not been uncommon. However, a single biomarker lacks sufficient credibility to predict the prognosis of patients (53). Therefore, a predictive model composed of multiple biomarkers is necessary.

Using Lasso regression, we constructed a prognostic risk model based on two MCM genes (MCM4 and MCM6). Using this model, each CCRCC patient is assigned a risk score. Subsequently, the model was validated in the E-MTAB-1980-ccRCC validation set. In the validation group, the survival rate of patients with low and high scores was significantly different. The ROC curve and AUC show that the model performs well. In addition, a highly accurate predictive nomogram was constructed integrating the risk score and conventional clinical prognostic parameters including age, gender, and lymph. It could be used to predict the individual 1-year, 3-year and 5-year OS probability for ccRCC patients according to the risk score and other conventional clinical prognostic parameters.

In the study, we demonstrate the relationship between drug sensitivity and the relative expression levels of MCM2-7 using the GSCA. High MCM2-7 expression was associated with higher drug resistance to 17-AAG, RDEA119, Trametinib and selumetinib. RDEA119, Trametinib and selumetinib are MEK inhibitors, 17-AAG is HSP90 inhibitor. Studies have reported that the inhibition of MEK1 leads to a decrease in the phosphorylation of MCM2 and MCM3 (54). Drug sensitivity information can optimize the design of clinical trials by molecular stratification of the patient population.

## CONCLUSION

Overall, we revealed that high levels of MCM2, MCM3, MCM4, MCM6 and MCM7 were independent adverse prognostic factors. Knockdown of MCM7 can inhibit the proliferation of ccRCC cells. In addition, we have also established a clinically

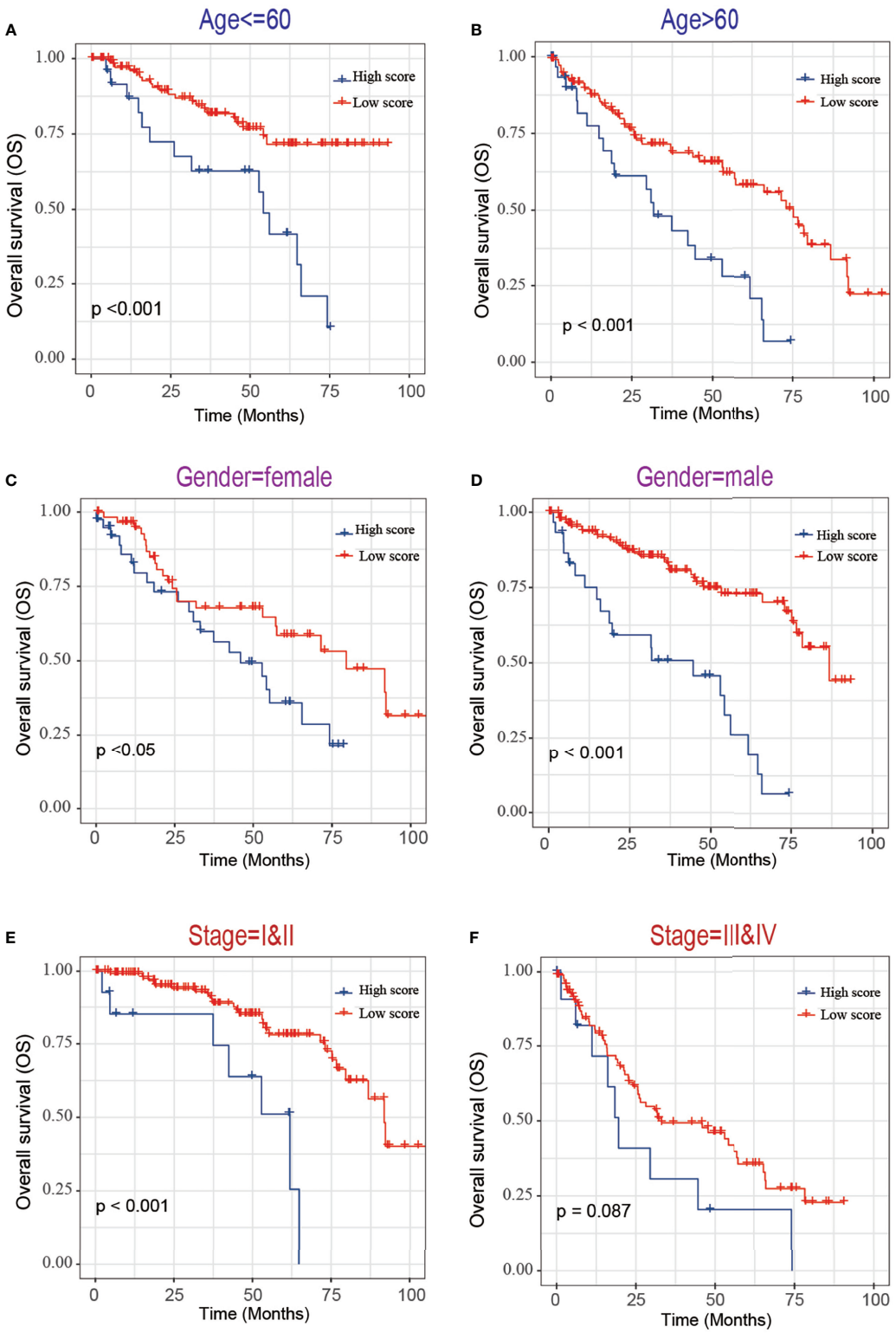



**FIGURE 9** | Kaplan-Maier survival curves of overall survival of ccRCC patients according to risk score model in different subgroups. **(A, B)** Prognosis analysis of the ccRCC patients with age<=60 **(A)** and age>60 **(B)** subgroup. **(C, D)** Prognosis analysis of the ccRCC patients with gender=female **(C)** and gender=male **(D)** subgroup. **(E, F)** Prognosis analysis of the ccRCC patients with stage=I&II **(E)** and stage=III& IV **(F)** subgroup. The Kaplan-Meier method was used to draw survival curves, and the log-rank test was performed to evaluate survival differences with the best cut-off value.

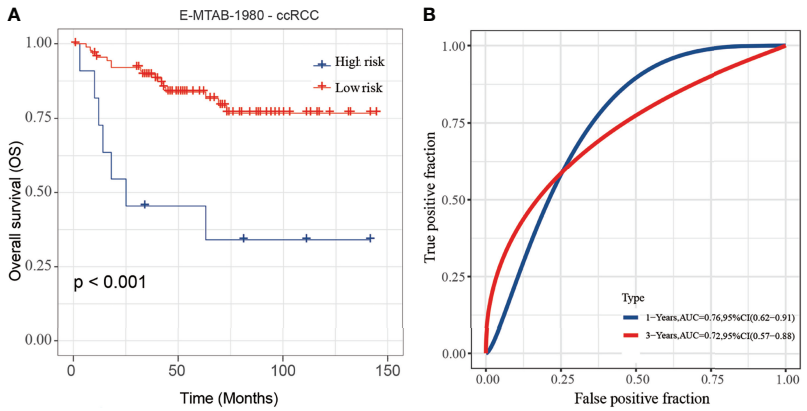



**FIGURE 10** | Validation of the risk score model by using E-MTAB-1980-ccRCC database. **(A, B)** The K-M plot **(A)** and 3-year survival ROC curve **(B)** of the risk score model by using E-MTAB-1980-ccRCC database.

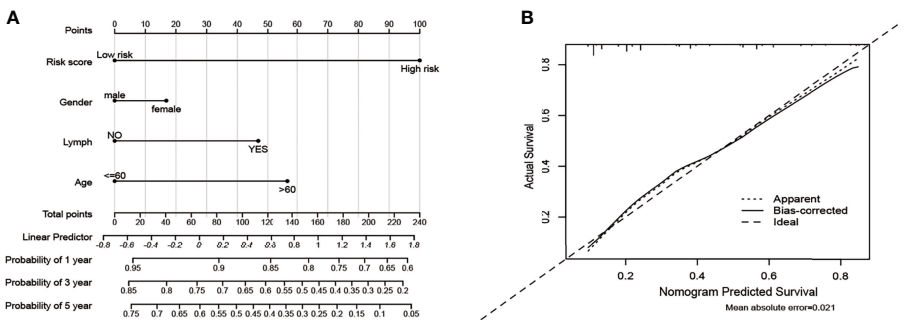



**FIGURE 11** | Nomogram and calibration plots for the prediction of outcomes in ccRCC patients based on risk score. **(A)** Nomogram for predicting 1-year, 3-year and 5-year events that combine clinical data with age, gender, lymph, and risk score. The line segment corresponding to each variable is marked with a scale, which represents the value range of the variable, and the length of the line segment reflects the contribution of the factor to the outcome event. The Point in the figure represents the individual score corresponding to each variable under different values, and the total score of the corresponding individual scores after all variables are taken. **(B)** The calibration plots for predicting overall survival.

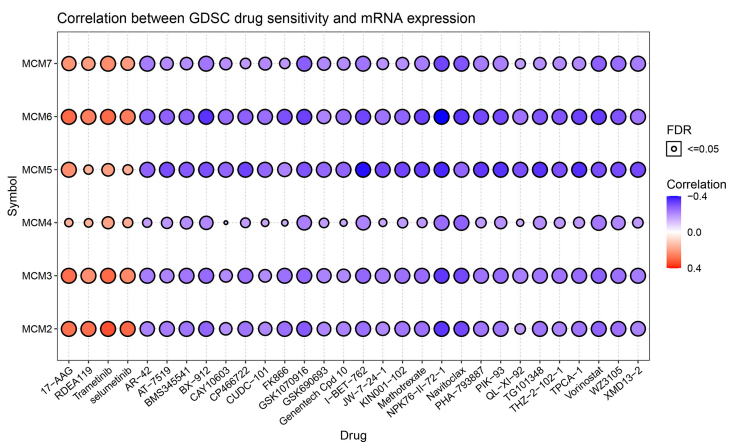



**FIGURE 12** | Drug sensitivity of the 6 MCM2-7 genes from GSCA. The correlations between the MCM2-7 expression and drugs. The positive spearman correlation coefficients indicate that high gene expression is resistant to the drug, and vice versa.

practical and easy-to-implement risk score model consisting of two MCM genes. This model can be a potential biomarker for predicting the prognosis of ccRCC patients.

## DATA AVAILABILITY STATEMENT

The original contributions presented in the study are included in the article/**Supplementary Material**. Further inquiries can be directed to the corresponding authors.

## ETHICS STATEMENT

The study was performed with the approval of the Ethics Committee of Fifth Hospital of Xiamen and complied with the Helsinki Declaration. Written informed consent was obtained from all patients involved.

## AUTHOR CONTRIBUTIONS

JZ and HZ drafted the manuscript. JZ performed the statistical analyses. QW and YW participated in the design of the study. QW and YW conceived of the study. HZ acquired the datasets. All authors read and approved the final manuscript.

## FUNDING

This work was supported by the Science and Technology Planning Projects of Xiamen Science & Technology Bureau (No. 3502Z20149025).

## SUPPLEMENTARY MATERIAL

The Supplementary Material for this article can be found online at: https://www.frontiersin.org/articles/10.3389/fonc.2021.782755/full#supplementary-material

## REFERENCES

1. Siegel RL, Miller KD, Jemal A. Cancer Statistics, 2019. *CA Cancer J Clin* (2019) 69(1):7–34. doi: 10.3322/caac.21551
2. Hsieh JJ, Purdue MP, Signoretti S, Swanton C, Albiges L, Schmidinger M, et al. Renal Cell Carcinoma. *Nat Rev Dis Primers* (2017) 3:17009. doi: 10.1038/nrdp.2017.9
3. Siegel RL, Miller KD, Jemal A. Cancer Statistics, 2020. *CA Cancer J Clin* (2020) 70(1):7–30. doi: 10.3322/caac.21590
4. Yang DC, Chen CH. Potential New Therapeutic Approaches for Renal Cell Carcinoma. *Semin Nephrol* (2020) 40(1):86–97. doi: 10.1016/j.semnephrol.2019.12.010
5. Simon NE, Schwacha A. The Mcm2-7 Replicative Helicase: A Promising Chemotherapeutic Target. *BioMed Res Int* (2014) 2014:549719. doi: 10.1155/2014/549719
6. Maine GT, Sinha P, Tye BK. Mutants of S. Cerevisiae Defective in the Maintenance of Minichromosomes. *Genetics* (1984) 106(3):365–85. doi: 10.1093/genetics/106.3.365
7. Vijayraghavan S, Schwacha A. The Eukaryotic Mcm2-7 Replicative Helicase. *Sub-Cellular Biochem* (2012) 62:113–34. doi: 10.1007/978-94-007-4572-8_7
8. Liu Z, Li J, Chen J, Shan Q, Dai H, Xie H, et al. MCM Family in HCC: MCM6 Indicates Adverse Tumor Features and Poor Outcomes and Promotes S/G2 Cell Cycle Progression. *BMC Cancer* (2018) 18(1):200. doi: 10.1186/s12885-018-4056-8
9. Favazza L, Chitale DA, Barod R, Rogers CG, Kalyana-Sundaram S, Palanisamy N, et al. Renal Cell Tumors With Clear Cell Histology and Intact VHL and Chromosome 3p: A Histological Review of Tumors From the Cancer Genome Atlas Database. *Modern Pathol an Off J United States Can Acad Pathol Inc* (2017) 30(11):1603–12. doi: 10.1038/modpathol.2017.72
10. Wang S, Xiang T, Yu L, Wen J, Liu F, Yang D, et al. Novel Molecular Subtypes and Related Score Based on Histone Acetylation Modification in Renal Clear Cell Carcinoma. *Front Cell Dev Biol* (2021) 9:668810. doi: 10.3389/fcell.2021.668810
11. Wang Q, Ye Y, Lin R, Weng S, Cai F, Zou M, et al. Analysis of the Expression, Function, Prognosis and Co-Expression Genes of DDX20 in Gastric Cancer. *Comput Struct Biotechnol J* (2020) 18:2453–62. doi: 10.1016/j.csbj.2020.09.002
12. Yuan H, Yan M, Zhang G, Liu W, Deng C, Liao G, et al. CancerSEA: A Cancer Single-Cell State Atlas. *Nucleic Acids Res* (2019) 47(D1):D900–8. doi: 10.1093/nar/gky939
13. Zheng R, Wan C, Mei S, Qin Q, Wu Q, Sun H, et al. Cistrome Data Browser: Expanded Datasets and New Tools for Gene Regulatory Analysis. *Nucleic Acids Res* (2019) 47(D1):D729–35. doi: 10.1093/nar/gky1094
14. Meyers RM, Bryan JG, McFarland JM, Weir BA, Sizemore AE, Xu H, et al. Computational Correction of Copy Number Effect Improves Specificity of CRISPR-Cas9 Essentiality Screens in Cancer Cells. *Nat Genet* (2017) 49(12):1779–84. doi: 10.1038/ng.3984
15. Tsherniak A, Vazquez F, Montgomery PG, Weir BA, Kryukov G, Cowley GS, et al. Defining a Cancer Dependency Map. *Cell* (2017) 170(3):564–76.e516. doi: 10.1016/j.cell.2017.06.010
16. Shi B, Ding J, Qi J, Gu Z. Characteristics and Prognostic Value of Potential Dependency Genes in Clear Cell Renal Cell Carcinoma Based on a Large-Scale CRISPR-Cas9 and RNAi Screening Database DepMap. *Int J Med Sci* (2021) 18(9):2063–75. doi: 10.7150/ijms.51703
17. Schwacha A, Bell SP. Interactions Between Two Catalytically Distinct MCM Subgroups Are Essential for Coordinated ATP Hydrolysis and DNA Replication. *Mol Cell* (2001) 8(5):1093–104. doi: 10.1016/S1097-2765(01)00389-6
18. Ramnath N, Hernandez FJ, Tan DF, Huberman JA, Natarajan N, Beck AF, et al. MCM2 Is an Independent Predictor of Survival in Patients With Non-Small-Cell Lung Cancer. *J Clin Oncol Off J Am Soc Clin Oncol* (2001) 19(22):4259–66. doi: 10.1200/JCO.2001.19.22.4259
19. Zhang X, Teng Y, Yang F, Wang M, Hong X, Ye LG, et al. MCM2 Is a Therapeutic Target of Lovastatin in Human Non-Small Cell Lung Carcinomas. *Oncol Rep* (2015) 33(5):2599–605. doi: 10.3892/or.2015.3822
20. Hanna-Morris A, Badvie S, Cohen P, McCullough T, Andreyev HJ, Allen-Mersh TG. Minichromosome Maintenance Protein 2 (MCM2) Is a Stronger Discriminator of Increased Proliferation in Mucosa Adjacent to Colorectal Cancer Than Ki-67. *J Clin Pathol* (2009) 62(4):325–30. doi: 10.1136/jcp.2007.054643
21. Luhtala S, Haapaniemi T, Staff S, Isola J. Fluoro-Chromogenic Labelling for Detection of MCM2 to Assess Proliferation Activity in HER2-Amplified Breast Carcinomas. *Appl Immunohistochem Mol Morphol AIMM* (2020) 28(3):175–86. doi: 10.1097/PAI.0000000000000716
22. Issac MSM, Yousef E, Tahir MR, Gaboury LA. MCM2, MCM4, and MCM6 in Breast Cancer: Clinical Utility in Diagnosis and Prognosis. *Neoplasia (New York NY)* (2019) 21(10):1015–35. doi: 10.1016/j.neo.2019.07.011
23. Lau KM, Chan QK, Pang JC, Li KK, Yeung WW, Chung NY, et al. Minichromosome Maintenance Proteins 2, 3 and 7 in Medulloblastoma: Overexpression and Involvement in Regulation of Cell Migration and Invasion. *Oncogene* (2010) 29(40):5475–89. doi: 10.1038/onc.2010.287
24. Gao Z, Man X, Li Z, Bi J, Liu X, Li Z, et al. PLK1 Promotes Proliferation and Suppresses Apoptosis of Renal Cell Carcinoma Cells by Phosphorylating MCM3. *Cancer Gene Ther* (2020) 27(6):412–23. doi: 10.1038/s41417-019-0094-x

25. Li HT, Wei B, Li ZQ, Wang X, Jia WX, Xu YZ, et al. Diagnostic and Prognostic Value of MCM3 and Its Interacting Proteins in Hepatocellular Carcinoma. *Oncol Lett* (2020) 20(6):308. doi: 10.3892/ol.2020.12171
26. Maiorano D, Lutzmann M, Méchali M. MCM Proteins and DNA Replication. *Curr Opin Cell Biol* (2006) 18(2):130–6. doi: 10.1016/j.ceb.2006.02.006
27. Stewart PA, Khamis ZI, Zhau HE, Duan P, Li Q, Chung LWK, et al. Upregulation of Minichromosome Maintenance Complex Component 3 During Epithelial-to-Mesenchymal Transition in Human Prostate Cancer. *Oncotarget* (2017) 8(24):39209–17. doi: 10.18632/oncotarget.16835
28. Chevalier S, Blow JJ. Cell Cycle Control of Replication Initiation in Eukaryotes. *Curr Opin Cell Biol* (1996) 8(6):815–21. doi: 10.1016/S0955-0674(96)80082-2
29. Huang XP, Rong TH, Wu QL, Fu JH, Yang H, Zhao JM, et al. MCM4 Expression in Esophageal Cancer From Southern China and its Clinical Significance. *J Cancer Res Clin Oncol* (2005) 131(10):677–82. doi: 10.1007/s00432-005-0011-6
30. Aaberg TM, Covington KR, Tsai T, Shildkrot Y, Plasseraud KM, Alsina KM, et al. Gene Expression Profiling in Uveal Melanoma: Five-Year Prospective Outcomes and Meta-Analysis. *Ocular Oncol Pathol* (2020) 6(5):360–7. doi: 10.1159/000508382
31. Zheng R, Lai G, Li R, Hao Y, Cai L, Jia J. Increased Expression of MCM4 Is Associated With Poor Prognosis in Patients With Hepatocellular Carcinoma. *J Gastrointest Oncol* (2021) 12(1):153–73. doi: 10.21037/jgo-20-574
32. Kikuchi J, Kinoshita I, Shimizu Y, Kikuchi E, Takeda K, Aburatani H, et al. Minichromosome Maintenance (MCM) Protein 4 as a Marker for Proliferation and Its Clinical and Clinicopathological Significance in non-Small Cell Lung Cancer. *Lung Cancer (Amsterdam Netherlands)* (2011) 72 (2):229–37. doi: 10.1016/j.lungcan.2010.08.020
33. Yu SY, Wang YP, Chang JY, Shen WR, Chen HM, Chiang CP. Increased Expression of MCM5 Is Significantly Associated With Aggressive Progression and Poor Prognosis of Oral Squamous Cell Carcinoma. *J Oral Pathol Med Off Publ Int Assoc Oral Pathol Am Acad Oral Pathol* (2014) 43(5):344–9. doi: 10.1111/jop.12134
34. Liu YZ, Wang BS, Jiang YY, Cao J, Hao JJ, Zhang Y, et al. MCMs Expression in Lung Cancer: Implication of Prognostic Significance. *J Cancer* (2017) 8 (18):3641–7. doi: 10.7150/jca.20777
35. Giaginis C, Giagini A, Tsourouflis G, Gatzidou E, Agapitos E, Kouraklis G, et al. MCM-2 and MCM-5 Expression in Gastric Adenocarcinoma: Clinical Significance and Comparison With Ki-67 Proliferative Marker. *Digestive Dis Sci* (2011) 56(3):777–85. doi: 10.1007/s10620-010-1348-5
36. Wang D, Li Q, Li Y, Wang H. The Role of MCM5 Expression in Cervical Cancer: Correlation With Progression and Prognosis. *BioMed Pharmacother* (2018) 98:165–72. doi: 10.1016/j.biopha.2017.12.006
37. Atwell RB, Sutton RH, Moodie EW. Pulmonary Changes Associated With Dead Filariae (Dirofilaria Immitis) and Concurrent Antigenic Exposure in Dogs. *J Comp Pathol* (1988) 98(3):349–61. doi: 10.1016/0021-9975(88)90043-6
38. Zhang LL, Li Q, Zhong DS, Zhang WJ, Sun XJ, Zhu Y. MCM5 Aggravates the HDAC1-Mediated Malignant Progression of Lung Cancer. *Front Cell Dev Biol* (2021) 9:669132. doi: 10.3389/fcell.2021.669132
39. Gong B, Ma M, Yang X, Xie W, Luo Y, Sun T. MCM5 Promotes Tumour Proliferation and Correlates With the Progression and Prognosis of Renal Cell Carcinoma. *Int Urol Nephrol* (2019) 51(9):1517–26. doi: 10.1007/s11255-019-02169-3
40. Hotton J, Agopiantz M, Leroux A, Charra-Brunaud C, Marie B, Busby-Venner H, et al. Minichromosome Maintenance Complex Component 6 (MCM6) Expression Correlates With Histological Grade and Survival in Endometrioid Endometrial Adenocarcinoma. *Virchows Archiv an Int J Pathol* (2018) 472 (4):623–33. doi: 10.1007/s00428-017-2278-9
41. Vigouroux C, Casse JM, Battaglia-Hsu SF, Brochin L, Luc A, Paris C, et al. Methyl(R217)HuR and MCM6 Are Inversely Correlated and Are Prognostic Markers in Non Small Cell Lung Carcinoma. *Lung Cancer (Amsterdam Netherlands)* (2015) 89(2):189–96. doi: 10.1016/j.lungcan.2015.05.008
42. Xu J, Zhang S, You C, Huang S, Cai B, Wang X. Expression of Human MCM6 and DNA Topo II Alpha in Craniopharyngiomas and Its Correlation With Recurrence of the Tumor. *J Neuro-Oncol* (2007) 83(2):183–9. doi: 10.1007/s11060-006-9284-0
43. Helfenstein A, Frahm SO, Krams M, Drescher W, Parwaresch R, Hassenpflug J. Minichromosome Maintenance Protein (MCM6) in Low-Grade Chondrosarcoma: Distinction From Enchondroma and Identification of Progressive Tumors. *Am J Clin Pathol* (2004) 122(6):912–8. doi: 10.1309/G638TKNNG2CJUXWL
44. Wang H, Zhou C, Su B, Teng G, Zheng Y, Zhou X, et al. MCM7 Expression is Correlated With Histological Subtypes of Lung Adenocarcinoma and Predictive of Poor Prognosis. *Int J Clin Exp Pathol* (2017) 10(12):11747–53.
45. Yang JY, Li D, Zhang Y, Guan BX, Gao P, Zhou XC, et al. The Expression of MCM7 Is a Useful Biomarker in the Early Diagnostic of Gastric Cancer. *Pathol Oncol Res POR* (2018) 24(2):367–72. doi: 10.1007/s12253-017-0251-1
46. Kang W, Tong JH, Chan AW, Cheng AS, Yu J, To K. MCM7 Serves as a Prognostic Marker in Diffuse-Type Gastric Adenocarcinoma and siRNA-Mediated Knockdown Suppresses Its Oncogenic Function. *Oncol Rep* (2014) 31(5):2071–8. doi: 10.3892/or.2014.3094
47. Yang Y, Ma S, Ye Z, Zhou X. MCM7 Silencing Promotes Cutaneous Melanoma Cell Autophagy and Apoptosis by Inactivating the AKT1/mTOR Signaling Pathway. *J Cell Biochem* (2020) 121(2):1283–94. doi: 10.1002/jcb.29361
48. Zhong H, Chen B, Neves H, Xing J, Ye Y, Lin Y, et al. Expression of Minichromosome Maintenance Genes in Renal Cell Carcinoma. *Cancer Manag Res* (2017) 9:637–47. doi: 10.2147/CMAR.S146528
49. Mehdi MZ, Nagi AH, Naseem N. MCM - 2 and Ki - 67 as Proliferation Markers in Renal Cell Carcinoma: A Quantitative and Semi - Quantitative Analysis. *Int Braz J Urol Off J Braz Soc Urol* (2016) 42(6):1121–8. doi: 10.1590/s1677-5538.ibju.2015.0388
50. Dudderidge TJ, Stoeber K, Loddo M, Atkinson G, Fanshawe T, Griffiths DF, et al. Mcm2, Geminin, and KI67 Define Proliferative State and Are Prognostic Markers in Renal Cell Carcinoma. *Clin Cancer Res an Off J Am Assoc Cancer Res* (2005) 11(7):2510–7. doi: 10.1158/1078-0432.CCR-04-1776
51. Jang NR, Baek J, Ko Y, Song PH, Gu MJ. High MCM6 Expression as a Potential Prognostic Marker in Clear-Cell Renal Cell Carcinoma. *In Vivo (Athens Greece)* (2021) 35(1):299–306. doi: 10.21873/invivo.12259
52. Vogelstein B, Papadopoulos N, Velculescu VE, Zhou S, Diaz LA Jr., Kinzler KW. Cancer Genome Landscapes. *Science* (2013) 339(6127):1546–58. doi: 10.1126/science.1235122
53. Sankin A, Hakimi AA, Mikkilineni N, Ostrovnaya I, Silk MT, Liang Y, et al. The Impact of Genetic Heterogeneity on Biomarker Development in Kidney Cancer Assessed by Multiregional Sampling. *Cancer Med* (2014) 3(6):1485–92. doi: 10.1002/cam4.293
54. Najar MA, Aravind A, Dagamajalu S, Sidransky D, Ashktorab H, Smoot DT, et al. Hyperactivation of MEK/ERK Pathway by Ca(2+) /Calmodulin-Dependent Protein Kinase Kinase 2 Promotes Cellular Proliferation by Activating Cyclin-Dependent Kinases and Minichromosome Maintenance Protein in Gastric Cancer Cells. *Mol Carcinog* (2021) 60(11):769–83. doi: 10.1002/mc.23343


**Conflict of Interest:** The authors declare that the research was conducted in the absence of any commercial or financial relationships that could be construed as a potential conflict of interest.

**Publisher's Note:** All claims expressed in this article are solely those of the authors and do not necessarily represent those of their affiliated organizations, or those of the publisher, the editors and the reviewers. Any product that may be evaluated in this article, or claim that may be made by its manufacturer, is not guaranteed or endorsed by the publisher.

*Copyright © 2021 Zhang, Zhang, Wang and Wang. This is an open-access article distributed under the terms of the Creative Commons Attribution License (CC BY). The use, distribution or reproduction in other forums is permitted, provided the original author(s) and the copyright owner(s) are credited and that the original publication in this journal is cited, in accordance with accepted academic practice. No use, distribution or reproduction is permitted which does not comply with these terms.*

frontiers in Oncology

ORIGINAL RESEARCH
published: 09 March 2022
doi: 10.3389/fonc.2022.781932

# Adipogenic Transdifferentiation and Regulatory Factors Promote the Progression and the Immunotherapy Response of Renal Cell Carcinoma: Insights From Integrative Analysis

*Shuai Wang*[1†], *Xiyi Wei*[1†], *Chengjian Ji*[1†], *Yichun Wang*[1], *Xi Zhang*[1], *Rong Cong*[1] *and Ninghong Song*[1,2*]

[1] The State Key Lab of Reproductive Medicine, Department of Urology, The First Affiliated Hospital of Nanjing Medical University, Nanjing, China, [2] Department of Urology, The Affiliated Kezhou People's Hospital of Nanjing Medical University, Kezhou, China

OPEN ACCESS

**Edited by:**
Andrea Mari,
Careggi University Hospital, Italy

**Reviewed by:**
Carlo Augusto Mallio,
Campus Bio-Medico University, Italy
Anna Cadenar,
Careggi University Hospital, Italy

***Correspondence:**
Ninghong Song
songninghong@126.com

[†]These authors have contributed equally to this work

**Specialty section:**
This article was submitted to Genitourinary Oncology, a section of the journal Frontiers in Oncology

**Received:** 23 September 2021
**Accepted:** 09 February 2022
**Published:** 09 March 2022

**Citation:**
Wang S, Wei X, Ji C, Wang Y, Zhang X, Cong R and Song N (2022) Adipogenic Transdifferentiation and Regulatory Factors Promote the Progression and the Immunotherapy Response of Renal Cell Carcinoma: Insights From Integrative Analysis. Front. Oncol. 12:781932. doi: 10.3389/fonc.2022.781932

**Background:** Adipogenic transdifferentiation was an important carcinogenic factor in various tumors, while studies on its role in clear cell renal cell carcinoma (ccRCC) were still relatively few. This study aimed to investigate its prognostic value and mechanism of action in ccRCC.

**Methods:** Gene expression profiles and clinical data of ccRCC patients were obtained from The Cancer Genome Atlas database. Nonnegative matrix factorization was used for clustering. Gene set variation analysis (GSVA) and gene set enrichment analysis (GSEA) were used to analyze the pathways and biological process activities. single-sample GSEA (ssGSEA) was utilized to quantify the relative abundance of each immune cell. Tumor Immune Estimation Resource (TIMER) was used to evaluate the proportion of various immune infiltrating cells across diverse cancer types. Real-Time PCR was performed to examine the gene expression. R software was utilized to analyze the expression and prognostic role of genes in ccRCC.

**Results:** A total of 49 adipose-related genes (ARGs) were screened for differential expression between normal and ccRCC tissues. Based on differentially expressed ARGs, patients with ccRCC were divided into two adipose subtypes with different clinical, molecular, and pathway characteristics. Patients in cluster A exhibited more advanced pathological stages, higher expressions of RARRES2 and immune checkpoint genes, higher immune infiltration scores, and less nutrient metabolism pathways. Adipose differentiation index (ADI) was constructed according to the above ARGs and survival data, and its robustness and accuracy was validated in different cohorts. In addition, it was found that the expression of ARGs was associated with immune cell infiltration and immune checkpoint in ccRCC, among which GBP2 was thought to be the most relevant

gene to the tumor immune microenvironment and play a potential role in carcinogenesis and invasion of tumor cells.

**Conclusion:** Our analysis revealed the consistency of higher adipogenic transdifferentiation of tumor cells with worse clinical outcomes in ccRCC. The 16-mRNA signature could predict the prognosis of ccRCC patients with high accuracy. ARGs such as GBP2 might shed light on the development of novel biomarkers and immunotherapies of ccRCC.

**Keywords: adipogenic transdifferentiation, adipose-related gene, clear cell renal cell carcinoma, prognostic model, GBP2, immunotherapy**

## INTRODUCTION

Renal cell carcinoma (RCC) influences more than 400,000 individuals per year, accounting for approximately 2.2% of all cancer diagnoses and 1.8% of all cancer deaths worldwide (1). In 2021, approximately 76,000 cancer cases and 13,700 mortalities were estimated to occur in the United States (2). 16% of RCC patients would present with or develop distant metastases and have a 5-year survival rate of 11.6% according to the Surveillance, Epidemiology, and End Results (SEER) database (3).

RCC is categorized generally into two major groups: clear cell renal cell carcinoma (ccRCC) and non-clear cell renal cell carcinoma (non-ccRCC), among which ccRCC makes up about 70% of all cancers of the kidney (4). ccRCC is defined by malignant renal cells with a clear cytoplasm historically, derived from the epithelium of the renal tubules. ccRCC cells possessed an mixture of glycogen and lipid droplets in cytoplasm, accounting for their "clear cell" style under HE staining (5). Reports have shown that ccRCC cells were capable of pluripotent differentiation *in vitro* and underwent adipogenic differentiation preferentially *in vivo* in human patients (6). Meanwhile, lipid deposition in cancer cells promotes a selective advantage to cancer cells, especially in ccRCC (7). Considering that the adipogenic process might play a deleterious role in driving tumorigenesis in lipid-laden ccRCC, Tan et al. assessed the expression of adipokines in ccRCC and discovered the adipokine chemerin, which was encoded by the retinoic acid receptor responder 2 (RARRES2) gene (8). The functions of this chemerin were verified as inhibiting fatty acid oxidation, maintaining intracellular fatty acid levels, preventing ferroptosis, and promoting cellular adipogenic transdifferentiation (8, 9). Their research data suggested that obesity and tumor cells would promote the occurrence of ccRCC through the adipokine chemerin.

The purpose of this study was to explore the role of adipogenic transdifferentiation in the occurrence and development of ccRCC and develop a model to predict prognosis and therapeutic responses in ccRCC patients. Based on the clustering of genes encoding proteins secreted from brown and white adipocytes, we defined two adipose subtypes. Each adipose subtype corresponded to different clinical and molecular characteristics. We developed and validated a combined adipose-related gene (ARG) expression-based adipogenic differentiation index (ADI) for predicting the overall survival (OS) of ccRCC, which was worth getting validated prospectively and utilized in further clinical practice. In addition, we found out one key ARG—GBP2, which might be a potential biomarker in the prediction of the survival of ccRCC patients.

## METHODS

### Acquisition of Data Resource

Publicly available transcriptome data and somatic mutation information of patients with ccRCC were downloaded from The Cancer Genome Atlas (TCGA) database (https://portal.gdc.cancer.gov/), including 72 normal cases and 539 tumor cases. Meanwhile, corresponding clinical feature information of ccRCC were also acquired (**Table 1**). A list of 151 genes encoding 143 differentially regulated proteins secreted from brown and white adipocytes were collected from the previous research (10). We defined these genes as adipose-related genes (ARGs).

A dataset NIHMS1611472 in Excel format was acquired from the National Center for Biotechnology Information (NCBI) as a cohort for validating the prognostic potential of our model. This dataset was submitted by Braun et al. and included 1006 patients' clinical data and 311 tissue samples (11).

### Identification of Differentially Expressed ARGs

In the preprocessing of the raw data, the "*Limma*" package was used to correct the data and handle the repeated data. Wilcoxon test was applied to analyze the ARG expression profile in tumor samples compared with normal tissue controls. Adjusted $P < 0.05$ and $|\log2 \text{ fold changes (FC)}| > 1$ were used as the criteria for screening differentially expressed ARGs. All the above operations were carried out in R software (version 4.1.0).

### Establishment of Adipose Subtypes

As an unsupervised clustering algorithm, Nonnegative matrix factorization (NMF) was used to cluster the ccRCC samples (12). To select the best number of clustering, "Brunet" method was adopted. The number of iterations was 30. The point before the greatest variation in cophenetic values was considered as the optimal number of adipose subtypes. To assess the reliability of the clustering results, the "Kaplan-Meier" method was used to calculate the overall survival and median survival time for each subtype. The log-rank test with a criteria level of $P < 0.05$ was

**TABLE 1** | Clinical characteristics of clear cell renal cell carcinoma patients in TCGA database.

| Clinical features | Variables | Total (n = 539) | Percentages (%) |
|---|---|---|---|
| Age (year) | ≤65 | 353 | 65.49 |
| | >65 | 186 | 34.51 |
| Gender | Female | 186 | 34.51 |
| | Male | 353 | 65.49 |
| Histological grade | G1 | 14 | 2.60 |
| | G2 | 235 | 43.60 |
| | G3 | 207 | 38.40 |
| | G4 | 75 | 13.91 |
| | Gx | 5 | 0.93 |
| | Unknown | 3 | 0.56 |
| T classification | T1 | 278 | 51.58 |
| | T2 | 71 | 13.17 |
| | T3 | 179 | 33.21 |
| | T4 | 11 | 2.04 |
| Lymph nodes | N0 | 241 | 44.71 |
| | N1 | 16 | 2.97 |
| | NX | 282 | 52.32 |
| Distant metastasis | M0 | 428 | 79.41 |
| | M1 | 78 | 14.47 |
| | MX | 31 | 5.75 |
| | Unknown | 2 | 0.37 |
| Clinical stage | Stage I | 272 | 50.46 |
| | Stage II | 59 | 10.95 |
| | Stage III | 123 | 22.82 |
| | Stage IV | 82 | 15.21 |
| | Unknown | 3 | 0.56 |

applied to analyze the difference in survival between different clusters. Clinical features (T classification, lymph nodes, distant metastasis, clinical stage, histological grade, gender, age, and survival time) were also included in the comparison between adipose subtypes.

## Evaluation of Biological Process Activities and Immune Characteristics of Subtypes

To estimate the variation in pathways and biological process activities between different adipose subtypes, we performed gene set variation analysis (GSVA) with the gene sets of "c2.cp.kegg.v7.4.symbols" downloaded from the Molecular Signatures Database (MSigDB). Adjusted $P$ value < 0.05 and |log2FC| > 0.1 indicated a significant difference between two groups of data. The heatmap was drawn with "*pheatmap*" R packages. We applied single-sample gene set enrichment analysis (ssGSEA) to quantify the relative abundance of each immune cell in the ccRCC tumor microenvironment. The gene set was obtained from the research of Charoentong et al. (13), which provided a variety of human immune cell subtypes. We also utilized student's t-test to identify differential expression of immune checkpoint blockade genes between adipose subtypes.

## Construction of the ADI Based on ARGs

Univariate Cox regression analyses were conducted to find out candidate ARGs, of which expressions were related to the OS of ccRCC patients. Then, LASSO regression analysis was used to obtain several genes with the significant prognosis that could be an independent indicator. In the end, 16 ARGs were screened to construct the ADI, and a multivariable Cox proportional hazards model was used to calculate the risk coefficients of ARGs. The establishment of ADI based on a linear combination of the relative expression level of genes multiplied regression coefficients. After that, patients with ccRCC were stratified into the low risk and high risk groups according to the median ADI value as the risk cutoff value. Kaplan-Meier method was utilized to analyze the OS of these two groups, and log-rank test was used to evaluate the difference between low and high groups. To verify the prediction value of the model, we plotted receiver operating characteristic curves (ROCs). Finally, we validated our model on a dataset provided by another research (11).

## Evaluation of Modeling Gene Correlation and Function

To investigate the relationships of expression between the modeling genes and the immune checkpoint genes in ccRCC, correlation analysis was performed using Spearman's method. And we observed that the expression of GBP2 positively correlated with most immune checkpoint genes. Using data from Tumor Immune Estimation Resource (TIMER, http://timer.comp-genomics.org/), which was an open resource for evaluating the proportion of various immune infiltrating cells across diverse cancer types, we visualized the correlation between the $CD8^+$ T cell and the expression of GBP2 with the method of "quanTIseq". $P < 0.05$ was as the threshold, and the correlation value varied from -1 to 1, the larger the absolute value, the more relevant. Stratified analyses between clinical features and the expression of GBP2 were also investigated with the log-rank test respectively. Gene set enrichment analysis (GSEA) was

conducted using GSEA v4.0.3 (http://www.broadinstitute.org/gsea).

## RT-qPCR and External Validation of Expression Level

The proteomics data and clinical features of cancer patients from the Clinical Proteomic Tumor Analysis Consortium (CPTAC, https://proteomics.cancer.gov/programs/cptac) and the Human Protein Atlas database (HPA, https://www.proteinatlas.org/) were utilized to analyze the protein expression between ccRCC and normal tissues. The real time quantitative polymerase chain reaction (RT-qPCR) was performed for comparison of gene expressions in different ccRCC cell lines and tissues. The PCR run conditions for the detection of GBP2 were used as previously described (14). The primers applied for GBP2 were displayed follow: "Forward: CTATCTGCAATTACGCAGCCT; Reverse: TGTTCTGGCTTCTTGGGATGA".

## Statistical Analysis

R software (R version 4.1.0) was used to perform all statistical analyses and graphics. The associations of clinical features between different clusters or groups were examined by the chi-square test or Fisher's exact test. Differences between the two groups of samples were compared by the Wilcox test, while continuous variables were compared by Student's t-test. Kaplan-Meier method was utilized to analyze the survival curve, and the significance of the difference was determined by the log-rank test. Our scores with a $P$-value < 0.05 and Spearman correlation coefficient > 0.3 were considered to be statistically significant if not specifically stated.

# RESULT

## Identification of the ccRCC Characteristic of Adipogenic Transdifferentiation

To ascertain whether ccRCC was typified by accumulation of neutral lipids and adipogenic transdifferentiation, we firstly investigated the mRNA expression of RARRES2 gene between normal and ccRCC samples. Compared to normal kidney tissues, RARRES2 demonstrated higher expression in ccRCC tissues (**Figure 1A**). We next explored whether RARRES2 expression

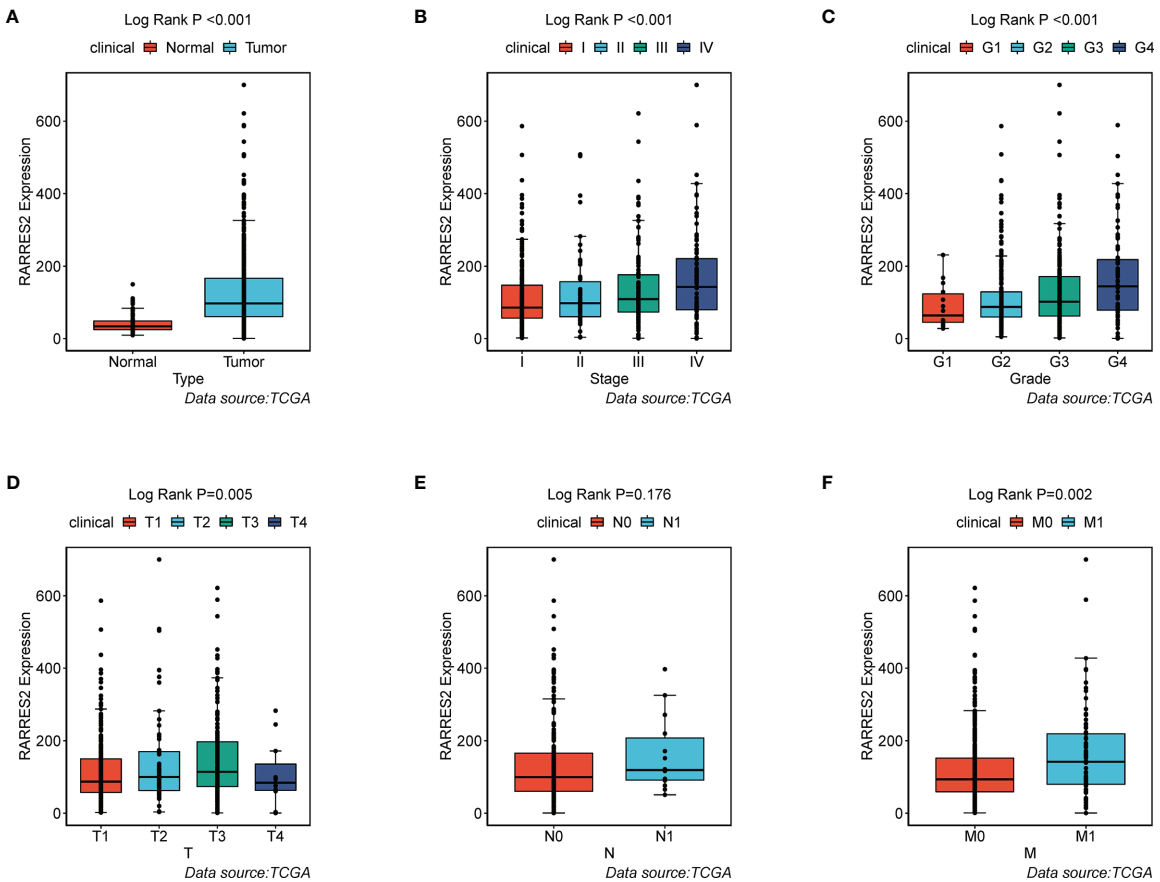



**FIGURE 1** | Association of RARRES2 mRNA expression with clinical parameters (data source: TCGA). **(A)** Type (wilcoxon test, $p < 0.001$); **(B)** Clinical stage (K-W test, $p < 0.001$); **(C)** Histological grade (K-W test, $p = 0.001$); **(D)** T classification (K-W test, $p = 0.005$); **(E)** Lymph nodes (wilcoxon test, $p = 0.176$); **(F)** Distant metastasis (wilcoxon test, $p = 0.002$).

was associated with clinical features. As was shown in **Figure 1B**, the expression of RARRES2 was correlated positively with the TNM stage of ccRCC patients ($p < 0.001$). There was a significant positive correlation between RARRES2 expression and the histological grade ($p = 0.001$), T classification ($p = 0.005$), distant metastasis ($p = 0.002$), while no significant correlation was found between RARRES2 expression and the lymph nodes ($p = 0.176$) (**Figures 1C–F**). And RARRES2 showed a consistent increase in gene expression and disease severity in all clinical characteristics other than lymph nodes stage or T4 stage.

## Identification of Differentially Expressed ARGs and Molecular Subtypes

A total of 49 ARGs were finally screened for differential expression between normal and ccRCC tissues. Compared to normal kidney tissues, 33 ARGs demonstrated markedly higher expression in ccRCC tissues (e.g., APOC1 and ENO2), while the rest were on the contrary (e.g., SFRP1 and DAG1) (**Figure 2A**). The above analyses indicated that the expression imbalance of ARGs played a crucial role in the occurrence, progression and adipogenic transdifferentiation of ccRCC. According to the cophenetic, dispersion and silhouette indicators, two clusters were eventually identified using NMF clustering (**Figures 2B, C**), including 169 cases in cluster A and 370 cases in cluster B. Then, we integrated the clinical information and found that patients in cluster A showed a significantly worse OS than cluster B (log-rank $p = 0.003$; **Figures 2D**). **Figure 2E** showed a heatmap displaying the clinicopathological features and expression distributions of differentially expressed ARGs. Furthermore, we explored the proportion of different levels of pathological stages in two subtypes, as well as the expression of RARRES2. And it turned out that patients in cluster A exhibited significantly more advanced clinical stages ($p = 0.009$) and a markedly higher RARRES2 expression ($p < 0.001$) than those in cluster B (**Figure 2F**).

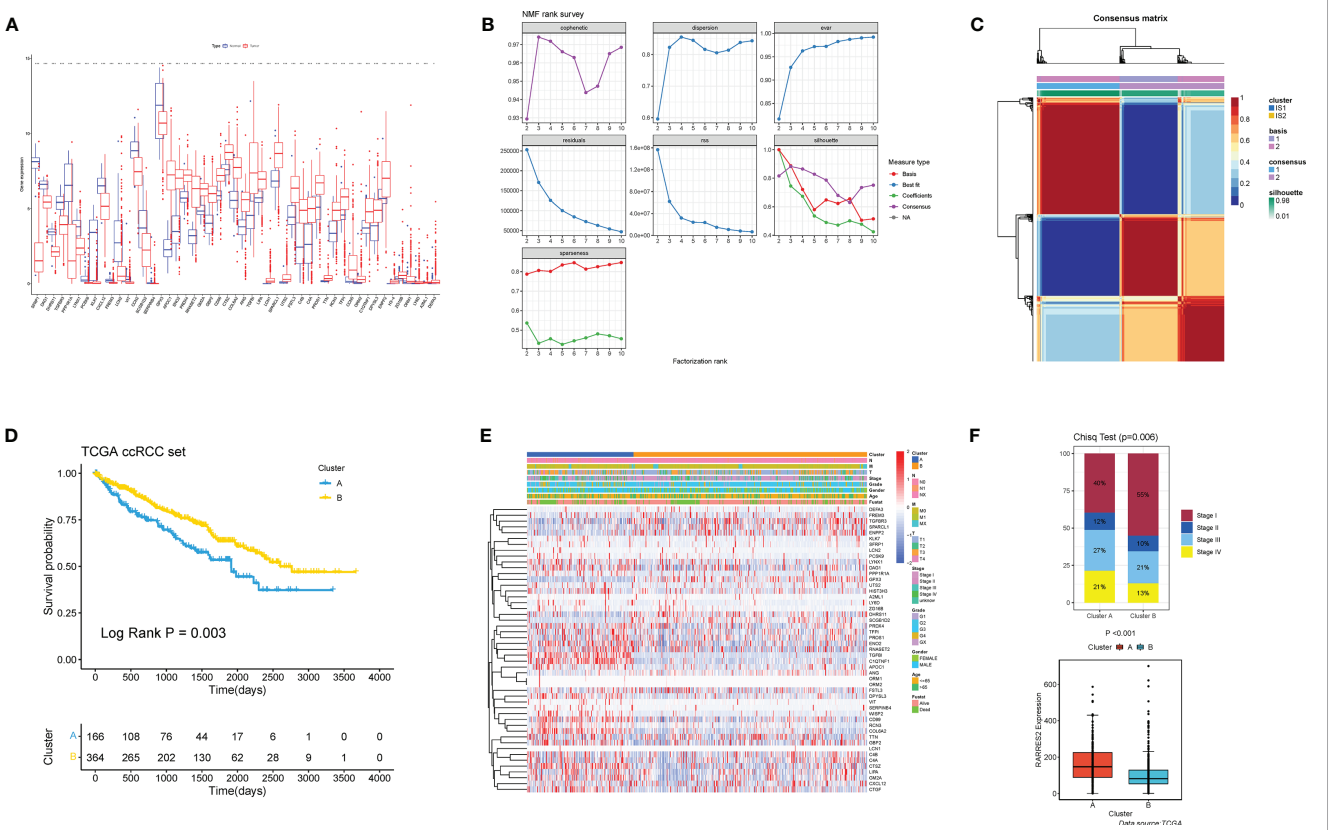



**FIGURE 2** | Nonnegative matrix factorization clustering identified two adipose subtypes based on differentially expressed ARGs. **(A)** The expression of 49 differentially expressed ARGs between normal tissues and ccRCC tissues. Tumor, red; Normal, blue. The upper and lower ends of the boxes represented interquartile range of values. The lines in the boxes represented median value. Adjusted $p < 0.05$ and |log2 fold changes (FC)| > 1 were used as the criteria for screening differentially expressed ARGs. The asterisks represented the statistical p value (*$p < 0.05$, **$p < 0.01$, ***$p < 0.001$). **(B)** The cophenetic, RSS and dispersion distributions with rank = 2–10; combining these indicators results in the optimal number of clusters of 2. **(C)** Consensus map of NMF clustering. **(D)** Survival analyses for the two adipose subtypes based on 530 patients with ccRCC from TCGA cohorts including 166 cases in cluster A, and 364 cases in cluster B Kaplan-Meier curves with log-rank $p = 0.003$ showed a significant survival difference among two adipose clusters. The cluster A showed significantly worse overall survival than the cluster B. **(E)** NMF clustering of 49 ARGs in the TCGA ccRCC cohort. The adipose subtypes, TNM stages, clinical stages, survival status and age were used as patient annotations. Red represented high expression of ARGs and blue represented low expression. **(F)** Proportion of cases with different stages (chi-square test, $p = 0.006$) and difference of RARRES2 mRNA expression (wilcoxon test, $p < 0.001$) in the two adipose subtypes.

## Biological and Immune-Related Features in Adipose Subtypes

To investigate the molecular differences in participating KEGG pathways between the two subtypes, we utilized GSVA to analyze the enriched pathways in each cluster. Some of the results were shown in **Figure 3A** (**Table S1** for more details). Cluster A was enriched with less nutrient metabolism pathways, for instance, metabolisms of pyruvate (adjusted *p* value = 2.05E-15), glycine, serine and threonine (adjusted *p* value = 1.67E-12), and fatty acid (adjusted *p* value = 9.99E-26). In addition, we noticed that PPAR signaling pathway also presented less in cluster A (adjusted *p* value = 3.95E-16), which was involved biological processes such as lipid metabolism gene expression, lipid oxidation, and promotion of adipocyte differentiation. ssGSEA was performed to analyze the proportion of 23 kinds of immune cells in immune infiltration microenvironment between adipose subtypes. As was shown in **Figure 3B**, all immune cells have some degree of difference between samples in cluster A and B, except the CD56dim natural killer cell, Eosinophil, and Immature dendritic cell. ccRCC patients in cluster A had higher scores in 19 kinds of immune cells, among which Myeloid-derived suppressor cells (MDSC), Monocyte and Activated CD8 T cell appeared to be the top three cell types. Previous studies have shown that immune checkpoints (ICPs) played a vital role in tumor immunity. Therefore, we explored the expression of ICPs in two clusters. Compared to samples in cluster B, 25 ICP genes demonstrated markedly higher expression in cluster A (e.g., CTLA4 and PDCD1), while 6 expressed significantly less (e.g., BTN2A1 and ADORA2A) (**Figure 3C**). These results indicated that immune surveillance of T cells was repressed in cluster A patients, thus promoting the growth of tumor.

## Construction of ADI Model Based on ARGs

For these differentially expressed ARGs and survival data, a univariate Cox regression was performed, and 18 genes with

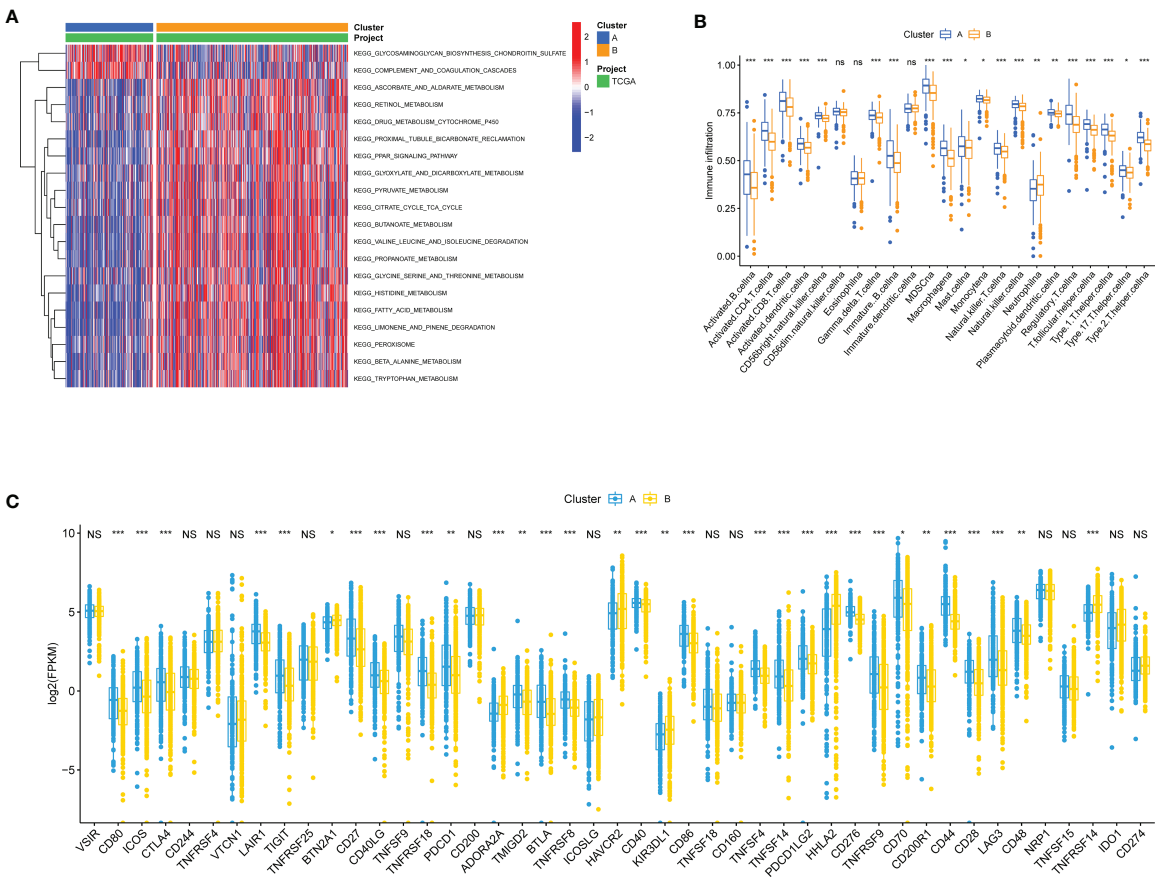



**FIGURE 3** | Biological and immune-related characteristics in different clusters. **(A)** GSVA showing the activation states of biological pathways in two clusters. The heatmap was used to visualize these biological processes, and red represented activated pathways and blue represented inhibited pathways. **(B)** The abundance of each TME infiltrating cell in cases in two clusters. The upper and lower ends of the boxes represented interquartile range of values. The lines in the boxes represented median value, and colorful dots showed outliers. The asterisks represented the statistical *p* value (*$p < 0.05$, **$p < 0.01$, ***$p < 0.001$; ns, Not Statistically Significant). **(C)** The expression of ICP mRNAs in two clusters. The upper and lower ends of the boxes represented interquartile range of values. The lines in the boxes represented median value. The asterisks represented the statistical *p* value (*$p < 0.05$, **$p < 0.01$, ***$p < 0.001$; NS, Not Statistically Significant).

significant prognostic differences were identified (**Figure 4A**). We then utilized a Lasso-Cox regression model to further select the ARGs with the highest prognostic value. (**Figure 4B**) Finally, a prognosis signature based on the personalized expression level of 16 ARGs was constructed. Using the coefficients obtained from the Lasso Cox regression model, we defined an index–ADI to calculate the risk score of each patient. The formula was as follows:

$$ADI = (-0.124031) \times \exp^{TGFBR3} + 0.001859 \times \exp^{PPP1R1A} + 1.167980 \times \exp^{SERPINB4} + 0.004887 \times \exp^{ENO2} + 0.003922 \times \exp^{RNASET2} + 0.004879 \times \exp^{GBP2} + (-0.006205) \times \exp^{CD99} + 0.000408 \times \exp^{COL6A2} + 0.0000187 \times \exp^{TGFBI} + (-0.008569 \times \exp^{LIPA} + (-0.000721) \times \exp^{SPARCL1} + 0.006734 \times \exp^{RCN3} + (-0.011232) \times \exp^{WISP2} + 0.004721 \times \exp^{C1QTNF1} + 0.018172 \times \exp^{DPYSL3} + 0.0000054 \times \exp^{ENPP2}$$

Based on the median ADI, ccRCC patients with ADIs higher than the median were defined as a high-risk group, and ADIs lower than the median were defined as a low-risk group. The ADI distribution, survival time and survival status, and expression of 16 genes in the training cohort were shown in **Figures 4C** and **D**. Samples with high ADIs had significantly lower OS than those with low ADIs, indicating that the patients with high ADIs had a worse prognosis. High expression of 12 ARGs (PPP1R1A, SERPINB4, ENO2, RNASET2, GBP2, COL6A2, COL6A2, TGFBI, RCN3, WISP2, C1QTNF1, DPYSL3, and ENPP2) was associated with high risk, consistent with their positive coefficients in our formula, so these genes were considered risk factors.

## Validation of the Robustness of the Model in Both Internal and External Cohorts

60% of the 530 TCGA preprocessed samples were randomly selected as the training cohort to construct the above model. As was revealed in the Kaplan-Meier (KM) curve, patients in the high-risk group had a worse prognosis compared to those in the low-risk group in the training cohort (log-rank $p < 0.001$) (**Figure 5A**). The rest 40% samples were taken as the testing cohort. We applied the same model and coefficients as the training cohort to generate the ADI of each patient in both the testing cohort and the whole cohort from TCGA. Consistent with the results from the training set, significantly higher survival rates were observed in low-risk groups in comparison with the high-risk ones, both in the testing cohort (log-rank $p < 0.001$; **Figure 5B**), and the whole cohort (log-rank $p < 0.001$; **Figure 5C**). The survival time-dependent receiver operating characteristic (ROC) curves in the training, testing, and whole cohorts were also performed. **Figures 5D–F** exhibited the

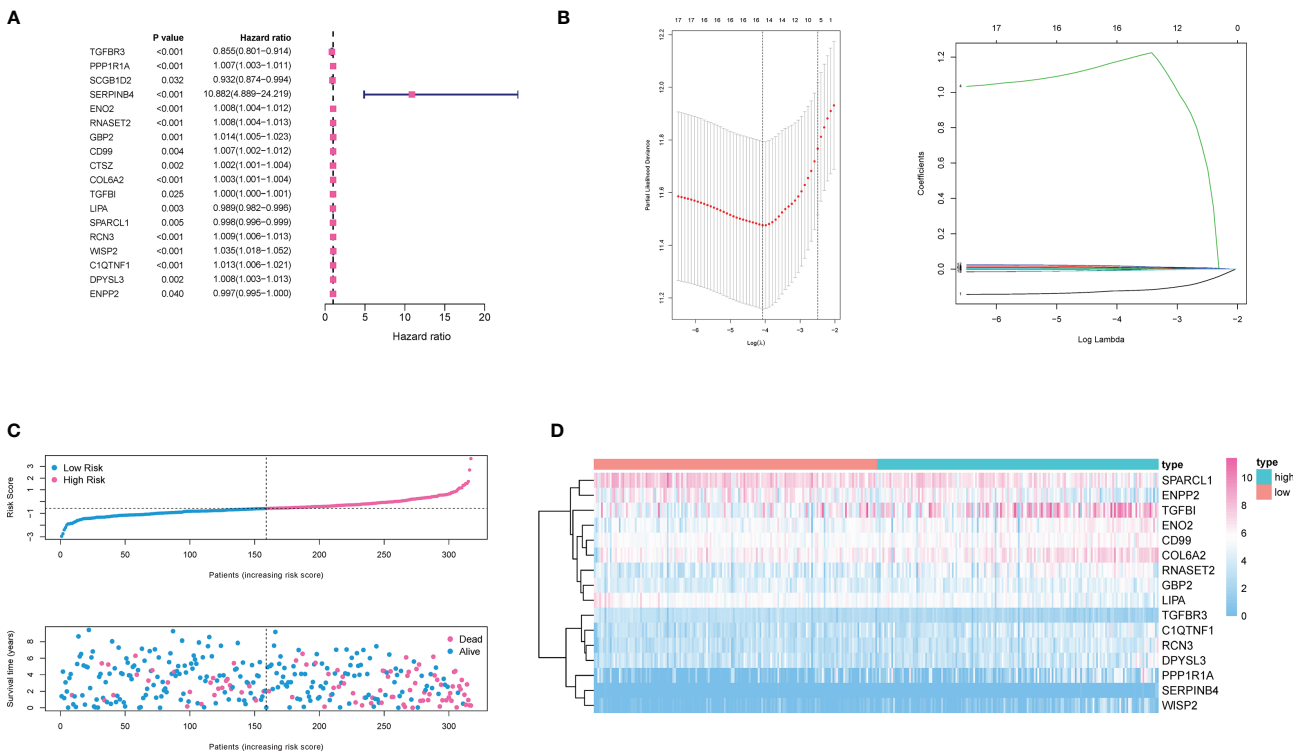



**FIGURE 4** | Construction of ADI model. **(A)** 18 genes associated with OS of ccRCC patients were obtained through univariate Cox regression analysis. **(B)** A 16-mRNA signature was constructed by LASSO Cox regression. **(C)** Prognostic analysis of 16-gene signature in the training set. The dotted line represented the median risk score and divided the patients into low- and high-risk group. More dead patients corresponded to the higher risk score according to the curve of risk score and survival status of the patients. **(D)** Heatmap of the expression profiles of the 16 prognostic genes in low- and high-risk group.

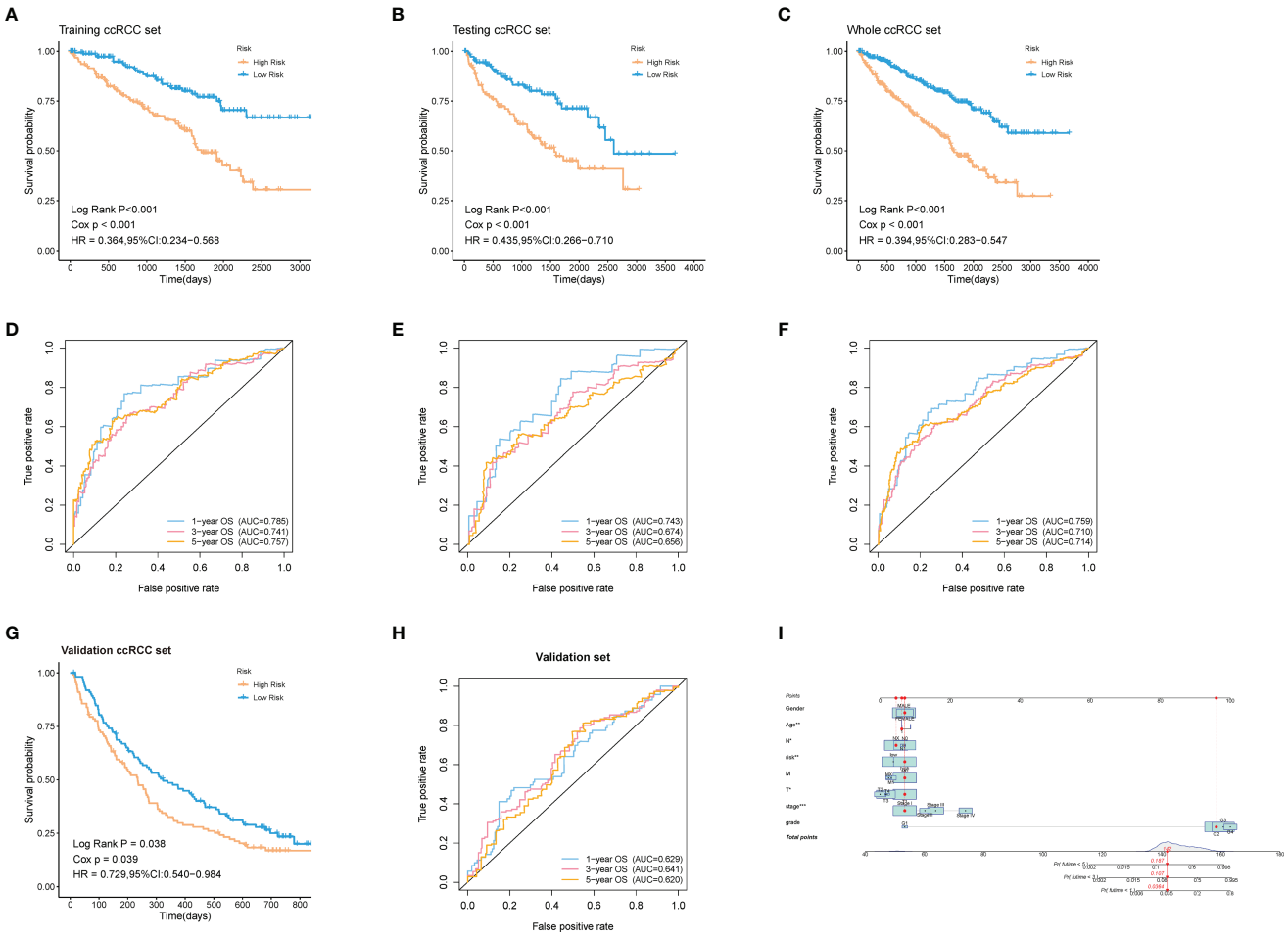



**FIGURE 5** | Validation of the robustness of the model in both internal and external cohorts. **(A–C, G)** Kaplan–Meier survival analysis of the training ccRCC set, testing ccRCC set, whole ccRCC set, and validation set (NIHMS1611472 from NCBI). The survival rate of the patients in the high-risk group was significantly lower than those in the low-risk group respectively. **(D–F, H)** Time-dependent ROC analysis of the training ccRCC set, testing ccRCC set, whole ccRCC set, and validation set (NIHMS1611472 from NCBI). The AUC suggested that the prognostic accuracy of the 16-mRNA signatures in the discovery set was robust and accurate. **(I)** The nomogram for predicting proportion of patients with 3- or 5-year OS. The asterisks represented the statistical p value (*p < 0.05, **p < 0.01, ***p < 0.001).

prognostic classification efficiency in three cohorts at 1-year, 3-years, and 5-years respectively. The areas under the curve (AUC) of the 1 year, 3 years, and 5 years ROC curve in the training cohort were 0.785, 0.741, and 0.757, with 0.743, 0.674, and 0.656 in the testing cohort and 0.759, 0.710, and 0.714 in the whole cohort. Using data from the NIHMS1611472 dataset, we also drew KM survival curve distribution of 16 ARGs signature (**Figure 5G**) and performed the ROC analysis of the prognostic classification of the risk score (**Figure 5H**). The AUC for 1-year, 3-years, and 5-years were 0.629, 0.641, and 0.620. There was a significant difference between the high- and low-risk groups (log-rank $p = 0.038$). The results of validation of the robustness of our model in both internal and external cohorts advocated that our risk model was accurate in the forecasting of survival. In addition, a nomogram including our risk signature and some clinic-pathological factors was established to improve clinical feasibility (**Figure 5I**).

## Survival Analysis in Stratification of Different Clinical Features

To explore whether patients at different risks presented a distinct prognosis, patients were further stratified into subgroups of age ≤ 65 and age> 65 years old, male and female, histological grade I/II and grade III/IV, stage I/II and stage III/IV, T1/2 and T3/4, N0 and N1, M0 and M1. As was shown in **Figure 6**, except for the subgroup of histological grade I/II (log-rank $p = 0.23$), clinical stage I/II (log-rank $p = 0.112$), and N1 (log-rank $p = 0.809$), patients in high-risk group showed a worse prognosis than those in low-risk groups. This further indicated that our model still had a strong predictive ability in different clinical signs.

## Immune-Related Feature and Prognostic Value of the Key Modeling Gene

During the growth and progression of tumors, they often exhibited immunosuppression. Considered as the main

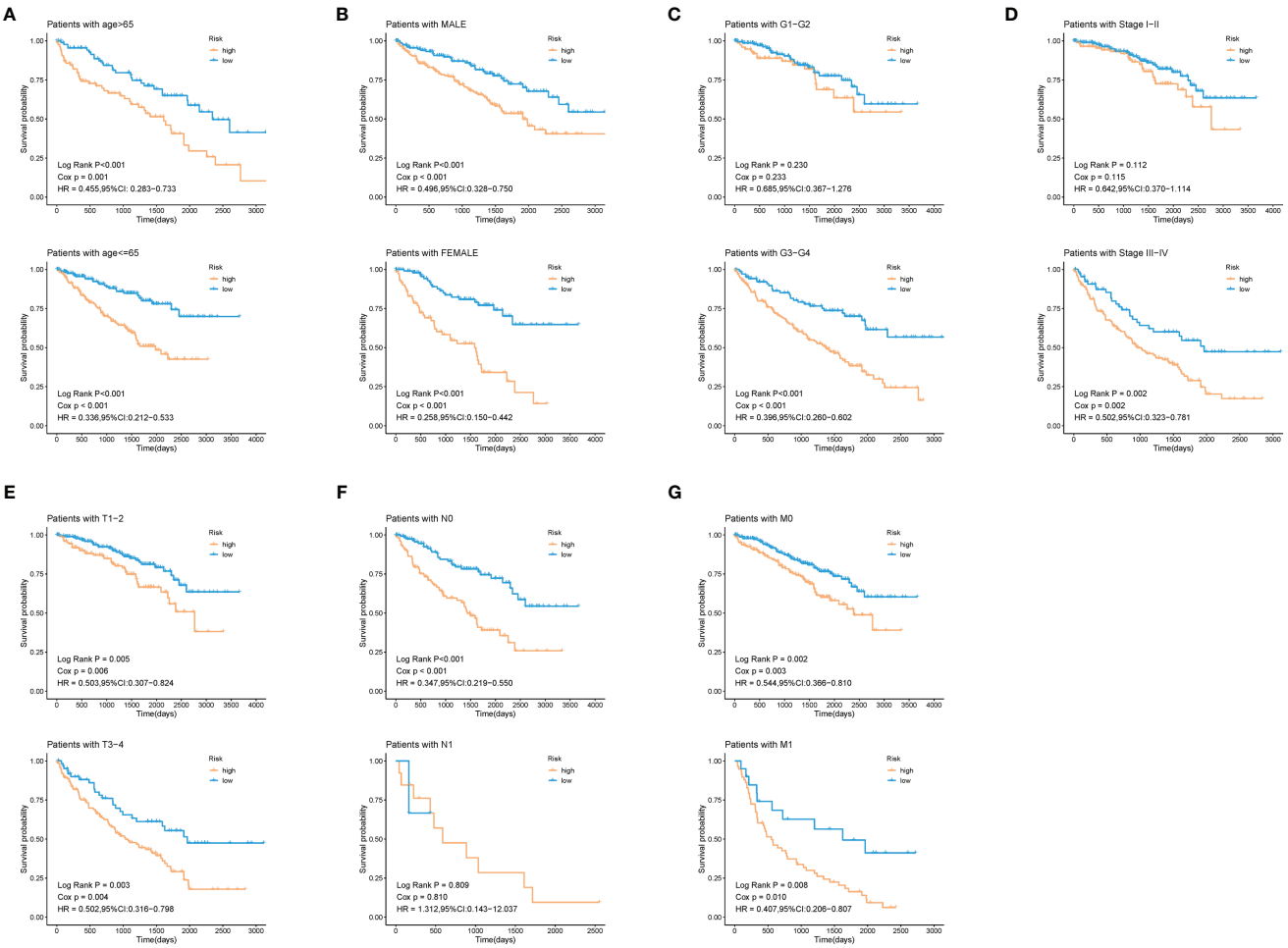



**FIGURE 6** | Validation of the prognostic efficacy of our model under the stratifications of different clinical parameters. **(A)** age > 65 and age <=65, **(B)** male and female, **(C)** histological grade 1/2 and 3/4, **(D)** clinical stage I/II and III/IV, **(E)** T 1/2 and 3/4, **(F)** N 0 and 1, **(G)** M 0 and 1.

mechanism of tumor immune resistance, the immune checkpoint pathways allowed tumors to negatively regulate T cells to escape immune surveillance. As a promising immunotherapy, the immune checkpoint blockade has been applied to various tumors including ccRCC. Therefore, we investigated the correlation between expressions of ICPs and risk scores and expressions of our modeling genes by using Pearson correlation analysis in TCGA cohort (**Figure 7A**). And we noticed that one gene GBP2 was correlated positively with the expressions of all listed immune checkpoint except CD155 or OX40. Speculating that GBP2 might play a role in the tumor microenvironment, we analyzed its correlation with the $CD8^+$ T cells, the most potent effector cell in immunotherapy. As was shown in **Figure 7B**, GBP2 and $CD8^+$ T cell represented good correlation in ccRCC samples ($R = 0.65$, $p < 0.05$). Similarly, the significant correlation coefficients of GBP2 expression with classical immune checkpoints PD-1 and PD-L1 were presented in **Figure 7C**. We also evaluated the relationship between GBP2 expression and clinical characteristic subtypes in TCGA ccRCC samples. Other than age, the expression of GBP2 was significantly higher in subgroups with more severe clinical predictors, including histological grade (log-rank $p < 0.001$), clinical stage (log-rank $p < 0.001$), T classification (log-rank $p < 0.001$), lymph nodes (log-rank $p = 0.016$), and distant metastasis (log-rank $p = 0.017$) (**Figure 7D**). GSEA was utilized to biological changes associated with the expression of GBP2. **Figures 8A–F** revealed the markedly different signaling pathways, including the TNFα signaling *via* NF-κB, IL6-JAK-STAT3 signaling, KRAS signaling, PI3K-AKT-mTOR signaling, apoptosis, and p53 pathway. These were primarily correlated with carcinogenesis, invasion, and the immune microenvironment of tumor cells.

## Validation of the Role of GBP2 at the Translational Level and Through Experiments

The HPA database was used to confirm the protein expression between ccRCC and normal tissues. The protein expression of GBP2 was higher in the tumor tissues compared to the normal

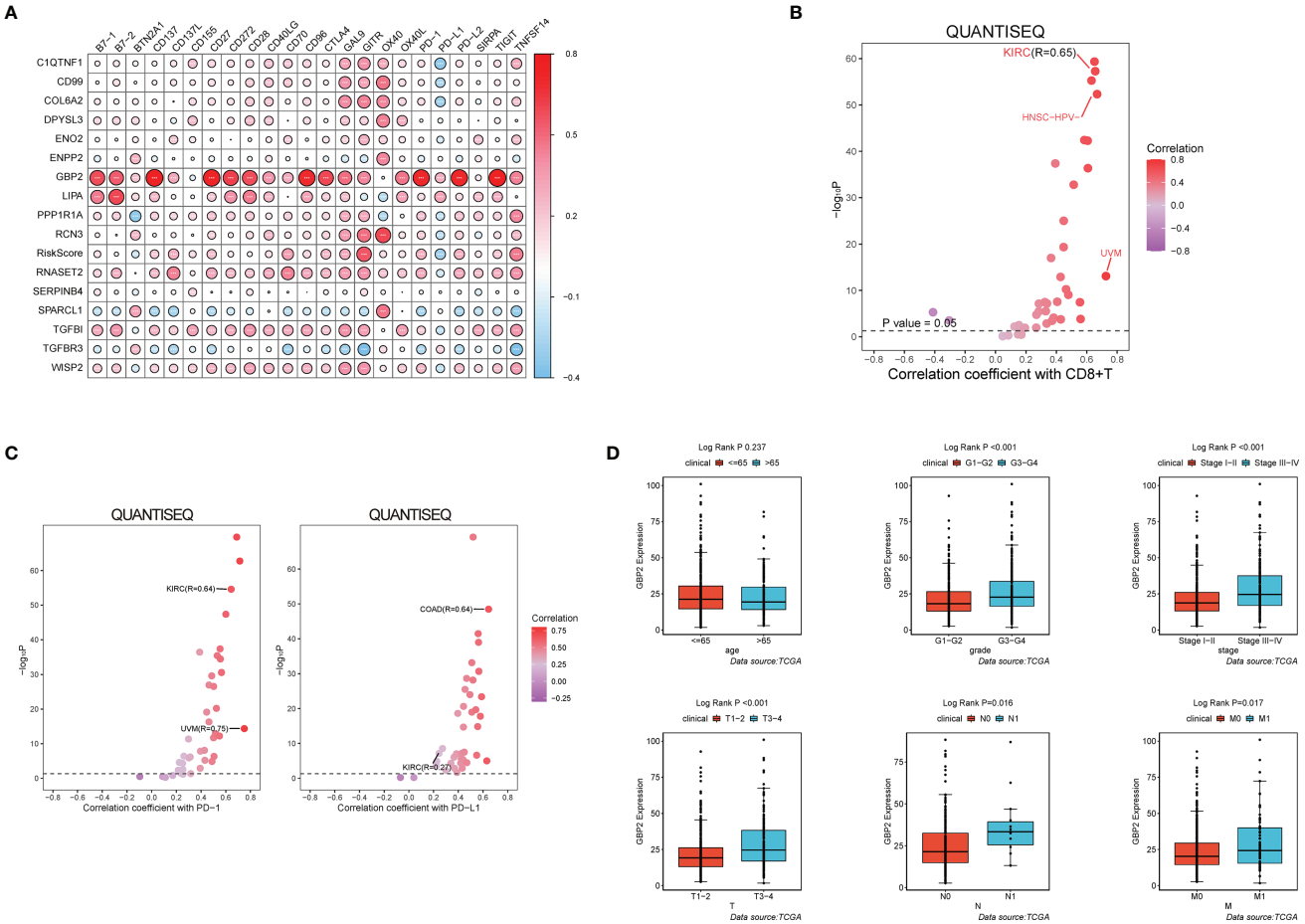



**FIGURE 7** | GBP2 was associated with the tumor microenvironment of ccRCC. **(A)** The correlation matrix of each immune checkpoint in modeling genes. (*$p$ < 0.05, **$p$ < 0.01, ***$p$ < 0.001). QuanTIseq analysis of RNA-seq data from 19 TCGA solid cancers: **(B)** Correlation of GBP2 expression with $CD8^+$ T cells, **(C)** Correlation of GBP2 expression with immune checkpoint PD-1 and PD-L1. **(D)** Higher GBP2 expression was associated with more severe clinical parameters in ccRCC patients such as histological grade, clinical stage, T classification., lymph nodes, distant metastasis according to data from TCGA.

tissue, which was consistent with our results from RT-qPCR (**Figures 9A, B**). In addition, the expression of GBP2 was always significantly elevated in kidney cancer cell lines (769-P, Caki-2, and ACHN) compared to the normal human renal tubular epithelial HK-2 cells (**Figure 9B**). It was insufficient to use genomic data to predict cancer prognosis while proteomics could improve our understanding of the etiology and progression of cancer and improve the assessment of cancer prognosis. The data from CPTAC showed that there were significant differences in the translational level of GBP2 between normal tissues and ccRCC (**Figure 9C**).

## DISCUSSION

Traditional prognostic factors for ccRCC mainly included tumor-node-metastasis (TNM) stage, histological grade, and clinical stage. Although these indicators have been progressively refined over the past decades, there are still many difficulties in reducing the mortality and improving prognosis of patients with ccRCC. The identification of novel diagnostic and prognostic biomarkers for ccRCC is a necessity at present.

Dysregulated metabolism was a hallmark of malignant tumor, manifested through alterations in metabolites. Based on metabolomic profiling, Hakimi et al. found that ccRCC characterized broad shifts of central carbon metabolism, one-carbon metabolism and anti-oxidant response (15). Many prognostic models were developed according to the important alterations in metabolic processes in ccRCC. Gui et al. (16) developed a hypoxia-immune–based multiomics signature since they noticed both the hypoxia and immune status of the tumor microenvironment in ccRCC. A predictive model consisting of 13 glycolysis-related genes was also constructed by Zhang et al. (17) based on the high levels of glycolysis in tumor cells even under aerobic conditions. Moreover, recent studies shed light on the possible mechanisms by which deregulated lipid metabolism promotes malignant proliferation and adipogenic transdifferentiation in ccRCC (7, 18, 19), while the relationship

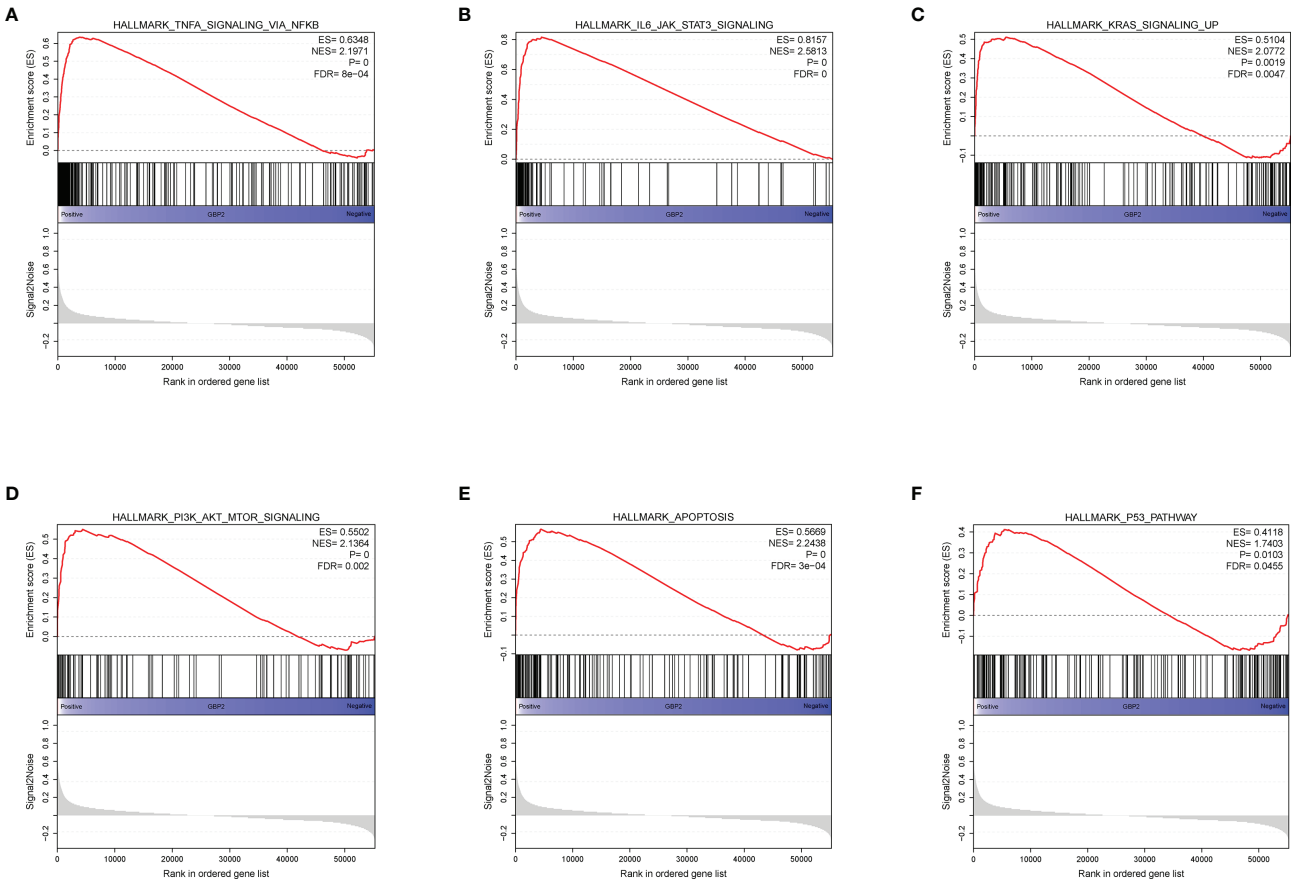



**FIGURE 8** | GSEA analysis revealed several activated oncogenic pathways associated with the expression of GBP2. **(A)** TNF-α signaling *via* NF-κB. **(B)** IL-6-JAK-STAT3 signaling. **(C)** KRAS signaling. **(D)** PI3K/AKT/mTOR signaling. **(E)** Apoptosis. **(F)** P53 pathway.

between the degree of adipogenic transdifferentiation of tumor cells and the disease prognosis of ccRCC still remained unclear. These results brought us a novel research direction.

In the current study, we first verified that the distribution of adipokine chemerin promoting cellular adiposity differentiation differed significantly between clinical subgroups, and that the gene RARRES2 was expressed more in the advanced subgroups. This demonstrated a positive correlation between the degree of tumor cell adipogenic transdifferentiation and the severity of the disease, which was consistent with the previous findings (8). Next, based on extracted 49 differentially expressed genes from genes encoding specific proteins secreted by adipocytes, we defined two subtypes with distinct clinical and biological features in ccRCC. The results showed that patients in cluster A had worse clinical outcomes and a greater proportion of advanced stages. Moreover, cluster A exhibited a significant lipid metabolism inactivation status, including the poorly expressed fatty acid metabolism and PPAR signaling pathways, which played a role in clearing cellular lipids in kidney tissues. Previous studies have demonstrated that the infiltrating immune cells were essential for tumor growth, metastasis, and drug resistance (20, 21). When we performed immune cell infiltration analysis of the tumor microenvironment for both clusters, we found that cluster A was enriched in both innate and acquired immune cell infiltration, while patients in cluster A didn't show a matching survival advantage. Given that samples in cluster A expressed significantly more immune checkpoints, we hypothesized that immunotherapy might have good efficacy for ccRCC patients with high adipogenic transdifferentiation and severe condition.

Based on the results of univariate Cox regression analysis, 18 ARGs associated with OS were picked out. To eliminate the limitation of overfitting and further optimize gene selection, Lasso regression analysis was performed and finally 16 independent prognostic ARGs (TGFBR3, PPP1R1A, SERPINB4, ENO2, RNASET2, GBP2, CD99, COL6A2, TGFBI, LIPA, SPARCL1, RCN3, WISP2, C1QTNF1, DPYSL3 and ENPP2) were screened out to develop the ADI. After constructing the 16-gene signature, patients were separated into high-risk and low-risk groups. Our results showed that high risk-score patients had an inferior survival probability and clinical outcomes. Not only that, but we also verified that our model had a strong predictive efficacy through the validation of its robustness in both internal and external cohorts.

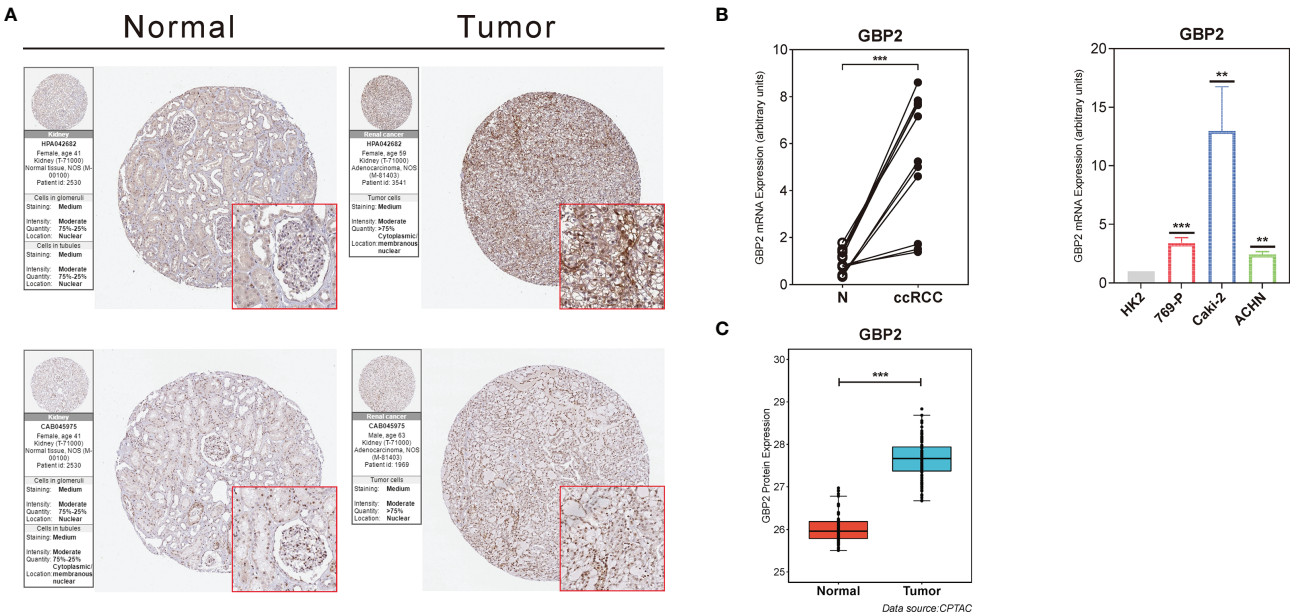



**FIGURE 9** | Validation of the role of GBP2 at the translational and transcriptional levels. **(A)** Immunohistochemical images from the HPA database show GBP2 protein expression in normal kidney (Normal) and KIRC (Tumor) tissues by different antibodies. **(B)** The mRNA expression of GBP2 was significantly different between normal kidney and ccRCC tissues according to the PCR results, as well as non-renal cancer cell line and several RCC cell lines. **(C)** The protein GBP2 expression of GBP2 was significantly different between normal kidney and ccRCC tissues according to the data from CPTAC. The asterisks represented the statistical p value (**p < 0.01, ***p < 0.001).

The guanylate-binding proteins (GBPs) were a large subfamily within the dynamin superfamily of large guanosine triphosphatase (GTPases) and involved in the regulation of intracellular immunity and basic physiological processes (22). As a member of the GBPs, GBP2 was important for protective immunity against microorganisms and viral pathogens (23). Our results showed that the expression GBP2 was significantly and positively correlated with both the expression of most immune checkpoints (such as PD-1 and PD-L1) and the distribution of $CD8^+$ T cells in the RCC tumor microenvironment. In addition, stratified analysis revealed that ccRCC patients with significantly upregulated expression of GBP2 tended to be at a more advanced stage. These findings suggested that GBP2 might be a potential biomarker for ccRCC disease assessment and immunotherapy response prediction. To investigate the molecular mechanisms underlying the regulation of GBP2 in ccRCC, we performed GSEA analysis to identify the GBP2-related enriched biological processes and pathways. The GSEA results suggested that TNFα signaling *via* NF-κB, IL6-JAK-STAT3 signaling, KRAS signaling, PI3K-AKT-mTOR signaling, correlated with progression of ccRCC. It has been showed that there was a direct correlation between tumor grade, invasion and metastasis of RCC and the expression and activation of NF-κB (24). Su et al. have found that insulin-like growth factor I (IGF-I) exerted stimulative role in RCC cell growth and had suppressive effects on RCC cell apoptosis through JAK2/STAT3 pathway (25). While mutation of KRAS was a rare event in RCC, wild type KRAS could exert tumor suppressor effects on RCC cell proliferation and tumor growth (26). Overactivation of PI3K-Akt-mTOR signaling has been suggested to correlate with aggressive behavior and poor prognosis in RCC tumors (27). All these results suggested that GBP2 promoted oncogenesis and progression of ccRCC through regulating multiple signaling pathways and it was validated at both the transcriptional and translational level.

Recent studies have explored the role of GBP2 on carcinogenesis and found that GBP2 could enhance the invasive ability of glioblastoma *via* the GBP2/Stat3/FN1 signal cascade (28). It was reported that the overexpression of GBP2 was correlated with an advanced T classification and poor OS in pancreatic adenocarcinoma (29). However, when it comes to colorectal cancer, GBP2 was proven to inhibit the growth of cancer cells by interfering with Wnt signal transduction. Godoy et al. found that the high expression of GBP2 was associated with a better prognosis in breast cancer (30). This might be due to the fact that GBP2 could prevent dynamin-related protein 1 (Drp1) translocating from the cytoplasm to the mitochondria, thus weakening the Drp1-dependent mitochondrial fission and the invasion of breast cancer cells (31). Additionally, in the present study, we found that GBP2 was a promising biomarker for the prediction of ccRCC prognosis and response to immunotherapy.

The association between excess body weight and risk of renal cell carcinoma has been widely reported in large prospective cohorts (32, 33). Tan and his colleagues found that chemerin could promote the progression of ccRCC by inducing the adipogenic transdifferentiation of tumor cells. Meanwhile, the level of chemerin in the peripheral circulation was positively

correlated with the body mass index (BMI) of patients, confirming a positive relationship between obesity and adipogenic transdifferentiation of ccRCC (8). However, the BMI cannot provide any information about the distribution of adipose tissues. Federico et al. explored the relationship between the distribution of adipose tissues and subtypes of RCC, and confirmed that ccRCC patients tended to exhibit a greater amount of abdominal fat, especially visceral adipose tissues (VATs) (34). The current theory suggests that adipose tissue is an endocrine/metabolic organ (35). Indeed, VATs possess higher hormonal and metabolic functions compared to subcutaneous adipose tissues (SATs) and can secrete a variety of factors conducive to the adipogenic transdifferentiation of surrounding cells (8, 34). Therefore, visceral obesity, especially perirenal fat, may serve as a positive role in promoting the adipogenic transdifferentiation of ccRCC (36, 37). In essence, kidney cancer cells and perirenal adipose tissue can interact through genomic changes and regulation (8, 38). In addition, Greco's study found a different distribution of perirenal adipose tissues between ccRCC and non-ccRCC. Specifically, ccRCC had more abundant perirenal fat, which might partly explain the mild degree of adipogenic transdifferentiation and the low expression level of chemerin in non-ccRCC cases, where perirenal adipose tissues were less distributed (8, 39).

The advantages of our study lied in our statistical analysis of adipokine-related genetic prognostic signature using high-throughput data and large-scale databases, which catered to the urgent need for validated index of ccRCC. In addition, our study could contribute to a better understanding of the role of adipogenic differentiation in ccRCC. Inevitably, our study also has several limitations. Firstly, clinical parameters such as age, pathological stage were not integrated into our ADI formula. Secondly, the clinical data in TCGA database was not comprehensive, and we were unable to obtain more parameters to validate our model, such as CT images and nephrometry scores. Thirdly, the mechanism of ARGs such as GBP2 affecting the occurrence and development of ccRCC needed further study *in vivo* and in *vito*.

## CONCLUSION

In conclusion, the adipogenic transdifferentiation status of tumor cells in patients with ccRCC was closely related to prognosis. We have presented a comprehensive analysis for ARG expression profiles and clinical data and identified a 16-mRNA signature that could effectively predict the prognosis of patients in ccRCC patients. ARGs such as GBP2 could helpfully provide insights into the underlying mechanism of ccRCC and may be a novel independent biomarker in the prediction of the survival of ccRCC patients.

## DATA AVAILABILITY STATEMENT

The original contributions presented in the study are included in the article/**Supplementary Material**. Further inquiries can be directed to the corresponding author.

## ETHICS STATEMENT

The studies involving human participants were reviewed and approved by The Ethical Committee of The First Affiliated Hospital of Nanjing Medical University. The patients/participants provided their written informed consent to participate in this study.

## AUTHOR CONTRIBUTIONS

NS designed this work. SW and XW wrote the manuscript. CJ performed the bioinformatics analysis. YW, XZ, and RC performed the data review. All authors have read and approved the manuscript.

## FUNDING

This work was supported by the National Natural Science Foundation of China (grant number 82071638).

## SUPPLEMENTARY MATERIAL

The Supplementary Material for this article can be found online at: https://www.frontiersin.org/articles/10.3389/fonc.2022.781932/full#supplementary-material

## REFERENCES

1. Bray F, Ferlay J, Soerjomataram I, Siegel RL, Torre LA, Jemal A. Global Cancer Statistics 2018: GLOBOCAN Estimates of Incidence and Mortality Worldwide for 36 Cancers in 185 Countries. *CA: Cancer J Clin* (2018) 68 (6):394–424. doi: 10.3322/caac.21492
2. Siegel RL, Miller KD, Fuchs HE, Jemal A. Cancer Statistics, 2021. *CA: Cancer J Clin* (2021) 71(1):7–33. doi: 10.3322/caac.21654
3. Garje R, An J, Greco A, Vaddepally RK, Zakharia Y. The Future of Immunotherapy-Based Combination Therapy in Metastatic Renal Cell Carcinoma. *Cancers (Basel)* (2020) 12(1):143. doi: 10.3390/cancers 12010143
4. Hsieh JJ, Purdue MP, Signoretti S, Swanton C, Albiges L, Schmidinger M, et al. Renal Cell Carcinoma. *Nat Rev Dis Primers* (2017) 3:17009. doi: 10.1038/nrdp.2017.9
5. Oberling C, Riviere M, Haguenau F. Ultrastructure of the Clear Cells in Renal Carcinomas and its Importance for the Demonstration of Their Renal Origin. *Nature* (1960) 186:402–3. doi: 10.1038/186402a0
6. Tun HW, Marlow LA, von Roemeling CA, Cooper SJ, Kreinest P, Wu K, et al. Pathway Signature and Cellular Differentiation in Clear Cell Renal Cell Carcinoma. *PloS One* (2010) 5(5):e10696. doi: 10.1371/journal.pone.0010696
7. Du W, Zhang L, Brett-Morris A, Aguila B, Kerner J, Hoppel CL, et al. HIF Drives Lipid Deposition and Cancer in ccRCC *via* Repression of Fatty Acid Metabolism. *Nat Commun* (2017) 8(1):1769. doi: 10.1038/s41467-017-01965-8

8. Tan SK, Mahmud I, Fontanesi F, Puchowicz M, Neumann CKA, Griswold AJ, et al. Obesity-Dependent Adipokine Chemerin Suppresses Fatty Acid Oxidation to Confer Ferroptosis Resistance. *Cancer Discovery* (2021) 11 (8):2072–93. doi: 10.1158/2159-8290.CD-20-1453
9. Helfer G, Wu QF. Chemerin: A Multifaceted Adipokine Involved in Metabolic Disorders. *J Endocrinol* (2018) 238(2):R79–r94. doi: 10.1530/JOE-18-0174
10. Deshmukh AS, Peijs L, Beaudry JL, Jespersen NZ, Nielsen CH, Ma T, et al. Proteomics-Based Comparative Mapping of the Secretomes of Human Brown and White Adipocytes Reveals EPDR1 as a Novel Batokine. *Cell Metab* (2019) 30(5):963–75.e967. doi: 10.1016/j.cmet.2019.10.001
11. Braun DA, Hou Y, Bakouny Z, Ficial M, Sant' Angelo M, Forman J, et al. Interplay of Somatic Alterations and Immune Infiltration Modulates Response to PD-1 Blockade in Advanced Clear Cell Renal Cell Carcinoma. *Nat Med* (2020) 26(6):909–18. doi: 10.1038/s41591-020-0839-y
12. Brunet JP, Tamayo P, Golub TR, Mesirov JP. Metagenes and Molecular Pattern Discovery Using Matrix Factorization. *Proc Natl Acad Sci United States America* (2004) 101(12):4164–9. doi: 10.1073/pnas.0308531101
13. Charoentong P, Finotello F, Angelova M, Mayer C, Efremova M, Rieder D, et al. Pan-Cancer Immunogenomic Analyses Reveal Genotype-Immunophenotype Relationships and Predictors of Response to Checkpoint Blockade. *Cell Rep* (2017) 18(1):248–62. doi: 10.1016/j.celrep.2016.12.019
14. Ohl F, Jung M, Radonić A, Sachs M, Loening SA, Jung K. Identification and Validation of Suitable Endogenous Reference Genes for Gene Expression Studies of Human Bladder Cancer. *J Urol* (2006) 175(5):1915–20. doi: 10.1016/S0022-5347(05)00919-5
15. Hakimi AA, Reznik E, Lee CH, Creighton CJ, Brannon AR, Luna A, et al. *Et Al*: An Integrated Metabolic Atlas of Clear Cell Renal Cell Carcinoma. *Cancer Cell* (2016) 29(1):104–16. doi: 10.1016/j.ccell.2015.12.004
16. Gui CP, Wei JH, Chen YH, Fu LM, Tang YM, Cao JZ, et al. A New Thinking: Extended Application of Genomic Selection to Screen Multiomics Data for Development of Novel Hypoxia-Immune Biomarkers and Target Therapy of Clear Cell Renal Cell Carcinoma. *Briefings Bioinf* (2021) 22(6):bbab173. doi: 10.1093/bib/bbab173
17. Zhang Y, Chen M, Liu M, Xu Y, Wu G. Glycolysis-Related Genes Serve as Potential Prognostic Biomarkers in Clear Cell Renal Cell Carcinoma. *Oxid Med Cell Longevity* (2021) 2021:6699808. doi: 10.1155/2021/6699808
18. Sundelin JP, Ståhlman M, Lundqvist A, Levin M, Parini P, Johansson ME, et al. Increased Expression of the Very Low-Density Lipoprotein Receptor Mediates Lipid Accumulation in Clear-Cell Renal Cell Carcinoma. *PloS One* (2012) 7(11):e48694. doi: 10.1371/journal.pone.0048694
19. Qiu B, Ackerman D, Sanchez DJ, Li B, Ochocki JD, Grazioli A, et al. Hif2α-Dependent Lipid Storage Promotes Endoplasmic Reticulum Homeostasis in Clear-Cell Renal Cell Carcinoma. *Cancer Discovery* (2015) 5(6):652–67. doi: 10.1158/2159-8290.CD-14-1507
20. Díaz-Montero CM, Rini BI, Finke JH. The Immunology of Renal Cell Carcinoma. *Nat Rev Nephrol* (2020) 16(12):721–35. doi: 10.1038/s41581-020-0316-3
21. Vuong L, Kotecha RR, Voss MH, Hakimi AA. Tumor Microenvironment Dynamics in Clear-Cell Renal Cell Carcinoma. *Cancer Discovery* (2019) 9 (10):1349–57. doi: 10.1158/2159-8290.CD-19-0499
22. Guenzi E, Töpolt K, Cornali E, Lubeseder-Martellato C, Jörg A, Matzen K, et al. The Helical Domain of GBP-1 Mediates the Inhibition of Endothelial Cell Proliferation by Inflammatory Cytokines. *EMBO J* (2001) 20(20):5568–77. doi: 10.1093/emboj/20.20.5568
23. Vestal DJ, Jeyaratnam JA. The Guanylate-Binding Proteins: Emerging Insights Into the Biochemical Properties and Functions of This Family of Large Interferon-Induced Guanosine Triphosphatase. *J Interferon Cytokine Res Off J Int Soc Interferon Cytokine Res* (2011) 31(1):89–97. doi: 10.1089/jir.2010.0102
24. Oya M, Takayanagi A, Horiguchi A, Mizuno R, Ohtsubo M, Marumo K, et al. Increased Nuclear Factor-Kappa B Activation is Related to the Tumor Development of Renal Cell Carcinoma. *Carcinogenesis* (2003) 24(3):377–84. doi: 10.1093/carcin/24.3.377
25. Su Y, Zhao A, Cheng G, Xu J, Ji E, Sun W. The IGF-I/JAK2-STAT3/miR-21 Signaling Pathway may be Associated With Human Renal Cell Carcinoma Cell Growth. *Cancer Biomarkers section A Dis Markers* (2017) 19(3):289–96. doi: 10.3233/CBM-160449
26. Li F, Aljahdali IAM, Zhang R, Nastiuk KL, Krolewski JJ, Ling X. Kidney Cancer Biomarkers and Targets for Therapeutics: Survivin (BIRC5), XIAP, MCL-1, Hif1α, Hif2α, NRF2, MDM2, MDM4, P53, KRAS and AKT in Renal Cell Carcinoma. *J Exp Clin Cancer Res CR* (2021) 40(1):254. doi: 10.1186/s13046-021-02026-1
27. Pal SK, Quinn DI. Differentiating mTOR Inhibitors in Renal Cell Carcinoma. *Cancer Treat Rev* (2013) 39(7):709–19. doi: 10.1016/j.ctrv.2012.12.015
28. Yu S, Yu X, Sun L, Zheng Y, Chen L, Xu H, et al. GBP2 Enhances Glioblastoma Invasion Through Stat3/fibronectin Pathway. *Oncogene* (2020) 39(27):5042–55. doi: 10.1038/s41388-020-1348-7
29. Liu B, Huang R, Fu T, He P, Du C, Zhou W, et al. GBP2 as a Potential Prognostic Biomarker in Pancreatic Adenocarcinoma. *PeerJ* (2021) 9:e11423. doi: 10.7717/peerj.11423
30. Godoy P, Cadenas C, Hellwig B, Marchan R, Stewart J, Reif R, et al. Interferon-Inducible Guanylate Binding Protein (GBP2) is Associated With Better Prognosis in Breast Cancer and Indicates an Efficient T Cell Response. *Breast Cancer (Tokyo Japan)* (2014) 21(4):491–9. doi: 10.1007/s12282-012-0404-8
31. Zhang J, Zhang Y, Wu W, Wang F, Liu X, Shui G, et al. Guanylate-Binding Protein 2 Regulates Drp1-Mediated Mitochondrial Fission to Suppress Breast Cancer Cell Invasion. *Cell Death Dis* (2017) 8(10):e3151. doi: 10.1038/cddis.2017.559
32. Wang F, Xu Y. Body Mass Index and Risk of Renal Cell Cancer: A Dose-Response Meta-Analysis of Published Cohort Studies. *Int J Cancer* (2014) 135 (7):1673–86. doi: 10.1002/ijc.28813
33. Bhaskaran K, Douglas I, Forbes H, dos-Santos-Silva I, Leon DA, Smeeth L. Body-Mass Index and Risk of 22 Specific Cancers: A Population-Based Cohort Study of 5·24 Million UK Adults. *Lancet (London England)* (2014) 384 (9945):755–65. doi: 10.1016/S0140-6736(14)60892-8
34. Greco F, Quarta LG, Grasso RF, Beomonte Zobel B, Mallio CA. Increased Visceral Adipose Tissue in Clear Cell Renal Cell Carcinoma With and Without Peritumoral Collateral Vessels. *Br J Radiol* (2020) 93 (1112):20200334. doi: 10.1259/bjr.20200334
35. Wozniak SE, Gee LL, Wachtel MS, Frezza EE. Adipose Tissue: The New Endocrine Organ? A Review Article. *Digestive Dis Sci* (2009) 54(9):1847–56. doi: 10.1007/s10620-008-0585-3
36. Després JP, Lemieux I. Abdominal Obesity and Metabolic Syndrome. *Nature* (2006) 444(7121):881–7. doi: 10.1038/nature05488
37. Zhang HP, Zou J, Xu ZQ, Ruan J, Yang SD, Yin Y, et al. Association of Leptin, Visfatin, Apelin, Resistin and Adiponectin With Clear Cell Renal Cell Carcinoma. *Oncol Lett* (2017) 13(1):463–8. doi: 10.3892/ol.2016.5408
38. Greco F, Mallio CA. Relationship Between Visceral Adipose Tissue and Genetic Mutations (VHL and KDM5C) in Clear Cell Renal Cell Carcinoma. *La Radiologia Med* (2021) 126(5):645–51. doi: 10.1007/s11547-020-01310-y
39. Greco F, Mallio CA, Grippo R, Messina L, Vallese S, Rabitti C, et al. Increased Visceral Adipose Tissue in Male Patients With non-Clear Cell Renal Cell Carcinoma. *La Radiologia Med* (2020) 125(6):538–43. doi: 10.1007/s11547-020-01146-6


**Conflict of Interest:** The authors declare that the research was conducted in the absence of any commercial or financial relationships that could be construed as a potential conflict of interest.

**Publisher's Note:** All claims expressed in this article are solely those of the authors and do not necessarily represent those of their affiliated organizations, or those of the publisher, the editors and the reviewers. Any product that may be evaluated in this article, or claim that may be made by its manufacturer, is not guaranteed or endorsed by the publisher.

*Copyright © 2022 Wang, Wei, Ji, Wang, Zhang, Cong and Song. This is an open-access article distributed under the terms of the Creative Commons Attribution License (CC BY). The use, distribution or reproduction in other forums is permitted, provided the original author(s) and the copyright owner(s) are credited and that the original publication in this journal is cited, in accordance with accepted academic practice. No use, distribution or reproduction is permitted which does not comply with these terms.*

frontiers | Frontiers in Oncology

TYPE Original Research
PUBLISHED 16 August 2022
DOI 10.3389/fonc.2022.834524

Check for updates

OPEN ACCESS

EDITED BY
James H. Finke,
Case Western Reserve University,
United States

REVIEWED BY
Miriam Ficial,
Barts Health NHS Trust,
United Kingdom
Nur Damayanti,
Purdue University Indianapolis,
United States
Qian Du,
GNS Healthcare, United States

*CORRESPONDENCE
Tengcheng Li
litengch@mail2.sysu.edu.cn
Jieying Wu
wujying@mail.sysu.edu.cn

†These authors have contributed equally to this work

SPECIALTY SECTION
This article was submitted to Genitourinary Oncology, a section of the journal Frontiers in Oncology

RECEIVED 13 December 2021
ACCEPTED 14 July 2022
PUBLISHED 16 August 2022

CITATION
Wang Y, Sun Z, Lu S, Zhang X, Xiao C, Li T and Wu J (2022) Identification of PLAUR-related ceRNA and immune prognostic signature for kidney renal clear cell carcinoma.
*Front. Oncol.* 12:834524.
doi: 10.3389/fonc.2022.834524

COPYRIGHT
© 2022 Wang, Sun, Lu, Zhang, Xiao, Li and Wu. This is an open-access article distributed under the terms of the Creative Commons Attribution License (CC BY). The use, distribution or reproduction in other forums is permitted, provided the original author(s) and the copyright owner(s) are credited and that the original publication in this journal is cited, in accordance with accepted academic practice. No use, distribution or reproduction is permitted which does not comply with these terms.

# Identification of PLAUR-related ceRNA and immune prognostic signature for kidney renal clear cell carcinoma

Yu Wang[1†], Zhuolun Sun[1†], Shuo Lu[1], Xu Zhang[2], Chutian Xiao[3], Tengcheng Li[1*] and Jieying Wu[1*]

[1]Department of Urology, The Third Affiliated Hospital, Sun Yat-sen University, Guangzhou, China, [2]Department of Gynecology, The Third Affiliated Hospital, Sun Yat-sen University, Guangzhou, China, [3]Department of Urology, The Sixth Affiliated Hospital, Sun Yat-sen University, Guangzhou, China

Kidney renal clear cell carcinoma (KIRC) represents one of the most fatal cancers, usually showing malignant progression and a high tumor recurrence rate. The urokinase-type plasminogen activator receptor (PLAUR) plays a critical role in the initiation and progression of several cancers, including KIRC. However, the function and mechanism of PLAUR in patients with KIRC are still unclear and require further investigation. In the present study, we first explored the expression profile and prognostic values of PLAUR in pan-cancer based on The Cancer Genome Atlas and Genotype-Tissue Expression databases. PLAUR was upregulated in multiple cancers and was significantly associated with poor overall survival and disease-free survival only in patients with KIRC. Subsequently, the PVT1/SNHG15-hsa-miR-532-3p axis was identified as the most potential upstream regulatory network of PLAUR in KIRC. In addition, PLAUR expression was closely associated with tumor-infiltrating immune cells, tumor immunity biomarkers, and immunomodulator expression. Furthermore, we constructed a multiple-gene risk prediction signature according to the PLAUR-related immunomodulators (PRIs). A prognostic nomogram was then developed to predict the 1-, 3-, and 5-year survival probabilities of individuals. In conclusion, our study identified the PVT1/SNHG15-hsa-miR-532-3p-PLAUR axis and a prognostic signature of PRIs, which could be a reference for future clinical research.

KEYWORDS

**ceRNA, immunomodulators, kidney renal clear cell carcinoma, PLAUR, prognostic signature**

# Introduction

Renal cell carcinoma (RCC) is a common urinary malignancy originating from the epithelium of renal tubules, the incidence of which has recently increased. Approximately 76,080 new cases of RCC were diagnosed each year in the United States in 2021, of which 13,780 cases resulted in death (1). Kidney renal clear cell carcinoma (KIRC) is the most common subtype (representing approximately 80–90% of RCC), characterized by a high metastasis rate and resistance to radiotherapy and chemotherapy (2, 3). Approximately 25–30% of patients with KIRC are diagnosed with distant metastases, and the 5-year survival rate drops to approximately 10% (4). With the development of modern medicine, a multi-modal tumor strategy including surgical resection, molecular targeted therapy, and immunotherapy has dramatically optimized the clinical efficacy (5). Nevertheless, 30% of patients with localized KIRC inevitably developed local recurrence or tumor progression (2, 6). Although some promising biomarkers have been discovered, the underlying mechanism of recurrence and metastasis of KIRC is unclear (7). Therefore, new molecular-based research and effective therapies are urgently needed as they would be of great value for guiding the clinical management of patients with KIRC.

The urokinase-type plasminogen activator receptor (PLAUR, also known as CD87), a component of the urokinase-type plasminogen activator (PLAU) system, contains three structurally homologous domains and anchors on the cell surface through a glycosylated glycan-lipid (8, 9). PLAUR is involved in the pericellular network of interacting proteolytic systems and drives various malignancy-related processes, including angiogenesis, cell differentiation, proliferation, and migration (10–12). PLAUR overexpression has been reported in several hematologic and most solid malignancies, including acute lymphocytic leukemia, myeloma (13), breast cancer (14), non-small cell lung cancer (15), bladder cancer (16), and colon cancer (9). Additionally, Bhuvarahamurthy et al. revealed that PLAUR expression was upregulated in KIRC samples, and its expression appeared to increase with tumor grade or stage (17). PLAUR expression is mostly confined to the tumor tissue (11). PLAUR plays an important role in innate and adaptive immune responses (18). Rijneveld et al. reported that lymphocyte migration and macrophage and neutrophil infiltration were affected in infected tissues without PLAUR (19). Furthermore, PLAUR promotes activated T cell recruitment (18). Moreover, the composition of tumor-infiltrating immune cells may modulate tumor progression and determine outcomes (20). Therefore, it is clinically useful to investigate further the relationship between PLAUR expression and tumor immune infiltration in KIRC.

The regulatory mechanism of competing endogenous RNAs (ceRNAs) was presented for the first time by Salmena et al. in 2011 (21). This theory holds that ceRNA can competitively bind to microRNAs (miRNAs) and indirectly affect the gene silencing caused by miRNA. Long noncoding RNAs (lncRNAs) can adsorb onto miRNAs to regulate target gene expression (22). Currently, the ceRNA network has been shown to play a vital role in the occurrence and progression of multiple cancers (23). However, the significance of the key lncRNA–miRNA–PLAUR ceRNA network in KIRC needs further investigation.

In the present study, we first evaluated the differential expression and prognostic values of PLAUR in multiple cancers. Next, upstream miRNAs of PLAUR and upstream lncRNAs of candidate miRNAs were explored in KIRC. The associations between PLAUR and immune cell infiltration as well as biomarkers of immune cells were investigated using diverse authoritative databases. Further, we constructed a ceRNA (PVT1/SNHG15-hsa-miR-532-3p-PLAUR) regulatory network and a PLAUR-related immunomodulators (PRIs) signature to predict the prognosis of KIRC. The results of this study will enhance our understanding of the pathogenesis of KIRC and provide new molecular and therapeutic strategies for patients with KIRC.

# Materials and methods

## Data acquisition and pan-cancer PLAUR expression profile analysis

The mRNA expression profiles of 20 cancers were obtained from the University of California Santa Cruz Xena Browser (https://xenabrowser.net) (24). These transcriptomics data were normalized and analyzed using the "limma" R package. The differential expression levels of PLAUR in the different tumor and normal samples were analyzed using the Kruskal–Wallis test. The full list of 20 cancer types and their abbreviations is presented in Table S1.

## GEPIA database analysis

Based on The Cancer Genome Atlas (TCGA, https://portal.gdc.cancer.gov/) and Genotype-Tissue Expression (GTEx, https://gtexportal.org/) data, the Gene Expression Profiling Interactive Analysis (GEPIA, http://gepia.cancer-pku.cn/) is a free tool that delivers customizable functionalities, including differential expression and survival analyses (25). Additionally, we utilized the "Boxplots" module of GEPIA2 to analyze the expression profiles of PLAUR in diverse cancer types. Similarly, PLAUR-related lncRNA expression was also examined in KIRC. In addition, the "Survival Plots" module was applied to investigate overall survival (OS) and disease-free survival (DFS) data of the individual cancers in detail. Hazard ratios (HR) and *P* values were calculated using the log-rank test.

## StarBase database analysis

The miRNA–mRNA and lncRNA–miRNA interactions were predicted using the StarBase (http://starbase.sysu.edu.cn/) database (26). First, we used the StarBase database, which contained seven prediction algorithms (PITA, RNA22, miRmap, microT, miRanda, PicTar, and TargetScan), to predict the potential upstream binding miRNAs of PLAUR. Only the predicted miRNAs observed in one or more algorithms were regarded as potential miRNAs of PLAUR for the subsequent analysis. Furthermore, StarBase was employed to predict the potential lncRNAs that might bind to the above potential miRNAs. Furthermore, we explored the expression levels of miRNAs and lncRNAs in the KIRC samples and compared them with the controls. Moreover, the Kaplan–Meier survival analysis was used to assess the prognostic value of the potential targets. The expression correlation analysis for miRNA–mRNA, lncRNA–miRNA, and lncRNA–mRNA was further analyzed in the KIRC samples.

## Immune cell infiltration of PALUR in KIRC patients

CIBERSORT, a deconvolution algorithm developed by Newman (27), was employed to quantify the relative abundance of the 22 immune cell types in individual KIRC samples with the RNA-sequencing data from TCGA database. Only samples with CIBERSORT $P< 0.05$ were enrolled in this analysis. According to the median PLAUR expression, the KIRC samples were split into low- and high-expression groups. The infiltration levels of the immune cells were compared between the two groups and analyzed using the Wilcoxon rank-sum test. The correlation analysis among these infiltrating immune cells was performed using the Spearman test.

## TIMER database analysis

Tumor Immune Estimation Resource (TIMER, https://cistrome.shinyapps.io/timer/) is an integrative web interface used for the comprehensive analysis of tumor-infiltrating immune cells (28). We obtained six infiltrating immune cells (B cells, CD4+ T cells, CD8+ T cells, neutrophils, macrophages, and dendritic cells) in the KIRC samples using this dataset. The "somatic copy number alternation (SCNA)" module was used to compare the tumor infiltration levels under diverse SCNAs of PLAUR. The correlations between PLAUR expression and levels of immune cell infiltration were analyzed using TIMER.

## PLAUR-related immunomodulators

The immunophenoscore (IPS) was used to predict the immunotherapeutic responses by The Cancer Immunome Atlas (TCIA; https://tcia.at/), as described previously (29). TISIDB (http://cis.hku.hk/TISIDB) is one of the most comprehensive web portals for data on tumor and immune system interactions, comprising several types of data resources in onco-immunology (30). We utilized this database to retrieve the immunomodulators (immunopotentiators and immunosuppressants) associated with PLAUR. Immunomodulators closely correlated with the expression level of PLAUR were identified for further analysis (Spearman analysis, $P< 0.05$). The protein–protein interaction (PPI) networks of PLAUR-related immunomodulators (PRIs) were then generated using the STRING database (https://string-db.org/) (31). Gene Ontology (GO) and Kyoto Encyclopedia of Genes and Genomes (KEGG) pathway enrichment analyses were performed using the resulting protein network genes with the Metascape database (http://metascape.org) (32).

## Construction and validation of PRIs signature

Subsequently, we sought to construct a prognostic signature from the PRIs to assess the outcomes of patients with KIRC based on TCGA database. The differentially expressed PRIs (DEPRIs) between the 536 KIRC and normal samples were selected with a preset threshold of $|\log2 \text{ fold change (FC)}| \geq 2$ and false discovery rate (FDR) $< 0.05$. The DEPRIs highly associated with OS were then determined as prognostic DEPRIs ($P< 0.05$) *via* univariate Cox regression. Further, the least absolute shrinkage and selection operator (Lasso) regression was applied to these prognostic DEPRIs to reduce the complexity of the model and control overfitting. We constructed the prognostic signature according to the expression levels and corresponding coefficients with the multivariate Cox regression. The risk score formula for each patient was as follows: risk score = $\sum_{i=1}^{n} \beta(i) \times x(i)$, where $\beta(i)$ and $x(i)$ indicate the expression level and coefficient of gene, respectively. The Kaplan–Meier survival curve, the time-dependent receiver operating characteristic (ROC) curves and the area under the curve (AUC), principal component analysis (PCA), and t-distributed stochastic neighbor embedding (t-SNE) were employed to evaluate the performance of the constructed PRIs signature in TCGA cohort. E-MTAB-1980 with OS data downloaded from the EMBL-EBI database (https://www.ebi.ac.uk/) was used as an independent validation cohort.

## Development of nomogram

Independent prognostic factors were evaluated by Cox regression. In clinical research, nomograms are widely utilized as a quantitative tool to accurately assess cancer patients' outcomes (33). In this study, a nomogram was developed to optimize the predictive performance for patients with KIRC by incorporating risk scores and the above independent prognostic factors. Afterward, the calibration and ROC curves were drawn, and decision curve analysis (DCA) was conducted to evaluate the accuracy, discrimination, and practicality of the nomogram, respectively.

## Statistical analysis

All statistical examinations in this study were performed using database-derived tools or the R language (34). Values of $P< 0.05$ and log-rank $P< 0.05$ were regarded as statistically significant.

# Results

## Expression profile of PLAUR in pan-cancer

As the expression level of the PLAUR gene in pan-cancer has not yet been precisely determined, we utilized TCGA and GTEx databases for the differential expression analysis of PLAUR mRNA in the 20 most prevalent types of human cancer. Based on TCGA database, we discovered that PLAUR was significantly upregulated in 11 cancer types, including BRCA, CHOL, COAD, ESCA, GBM, HNSC, KIRC, KIRP, STAD, THCA, and UCEC, as compared to that in normal tissues; however, the PLAUR mRNA was downregulated in two cancers, i.e., KICH and LUSC ($P< 0.05$) (Figure 1A). No statistically significant difference was observed in the regulation of PLAUR in BLCA, LGG, LIHC, LUAD, PAAD, PRAD, and READ. Considering that TCGA database lacks normal tissue data for some cancers, we then utilized the GEPIA database (including TCGA and GTEx databases) to verify further the differences in the expression of PLAUR in these 20 cancers. On combining the RNA-sequencing data of the normal and tumor tissues from the GTEx and TCGA databases, PLAUR expression in tumor tissues of BRCA, CHOL, COAD, ESCA, GBM, HNSC, KIRC, KIRP, PAAD, READ, STAD, and THCA was found to be significantly higher than that in the corresponding control tissues (Figure 1B). Taken together, PLAUR may play a key regulatory role in the carcinogenesis of the 10 types of cancer, i.e., BRCA, CHOL, COAD, ESCA, GBM, HNSC, KIRC, KIRP, STAD, and THCA.

## Prognostic analysis of PLAUR in pan-cancer

To understand the association between PLAUR and tumor prognosis, Kaplan–Meier curves were constructed to evaluate the OS and DFS of the above 10 cancer types (BRCA, CHOL, COAD, ESCA, GBM, HNSC, KIRC, KIRP, STAD, and THCA) using the GEPIA database. The cancer samples were sorted into high and low PLAUR expression groups, using the median expression value of PLAUR. The OS curves showed that cases with higher PLAUR expression such as GBM, HNSC, and KIRC were associated with poor prognoses (Figure 2). Furthermore, the DFS curves suggested a correlation between high PLAUR expression and poor prognosis in the KIRC samples (Figure 3). The other cancers did not show any statistically significant difference indicating an association between PLAUR expression and survival-predicting ability. Taken together, these results revealed that PLAUR might serve as a biomarker for unfavorable outcomes in KIRC.

## Prediction of upstream miRNAs of PLAUR

To determine whether PLAUR was regulated by certain noncoding RNAs (ncRNAs), we first investigated the upstream regulatory miRNAs that possibly target PLAUR and ultimately identified 23 miRNAs. An miRNA–RNA regulatory network, consisting of 23 miRNA–PLAUR relationships, was established and visualized using Cytoscape (Figure 4A). Based on the ceRNA hypothesis, the level of miRNA expression should be inversely correlated with that of mRNA expression (21). Therefore, the expression correlation between PLAUR and the 23 upstream regulatory miRNAs was further analyzed in patients with KIRC using the StarBase database (Table 1). We noticed two significant inverse correlation pairs, i.e., hsa-miR-328-3p-PALUR and hsa-miR-532-3p-PLAUR (all $P< 0.05$) (Figure 4B). No difference was found in the correlation of expression between PLAUR and the other 21 predicted miRNAs (Table 1). To further confirm whether hsa-miR-328-3p and hsa-miR-532-3p influenced KIRC, the expression levels of these two miRNAs in KIRC and normal tissues were analyzed. Significant differences in hsa-miR-532-3p were found in the KIRC samples compared to normal kidney tissues (Figure 4C), but not in hsa-miR-328-3p. Notably, combined with the OS analysis, hsa-miR-532-3p was significantly downregulated, and its downregulation was correlated with poor clinical outcomes in patients with KIRC (Figure 4D). The above results suggest that hsa-miR-532-3p may be the most potentially regulated miRNA of PLAUR in KIRC.

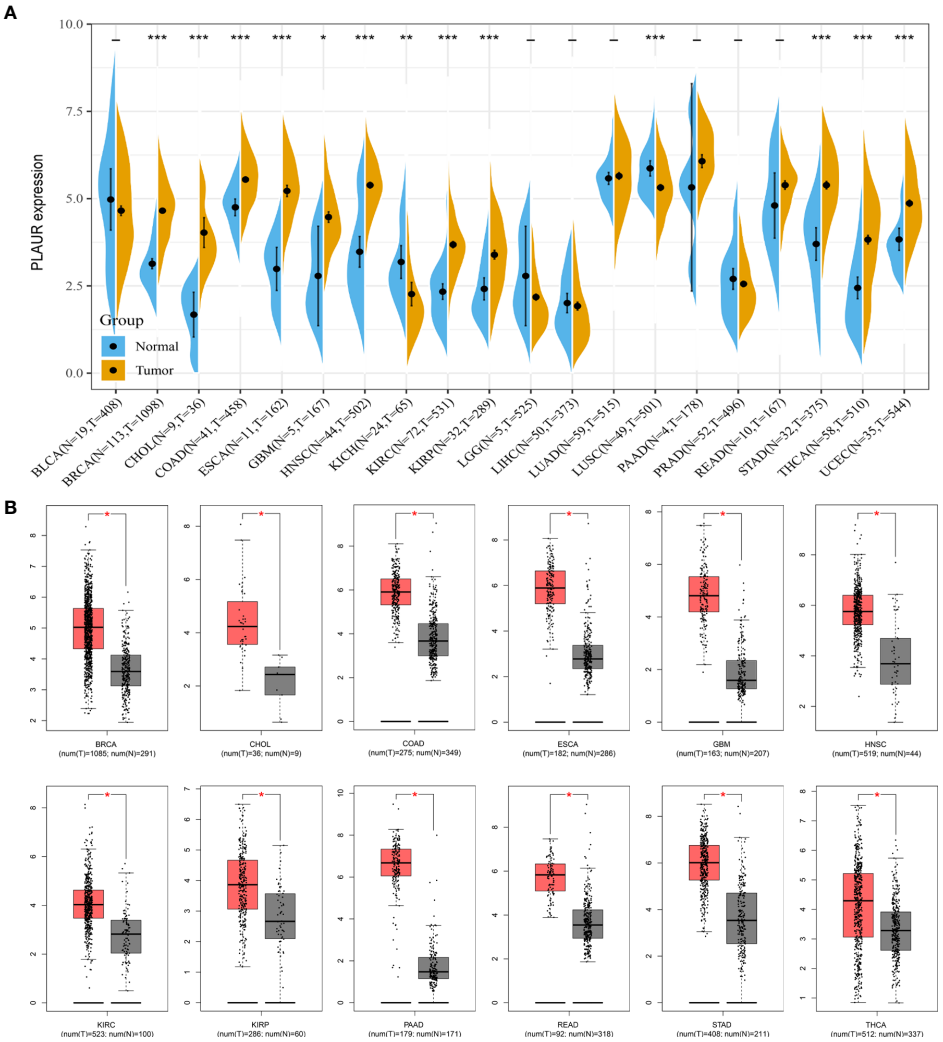



FIGURE 1
Expression analysis of PLAUR in pan-cancer. **(A)** The expression of PLAUR in 20 neoplastic tissues based on TCGA database. **(B)** The expression of PLAUR was higher in 12 cancer tissues compared with corresponding TCGA and GTEx normal tissues. *$P$ value< 0.05; **$P$ value< 0.01; ***$P$ value < 0.001.

## Prediction of upstream lncRNAs of hsa-miR-532-3p

We used the StarBase database to identify the potential upstream lncRNAs that regulated hsa-miR-532-3p and determined 121 possible lncRNAs. Accordingly, we established hsa-miR-532-3p-lncRNA regulatory networks (Table S2). The differential expression levels of these lncRNAs in KIRC were then detected using GEPIA. Among all the 121 potential upstream lncRNAs, only PVT1 and SNHG15 expression levels were remarkably upregulated in the KIRC samples compared to those in the controls (Figures 5A, B). Afterward, we evaluated the prognostic values of PVT1 and SNHG15 in KIRC. The Kaplan–Meier survival analysis suggested high expression levels of PVT1 and SNHG15, indicating poor OS and DFS in patients with KIRC (Figure 5C–F). Based on the theory proposed by Salmena et al., lncRNAs might act as ceRNAs by sponging miRNA to regulate mRNA expression (21). Thus, lncRNA expression should be positively correlated with mRNA expression and negatively correlated with miRNA expression. Further, we investigated the correlation between the expression levels of two lncRNAs (PVT1 and SNHG15) and hsa-miR-532-3p or PLAUR in KIRC (Figures 5G–J). The result was consistent with the theoretical prediction of Salmena et al. According to the differential expression, survival, and correlation analyses, PVT1 and SNHG15 were predicted to be the most potential upstream lncRNAs of the hsa-miR-532-3p/PLAUR axis in KIRC.

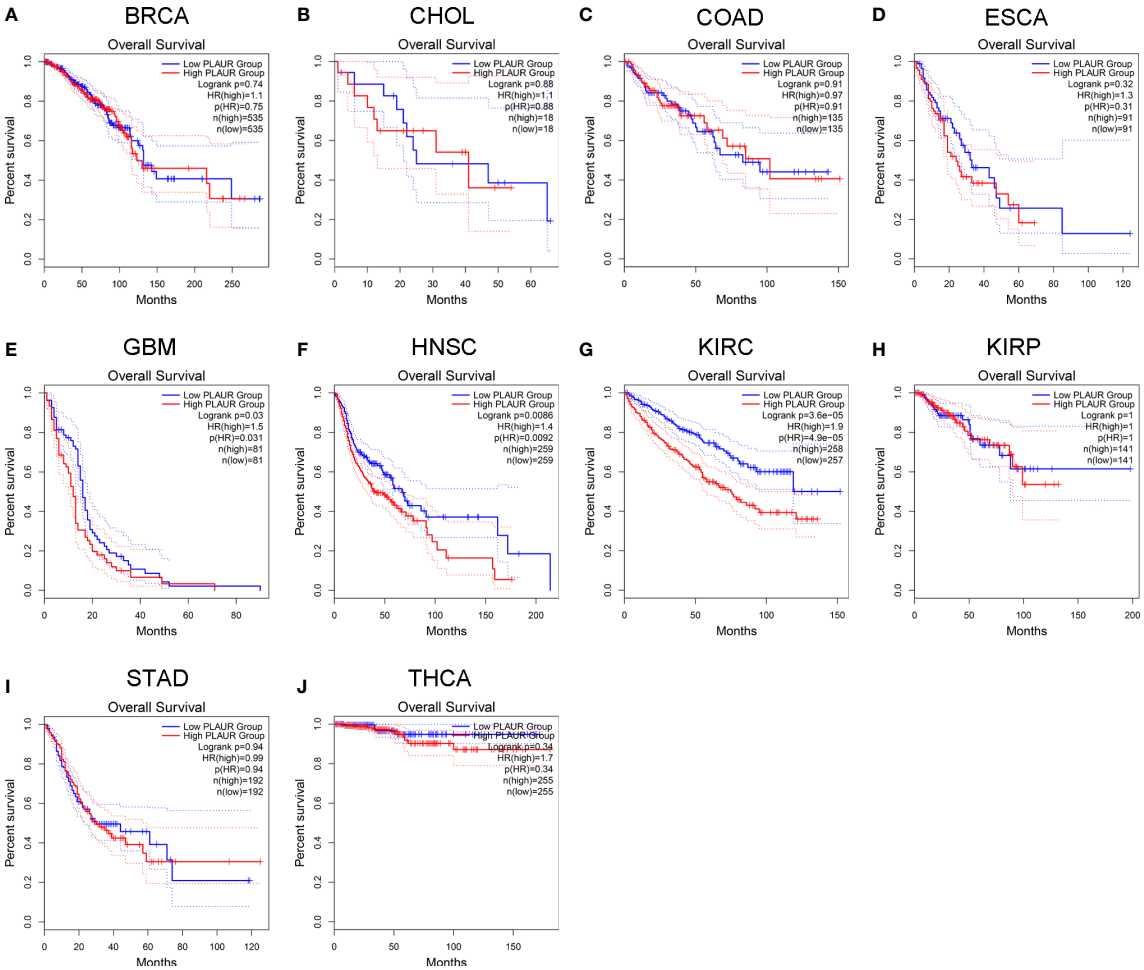



FIGURE 2
Kaplan-Meier survival curve for OS in 10 different tumor types using the GEPIA database. **(A–J)** BRCA, CHOL, COAD, ESCA, GBM, HNSC, KIRC, KIRP, STAD, THCA.

## The relationship between PLAUR Expression and immune cell infiltration

The expression spectrums and the relative proportions of the 22 immune cells in KIRC were explored and assessed through the CIBERSORT algorithm to investigate the infiltrations of specific immune cell subpopulations. Then, we constructed a bar plot to display the landscapes of different cell subtypes in each sample after screening the samples with $P \geq 0.05$ (Figure S1A). The correlation analyses of the 22 cell subtypes showed weak-to-moderate correlation, and the strongest positive correlations were found between memory-resting CD8+ and CD4+ T cells (Figure S1B). Additionally, compared with the PLAUR low expression group, the fractions of plasma cells, memory-activated CD4 T cells, regulatory T cells (Tregs), M0 macrophages, activated mast cells, and neutrophils were significantly higher, whereas those of memory-resting CD4+ T cells, resting NK cells, monocytes, macrophages M1, and resting mast cells were significantly lower in the PLAUR high expression group (Figure S1C). These findings indicated that the activation of some immune cells appeared to reflect the impact of PLAUR on the immune system.

The PLAUR gene is a key gene involved in coagulation and fibrinolysis, which are under complex regulation by inflammation and the local recruitment of leukocytes in the tumor microenvironment (35, 36). Hence, using the TIMER database, we further explored the underlying relationships between the SCNA of PLAUR and six different infiltrating immune cells. Besides macrophages, the copy numbers of PLAUR varied significantly in all the infiltrating immune cells, including B cells, CD8+ T cells, CD4+ T cells, neutrophils, and dendritic cells in the KIRC samples (Figure 6A). Moreover, we found that samples with arm-level deletion by PLAUR showed lower levels of immune infiltrates than diploid/normal samples,

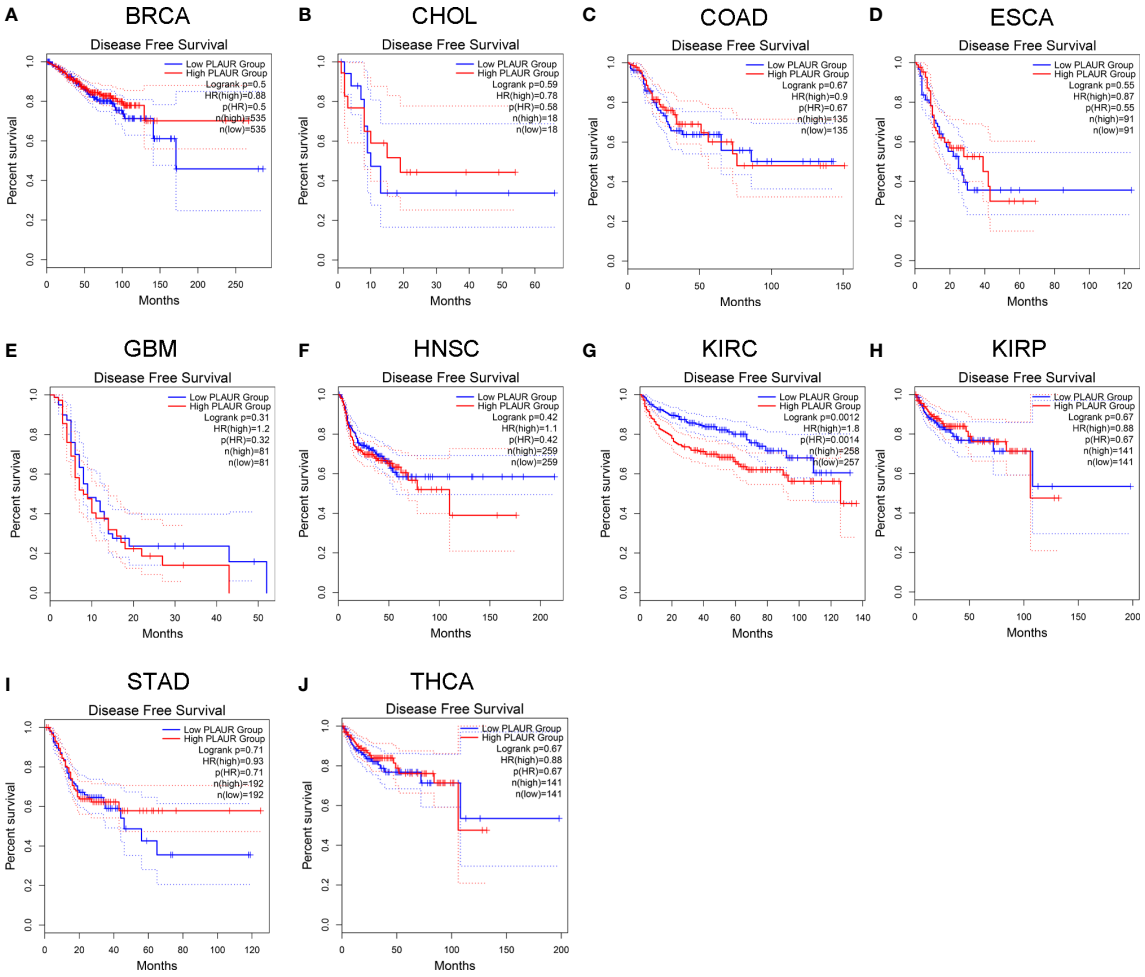



FIGURE 3
Kaplan-Meier survival curve for DFS in 10 different tumor types using the GEPIA database. **(A–J)** BRCA, CHOL, COAD, ESCA, GBM, HNSC, KIRC, KIRP, STAD, THCA.

indicating the effect of arm-level deletion on the infiltration level of immune cells in KIRC. A correlation analysis provided more insights into the mechanism of PLAUR in KIRC. The correlation analysis of PLAUR expression with infiltrating immune cells demonstrated that PLAUR expression was positively correlated with the infiltration of all immune cells except CD8+ T cells (Figures 6B). To further clarify the influence of PLAUR expression on tumor immune cells, we conducted an expression correlation analysis between PLAUR expression and the biomarkers released by various infiltrating immune cells. PLAUR expression was significantly linked to most (20/22) biomarkers (Table 2). Except NOS2 (r< 0), all the 19 biomarkers of infiltrating immune cells presented positive correlations with PLAUR expression. This confirmed the PLAUR expression was positively linked to immune cell infiltration.

## Association analysis between PLAUR and immunomodulators

We aimed to investigate whether PLAUR was related to immunomodulators, as the introduction of immunotherapy has considerably transformed the cancer treatment landscape. To explore the association with response to immunotherapy, we investigated the association between PLAUR-high vs PLAUR-low expression groups in some established immune-related signatures introduced by Braun et al. (37). The signature analysis was performed using four immune-related signatures listed in Table S3. There was a significant difference in myeloid cell infiltration (IMmotion150 Myeloid) (38) between the high- and low- PLAUR expression groups for either the Anti-PD1 treatment or the mTOR treatment (Figures S2A, S2B). No significant difference was detected in IMmotion150 Angio

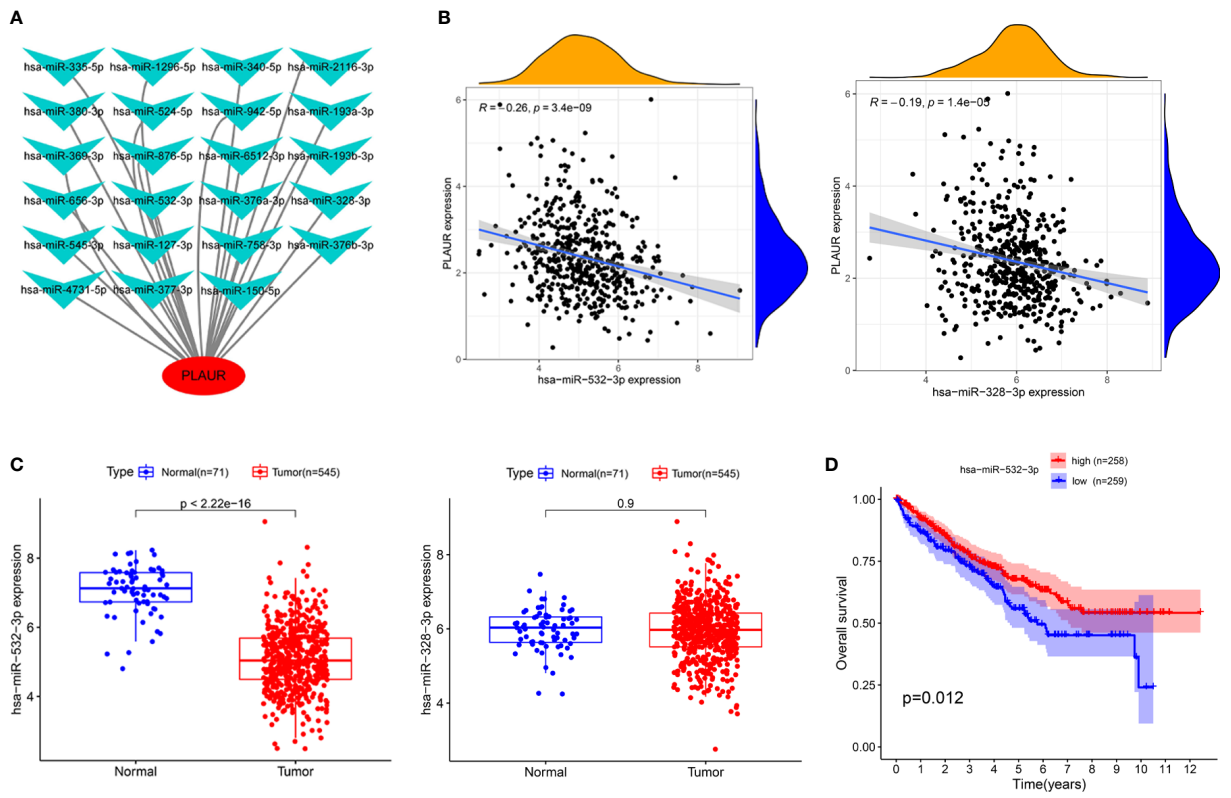



FIGURE 4
Identification of hsa-miR-532-3p as a potential upstream miRNA of PLAUR in KIRC using the StarBase database. **(A)** The miRNA-PLAUR regulatory network. **(B)** The expression correlation between hsa-miR-532-3p, hsa-miR-328-3p and PLAUR in KIRC. **(C)** The expression of hsa-miR-532-3p and hsa-miR-328-3p in KIRC tissues compared with normal controls. **(D)** The prognostic value of hsa-miR-532-3p in KIRC.

(38), T effector cell infiltration (IMmotion150 Teff) (38), and Javelin (39).

In addition, on investigating the significance of PLAUR to assess the effect of immunotherapy using TCIA, the results illustrated that the relative probabilities of responding to CTLA4-positive/PDL1-negative treatments in the low PLAUR group were higher than those in the high PLAUR group (Figures S2C–S2E).

Subsequently, the Spearman correlations between PLAUR expression and immunopotentiators as well as immunosuppressants were analyzed using the TISIDB database. A total of 38 immunopotentiators (Figure 7A) and 17 immunosuppressants (Figure 7B) were identified to be significantly correlated with PLAUR expression in KIRC ($P< 0.05$). The PPI of these 55 PRIs is presented in Figure 7C. As per the Metascape database, the most abundant biological process related to the 55 PRIs were immune events, particularly lymphocyte activation (Figure 7D). In terms of cellular component and molecular function analyses, these PRIs were mainly enriched in the external side of the plasma membrane and tumor necrosis factor receptor binding, respectively (Figure 7D). The result from the KEGG analysis revealed that the intestinal immune networks for IgA production, natural killer cell-mediated cytotoxicity, cell adhesion molecules, and Jak-STAT signaling pathways were associated with PLAUR-mediated immune system processes (Figure 7E).

## Construction and validation of the PRIs signature for KIRC

Compared with normal samples, 26 out of 55 PRIs were differentially expressed in tumor samples using the screening criteria (|log2FC|>2 and FDR<0.05). A heatmap was generated to illustrate the expression profiles of these 26 DEPRIs in KIRC (Figure 8A). Among them, only one gene, HHLA2, was downregulated in the KIRC tissues, whereas the remaining 25 genes were upregulated. The univariate Cox regression analysis was employed to investigate the prognostic values of these 26 DEPRIs in KIRC in TCGA database, and 17 DEPRIs were found to be closely related to OS ($P< 0.05$) (Figure 8B). The 17 candidate genes were further studied using LASSO (Figure 8C) and a multivariate (Figure 8D) Cox regression analysis.

TABLE 1 The expression correlation analysis between predicted miRNAs and PLAUR and the differential expression analysis of predicted miRNAs.

| Gene | miRNA | cor | pvalue | logFC | diffPval |
|---|---|---|---|---|---|
| PLAUR | hsa-miR-532-3p | -0.257 | 3.36E-09 [a] | -1.98 | 1.66E-34 [a] |
| PLAUR | hsa-miR-328-3p | -0.190 | 1.39E-05 [a] | -0.024 | 9.02E-02 |
| PLAUR | hsa-miR-1296-5p | -0.054 | 2.16E-01 | -0.691 | 1.67E-13 [a] |
| PLAUR | hsa-miR-524-5p | -0.054 | 2.21E-01 | 0.002 | 4.71E-01 |
| PLAUR | hsa-miR-545-3p | -0.002 | 9.68E-01 | 0.022 | 5.66E-02 |
| PLAUR | hsa-miR-6512-3p | 0.003 | 9.44E-01 | -0.069 | 3.07E-09 [a] |
| PLAUR | hsa-miR-340-5p | 0.042 | 3.37E-01 | 0.644 | 1.68E-07 [a] |
| PLAUR | hsa-miR-876-5p | 0.055 | 2.11E-01 | -0.053 | 5.11E-06 [a] |
| PLAUR | hsa-miR-4731-5p | 0.059 | 1.79E-01 | 0.012 | 3.47E-02 [a] |
| PLAUR | hsa-miR-127-3p | 0.084 | 5.65E-02 | -1.30 | 1.80E-16 [a] |
| PLAUR | hsa-miR-380-3p | 0.096 | 2.91E-02 | -0.027 | 3.84E-02 [a] |
| PLAUR | hsa-miR-2116-3p | 0.127 | 3.84E-03 [a] | 0.088 | 1.23E-01 |
| PLAUR | hsa-miR-758-3p | 0.127 | 3.82E-03 [a] | -0.622 | 6.67E-08 [a] |
| PLAUR | hsa-miR-335-5p | 0.141 | 1.33E-03 [a] | -1.54 | 4.55E-24 [a] |
| PLAUR | hsa-miR-656-3p | 0.150 | 6.00E-04 [a] | -0.097 | 3.46E-03 [a] |
| PLAUR | hsa-miR-376a-3p | 0.158 | 3.01E-04 [a] | -0.096 | 3.83E-03 [a] |
| PLAUR | hsa-miR-369-3p | 0.174 | 7.15E-05 [a] | -0.071 | 3.53E-01 |
| PLAUR | hsa-miR-376b-3p | 0.176 | 5.71E-05 [a] | -0.256 | 1.02E-05 [a] |
| PLAUR | hsa-miR-377-3p | 0.194 | 8.66E-06 [a] | -0.204 | 3.10E-05 [a] |
| PLAUR | hsa-miR-942-5p | 0.208 | 1.86E-06 [a] | 0.544 | 7.70E-10 [a] |
| PLAUR | hsa-miR-150-5p | 0.213 | 1.13E-06 [a] | 0.713 | 2.04E-06 [a] |
| PLAUR | hsa-miR-193b-3p | 0.263 | 1.37E-09 [a] | -0.197 | 7.16E-02 |
| PLAUR | hsa-miR-193a-3p | 0.267 | 7.65E-10 [a] | 0.856 | 1.48E-17 [a] |

[a]These results are statistically significant.

Ultimately, five target genes were retained to construct the prognostic PRIs signature. Then, the coefficient values were extracted to calculate the risk score for each patient with the following formula: risk score = (-0.0196 × the expression value of HHLA2) + (0.0245× the expression value of IL2RA) + (0.0855× the expression value of TNFRSF18) + (0.0407× the expression value of TNFSF14) + (0.1404× the expression value of CTLA4).

The median risk score was used to classify patients into the low- and high-risk groups. The Kaplan–Meier curve showed that patients of the high-risk group suffered a poor prognosis compared to those of the low-risk group (Figure 8E). Time-dependent ROC curves showed that the PRIs signature harbored a satisfactory performance to predict OS in patients with KIRC (1-, 3-, and 5-year AUC was 0.697, 0.656, and 0.707, respectively) (Figure 8F). The scatterplot of the risk score and survival status showed that the mortality rate of patients increased with the increase in risk score (Figure 8G). Moreover, PCA and t-SNE analyses were performed to confirm the diverse directions between the two risk groups (Figure 8H). We performed the same analyses in an independent validation cohort to determine whether the PRIs have prognostic significance in other populations. Analogous results were achieved in the E-MTAB-1980 cohort (Figures 9A–D). The above results reflected that the PRIs signature might precisely and steadily predict survival outcomes in patients with KIRC.

## Independent prognostic value of the PRIs signature

We performed univariate and multivariate Cox regression analyses to investigate whether the PRIs signature was a clinically independent prognostic factor for KIRC. The univariate Cox regression analysis showed that the signature-based risk score was closely related to the OS of patients with KIRC (HR = 1.282, $P<0.001$) in TCGA database (Figure S3A). In contrast, the multivariate Cox analysis revealed that the signature could work as an independent prognostic factor (HR = 1.196, $P = 0.002$) (Figure S3B). These results were validated in the E-MTAB-1980 cohort (Figure S3C, S3D).

## Development of the nomogram and the evaluation of predictive effectiveness

To provide clinicians with a quantitative approach to assessing the individual survival probability in patients with

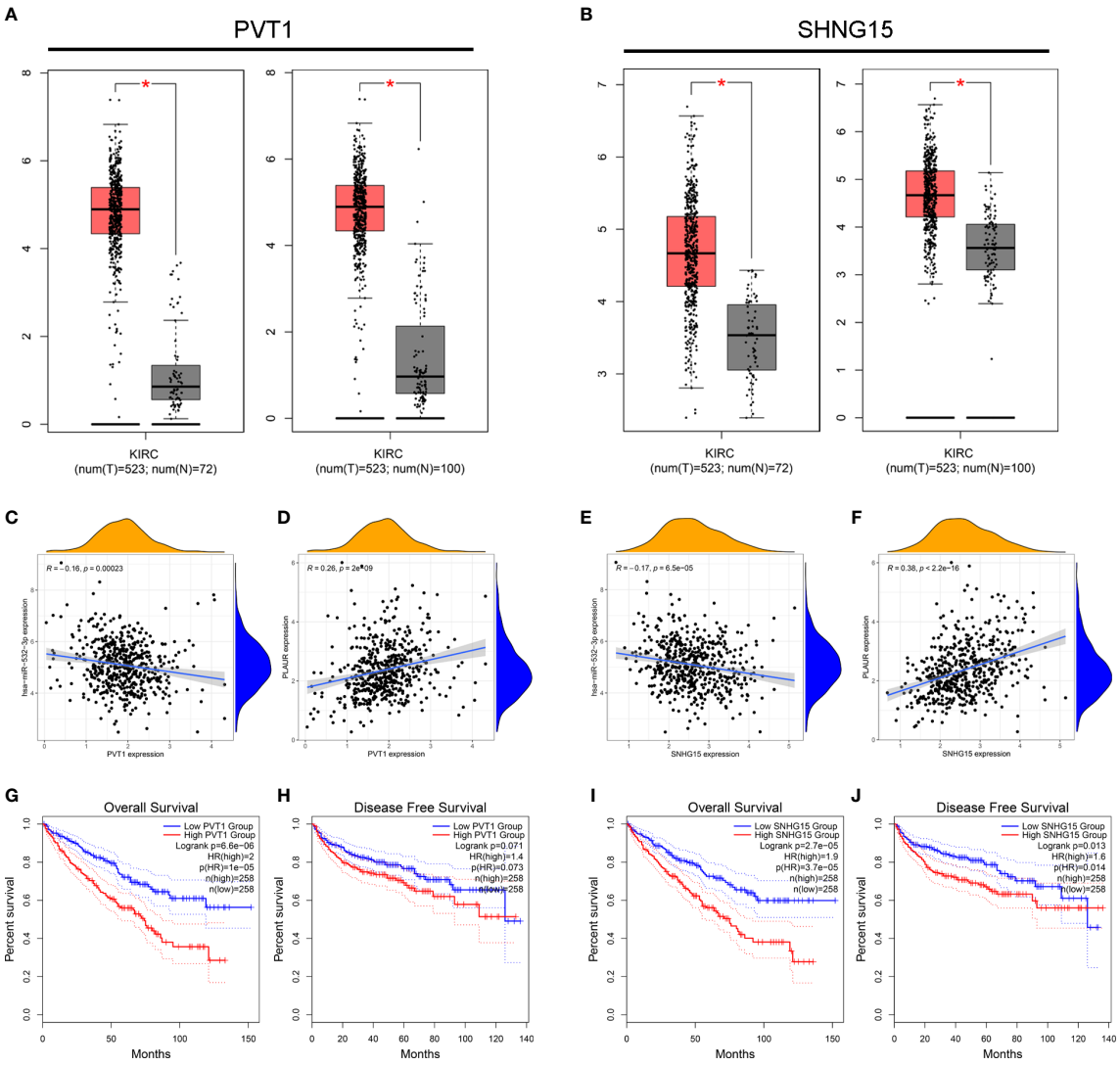



FIGURE 5
Identification of PVT1 and SNHG15 as two potential upstream lncRNAs of hsa-miR-532-3p-PLAUR axis in KIRC using the StarBase database. **(A–B)** The differential expression of PVT1 **(A)** and SNHG15 **(B)** in KIRC samples and "TCGA normal" or "TCGA and GTEx normal" samples. **(C-D)** The expression correlation between PVT1 and hsa-miR-532-3p **(C)**, PVT1 and PLAUR **(D)** in KIRC. **(E–F)** The expression correlation between SNHG15 and hsa-miR-532-3p **(E)**, SNHG15 and PLAUR **(F)** in KIRC. **(G–H)** Kaplan-Meier survival curve of OS for PVT1 **(G)** and SNHG15 **(H)**. **(I–J)** Kaplan-Meier survival curve of DFS for PVT1 **(G)** and SNHG15 **(H)** *p<0.05.

KIRC, we developed a nomogram incorporating the risk score and clinical features (including age, gender, grade, and AJCC stage) in TCGA cohort (Figure 10A). The calibration curves of the nomogram exhibited good concordance between the predicted and actual outcomes, revealing that the nomogram possessed better predictive ability (Figures 10B–D). The AUC values predicting the 1-, 3-, and 5-year OS of the nomogram were 0.833, 0.801, and 0.760, respectively, which outperformed all clinicopathological features (Figures 10E–G). The DCA suggested that the nomogram provided a higher overall net benefit than other clinical features for most threshold probabilities, demonstrating the potential clinical usefulness of the predictive nomogram (Figures 10H–J). Altogether, the nomogram might increase the predicted probability and confer some net benefit, enabling individualized prognosis prediction and helping clinical practice.

## Discussion

KIRC is one of the most lethal cancers, usually showing malignant progression and a high tumor recurrence rate (6).

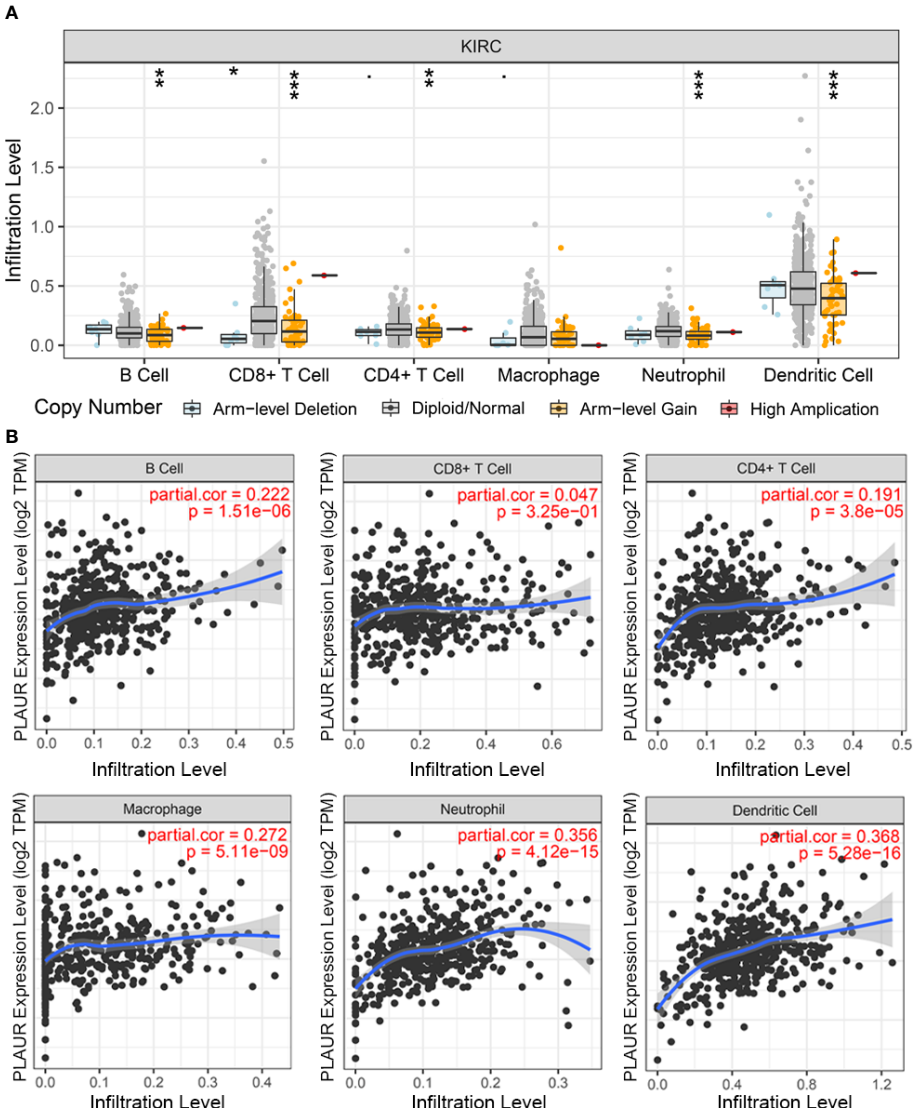



FIGURE 6
The relationship between expression of PLAUR and immune cell infiltration in KIRC. **(A)** Association between PLAUR gene copy number and immune cell infiltration levels in KIRC. **(B)** The relationship of PLAUR expression with six various infiltrating immune cells in KIRC. *p<0.05; **p<0.01; ***p<0.001.

Although various therapeutic strategies are available for KIRC, patient survival rates remain poor (2, 5) Elucidating the molecular mechanism underlying KIRC pathogenesis and seeking potential biomarkers are critical for identifying novel therapeutic targets and improving the prognosis of patients with KIRC. PLAUR plays a crucial role in the initiation and progression of various cancers, including KIRC (11). However, the function and mechanism of PLAUR in patients with KIRC are still unclear and require further investigation.

In this study, we first analyzed the expression of PLAUR in pan-cancer using data from TCGA database, after which we used the GEPIA database to confirm the expression and prognostic potential of PLAUR. The survival analysis for PLAUR across 20 human cancers demonstrated that high PLAUR expression was significantly correlated with poor OS and DFS only in patients with KIRC. Two previous studies indicated that PLAUR expression was upregulated in KIRC tissues compared to normal tissues, and the expression appeared to increase with tumor grade or stage (17, 40). Concomitant to these reports, our results revealed the tumorigenic effect of PLAUR in KIRC.

LncRNA can interact with miRNA to participate in the regulation of target gene expression based on the ceRNA hypothesis (21, 41). Through the StarBase database, we

TABLE 2 Correlation analysis between PLAUR and biomarkers of immune cells in KIRC.

| Immune cell | Biomarker | cor | pvalue |
|---|---|---|---|
| B cell | CD19 | 0.377 | 0 [a] |
| B cell | CD79A | 0.368 | 0 [a] |
| CD8+ T cell | CD8A | 0.217 | 4.36E-07 [a] |
| CD8+ T cell | CD8B | 0.215 | 5.84E-07 [a] |
| CD4+ T cell | CD4 | 0.442 | 0 [a] |
| M1 macrophage | NOS2 | -0.132 | 2.27E-03 [a] |
| M1 macrophage | IRF5 | 0.193 | 7.57E-06 [a] |
| M1 macrophage | PTGS2 | 0.288 | 1.41E-11 [a] |
| M2 macrophage | CD163 | 0.329 | 7.31E-15 [a] |
| M2 macrophage | VSIG4 | 0.440 | 0 [a] |
| M2 macrophage | MS4A4A | 0.399 | 0 [a] |
| Neutrophil | CEACAM8 | -0.026 | 5.52E-01 |
| Neutrophil | ITGAM | 0.371 | 0 [a] |
| Neutrophil | CCR7 | 0.370 | 0 [a] |
| Dendritic cell | HLA-DPB1 | 0.311 | 2.31E-13 [a] |
| Dendritic cell | HLA-DQB1 | 0.199 | 3.71E-06 [a] |
| Dendritic cell | HLA-DRA | 0.308 | 4.43E-13 [a] |
| Dendritic cell | HLA-DPA1 | 0.240 | 2.02E-08 [a] |
| Dendritic cell | CD1C | 0.120 | 5.45E-03 [a] |
| Dendritic cell | NRP1 | -0.058 | 1.80E-01 |
| Dendritic cell | ITGAX | 0.432 | 0 [a] |

[a]These results are statistically significant.

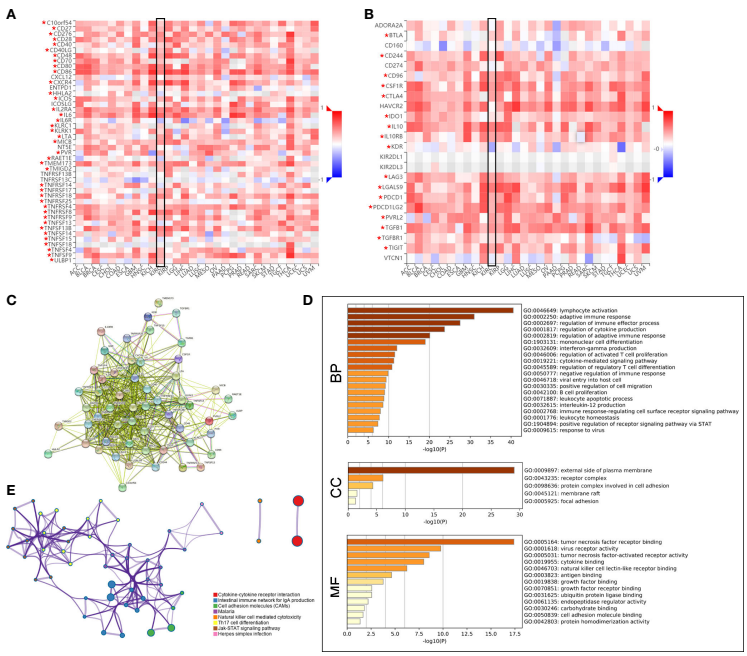



FIGURE 7
Identification of PLAUR-related immunomodulators (PRIs). **(A–B)** The correlation heatmaps of PLAUR with immunopotentiators **(A)** and immunosuppressants **(B)**. **(C)** Protein–protein network of 55 PRIs. **(D)** Gene Ontology annotation of 55 PRIs. **(E)** Kyoto Encyclopedia of Genes and Genomes pathway analysis of 55 PRIs. **P* value< 0.05.

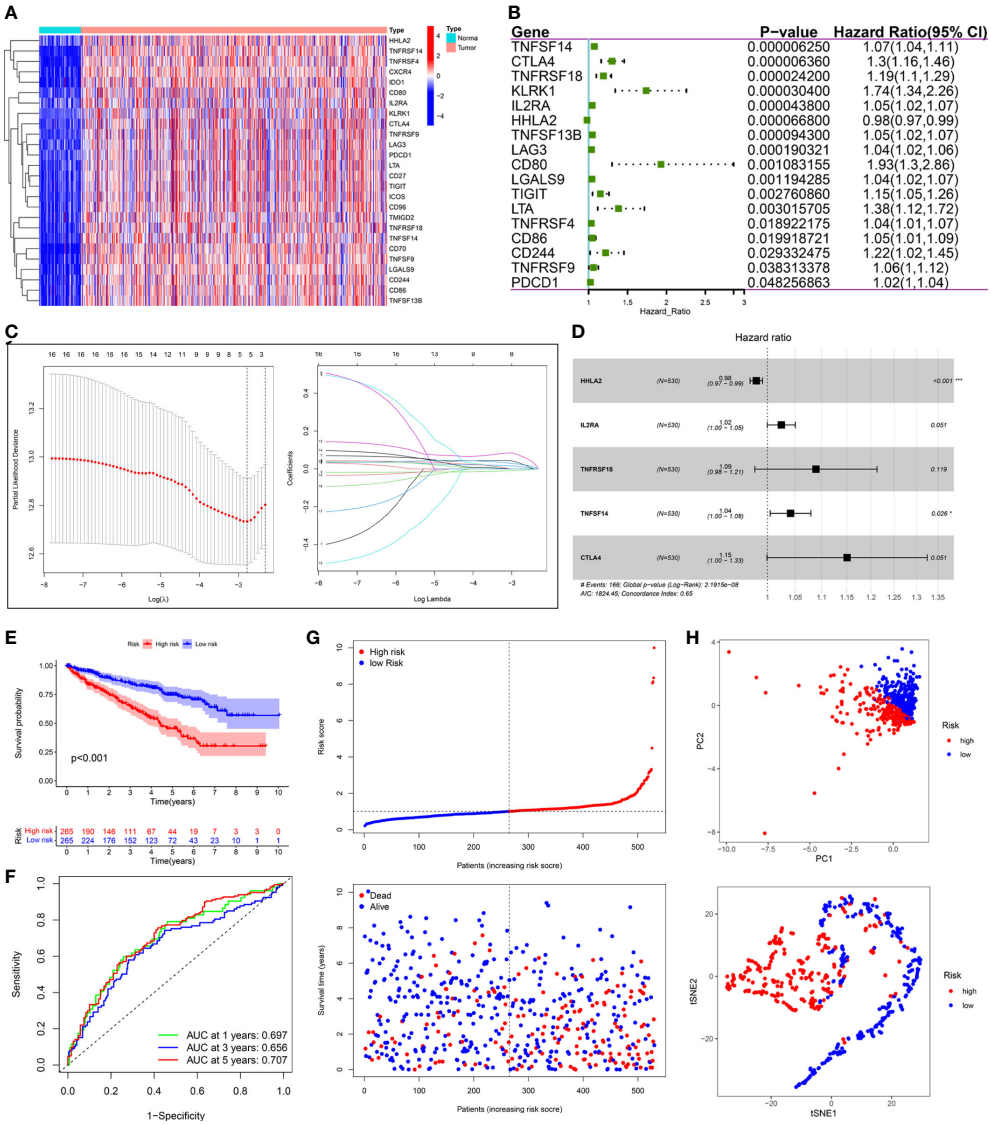



FIGURE 8
Construction of prognostic PRIs signature based on the TCGA KIRC cohort. **(A)** The heatmaps of 26 differentially expressed PRIs in KIRC tissues and normal tissues. **(B)** Forest plot of univariate Cox regression analysis of PRIs related to the OS. **(C)** LASSO coefficients profiles of the 5 PRIs in KIRC. **(D)** Forest plot of multivariate Cox regression analysis of 5 PRIs in KIRC. **(E)** Kaplan-Meier analysis of KIRC patients stratified by the median risk score in the TCGA cohort. **(F)** The time-dependent ROC curve for OS in the TCGA cohort. **(G)** The distribution of the risk score and OS status in the TCGA cohort. **(H)** PCA and t-SNE analyses in the TCGA cohort.

predicted that upstream regulatory miRNAs potentially bind to PLAUR and determined 23 candidate miRNAs. Most of these miRNAs might serve as tumor suppressors in KIRC. For example, miR-127-3p inhibited the proliferation and metastasis of KIRC by targeting the CDKN3/E2F1 axis (42), and miR-335-5p suppressed KIRC cell proliferation and invasion by repressing BCL-W expression (43). After a series of analyses for these 23 miRNAs, miR-532-3p was identified as the most potential miRNA of PLAUR, which was negatively associated with PLAUR expression; it was overexpressed and predicted a bad outcome in KIRC. Moreover, Han et al. suggested that miR-532-3p inhibited the malignant progression of KIRC by downregulating the expression of ETS1, an oncogene associated with unfavorable prognosis in KIRC (44).

Subsequently, 121 upstream potential lncRNAs of the miR-532-3p-PLAUR axis were discovered. Two of the most potentially upregulated lncRNAs (PVT1 and SNHG15) were then determined by a series analysis. Emerging research has revealed that PVT1 and SNHG15 play important roles in the

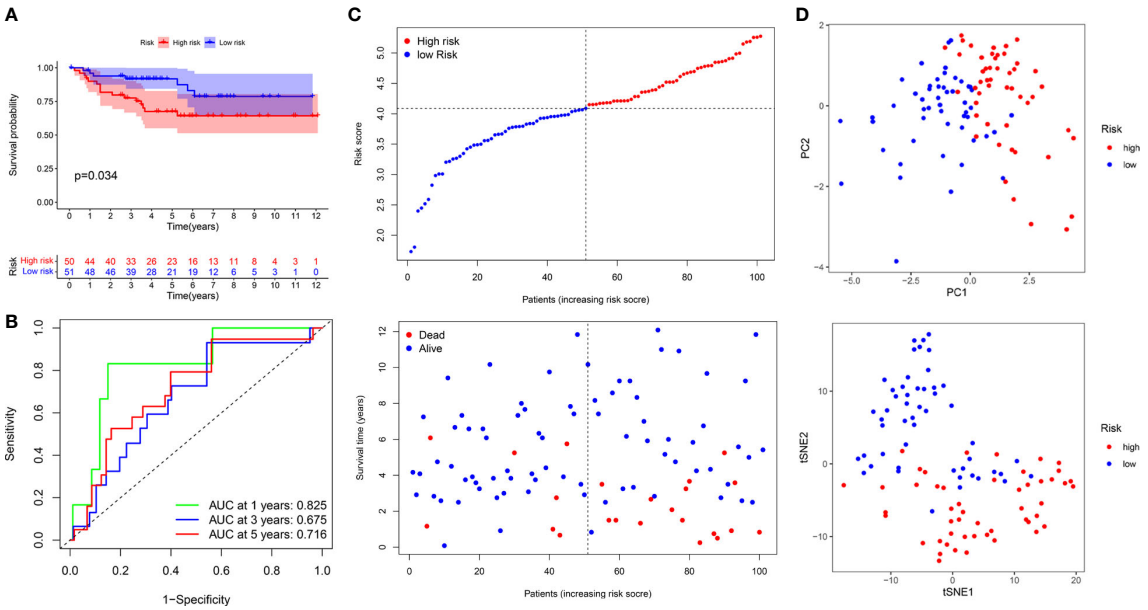



FIGURE 9
The prognostic value of PRIs prognostic for KIRC patients in an independent E-MTAB-1980 validation cohort. **(A)** Kaplan-Meier analysis of KIRC patients stratified by the median risk score in the E-MTAB-1980 cohort. **(B)** The time-dependent ROC curve for OS in the E-MTAB-1980 cohort. **(C)** The distribution of the risk score and OS status in the E-MTAB-1980 cohort. **(D)** PCA and t-SNE analyses in the E-MTAB-1980 cohort.

progression of various cancers, including KIRC. Yang et al. reported that PVT1 could serve as ceRNA in the context of KIRC and promoted cancer proliferation and migration *in vitro* and *in vivo* experiments (45). In addition, another study confirmed that the upregulated expression of SNHG15 induced the epithelial-mesenchymal transition process and accelerated the invasion and migration of KIRC by regulating the nuclear factor κB signaling pathway (46). Based on the above results, the PVT1/SNHG15-hsa-miR-532-3p-PLAUR axes were considered potential regulatory pathways in KIRC.

The infiltration of immune cells in the TME has previously been associated with the prognosis and immunotherapy outcomes of various human tumors, especially in patients with KIRC. The present study showed a significant positive correlation of PLAUR expression with various immune cells in KIRC. The activation of dendritic cells and CD8+ T cells was correlated with favorable prognoses in the majority of solid tumors, but with the poor prognosis of KIRC (47), which indicated that KIRC possessed a unique TME. Additionally, infiltrating CD4+ T cells and macrophages enhanced KIRC cell proliferation and invasion, respectively (48). PLAUR expression was also significantly positively correlated with the biomarkers of various infiltrating immune cells. These results suggest that tumor immune infiltration may influence PLAUR-mediated KIRC progression.

IMmotion150 is the first randomized study to evaluate the clinical activity of a combination of antiangiogenic agents and immune checkpoint inhibitors in untreated patients with mRCC (38). In this study, we observed that the relative probabilities of responding to ICI in the low PLAUR group were higher than those in the high PLAUR group using the TCIA database. Another interesting finding was the high PLAUR cases are enriched in the IMmotion150 myeloid signature, which has been previously associated with resistance to single-agent atezolizumab in the IMmotion150 trial (38, 49). Taken together, this data corroborate previous findings from the IMmotion150 trial and add further insights into the possible mechanisms of resistance to ICI in tumors with high myeloid inflammation.

The expression of immunomodulators substantially affects cancer treatment. Therefore, we further examined the relationship between PLAUR and immunomodulators (including 45 immunopotentiators and 24 immunosuppressants) and identified 55 PRIs using the TISIDB database. We performed functional enrichment analyses to investigate further the underlying biological processes and pathways associated with PLAUR in KIRC. A GO enrichment analysis suggested that the 55 PRIs were mainly involved in multiple immune responses. A KEGG pathway analysis of these PRIs showed that the Jak-STAT signaling pathway and cell adhesion molecules might be associated with PLAUR-mediated immune response. PLAUR blockade was reported to inhibit nasopharyngeal carcinoma cell migration and invasion by affecting the expression of phosphorylating Jak1 and STAT1 (50). Unsurprisingly, the Jak-STAT signaling pathway

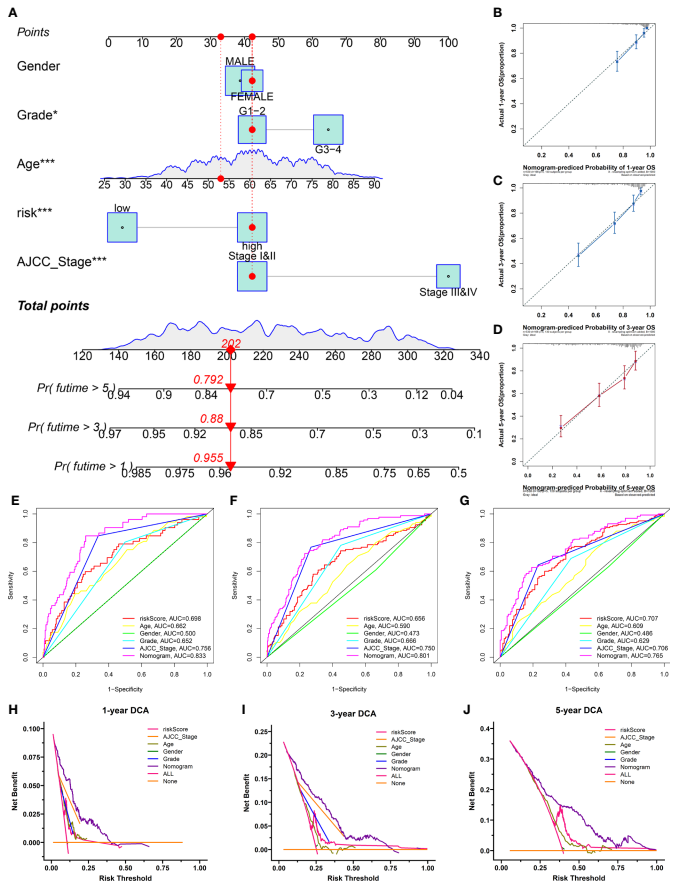



FIGURE 10
The nomogram was developed for prognostic probabilities prediction in the TCGA database. **(A)** Development of a nomogram for predicting survival probability of KIRC patients at 1-, 3-, and 5-years. **(B–D)** The calibration curves of the nomogram at 1-, 3-, and 5-years. **(E–G)** The time-dependent ROC curves of the nomogram at 1-, 3-, and 5-years. **(H–J)** The DCA curves of the nomogram at 1-, 3-, and 5-years. *p<0.05; ***p<0.001.

participates in almost all immunomodulatory processes, such as immune surveillance, inflammation, and tumor-driven immune escape (51). In addition, PLAUR could mediate cell adhesion and initiate intracellular signal transduction pathways (52). Cell adhesion molecules are important for cell-based tissue integrity and immune responses (53).

In this study, we also successfully constructed a PRIs signature to evaluate the prognosis of patients with KIRC. The patients were classified as low- and high-risk based on the median risk score. The Kaplan–Meier curve showed a great difference between the risk groups, and patients of the high-risk group had an unfavorable prognosis compared to those of the low-risk group. The time-dependent ROC curves, scatterplots of the risk score, and PCA analyses confirmed the favorable performance of the signature. Analogous results were achieved in an independent validation cohort. In addition, five PRIs (HHLA2, IL2RA, TNFRSF18, TNFSF14, and CTLA4) included in the signature were regarded as potential PLAUR-related biomarkers in KIRC, which were studied in other cancers including KIRC based on the current literature (7, 54–57). Finally, we developed a nomogram for personalized prognosis prediction by combining signature-based risk scores with various clinical features. These results demonstrated that the PRIs signature has significant prognostic implications in patients with KIRC.

The main strengths of our study are that we have identified the PVT1/SNHG15-hsa-miR-532-3p-PLAUR axis for the first time and constructed a prognostic PRIs signature for patients with KIRC (Figure 11). However, this study does have certain limitations. First, the function and mechanism of the PVT1/SNHG15-hsa-miR-532-3p-PLAUR axis should be further studied experimentally. Second, the clinical application of the PLAUR axis needs to be validated and verified in clinical practice. Third, an independent study with larger sample size is warranted to validate the predictive power of the PRIs signature.

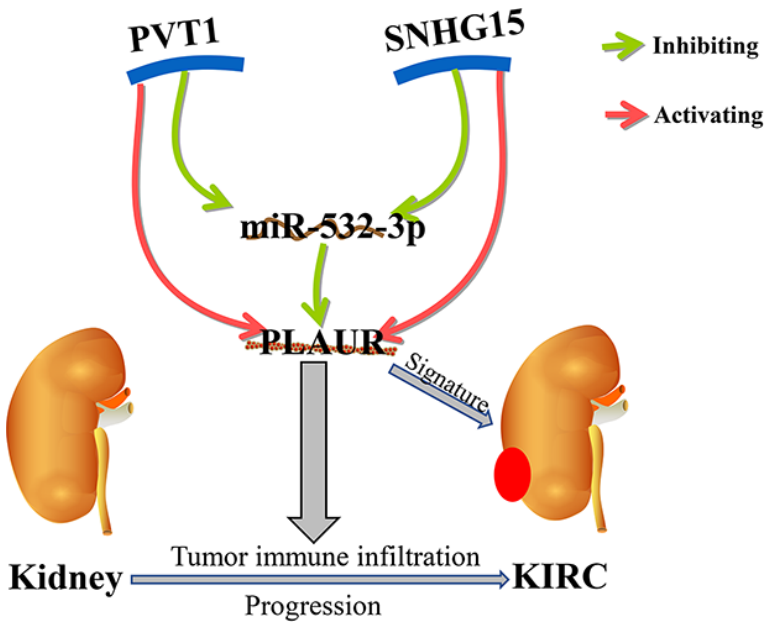



FIGURE 11
The model of PVT1/SNHG15-hsa-miR-532-3p-PLAUR axis in carcinogenesis of KIRC.

## Conclusion

High PLAUR expression was frequently observed in most common cancers and was significantly related to unfavorable outcomes (including OS and DFS) in KIRC. We constructed a PLAUR-related ceRNA regulatory network in KIRC, namely the PVT1/SNHG15-hsa-miR-532-3p-PLAUR axis. In addition, the current study suggested that PLAUR might exert its tumorigenic effect by regulating tumor immune cell infiltration and immunomodulatory expression. The risk signatures derived from PRIs were independently predictive of OS for patients with KIRC and have potentially substantial clinical significance.

## Data availability statement

Publicly available datasets were analyzed in this study. This data can be found here: UCSC Xena Browser (https://xenabrowser.net), and EMBL-EBI database (https://www.ebi.ac.uk/).

## Author contributions

YW and ZS designed the study and wrote this manuscript. SL organized the database. XZ and CX performed the statistical analysis. TL and JW revised the manuscript. All authors have seen and approved the final version of the manuscript. All authors contributed to the article and approved the submitted version.

## Funding

This work was supported by Natural Science Foundation of Guangdong Province (2018A030313261).

## Conflict of interest

The authors declare that the research was conducted in the absence of any commercial or financial relationships that could be construed as a potential conflict of interest.

## Publisher's note

All claims expressed in this article are solely those of the authors and do not necessarily represent those of their affiliated organizations, or those of the publisher, the editors and the reviewers. Any product that may be evaluated in this article, or claim that may be made by its manufacturer, is not guaranteed or endorsed by the publisher.

## Supplementary material

The Supplementary Material for this article can be found online at: https://www.frontiersin.org/articles/10.3389/fonc.2022.834524/full#supplementary-material

# References


1. Siegel RL, Miller KD, Fuchs HE, Jemal A. Cancer statistics, 2021. *CA: Cancer J Clin* (2021) 71(1):7–33. doi: 10.3322/caac.21654

2. Tahbaz R, Schmid M, Merseburger AS. Prevention of kidney cancer incidence and recurrence: lifestyle, medication and nutrition. *Curr Opin Urol* (2018) 28(1):62–79. doi: 10.1097/mou.0000000000000454

3. Hakimi AA, Voss MH, Kuo F, Sanchez A, Liu M, Nixon BG, et al. Transcriptomic profiling of the tumor microenvironment reveals distinct subgroups of clear cell renal cell cancer: Data from a randomized phase III trial. *Cancer Discovery* (2019) 9(4):510–25. doi: 10.1158/2159-8290.cd-18-0957

4. Mitchell TJ, Turajlic S, Rowan A, Nicol D, Farmery JHR, O'Brien T, et al. Timing the landmark events in the evolution of clear cell renal cell cancer: TRACERx renal. *Cell* (2018) 173(3):611–23.e17. doi: 10.1016/j.cell.2018.02.020

5. Rini BI, Battle D, Figlin RA, George DJ, Hammers H, Hutson T, et al. The society for immunotherapy of cancer consensus statement on immunotherapy for the treatment of advanced renal cell carcinoma (RCC). *J Immunother Cancer* (2019) 7(1):354. doi: 10.1186/s40425-019-0813-8

6. Capitanio U, Bensalah K, Bex A, Boorjian SA, Bray F, Coleman J, et al. Epidemiology of renal cell carcinoma. *Eur Urol* (2019) 75(1):74–84. doi: 10.1016/j.eururo.2018.08.036

7. Zhang Z, Liu J, Zhang C, Li F, Li L, Wang D, et al. Over-expression and prognostic significance of HHLA2, a new immune checkpoint molecule, in human clear cell renal cell carcinoma. *Front Cell Dev Biol* (2020) 8:280. doi: 10.3389/fcell.2020.00280

8. Llinas P, Le Du MH, Gårdsvoll H, Danø K, Ploug M, Gilquin B, et al. Crystal structure of the human urokinase plasminogen activator receptor bound to an antagonist peptide. *EMBO J* (2005) 24(9):1655–63. doi: 10.1038/sj.emboj.7600635

9. Li D, Wei P, Peng Z, Huang C, Tang H, Jia Z, et al. The critical role of dysregulated FOXM1-PLAUR signaling in human colon cancer progression and metastasis. *Clin Cancer Res* (2013) 19(1):62–72. doi: 10.1158/1078-0432.CCR-12-1588

10. Wang Y. The role and regulation of urokinase-type plasminogen activator receptor gene expression in cancer invasion and metastasis. *Medicinal Res Rev* (2001) 21(2):146–70. doi: 10.1002/1098-1128(200103)21:2<146::aid-med1004>3.0.co;2-b. PubMed PMID: 11223863

11. Mazar AP. Urokinase plasminogen activator receptor choreographs multiple ligand interactions: implications for tumor progression and therapy. *Clin Cancer Res* (2008) 14(18):5649–55. doi: 10.1158/1078-0432.ccr-07-4863

12. Hu X, Mandika C, He L, You Y, Chang Y, Wang J, et al. Construction of urokinase-type plasminogen activator receptor-targeted heterostructures for efficient photothermal chemotherapy against cervical cancer to achieve simultaneous anticancer and antiangiogenesis. *ACS Appl materials interfaces* (2019) 11(43):39688–705. doi: 10.1021/acsami.9b15751

13. Béné MC, Castoldi G, Knapp W, Rigolin GM, Escribano L, Lemez P, et al. CD87 (urokinase-type plasminogen activator receptor), function and pathology in hematological disorders: a review. *Leukemia* (2004) 18(3):394–400. doi: 10.1038/sj.leu.2403250

14. Indira Chandran V, Eppenberger-Castori S, Venkatesh T, Vine KL, Ranson M. HER2 and uPAR cooperativity contribute to metastatic phenotype of HER2-positive breast cancer. *Oncoscience* (2015) 2(3):207–24. doi: 10.18632/oncoscience.146

15. Salden M, Splinter TA, Peters HA, Look MP, Timmermans M, van Meerbeeck JP, et al. The urokinase-type plasminogen activator system in resected non-small-cell lung cancer. Rotterdam oncology thoracic study group. *Ann Oncol* (2000) 11(3):327–32. doi: 10.1023/a:1008312801800

16. Bhuvarahamurthy V, Schroeder J, Denkert C, Kristiansen G, Schnorr D, Loening SA, et al. *In situ* gene expression of urokinase-type plasminogen activator and its receptor in transitional cell carcinoma of the human bladder. *Oncol Rep* (2004) 12(4):909–13. doi: 10.3892/or.12.4.909

17. Bhuvarahamurthy V, Schroeder J, Kristiansen G, Roigas J, Denkert C, Johannsen M, et al. Differential gene expression of urokinase-type plasminogen activator and its receptor in human renal cell carcinoma. *Oncol Rep* (2005) 14(3):777–82. doi: 10.3892/or.14.3.777

18. Mondino A, Blasi F. uPA and uPAR in fibrinolysis, immunity and pathology. *Trends Immunol* (2004) 25(8):450–5. doi: 10.1016/j.it.2004.06.004

19. Rijneveld AW, Levi M, Florquin S, Speelman P, Carmeliet P, van der Poll T. Urokinase receptor is necessary for adequate host defense against pneumococcal pneumonia. *J Immunol (Baltimore Md 1950)* (2002) 168(7):3507–11. doi: 10.4049/jimmunol.168.7.3507

20. Yang F, Zeng Z, Li J, Zheng Y, Wei F, Ren X. PD-1/PD-L1 axis, rather than high-mobility group alarmins or CD8+ tumor-infiltrating lymphocytes, is associated with survival in head and neck squamous cell carcinoma patients who received surgical resection. *Front Oncol* (2018) 8:604. doi: 10.3389/fonc.2018.00604

21. Salmena L, Poliseno L, Tay Y, Kats L, Pandolfi PP. A ceRNA hypothesis: The Rosetta stone of a hidden RNA language? *Cell* (2011) 146(3):353–8. doi: 10.1016/j.cell.2011.07.014

22. Schmitz SU, Grote P, Herrmann BG. Mechanisms of long noncoding RNA function in development and disease. *Cell Mol Life Sci* (2016) 73(13):2491–509. doi: 10.1007/s00018-016-2174-5

23. Fontemaggi G, Turco C, Esposito G, Di Agostino S. New molecular mechanisms and clinical impact of circRNAs in human cancer. *Cancers* (2021) 13(13):3154. doi: 10.3390/cancers13133154

24. Liu TT, Li R, Huo C, Li JP, Yao J, Ji XL, et al. Identification of CDK2-related immune forecast model and ceRNA in lung adenocarcinoma, a pan-cancer analysis. *Front Cell Dev Biol* (2021) 9:682002. doi: 10.3389/fcell.2021.682002

25. Tang Z, Li C, Kang B, Gao G, Li C, Zhang Z. GEPIA: a web server for cancer and normal gene expression profiling and interactive analyses. *Nucleic Acids Res* (2017) 45(W1):W98–w102. doi: 10.1093/nar/gkx247

26. Li JH, Liu S, Zhou H, Qu LH, Yang JH. starBase v2.0: decoding miRNA-ceRNA, miRNA-ncRNA and protein-RNA interaction networks from large-scale CLIP-seq data. *Nucleic Acids Res* (2014) 42(Database issue):D92–7. doi: 10.1093/nar/gkt1248

27. Newman AM, Steen CB, Liu CL, Gentles AJ, Chaudhuri AA, Scherer F, et al. Determining cell type abundance and expression from bulk tissues with digital cytometry. *Nat Biotechnol* (2019) 37(7):773–82. doi: 10.1038/s41587-019-0114-2

28. Li T, Fan J, Wang B, Traugh N, Chen Q, Liu JS, et al. TIMER: A web server for comprehensive analysis of tumor-infiltrating immune cells. *Cancer Res* (2017) 77(21):e108–e10. doi: 10.1158/0008-5472.can-17-0307

29. Charoentong P, Finotello F, Angelova M, Mayer C, Efremova M, Rieder D, et al. Pan-cancer immunogenomic analyses reveal genotype-immunophenotype relationships and predictors of response to checkpoint blockade. *Cell Rep* (2017) 18(1):248–62. doi: 10.1016/j.celrep.2016.12.019

30. Ru B, Wong CN, Tong Y, Zhong JY, Zhong SSW, Wu WC, et al. TISIDB: an integrated repository portal for tumor-immune system interactions. *Bioinf (Oxford England)* (2019) 35(20):4200–2. doi: 10.1093/bioinformatics/btz210

31. Szklarczyk D, Gable AL, Lyon D, Junge A, Wyder S, Huerta-Cepas J, et al. STRING v11: Protein-protein association networks with increased coverage, supporting functional discovery in genome-wide experimental datasets. *Nucleic Acids Res* (2019) 47(D1):D607–d13. doi: 10.1093/nar/gky1131

32. Liao Y, Wang J, Jaehnig EJ, Shi Z, Zhang B. WebGestalt 2019: Gene set analysis toolkit with revamped UIs and APIs. *Nucleic Acids Res* (2019) 47(W1):W199–w205. doi: 10.1093/nar/gkz401

33. Iasonos A, Schrag D, Raj GV, Panageas KS. How to build and interpret a nomogram for cancer prognosis. *J Clin Oncol* (2008) 26(8):1364–70. doi: 10.1200/jco.2007.12.9791

34. Ross I, Robert G. R. A language and environment for statistical computing R foundation for statistical computing. *J Comput Graph Stat* 5:299–314. doi: 10.1890/0012-9658 (2002)083 [3097:CFHIWS]2.0.CO;2.

35. Foley JH, Conway EM. Cross talk pathways between coagulation and inflammation. *Circ Res* (2016) 118(9):1392–408. doi: 10.1161/CIRCRESAHA.116.306853

36. Date K, Ettelaie C, Maraveyas A. Tissue factor-bearing microparticles and inflammation: a potential mechanism for the development of venous thromboembolism in cancer. *J Thromb Haemost* (2017) 15(12):2289–99. doi: 10.1111/jth.13871

37. Braun DA, Hou Y, Bakouny Z, Ficial M, Sant' Angelo M, Forman J, et al. Interplay of somatic alterations and immune infiltration modulates response to PD-1 blockade in advanced clear cell renal cell carcinoma. *Nat Med* (2020) 26(6):909–18. doi: 10.1038/s41591-020-0839-y

38. McDermott DF, Huseni MA, Atkins MB, Motzer RJ, Rini BI, Escudier B, et al. Clinical activity and molecular correlates of response to atezolizumab alone or in combination with bevacizumab versus sunitinib in renal cell carcinoma. *Nat Med* (2018) 24(6):749–57. doi: 10.1038/s41591-018-0053-3

39. Choueiri TK, Albiges L, Haanen JBAG, Larkin JMG, Uemura M, Pal SK, et al. Biomarker analyses from JAVELIN renal 101: Avelumab + axitinib (A+Ax) versus sunitinib (S) in advanced renal cell carcinoma (aRCC). *J Clin Oncol* (2019) 37(15_suppl):101–. doi: 10.1200/JCO.2019.37.15_suppl.101

40. Swiercz R, Wolfe JD, Zaher A, Jankun J. Expression of the plasminogen activation system in kidney cancer correlates with its aggressive phenotype. *Clin Cancer Res* (1998) 4(4):869–77.

41. Lou W, Wang W, Chen J, Wang S, Huang Y. ncRNAs-mediated high expression of SEMA3F correlates with poor prognosis and tumor immune infiltration of hepatocellular carcinoma. *Mol Ther Nucleic Acids* (2021) 24:845–55. doi: 10.1016/j.omtn.2021.03.014

42. Cen J, Liang Y, Huang Y, Pan Y, Shu G, Zheng Z, et al. Circular RNA circSDHC serves as a sponge for miR-127-3p to promote the proliferation and metastasis of renal cell carcinoma *via* the CDKN3/E2F1 axis. *Mol Cancer* (2021) 20 (1):19. doi: 10.1186/s12943-021-01314-w

43. Wang K, Chen X, Zhan Y, Jiang W, Liu X, Wang X, et al. miR-335 inhibits the proliferation and invasion of clear cell renal cell carcinoma cells through direct suppression of BCL-W. *Tumour Biol* (2015) 36(9):6875–82. doi: 10.1007/s13277-015-3382-6

44. Han M, Yan H, Yang K, Fan B, Liu P, Yang H. Identification of biomarkers and construction of a microRNA–mRNA regulatory network for clear cell renal cell carcinoma using integrated bioinformatics analysis. *PloS One* (2021) 16(1): e0244394. doi: 10.1371/journal.pone.0244394

45. Yang T, Zhou H, Liu P, Yan L, Yao W, Chen K, et al. lncRNA PVT1 and its splicing variant function as competing endogenous RNA to regulate clear cell renal cell carcinoma progression. *Oncotarget* (2017) 8(49):85353–67. doi: 10.18632/oncotarget.19743

46. Du Y, Kong C, Zhu Y, Yu M, Li Z, Bi J, et al. Knockdown of SNHG15 suppresses renal cell carcinoma proliferation and EMT by regulating the NF-κB signaling pathway. *Int J Oncol* (2018) 53(1):384–94. doi: 10.3892/ijo.2018.4395

47. Tabei T, Nakaigawa N, Kaneta T, Ikeda I, Kondo K, Makiyama K, et al. Early assessment with (18)F-2-fluoro-2-deoxyglucose positron emission tomography/computed tomography to predict short-term outcome in clear cell renal carcinoma treated with nivolumab. *BMC Cancer* (2019) 19(1):298. doi: 10.1186/s12885-019-5510-y

48. Wang Y, Yin C, Geng L, Cai W. Immune infiltration landscape in clear cell renal cell carcinoma implications. *Front Oncol* (2020) 10:491621. doi: 10.3389/fonc.2020.491621

49. Lavacchi D, Pellegrini E, Palmieri VE, Doni L, Mela MM, Di Maida F, et al. Immune checkpoint inhibitors in the treatment of renal cancer: Current state and future perspective. *Int J Mol Sci* (2020) 21(13):4691. doi: 10.3390/ijms21134691

50. Bao YN, Cao X, Luo DH, Sun R, Peng LX, Wang L, et al. Urokinase-type plasminogen activator receptor signaling is critical in nasopharyngeal carcinoma cell growth and metastasis. *Cell Cycle (Georgetown Tex)* (2014) 13(12):1958–69. doi: 10.4161/cc.28921

51. Owen KL, Brockwell NK, Parker BS. JAK-STAT signaling: A double-edged sword of immune regulation and cancer progression. *Cancers* (2019) 11(12):2002. doi: 10.3390/cancers11122002

52. Cancello R, Rouault C, Guilhem G, Bedel JF, Poitou C, Di Blasio AM, et al. Urokinase plasminogen activator receptor in adipose tissue macrophages of morbidly obese subjects. *Obes facts* (2011) 4(1):17–25. doi: 10.1159/000324587

53. Läubli H, Borsig L. Altered cell adhesion and glycosylation promote cancer immune suppression and metastasis. *Front Immunol* (2019) 10:2120. doi: 10.3389/fimmu.2019.02120

54. Nukui A, Masuda A, Abe H, Arai K, Yoshida KI, Kamai T. Increased serum level of soluble interleukin-2 receptor is associated with a worse response of metastatic clear cell renal cell carcinoma to interferon alpha and sequential VEGF-targeting therapy. *BMC Cancer* (2017) 17(1):372. doi: 10.1186/s12885-017-3369-3

55. Yu N, Fu S, Xu Z, Liu Y, Hao J, Zhang A, et al. Synergistic antitumor responses by combined GITR activation and sunitinib in metastatic renal cell carcinoma. *Int J Cancer* (2016) 138(2):451–62. doi: 10.1002/ijc.29713

56. Xu F, Guan Y, Zhang P, Xue L, Yang X, Gao K, et al. The impact of TNFSF14 on prognosis and immune microenvironment in clear cell renal cell carcinoma. *Genes Genomics* (2020) 42(9):1055–66. doi: 10.1007/s13258-020-00974-0

57. Bedke J, Kruck S, Gakis G, Stenzl A, Goebell PJ. Checkpoint modulation–a new way to direct the immune system against renal cell carcinoma. *Hum Vaccines immunotherapeutics* (2015) 11(5):1201–8. doi: 10.1080/21645515.2015.1016657

# Advantages of publishing in Frontiers

**OPEN ACCESS**
Articles are free to read for greatest visibility and readership

**FAST PUBLICATION**
Around 90 days from submission to decision

**HIGH QUALITY PEER-REVIEW**
Rigorous, collaborative, and constructive peer-review

**TRANSPARENT PEER-REVIEW**
Editors and reviewers acknowledged by name on published articles

**Frontiers**
Avenue du Tribunal-Fédéral 34
1005 Lausanne | Switzerland

**Visit us:** www.frontiersin.org
**Contact us:** frontiersin.org/about/contact

**REPRODUCIBILITY OF RESEARCH**
Support open data and methods to enhance research reproducibility

**DIGITAL PUBLISHING**
Articles designed for optimal readership across devices

**FOLLOW US**
@frontiersin

**IMPACT METRICS**
Advanced article metrics track visibility across digital media

**EXTENSIVE PROMOTION**
Marketing and promotion of impactful research

**LOOP RESEARCH NETWORK**
Our network increases your article's readership